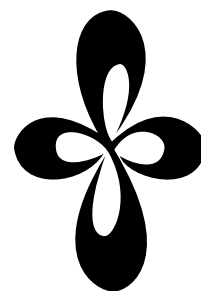


ANNUAL REVIEW

***INSTITUTE
FOR
MOLECULAR
SCIENCE***



2006
(Sep. 2005 ~ Aug. 2006)

Published by

Institute for Molecular Science

National Institutes of Natural Sciences

Myodaiji, Okazaki 444-8585, Japan

Phone: +81-564-55-7418 (Secretary Room)

Fax: +81-564-54-2254 (Secretary Room)

URL: <http://www.ims.ac.jp/>

Editorial Committee 2006

Chairperson

TSUKUDA, Tatsuya

Vice-Chairperson

KAWAGUCHI, Hiroyuki

YAMASHITA, Yasufumi

IMURA, Kohei

JUDAI, Ken

FURUKAWA, Ko

ISHIZUKA, Tomoya

TERO, Ryugo

MIURA, Shinichi

ISHIDA, Tateki

MATSUO, Tsukasa

TANAKA, Hirofumi

WATANABE, Kazuya

ITO, Takahiro

ISHIZUKI, Hideki

YOSHIOKA, Shiro

KAMO, Kyoko

NAKAMURA, Rie

IMS 2006

The newly established National Institutes of Natural Sciences (NINS), the parent organization of The Institute for Molecular Science, has entered its third year.

In the current unfortunate trend that society does not attach much importance to “basic sciences,” we have to strive to appeal to the public for recognizing the significance. After the incorporation of national universities and institutes, this has become one of the most important roles that the Inter-University Research Institutes (IURIs) like IMS should play. In order to explain the roles and significance of IURIs, we have written up “What is an IURI?” and put it on the home page.

Currently at the IMS the following four special programs are successfully going on, although the supports should further be strengthened: (i) Extreme Photonics in collaboration with RIKEN, (ii) COE of molecular and materials simulations as a joint research program of NINS, (iii) Nanotechnology support project, including the joint research initiatives using the cutting-edge 920 MHz NMR machine, and (iv) Development of nano-science simulations for the “Grand Challenge Applications” in the Petaflops super-computer project.

The IMS international collaboration program has gotten on the track and many fruitful collaborative researches are now underway. In addition, the new Asian Core Program has been approved. This enables us to conduct collaborative researches among Asian countries and also to bring up young Asian scientists.

In order to confront the present severe financial circumstances, we are planning to establish a network with universities so that we can work together to purchase new and revive old experimental equipments efficiently.

In order to convince the society of the importance of basic sciences and also to repay the government support, it is essential to conduct excellent research as a Center of Excellence. All members of IMS must strive to further their studies.

This volume of Annual Review is a comprehensive summary of research activities carried out at the IMS in the period of September 2005–August 2006. As usual, a lot of activities are going on and we are proud of that. Any constructive comments and/or questions are heartily welcome. It is also a great pleasure to announce that many colleagues received various prizes as explained in the end of this volume.

October, 2006



H. Nakamura

NAKAMURA, Hiroki
Director General, Institute for Molecular Science

CONTENTS

IMS 2006 -----	iii
CONTENTS -----	v
ORGANIZATION AND STAFF-----	1
COUNCIL -----	11
BUILDINGS AND CAMPUS -----	13
RESEARCH ACTIVITIES I-----	15

Department of Theoretical Studies

I-A Theoretical Study and Design of Functional Molecular Systems:

New Bonding, Structures, and Reactions -----	15
I-A-1 Effect of the Axial Cysteine Ligand on the Electronic Structure and Reactivity of High-Valent Iron (IV) Oxo-Porphyrins (Compound I): A Theoretical Study -----	15
I-A-2 $\text{Sc}_3\text{N@C}_{80}$: Computations on the Two-Isomer Equilibrium at High Temperatures -----	15
I-A-3 The Aromaticity of the Stannole Dianion-----	15
I-A-4 Reversible and Regioselective Reaction of La@C_{82} with Cyclopentadiene-----	15
I-A-5 Structural Determination of Metallofullerene Sc_3C_{82} Revisited: A Surprising Finding -----	16
I-A-6 Electronic Structures of Semiconducting Double-Walled Carbon Nanotubes: Important Effect of Interlayer Interaction -----	16
I-A-7 Positional Control of Encapsulated Atoms inside a Fullerene Cage by Exohedral Addition---	16
I-A-8 A Singly Bonded Derivative of Endohedral Metallofullerene: $\text{La@C}_{82}\text{CBr}(\text{COOC}_2\text{H}_5)_2$ -----	16
I-A-9 S-Heterocyclic Carbene with a Disilane Backbone -----	16
I-A-10 Ab Initio and DFT Study of the ^{29}Si NMR Chemical Shifts in $\text{RSi}\equiv\text{SiR}$ -----	17
I-A-11 A New Parallel Algorithm of MP2 Energy Calculations-----	17
I-A-12 Synthesis and Properties of a New Kinetically Stabilized Digermyne: New Insights for a Germanium Analogue of an Alkyne -----	17
I-A-13 Computational Modelling for the Clustering Degree in the Saturated Steam and the Water-Containing Complexes in the Atmosphere -----	17
I-A-14 Analysis of Lanthanide-Induced NMR Chemical Shifts of the Ce@C_{82} Anion-----	17
I-A-15 Synthesis and Structural Characterization of Endohedral Pyrrolidinometallofullene: $\text{La}_2\text{@C}_{80}(\text{CH}_2)_2\text{NTrt}$ -----	18
I-A-16 $\text{La}_2\text{@C}_{72}$ and $\text{Sc}_2\text{@C}_{72}$: Computational Characterizations -----	18
I-A-17 Reactivity of 1-Hydro-5-Carbaphosphatrane Based on Tautomerization between Pentavalent Phosphorane and Trivalent Cyclic Phosphonite-----	18
I-A-18 Evolution of the Electronic Properties of Metallic Single-Walled Nanotubes with the Degree of CCl_2 Covalent Functionalization -----	18
I-A-19 Stability Computations for Ba@C_{74} Isomers -----	18
I-A-20 Comment on Disproving a Silicon Analog of an Alkyne with the Aid of Topological Analyses of the Electronic Structure and Ab Initio Molecular Dynamics Calculations -----	18
I-A-21 Selective Interaction of Larger or Charge-Transfer Aromatic Molecules with Metallic Single-Wall Carbon Nanotubes: Critical Role of the Molecular Size and Orientation-----	19
I-A-22 Excited Electronic States and Relative Stabilities of C_{80} Isomers-----	19
I-A-23 Synthesis and Characterization of a Bisadduct of La@C_{82} -----	19
I-A-24 ^{13}C NMR Spectroscopic Study of Scandium Dimetallofullerene, $\text{Sc}_2\text{@C}_{84}$ vs. $\text{Sc}_2\text{C}_2\text{@C}_{82}$ -----	19
I-A-25 H_2 , Ne, and N_2 Energies of Encapsulation into C_{60} Evaluated with the MPWB1K Functional-----	19
I-A-26 Host-Guest Complexation of Endohedral Metallofullerene with Azacrown Ether and Its Application -----	20
I-A-27 Synthesis of Stannaindenyl Anions and a Dianion -----	20
I-A-28 The Bingel Monoadducts of La@C_{82} : Synthesis, Characterization, and Electrochemistry---	20
I-A-29 Syntheses, Structures, and Reactions of Heptacoordinate Trihalogermanes Bearing a Triarylmethyl-Type Tetradentate Ligand-----	20
I-A-30 Structural and Electronic Properties of Fluorinated Boron Nitride Nanotubes -----	20
I-A-31 Characterization of the Bis-Silylated Endofullerene $\text{Sc}_3\text{N@C}_{80}$ -----	20
I-A-32 Synthesis and Characterization of Dimetallostannafluorenes -----	21
I-A-33 Carbon Monoxide inside an Open-Cage Fullerene-----	21

I-B Applications of the Zhu-Nakamura Theory to Nonadiabatic Chemical Dynamics -----	22
I-B-1 Generalized Trajectory Surface Hopping Method Based on the Zhu-Nakamura Theory -----	22
I-B-2 Semiclassical Treatment of Thermally Activated Electron Transfer in the Intermediate to Strong Electronic Coupling Regime under the Fast Dielectric Relaxation -----	22
I-B-3 Electron Transfer Rate Uniformly Valid from Nonadiabatic to Adiabatic Regime Based on the Zhu-Nakamura Theory -----	22
I-B-4 Incorporation of Nonadiabatic Transition into Wave-Packet Dynamics-----	22
I-B-5 Dynamics of Nonadiabatic Chemical Reactions -----	22
I-C Theory of Multi-Dimensional Tunneling -----	23
I-C-1 Tunneling Splitting of Energy Levels and Rotational Constants in the Vinyl Radical C_2H_3 ---	23
I-D Laser Control of Molecular Processes and Development of Molecular Functions -----	23
I-D-1 Semiclassical Guided Optimal Control of Molecular Dynamics-----	23
I-D-2 Selective Transition to the Closely-Lying States $Cs(7D_{3/2})$ and $Cs(7D_{5/2})$ by Femtosecond Laser Pulses-----	23
I-D-3 Ab Initio Nonadiabatic Quantum Dynamics of Cyclohexadiene/Hexatriene Ultrafast Photoisomerization-----	24
I-D-4 Atomic Hydrogen Transmission through Five-Membered Carbon Ring by the Mechanism of Non-Adiabatic Tunneling -----	24
I-D-5 Laser Control of Reactions of Photoswitching Functional Molecules -----	24
I-D-6 Laser Control of Chemical Dynamics: Control of Electronic Transitions by Quadratic Chirping-----	24
I-D-7 Laser Control of Chemical Dynamics: Control of Wave Packet Motion-----	25
I-E Theoretical Studies of Electron Dynamics -----	26
I-E-1 Photoinduced Electric Currents in Ring-Shaped Molecules by Circularly Polarized Laser Pulses -----	26
I-E-2 An Efficient Numerical Method for Exciton States in Quantum Boxes -----	26
I-F Electronic Structure Theory of Quantum Dissipative Systems -----	26
I-F-1 Electronic Structure Theory of Adsorbate-Surface Systems -----	26
I-F-2 Electronic Structure Calculations at Constant Chemical Potential toward the Application to Electrochemistry -----	27
I-G Electronic Structures and Photochemical Properties of Nanometer-Sized Metal Clusters -----	27
I-G-1 Theoretical Investigation of Optimized Structures of Thiolated Gold Cluster $[Au_{25}(SCH_3)_{18}]^+$ -----	27
I-G-2 Gold-Thiolate Nanoring: Electronic Structure and Photochemical Properties-----	27
I-H Electronic Structure of a Molecule in Solution -----	28
I-H-1 A New Method to Determine Electrostatic Potential around a Macromolecule in Solution from Molecular Wave Function-----	28
I-H-2 Ab Initio Theoretical Study of Temperature and Density Dependence of Molecular and Thermodynamic Properties of Water in the Entire Fluid Region: Autoionization Processes-----	28
I-H-3 Conformational Equilibrium of 1,2-Dichloroethane in Water: Comparison of PCM and RISM-SCF Methods -----	28
I-I Solvation Thermodynamics of Protein and Related Molecules -----	29
I-I-1 Locating Missing Water Molecules in Protein Cavities by the Three-Dimensional Reference Interaction Site Model (3D-RISM) Theory of Molecular Solvation-----	29
I-I-2 Conformational Equilibria in Liquids Consisting of Small Chain Molecules -----	29
I-I-3 Theoretical Study of Volume Changes Accompanying Xenon-Lysozyme Binding: Implication for Molecular Mechanism of Pressure Reversal of Anesthesia-----	30
I-I-4 A Theoretical Analysis on Hydration Thermodynamics of Proteins-----	30
I-I-5 Selective Ion-Binding by Protein Probed with the 3D-RISM Theory -----	30
I-J Collective Density Fluctuations in Polar Liquids and Their Response to Ion Dynamics -----	30
I-J-1 Study of Anomalous Mobility of Polar Molecular Solutions by Means of the Site-Site Memory Equation Formalism -----	31
I-K Statistical Mechanics of Interfacial Fluids -----	31
I-K-1 Criticality of a Liquid-Vapor Interface from an Inhomogeneous Integral Equation Theory ---	31
I-L Photoinduced Phase Transitions in Molecular Materials -----	32
I-L-1 Interchain Coupling Effects on Photoinduced Phase Transitions between Neutral and Ionic Phases in an Extended Hubbard Model with Alternating Potentials and an Electron-Lattice Coupling -----	32
I-L-2 Inter-Chain Coulomb-Lattice Relaxation and Multicriticality in Charge Transfer Organic Complexes -----	32
I-L-3 Quantum Paraelectricity near the Neutral-Ionic Critical Point -----	32
I-L-4 Dynamics of Photoexcited States in One-Dimensional Dimerized Mott Insulators -----	33

I-L-5 Charge Ordering in θ -(BEDT-TTF) ₂ RbZn(SCN) ₄ : Cooperative Effects of Electron Correlations and Lattice Distortions -----	33
I-M Collective Transport through Metal-Insulator Interfaces-----	33
I-M-1 Mechanism of Ambipolar Field-Effect Transistors on One-Dimensional Organic Mott Insulators-----	33
I-N Polyamorphism in Molecular Liquids -----	35
I-N-1 Murnaghan's Equation of Motion Revisited -----	35
I-N-2 Polyamorphism in Tin Tetraiodide -----	35
I-N-3 New Method for Inversion from Structure Factors to Radial Distributions-----	35
I-N-4 Changes in Orientational Correlations in a Molecular Liquid on Compression -----	36
I-O Molecular Dynamics Simulations of Proteins-----	37
I-O-1 Determinants of Water Permeability in Aquaporin Family: A Comparative Simulation Study -----	37
I-P Bioinformatics Studies of Proteins-----	37
I-P-1 Normal Mode Analysis Fixing the External Degrees of Freedom for Any Portion of a System-----	37
I-P-2 Probabilistic Alignment Detects Remote Homology in a Pair of Protein Sequences without Homologous Sequence Information -----	37
I-Q Theoretical Studies on Dynamical Foundation of Chemical Reactions and Proteins-----	39
I-Q-1 Dynamical Hierarchy in Transition States of Reactions-----	39
I-Q-2 Definability of No-Return Transition States in High Energy Regime above Reaction Threshold-----	39
I-Q-3 Wavelet Analysis and Arnold Web Picture for Detecting Energy Transfer in a Hamiltonian Dynamical System-----	39
I-Q-4 Foundation and Limitations of Statistical Reaction Theory -----	40
I-Q-5 Bifurcation of Transition States in Many-Degrees of Freedom Chemical Reactions: Non-Collinear H ₂ +H Exchange Reaction-----	40
I-Q-6 Fractional Behavior in Nonergodic Reaction Processes of Isomerization -----	40
I-Q-7 Mechanism of Fast Energy Exchange between Two NO Vibrations in a Short Lifetime Path of O(1D)+N ₂ O→NO+NO: Analyses by the Normal Form Theory-----	40
I-Q-8 Topographical Complexity of Multidimensional Energy Landscapes-----	40
I-Q-9 A New Scheme to Construct Multidimensional Effective Free Energy Landscape from Single Molecule Time Series-----	41
I-R Analysis Method of Electronic Structure-----	42
I-R-1 Analysis on Solvated Molecule with a New Energy Partitioning Scheme for Intra- and Intermolecular Interactions-----	42
I-R-2 A New Analysis of Molecular Orbital Wavefunctions Based on Resonance Theory -----	42
I-R-3 Solvation Effect on Resonance Structure. Extracting Valence Bond-Like Character from Molecular Orbitals-----	42
I-S Solvation Structure and Its Effect on Electronic Structure-----	42
I-S-1 A New Method to Reconstruct Three-Dimensional Spatial Distribution Function from Radial Distribution Function in Solvation Structure -----	42
I-S-2 New Evaluation of Reconstructed Spatial Distribution Function from Radial Distribution Functions -----	43
RESEARCH ACTIVITIES II-----	45

Department of Molecular Structure

II-A Development of Dynamic Near-Field Spectroscopy and Application to Nanometric Systems ----	45
II-A-1 Photoluminescence from Gold Nanoplates Induced by Near-Field Two-Photon Absorption-----	45
II-A-2 Near-Field Imaging of SERS-Active Hot Spots on Metal-Nanoparticle Aggregates-----	46
II-A-3 Reciprocity in Scanning Near-Field Optical Microscopy: Illumination and Collection Modes of Transmission Measurements-----	46
II-A-4 Near-Field Raman Study on the Close-Packed 2D Nanostructures of Gold Nanoparticles ---	47
II-A-5 Enhancement and Quenching of Fluorescence from Dye Molecules by Single Gold Nanoparticles-----	47
II-A-6 Near-Field Two-Photon-Induced Photoluminescence from Single Gold Nanorods -----	47
II-A-7 Ultrafast Near-Field Transient Imaging of Single Gold Nanorods-----	47
II-A-8 Scanning Near-Field Optical Microscopic Study of Porphyrin Nanowire-----	48
II-B Development of a Novel Solid-State NMR Technique -----	49
II-B-1 Remarkable Reduction of RF Power by ATANSEMA and DATANSEMA Separated Local Field in Solid-State NMR Spectroscopy -----	49

II-B-2 Reduction of RF Power by Duration and Amplitude Time-Averaged Nutation Cross Polarization in Solid State NMR Spectroscopy	49
II-C Structural Characterization of Biomolecules by Solid State NMR	50
II-C-1 Histidines, Heart of the Hydrogen Ion Channel from Influenza A Virus: Toward an Understanding of Conductance and Proton Selectivity	50
II-C-2 Conformational Changes of Adrenocorticotrophic Hormone, ACTH (1-24), Bound to Lipid Bilayers, Dependent upon Proportion of Lipids Composition, as Studied by Solid State NMR ..	50
II-D Structure and Function of Metalloproteins and Its Molecular Design	51
II-D-1 Absence of a Detectable Intermediate in the Compound I Formation of Horseradish Peroxidase at Ambient Temperature	51
II-D-2 Dehydration in the Folding of Reduced Cytochrome <i>c</i> Revealed by the Electron-Transfer-Triggered Folding under High Pressure	51
II-D-3 Time-Resolved Small Angle X-Ray Scattering Investigation on the Folding Dynamics of Heme Oxygenase: Implication of the Scaling Relationship for the Submillisecond Intermediates of Protein Folding	52
II-E Structure and Energy Changes during Protein Reaction Dynamics	53
II-E-1 Time-Resolved Thermodynamics: Heat Capacity Change of Transient Species during Photo-Reaction of PYP	53
II-E-2 Conformational Changes of PYP Monitored by Diffusion Coefficient: Effect of N-Terminal α -Helices	53
II-E-3 Diffusion Coefficient and the Secondary Structure of Poly-L-Glutamic Acid in Aqueous Solution	53
II-F Surface Magnetism of Ultrathin Films:	
Search of New Phenomena and Exploitation of New Techniques	54
II-F-1 Effect of Adsorbate Carbon on Spin Reorientation Transitions in Cu-Capped Ultrathin Ni Films on Cu(001)	54
II-F-2 Effect of Surface Chemisorption on the Spin Reorientation Transition in Magnetic Ultrathin Fe Film on Ag(001)	54
II-F-3 Magnetic Circular Dichroism near the Fermi Level: Possibility of UV MCD PEEM	55
II-G Development of Fluorescent and Bioluminescent Proteins for Imaging Biomolecules	57
II-G-1 A Short Peptide Sequence that Targets Fluorescent and Functional Proteins into the Mitochondrial Intermembrane Space	57
II-G-2 Intein-Mediated Reporter Gene Assay for Detecting Protein-Protein Interactions in Living Mammalian Cells	57
II-G-3 A Genetically Encoded Indicator for Assaying Bioactive Chemicals that Induce Nuclear Transport of Glucocorticoid Receptor	57
II-G-4 A Method for Determining the Activities of Cytokines Based on the Nuclear Transport of Nuclear Factor- κ B	58

RESEARCH ACTIVITIES III **59**

Department of Electronic Structure

III-A Synthesis and Characterization of Exotic Molecule Based Nano-Crystals of Metal Acetylides: Toward Carbon Encapsulated Metal Dot Array, Metal Nano-Networks and Metal-Carbon Hybrid Devices	59
III-A-1 Electric Conductivity of Self-Assembled Copper Acetylide Nanowires and Nanocables	59
III-A-2 Crystal Structure of C_2Cu_2 Nanowires by X-Ray Diffraction and DFT Calculation	60
III-A-3 Photoconversion of Organometallic Cluster Thin Films to Metallic Copper-Sheets Sandwiched in Polymers	60
III-A-4 Synthesis of Carbon-Encapsulated Nanoparticles <i>via</i> Thermal Decomposition of Metal Acetylide	61
III-A-5 Synthesis, Structure and Magnetic Properties of a New Low-Spin Iron(III) Complex $[FeL_3]$ $\{L = [HNC(CH_3)_2C(CN)]\}$	61
III-A-6 Preparation and Characterization of Gold Nanoparticles with Reactive Thiocarbonyls: A Proposal for Active Size Control of Nanoparticles	62
III-B Ultrafast Dynamics and Scanning Tunneling Microscopy	62
III-B-1 Ultrafast Dynamics of Excited States of Chromium(III) Porphyrin Complexes in Solution ..	62
III-B-2 Scanning-Tunneling Microscopy, Near-Edge X-Ray-Absorption Fine Structure, and Density-Functional Theory Studies of N_2O Orientation on Pd(110)	63
III-C Spectroscopic and Dynamical Studies of Molecular Cluster Ions	63
III-C-1 IR Photodissociation Spectroscopy of Hydrated Noble Metal Ions: Coordination and Solvation Structures	63
III-D Development of High-Precision Coherent Control and Its Applications	64
III-D-1 Visualizing Picometric Quantum Ripples of Ultrafast Wave-Packet Interference	64

III-D-2	Real-Time Observation of Phase-Controlled Molecular Wave-Packet Interference	64
III-D-3	Implementation of Quantum Gate Operations in Molecules with Weak Laser Fields	65
III-E	Quantum-State Manipulation of Molecular Motions	66
III-E-1	Nonadiabatic Population Transfer by Intense Femtosecond Laser Light	66
III-E-2	Wavepacket Observation of Methyl Internal Rotation in Substituted Toluenes	66
III-E-3	Development of High-Resolution Coherent Pulsed Lasers	67
III-E-4	Laser Spectroscopy of the van der Waals Vibrations of Benzene–Water	67
III-F	Spectroscopy of Jet-Cooled Aromatic Molecules and Photochemical Reaction of Aza- and Thio-Substituted Nucleobases	68
III-F-1	Conformation of 2-Aminoindan in a Supersonic Jet: The Role of N–H··· π Hydrogen Bonding	68
III-F-2	Conformation of Thioanisole in a Supersonic Jet	68
III-F-3	Excited-State Dynamics of 6-Azauracil with UVA Light Irradiation	68
III-F-4	Ultrafast Excited-State Dynamics of 4-Thiothymidine in Aqueous Solution	68
III-G	Photochemical Reactions in Microreactors	69
III-G-1	Application of Microreactors for Photoreactions	69
III-G-2	Photocatalytic Reduction in Microreactors	69
III-H	Coherent Phonon Dynamics in Crystals	71
III-H-1	Femtosecond Pump-Probe Study of Coherent Soft Phonon in Ferroelectric Materilas	71
III-H-2	Temperature Dependence of Coherent A_{1g} and E_g Phonons of Bismuth	71
III-I	In-Situ Observation of Surface Reactions by Variable Temperature Scanning Tunneling Microscopy	72
III-I-1	Spontaneous Formation of Stripe Phase under the Dynamic Equilibrium between Adsorption and Desorption of H ₂ O on O-Covered Ag(110) Surfaces	72
III-I-2	Direct Observation of a Propagating Chemical Wave in Disproportionation Reactions of Water on Oxidized Ag(110) Surface by Scanning Tunneling Microscopy	72
III-J	High-Resolution Spectroscopy and Excited-State Dynamics of Jet-Cooled Molecules	73
III-J-1	Vibronic Structure in the S_1 – S_0 Transition of Jet-Cooled Dibenzofuran	73
III-J-2	Energy Levels of CH ₃ Rotation in the S_1 and S_0 States of 9-Methylantracene	73
III-J-3	High-Resolution Spectroscopy of the T_1 $^3A_u(n\pi^*)$ State of Oxalyl Chloride	73
RESEARCH ACTIVITIES IV		75
Department of Molecular Assemblies		
IV-A	Optical Study of Charge Ordering States in Organic Conductors	75
IV-A-1	Charge Ordering State of β'' -(ET) ₃ (HSO ₄) ₂ and β'' -(ET) ₃ (ClO ₄) ₂ by Temperature-Dependent Infrared and Raman Spectroscopy	75
IV-A-2	Infrared and Raman Studies of the Charge-Ordering Phase Transition at ~170 K in the Quarter-Filled Organic Conductor, β'' -(ET)(TCNQ)	76
IV-A-3	Unusual Intermediate State between Metallic and Charge-Ordered States in θ -Type ET Salts	76
IV-A-4	Photo-Gatable Second Harmonic Generation in Ferroelectric Organic Conductor with Strongly Correlated Electrons	77
IV-A-5	Evaluation of Charge Transfer Degree in the Bis(ethylenethio) Tetrathiafulvalene Salts by Raman Spectroscopy	77
IV-A-6	Installation of a Cryostat to the Far-Infrared Spectrometer and the Transmission Measurement of α -(BEDT-TTF) ₂ I ₃	77
IV-A-7	Mechanism of the Phase Separation in the Monovalent-to-Divalent Phase Transition of Biferrocenium-(F ₁ TCNQ) ₃	77
IV-B	Magnetic Resonance Studies for Molecular-Based Conductors	79
IV-B-1	Deuteration Effect and Possible Origin of the Charge-Ordering Transition of (TMTTF) ₂ X	79
IV-B-2	¹³ C NMR Analyses of Successive Charge Ordering in (TMTTF) ₂ ReO ₄	80
IV-B-3	Redistribution of Electronic Charges in the Spin-Peierls State in (TMTTF) ₂ AsF ₆ Observed by ¹³ C NMR	80
IV-B-4	The Effect of Deuteration on the Transition into a Charge Ordered State of (TMTTF) ₂ X Salts	81
IV-B-5	Magnetic Properties of Hexa- <i>peri</i> -hexabenzocoronene Nanotube Investigated by Magnetic Resonance	81
IV-B-6	X-Ray Structural Study of Charge and Anion Orderings of TMTTF Salts	81
IV-B-7	Depinning of the Spin-Density Wave in (TMTTF) ₂ Br under Pressure	82
IV-B-8	Pulsed ESR Measurements for (TMTTF) ₂ X	82
IV-B-9	Synchrotron X-Ray Diffraction Experiments and MEM Analyses for the Charge-Ordering State of (TMTTF) ₂ PF ₆	82

IV-B-10	<i>g</i> -Anisotropy of the S ₂ -State Manganese Cluster in Single Crystals of Cyanobacterial Photosystem II Studied by W-Band Electron Paramagnetic Resonance Spectroscopy	83
IV-C	Development of Multi-Functional Molecular Systems	84
IV-C-1	Phase Diagram and Anomalous Resistivity Behavior of λ -(BETS) ₂ Fe _x Ga _{1-x} Cl ₄	84
IV-C-2	Magnetic Transitions of Single-Component Molecular Metal [Au(tmdt) ₂] and Its Alloy Systems	84
IV-C-3	Molecular Design and Physical Properties of Single-Component Molecular Metals	85
IV-C-4	A Molecular Conductor Based on Monoanionic Nickel Complex with Extended-TTF Type Ligands, (tBu ₄ N)[Ni(dmstfdt) ₂] Exhibiting Weakly Metallic Behavior at High Temperature and Weak Ferromagnetism at Low Temperature	85
IV-C-5	Ferroelectric Porous Molecular Crystal, [Mn ₃ (HCOO) ₆](C ₂ H ₅ OH)	86
IV-C-6	Antiferroelect Porous Molecular Crystal with Guest Water Molecules	86
IV-C-7	High-Pressure Four-Probe Resistivity Measurements of Organic Crystals	87
IV-C-8	Electrical Conductivity Modulation Coupled to a High-Spin–Low-Spin Conversion in the Molecular System [Fe ^{III} (qsal) ₂][Ni(dmit) ₂] ₃ ·CH ₃ CN·H ₂ O	87
IV-C-9	Structural Modifications Accompanying a Reproducible Spin-Crossover Phenomenon in [Fe(qsal) ₂][Ni(dmise) ₂]·2CH ₃ CN	88
IV-C-10	A Magnetic Organic Conductor Based on a π Donor with a Stable Radical and a Magnetic Anion—A Step to Magnetic Organic Metals with Two Kinds of Localized Spin Systems	88
IV-C-11	Synthesis and Characterization of Novel PROXYL-Fused π -Electron Donors	89
IV-D	Progress of Conjugated Phenomena Coupled with Spin, Charge and Photon for Assembled Hetero-Molecular System	90
IV-D-1	Enhancement of the Curie Temperature by Photoisomerization of Diaryl-Ethene (DAE) for an Organic–Inorganic Hybrid System: Co ₄ (OH) ₇ (DAE) _{0.5} ·3H ₂ O	90
IV-D-2	Charge Transfer Phase Transition and Ferromagnetism in Organic-Inorganic Hybrid System, A[Fe ^{II} Fe ^{III} (dto) ₃](A = (C _n H _{2n+1}) ₄ N, Spiropyran, <i>etc.</i> ; dto = C ₂ O ₂ S ₂)	90
IV-E	Charge and Spin Dynamics of Organic Conductors	92
IV-E-1	Charge Ordering State on Organic Conductors	92
IV-E-2	¹³ C-NMR Study of Single Crystal of β' -(BEDT-TTF)(TCNQ) under Pressure	92

RESEARCH ACTIVITIES V ----- 93

Department of Applied Molecular Science

V-A	Design of Spin-Functional Nanomaterials through Molecular Programming and Nanostructuring	93
V-A-1	Molecular Design and Functions of Spin-Active Dendrimers	93
V-A-2	Molecular Design and Functions of Spin-Active One-Dimensional Nano-Channels	93
V-B	Bioinorganic Chemistry and Structural Biology of Heme Proteins	94
V-B-1	Compound I of Heme Oxygenase Can Not Hydroxylate Its Heme <i>meso</i> -Carbon	94
V-C	Electronic Structure and Phase Stability of Bulk Metallic Glass	95
V-C-1	Electronic Structure of Bulk Metallic Glass Zr ₅₅ Al ₁₀ Cu ₃₀ Ni ₅	95
V-C-2	Free-Energy Estimation of the Zr-Ni-Al Bulk Metallic Glass from the Local Atomic Arrangements of the Relevant Crystals	95
V-C-3	Investigation of Stability of the Zr-Ni-Al Bulk Amorphous Phase from Local Atomic Arrangements of the Relevant Crystals	95
V-C-4	Electronic Structure of Zr-TM-Al (TM = Ni, Cu) Bulk Metallic Glasses	96
V-D	Electronic Structures of Fe₂VAl Intermetallic Compound and Its Related Alloys	96
V-D-1	Surface and Bulk Electronic Structures of Heusler-Type Fe ₂ VAl	96
V-E	Phase Dynamics under Ultra-High Pressures	97
V-E-1	Nanosecond Rapid Freezing of Liquid Benzene under Shock Compression Studied by Time-Resolved Coherent Anti-Stokes Raman Spectroscopy	97
V-E-2	Time-Resolved Coherent Anti-Stokes Raman Scattering of Cyclohexane under Shock Compression	97
V-F	Pyrrrole-Based Molecular Assemblies and Supramolecular Structures	98
V-F-1	Dipyrrolyldiketone Difluoroboron Complexes: Novel Anion Sensors with C–H···X [−] Interactions	98
V-F-2	CH···Anion Interaction in BF ₂ Complexes of C ₃ -Bridged Oligopyrroles	98
V-F-3	BF ₂ Complex of Fluorinated Dipyrrolyldiketone: A New Class of Efficient Receptor for Acetate Anions	98
V-F-4	Dipyririn-Porphyrin Hybrids: Potential π -Conjugated Platform to Fabricate Coordination Oligomers	99
V-F-5	Nanoscale Spherical Architectures Fabricated by Metal Coordination of Multiple Dipyririn Moieties	99

RESEARCH ACTIVITIES VI-----101**Department of Vacuum UV PhotoScience**

VI-A Electronic Structure and Decay Mechanism of Inner-Shell Excited Molecules-----	101
VI-A-1 Improvement of the Energy Resolution of Transmission Grating Soft X-Ray Emission Spectrometer-----	101
VI-A-2 Development of a Sub-Pixel Resolution CCD for High Resolution Soft X-Ray Emission Spectrometer-----	101
VI-B Soft X-Ray Photoelectron-Photoabsorption Spectroscopy and Electronic Structure of Molecular Solids and Clusters-----	102
VI-B-1 Orbital-Dependent Stabilization in the Valence Ionization of CS ₂ Cluster-----	102
VI-B-2 Absence of Symmetry Breaking Observed for O 1s Core-Excited SO ₂ Molecule-----	102
VI-B-3 Radiation Damage Effects on the Electronic Structure of Glycine-----	102
VI-C Molecules in Few-Cycle Intense Laser Fields-----	104
VI-C-1 Electronic and Nuclear Responses of Fixed-in-Space H ₂ S in Ultrashort Intense Laser Fields-----	104
VI-C-2 Coulomb Explosion Imaging of Molecular Structures with Ultrashort Intense Laser Pulses-----	104
VI-D Synchrotron Radiation Stimulated High-Speed Etching on Silicon Surfaces-----	105
VI-D-1 Construction of High-Speed Synchrotron Radiation Etching System Using XeF ₂ -----	105
VI-D-2 Vapor-Phase Etching of Silicon Substrates Using XeF ₂ -----	105
VI-E Fabrication of Silicon-Based Planar Ion-Channel Biosensors-----	106
VI-E-1 Fabrication of Circular Through-Hole on Si(100)-SOI Substrate-----	106
VI-E-2 Channel Current Measurement Using Silicon-Based Planar Type Biosensor-----	106
VI-E-3 Noise Analysis in the Planar-Type Ion-Channel Biosensors-----	107
VI-F Integration and Characterization of Bio-Functional Materials on Silicon Surfaces-----	107
VI-F-1 Supported Phospholipid Bilayer Formation on Hydrophilicity-Controlled Silicon Dioxide Surfaces-----	108
VI-F-2 Orientation of Avidin Molecules Immobilized on COOH-Modified SiO ₂ /Si(100) Surfaces-----	108
VI-F-3 AFM Characterization of Gramicidin-A in Tethered Lipid Membrane on Silicon Surface--	108
VI-F-4 In-Situ Infrared Reflection Absorption Spectroscopy System Using Buried Metal Layer Substrate (BML-IRRAS) for Biomaterials under Water-----	109
VI-G Extreme UV Photoionization Studies of Fullerenes by Using a Grazing-Incidence Monochromator and High-Temperature Mass Spectrometer-----	110
VI-G-1 Refinements of the Estimation of Photoabsorption Cross Sections of Metallofullerenes ---	110
VI-G-2 Fragmentation Mechanism of Highly Excited C ₇₀ Cations in the Extreme Ultraviolet-----	110
VI-H Photoionization and Fragmentation Mechanisms of C₆₀ and C₇₀ in the Extreme Ultraviolet-----	111
VI-H-1 Kinetic Energy Analysis of the Fragment Ions Produced from C ₆₀ and C ₇₀ -----	111
VI-H-2 Photofragment Imaging Apparatus for Measuring Momentum Distributions in Dissociative Photoionization of Fullerenes-----	111
VI-H-3 Simulated Image of Fragment Ions Produced from C ₆₀ -----	112
VI-H-4 Scattering Distributions of the Photofragments from C ₆₀ in the Extreme Ultraviolet-----	112
VI-H-5 Why We Wish to Measure the Yield Curves of the Photofragments from C ₆₀ in Coincidence with Threshold Electrons-----	113
VI-H-6 ZEKE Photoelectron Spectroscopy Utilizing the Dark Gap of UVSOR Storage Ring-----	113
VI-H-7 New Design of a ZEKE Photoelectron Spectrometer for Photofragmentation Studies of Fullerenes-----	113
VI-H-8 High Resolution Photoelectron Spectroscopy of Gaseous Fullerenes-----	114
VI-H-9 Construction of an End Station of BL2B to Study Dissociative Photoionization of Fullerenes and VUV Spectroscopy of Ionic Liquids-----	114
VI-I Ray-Tracing for the Branch Beam Line of the 10-m Normal Incidence Monochromator Developed for Gas-Phase Photochemistry-----	115
VI-I-1 Layout of the Branch Beam Line of BL7U-----	115
VI-I-2 Ray-Tracing for the Branch Beam Line of BL7U of UVSOR-----	115

RESEARCH ACTIVITIES VII-----117**Department of Computational Molecular Science**

VII-A Computer Simulation of Quantum Systems in Condensed Phase-----	117
VII-A-1 A Surface Hopping Method for Chemical Reaction Dynamics in Solution Described by Diabatic Representation: An Analysis of Tunneling and Thermal Activation-----	117

VII-B Molecular Dynamics Study of Classical Complex Systems	117
VII-B-1 A Molecular Dynamics Study of Sodium Chenodeoxycholate in an Aqueous Solution----	117
VII-B-2 A Molecular Dynamics Study of Free Energy of Micelle Formation for Sodium Dodecyl Sulfate in Water and Its Size Distribution-----	117
VII-B-3 A Molecular Dynamics Study of Structural Stability of Spherical SDS Micelle as a Function of Its Size	117
VII-B-4 A Molecular Dynamics Study of Surface Structure of Spherical SDS Micelles	118
VII-C Development of Simulation Algorithms for Quantum Many-Body Systems	118
VII-C-1 Path Integral Hybrid Monte Carlo Study on Structure of Small Helium-4 Clusters Doped with a Linear Molecule	118
VII-D Development of Polarizable Molecular Modeling for Simulation Studies	119
VII-D-1 Polarizable Solute in Polarizable and Flexible Solvents: Simulation Study of Electron Transfer Reaction Systems	119
VII-D-2 Extended Treatment of Charge Response Kernel Comprising the Density Functional Theory and Charge Regulation Procedures	119
VII-E Computational Analysis of Sum Frequency Generation Spectroscopy	119
VII-E-1 Intermolecular Correlation Effect in Sum Frequency Generation Spectroscopy of Electrolyte Aqueous Solution-----	120
VII-F Theoretical Study of Condensed Phase Dynamics by Using Multi-Dimensional Spectroscopy	121
VII-F-1 Fifth-Order Two-Dimensional Raman Spectroscopy of Liquid Water, Crystalline Ice Ih and Amorphous Ices: Sensitivity to Anharmonic Dynamics and Local Hydrogen Bond Network Structure	121
VII-G Theoretical Study of Dynamics in Biological Systems	121
VII-G-1 Mechanism of Ion Permeation in Model Channel; Free Energy Surface and Dynamics of K ⁺ Ion Transport in Anion-Doped Carbon Nanotube ----	121
VII-H Theoretical Study of Origin of Slow Relaxation in Liquid Water	121
VII-H-1 Origin of Slow Relaxation in Liquid Water Dynamics: A Possible Scenario for the Presence of Bottleneck in Phase Space	121
RESEARCH ACTIVITIES VIII	123

Coordination Chemistry Laboratories

VIII-A Metal Complexes Aimed at Conversion between Chemical and Electrochemical Energies---	123
VIII-A-1 Structural Characterization of Ruthenium–Dioxolene Complexes with Ru ^{II} -SQ and Ru ^{II} -Cat Frameworks-----	123
VIII-A-2 Reversible Bond Formation and Cleavage of the Oxo Bridge of [Ru ₂ (μ-O) (dioxolene) ₂ (btpyxa)] ³⁺ [btpyxa = 2,7-Di-tert-butyl-9,9-dimethyl-4,5-bis(2,2':6',2''-terpyrid-4'-yl)xanthene] Driven by a Three-Electron Redox Reaction	123
VIII-A-3 A New Series of Molybdenum-(IV), -(V), and -(VI) Dithiolate Compounds as Active Site Models of Molybdoenzymes: Preparation, Crystal Structures, Spectroscopic/Electrochemical Properties and Reactivity in Oxygen Atom Transfer	124
VIII-A-4 Reversible Hydride Generation and Release from the Ligand of [Ru(pbn)(bpy) ₂](PF ₆) ₂ Driven by a Pbn-Localized Redox Reaction	124
VIII-A-5 Mononuclear Five-Coordinate Molybdenum(IV) and -(V) Monosulfide Complexes Coordinated with Dithiolene Ligands: Reversible Redox of Mo(V)/Mo(IV) and Irreversible Dimerization of [Mo ^V S] ⁻ Cores to a Dinuclear [Mo ^V ₂ (μ-S) ₂] ²⁻ Core	124
VIII-A-6 Synthesis and Crystal Structures of [W(3,6-dichloro-1,2-benzenedithiolate) ₃] ⁿ⁻ (n = 1, 2) and [Mo(3,6-dichloro-1,2-benzenedithiolate) ₃] ²⁻ : Dependence of the Coordination Geometry on the Oxidation Number and Counter-Cation in Trigonal-Prismatic and Octahedral Structures-----	124
VIII-A-7 Synthesis, Structures and Electrochemical Properties of Ruthenium (II) Complexes Bearing Bidentate 1,8-Naphthyridine and Terpyridine Analogous (N,N,C)-Tridentate Ligands	125
VIII-A-8 Dioxo-Molybdenum(VI) and Mono-Oxo-Molybdenum(IV) Complexes Supported by New Aliphatic Dithiolene Ligands: New Models with Weakened Mo:O Bond Characters for the Arsenite Oxidase Active Site	125
VIII-A-9 Electronic Structural Changes between Nickel(II)–Semiquinonato and Nickel(III)–Catecholato States Driven by Chemical and Physical Perturbation	125
VIII-A-10 Electrochemical Hydrogenation of [Ru(bpy) ₂ (napy-κN)(CO)] ²⁺ : Inhibition of Reductive Ru–CO Bond Cleavage by a Ruthenacycle	125
VIII-A-11 Synthesis, Chemical- and Electrochemical Properties of Ruthenium(II) Complexes Bearing 2,6-Bis(2-naphthyridyl)pyridine	126

VIII-A-12 Synthesis and Electrochemical Properties of Bis(bipyridine)ruthenium(II) Complexes Bearing Pyridinyl- and Pyridinylidene Ligands Induced by Cyclometalation of N-Methylated Bipyridinium Analogs	126
VIII-A-13 Stabilization and Destabilization of the Ru–CO Bond during the 2,2'-Bipyridin-6-Onato (bpyO)-Localized Redox Reaction of [Ru(terpy)(bpyO)(CO)](PF ₆)	126
VIII-A-14 Electronic Structural Changes between Nickel(II)–Semiquinonato and Nickel(III)–Catecholato States Driven by Chemical and Physical Perturbation	126
VIII-B Coordination Chemistry of Sterically Hindered Ligands and Multidentate Ligands, and Activation of Small Molecules	128
VIII-B-1 Complexes of Tantalum with Triaryloxides: Ligand and Solvent Effects on Formation of Hydride Derivatives	128
VIII-B-2 A Synthetic Cycle for H ₂ /CO Activation and Allene Synthesis Using Recyclable Zirconium Complexes	128
VIII-B-3 A Tantalum(V) Carbene Complex: Formation of a Carbene-Bis(phenoxide) Ligand by Sequential Proton and Hydride Abstraction	128
VIII-C Physicochemical Properties of Hemoprotein Reconstituted with Artificially Created Hemins	130
VIII-C-1 Preparation and O ₂ Binding Study of Myoglobin Having a Cobalt Porphycene	130
VIII-C-2 Iron Porphyrin–Cyclodextrin Supramolecular Complex as a Functional Model of Myoglobin in Aqueous Solution	130
VIII-C-3 Crystal Structure and Peroxidase Activity of Myoglobin Reconstituted with Iron Porphycene	131
VIII-C-4 Construction of Glycosylated Myoglobin by Reconstitutive Method	131
VIII-C-5 Structure and Ligand Binding Properties of Sperm Whale Myoglobins Reconstituted with Two Monopropionated Hemin: Role of Each Heme-Propionate Side Chain in Myoglobin	131
VIII-C-6 Ligand Binding Properties of Two Kinds of Reconstituted Myoglobins with Iron Porphycene Having Propionates: Effect of β-Pyrrolic Position of Two Propionate Side Chains in Porphycene Framework	132
VIII-D Syntheses, Structures, and Reactivities of Multinuclear Transition Metal Complexes with O- and N-Donor Ligands	133
VIII-D-1 Syntheses and Properties of NCN-Bridged Tri- and Tetranuclear Complexes of Cobalt and Rhodium	133
VIII-D-2 Electrophilic O-Methylation of a Terminal Nitrosyl Ligand Attained by Early–Late Heterobimetallic Effect	133
VIII-E Transition Metal Cluster Chemistry	134
VIII-E-1 Metathesis Approach to Linkage of Two Tetraplatinum Cluster Units: Synthesis, Characterization, and Dimerization of [Pt ₄ (μ-OCOCH ₃) ₇ (μ-OCO(CH ₂) _n CH=CH ₂)] (n = 0–3)	134
VIII-E-2 Hexapalladium Cluster: Unique Reaction of Cyclic Pd ₃ (CNC ₆ H ₃ Me _{2-2,6}) ₆ and Linear [Pd ₃ (CNC ₆ H ₃ Me _{2-2,6}) ₈] ²⁺	134
VIII-F Synthesis of Transition Metal Catalysts for Organic Transformations	135
VIII-F-1 Oxidative Addition of RCO ₂ H and HX to Chiral Diphosphine Complexes of Iridium(I): Convenient Synthesis of Mononuclear Halo-Carboxylate Iridium(III) Complexes and Cationic Dinuclear Triply Halogen-bridged Iridium(III) Complexes and Their Catalytic Performance in Asymmetric Hydrogenation of Cyclic Imines and 2-Phenylquinoline	135
VIII-G Early Transition Metal Complexes	135
VIII-G-1 Synthesis, Structure, and Reactivity of Tantalum and Tungsten Homoenoate Complexes	135
VIII-H Creation of Novel Functional Nano Materials Based on Proton-Coupled Electronic Properties	136
VIII-H-1 Most Stable Metallic Phase of the Mixed-Valence MMX-Chain, Pt ₂ (dtp) ₄ I (dtp: C ₂ H ₅ CS ₂ ⁻) in Purely d-Electronic Conductors Based on the Transition-Metal Complex	136
VIII-H-2 Direct Determination of Low-Dimensional Structures: Synchrotron X-Ray Scattering on One-Dimensional Charge-Ordered MMX-Chain Complexes	136
VIII-H-3 Pressure-Induced Metal–Semiconductor–Metal Transitions in an MMX-Chain Complex, Pt ₂ (C ₂ H ₅ CS ₂) ₄ I	136
VIII-H-4 Synthesis of a One-Dimensional Metal-Dimer Assembled System with Interdimer Interaction, M ₂ (dtp) ₄ (M = Ni, Pd; dtp = Dithiopropionato)	136
VIII-H-5 Galvanostatic Transient Studies on Copper Coordination Polymer under Hydrogen Absorption	137

VIII-I Development of Metal-Cojugated Redox Systems in Metal-Dioxolene Complexes and Electrochemical Activation of Water Ligand -----	138
VIII-I-1 Synthesis of a Water-Soluble Ruthenium–Terpyridine–Dioxolene and the Electrochemical Activation of Water Molecules-----	138
VIII-J Syntheses, Structures, and Redox Properties of New Multinuclear Coordination Materials with Metallocene Units -----	139
VIII-J-1 Synthesis of Coordination Polymers with Cobaltocenium and Rhodocenium Units-----	139
VIII-J-2 Synthesis of Coordination Networks with Ruthenocene Units-----	139
RESEARCH ACTIVITIES IX -----	141
Research Center for Molecular-Scale Nanoscience	
IX-A Nano-Science and Nano-Technology toward Molecular Scale Electronics -----	141
IX-A-1 Synthesis and Self-Assembly of Novel Porphyrin Molecular Wires-----	141
IX-A-2 Molecular Junctions Composed of Oligothiophene Dithiol Bridged Gold Nanoparticles Exhibiting Photoresponsive Properties-----	141
IX-A-3 Simple Preparation Method for Supramolecular Porphyrin Arrays on Mica Using Air/Water Interface-----	141
IX-A-4 Porphyrin Molecular Nanodevices Wired Using Single-Walled Carbon Nanotubes-----	142
IX-A-5 Electronic Properties of Single-Walled Carbon Nanotube/150mer-Porphyrin System Measured by Point-Contact Current Imaging Atomic Force Microscopy-----	142
IX-A-6 Preparation of Very Reactive Thiol-Protected Gold Nanoparticles: Revisiting the Brust-Schiffrin Method-----	142
IX-A-7 Spontaneous Resolution of Delta and Gamma Enantiomeric Pair of [Ru(phen)(bpy) ₂](PF ₆) ₂ (phen = 1,10-phenanthroline, bpy = 2,2'-bipyridine) by Racemic Conglomerate Crystallization-----	142
IX-A-8 Structural and Spectroscopic Characterizations of Low-Spin [Fe(4,4-dimethyl-2,2'-bipyridine) ₃](NCS) ₂ /H ₂ O Prepared from High-Spin Iron(II) Dithiocyanate Tetrapyrindine-----	143
IX-A-9 Morphology and Electric Properties of Nonathiophene/Au Nano-Composite Thin Films Formed between 1 μm Gapped Electrodes-----	143
IX-A-10 Synthesis of End-Functionalized π-Conjugated Porphyrin Oligomers-----	143
IX-A-11 Fabrication of Nanoscale Gaps Using a Combination of Self-Assembled Monomolecular and Electron Beam Lithographic Techniques-----	143
IX-A-12 Synthesis and Photochemical Behavior of Metalloporphyrin Complexes Containing a Photochromic Axial Ligand-----	143
IX-B Development of Organic Semiconductors for Molecular Thin-Film Devices -----	144
IX-B-1 Synthesis and Characterization of Three Novel Perfluoro-Oligothiophenes Ranging in Length from the Trimer to the Pentamer-----	144
IX-C Development of Multi-Function Integrated Macromolecules and Their Organization on Substrate Surfaces for Planar Molecular-Scale Electronics Circuits -----	145
IX-C-1 Stepwise Synthesis of Molecular Wire with a Double-Tunnel Junction-----	145
IX-C-2 Direct Identification of Conformational Isomers of Adsorbed Oligothiophene on Cu(100)-----	145
IX-D Nano- and Complex-Catalysis -----	146
IX-D-1 NCN Pincer Palladium Complexes: Their Preparation <i>via</i> a Ligand Introduction Route and Their Catalytic Properties-----	146
IX-D-2 Asymmetric P-Allylic Etherification of Cycloalkenyl Esters with Phenols in Water Using a Resin-Supported Chiral Palladium Complex-----	146
IX-D-3 A Solid-Phase Self-Organized Catalyst of Nanopalladium with Main-Chain Viologen Polymers: α-Alkylation of Ketones with Primary Alcohols-----	146
IX-E Development of New Nanomaterials as Components in Advanced Molecular Systems -----	147
IX-E-1 Automated Design of Protecting Molecules for Metal Nanoparticles by Combinatorial Molecular Simulations-----	147
IX-F Designing Artificial Photosynthesis at Molecular Dimensions -----	147
IX-F-1 Elucidation of Solution Structures of Dendrimer-Linked Porphyrins-----	148
IX-F-2 Reconstitution of the Water-Oxidizing Complex in Manganese-Depleted Photosystem II Preparations Using Binuclear Mn(II) and Mn(IV) Complexes-----	149
IX-G Development of New Metal Complexes as Redox Catalysts -----	149
IX-G-1 Syntheses and Structures of Co(I) Complexes Having Cyclopentadienyl Auxiliaries and C–P Bond Cleavage of the Coordinated Phosphine-----	149
IX-H Synthesis of Buckybowls and Heterobuckybowls -----	151
IX-H-1 Regio- and Stereo-Selective Synthesis of Multi-Substituted Benzene Derivatives by Cyclotrimerization of Haloalkene Derivatives-----	151

IX-I Spectroscopy and Chemistry of Metal Nanoclusters on Surfaces -----	152
IX-I-1 STM Observation and Fabrication of Films of Gold Nanoclusters with and without Alkanethiolate Ligands on TiO ₂ (110) -----	152
IX-J Photochemistry on Well-Defined Surfaces -----	152
IX-J-1 Photochemistry of Cyclohexane on Cu(111) -----	152
IX-J-2 Photochemistry and Post-Irradiation Chemistry of Cyclohexane on Pt(111) -----	153
IX-K Ultrafast Dynamics at Well-Defined Surfaces -----	153
IX-K-1 Coherent Surface Phonon Dynamics at K-Covered Pt(111) Surfaces Investigated by Time-Resolved Second Harmonic Generation -----	153
IX-K-2 Excitation Mechanism of Coherent Surface Phonons on Na-Covered Cu(111) -----	153
IX-K-3 Electron Transfer Dynamics from Organic Adsorbate to a Semiconductor Surface: Zinc-Phthalocyanine on TiO ₂ (110) -----	154
IX-L Vibrational Dynamics at Surfaces and Interfaces Studied by Time-Resolved Sum Frequency Spectroscopy -----	154
IX-L-1 Vibrational Energy Relaxation at the Interface of Ice/CO/Pt(111) Studied by fs Time-Resolved Sum Frequency Generation-----	154
IX-M Chemistry of One-Dimensional Nano-Surface Compounds Studied by Scanning Tunneling Microscopy -----	155
IX-M-1 Direct Observation of a Propagating Chemical Wave in Disproportionation Reactions of Water on Oxidized Ag(110) Surface by Scanning Tunneling Microscopy -----	155
IX-N Structures, Stabilities and Physicochemical Properties of Organometallic Hybrid Clusters ---	156
IX-N-1 Aerobic Oxidation Catalyzed by Gold Nanoclusters as <i>quasi</i> -Homogeneous Catalysts: Generation of Hydrogen Peroxide Using Ammonium Formate-----	156
IX-N-2 Spectroscopic Investigation of Dendrimer-Encapsulated Gold Clusters-----	156
IX-N-3 Chromatographic Isolation of “Missing” Au ₅₅ Clusters Protected by Alkanethiolates -----	156
IX-N-4 Chiroptical Activity of BINAP-Stabilized Undecagold Clusters-----	156
IX-N-5 Kinetic Stabilization of Growing Gold Clusters by Passivation with Thiolates -----	157
IX-N-6 Size Effect on the Catalysis of Gold Clusters Dispersed in Water for Aerobic Oxidation of Alcohol -----	157
IX-N-7 X-Ray Magnetic Circular Dichroism of Size-Selected, Thiolated Gold Clusters -----	157
IX-N-8 Mechanism of Selective Formation of Thiolated Au ₂₅ Clusters in Ligand Exchange of Phosphine-Stabilized Gold Clusters: Size Focusing <i>via</i> Core Etching-----	158
IX-O Structural Analyses of Biological Macromolecules by Ultra-High Field NMR Spectroscopy --	159
IX-O-1 Solution Structure and Dynamics of Ufm1, a Ubiquitin-Fold Modifier 1 -----	159
IX-O-2 Glycoform-Dependent Conformational Alteration of the Fc Region of Human Immunoglobulin G1 as Revealed by NMR Spectroscopy -----	159

UVSOR Facility

IX-P Development of the UVSOR Light Source -----	161
IX-P-1 Design and Construction of Variably Polarized Undulator-----	161
IX-P-2 Upgrade of Booster Synchrotron Magnet Power Supplies -----	161
IX-P-3 One Watt Lasing in Deep UV Region of UVSOR-II Free Electron Laser -----	161
IX-P-4 Production of Coherent Terahertz Radiation by Laser Bunch Slicing Method -----	161
IX-P-5 Coherent Harmonic Generation by Using Ultra-Short Pulse Laser -----	162
IX-Q Researches by the Use of UVSOR -----	162
IX-Q-1 Experimental Investigation of Core-Valence Double Photoionization -----	162
IX-Q-2 Efficient Production of Metastable Fragments around the 1s Ionization Threshold in N ₂ --	162
IX-Q-3 Anisotropic Fragment Emission on Valence Photoionization of CF ₄ -----	162
IX-Q-4 Auger Decay of Ne 1s Photoionization Satellites Studied by a Multi-Electron Coincidence Method-----	162
IX-Q-5 Inner-Valence States of N ²⁺ and the Dissociation Dynamics Studied by Threshold Photoelectron Spectroscopy and Configuration Interaction Calculation-----	163
IX-Q-6 Electron Correlation in Xe 4d Auger Decay Studied by Slow Photoelectron–Auger Electron Coincidence Spectroscopy -----	163
IX-Q-7 Development of Symmetry-Resolved Zero-Kinetic-Energy Photoelectron Spectroscopy for Probing Multielectron Processes -----	163
IX-Q-8 Iron-Based Heavy Quasiparticles in SrFe ₄ Sb ₁₂ : An Infrared Spectroscopic Study -----	163
IX-Q-9 Optical Pseudogap from Iron States in Filled Skutterudites AFe ₄ Sb ₁₂ (A = Yb and Ca, Ba) -----	163
IX-Q-10 Continuity of Ce 4f Electronic Structure across the Quantum Critical Point: A Resonant Photoemission Study on CeNi _{1-x} Co _x Ge ₂ -----	164
IX-Q-11 Optical Study on Clathrates Sr ₈ Ga ₁₆ Ge ₃₀ and β-Eu ₈ Ga ₁₆ Ge ₃₀ -----	164
IX-Q-12 Infrared Study on Electronic Structure of SrT ₄ Sb ₁₂ (T = Fe, Ru) -----	164
IX-Q-13 Angle-Resolved Photoemission Study on CeTe ₂ -----	164

IX-Q-14 High-Resolution Photoemission Spectroscopy of CeNiGe ₂ and CeCoGe ₂ -----	164
IX-Q-15 Infrared Absorption in Heavy Fermion System CeNi _{1-x} Co _x Ge ₂ -----	165

Laser Research Center for Molecular Science

IX-R Developments and Researches of New Laser Materials -----	166
IX-R-1 Photonic-Crystal-Fiber Pigtail Device Integrated with Lens-Duct Optics for Terahertz Radiation Coupling -----	166
IX-R-2 Band-Structure Design of Fluoride Complex Materials for Deep-Ultraviolet Light-Emitting Diodes-----	166
IX-R-3 Ce ³⁺ -Doped LiCaAlF ₆ Crystals as a Solid-State Ultraviolet Saturable Absorber and Role of Excited State Absorption -----	166
IX-R-4 Generation of Terahertz Radiation Using Zinc Oxide as Photoconductive Material Excited by Ultraviolet Pulses -----	166
IX-R-5 Ultraviolet Irradiation Effect of Ce ³⁺ -Doped BaMgF ₄ Crystals-----	166
IX-R-6 Vacuum Ultraviolet and Ultraviolet Spectroscopy of BaMgF ₄ Codoped with Ce ³⁺ and Na ⁺ -----	167
IX-R-7 Vacuum Ultraviolet Spectroscopy of Ce ³⁺ -Doped SrMgF ₄ with Superlattice Structure-----	167
IX-S Development and Research of Advanced Tunable Solid State Lasers -----	168
IX-S-1 300W Continuous-Wave Operation of Diode Edge-Pumped, Hybrid Composite Yb:YAG Microchip Laser -----	168
IX-S-2 Spectroscopic Properties and Laser Emission in Layer-by-Layer Type Nd:Y ₃ ScAl ₄ O ₁₂ /Nd:Y ₃ Al ₅ O ₁₂ Composite Ceramics -----	168
IX-S-3 Thermal Properties of Y ₃ Al ₅ O ₁₂ , GdVO ₄ , and YVO ₄ -----	168
IX-S-4 Spectroscopic Properties and Laser Operation of RE ³⁺ -Ion Doped Garnet Materials-----	169
IX-S-5 Comparative Study on the Spectroscopic Properties of Nd:GdVO ₄ and Nd:YVO ₄ with Hybrid Process-----	169
IX-S-6 High-Energy, Narrow-Bandwidth 2- μ m Optical Parametric Oscillator/Power Amplifier Based on Periodically Poled MgO:LiNbO ₃ -----	169
IX-S-7 High-Energy Quasi-Phase Matched Optical-Parametric Oscillation in Periodically Poled MgO:LiNbO ₃ Device with 5 mm \times 5 mm Aperture -----	170

Equipment Development Center

IX-T Development of New Instruments and Experimental Devices -----	171
IX-T-1 Manufacture of a Mold for a Microchip Using a Surface Impression Agent -----	171
IX-T-2 A Compact Mechanical Velocity Selector to Analyze Molecular Alignment -----	171

Safety Office

IX-U Development of Novel Heterocyclic Compounds and Their Molecular Assemblies for Advanced Materials -----	173
IX-U-1 TTF Derivatives Containing Fused-Pyrazine Rings for Novel Donor-Acceptor Systems---	173

RESEARCH ACTIVITIES X ----- 175

Okazaki Institute for Integrative Bioscience

X-A Bioinorganic Chemistry of Heme-Based Sensor Proteins -----	175
X-A-1 Effect of Mutation on the Dissociation and Recombination Dynamics of CO in Transcriptional Regulator CooA: A Picosecond Infrared Transient Absorption Study -----	175
X-A-2 Evidence for Displacements of the C-Helix by CO Ligation and DNA Binding to CooA Revealed by UV Resonance Raman Spectroscopy -----	175
X-A-3 Crystallization and Preliminary X-Ray Analysis of CooA from <i>Carboxydotherrmus hydrogenoformans</i> -----	175
X-A-4 Specific Hydrogen-Bonding Networks Responsible for Selective O ₂ Sensing of the Oxygen Sensor Protein HemAT from <i>Bacillus subtilis</i> -----	176
X-A-5 Recognition and Discrimination of Gases by the Oxygen-Sensing Signal Transducer Protein HemAT as Revealed by FTIR Spectroscopy -----	176
X-A-6 Biophysical Properties of a c-Type Heme in Chemotaxis Signal Transducer Protein DcrA -----	176
X-B Bioinorganic Chemistry of a Novel Heme Enzyme that Catalyzes the Dehydration Reaction --	177
X-B-1 Spectroscopic and Substrate Binding Properties of Heme-Containing Aldoxime Dehydratases, OxdB and OxdRE -----	177
X-C Reaction Mechanism of Metalloenzymes Related to Oxygen Activation -----	178
X-C-1 Oxidizing Intermediates from the Sterically Hindered Salen Iron Complexes Related to the Oxygen Activation by Nonheme Iron Enzymes -----	178

X-C-2	A Trigonal-Bipyramidal Geometry Induced by an External Water Ligand in a Sterically Hindered Iron Salen Complex, Related to the Active Site of Protocatechuate 3,4-Dioxygenase-----	178
X-C-3	O ₂ - and H ₂ O ₂ -Dependent Verdoheme Degradation by Heme Oxygenase: Reaction Mechanisms and Potential Physiological Roles of the Dual Pathway Degradation-----	178
X-C-4	¹³ C and ¹⁵ N NMR Studies of Iron-Bound Cyanides of Heme Proteins and Related Model Complexes: Sensitive Probe for Detecting Hydrogen Bonding Interactions at the Proximal and Distal Sides-----	179
X-C-5	Roles of the Heme Distal Residues of FixL in O ₂ Sensing: A Single Convergent Structure of the Heme Moiety Is Relevant to the Downregulation of Kinase Activity -----	179
X-C-6	¹⁷ O NMR Study of Oxo Metalloporphyrin Complexes: Correlation with Electronic Structure of M=O Moiety-----	179
X-D	Reaction Mechanism of Metalloenzymes Related to Global Nitrogen Cycle -----	180
X-D-1	Kinetic Isotope Effects on the Rate-Limiting Step of Heme Oxygenase Catalysis Indicate Concerted Proton Transfer/Heme Hydroxylation -----	180
X-D-2	⁶³ Cu NMR Spectroscopy of Copper(I) Complexes with Various Tridentate Ligands: CO as a Useful ⁶³ Cu NMR Probe for Sharpening ⁶³ Cu NMR Signals and Analyzing the Electronic Donor Effect of a Ligand -----	180
X-E	Biomolecular Science -----	182
X-E-1	Kinetics and DFT Studies on the Reaction of Copper(II) Complexes and H ₂ O ₂ -----	182
X-E-2	Detection of the His-Heme Fe ²⁺ -NO Species in the Reduction of NO to N ₂ O by <i>ba</i> ₃ -Oxidase from <i>Thermus thermophilus</i> -----	182
X-E-3	Structural Studies Reveal that the Diverse Morphology of β ₂ -Microglobulin Aggregates is a Reflection of Different Molecular Architectures -----	183
X-E-4	Biophysical Properties of a <i>c</i> -Type Heme in Chemotaxis Signal Transducer Protein DcrA -----	183
X-E-5	Discovery of a Reaction Intermediate of Aliphatic Aldoxime Dehydratase Involving Heme as an Active Center-----	183
X-E-6	Intramolecular Arene Hydroxylation <i>versus</i> Intermolecular Olefin Epoxidation by (μ-η ² :η ² -Peroxo)dicopper(II) Complex Supported by Dinucleating Ligand -----	184
X-E-7	Significance of the Molecular Shape of Iron Corrophycene in a Protein Pocket -----	184
X-E-8	Sequential Reaction Intermediates in Aliphatic C-H Bond Functionalization Initiated by a Bis(μ-oxo)dinickel(III) Complex -----	184
X-E-9	¹⁷ O NMR Study of Oxo Metalloporphyrin Complexes: Correlation with Electronic Structure of M=O Moiety-----	185
X-E-10	Nonheme Iron(II) Complexes of Macrocyclic Ligands in the Generation of Oxoiron(IV) Complexes and the Catalytic Epoxidation of Olefins-----	185
X-E-11	Resonance Raman Enhancement of Fe ^{IV} =O Stretch in High-Valent Iron Porphyrins: An Insight from TD-DFT Calculations-----	185
X-E-12	Spectroscopic and Substrate Binding Properties of Heme-Containing Aldoxime Dehydratases, OxdB and OxdRe -----	185
X-E-13	Spectroscopic and DNA-Binding Characterization of the Isolated Heme-Bound Basic Helix-Loop-Helix-PAS-A Domain of Neuronal PAS Protein 2 (NPAS2), a Transcription Activator Protein Associated with Circadian Rhythms -----	186
X-E-14	Specific Hydrogen-Bonding Networks Responsible for Selective O ₂ Sensing of the Oxygen Sensor Protein HemAT from <i>Bacillus subtilis</i> -----	186
X-E-15	Raman Evidence for Specific Substrate-Induced Structural Changes in the Heme Pocket of Human Cytochrome P450 Aromatase during the Three Consecutive Oxygen Activation Steps -----	186
X-E-16	Evidence for Displacement of the C-Helix by CO Ligation and DNA Binding to CooA Revealed by UV Resonance Raman Spectroscopy -----	187
X-E-17	On the Relationship of Coral Allene Oxide Synthase to Catalase: A Single Active Site Mutation that Induces Catalase Activity in Coral Allene Oxide Synthase--	187
X-E-18	Similarities and Differences between Cyclobutane Pyrimidine Dimer (CPD) Photolyase and (6-4) Photolyase as Revealed by Resonance Raman Spectroscopy: Electron Transfer from FAD Cofactor to UV-Damaged DNA -----	187
X-E-19	Structure of Interacting Segments in the Growing Amyloid Fibril of β ₂ -Microglobulin Probed with IR Spectroscopy -----	188
X-E-20	Pathway of Information Transmission from Heme to Protein upon Ligand Binding/ Dissociation in Myoglobin Revealed by UV Resonance Raman Spectroscopy -----	188
X-E-21	Characteristic Structure and Environment in FAD Cofactor of (6-4) Photolyase along Function Revealed by Resonance Raman Spectroscopy-----	188

X-E-22 Time-Resolved Raman Evidence for Energy Funneling through Propionate Side Chains in Heme Cooling Upon Photolysis of Carbonmonoxy Myoglobin -----	189
X-E-23 Characterization of the Phenoxy Radical in Model Complexes for the Cu _B Site of Cytochrome <i>c</i> Oxidase: Steady-State and Transient Absorption Measurements, UV Resonance Raman Spectroscopy, EPR Spectroscopy, and DFT Calculations for M ^{II} -BIAIP-----	189
X-E-24 Ultraviolet Resonance Raman Evidence for Utilization of the Heme 6-Propionate Hydrogen Bond Network in Signal Transmission from Heme to Protein in <i>Ec</i> DOS Protein ----	189
X-E-25 Identification of an “End-on” Nickel-Superoxo Adduct, [Ni(tmc)(O ₂)] ⁺ -----	189
X-E-26 Regioselective Arene Hydroxylation Mediated by a (μ-Peroxo)diiron(III) Complex: A Functional Model for Toluene Monooxygenase-----	190
X-E-27 A Novel Mononuclear Ligand-Based Alkylperoxo Copper(II) Complex as a Reaction Intermediate in the Oxidation of the Methyl Group of the Supporting Ligand-----	190
X-E-28 Synthesis, Characterization, and Reactivities of Manganese(V)-Oxo Porphyrin Complexes -----	190
RESEARCH FACILITIES -----	191
Research Center for Molecular-scale Nanoscience -----	191
UVSOR Facility -----	191
Laser Research Center for Molecular Science -----	192
Equipment Development Center-----	192
Safety Office-----	192
Research Center for Computational Science-----	193
SPECIAL RESEARCH PROJECTS-----	195
(a) —Grand Challenge in Nanoscience—Next Generation Integrated Nanoscience Simulation Software Development & Application of Advanced High-Performance Supercomputer Project -----	195
(b) Formation of Interdisciplinary and International Bases for Natural Sciences, NINS “Development of New Computational Methods for Large-Scale Systems and Establishment of Advanced Simulation Center for Molecules and Materials” -----	196
(c) Nanotechnology Support Project: Molecular Synthesis and Analysis Group-----	196
(d) Extreme Photonics-----	197
OKAZAKI CONFERENCE -----	199
JOINT STUDIES PROGRAMS-----	201
(1) Special Projects -----	201
(2) Research Symposia -----	202
(3) Cooperative Research-----	202
(4) Use of Facility -----	202
(5) Use of UVSOR Projects -----	202
(6) Use of Facility Program of the Computer Center-----	203
COLLABORATION PROGRAMS-----	205
FOREIGN SCHOLARS -----	207
AWARDS -----	211
LIST OF PUBLICATIONS -----	217
REVIEW ARTICLES AND TEXTBOOKS-----	233
AUTHOR INDEX -----	235

Abbreviations

IMS: Institute for Molecular Science
SOKENDAI: The Graduate University for Advanced Studies

ORGANIZATION AND STAFF

Organization

The Institute for Molecular Science comprises twenty research laboratories, each staffed by a professor, an associate professor, two research associates and several technical associates, and two research laboratories with foreign visiting professors and five research facilities.

The laboratories are grouped into seven departments and one facility for coordination chemistry:

Department of Theoretical Studies	Theoretical Studies I Theoretical Studies II Theoretical Studies III Theoretical Studies IV ¹⁾
Department of Molecular Structure	Molecular Structure I Molecular Structure II ¹⁾ Molecular Dynamics
Department of Electronic Structure	Excited State Chemistry Excited State Dynamics Electronic Structure ¹⁾ Molecular Energy Conversion ²⁾
Department of Molecular Assemblies	Solid State Chemistry Molecular Assemblies Dynamics Molecular Assemblies ¹⁾
Department of Applied Molecular Science	Applied Molecular Science I Applied Molecular Science II ¹⁾
Department of Vacuum UV Photoscience	Photochemistry Chemical Dynamics Synchrotron Radiation Research ²⁾
Department of Computational Molecular Science	Computational Molecular Science I Computational Molecular Science II Computational Molecular Science III ¹⁾
Coordination Chemistry Laboratories	Functional Coordination Chemistry Coordination Bond ¹⁾ Complex Catalysis

The research facilities are:

- Research Center for Molecular-scale Nanoscience Molecular-scale Electronics
Nanocatalysis and Biomolecular Devices
Nano-scale Photoscience
Advanced Molecular Science³⁾
- UVSOR Facility
- Laser Research Center for Molecular Science Advanced Lasers for Chemical Reaction Studies
Advanced Lasers for Synchrotron Radiation Applications
Advanced UV and IR Tunable Lasers
- Equipment Development Center
- Safety Office

Okazaki research facilities (related to IMS) are:

- Okazaki Institute for Integrative Bioscience
- Research Center for Computational Science

1) Professors and associate professors are visiting professors from other universities.

2) Research laboratories with foreign visiting professors.

3) Professors, associate professors, and research associates, along with their positions, are transferred from other universities.

Scientific Staff

NAKAMURA, Hiroki

Professor, Director-General

NAGAKURA, Saburo
HIROTA, Eizi
KIMURA, Katsumi

Emeritus Professors

The Japan Academy
Professor Emeritus, The Graduate University for Advanced Studies
IMS, Professor Emeritus, Japan Advanced Institute of Science and Technology

MOROKUMA, Keiji
INOKUCHI, Hiroo

Professor, Emory University, U. S. A.
Chief Scientist of Space Utilization Research Program, Japan Aerospace Exploration Agency

MARUYAMA, Yusei
YOSHIHARA, Keitaro
HANAOKI, Ichiro
IWAMURA, Hiizu
SAITO, Shuji
IWATA, Suehiro
ITO, Mitsuo

Professor, Hosei University
Professor, Japan Advanced Institute of Science and Technology
Professor Emeritus, The Graduate University for Advanced Studies
Professor, University of the Air
Professor, Fukui University
Professor, National Institution for Academic Degree
Professor Emeritus, The Graduate University for Advanced Studies, Tohoku University
Director, RIKEN Wako Institute, RIKEN Discovery Institute
Fellow, Toyota Physical and Chemical Research Institute

KAYA, Koji
KITAGAWA, Teizo

Department of Theoretical Studies

Theoretical Studies I

NAGASE, Shigeru
KOBAYASHI, Kaoru
OHTSUKA, Yuki
ISHIMURA, Kazuya
SLANINA, Zdenek
TAKAGI, Nozomi
KATOUDA, Michio
GAO, Xingfa
MIZOROGI, Naomi

Professor
Research Associate (–December '05)
Research Associate (April '06–)
Technical Associate
Post-Doctoral Fellow
Post-Doctoral Fellow
Post-Doctoral Fellow
Post-Doctoral Fellow (August '06–)
Graduate Student

Theoretical Studies II

NAKAMURA, Hiroki
NOBUSADA, Katsuyuki
MIL'NIKOV, Gennady

YASUIKE, Tomokazu
KONDORSKY, Alexey
CHIKAZUMI, Shinpei
TAMURA, Hiroyuki

KUBOTA, Youji
OLOYEDE, Oluwaponmile

SHIRATORI, Kazuya
IWASA, Takeshi

Professor (–March '06)
Associate Professor
Research Associate (–October '05), Post-Doctoral Fellow (November '05–March '06)
Research Associate
Post-Doctoral Fellow (–March '06)
Post-Doctoral Fellow (–March '06)
Post-Doctoral Fellow (–March '06), Research Fellow (April–May '06)
Post-Doctoral Fellow
Graduate Student (–September '05), Post-Doctoral Fellow (October–November '05)
Graduate Student
Graduate Student (from Hokkaido University)* (–March '06),
Graduate Student (April '06–)

Theoretical Studies III

HIRATA, Fumio
YONEMITSU, Kenji
CHONG, Song-Ho
YAMASHITA, Yasufumi
KOBRYN, Oleksandr
MARUYAMA, Yutaka
MIYATA, Tatsuhiko
YOSHIDA, Norio
IKUTA, Yasuhiro

Professor
Associate Professor
Research Associate
Research Associate
IMS Fellow
Post-Doctoral Fellow
Post-Doctoral Fellow
Post-Doctoral Fellow
Post-Doctoral Fellow

TANIMURA, Ayumi	Post-Doctoral Fellow (–March '06)
MAESHIMA, Nobuya	Post-Doctoral Fellow
MIYASHITA, Satoshi	Post-Doctoral Fellow
TANAKA, Yasuhiro	Post-Doctoral Fellow (April '06–)
MATSUGAMI, Masaru	Graduate Student
ISHIZUKA, Ryosuke	Graduate Student
PHONGPHANPHANEE, Saree	Graduate Student (April '06–)

Theoretical Studies IV

FUCHIZAKI, Kazuhiro	Visiting Professor (from Ehime University) (–March '06)
KIDERA, Akinori	Visiting Professor (from Yokohama City University) (April '06–)
KOMATSUZAKI, Tamiki	Visiting Associate Professor (from Kobe University) (–March '06)
SATO, Hirofumi	Visiting Associate Professor (from Kyoto University) (April '06–)

Department of Molecular Structure*Molecular Structure I*

OKAMOTO, Hiromi	Professor
NISHIMURA, Katsuyuki	Associate Professor (April '06–)
IMURA, Kohei	Research Associate
HORIMOTO, Noriko	IMS Fellow
WU, Hui Jun	Graduate Student (April '06–)

Molecular Structure II

TERAZIMA, Masahide	Visiting Professor (from Kyoto University)
ISHIMORI, Koichiro	Visiting Professor (from Hokkaido University) (–March '06)
KATAYAMA, Mutsumi	Visiting Associate Professor (from RIKEN) (April '06–)

Molecular Dynamics

KITAGAWA, Teizo	Professor (Okazaki Institute for Integrative Bioscience) (–March '06)
YOKOYAMA, Toshihiko	Professor
OZAWA, Takeaki	Associate Professor
UCHIDA, Takeshi	Research Associate (–September '05)
NAKAGAWA, Takeshi	Research Associate
TAKEUCHI, Masaki	Research Associate (December '05–)
WATANABE, Hirokazu	Technical Associate
HIDA, Naoki	IMS Fellow (April '06–)
AWAIS, Muhammad	Post-Doctoral Fellow (April '06–)
MA, Xiaodong	Graduate Student
NAGAOKA, Yasutaka	Graduate Student (April '06–)
HATTORI, Naoshi	Graduate Student (April '06–)
TERASAKA, Chie	Research Fellow (August '06–)

Department of Electronic Structure*Excited State Chemistry*

NISHI, Nobuyuki	Professor
BOO, Bong Hyun	Visiting Professor (from Chungnam National University, South Korea) (July '06)
JUDAI, Ken	Research Associate
NISHIJO, Junichi	Research Associate
OISHI, Osamu	Technical Associate
OKABE, Chie	IMS Fellow
WATANABE, Michio	Research Fellow (–March '06)

Excited State Dynamics

OHMORI, Kenji	Professor
OHSHIMA, Yasuhiro	Professor
KATSUKI, Hiroyuki	Research Associate
HASEGAWA, Hirokazu	Research Associate
HOSAKA, Kouichi	IMS Fellow
MIYAZAKI, Mitsuhiro	IMS Fellow (–October '05) ¹⁾
SUMA, Kohsuke	JSPS Post-Doctoral Fellow (April '06–)

* persons carrying out graduate research of IMS on Cooperative Education Program of IMS with other graduate schools

DELANGNES, Jean-Christophe	Post-Doctoral Fellow (April '06–)
SHIMADA, Hiroyuki	Post-Doctoral Fellow (May '06–)
MIYAKE, Shinichiro	Graduate Student (from Kyoto University)* (–March '06)
KITANO, Kenta	Graduate Student (from Kyoto University)* (September '05–August '06)

Electronic Structure

ICHIMURA, Teijiro	Visiting Professor (from Tokyo Institute of Technology) (–March '06)
KITAJIMA, Masahiro	Visiting Professor (from National Institute for Materials Science) (April '06–)
TAKAGI, Noriaki	Visiting Associate Professor (from the University of Tokyo) (–March '06)
BABA, Masaaki	Visiting Associate Professor (from Kyoto University) (April '06–)

Molecular Energy Conversion

SWIETLIK, Roman	Visiting Professor (from Polish Academy of Science, Poland) (March–August '06)
GAO, Yongli	Visiting Professor (from University of Rochester, U.S.A.) (June '06–)
TANATAR, Makariy	Visiting Associate Professor (from National Ukrainian Academy of Sciences, Ukraine) (–January '06)
ALLAKHVERDIEV, Suleyman I.	Visiting Associate Professor (from Institute of Basic Biological Problems, Russia) (April–June '06)
PAL, Tarasankar Nil	Visiting Associate Professor (from Indian Institute of Technology, India) (May–August '06)

Department of Molecular Assemblies*Solid State Chemistry*

YAKUSHI, Kyuya	Professor
NAKAMURA, Toshikazu	Associate Professor
YAMAMOTO, Kaoru	Research Associate
FURUKAWA, Ko	Research Associate
URUICHI, Mikio	Technical Associate
HARA, Toshifumi	IMS Fellow
NAKANO, Chikako	Research Fellow
DROZDOVA, Olga	Research Fellow (–November '05) ²⁾
MATSUOKA, Hideto	Research Fellow (–January '06) ³⁾
MAEDA, Keisuke	Graduate Student
TANAKA, Masayuki	Graduate Student

Molecular Assemblies Dynamics

KOBAYASHI, Hayao	Professor
TAKAHASHI, Kazuyuki	Research Associate
OKANO, Yoshinori	Technical Associate
CUI, Heng-Bo	Post-Doctoral Fellow
SUN, Hao-Lin	Post-Doctoral Fellow (September '05–August '06) ⁴⁾
MIYAMOTO, Akihito	Visiting Scientist
OTUBO, Saika	Graduate Student (–March '06) ⁵⁾

Molecular Assemblies

KOJIMA, Norimichi	Visiting Professor (from the University of Tokyo)
KAWAMOTO, Atsushi	Visiting Associate Professor (from Hokkaido University)

Department of Applied Molecular Science*Applied Molecular Science I*

AONO, Shigetoshi	Professor (Okazaki Institute for Integrative Bioscience)
JIANG, Donglin	Associate Professor
AKITA, Motoko	Research Associate (–September '05)
YOSHIOKA, Shiro	Research Associate (Okazaki Institute for Integrative Bioscience)
ISHIZUKA, Tomoya	Research Associate (February '06–)
HE, Jiang	IMS Fellow (April '06–)

ISHIJIMA, Ryo
WAN, Shun
NIU, Yinghui

Graduate Student (April '06–)
Graduate Student (April '06–)
Graduate Student (April '06–)

Applied Molecular Science II

IKEDA-SAITO, Masao
SODA, Kazuo
NAKAMURA, Kazutaka

Visiting Professor (from Tohoku University) (–March '06)
Visiting Professor (from Nagoya University) (April '06–)
Visiting Associate Professor (from Tokyo Institute of Technology) (–March '06)
Visiting Associate Professor (from Ritsumeikan University) (April '06–)

MAEDA, Hiromitsu

Department of Vacuum UV Photoscience

Photochemistry

KOSUGI, Nobuhiro
HISHIKAWA, Akiyoshi
HATSUI, Takaki
TAKAHASHI, Eiji
HIYAMA, Miyabi
FUSHITANI, Mizuho
MATSUDA, Akitaka

Professor
Associate Professor
Research Associate
Research Associate (–December '05)
Research Associate (–March '06)
Research Associate (August '06–)
IMS Fellow

Chemical Dynamics

URISU, Tsuneo
MITSUKE, Koichiro
KATAYANAGI, Hideki
TERO, Ryugo
MAO, Yanli
HUANG, Chaoqun
UNO, Hidetaka
YAGI, Hajime
CHIANG, Tsung-Yi
MISAWA, Nobuo
SAYED, Md. Abu
ZHANG, Zhenlong
KAFLE, Bhim Prasad
NAKAI, Naohito
PRODHAN, Md Serajul Islam
ASANO, Toshifumi
KIM, Yong-Hoon
RAHMAN, Mashuur

Professor
Associate Professor
Research Associate
Research Associate
IMS Fellow (April '06–)
IMS Fellow (August '06–)
Research Fellow
Research Fellow
Research Fellow (April '06–)
Graduate Student
Graduate Student
Graduate Student
Graduate Student
Graduate Student
Graduate Student (October '05–)
Graduate Student (April '06–)
Graduate Student (–September '05)
Graduate Student (–October '05)

Synchrotron Radiation Research

ARAKI, Koiti

LU, Xin
LONG, La-Sheng

WANG, Wenping

Visiting Professor (from Universidade de Sao Paulo) (November '05–January '06)
Visiting Professor (from Xiamen University) (–June '06)
Visiting Associate Professor (from Xiamen University) (–April '06)
Visiting Associate Professor (from Hefei University of Technology) (April '06–)

Department of Computational Molecular Science

Computational Molecular Science I

OKAZAKI, Susumu
MORITA, Akihiro
MIURA, Shinichi
ISHIDA, Tateki
IWAHASHI, Kensuke
YOSHII, Noriyuki
YAMADA, Atsushi
MIKAMI, Taiji
ISHIYAMA, Tatsuya

Professor (Research Center for Computational Science)
Associate Professor (Research Center for Computational Science)
Research Associate
Research Associate
Post-Doctoral Fellow (–February '06)
Post-Doctoral Fellow
Post-Doctoral Fellow
Post-Doctoral Fellow
Post-Doctoral Fellow

LI, Hongzhen Post-Doctoral Fellow (–August '06)
 SOKOLOV, Vladimir V. Post-Doctoral Fellow (April '06–)

Computational Molecular Science II

SAITO, Shinji Professor (October '05–)
 KIM, Kang Research Associate (June '06–)
 KOBAYASHI, Chigusa Post-Doctoral Fellow (April '06–)
 YAGASAKI, Takuma Post-Doctoral Fellow (April '06–)

Coordination Chemistry Laboratories

TANAKA, Koji Director

Functional Coordination Chemistry

TANAKA, Koji Professor
 KAWAGUCHI, Hiroyuki Associate Professor
 WADA, Tohru Research Associate
 MATSUO, Tsukasa Research Associate
 MIYASATO, Yuji IMS Fellow
 WATANABE, Takahito IMS Fellow
 TANNAI, Hidenori Post-Doctoral Fellow
 AKAGI, Fumio Post-Doctoral Fellow
 OKAMURA, Rei Post-Doctoral Fellow (–January '06)⁶⁾
 HINO, Takami Post-Doctoral Fellow (–January '06)⁷⁾
 FUJITA, Mitsuharu Post-Doctoral Fellow (–March '06)⁸⁾
 TAKUMA, Motoki Post-Doctoral Fellow (–March '06)⁹⁾
 KIMURA, Masahiro Post-Doctoral Fellow (June '06–)
 ARII, Hidekazu Post-Doctoral Fellow (June '06–)
 FUKAWA, Tomohide Post-Doctoral Fellow (July '06–)
 TSUTSUI, Kanako Research Fellow (–March '06)¹⁰⁾
 INOUE, Ayako Graduate Student
 FUKUSHIMA, Takashi Graduate Student

Coordination Bond

ISHII, Yoichi Visiting Professor (from Chuo University)
 HAYASHI, Takashi Visiting Professor (from Osaka University)

Complex Catalysis

MASHIMA, Kazushi Visiting Professor (from Osaka University) (–March '06)
 KITAGAWA, Hiroshi Visiting Professor (from Kyushu University) (April '06–)
 KURIHARA, Masato Visiting Associate Professor (from Yamagata University) (–March '06)
 KONDO, Mitsuru Visiting Associate Professor (from Shizuoka University) (April '06–)

Research Facilities***Research Center for Molecular-scale Nanoscience***

OGAWA, Takuji Director

Molecular-scale Electronics

OGAWA, Takuji Professor
 SUZUKI, Toshiyasu Associate Professor
 TANAKA, Shoji Research Associate
 SAKAMOTO, Youichi Research Associate
 TANAKA, Hirohumi Research Associate
 HUANG, Wei IMS Fellow
 HINO, Takami Post-Doctoral Fellow (February '06–)
 SUGAWARA, Yoshitaka Post-Doctoral Fellow (May '06–)
 SATO, Hirokazu Research Fellow (–March '06)
 TANEMURA, Hiroyo Research Fellow (April '06–)
 IIDA, Yuko Research Fellow (May '06–)
 OZAWA, Hiroaki Graduate Student
 YAJIMA, Takashi Graduate Student
 KAWAO, Masahiro Graduate Student
 OKUBO, Kimitaka Graduate Student

MIYAKE, Yusuke	Graduate Student (April '06–)
<i>Nanocatalysis and Biomolecular Devices</i>	
UOZUMI, Yasuhiro	Professor
NAGATA, Toshi	Associate Professor
SAKURAI, Hidehiro	Associate Professor
NAGASAWA, Takayuki	Research Associate
YAMADA, Yoichi	Research Associate
HIGASHIBAYASHI, Shuhei	Research Associate
KAMIYA, Ikuyo	IMS Fellow
OE, Yohei	IMS Fellow (April '06–)
MAKI, Suguru	IMS Fellow (–September '05)
TAKENAKA, Kazuhiro	Post-Doctoral Fellow (–October '05)
SUZUKA, Toshimasa	Post-Doctoral Fellow
KIMURA, Tsutomu	Post-Doctoral Fellow
OHTAKA, Atsushi	Post-Doctoral Fellow (–March '06)
MAEDA, Yasunari	Post-Doctoral Fellow (–March '06)
KIMURA, Masahiro	Graduate Student (–March '06), Post-Doctoral Fellow (April–May '06)
MINAGAWA, Maki	Graduate Student (–March '06), Post-Doctoral Fellow (April '06–)
NAKANO, Sachiko	Research Fellow (October '05–)
TAKENAKA, Hiroe	Research Fellow (May '06–)
SAKAMAKI, Junichiro	Graduate Student (–September '05)
ARAKAWA, Takayasu	Graduate Student
BEPPU, Tomohiko	Graduate Student
KAWADE, Rei	Graduate Student
FUKUYAMA, Naoshi	Graduate Student (–November '05)
TAKIZAWA, Ryu	Graduate Student
<i>Nano-scale Photoscience</i>	
MATSUMOTO, Yoshiyasu	Professor
TSUKUDA, Tatsuya	Associate Professor
NEGISHI, Yuichi	Research Associate
WATANABE, Kazuya	Research Associate
MATSUMOTO, Taketoshi	Research Associate
TSUNOYAMA, Hironori	IMS Fellow
CHAKI, Nirmalya Kumar	IMS Fellow
NAGAO, Masashi	IMS Fellow (–August '06)
SAWADA, Takeshi	Post-Doctoral Fellow (–September '05)
NAKAI, Ikuyo	Post-Doctoral Fellow (April '06–)
YANAGIMOTO, Yasushi	Post-Doctoral Fellow (Inoue Fellow)
SHICHIBU, Yukatsu	Post-Doctoral Fellow
NAKAO, Satoru	Research Fellow
YAMAGUCHI, Dai	Graduate Student (–March '06)
FUYUKI, Masanori	Graduate Student
<i>Advanced Molecular Science</i>	
KATO, Koichi	Visiting Professor (from Nagoya City University)
SASAKAWA, Hiroaki	Research Associate
YAGI, Hirokazu	Graduate Student (from Nagoya City University)*
NAGANO, Mayumi	Graduate Student (from Nagoya City University)* (–March '06)
SUMIYOSHI, Akira	Graduate Student (from Nagoya City University)* (–March '06)
SUZUKI, Maiko	Graduate Student (from Nagoya City University)* (–March '06)
KAMIYA, Yukiko	Graduate Student (from Nagoya City University)* (–March '06)
MAENO, Aya	Graduate Student (from Nagoya City University)* (–March '06)
OKAMOTO, Kenta	Graduate Student (from Nagoya City University)* (April '06–)
SAHASHI, Hiroki	Graduate Student (from Nagoya City University)* (April '06–)
KAMIYA, Daiki	Graduate Student (from Nagoya City University)* (April '06–)
UTSUMI, Maho	Graduate Student (from Nagoya City University)* (April '06–)
MASUKANE, Naoya	Graduate Student (from Nagoya City University)* (April '06–)
MIMURA, Shunsuke	Graduate Student (from Nagoya City University)* (April '06–)
TSUKAKOSHI, Haruko	Graduate Student (from Nagoya City University)* (April '06–)

* persons carrying out graduate research of IMS on Cooperative Education Program of IMS with other graduate schools

UVSOR Facility

KOSUGI, Nobuhiro	Director
KATOH, Masahiro	Professor
SHIGEMASA, Eiji	Associate Professor
KIMURA, Shin-ichi	Associate Professor
HARA, Toru	Visiting Associate Professor (from RIKEN)
HOSAKA, Masahito	Research Associate
MOCHIHASHI, Akira	Research Associate
ITO, Takahiro	Research Associate
HIKOSAKA, Yasumasa	Research Associate
SAKURAI, Yoko	IMS Fellow
KANAYASU, Tatsuo	IMS Fellow
SHIMADA, Miho	IMS Fellow (April '06–)
YOSHIMURA, Daisuke	Post-Doctoral Fellow (–October '05)
SUMII, Ryohei	Post-Doctoral Fellow (September '05–)
KIM, Hyeong-Do	Visiting Scientist (from Pohang Accelerator Laboratory, Korea) (September '05)
COUPRIE, Marie-Emmanuelle	Visiting Scientist (from CEA/DSM/DRECAM/SPAM, France) (November '05)
MEYER, Michael	Visiting Professor (from LURE, Centre Universitaire Paris-Sud, France) (November '04–December '05)
BIELAWSKI, Serge	Visiting Scientist (from Universite des Sciences et Technologies de Lille, France) (November–December '05)
SZWAJ, Christophe	Visiting Scientist (from Universite des Sciences et Technologies de Lille, France) (November–December '05)
RUEHL, Eckart	Visiting Scientist (from Wuerzburg University, France) (November–December '05)
PLENGE, Juergen	Visiting Scientist (from Wuerzburg University, France) (December '05)
SIMON, Marc	Visiting Scientist (from LCPMR, France) (January '06)
GUILLEMIN, Renand	Visiting Scientist (from LCPMR, France) (January '06)
HOLLAND, Andrew	Visiting Scientist (from Brunel University, U.K.) (March '06)
INGLEY, Richard	Visiting Scientist (from Brunel University, U.K.) (March '06)
KWON, Yong-Seung	Visiting Scientist (from Sungkyunkwan University, Korea) (March, July '06)
SICHELSCHMIT, Joerg	Visiting Scientist (from Max Planck Institut fuer Chemische Physik fester Stoffe, Germany) (August '06)
NISHI, Tatsuhiko	Graduate Student (–March '06)
IM, Hojun	Graduate Student
MIZUNO, Takafumi	Graduate Student
MIYAZAKI, Hidetoshi	Graduate Student (from Nagoya University)* (April '06–)
MIZUNUMA, Tatsuro	Graduate Student (from Meiji University)* (April '06–)
OTA, Shunji	Graduate Student (from Nagoya University)* (April '06–)
SUZUMURA, Kosuke	Graduate Student (from Nagoya University)* (April '06–)

Laser Research Center for Molecular Science

MATSUMOTO, Yoshiyasu Director

*Advanced Lasers for Chemical Reaction Studies**Advanced Lasers for Synchrotron Radiation Applications*

SARUKURA, Nobuhiko	Associate Professor (–December '05), Professor (January '06–)
ONO, Shingo	Research Associate
ESTACIO, Elmer	IMS Fellow
QUEMA, Alex	JSPS Post-Doctoral Fellow (–March '06)
MURAKAMI, Hidetoshi	Research Fellow (–March '06)
DIWA, Gilbert	Graduate Student (–March '06)
PONSECA, Carlito Jr.	Graduate Student (–March '06)
de los REYES, Glenda	Graduate Student (–March '06)
PHAM, Minh	Graduate Student (October '05–March '06)
CADATAL, Marilou	Graduate Student (October '05–March '06)

Advanced UV and IR Tunable Lasers

TAIRA, Takunori	Associate Professor
ISHIZUKI, Hideki	Research Associate
TSUNEKANE, Masaki	Post-Doctoral Fellow
SATO, Yoichi	Post-Doctoral Fellow
SAIKAWA, Jiro	Post-Doctoral Fellow (from Tokyo Institute of Technology)

Equipment Development Center

URISU, Tsuneo	Director
---------------	----------

Safety Office

OGAWA, Takuji	Director
TOMURA, Masaaki	Research Associate

Okazaki Research Facilities (related to IMS)*Okazaki Institute for Integrative Bioscience**Department of Strategic Methodology*

AONO, Shigetoshi	Professor
FUJII, Hiroshi	Associate Professor
YOSHIOKA, Shiro	Research Associate
KOBAYASHI, Katsuaki	IMS Fellow (–March '06)
KUJIME, Masato	Post-Doctoral Fellow
OZAWA, Kazumichi	Post-Doctoral Fellow (–March '06)
SAWAI, Hitomi	IMS Fellow (April '06–)
IURA, Takafumi	Visiting Scientist (from Yazaki Corporation)(June '06–)
INAGAKI, Sayaka	Graduate Student (–March '06), Research Fellow (April–May '06)
YOSHIMURA, Hideaki	Graduate Student
NISHIMURA, Muneto	Graduate Student
TAKAHASHI, Akihiro	Graduate Student (April '06–)

Department of Bio-environmental Science

KITAGAWA, Teizo	Professor (–March '06)
TAKAGI, Junichi	Visiting Professor (from Osaka University)
KUBO, Minoru	IMS Fellow (–March '06), Post-Doctoral Fellow (April '06–)
GU, Yuzong	Visiting Scientist; JSPS Post-Doctoral Fellow (from Henan University, China) (–July '06)
KOUTSOUPAKIS, Constantinos	Visiting Scientist; JSPS Post-Doctoral Fellow (November '05–)
EL-MASHTOLY, Samir Fathy Abd El-Monem	Visiting Scientist; JSPS Post-Doctoral Fellow
TOSHA, Takehiko	JSPS Post-Doctoral Fellow
NAGANO, Yasutomo	JSPS Post-Doctoral Fellow (–March '06)
LI, Zhengqiang	Research Fellow (from Jilin University) (September–December '05)
VAROTSIS, Constantinos	Visiting Scientist (from University of Crete, Greece) (October–November '05)
GAO, Ying	Graduate Student
LI, Jiang	Graduate Student
LU, Ming	Graduate Student

Research Center for Computational Science

NAGASE, Shigeru	Director (–March '06)
OKAZAKI, Susumu	Director (April '06–)
SAITO, Shinji	Professor (Department of Computational Molecular Science) (October '05–)
MORITA, Akihiro	Associate Professor
OONO, Hitoshi	Research Associate
MIURA, Shinichi	Research Associate (Department of Computational Molecular Science)
ISHIDA, Tateki	Research Associate (Department of Computational Molecular Science)
KIM, Kang	Research Associate (Department of Computational Molecular Science) (June '06–)

* persons carrying out graduate research of IMS on Cooperative Education Program of IMS with other graduate schools

Technical Staff

KATO, Kiyonori	Technical Division Head
SUZUI, Mitsukazu	Technical Section Chief
YOSHIDA, Hisashi	Technical Section Chief
HORIGOME, Toshio	Technical Section Chief
YAMANAKA, Takaya	Technical Section Chief
MIZUTANI, Fumiyasu	Technical Section Chief
TAKAYAMA, Takashi	Technical Section Chief
MIZUTANI, Nobuo	Equipment Development Center (Unit Chief)
AOYAMA, Masaki	Equipment Development Center (Unit Chief)
YANO, Takayuki	Equipment Development Center
KONDOU, Takuhiko	Equipment Development Center
NAGATA, Masaaki	Equipment Development Center (Unit Chief)
UCHIYAMA, Kouichi	Equipment Development Center
TOYODA, Tomonori	Equipment Development Center
HASUMOTO, Masami	UVSOR facility (Unit Chief)
YAMAZAKI, Jun-ichiro	UVSOR facility (Unit Chief)
NAKAMURA, Eiken	UVSOR facility (Unit Chief)
SAKAI, Masahiro	UVSOR facility
KONDOU, Naonori	UVSOR facility
HAYASHI, Kenji	UVSOR facility
CHIBA, Hisashi	Laser Research Center for Molecular Science
UEDA, Tadashi	Laser Research Center for Molecular Science
TESHIMA, Fumitsuna	Research Center for Computational Science
NAITOU, Shigeki	Research Center for Computational Science
SAWA, Masataka	Research Center for Computational Science
IWAHASHI, Kensuke	Research Center for Computational Science
MIZUKAWA, Tetsunori	Research Center for Molecular-scale Nanoscience
MAKITA, Seiji	Research Center for Molecular-scale Nanoscience
FUJIWARA, Motoyasu	Research Center for Molecular-scale Nanoscience
NAKANO, Michiko	Research Center for Molecular-scale Nanoscience
HARADA, Miyuki	Public Affairs Office
MINAMINO, Satoshi	Archives

List of Present Addresses

- 1) Chemical Spectroscopy Division, Chemical Resources Laboratory, Tokyo Institute of Technology, 4259 Nagatsuta, Midori-ku, Yokohama, Kanagawa 226-8503
- 2) NISSAN ARC, LTD., 1 Natsushima-cho, Yokosuka, Kanagawa 237-0061
- 3) RIKEN, 2-1, Hirosawa, Wako, Saitama 351-0198
- 4) Institute for Materials Chemistry and Engineering, Kyushu University, 6-1, Kasuga-koen, Kasuga, Fukuoka 816-8508
- 5) Mitsubishi Chemical Corporation, 5-33-8, Shiba, Minato-ku, Tokyo 108-0014
- 6) Sumitomo Chemical, Sodegaura 299-0295
- 7) Ogawa group, IMS, Okazaki 444-8787
- 8) Kyushu University, Fukuoka 819-1395
- 9) Münster University, 48149 Münster, Germany
- 10) Shiga International Patent Office, Tokyo 104-8543

COUNCIL

NAKAMURA, Hiroki

Director-General

Councillors

ESAKI, Nobuyoshi
KATO, Shinichi

Director, Institute for Chemical Research, Kyoto University
Chief Executive Officer, Toyota Central Research &
Development Laboratories, Inc.

TSUCHIYA, Soji
NOGUCHI, Hiroshi
NORDGREN, Joseph*

Invited Professor, Josai University
Culture News Editor, The Chunichi Shinbun Press
Professor, Uppsala University

CASTLEMAN, A. Welford Jr.*

Professor, The Pennsylvania State University

The Council is the advisory board for the Director-General.

* Two of the councillors are selected among distinguished foreign scientists.

Distinguished Consultants

NAGAKURA, Saburo
INOKUCHI, Hiroo

The Japan Academy
Chief Scientist of Space Utilization Research Program,
Japan Aerospace Exploration Agency

ITO, Mitsuo

Professor Emeritus, Institute for Molecular Science, The
Graduate University for Advanced Studies, Tohoku
University

KAYA, Koji

Director, RIKEN Discovery Research Institute

Research Consultants

HIROTA, Noboru
KONDOW, Tamotsu
TAMAO, Kohei

Professor Emeritus, Kyoto University
Visiting Professor, Toyota Technological Institute
Director, RIKEN Frontier Research System

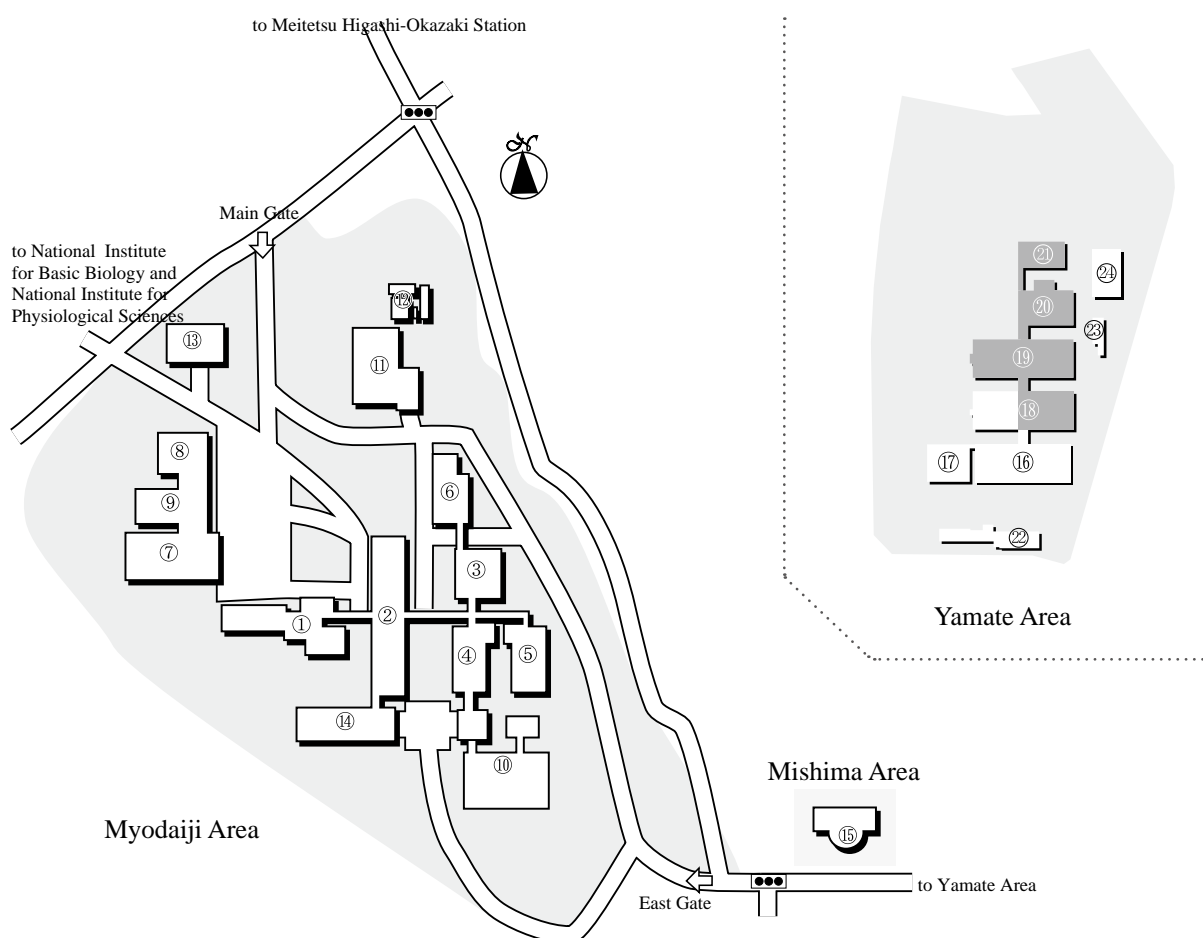
Administration Bureau

KURIKI, Shigeo	Director, Okazaki Administration Office
	Director, General Affairs Department
HARUHATA, Fumio	Director, Financial Affairs Department
TAKYOU, Moriyasu	Head, General Affairs Division
HIRAO, Koji	Head, International Relations and Research Cooperation Division
HAYASHI, Masanori	Head, Financial Affairs Division
KASSAI, Isamu	Head, Procurement Division
WATANABE, Toshio	Head, Facilities Division

BUILDINGS AND CAMPUS

The IMS campus covering 62,343 m² is situated on a low hill in the midst of Okazaki city. The inequality in the surface of the location, the hill and growing trees are preserved as much as possible, and low-storied buildings are adopted for conservation of the environment. The buildings of IMS are separated according to their functions as shown in the map below. The Research Office Building and all Research Facilities, except for the Computer Center, are linked organically to the Main Laboratory Buildings by corridors. The computer Center, Library and Administration Buildings are situated between IMS and neighboring National Institute for Basic Biology and National Institute for Physiological Sciences, since the latter two facilities are for common use amongst these three institutes.

The lodging facility of IMS called Yamate Lodge, located within ten minutes' walk, has sleeping accommodations for 15 guests and two families. Mishima Lodge, located within four minutes' walk east of IMS can accommodate 74 guests and 20 families. Scientists visiting IMS, as well as the two other institutes, can make use of these facilities. Foreign visiting scientists can also live in these lodgings with their families during their stays. The Okazaki Conference Center, with four conference rooms capable of attendance between 50~250, was built in April, 1997 in the Mishima area. The two buildings, Center for Integrative Bioscience, and Research Center for Computational Science, and research facilities of ONRI were built in February, 2002 in the Yamate Area. Four other buildings were also built in March, 2004 in the Yamate Area.



- | | |
|--|--|
| 1. Research Office Building | 13. Faculty Club |
| 2. Main Laboratory Building | 14. South Laboratory Building |
| 3. Equipment Development Center | 15. Okazaki Conference Center |
| 4. Laser Research Center for Molecular Science | 16. Yamate Bldg. 1A |
| 5. Research Center for Molecular-scale Nanoscience | 17. Yamate Bldg. 1B |
| 6. Low-Temperature Facilities Building | 18. Yamate Bldg. 2 |
| 7. Computer Center | 19. Yamate Bldg. 3 |
| 8. Library | 20. Yamate Bldg. 4 |
| 9. Central Administration | 21. Yamate Bldg. 5 |
| 10. UVSOR Facility | 22. Yamate Lodge |
| 11. Power Station | 23. Waste-Water Disposition Facilities |
| 12. Waste-Water Disposition Facilities | 24. Power Station |



Okazaki (population 351,000) is 260 km west of Tokyo, and can be reached by train in approximately 3 hours from Tokyo via Shinkansen and the Meitetsu Line. The nearest large city is Nagoya, about 40 km northwest of Okazaki.



RESEARCH ACTIVITIES I

Department of Theoretical Studies

I-A Theoretical Study and Design of Functional Molecular Systems: New Bonding, Structures, and Reactions

In theoretical and computational chemistry, it is an important goal to develop functional molecules with novel bonding and structures before or in cooperation with experiment. Thus, novel bonds and structures provided by heavier atoms are investigated. In addition, unique spaces and flexible structures provided by large molecules and clusters are investigated. Efficient computational methods are investigated to perform reliable quantum chemistry calculations of large molecular systems.

I-A-1 Effect of the Axial Cysteine Ligand on the Electronic Structure and Reactivity of High-Valent Iron (IV) Oxo-Porphyrins (Compound I): A Theoretical Study

CHOE, Yoong-Kee¹; NAGASE, Shigeru
(¹AIST)

[*J. Comput. Chem.* **26**, 1600–1611 (2005)]

The effects of axial ligands on the alkane hydroxylation of high-valent iron (IV) oxo-porphyrins (Compound I) are investigated using hybrid density functional theory at the B3LYP level. As axial ligands, thiolate, imidazole, phenolate, and chloride anions are investigated; the first three are the models of cysteinate, histidine, and tyrosinate, respectively. The alkane hydroxylation proceeds *via* several steps. A remarkable effect of axial ligands is found in the final product release step. The thiolate ligand weakens a bond between heme and an alcohol. In contrast, the imidazole ligand significantly increases the interaction between heme and an alcohol, which causes the catalytic cycle to be less efficient.

I-A-2 Sc₃N@C₈₀: Computations on the Two-Isomer Equilibrium at High Temperatures

SLANINA, Zdenek; NAGASE, Shigeru

[*ChemPhysChem* **6**, 2060–2063 (2005)]

The relative concentrations of the two isomers (I_h and D_{5h}) of Sc₃N@C₈₀, are investigated by calculating Gibbs free energies at the B3LYP level. When a relatively free motion of Sc₃N inside C₈₀ is allowed, the observed populations of 10 and 17% for the minor D_{5h} isomer are reached at 2100 and 2450 K, respectively. The entropy term plays an essential role, since, if it is neglected, the D_{5h} population at 2100 K is only 1%, owing to the relatively large interisomeric separation potential energy of 19 kcal/mol.

I-A-3 The Aromaticity of the Stannole Dianion

SAITO, Masaichi¹; HAGA, Ryuta¹; YOSHIOKA,

Michikazu¹; ISHIMURA, Kazuya; NAGASE, Shigeru
(¹Saitama Univ.)

[*Angew. Chem., Int. Ed.* **44**, 6553–6556 (2005)]

Neither monoanions nor dianions of stannoles have been well characterized, unlike the cases of the silole and germole anions. Thus, the lithium salt of a stannole dianion is isolated and investigated by NMR, X-ray crystal analysis, and theoretical calculations as the first tin-containing carbocyclic aromatic compound. The aromaticity of the stannole dianion is characterized by calculating charge delocalization and NICS (nucleus-independent chemical shift) values.

I-A-4 Reversible and Regioselective Reaction of La@C₈₂ with Cyclopentadiene

MAEDA, Yutaka¹; MIYASHITA, Jun¹;
HASEGAWA, Tadashi¹; WAKAHARA, Takatsugu²;
TSUCHIYA, Takahiro²; NAKAHODO, Tsukasa²;
AKASAKA, Takeshi²; MIZOROGI, Naomi;
KOBAYASHI, Kaoru; NAGASE, Shigeru; KATO,
Tatsuhisa³; BAN, Noritaka⁴; NAKAJIMA, Hiroshi⁴;
WATANABE, Yoshihito⁴
(¹Tokyo Gakugei Univ.; ²Univ. Tsukuba; ³Josai Univ.;
⁴Nagoya Univ.)

[*J. Am. Chem. Soc.* **127**, 12190–12191 (2005)]

The reversible and regioselective reaction of La@C₈₂ with cyclopentadiene is demonstrated in comparison with the corresponding reaction of C₆₀. Theoretical calculations show that La@C₈₂ reacts faster with cyclopentadiene than C₆₀, because La@C₈₂ has a lower LUMO than C₆₀. The low yield of the adduct of La@C₈₂ and cyclopentadiene is due to the presence of the fast retro-reaction. The rate constant for the consumption of La@C₈₂ is 2200 times slower than that of C₆₀ at 293 K.

I-A-5 Structural Determination of Metallofullerene Sc₃C₈₂ Revisited: A Surprising Finding

IIDUKA, Yuko¹; WAKAHARA, Takatsugu¹; NAKAHODO, Tsukasa¹; TSUCHIYA, Takahiro¹; SAKURABA, Akihiro²; MAEDA, Yutaka³; AKASAKA, Takeshi¹; YOZA, Kenji⁴; HORN, Ernst⁵; KATO, Tatsuhisa⁶; LIU, Michael T. H.⁷; MIZOROGI, Naomi; KOBAYASHI, Kaoru; NAGASE, Shigeru
(¹Univ. Tsukuba; ²Niigata Univ.; ³Tokyo Gakugei Univ.; ⁴Bruker AXS K.K.; ⁵Rikkyo Univ.; ⁶Josai Univ.; ⁷Univ. Prince Edward Island)

[*J. Am. Chem. Soc.* **127**, 12500–12501 (2005)]

It is widely accepted that the maximum-entropy-method (MEM)/Rietveld analysis of synchrotron X-ray powder diffraction data is powerful for structural determination of endohedral metallofullerenes. For example, the MEM/Rietveld analysis of Sc₃C₈₂ has shown that three Sc atoms are encapsulated inside a C_{3v} isomer of C₈₂ as a trimer with extremely short Sc–Sc distances. For Sc₃C₈₂, however, theoretical calculations reveal that two C atoms as well as three Sc atoms are encapsulated inside the I_h-C₈₀ (not C₈₂) fullerene, this Sc₂C₂@C₈₀ structure being much more stable than the Sc₃@C₈₂ structure determined by MEM/Rietveld analysis. The Sc₂C₂@C₈₀ structure is also verified by the NMR analysis of the anion and X-ray crystal analysis of a Sc₂C₂@C₈₀ derivative. It is suggested that the widely used MEM/Rietveld analysis is not reliable enough to determine the structures of endohedral metallofullerenes.

I-A-6 Electronic Structures of Semiconducting Double-Walled Carbon Nanotubes: Important Effect of Interlayer Interaction

SONG, Wei¹; NI, Ming¹; LU, Jing¹; GAO, Zhengxiang¹; NAGASE, Shigeru; YU, Dapeng¹; YE, Hengqiang¹; ZHANG, Xinwei²
(¹Peking Univ.; ²Inst. Appl. Phys. Comput. Math.)

[*Chem. Phys. Lett.* **414**, 429–433 (2005)]

Electronic structures of zigzag (7, 0)@(15, 0), zigzag (7, 0)@(18, 0), zigzag (8, 0)@(16, 0), and chiral (4, 2)@(10, 5) double-walled carbon nanotubes (DWNTs) are investigated by using first-principle calculations. The π and π^* states of inner (7, 0) and (4, 2) single-walled carbon nanotubes (SWNTs) exhibit a larger downward shift with respect to those of the outer (15, 0), (18, 0) and (10, 5) SWNTs. For (7, 0)@(15, 0), (8, 0)@(16, 0), and (4, 2)@(10, 5) DWNTs, it is notable that the interlayer π - π stacking interaction causes a significant band reconstruction of the inner SWNT.

I-A-7 Positional Control of Encapsulated Atoms inside a Fullerene Cage by Exohedral Addition

YAMADA, Michio¹; NAKAHODO, Tsukasa¹;

WAKAHARA, Takatsugu¹; TSUCHIYA, Takahiro¹; MAEDA, Yutaka²; AKASAKA, Takeshi¹; KAKO, Masahiro³; YOZA, Kenji⁴; HORN, Ernst⁵; MIZOROGI, Naomi; KOBAYASHI, Kaoru; NAGASE, Shigeru

(¹Univ. Tsukuba; ²Tokyo Gakugei Univ.; ³Univ. Electro-Communications; ⁴Bruker AXS K.K.; ⁵Rikkyo Univ.)

[*J. Am. Chem. Soc.* **127**, 14570–14571 (2005)]

Theoretical calculations shows that the three-dimensional random motion of two La atoms in La₂C₈₀ can be restricted to the circular motion in a plane by attaching an electron-donating molecules such as disilirane on the outer surface of the C₈₀ cage. Thus, the exohedral chemical functionalization of Ce@C₈₂ by disilirane is performed to fix the random motion of two Ce atoms at specific positions. The exohedral attachment of disilirane regulates the Ce positions under the equator of the C₈₀ cage.

I-A-8 A Singly Bonded Derivative of Endohedral Metallofullerene:La@C₈₂CBr(COOC₂H₅)₂

FENG, Lai¹; NAKAHODO, Tsukasa¹; WAKAHARA, Takatsugu¹; TSUCHIYA, Takahiro¹; MAEDA, Yutaka²; AKASAKA, Takeshi¹; KATO, Tatsuhisa³; HORN, Ernst⁴; YOZA, Kenji⁵; MIZOROGI, Naomi; NAGASE, Shigeru
(¹Univ. Tsukuba; ²Tokyo Gakugei Univ.; ³Josai Univ.; ⁴Rikkyo Univ.; ⁵Bruker AXS K.K.)

[*J. Am. Chem. Soc.* **127**, 17136–17137 (2005)]

A novel singly bonded derivative of La@C₈₂ is obtained by the reaction with diethyl bromomalonate. Theoretical calculations show that the reaction center of La₂@C₈₂ is most positively charged and has the second largest local strain, which is most reactive toward a nucleophilic attack. This suggests that a nucleophilic reaction takes place at the first step, followed by the oxidation of an intermediate, [La@C₈₂CBr(COOC₂H₅)₂], to afford the singly-bonded adduct.

I-A-9 S-Heterocyclic Carbene with a Disilane Backbone

NIKAWA, Hidefumi¹; NAKAHODO, Tsukasa¹; TSUCHIYA, Takahiro¹; WAKAHARA, Takatsugu¹; RAHMAN, G. M. Aminur¹; AKASAKA, Takeshi¹; MAEDA, Yutaka²; LIU, Michael T. H.³; MEGURO, Akira⁴; KYUSHIN, Soichiro⁴; MATSUMOTO, Hideyuki⁴; MIZOROGI, Naomi; NAGASE, Shigeru
(¹Univ. Tsukuba; ²Tokyo Gakugei Univ.; ³Univ. Prince Edward Island; ⁴Gunma Univ.)

[*Angew. Chem., Int. Ed.* **44**, 7567–7570 (2005)]

Heterocyclic carbenes have attracted considerable interest as ligands, catalysis, and spin sources. It is found that S-heterocyclic carbene can be generated by the [2 + 3] addition of cyclotetrasilene with CS₂, which is trapped by C₆₀ as a chemical probe. The structure and

electronic state of the S-heterocyclic carbene are determined by density functional calculations. It is calculated that the singlet state is 23.4 kcal/mol stable than the triplet state, and has a high nucleophilicity.

I-A-10 Ab Initio and DFT Study of the ^{29}Si NMR Chemical Shifts in $\text{RSi}\equiv\text{SiR}$

KARNI, Miriam¹; APELOIG, Yitzhak¹; TAKAGI, Nozomi; NAGASE, Shigeru
(¹Technion-Israel Inst. Tech.)

[*Organometallics* **24**, 6319–6330 (2005)]

The first DFT and ab-initio calculations of the ^{29}Si NMR chemical shifts of triply bonded silicon atoms are reported for $\text{RSi}\equiv\text{SiR}$ ($\text{R} = \text{H}, \text{CH}_3, \text{SiH}_3, \text{SiMe}(\text{SiH}_3)_2, \text{SiMe}(\text{SiMe}_3)_2, \text{SiMe}(\text{Si}t\text{Bu}_3)_2, \text{and Si}i\text{Pr}[\text{CH}(\text{SiMe}_3)_2]_2$). Small changes in geometries (the central Si–Si bond distance, the RSiSi bond angle and the RSiSiR twisting angle) strongly affect the chemical shifts. Inclusion of electron correlation by using MP2 and CCSD methods is found to be very important for reliable chemical shift calculations of $\text{RSi}\equiv\text{SiR}$. The chemical shifts calculated using the HCTH407 GGA functional are in good agreement with those calculated at the MP2 and CCSD levels. In contrast, a poor agreement is obtained when the popular B3LYP functional is used. The chemical shift of the triply-bonded silicon atoms in $\text{RSi}\equiv\text{SiR}$ ($\text{R} = \text{SiMe}(\text{Si}t\text{Bu}_3)_2$) is calculated to be in the range of 88 ± 5 ppm, this agreeing well with the observed chemical shift.

I-A-11 A New Parallel Algorithm of MP2 Energy Calculations

ISHIMURA, Kazuya; PULAY, Peter¹; NAGASE, Shigeru
(¹Univ. Arkansas)

[*J. Comput. Chem.* **27**, 407–413 (2006)]

A new parallel algorithm is developed for second order Møller-Plesset perturbation theory (MP2) energy calculations. Its main projected applications are for large molecules, for instance for the calculation of dispersion interaction. Tests on a moderate number of processors (2-16) show that the program has high CPU and parallel efficiency. Timings are presented for two relatively large molecules, taxol ($\text{C}_{47}\text{H}_{51}\text{NO}_{14}$) and luciferin ($\text{C}_{11}\text{H}_8\text{N}_2\text{O}_3\text{S}_2$), the former with the 6-31G* and 6-311G** basis sets (1032 and 1484 basis functions, 164 correlated orbitals), and the latter with the aug-cc-pVDZ and aug-cc-pVTZ basis sets (530 and 1198 basis functions, 46 correlated orbitals). An MP2 energy calculation on $\text{C}_{130}\text{H}_{10}$ (1970 basis functions, 265 correlated orbitals) completes in less than 2 hours on 128 processors.

I-A-12 Synthesis and Properties of a New Kinetically Stabilized Digermyne: New Insights for a Germanium Analogue of an Alkyne

SUGIYAMA, Yusuke¹; SASAMORI, Takahiro¹; HOSOI, Yoshinobu¹; FURUKAWA, Yukio²; TAKAGI, Nozomi; NAGASE, Shigeru; TOKITOH,

Norihiko¹
(¹Kyoto Univ.; ²Waseda Univ.)

[*J. Am. Chem. Soc.* **128**, 1023–1031 (2006)]

The reduction of an overcrowded (E)-1,2-dibromodigermyne, $\text{Bbt}(\text{Br})\text{Ge}=\text{Ge}(\text{Br})\text{Bbt}$ [$\text{Bbt} = 2,6$ -bis[bis(triethylsilyl)methyl]-4-[tris(trimethylsilyl)methyl]phenyl], with KC_8 affords a stable digermene, $\text{BbtGe}\equiv\text{GeBbt}$. The Ge–Ge triple bond distance of $\text{BbtGe}\equiv\text{GeBbt}$ is significantly shorter than that in the previously reported digermene, $\text{Ar}'\text{Ge}\equiv\text{GeAr}'$ ($\text{Ar}' = 2,6$ -Dip₂C₆H₃, Dip = 2,6-diisopropylphenyl). The nature of the Ge–Ge triple bond in $\text{BbtGe}\equiv\text{GeBbt}$ is disclosed by density functional calculations with large basis sets.

I-A-13 Computational Modelling for the Clustering Degree in the Saturated Steam and the Water-Containing Complexes in the Atmosphere

SLANINA, Zdenek; UHLIK, Filip¹; LEE, Shyi-Long²; NAGASE, Shigeru
(¹Charles Univ.; ²Natl. Chung-Cheng Univ.)

[*J. Quant. Spectrosc. Radiat. Transfer* **97**, 415–423 (2006)]

Recent computational findings of temperature increase of clustering degree in several different saturated vapors are analyzed further. A thermodynamic proof is presented, showing that this event should be rather common, if not general. Illustrations are based on the saturated steam and consequences for the atmosphere are discussed with both homo- and hetero-clustering. The best stabilization energies of $\text{H}_2\text{O}\cdot\text{N}_2$, $\text{H}_2\text{O}\cdot\text{O}_2$, and $(\text{O}_2)_2$ are reported. The water-dimer thermodynamics is recomputed in an anharmonic regime and a remarkable agreement with experiment is found. The results have some significance for the atmospheric greenhouse effect.

I-A-14 Analysis of Lanthanide-Induced NMR Chemical Shifts of the $\text{Ce}@C_{82}$ Anion

YAMADA, Michio¹; WAKAHARA, Takatsugu¹; LIAN, Yongfu¹; TSUCHIYA, Takahiro¹; AKASAKA, Takeshi¹; WAELCHLI, Markus²; MIZOROGI, Naomi; NAGASE, Shigeru; KADISH, Karl M.³
(¹Univ. Tsukuba; ²Bruker Biospin K.K.; ³Univ. Houston)

[*J. Am. Chem. Soc.* **128**, 1400–1401 (2006)]

From paramagnetic NMR spectra analysis and density functional calculations, it is found that the Ce atom in $\text{Ce}@C_{82}$ as well as $[\text{Ce}@C_{82}]^-$ is located at an off-centered position near a hexagonal ring of the C_{2v} - C_{82} cage along the C_2 axis, as found for $\text{M}@C_{82}$ ($\text{M} = \text{Sc}, \text{Y}, \text{and La}$). This is in sharp contrast with the Eu and Gd positions determined recently by the MEM/Rietveld method for $\text{Eu}@C_{82}$ and $\text{Gd}@C_{82}$.

I-A-15 Synthesis and Structural Characterization of Endohedral Pyrrolidinodimetallfullene: $\text{La}_2@C_{80}(\text{CH}_2)_2\text{NTrt}$

YAMADA, Michio¹; WAKAHARA, Takatsugu¹; NAKAHODO, Tsukasa¹; TSUCHIYA, Takahiro¹; MAEDA, Yutaka²; AKASAKA, Takeshi¹; YOZA, Kenji³; HORN, Ernst⁴; MIZOROGI, Naomi; NAGASE, Shigeru
(¹Univ. Tsukuba; ²Tokyo Gakugei Univ.; ³Bruker AXS K.K.; ⁴Rikkyo Univ.)

[*J. Am. Chem. Soc.* **128**, 1402–1403 (2006)]

The reaction of $\text{La}_2@C_{82}$ with 3-triphenylmethyl-5-oxazolidinone leads to the 6,6- and 5,6-adducts, $\text{La}_2@C_{80}(\text{CH}_2)_2\text{NTrt}$ (Trt = triphenylmethyl). The structure of the 6,6 adduct is determined by X-ray crystal structure and density functional calculations. As suggested by the electrostatic potential maps calculated for $[\text{C}_{80}(\text{CH}_2)_2\text{NH}]^-$, the two La atoms in $\text{La}_2@C_{80}(\text{CH}_2)_2\text{NTrt}$ are fixed, unlike the random motion in $\text{La}_2@C_{80}$, and can be regulated by addition positions.

I-A-16 $\text{La}_2@C_{72}$ and $\text{Sc}_2@C_{72}$: Computational Characterizations

SLANINA, Zdenek; CHEN, Zhongfang¹; SCHLEYER, Paul v. R.¹; UHLIK, Filip²; LU, Xin³; NAGASE, Shigeru
(¹Univ. Georgia; ²Charles Univ.; ³Xiamen Univ.)

[*J. Phys. Chem. A* **110**, 2231–2234 (2006)]

The $\text{La}_2@C_{72}$ and $\text{Sc}_2@C_{72}$ metallofullerenes are characterized by systematic density functional computations. On the basis of the most stable geometry of 39 C_{72} hexaanions and the computed energies of the best endofullerene candidates, the experimentally isolated $\text{La}_2@C_{72}$ has the structure coded #10611 that invalidates the so-called isolated pentagon (IPR) rule. The good agreement between the computed and the experimental ¹³C chemical shifts for $\text{La}_2@C_{72}$ further supports the literature assignment. The geometry, IR vibrational frequencies, and ¹³C chemical shifts of $\text{Sc}_2@C_{72}$ are predicted to assist its future experimental characterization.

I-A-17 Reactivity of 1-Hydro-5-Carbaphosphatrane Based on Tautomerization between Pentavalent Phosphorane and Trivalent Cyclic Phosphonite

KOBAYASHI, Junji¹; GOTO, Kei¹; KAWASHIMA, Takayuki¹; SCHMIDT, Michael W.²; NAGASE, Shigeru
(¹Univ. Tokyo; ²Iowa State Univ.)

[*Chem. Eur. J.* **12**, 3811–3820 (2006)]

Several reactions of 1-hydro-5-carbaphosphatrane based on tautomerization to the trivalent *t* cyclic phosphonite, not definitively observed by spectroscopic

methods, are investigated experimentally and analyzed by ab initio theoretical calculations. The calculated potential energy surfaces (reaction intermediates and transition states) provide insight into the reaction mechanism.

I-A-18 Evolution of the Electronic Properties of Metallic Single-Walled Nanotubes with the Degree of CCl_2 Covalent Functionalization

LU, Jing¹; WANG, Dan²; NAGASE, Shigeru; NI, Ming¹; ZHANG, Xinwei³; MAEDA, Yutaka⁴; WAKAHARA, Takatsugu⁵; NAKAHODO, Tsukasa⁵; TSUCHIYA, Takahiro⁵; AKASAKA, Takeshi⁵; GAO, Zhengxiang¹; YU, Dapeng¹; YE, Hengqiang¹; ZHOU, Yunsong²; MEL, W. N.⁶
(¹Peking Univ.; ²Capital Normal Univ.; ³Inst. Appl. Phys. Comput. Math.; ⁴Tokyo Gakugei Univ.; ⁵Univ. Tsukuba; ⁶Univ. Nebraska)

[*J. Phys. Chem. B* **110**, 5655–5658 (2006)]

The changes in energetic, structural, and electronic properties of the metallic (5, 5) single-walled carbon nanotube (SWNT) with the degree of sidewall covalent functionalization of CCl_2 are investigated by using density functional calculations. The saturation concentration of CCl_2 covalent functionalization is predicted to be 33.3%. The cycloadducts always adopt an open structure. A band gap opens as the functionalization concentration reaches 11% and then basically increases with increasing functionalization concentration. These results are in agreement with available experiments and can be applied to predict the band gap of metallic SWNTs produced by the HiPco method at a given CCl_2 functionalization concentration.

I-A-19 Stability Computations for $\text{Ba}@C_{74}$ Isomers

SLANINA, Zdenek; NAGASE, Shigeru

[*Chem. Phys. Lett.* **422**, 133–136 (2006)]

Relative concentrations of six isomers of $\text{Ba}@C_{74}$ are evaluated: one cage with isolated pentagons, three isomers with a pentagon–pentagon junction, two structures with one pentagon–pentagon pair and one heptagon. The density functional calculations of Gibbs free energies show that $\text{Ba}@C_{82}$ has a D_{3h} - C_{74} cage that satisfies the isolated pentagon rule. The stability computations are in agreement with recent observations.

I-A-20 Comment on Disproving a Silicon Analog of an Alkyne with the Aid of Topological Analyses of the Electronic Structure and Ab Initio Molecular Dynamics Calculations

FRENKING, Gernot¹; KRAPP, Andreas¹; NAGASE, Shigeru; TAKAGI, Nozomi; SEKIGUCHI, Akira²
(¹Philipps-Univ.; ²Univ. Tsukuba)

[*ChemPhysChem* **7**, 799–800 (2006)]

As the first example of the silicon analogues of alkynes, $\text{RSi}\equiv\text{SiR}$ ($\text{R} = \text{SiPr}[\text{CH}(\text{SiMe}_3)_2]_2$) has been isolated. From the topological analysis of electron density distributions, it is recently claimed that only two electron pairs participate in the Si–Si bonding. In view of donor-acceptor interactions, however, it is commented that the Si–Si bond can be described as a triple bond.

I-A-21 Selective Interaction of Larger or Charge-Transfer Aromatic Molecules with Metallic Single-Wall Carbon Nanotubes: Critical Role of the Molecular Size and Orientation

LU, Jing¹; NAGASE, Shigeru; ZHANG, Xinwei²; WANG, Dan³; NI, Ming¹; MAEDA, Yutaka⁴; WAKAHARA, Takatsugu⁵; NAKAHODO, Tsukasa⁵; TSUCHIYA, Takahiro⁵; AKASAKA, Takeshi⁵; GAO, Zhengxiang¹; YU, Dapeng¹; YE, Hengqiang¹; MEI, W. N.⁶; ZHOU, Yunsong³
(¹Peking Univ.; ²Inst. Appl. Phys. Comput. Math.; ³Capital Normal Univ.; ⁴Tokyo Gakugei Univ.; ⁵Univ. Tsukuba; ⁶Univ. Nebraska)

[*J. Am. Chem. Soc.* **128**, 5114–5118 (2006)]

Using first principles calculations, we report for the first time that large nearly neutral aromatic molecules, such as naphthalene and anthracene, and small charge-transfer aromatic molecules, such as TCNQ and DDQ, interact more strongly with metallic single-walled carbon nanotubes (SWNTs) *vs.* their semiconducting counterparts as the molecular orientation of DDQ is taken into account. Two new mechanisms for separating metallic and semiconducting SWNTs *via* noncovalent π - π stacking or charge-transfer interaction are suggested.

I-A-22 Excited Electronic States and Relative Stabilities of C_{80} Isomers

SLANINA, Zdenek; LEE, Shyi-Long¹; UHLIK, Filip²; ADAMOWICZ, Ludwik³; NAGASE, Shigeru
(¹Natl. Chung-Cheng Univ.; ²Charles Univ.; ³Univ. Arizona)

[*Int. J. Quantum Chem.* **106**, 2222–2228 (2006)]

The synthesis of fullerenes at very high temperatures allows for a significant population of excited electronic states and thus for non-negligible electronic partition functions. This issue is studied for seven isomers of C_{80} that satisfy the isolated pentagon rule. It is calculated that the effects of electronic excited states are larger than those in the previously tested examples. For the special conditions of fullerene synthesis/isolation, the electronic partition function based on the singlet excited states only reflect better the experimental population findings.

I-A-23 Synthesis and Characterization of a Bisadduct of La@C_{82}

FENG, Lai¹; TSUCHIYA, Takahiro¹; WAKAHARA, Takatsugu¹; NAKAHODO, Tsukasa¹; PIAO, Qiuyue¹; MAEDA, Yutaka²; AKASAKA, Takeshi¹; KATO, Tatsuhisa³; YOZA, Kenji⁴; HORN, Ernst⁵;

MIZOROGI, Naomi; NAGASE, Shigeru
(¹Univ. Tsukuba; ²Tokyo Gakugei Univ.; ³Josai Univ.; ⁴Bruker AXS K.K.; ⁵Rikkyo Univ.)

[*J. Am. Chem. Soc.* **128**, 5990–5991 (2006)]

Up to now, no direct evidence has been reported for the dimerization of endohedral metallofullerenes. By synthesizing the bisadduct of La@C_{82} , it is demonstrated that the bisadduct forms a dimer in the single crystal. From the density functional calculations, it is evaluated which carbons in the bisadduct have large spin densities and POAV (p orbital axis vector) values to predict the most favorable position for dimerization. The intermolecular C–C distance of 1.635 Å calculated at the B3LYP level for the dimer agrees very well with the value of 1.638 (9) Å determined by the X-ray crystal analysis.

I-A-24 ¹³C NMR Spectroscopic Study of Scandium Dimetallofullerene, $\text{Sc}_2\text{@C}_{84}$ vs. $\text{Sc}_2\text{C}_2\text{@C}_{82}$

IIDUKA, Yuko¹; WAKAHARA, Takatsugu¹; NAKAJIMA, Koji¹; TSUCHIYA, Takahiro¹; NAKAHODO, Tsukasa¹; MAEDA, Yutaka²; AKASAKA, Takeshi¹; MIZOROGI, Naomi; NAGASE, Shigeru
(¹Univ. Tsukuba; ²Tokyo Gakugei Univ.)

[*Chem. Commun.* 2057–2059 (2006)]

It has been widely believed that the typical dimetallofullerene, Sc_2C_{84} , takes the form of $\text{Sc}_2\text{@C}_{84}$ in which two Sc atoms are engaged inside the C_{84} fullerene. However, it is found that the endohedral structure is not $\text{Sc}_2\text{@C}_{84}$ but $\text{Sc}_2\text{C}_2\text{@C}_{80}$. This finding is in sharp contrast with the previous NMR and power X-ray MEM/Rietvelt analysis.

I-A-25 H_2 , Ne, and N_2 Energies of Encapsulation into C_{60} Evaluated with the MPWB1K Functional

SLANINA, Zdenek; PULAY, Peter¹; NAGASE, Shigeru
(¹Univ. Arkansas)

[*J. Chem. Theory Comput.* **2**, 782–785 (2006)]

The recently suggested MPWB1K functional is tested on $\text{H}_2\text{@C}_{60}$, Ne@C_{60} , and $\text{N}_2\text{@C}_{60}$ as a tool for evaluations of stabilization energies upon encapsulation of nonmetallic species into fullerenes. It is found that the MPWB1K (modified Perdew-Wang and Becke functionals) values can be within a few kilocalories per mole from the MP2 or SCS-MP2 (spin-component scaled MP2) values so that further applications of the functional are clearly encouraged. The best estimates of the encapsulation-energy gains found for $\text{H}_2\text{@C}_{60}$, Ne@C_{60} , and $\text{N}_2\text{@C}_{60}$ are at least 4 kcal/mol, slightly less than 4 kcal/mol, and about 9 kcal/mol, respectively.

I-A-26 Host-Guest Complexation of Endohedral Metallofullerene with Azacrown Ether and Its Application

TSUCHIYA, Takahiro¹; SATO, Kumiko¹;
 KURIHARA, Hiroki¹; WAKAHARA, Takatsugu¹;
 NAKAHODO, Tsukasa¹; MAEDA, Yutaka²;
 AKASAKA, Takeshi¹; OHKUBO, Kei³;
 FUKUZUMI, Shunich³; KATO, Tatsuhisa⁴;
 MIZOROGI, Naomi; KOBAYASHI, Kaoru;
 NAGASE, Shigeru
 (¹Univ. Tsukuba; ²Tokyo Gakugei Univ.; ³Osaka Univ.;
⁴Josai Univ.)

[*J. Am. Chem. Soc.* **128**, 6699–6703 (2006)]

Complexation of La@C₈₂-A with macrocyclic compounds, such as 1,4,7,10,13,16-hexaazacyclooctadecane, 1,4,7,10,13,16-hexamethyl-1,4,7,10,13,16-hexaazacyclooctadecane, mono-aza-18-crown-6 ether, 18-crown-6 ether, and *p-tert*-butylcalix[*n*]arenes (*n* = 4–8) is investigated.

I-A-27 Synthesis of Stannaindenyl Anions and a Dianion

SAITO, Masaichi¹; SHIMOSAWA, Masakazu¹;
 YOSHIOKA, Michikazu¹; ISHIMURA, Kazuya;
 NAGASE, Shigeru
 (¹Saitama Univ.)

[*Organometallics* **25**, 2967–2971 (2006)]

Reduction of 1,1-diphenylstannaindene with lithium gives the 1-phenyl-1-stannaindenyl anion, which is further reduced to provide the 1-stannaindenyl dianion. The remarkable upfield ⁷Li NMR resonance in the dianion and theoretical calculations suggest that the 1-stannaindenyl dianion has considerable aromatic character, as is observed in the sila- and germaindenyl dianions. The structure, charge distribution, NMR chemical shifts of the unsolvated and solvated 1-stannaindenyl dianion are calculated at the B3LYP level.

I-A-28 The Bingel Monoadducts of La@C₈₂: Synthesis, Characterization, and Electrochemistry

FENG, Lai¹; WAKAHARA, Takatsugu¹;
 NAKAHODO, Tsukasa¹; TSUCHIYA, Takahiro¹;
 PIAO, Qiuyue¹; MAEDA, Yutaka²; LIAN, Yongfu¹;
 AKASAKA, Takeshi¹; HORN, Ernst³; YOZA,
 Kenji⁴; KATO, Tatsuhisa⁵; MIZOROGI, Naomi;
 NAGASE, Shigeru
 (¹Univ. Tsukuba; ²Tokyo Gakugei Univ.; ³Rikkyo Univ.;
⁴Bruker AXS K.K.; ⁵Josai Univ.)

[*Chem. Eur. J.* **12**, 5578–5586 (2006)]

The reaction of La@C₈₂ with diethyl bromomalonate provides five monoadducts. Four of the five adducts are ESR inactive and singly bonded regioisomers, while the remaining adduct is ESR active and possesses a cyclic moiety between the malonate group and the C₈₂ cage.

Addition sites, thermal stabilities, and electrochemical properties are investigated with the help of density functional calculations.

I-A-29 Syntheses, Structures, and Reactions of Heptacoordinate Trihalogermanes Bearing a Triarylmethyl-Type Tetradentate Ligand

IWANAGA, Kohei¹; KOBAYASHI, Junji¹;
 KAWASHIMA, Takayuki¹; TAKAGI, Nozomi;
 NAGASE, Shigeru
 (¹Univ. Tokyo)

[*Organometallics* **25**, 3388–3393 (2006)]

Heptacoordinate trihalogermanes are synthesized by the reaction of the (triarylmethyl)lithium species and with tetrachlorogermane. The bonding nature of the central heptacoordinate Ge atom and the surrounding O atoms is investigated by the AIM (atoms-in-molecules) analysis at the B3PW1 level. The small electron density ($\rho(r_c)$) value and the small positive Laplacian ($\nabla^2\rho(r_c)$) value at the bond critical point (r_c) value suggest that the Ge–O bonds are weak and have ionic character.

I-A-30 Structural and Electronic Properties of Fluorinated Boron Nitride Nanotubes

LAI, Lin¹; SONG, Wei¹; LU, Jing¹; GAO,
 Zhengxiang¹; NAGASE, Shigeru; NI, Ming¹; MEI,
 W. N.²; LIU, Jianjun²; YU, Dapeng¹; YE,
 Hengqiang¹
 (¹Peking Univ.; ²Univ. Nebraska)

[*J. Phys. Chem. B* **110**, 14092–14097 (2006)]

The effects of F doping on the structural and electronic properties of the (5,5) single-walled boron nitride nanotube (BNNT) are investigated by using the density functional theory method. The chemisorption of F maintains the hexagonal BN network, increases the lattice constant, and introduces acceptor impurity states. On the other hand, substitutional doping of F destroys the hexagonal BN network, decreases the lattice constant, but does not alter the insulating feature of the BNNT. The observed insulator-to-semiconducting transition, a lattice contraction, and a highly disordered atom arrangement in the sidewall of BNNTs upon F doping are most reasonably attributed to a codoping of dominating substitutional F over chemisorbed F, which can induce deep donor impurity states, a lattice contraction, and a destruction of the hexagonal BN network simultaneously.

I-A-31 Characterization of the Bis-Silylated Endofullerene Sc₃N@C₈₀

WAKAHARA, Takatsugu¹; IIDUKA, Yuko¹;
 IKENAGA, Ozora¹; NAKAHODO, Tsukasa¹;
 SAKURABA, Akihiro²; TSUCHIYA, Takahiro¹;
 MAEDA, Yutaka³; KAKO, Masahiro⁴; AKASAKA,
 Takeshi¹; YOZA, Kenji⁵; HORN, Ernst⁶;
 MIZOROGI, Naomi; NAGASE, Shigeru
 (¹Univ. Tsukuba; ²Niigata Univ.; ³Tokyo Gakugei Univ.;

⁴Univ. Electro-Communications; ⁵Bruker AXS K.K.;
⁶Rikkyo Univ.)

[*J. Am. Chem. Soc.* **128**, 9919–9925 (2006)]

The photochemical reaction of Sc₃N@C₈₀ with 1,1,2,2-tetramesityl-1,2-disilirane affords the bis-silylated adduct. This adduct was characterized by NMR spectroscopy and single-crystal X-ray structure analysis. The dynamic behavior of the disilirane moiety and the encapsulated Sc₃N cluster were also investigated. The unique redox property of the adduct is reported by means of CV and DPV. Experimental results were confirmed by density functional calculations.

I-A-32 Synthesis and Characterization of Dimetallostannafluorenes

SAITO, Masaichi¹; SHIMOSAWA, Masakazu¹;
 YOSHIOKA, Michikazu¹; ISHIMURA, Kazuya;
 NAGASE, Shigeru
 (¹Saitama Univ.)

[*Chem. Lett.* 940–941 (2006)]

There has been considerable interest in the chemistry of anions and dianions of group 14 metalloids as heavier congeners of cyclopentadienyl anions. The reaction of 9,9-bis(*p*-methoxyphenyl)-9-stannafluorene with lithium or potassium gives the corresponding dimetallostannafluorene. The structure and aromaticity are characterized by density functional calculations.

I-A-33 Carbon Monoxide inside an Open-Cage Fullerene

IWAMATSU, Sho-ichi¹; STANISKY, Christopher
 M.²; CROSS, R. James²; SAUNDERS, Martin²;
 MIZOROGI, Naomi; NAGASE, Shigeru; MURATA,
 Shizuaki¹
 (¹Nagoya Univ.; ²Yale Univ.)

[*Angew. Chem., Int. Ed.* **45**, 5337–5340 (2006)]

It is of considerable interest to store a molecule inside cage molecules by making an orifice on the cage surface. Thus, an orifice is made on C₆₀ by chemical modification, which is the largest known to date for fullerenes, and CO is inserted through the orifice. The binding energy and dynamic behaviors are investigated by density functional calculations. It is suggested that the stored CO molecule rotates rapidly on the NMR time scale but not on the IR time scale.

I-B Applications of the Zhu-Nakamura Theory to Nonadiabatic Chemical Dynamics

I-B-1 Generalized Trajectory Surface Hopping Method Based on the Zhu-Nakamura Theory

OLOYEDE, Ponnile¹; MIL'NIKOV, Gennady V.¹; NAKAMURA, Hiroki
(¹SOKENDAI)

[*J. Chem. Phys.* **124**, 144110 (2006)]

We present a generalized formulation of the trajectory surface hopping method applicable to a general multidimensional system. The method is based on the Zhu-Nakamura theory of a nonadiabatic transition and therefore includes the treatment of classically forbidden hops. The method uses a generalized recipe for the conservation of angular momentum after forbidden hops and an approximation for determining a nonadiabatic transition direction which is crucial when the coupling vector is unavailable. This method also eliminates the need for a rigorous location of the seam surface, thereby ensuring its applicability to a wide class of chemical systems. In a test calculation, we implement the method for the DH_2^+ system, and it shows a remarkable agreement with the previous results of C. Zhu, H. Kamisaka, and H. Nakamura, [*J. Chem. Phys.* **116**, 3234 (2002)]. We then apply it to a diatomic-in-molecule model system with a conical intersection, and the results compare well with exact quantum calculations. The successful application to the conical intersection system confirms the possibility of directly extending the present method to an arbitrary potential of general topology.

I-B-2 Semiclassical Treatment of Thermally Activated Electron Transfer in the Intermediate to Strong Electronic Coupling Regime under the Fast Dielectric Relaxation

ZHAO, Yi¹; LIANG, Wanzhen²; NAKAMURA, Hiroki
(¹IMS and Univ. Sci. Tech. China; ²Univ. Sci. Tech. China)

[*J. Phys. Chem. A* **110**, 8204 (2006)]

The generalized nonadiabatic transition-state theory (NA-TST) (Zhao, Y.; *et al. J. Chem. Phys.* **121**, 8854 (2004)) is used to study electron transfer with use of the Zhu-Nakamura (ZN) formulas of nonadiabatic transition in the case of fast dielectric relaxation. The rate constant is expressed as a product of the well-known Marcus formula and a coefficient which represents the correction due to the strong electronic coupling. In the case of general multidimensional systems, the Monte Carlo approach is utilized to evaluate the rate by taking into account the multidimensionality of the crossing seam surface. Numerical demonstration is made by using a model system of a collection of harmonic oscillators in the Marcus normal region. The results are naturally coincident with the perturbation theory in the weak

electronic coupling limit; while in the intermediate to strong electronic coupling regime where the perturbation theory breaks down the present results are in the good agreement with those from the quantum mechanical flux-flux correlation function within the model of effective one-dimensional mode.

I-B-3 Electron Transfer Rate Uniformly Valid from Nonadiabatic to Adiabatic Regime Based on the Zhu-Nakamura Theory

ZHAO, Yi¹; NAKAMURA, Hiroki
(¹IMS and Univ. Sci. Tech. China)

[*J. Theor. Comput. Chem.* **5**, Special Issue 1–8 (2006)]

On the basis of the generalized nonadiabatic transition state theory recently introduced to remedy the crucial deficiencies of the conventional transition state theory, we have presented a new formula for electron transfer rate, which can cover the whole range from adiabatic to nonadiabatic regime in the absence of solvent dynamics control. The rate is expressed as a product of the well-known Marcus theory and a new coefficient that represents the effects of nonadiabatic transition at the crossing seam surface. The numerical comparisons are performed with different approaches and the present approach shows an excellent agreement with the quantum mechanical numerical solutions from weak to strong electronic coupling. The explanation of the experimental data of Nelson *et al.* manifests the potential applicability of the present theory.

I-B-4 Incorporation of Nonadiabatic Transition into Wave-Packet Dynamics

MIL'NIKOV, Gennady V.; ZOU, Shiyang; NAKAMURA, Hiroki

[*J. Chem. Phys.* **123**, 141101 (2005)]

Nonadiabatic wave-packet dynamics is factorized into purely adiabatic propagation and instantaneous localized non-adiabatic transition. A general formula is derived for the quantum-mechanical local nonadiabatic operator which is implemented within the framework of the R- matrix method. The operator can be used for incorporating the nonadiabatic transition in semiclassical wave-packet dynamics.

I-B-5 Dynamics of Nonadiabatic Chemical Reactions

NAKAMURA, Hiroki

[*J. Phys. Chem. A* **110**, 10929 (2006)]

New methods are proposed to treat nonadiabatic chemical dynamics in realistic large molecular systems

by using the Zhu-Nakamura (ZN) theory of curve-crossing problems. They include the incorporation of the ZN formulas into the Herman-Kluk type semiclassical wave packet propagation method and the trajectory surface hopping (TSH) method, formulation of the nonadiabatic transition state theory, and its application to the electron transfer problem. Since the nonadiabatic coupling is a vector in multi-dimensional space, the one-dimensional ZN theory works all right. Even the classically forbidden transitions can be correctly treated by the ZN formulas. In the case of electron transfer, a new formula which can improve the celebrated Marcus theory in the case of normal regime is obtained so that it

can work nicely in the intermediate and strong electronic coupling regimes. All these formulations mentioned above are demonstrated to work well in comparison with the exact quantum mechanical numerical solutions and are expected to be applicable to large systems which cannot be treated quantum mechanically numerically exactly. In order to take into account another quantum mechanical effect, namely, tunneling effect, an efficient method to detect caustics from which tunneling trajectories emanate is proposed. All the works reported here are the results of recent activities carried out in the author's research group. Finally, the whole set of ZN formulas is presented in Appendix.

I-C Theory of Multi-Dimensional Tunneling

I-C-1 Tunneling Splitting of Energy Levels and Rotational Constants in the Vinyl Radical C_2H_3

MIL'NIKOV, Gennady V.; ISHIDA, Toshimasa¹;
NAKAMURA, Hiroki
(¹Kyoto Univ.)

[*J. Phys. Chem. A* **110**, 5430–5435 (2006)]

The instanton theory newly implemented by two of

the authors (G. V. M. and H. N.) is applied to hydrogen tunneling transfer in a vinyl radical. The converged instanton trajectory is found on the CCSD(T)/aug-cc-pVTZ level of an ab initio potential energy surface. The calculated ground-state energy splitting agrees with the recent high-resolution experimental data within 3% of discrepancy. The semiclassical wave function is used to estimate the splitting of the principal rotational constants of the radical.

I-D Laser Control of Molecular Processes and Development of Molecular Functions

I-D-1 Semiclassical Guided Optimal Control of Molecular Dynamics

KONDORSKIY, Alexey; MIL'NIKOV, Gennady V.;
NAKAMURA, Hiroki

[*Phys. Rev. A* **72**, 041401(R) (2005)]

An efficient semiclassical optimal control theory applicable to multidimensional systems is formulated for controlling wave packet dynamics on a single adiabatic potential energy surface. The approach combines advantages of different formulations of optimal control theory: quantum and classical on one hand and global and local on the other. Numerical applications to the control of NCH-CN₂ isomerization demonstrate that this theory can provide an efficient tool to manipulate molecular dynamics of many degrees of freedom by laser pulses.

I-D-2 Selective Transition to the Closely-Lying States $Cs(7D_{3/2})$ and $Cs(7D_{5/2})$ by Femtosecond Laser Pulses

YAMADA, H.²; YOKOYAMA, K.¹; TERANISHI,

Y.¹; SUGITA, A.¹; SHIRAI, T.¹; AOYAMA, M.¹;
AKAHANE, Y.¹; INOUE, N.¹; UEDA, H.¹;
YAMAKAWA, K.¹; YOKOYAMA, A.¹; KAWASAKI,
M.³; NAKAMURA, Hiroki
(¹Japan Atomic Energy Research Inst.; ²Japan Atomic
Energy Research Inst. and Kyoto Univ.; ³Kyoto Univ.)

[*Phys. Rev. A* **72**, 063404 (2005)]

A demonstration of coherent quantum control for ultrafast precise selection of closely-lying states is reported. A phase-locked pair of femtosecond laser pulses is generated through a pulse shaper to excite the ground-state cesium atom to the $Cs(7D_{3/2})$ and $Cs(7D_{5/2})$ states by two-photon absorption. The excited state population is measured by detecting fluorescence from each spin-orbit state. By controlling the phase-difference of the pulse pair, an ultrafast precise selection is accomplished. The contrast ratio of the maximal to minimal selection ratio exceeds 10^3 with the delay less than 400 fs.

I-D-3 Ab Initio Nonadiabatic Quantum Dynamics of Cyclohexadiene/Hexatriene Ultrafast Photoisomerization

TAMURA, Hiroyuki; NANBU, Shinkoh¹; ISHIDA, Toshimasa²; NAKAMURA, Hiroki
(¹Kyushu Univ.; ²Kyoto Univ.)

[*J. Chem. Phys.* **124**, 084313 (2006)]

Reaction mechanisms of the ultrafast photoisomerization between cyclohexadiene and hexatriene have been elucidated by the quantum dynamics on the *ab initio* potential energy surfaces calculated by multi-reference configuration interaction method. In addition to the quantum wave-packet dynamics along the two-dimensional reaction coordinates, the semiclassical analyses have also been carried out to correctly estimate the nonadiabatic transition probabilities around conical intersections in the full-dimensional space. The reaction time durations of radiationless decays in the wave-packet dynamics are found to be generally consistent with the femtosecond time-resolution experimental observations. The nonadiabatic transition probabilities among the ground (S_0), first (S_1), and second (S_2) excited states have been estimated by using the semiclassical Zhu-Nakamura formula considering the full-dimensional wave-packet density distributions in the vicinity of conical intersections under the harmonic normal mode approximation. The cyclohexadiene (CHD) ring-opening process proceeds descending on the $S_1(1^1B)$ potential after the photoexcitation. The major part of the wave-packet decays from $S_1(1^1B)$ to $S_1(2^1A)$ by the first seam line crossing along the C_2 -symmetry-breaking directions. The experimentally observed ultrafast S_1 - S_0 decay can be explained by the dynamics through the S_1 - S_0 conical intersection along the direction toward the five-membered ring. The CHD: hexatriene (HT) branching ratio is estimated to be approximately 5:5, which is in accordance with the experiment in solution. This branching ratio is found to be mainly governed by the location of the five-membered ring S_1 - S_0 conical intersection along the ground state potential ridge between CHD and HT.

I-D-4 Atomic Hydrogen Transmission through Five-Membered Carbon Ring by the Mechanism of Non-Adiabatic Tunneling

NANBU, Shinkoh¹; ISHIDA, Toshimasa²; NAKAMURA, Hiroki
(¹Kyushu Univ.; ²Kyoto Univ.)

[*Chem. Phys.* **324**, 721–732 (2006)]

A novel usage of the non-adiabatic effects is proposed. In this proposal, atomic hydrogen penetrates through a five-membered carbon ring with the help of the non-adiabatic tunneling phenomenon. The cyclopentadienyl radical (C_5H_5) and pentaboron-substituted corannulene radical ($C_{15}H_{10}B_5$) are used to illustrate the mechanism. To demonstrate the proposal, first principles calculations are performed for the non-adiabatic dynamics on potential energy surfaces determined by

multi-reference configuration interaction method. The results show that the non-adiabatic transitions between the ground and excited states essentially control the hydrogen atom transmission through the five-membered ring of a pentaboron-substituted corannulene radical. It is found that the transmission occurs more than once out of four incidences when an appropriate initial wave packet is chosen. The phenomenon can be interpreted in terms of the Zhu-Nakamura semiclassical theory of non-adiabatic transitions.

I-D-5 Laser Control of Reactions of Photoswitching Functional Molecules

TAMURA, Hiroyuki; NANBU, Shinkoh¹; ISHIDA, Toshimasa²; NAKAMURA, Hiroki
(¹Kyushu Univ.; ²Kyoto Univ.)

[*J. Chem. Phys.* **125**, 034307 (2006)]

Laser control schemes of reactions of photoswitching functional molecules are proposed based on the quantum mechanical wave-packet dynamics and the design of laser parameters. The appropriately designed quadratically chirped laser pulses can achieve nearly complete transitions of wave packet among electronic states. The laser parameters can be optimized by using the Zhu-Nakamura theory of nonadiabatic transition. This method is effective not only for the initial photoexcitation process but also for the pump and dump scheme in the middle of the overall photoswitching process. The effects of momentum of the wave packet crossing a conical intersection on the branching ratio of products have also been clarified. These control schemes mentioned above are successfully applied to the cyclohexadiene/hexatriene photoisomerization (ring-opening) process which is the reaction center of practical photoswitching molecules such as diarylethenes. The overall efficiency of the ring opening can be appreciably increased by using the appropriately designed laser pulses compared to that of the natural photoisomerization without any control schemes.

I-D-6 Laser Control of Chemical Dynamics: Control of Electronic Transitions by Quadratic Chirping

ZOU, Shiyang; KONDORSKIY, Alexey¹; MIL'NIKOV, Gennady V.; NAKAMURA, Hiroki
(¹IMS and Lebedev Phys. Inst.)

[*Progress in Ultrafast Intense Laser Science*, Springer-Verlag (2006)]

An effective scheme of the laser control of wave packet dynamics applicable to the systems of many degrees of freedom is discussed. It is demonstrated that by using specially designed quadratically chirped pulses fast and nearly complete excitation of wave packet can be achieved without significant distortion of its shape. The parameters of the laser pulse can be estimated analytically from the Zhu-Nakamura (ZN) theory of nonadiabatic transition. The scheme is applicable to various processes such as simple electronic excitation,

pump-dump, and selective bond breaking, and it is actually numerically demonstrated to work well by taking diatomic and triatomic molecules as examples.

I-D-7 Laser Control of Chemical Dynamics: Control of Wave Packet Motion

**KONDORSKIY, Alexey¹; MIL'NIKOV, Gennady V.;
NAKAMURA, Hiroki**

(¹IMS and Lebedev Phys. Inst.)

[Progress in Ultrafast Intense Laser Science, Springer-Verlag (2006)]

An efficient semiclassical optimal control theory for controlling wave packet dynamics on a single adiabatic potential energy surface applicable to the systems of many degrees of freedom is discussed with all the details. The approach combines advantages of different formulations of optimal control theory: quantum and classical on one hand and global and local on the other. The efficiency and reliability of the method is demonstrated by taking the systems of two and four dimensions as examples.

I-E Theoretical Studies of Electron Dynamics

Electron dynamics in nanometer-sized molecules and nanostructured materials is an intrinsic process related to a number of interesting phenomena such as linear and nonlinear optical response, electric conduction, and also chemical reaction. Despite the importance, the electron dynamics has not been understood in detail. We have developed a computational method simulating the electron dynamics in real time and real space, and revealed the dynamics in detail.

I-E-1 Photoinduced Electric Currents in Ring-Shaped Molecules by Circularly Polarized Laser Pulses

NOBUSADA, Katsuyuki; YABANA, Kazuhiro¹
(¹Univ. Tsukuba)

[*Phys. Rev. A* submitted]

We have theoretically demonstrated that circularly polarized laser pulses induce electric currents and magnetic moments in ring-shaped molecules Na₁₀ and benzene. The photoinduced electric currents are simulated in real space and real time within a time-dependent local density approximation. It has been found that the electric currents are induced efficiently and persist continuously even after the laser pulses were switched off provided the applied laser frequency is in tune with the dipole resonance frequency for each molecular system. The electric currents are definitely revealed to be a second order nonlinear optical response. The ring currents inevitably cause the magnetic dipole moment, so that the molecules are magnetized. The circularly polarized laser pulses induce the electric currents and the magnetic moment much more effectively than by using static magnetic fields.

I-E-2 An Efficient Numerical Method for Exciton States in Quantum Boxes

KUBOTA, Yoji; NOBUSADA, Katsuyuki

[*Phys. Lett. A* submitted]

We have developed an efficient numerical method for exciton states in thin quantum boxes. In our numerical method, the exciton wave function is expanded in terms of coordinate eigenstates on each grid point. This method is found to be much more efficient and promising for calculating the exciton states than the standard configuration-interaction (CI) approach. In the CI approach, the wave function is expanded in terms of single-particle electron and hole eigenfunctions. Then, the computations of the matrix elements of the Hamiltonian (Coulomb potential) require multidimensional numerical integrals. Thus, the CI approach needs huge computational costs due to the multidimensional integrals. It is practically difficult to apply the CI approach to the studies of multi-exciton states, dynamics of excitons, and excitons in complex microstructures. To overcome the drawback, we alternatively use the discrete variable representation (DVR) as the basis set for the wave function. The DVR is a coordinate eigenfunction localized on each grid point associated with the Gaussian quadrature rule. Taking the advantage of the DVR, the matrix of the multidimensional Coulomb integrals can be reduced to the diagonal matrix with single point values. Consequently, the computational time for the matrix elements decreases sharply. The matrix of the kinetic energy is also sparse. Then, we can deal with a large number of bases by using the Lanczos diagonalization. We obtained energy, eigenfunction, and electron-hole separation of the exciton for various widths L of the quantum box. Our numerical method has high potentialities for studying properties of bi- and tri-excitons in various microstructures.

I-F Electronic Structure Theory of Quantum Dissipative Systems

I-F-1 Electronic Structure Theory of Adsorbate-Surface Systems

YASUIKE, Tomokazu; NOBUSADA, Katsuyuki

In the conventional cluster model, the model cluster, which is constructed by subtracting a subsystem from the whole adsorbate-surface system, is isolated. The isolated cluster implicitly has the artificial boundary condition that the wave function should be zero at the edge of the cluster. Such an inaccurate boundary condition leads to discrete energy spectra, although adsorbate-

surface systems must have continuous ones. In the present work, we circumvent this problem by introducing the absorbing boundary condition (ABC) into the model cluster. The ABC model cluster was found to precisely reproduce the exact density of states (DOS) of a 1D periodic potential model. The improvement of DOS leads to an appropriate description for the adsorbate-surface chemical bonding. Moreover, it was also shown that the ABC model cluster allows us to reveal the dynamical properties such as an adsorbate-surface electron transfer rate and a lifetime of adsorbate electronic states.

I-F-2 Electronic Structure Calculations at Constant Chemical Potential toward the Application to Electrochemistry

SHIRATORI, Kazuya; NOBUSADA, Katsuyuki

We have developed the method of quantum chemistry calculations based on Mermin's finite temperature density functional theory (FT-DFT) to describe the electronic structures of molecular systems interacting with an electron reservoir. On the basis of the Kohn-Sham (KS) formalism of FT-DFT, the FT-KS equation is derived in a very similar form to the equation at zero-temperature. In the FT-KS equation, the exchange-correlation potential is intrinsically a function of temperature, and the occupation numbers are associated

with the Fermi-Dirac distribution. We practically approximate the exchange-correlation potential by the hybrid B3LYP functional given at zero-temperature. Then, the FT-KS equation can be solved by exploiting the same algorithm in the standard DFT calculations except that the effects of the temperature and the chemical potential are taken into account through the fractional occupation numbers. The numerical scheme for solving the FT-KS equation mentioned above was implemented in the quantum chemistry program GAMESS and applied to the reaction, $\text{Ag}^{2+} + e^- \rightleftharpoons \text{Ag}^+$ in aqueous solution. To estimate the effects of the aqueous solvent, the polarizable continuum model (PCM) was employed. The radii R of the cavities in PCM were adjusted to reproduce the experimental data of the hydration free energies.

I-G Electronic Structures and Photochemical Properties of Nanometer-Sized Metal Clusters

Nanometer-sized metal clusters provide interesting physicochemical properties such as optical response, catalysis, and reactivity, which are significantly different from those in corresponding bare metal clusters or bulk metals. We have investigated the electronic structures and the photochemical properties of monolayer-protected metal clusters with special emphasis on describing metal-molecule interactions.

I-G-1 Theoretical Investigation of Optimized Structures of Thiolated Gold Cluster $[\text{Au}_{25}(\text{SCH}_3)_{18}]^+$

IWASA, Takeshi; NOBUSADA, Katsuyuki

[*J. Phys. Chem. C* in press]

Geometric and electronic structures of a gold-methanethiolate $[\text{Au}_{25}(\text{SCH}_3)_{18}]^+$ are investigated by using density functional theory. Three types of optimized structures are derived from two different Au_{25} core clusters protected by 18 methanethiolates. The most probable optimized structure consists of a Au_7 core cluster and Au-S complex-like ring clusters, $\text{Au}_{12}(\text{SCH}_3)_{12}$ and $\text{Au}_3(\text{SCH}_3)_3$. The Au_7 core cluster is enclosed by the $\text{Au}_{12}(\text{SCH}_3)_{12}$ ring cluster and then the $\text{Au}_7\text{-Au}_{12}(\text{SCH}_3)_{12}$ core-ring subsystem is capped with the two $\text{Au}_3(\text{SCH}_3)_3$ ring clusters from both sides of the top and the bottom. This structural feature is in contrast to a general notion of gold-thiolate clusters that a core gold cluster is superficially protected by thiolate molecules. The optimized structure provides a large HOMO-LUMO gap, and its X-ray diffraction and absorption spectra successfully reproduce the experimental results.

plexes $\text{Au}_n(\text{SCH}_3)_n$. The complexes were found to be stable structures in the form of a circular ring. The characteristic Au-S interaction plays an important role in forming such a unique ring structure. The ring structure also provides interesting photochemical properties that are rather different from those of similar-sized gold-methanethiolate clusters.

I-G-2 Gold-Thiolate Nanoring: Electronic Structure and Photochemical Properties

NOBUSADA, Katsuyuki

We have studied the electronic structure and the photochemical properties of gold-methanethiolate com-

I-H Electronic Structure of a Molecule in Solution

Chemical reaction is undoubtedly the most important issue in the theoretical chemistry, and the electronic structure is a key to solve the problem. As long as molecules in the gas phase are concerned, the theory for the electronic structure has been enjoying its great success. However, when it comes to molecules in solution, the stage of theory is still an infant. Thirteen years ago, we have proposed a method refereed to as RISM-SCF based on the integral equation theory of molecular liquids (RISM) and the *ab initio* electronic structure theory (SCF).¹⁾ The method was applied successfully to a variety of chemical processes in solution including a number of different types of chemical reactions, S_N2 , acid-base, redox, and so on.

More recently, we have revised the theory so that the theory can account for the three dimensional distribution of solvent around solute.²⁾ (3D-RISM) This revision turns out to be essential when one tries to treat the solvent distribution around the native state of protein. The new theory allows us to handle the electronic structure of protein in water with appropriate theories for quantum chemistry.

One of the most complicated chemical reactions is that taking place in protein, or the enzymatic reaction. The reaction involves not only the electronic structure change of chemical species, but also recognition of substrates by host protein. The latest progress in our group is to develop a new approach for molecular recognition in host-guest systems. The progress is reported in the section I-I. Combining the approach with the 3D-RISM/SCF type theory will enable us to treat enzymatic reactions.

References

- 1) S. Ten-no, F. Hirata and S. Kato, *Chem. Phys. Lett.* **214**, 391 (1993); *J. Chem. Phys.* **100**, 7443 (1994); H. Sato, F. Hirata and S. Kato, *J. Chem. Phys.* **105**, 1546 (1996).
- 2) H. Sato, A. Kovalenko and F. Hirata, *J. Chem. Phys.* **112**, 9463 (2000).

I-H-1 A New Method to Determine Electrostatic Potential around a Macromolecule in Solution from Molecular Wave Function

YOSHIDA, Norio; HIRATA, Fumio

[*J. Comput. Chem.* **27**, 453 (2006)]

The three dimensional reference interaction site model integral equation theory (3D-RISM) combined with the *ab initio* molecular orbital method (3D-RISM-SCF) is applied to a solvated macro molecular system. The solvation structure around a solute molecule is obtained from the 3D-RISM integral equation under the electrostatic potential of the solute molecule, calculated by the *ab initio* molecular orbital theory.

The electrostatic potential should be calculated on each grid point in the three dimensional real space. Therefore, the calculation of the electrostatic potential is the most time consuming part in this method. In this paper, we propose a new procedure to save the computational cost for calculating the electrostatic potential and the solvated fock matrix.

I-H-2 Ab Initio Theoretical Study of Temperature and Density Dependence of Molecular and Thermodynamic Properties of Water in the Entire Fluid Region: Autoionization Processes

YOSHIDA, Norio; ISHIZUKA, Ryosuke; SATO, Hirofumi¹; HIRATA, Fumio
(¹Kyoto Univ.)

[*J. Phys. Chem.* **110**, 8451 (2006)]

The temperature and density dependence of the molecular and thermodynamic properties of water is investigated theoretically by means of the *ab initio*

electronic structure theory combined with the reference interaction site model method, so called as RISM-SCF. We consider the autoionization process ($H_2O + H_2O = H_3O^+ + OH^-$) by regarding H_2O , H_3O^+ and OH^- as "solute" molecules in an aqueous solution and evaluate molecular geometries, electronic structure, solvation structure, and ionic product of water (pK_w) of these species as functions of thermodynamical conditions. In our previous paper, we calculated these properties by using essentially the same method in a wide range of density (0.6–1.4 g/cm³). However, the calculation was limited in rather higher density (> 0.6 g/cm³) due to the difficulty of convergence, which is inherent to the hyper-netted chain (HNC) closure. The problem is overcome in this study by employing the Kovalenko-Hirata (KH) closure which hybridizes the HNC and mean spherical approximation (MSA). Here, we present the results for the thermodynamic range 0.025 g/cm³ to 1.0 g/cm³ and from 300 K to 800 K including a supercritical point.

I-H-3 Conformational Equilibrium of 1,2-Dichloroethane in Water: Comparison of PCM and RISM-SCF Methods

LEE, Jin Yong¹; YOSHIDA, Norio; HIRATA, Fumio
(¹Sungkyunkwan Univ.)

[*J. Phys. Chem. B* **110**, 16018 (2006)]

The RISM-SCF and polarizable continuum model (PCM) approaches have been applied to study the conformational equilibrium of 1,2-dichloroethane (DCE) in water. Both the electron correlation effect and basis sets play an important role to the relative energies of the gauche and trans conformers in gas and solution phases. Both PCM and RISM-MP2 methods resulted in the consistent trend with the previous experimental and theoretical studies that the population of the gauche

conformer increases in going from the gas phase to the aqueous solution. However, the PCM treatment could not describe the solvent effect completely in that the sign of relative free energy of the gauche and trans forms is opposite to the most recent experimental and theoretical data, while it is in good agreement by the RISM-MP2 method. We found that the larger excess chemical potential gain (by ~ -4.1 kcal/mol) for the gauche conformer is large enough to result in the gauche

preference of DCE in water, though it has to compensate the more solute reorganization energy (~ 1.7 kcal/mol) and overcome the energy difference (~ 1.6 kcal/mol) in the gas phase. The radial distribution functions between DCE and the nearest water shows that the electrostatic repulsion between chlorine and oxygen atoms is higher in trans conformer than gauche one, while the attractive interaction between chlorine and hydrogen of water is higher in gauche conformer.

I-I Solvation Thermodynamics of Protein and Related Molecules

Concerning biomolecules such as protein, it is a final goal for the biochemistry and biophysics to explore the relation between conformations and biological functions. The first important step toward the goal would be to explain the conformational stability of biomolecules in terms of the microscopic structure of the molecules in solvent. It is an extremely difficult problem by any means due to the overwhelmingly large degrees of freedom to be handled, including protein and solvent.

In the past 11 years, we have been developing a method to attack the problem based on the statistical mechanics of liquids, especially, on the RISM theory.¹⁾ Recently, we put forward our effort to apply the three dimensional (3D) RISM theory to biomolecules, and have succeeded for the first time to obtain thermodynamic quantities of "real" protein, which is in agreement with experiments not only qualitatively but also quantitatively in case of the partial molar volume.²⁾ The 3D-RISM theory turns out to be even more powerful to explore water molecules trapped in a cavity of protein.³⁾

References

- 1) M. Kinoshita, Y. Okamoto and F. Hirata, *J. Am. Chem. Soc.* **120**, 1855 (1998).
- 2) T. Imai, A. Kovalenko and F. Hirata, *Chem. Phys. Lett.* **395**, 1 (2004).
- 3) T. Imai, R. Hiraoka, A. Kovalenko and F. Hirata, *J. Am. Chem. Soc.* **127**, 15334 (2005).

I-I-1 Locating Missing Water Molecules in Protein Cavities by the Three-Dimensional Reference Interaction Site Model (3D-RISM) Theory of Molecular Solvation

IMAI, Takashi¹; HIRAOKA, Ryusuke¹;
KOVALENKO, Andriy F.²; HIRATA, Fumio
(¹Ritsumeikan Univ.; ²NRC, Canada)

[Protein in press]

Water molecules confined in protein cavities are of great importance in understanding the protein structure and functions. However, it is a nontrivial task to locate such water molecules in protein by ordinary molecular simulation and modeling techniques as well as experimental methods. The present study proves that the three-dimensional reference interaction site model (3D-RISM) theory, a recently developed statistical-mechanical theory of molecular solvation, has an outstanding advantage in locating such water molecules. In this paper, we demonstrate that the 3D-RISM theory was able to reproduce the structure and the number of water molecules in cavities of hen egg-white lysozyme observed commonly in the X-ray structures of different resolutions and conditions. Furthermore, it is shown that the theory successfully identified a water molecule in a cavity, even the existence of which had been ambiguous from the X-

ray results. In contrast, it was confirmed that molecular dynamics simulation is helpless to find such water molecules because the results substantially depend on the initial coordinates of water molecules. Possible applications of the theory to problems in the field of molecular biology are also discussed.

I-I-2 Conformational Equilibria in Liquids Consisting of Small Chain Molecules

ISHIZUKA, Ryosuke; HIRATA, Fumio

[*Chem. Phys. Lett.* **420**, 135 (2006)]

The conformational equilibrium in neat liquids consisting of small chain molecules, *n*-butane and 1,2-dichloroethane, are studied by means of a RISM-type integral equation theory formulated by Yoshida, Munakata and Hirata. Conformational shift toward the *gauche* isomer was observed upon transferring from gas to liquid phases in the both fluids in harmony with experiments. The equilibrium constant for 1,2-dichloroethane shows very small temperature dependence. The pressure dependence of the equilibrium constant indicates that the *gauche* isomer is in favor at higher temperature. The theoretical results are consistent with the experimental observations.

I-I-3 Theoretical Study of Volume Changes Accompanying Xenon-Lysozyme Binding: Implication for Molecular Mechanism of Pressure Reversal of Anesthesia

IMAI, Takashi¹; ISOGAI, Hideto¹; SETO, Tomoyoshi²; KOVALENKO, Andriy F.³; HIRATA, Fumio
(¹Ritsumeikan Univ.; ²Shiga Univ.; ³NRC, Canada)

[*J. Phys. Chem. B* **110**, 12149 (2006)]

The change in partial molar volume (PMV) accompanying the xenon-lysozyme binding was investigated for elucidating the molecular mechanism of the pressure reversal of general anesthesia, using the three-dimensional reference interaction site model (3D-RISM) theory. An increase of the PMV from xenon binding to the substrate binding site of lysozyme was found, and the binding is suppressed by pressure, while the internal site binding did not change the PMV. From the decomposition of the PMV change, combined with the analysis of the hydration change due to the binding, we propose a molecular mechanism of the PMV increase from anesthetic-protein binding, that is the mechanism of pressure reversal of general anesthesia.

I-I-4 A Theoretical Analysis on Hydration Thermodynamics of Proteins

IMAI, Takashi¹; HARANO, Yuichi²; KINOSHITA, Masahiro²; KOVALENKO, Andriy F.³; HIRATA, Fumio
(¹Ritsumeikan Univ.; ²Kyoto Univ.; ³NRC, Canada)

[*J. Chem. Phys.* **125**, 024911 (2006)]

The hydration free energy (HFE) is calculated for several proteins using the three-dimensional reference interaction site model (3D-RISM) theory, a recently developed integral equation theory of molecular solvation, combined with the all-atom potentials. The HFE is decomposed into the energetic and entropic components under the isochoric condition. The former comprises the protein-water interaction energy and the water reorgani-

zation energy (the energy arising from the structural changes induced in water). Each component is further decomposed into the non-electrostatic and electrostatic contributions. It is found that the HFE is governed by the non-electrostatic hydration entropy and the electrostatic hydration energy. The non-electrostatic hydration entropy is almost exclusively ascribed to the translational entropy loss of water upon the protein insertion. It asymptotically becomes proportional to the excluded volume (EV) for water molecules with increasing the protein size. The hydration energy is determined by the protein-water interaction energy which is half compensated by the water reorganization energy. These energy terms are approximately proportional to the water-accessible surface area (ASA). The energetic and entropic contributions are balanced with each other, and the HFE has no apparent linear relation with the EV and ASA.

I-I-5 Selective Ion-Binding by Protein Probed with the 3D-RISM Theory

YOSHIDA, Norio; PHONGPHANPHANEE, Saree; MARUYAMA, Yutaka; IMAI, Takashi¹; HIRATA, Fumio
(¹Ritsumeikan Univ.)

[*J. Am. Chem. Soc.* in press]

Selective ion-binding by human lysozyme and its mutants is probed with the three-dimensional interaction site model theory, which is the statistical mechanical integral equation theory. The three-dimensional distribution of ions as well as water molecules was calculated for aqueous solutions of three different electrolytes CaCl₂, NaCl and KCl, and for four different mutants of the human lysozyme: wild type, Q86D, A92D, Q86D/A92D that have been studied experimentally. For the wild type of the protein in the aqueous solutions of all the electrolytes studied, there are no distributions observed for the ions inside the active site. The A92D and Q86D/A92D mutants show a large peak of Na⁺ in the recognition site. Especially, holo-Q86D/A92D, one of the mutants, shows conspicuous peak of Ca²⁺. These behaviors are in accord with the experimental results.

I-J Collective Density Fluctuations in Polar Liquids and Their Response to Ion Dynamics

As to the model for molecular diffusion in polar liquids, there are two quite different points of view. One is the conventional rot-translation model, and the other the interaction-site description which sees the diffusion of a molecule as a correlated motion of each atom (site).¹⁾ It is clearly advantageous to use the interaction-site description compared to the rot-translation model to account for chemical characteristics of solvent as well as solute dynamics. However, the interaction-site description has its own disadvantage in interpreting physical meaning of the results, since it does not give an explicit picture for the rotational relaxation of molecules, which can be directly probed by many experimental means including the dielectric and NMR relaxation. We have solved the problem by extracting collective modes of the density fluctuation from the site-site density correlation functions. In our recent study for dynamics of molecular liquids based on the interaction-site model, we have succeeded to abstract the collective excitations in liquids, which can be identified as optical and acoustic modes, by diagonalizing the collective

frequency matrix appearing in the generalized Langevin equation. The two modes arise essentially from the rotational and translational motions of molecules.²⁾ We applied the method to the ion dynamics in a dipolar liquid, and could have explained successfully the peculiar size dependence of friction of alkali and halide ions in terms of response of the collective excitations in solvent to the solute displacement.³⁾

In the past year, we have elaborated the memory kernel in our generalized Langevin equation base on the mode coupling theory. We have also extended our treatment to dynamics of water and hydrated ions. Those studies as well as other related topics are reviewed below.

References

- 1) F. Hirata, *J. Chem. Phys.* **96**, 4619 (1992).
- 2) S. Chong and F. Hirata, *Phys. Rev. E* **57**, 1691 (1998).
- 3) S. Chong and F. Hirata, *J. Chem. Phys.* **108**, 7339 (1998).

I-J-1 Study of Anomalous Mobility of Polar Molecular Solutions by Means of the Site-Site Memory Equation Formalism

KOBRYN, Alexander; YAMAGUCHI, T.¹; HIRATA, Fumio

(¹Fukuoka Univ.)

[*J. Mol. Liq.* **125**, 14 (2006)]

In this work, the memory equation approach is applied for theoretical study of dynamics of polar molecular liquids described by the interaction site model. The study includes the temperature-density (pressure) dependence of the translational diffusion coefficients D and orientational relaxation times τ for infinitely dilute solutions of acetonitrile and methanol in water, and methanol in acetonitrile. Calculations are performed over the range of temperatures and densities employing

the SPC/E model for water and optimized site-site potentials for acetonitrile and methanol. Despite an approximate character of the model potentials and closure relation used, the theory is able to reproduce qualitatively all main features of temperature and density dependences of D and τ observed in computer and real experiments. In particular, anomalous behavior, *i.e.*, the increase in mobility with density (pressure), is obtained for D and τ of methanol in water, while acetonitrile in water or methanol in acetonitrile do not show deviations from the usual. The observed enhancement in the molecular mobility is interpreted in accordance with the concept by Yamaguchi *et al.* [*J. Chem. Phys.* **119**, 1021 (2003)], *i.e.*, in terms of two competing origins of friction, which interplay with each other as density increases: the collisional and dielectric frictions that have tendency, respectively, to strengthen and weaken with increasing density.

I-K Statistical Mechanics of Interfacial Fluids

Microscopic structure of fluid interfaces has been drawing a lot of attention due to recent development in the experimental techniques devised particularly to probe the interface. However, there are many open questions remained unanswered. For example, how wide is the interfacial region, how does it depend on the chemical species consisting the solution? Is the interface more or less homogeneous in terms of density or concentration of the two fluids, or is it spatially inhomogeneous? If it is inhomogeneous, what is the spatial extent of the inhomogeneity? Answering those questions is the most difficult and challenging tasks for theoretical physics and chemistry, and not much progress has been made in the past, especially from a molecular view point. We have been developing statistical mechanics for two different types of interfacial fluids: fluid-fluid interface and fluids in porous media. Following are the latest achievement in that direction.

I-K-1 Criticality of a Liquid-Vapor Interface from an Inhomogeneous Integral Equation Theory

OMELYAN, Igor¹; HIRATA, Fumio; KOVALENKO, Andriy F.²

(¹ICMP, Ukraine; ²NRC, Canada)

[*Phys. Chem. Chem. Phys.* **7**, 4132 (2005)]

A microscopic theory is developed to study the liquid-vapor interfacial properties of simple fluids with *ab initio* treatment of the inhomogeneous two-body

correlation functions, without any interpolation. It consists of the inhomogeneous Ornstein-Zernike equation coupled with the Duh-Henderson-Verlet closure and the Lovett-Mou-Buff-Wertheim equation. For the liquid-vapor interface of the Lennard-Jones fluid, we obtained the density profile and the surface tension, as well as their critical behaviour. In particular, we identified non-classical critical exponents. The theory accurately predicts the phase diagram and the interfacial properties in a very good agreement with simulations. We also showed that the method leads to true capillary-wave asymptotics in the macroscopic limit.

I-L Photoinduced Phase Transitions in Molecular Materials

Photoirradiation may create electrons, holes or excitons, which are often accompanied by local structural deformation. Sometimes it causes spatially large structural transformations with the help of cooperativity possessed by interacting electrons and molecules. Thus, a nonequilibrium phase can be generated, which may not be reached by simply changing temperature or pressure because the energy of a photon is much higher than thermal energies. Such photoinduced phase transitions have been studied extensively, both experimentally and theoretically. Thanks to the great progress in laser spectroscopy techniques, charge and lattice dynamics are being clarified in many molecular materials on different time scales including ultrafast and/or coherent dynamics. Now we need to treat relevant itinerant-electron models, whose transfer integrals give transition amplitudes. This is in contrast to stochastic dynamics in classical statistical models, where transition probabilities are determined by the Boltzmann factors at finite temperatures.

I-L-1 Interchain Coupling Effects on Photoinduced Phase Transitions between Neutral and Ionic Phases in an Extended Hubbard Model with Alternating Potentials and an Electron-Lattice Coupling

[*Synth. Met.* **154**, 257–260 (2005)]

YONEMITSU, Kenji

[*Phys. Rev. B* **73**, 155120 (7 pages) (2006)]

Dynamics of ionic-to-neutral and neutral-to-ionic phase transitions induced by intrachain charge-transfer photoexcitations are studied in a quasi-one-dimensional extended Hubbard model with alternating potentials and an electron-lattice coupling for mixed-stack charge-transfer complexes. For interchain couplings, we use electron-electron interactions previously estimated for TTF-CA. Photoexcitation is introduced by a pulse of oscillating electric field. The TDHF approximation is used for the electronic part, and the classical approximation for the lattice part. In the ionic-to-neutral transition, the transferred charge density is a strongly nonlinear function of the photoexcitation density, which is characterized by the presence of a threshold. With substantial interchain couplings comparable to those in TTF-CA, the interchain correlation is strong during the transition. Neutral domains in nearby chains simultaneously grow even if their nucleation is delayed by reducing the amplitude of the electric field. With weaker interchain couplings, the growing processes are in phase only when the amplitude of the electric field is large. Thus, the experimentally observed, coherent motion of a macroscopic neutral-ionic domain boundary is allowed to emerge by such substantial interchain couplings. In the neutral-to-ionic transition, by contrast, the transferred charge density is almost a linear function of the photoexcitation density. Interchain electron-electron interactions make the function slightly nonlinear, but the uncooperative situation is unchanged and consistent with the experimental findings.

I-L-2 Inter-Chain Coulomb-Lattice Relaxation and Multicriticality in Charge Transfer Organic Complexes

KISHINE, Jun-ichiro¹; OHARA, Tomoaki¹; LUTY, Tadeusz²; YONEMITSU, Kenji

(¹*Khushu Inst. Tech.*; ²*Tech. Univ. Wroclaw*)

We discuss the neutral-to-ionic phase transition and the emergence of multi-criticality in the quasi-one-dimensional charge-transfer salt TTF-CA under pressure. We stress that subtle interplay of Coulomb and lattice processes may be quite sensitive to pressure. Emergence or disappearance of the multi-critical point in a series of charge-transfer salts is understood through this interplay. What's behind is coexistence and coupling of non-symmetry-breaking and symmetry-breaking order parameters.

I-L-3 Quantum Paraelectricity near the Neutral-Ionic Critical Point

YAMASHITA, Yasufumi; YONEMITSU, Kenji

In a series of organic charge-transfer complexes DM-TTF-QBr_nCl_{4-n}, the neutral-ionic (NI) phase transition is observed in the chlorine rich complexes for $n < 2.1$. The neutral ground state of DM-TTF-QBr₄ is destabilized by applying hydrostatic pressure P , and the NI transition emerges when P exceeds P_c where $T_c = 0$; so-called the quantum critical point (QCP). In the vicinity of the QCP, the dielectric permittivity in the neutral phase follows the Barrett formula characteristic of quantum paraelectricity, which probably originates from charge-transfer fluctuations. In the present study, we have phenomenologically dealt with the NI phase transition by a quantum version of the Blume-Emery-Griffiths (QBEG) model. Applying the mean-field approximation to the QBEG model, the magnitude of ferroelectricity and ionicity as well as the dielectric permittivity are calculated with changing P . The paraelectric ground state with a finite ionicity is realized with the Barrett-type permittivity, which is consistent with the experimental results. In addition, the calculated permittivity agrees well with that of DM-TTF-QBr₄ under various pressures including the ionic phase. What we found is that the quantum dipole-flipping term is indispensable to reproduce the experimental results within our model. Therefore, it is highly suggested that charge transfer fluctuations due to the quantum tunneling allow a finite ionicity even in the neutral phase, which realizes the quantum paraelectric ground state near the quantum critical point.

I-L-4 Dynamics of Photoexcited States in One-Dimensional Dimerized Mott Insulators

MAESHIMA, Nobuya¹; YONEMITSU, Kenji
(¹IMS and Tohoku Univ.)

[*Phys. Rev. B* **74**, 155105 (11 pages) (2006)]

Dynamical properties of photoexcited states are theoretically studied in a one-dimensional Mott insulator dimerized by the spin-Peierls instability. Numerical calculations combined with a perturbative analysis have revealed that the lowest photoexcited state without nearest-neighbor interaction corresponds to an interdimer charge transfer excitation that belongs to dispersive excitations. This excited state destabilizes the dimerized phase, leading to a photoinduced inverse spin-Peierls transition. We discuss the purely electronic origin of midgap states that are observed in a latest photoexcitation experiment of an organic spin-Peierls compound, K-TCNQ.

I-L-5 Charge Ordering in θ -(BEDT-TTF)₂RbZn(SCN)₄: Cooperative Effects of Electron Correlations and Lattice Distortions

MIYASHITA, Satoshi¹; YONEMITSU, Kenji
(¹IMS and Tohoku Univ.)

We investigate combined effects of electron correlations and lattice distortions on the charge ordering (CO)

in θ -(BEDT-TTF)₂RbZn(SCN)₄ theoretically by the two-dimensional extended Hubbard model at 1/4-filling. It is well known that this material undergoes a phase transition from the high-symmetry to the low-symmetry structure by lowering temperature. The ground state is an insulator with the horizontal-stripe CO along t_{p4} (HCO- t_{p4}). The importance of long-range electron-electron interactions is well recognized and the mechanism for stabilizing the HCO- t_{p4} has been argued mainly on the basis of the low-symmetry structure. Because the lattice distortions are coupled with the electron system, giving rise to the first-order transition sensitive to the crystal structure, electron-phonon interactions are also important. Then, by means of the exact diagonalization, we have calculated the ground-state energy and local density of holes by adopting both electron-electron and electron-phonon couplings on the basis of the high-symmetry structure. For electron-phonon couplings, we consider three kinds of distortions: displacements along the c -direction (s_c), those along the a -direction (s_{p1}) and molecular rotations (s_{p4}), leading to linear modulations in the respective transfer integrals. The s_c -dependence of the local density of holes demonstrates that the coupling s_c induces the HCO- t_{p4} . The coupling s_{p4} also induces this CO, though s_{p1} does not. In this salt, the effects of displacements along the c -direction and molecular rotations are stronger than those along the a -direction. Thus, electron-phonon interactions are crucial to stabilize both the HCO- t_{p4} and the low-symmetry structure in θ -(BEDT-TTF)₂RbZn(SCN)₄.

I-M Collective Transport through Metal-Insulator Interfaces

Molecular materials are used in many device structures. Charge transport is always through an interface between two materials with different electronic states and work functions. In field-effect transistors fabricated on an insulating material with coherent charge transport under electric fields, the insulator-(source/drain) electrode interface barrier potentials, known as Schottky barriers, play an important role. For band insulators, the Schottky barriers indeed govern the current-voltage characteristics. Quite recently, ambipolar characteristics are found in field-effect transistor device structures based on organic single crystals of a quasi-one-dimensional Mott insulator. Thus, we need to take correlation effects into account in dealing with charge transport through electrostatic potentials that originate from the long-range Coulomb interaction.

I-M-1 Mechanism of Ambipolar Field-Effect Transistors on One-Dimensional Organic Mott Insulators

YONEMITSU, Kenji

[*Proc. Pacificchem* (2005) in press]

The characteristics of a field-effect transistor (FET) fabricated on a crystal of an organic charge-transfer complex depend on the electronic state of the crystal. Ambipolar characteristics are observed for Mott insulators, while unipolar ones for band insulators. We study them in one-dimensional models of electrons. The Hubbard model for a Mott insulator is attached to the tight-binding model for metallic electrodes. We solve

the Poisson equation and add its solution for the electrostatic potential to these models in order to reproduce Schottky barriers at the interfaces. We use both the mean-field approximation and the Lanczos exact-diagonalization method in solving the time-dependent Schrödinger equation to obtain essentially the same result. Mott insulators show the ambipolar FET characteristics irrespective of the difference between the work function of the channel and that of the metallic electrodes. In order to exclude the ambiguity introduced in the one-dimensional modeling of the effect of the gate electrode and to allow the direct observation of the correlation between the electronic state in the channel and that at the interfaces, we have removed the gate electrode and employ different metals for the electrodes among which only one interface possesses a large work-

function difference. In this case, the current-voltage characteristics are almost anti-symmetric for Mott insulators and very asymmetric for band insulators. These results are also consistent with recent experiments by T. Hasegawa and coworkers. The characteristics for Mott insulators are again caused by the correlation between the electronic state in the channel and that at the interface.

I-N Polyamorphism in Molecular Liquids

So far the only quantity known as the order parameter that distinguishes liquids from gases is density. However, a recent experimental confirmation of the very existence of the pressure-induced “structural” transition between stable liquids of black phosphorus lends strong impetus to reconsideration on the concepts of liquids. Recently, we have succeeded, through *in situ* synchrotron x-ray diffraction measurements under high pressures and temperatures, in unveiling the presence of a liquid-to-liquid structural phase transition in a molecular liquid SnI₄. This discovery offers the first evidence of the thermodynamically stable transition found in general compounds other than elements. The purpose of the present project is on the basis of theoretical, computational as well as experimental investigations to construct the statistical-mechanical model for the transition from which local order parameters characterizing the polyamorphism can be extracted.

I-N-1 Murnaghan’s Equation of Motion Revisited

FUCHIZAKI, Kazuhiro
(IMS and Ehime Univ.)

[*J. Phys. Soc. Jpn.* **75**, 034601 (4 pages) (2006)]

The expression known as Murnaghan’s equation of state in high-pressure research community is mathematically a correct solution to the equation of bulk modulus but is valid only within a very limited parameter space. Moreover, the equation of state in question exhibits a peculiar behavior at high pressures when fitted to compression data. An alternative expression with a much wider range of validity is given. No peculiarity appears in the resultant compression curve. The latter expression thus provides a new tool as an infinitesimal-strain equation of state for quick estimate of compression characteristics of substances.

I-N-2 Polyamorphism in Tin Tetraiodide

FUCHIZAKI, Kazuhiro¹; **HASE, Takaki**²;
YAMADA, Akihiro²; **HAMAYA, Nozomu**³;
KATAYAMA, Yoshinori⁴; **FUNAKOSHI, Ken-ichi**⁵
(¹IMS and Ehime Univ.; ²Ehime Univ.; ³Ochanomizu Univ.; ⁴JAEA; ⁵JASRI)

[*Science* submitted]

The experimental evidence for a thermodynamically stable liquid-to-liquid transition to occur has been given thus far only for liquid phosphorus. This transition is regarded as an allotropic transition in noncrystalline states. Then, one might ask whether there can be a general polymorphic transition in noncrystalline states. Such polyamorphism in equilibrium states has been searched for a long time. Here, we present firm evidence that there exist two types of phases in a molecular liquid SnI₄ below and above about 1.5 GPa, where the melting curve of the crystalline phase has an apparent break. Structure factors of the liquids were obtained through *in situ* synchrotron x-ray diffraction measurements performed under pressures from 1 atm up to 3.4 GPa. At lower pressures below 1.5 GPa higher-wavenumber components of the structure factor can be well explained by an ideal gas structure consisting of molecules with regular tetrahedral symmetry. The presence of molecules is also confirmed by the fact that the positions of the two

principal peaks in the reduced radial distribution functions inverted from the structure factors, which corresponds to two kinds of intramolecular separation, are almost independent of pressures applied as far as the pressure is below 1.5 GPa. However, with increasing pressure beyond 1.5 GPa, the two peaks are going to merge, the situation having been found in high-pressure amorphous structure in which molecular dissociation proceeds. We conclude from these observations that the lower-pressure liquid is a molecular liquid, whereas polymerization takes place on the higher-pressure side.

I-N-3 New Method for Inversion from Structure Factors to Radial Distributions

FUCHIZAKI, Kazuhiro
(IMS and Ehime Univ.)

[*J. Chem. Phys.* submitted]

Although one of the advantages of using synchrotron radiation is its wide energy range available to scattering experiments, the situation is a bit different in the energy-dispersive type of measurements employed upon high-pressure experiments utilizing a multi-anvil type apparatus. The effective energy range is restricted by scattering angles; it is limited down to several degrees to avoid strong forward scattering on the one hand while an upper bound is limited up to ~16 degrees to obtain scattered intensities with reasonable S/N ratio on the other. The actual wavenumber window, Λ , is thus limited both in low and high k directions. If the structure factors with a finite window Λ is naively Fourier transformed to obtain radial distribution functions, G , they will suffer from spurious peaks originated from this finite truncation. Applying some window functions to reduce the truncation effects is not recommended because it severely modifies the peak height of G . Hence, a new method has been devised in which no Fourier inversion is invoked. The method relies on the maximum entropy principle to yield G according to the relation involving an observed structure factor and a Lagrange’s multiplier, λ , as input. G determined based on the relation agrees well with that obtained through the reverse Monte Carlo calculations of the structure factor, and found to be robust against a choice of the value for λ .

I-N-4 Changes in Orientational Correlations in a Molecular Liquid on Compression

FUCHIZAKI, Kazuhiro¹; NEZBEDA, Ivo²;
KALYUZHNYI, Y. V.³

(¹IIMS and Ehime Univ.; ²Czech Acad. Sci.; ³Natl. Acad. Sci. Ukraine)

[*J. Chem. Phys.* submitted]

Evolution in local molecular configuration in a molecular liquid, especially in orientational correlations, with increasing pressure is of primary interest. This aspect was investigated conducting molecular dynamics simulations for a molecular liquid SnI₄. The method of the simulations is basically the same as that employed previously¹⁾ except that the shape of the MD cell was fixed to be cubic with only its size allowed to vary.

The structure factor, S , obtained at ambient pressure attains remarkable agreement with the experimental result. Moreover, its components with wavenumbers beyond $\sim 2.7 \text{ \AA}^{-1}$ are hardly affected by thermodynamic conditions applied as well as the precise nature of the intermolecular interactions. The region beyond $k \sim 2.7 \text{ \AA}^{-1}$ corresponds to the lengths within the intramolecular distance. In fact, the behavior of S over this length scale is quantitatively explained by the ideal gas model consisting of freely rotating tetrahedral molecules. However, the behavior in the low- k region is strongly affected by the intermolecular correlations. The primary peak shifts in higher- k direction upon compression, reflecting the shrinkage of the system as a whole, whereas the height of the peak increases, implying that the spatial correlation develops due to, mainly, hard-core repulsion between the molecules. The first small peak located at $\sim 1 \text{ \AA}^{-1}$, which diminishes in height, is from the spatial correlation between the central tins; in the structure factors obtained through RISM calculations with no interactions between tin atoms, the corresponding peak never appears. A unique orientational order parameter that can capture the intermolecular orientational correlation is discussed. We found on the basis of the behavior of the order parameter that population of nearest neighbor molecular pairs which are in vertex-to-face configuration increases on compression.

References

- 1) K. Fuchizaki and K. Nagai, *Solid State Commun.* **132**, 305–308 (2004).

I-O Molecular Dynamics Simulations of Proteins

Molecular functions of proteins are investigated by molecular dynamics (MD) simulations. Using parallel computing, the present-day computer resources allow us to simulate a dynamical process of a protein system consisting of $\sim 10^6$ atoms over $\sim 10^2$ ns. The studies go one step further to develop the method of deriving biologically significant information from the MD trajectories. Here, we report a result of such simulation study. Each specific protein function requires its specific way of description. The following example is a problem of the stationary transport process of water through narrow channels formed by proteins and lipid molecules. The results of the analysis stress the importance of the single-file characteristics for the efficient transport.

I-O-1 Determinants of Water Permeability in Aquaporin Family: A Comparative Simulation Study

HASHIDO, Masanori¹; IKEGUCHI, Mitsunori¹; KIDERA, Akinori²
(¹Yokohama City Univ.; ²IMS and Yokohama City Univ.)

Water permeation through the water channel, aquaporin (AQP), was studied by comparative molecular dynamics (MD) simulations of five members of the AQP family, AQP1, AQP4, AQPZ, GlpF, and AQP0, in the explicit membrane environment. Water permeability of the AQPs was determined from the MD trajectories in the form of the single-channel osmotic permeability p_f using the linear response formula. Comparing the p_f values of the five homologous proteins, we found several structural determinants of water permeability. First, the

wider channel containing more water simply appeared to transport more water. Second, water permeability through the AQP channel is related to the frequency of the jumping motion determined by the free-energy barrier height for water to jump between two adjacent preferential hydrogen bonding sites. The third factor is the correlation in the motions of the channel waters. In the analysis of the newly developed p_f matrix, we found that the water motion in AQPs was a perturbed single-file permeation, in which the two NPA motifs appear to interrupt the correlation in water motions, referring to the ideal single-file permeation in a carbon nanotube. This means that a smaller perturbation in the NPA region results in larger permeation. The importance of the single-file nature of water permeation was confirmed in MD simulations of three mutants of AQPZ mimicking AQP1.

I-P Bioinformatics Studies of Proteins

Database work on biological information, bioinformatics, is another important part of the theoretical studies of proteins. Molecular simulation focuses on each specific protein function. On the other hand, the database study treats the ensemble of proteins in the database. Here, we report two different types of bioinformatics study developing a new method. The first is about a method describing protein dynamics using the protein structure database and the elastic network model. This treats a problem of classical mechanics, or the separation of the internal and external degrees of freedom. The second is a method comparing two proteins using an analogy between dynamic programming and Ising model. Using the partition function of Ising model, we can further improve the conventional dynamic programming to detect remote homology in amino acid sequences.

I-P-1 Normal Mode Analysis Fixing the External Degrees of Freedom for Any Portion of a System

FUCHIGAMI, Sotaro¹; OMORI, Satoshi¹; IKEGUCHI, Mitsunori¹; KIDERA, Akinori²
(¹Yokohama City Univ.; ²IMS and Yokohama City Univ.)

Normal mode analysis, including the coarse-grained version of elastic network model, is most widely used to illustrate protein fluctuations. In the system with no external field, the external degrees of freedom are defined as the six normal modes with zero frequency. This definition is equivalent to those of the Eckart condition, or the Eckart frame. However, it has been recognized that the Eckart condition is not the best way to represent protein motions, but a relative motion to a

certain fixed part of the protein gives a more transparent representation. We call it the fixed-domain frame. Here, we derived the formula converting the Hessian matrix, or the covariance matrix, defined in the Eckart frame into the one in the fixed-domain frame. This formula was derived by imposing fictitious external forces to the molecule so as to eliminate the external motions of the domain without affecting the internal degrees of freedom. The validity of the formula was confirmed by a comparison with the superposition of many snapshots obtained from a molecular dynamics simulation.

I-P-2 Probabilistic Alignment Detects Remote Homology in a Pair of Protein Sequences without Homologous Sequence Information

KOIKE, Ryotaro¹; KINOSHITA, Kengo²; KIDERA,

Akinori³

(¹Tokyo Tech; ²Univ. Tokyo; ³IMS and Yokohama City Univ.)

Dynamic programming (DP) and its heuristic algorithms are the most fundamental methods for similarity searches of amino acid sequences. Their detection power has been improved by including supplemental information, such as homologous sequences in the profile method. Here, we describe a method, probabilistic alignment (PA) that gives improved detection power, but similarly to the original DP, uses only a pair of amino acid sequences. Receiver operating characteristic (ROC) analysis demonstrated that the PA method is far superior to BLAST, and that its sensitivity and selectivity approach to those of PSI-BLAST. Particularly for orphan proteins having few homologues in the database, PA exhibits much better performance than PSI-BLAST. Based on this observation, we applied the PA method to a homology search of two orphan proteins, Latexin and Resuscitation-promoting factor domain. Their molecular functions have been described based on structural similarities, but sequence homologues have not been identified by PSI-BLAST. PA successfully detected sequence homologues for the two proteins and confirmed that the observed structural similarities are the result of an evolutionary relationship.

I-Q Theoretical Studies on Dynamical Foundation of Chemical Reactions and Proteins

Recent experimental developments in single molecule spectroscopy have shed light on the distinct nonergodic features and the heterogeneity of the state space and non-Markovian process of biomolecules. This project focuses on the dynamical foundation of chemical reactions, *i.e.*, why and how the reacting systems climb through the saddle, and on the developments of new time series analyses to extract the dynamical information regarding the underlying state space structure from single molecule time series.

I-Q-1 Dynamical Hierarchy in Transition States of Reactions

LI, Chun Bui^{1,2}; **SHOUJIGUCHI, Akira**³; **TODA, Mikito**³; **KOMATSUZAKI, Tamiki**⁴
(¹Kobe Univ.; ²JST/CREST; ³Nara Women's Univ.; ⁴IMS, Kobe Univ. and JST/CREST)

[*Few-Body Systems* **38**,173–179 (2006)]

Recent theoretical developments^{1–4}) in chemical reactions have greatly improved our understanding of the definability of the no-return dividing hypersurface and the reaction path along which all reacting species follow. We present a partial normalization procedure of Lie canonical perturbation theory to elucidate the phase space geometry of the transition state in the multi-dimensional phase space for a wide range of energy above the threshold. State selectivity and dynamical correlation along the evolution of reactions are also discussed.

References

- 1) T. Komatsuzaki and R. S. Berry, *Proc. Natl. Acad. Sci. U.S.A.* **98**, 7666 (2001).
- 2) T. Komatsuzaki and R. S. Berry, *J. Chem. Phys.* **130**, 4105 (2001).
- 3) T. Komatsuzaki and R. S. Berry, *Adv. Chem. Phys.* **123**, 79 (2002).
- 4) M. Toda, T. Komatsuzaki, T. Konishi, R. S. Berry and S. A. Rice, Eds., "Geometrical Structures of Phase Space in Multidimensional Chaos: Applications to Chemical Reaction Dynamics in Complex Systems," *Adv. Chem. Phys.* **130A**, **130B** (2005).

I-Q-2 Definability of No-Return Transition States in High Energy Regime above Reaction Threshold

LI, Chun Bui^{1,2}; **SHOUJIGUCHI, Akira**³; **TODA, Mikito**³; **KOMATSUZAKI, Tamiki**⁴
(¹Kobe Univ.; ²JST/CREST; ³Nara Women's Univ.; ⁴IMS, Kobe Univ. and JST/CREST)

[*Phys. Rev. Lett.* **97**, 028302 (4 pages) (2006)]

No-return transition states (TSs) defined in multi-dimensional phase space, where *recrossing* trajectories through the commonly used "configuration" TS pass only *once*, robustly exist up to moderately high energy regime above the reaction threshold even when nonlinear resonances among the bath degrees of freedom perpen-

dicular to the reaction coordinate result in local chaos. However, at much higher energy when global chaos appears in the bath space, the separability of the reaction coordinate from the bath degrees of freedom ceases to hold locally. In the phase space near the saddles, it is found that the slower the system passes the TS, the more recrossing trajectories reappear. Their implications and mechanisms are discussed concerning to what extent one can define no-return TSs in high energy regime above the reaction threshold.

I-Q-3 Wavelet Analysis and Arnold Web Picture for Detecting Energy Transfer in a Hamiltonian Dynamical System

SHOUJIGUCHI, Akira¹; **BABA, Akinori**²; **LI, Chun Bui**²; **KOMATSUZAKI, Tamiki**³; **TODA, Mikito**¹
(¹Nara Women's Univ.; ²Kobe Univ.; ³IMS and Kobe Univ.)

[*Laser Phys.* **16**, 1097–1106 (2006)]

Our motivation is to understand how, in chemical reactions, the reaction coordinate effectively gains dynamical energy from the other degrees of freedom (*i.e.*, bath coordinates) avoiding thermalization of the redistributed energy. In such a system, the phase space structure should be not homogeneous; *i.e.*, the system is never ergodic. In this study, we introduce a way to capture the inhomogeneity of the phase space and to monitor energy transfers among their partial degrees of freedom in nonergodic systems using wavelet analysis and a picture of the Arnold web. First, we examine several simple energy transfer processes, *i.e.*, a motion on a resonance line, between resonance lines, and around a resonance junction in a simple three-degree-of-freedom (DOF) system and show how the elemental processes of the intramolecular vibrational energy redistribution (IVR) are detected by our tools. We especially note that the structure of the higher order resonance of the system can be detected by wavelet analysis and motion in the action space. Next, we analyze a reaction process in a simple Hamiltonian system of 3 DOF with a double-well potential, *i.e.*, a system with a transition state of the center-saddle-center type, and detect energy transfers in the reactive process. The aim of the study is to propose a way to characterize the inhomogeneity of the phase space, *e.g.*, the reactive doorway, which leads to controllability of the chemical reaction by light, *i.e.*, control of the reaction by selectively preparing an initial state in the reactive doorway by optical excitation.

I-Q-4 Foundation and Limitations of Statistical Reaction Theory

SHOUJIGUCHI, Akira¹; LI, Chun Bui²;
KOMATSUZAKI, Tamiki³; TODA, Mikito¹

(¹Nara Women's Univ.; ²Kobe Univ.; ³IMS and Kobe Univ.)

[Commun. Nonlinear Sci. Numerical Simulation in press]

We study the foundation and limitations of the statistical reaction theory. In particular, we focus our attention to the question of whether the rate *constant* can be defined for nonergodic systems. Based on the analysis of the Arnold web in the reactant well, we show that the survival probability exhibits two types of behavior: one where it depends on the residential time as the power-law decay and the other where it decays exponentially. The power-law decay casts a doubt on definability of the rate *constant* for nonergodic systems. We indicate that existence of the two types of behavior comes from subdiffusive motions in remote regions from the primary resonances. Moreover, based on the analysis of non-stationary features of the trajectories, we can understand how Normally Hyperbolic Invariant Manifolds (NHIM) is connected with the Arnold web. We propose that the following two features play a key role in understanding the reactions where ergodicity is broken, i.e., whether the Arnold web is nonuniform and how the NHIM is connected with the Arnold web.

I-Q-5 Bifurcation of Transition States in Many-Degrees of Freedom Chemical Reactions: Non-Collinear H₂+H Exchange Reaction

LI, Chun Bui^{1,2}; TODA, Mikito³; KOMATSUZAKI, Tamiki⁴

(¹Kobe Univ.; ²JST/CREST; ³Nara Women's Univ.; ⁴IMS, Kobe Univ. and JST/CREST)

A new method is presented to scrutinize the bifurcation of no-return transition states (TSs) at potential saddles for many degrees of freedom (dof) systems. The bifurcation can give rise to a short-lived intermediate state at the saddle resulting in the overestimation of the reaction rate from the TS. As an illustrative example of the method, the H₂+H exchange reaction is investigated. It is shown that the new action variable of bath dof defined in the multidimensional phase space also serves as a bifurcation control parameter for the no-return TS besides the total energy. This enables us to determine analytically when and how the no-return TS is ruined through the bifurcation. The definability of no-return TSs after the occurrence of bifurcation above the reaction threshold is also discussed.

I-Q-6 Fractional Behavior in Nonergodic Reaction Processes of Isomerization

SHOUJIGUCHI, Akira¹; LI, Chun Bui²;
KOMATSUZAKI, Tamiki³; TODA, Mikito¹

(¹Nara Women's Univ.; ²Kobe Univ.; ³IMS and Kobe Univ.)

We present numerical manifestation of fractional behavior in reaction processes for a prototype model of three-degree-of-freedom (3DOF) isomerization. Survival probability in the well exhibits two distinct ranges of time scale: One when it decreases in time with power-law and the other when it does exponentially. Trajectories with power-law decay exhibit $1/f$ spectra and subdiffusion in action space, and those with exponential decay do Lorentzian spectra and normal diffusion. The existence of these two types of behavior is explained based on nonergodicity on the network of nonlinear resonances (Arnold web) in the well, and connection between the saddle and the Arnold web. Implications of the fractional dynamics are discussed in terms of Maxwell's demon in molecules.

I-Q-7 Mechanism of Fast Energy Exchange between Two NO Vibrations in a Short Lifetime Path of O(1D)+N₂O→NO+NO: Analyses by the Normal Form Theory

KAWAI, Shinnosuke¹; FUJIMURA, Yo¹;
KAJIMOTO, Okitsugu¹; YAMASHITA, Takefumi²;
LI, Chun Bui³; KOMATSUZAKI, Tamiki⁴; TODA, Mikito⁵

(¹Kyoto Univ.; ²Univ. Tokyo; ³Kobe Univ.; ⁴IMS and Kobe Univ.; ⁵Nara Women's Univ.)

Normal form theory is applied to analyze classical dynamics of a short lifetime path in the reaction O(¹D) + N₂O → NO + NO, which was found to exhibit efficient energy exchange between the vibrational modes in spite of the short lifetime of the reaction intermediate as shown in our previous paper [S. Kawai *et al.*, *J. Chem. Phys.* **124**, 184315 (2006)]. The normal form procedure simplifies the analysis of the dynamics near the saddle point by significantly reducing the number of coupling terms in the Hamiltonian. By assessing the contribution of the remaining coupling terms, we reduce the system to a subsystem of two degrees of freedom, which describes the basic mechanism of the energy transfer near the saddle. The motion of the subsystem preserves the "normal mode picture" in spite of its high energy. Then the vibrational energy, which is initially localized in the new NO bond, is transferred to the old NO bond through the beat between the symmetric and antisymmetric stretching modes. Moreover, the period of the "beat" between the two normal modes is short enough for the energy transfer to take place near the saddle. Thus, the essence of the efficient energy transfer is explained by the robust preservation of the "normal mode picture" and the relatively large difference between the frequencies of the two modes.

I-Q-8 Topographical Complexity of Multidimensional Energy Landscapes

RYLANCE, Gareth J.¹; JOHNSTON, Roy L.¹;
MATSUNAGA, Yasuhiro²; LI, Chun Bui^{2,3}; BABA, Akinori^{2,3}; KOMATSUZAKI, Tamiki⁴

(¹Univ. Birmingham; ²Kobe Univ.; ³JST/CREST; ⁴IMS, Kobe Univ. and JST/CREST)

A new scheme for visualizing and quantifying the

complexity of multidimensional energy landscapes and multiple pathways is presented employing Principal Component (PC)-based disconnectivity graphs and the Shannon entropy of relative 'sizes' of superbasins. The PC-based disconnectivity graphs incorporate a metric relationship between the stationary points of the system, which enable us to capture not only the actual assignment of the superbasins but also the size of each superbasin in the multidimensional configuration space. The landscape complexity measure quantifies the degree of topographical complexity of a multidimensional energy landscape and tells us at which energy regime branching of a main path becomes significant, making the system more likely to be kinetically trapped in local minima. The path complexity measure quantifies the difficulty encountered by the system to reach a connected local minimum by the path in question, implying that the more significant the branching points along the path are the more difficult it is to end up with the desired local minimum. As an illustrative example, we apply this analysis to two kinds of small model protein systems exhibiting a highly frustrated, and an ideal funnel-like energy landscape.

I-Q-9 A New Scheme to Construct Multidimensional Effective Free Energy Landscape from Single Molecule Time Series

BABA, Akinori^{1,2}; KOMATSUZAKI, Tamiki³
(¹Kobe Univ.; ²JST/CREST; ³IMS, Kobe Univ. and
JST/CREST)

The questions "How can one learn from an ensemble of short single molecule time series about the underlying multidimensional free energy landscape or, in general, state space?" and "How can one differentiate molecular memory along several reaction paths, if it exists?" are among the most important and central subjects for analyzing single molecule time series. Here we present a concept of local ergodic state (LES) to explore free energy landscape picture. We introduce a working hypothesis on a given single molecule time series concerning LES: if LES exists, a unique distribution (not necessarily Gaussian) function for the observable can be assigned for the LES. To assign LESs from single molecule time series, we focus on the hierarchy of time scales, $t_{\text{cor}} \ll t_{\text{eq}} \ll t_{\text{obs}} \ll t_{\text{esc}}$, where t_{cor} is the time scale of the system to possess dynamic memory, t_{eq} the time scale to be "equilibrated" within each LES, t_{obs} the observation time, and t_{esc} the time scale of the system to escape from a LES to the other LES on multidimensional free energy landscape. Our methodology naturally leads to a free energy landscape whose topography depends on which time scale the system experiences the underlying landscape. For example two metastable states will be unified as one if the time scale of observation is longer than the escape time scale for which the system can visit mutually these two states. We present our recent analyses on time series of the end-to-end distance of 46-bead model protein.

I-R Analysis Method of Electronic Structure

Understanding of chemical bond has been one of the main subjects in physical chemistry since its foundation. Nowadays, it is easy for the modern quantum-chemical technique to compute bond energy, length or detailed information on wave functions. However, it is difficult to directly bridge between these results and traditional chemical concepts (or chemical intuition), because the wave function of a molecule is usually described in terms of molecular orbitals (MO) being de-localized over whole molecule. Even obtaining the wave function of the molecule, it is numerical description of the molecule, and is often far from chemical intuition. Various methods have been developed to make up for the deficiencies in MO method. One good example is population analysis, which provides the information on an atom in a molecule. In this project, we have developed new analysis methods abstracting chemical concepts from computational results of standard MO.

I-R-1 Analysis on Solvated Molecule with a New Energy Partitioning Scheme for Intra- and Intermolecular Interactions

SATO, Hirofumi¹; SAKAKI, Shigeyoshi²
(¹IMS and Kyoto Univ.; ²Kyoto Univ.)

[*J. Phys. Chem. B* **110**, 12714–12720 (2006)]

A new partitioning scheme for the total energy of molecules is presented. In the scheme, the Hartree-Fock total energy of a molecular system is represented as the sum of one- and two-center terms exactly. The present method provides physically reasonable behavior for a wide range of interactions, and intermolecular interaction is treated equivalently with intramolecular interaction. The method is applied to analysis on the inter- and intramolecular interactions of molecular complexes both in gas phase and in aqueous solution. The results strongly indicate that the present method is a powerful tool to understand not only the bonding nature of molecules but also interaction between molecules.

I-R-2 A New Analysis of Molecular Orbital Wavefunctions Based on Resonance Theory

IKEDA, Atsushi¹; NAKAO, Yoshihide¹; SATO, Hirofumi²; SAKAKI, Shigeyoshi¹
(¹Kyoto Univ.; ²IMS and Kyoto Univ.)

[*J. Phys. Chem. A* **110**, 9028–9030 (2006)]

A new method to evaluate the weights of resonance

structures from molecular orbital wave function is proposed, which is based on the second quantization of singlet-coupling. The present method is useful to analyze molecules of which the electronic structures are well localizable. The evaluation is carried out through localization of molecular orbitals followed by algebraic calculation of density matrices. This method is applied to H₂O, H₃O⁺, and BH₃. The calculated weights of covalent and ionic structures are in excellent agreement with those of the previous works and our chemical intuition.

I-R-3 Solvation Effect on Resonance Structure. Extracting Valence Bond-Like Character from Molecular Orbitals

IKEDA, Atsushi¹; YOKOGAWA, Daisuke¹; SATO, Hirofumi²; SAKAKI, Shigeyoshi¹
(¹Kyoto Univ.; ²IMS and Kyoto Univ.)

[*Chem. Phys. Lett.* **424**, 449–452 (2006)]

We have analyzed the resonance structure in the electronic structure for solvated molecules, which are computed by the RISM-SCF method. The analysis offers a bridge between modern quantum computational results and chemical intuitions. As expected, the contribution from the ionic structure tends to be enhanced in aqueous solutions on the electronic structure polarization due to solvation. The present procedure offers understanding of the nature of chemical bonds in a solvated molecule.

I-S Solvation Structure and Its Effect on Electronic Structure

It is well known that the electronic structure of a molecule considerably changes when the molecule is dissolved in solvent. Understanding the essential of this complex event requires three points of view, namely, the electronic structure of the molecule, solvation structure around it and these coupling. In this project, we have developed various types of methods to describe solvation processes and applied them to real systems.

I-S-1 A New Method to Reconstruct Three-Dimensional Spatial Distribution Function from Radial Distribution Function in Solvation Structure

YOKOGAWA, Daisuke¹; SATO, Hirofumi²; SAKAKI, Shigeyoshi¹
(¹Kyoto Univ.; ²IMS and Kyoto Univ.)

[*J. Chem. Phys.* **123**, 211102 (5 pages) (2005)]

Three-dimensional spatial distribution function SDF of solvent is a fundamental quantity for analysis of solvation. However, its calculation has been very limited because long computational time is required. We here developed a novel and robust method to construct approximated SDFs of solvent sites from radial distribution functions. In this method, the expansion of SDFs in real solid harmonics around atoms of solute leads to a linear equation, from which SDFs are evaluated with reasonable computational time. This method is applied to the analysis of the solvation structure of liquid water, as an example. The successful results clearly show that this method is very powerful to investigate solvation structure.

I-S-2 New Evaluation of Reconstructed Spatial Distribution Function from Radial Distribution Functions

**YOKOGAWA, Daisuke¹; SATO, Hirofumi²;
SAKAKI, Shigeyoshi¹**

(¹Kyoto Univ.; ²IMS and Kyoto Univ.)

[*J. Chem. Phys.* **125**, 114102 (2006)]

Although three dimensional (3D) solvation structure is much more informative than one dimensional structure, its evaluation is difficult experimentally and theoretically. In our previous communication [Yokogawa *et al. J. Chem. Phys.* **123**, 211102 (2005)], we proposed a new method to present reconstructed spatial distribution function (RC-SDF) from a set of radial distribution functions (RDFs). In this article, we successfully extended the method more accurately with new basis sets. This new method was applied to two liquid solvation structures, methanol and DMSO, as examples. Their RC-SDFs evaluated here clearly show that the former solvation structure is well-defined while the latter one is broad, which agrees well with the SDFs calculated directly from MD simulations. These results indicate that the method can reproduce well these 3D solvation structures in reasonable computational cost.

RESEARCH ACTIVITIES II

Department of Molecular Structure

II-A Development of Dynamic Near-Field Spectroscopy and Application to Nanometric Systems

There is much demand for the study of local optical properties of molecular assemblies and materials, to understand mesoscopic phenomena and/or to construct optoelectronic devices in the nanometric scale. Scanning near-field optical microscopy (SNOM), which enables spatial resolution beyond the diffraction limit of light, showed remarkable progress in technology in the past decade. Combination of this advanced optical technology with ultrafast/nonlinear spectroscopic methods may offer a direct probe of molecular dynamical processes in mesoscopic systems. It may bring essential and basic knowledge for analyzing origins of characteristic features and functionalities of mesoscopic systems. We have constructed apparatuses for near-field dynamic spectroscopy with the femtosecond temporal resolution and the nanometer spatial resolution. Using the apparatuses developed, we are observing the characteristic spatiotemporal behavior of various organic molecular systems and metal nanoparticles, for the purpose of understanding spatial coherence and dissipation of excitations, and their dynamics. We also investigate experimentally the basic characteristics of near-field microscopic measurements. Outlines of the experimental results obtained are summarized here.

II-A-1 Photoluminescence from Gold Nanoplates Induced by Near-Field Two-Photon Absorption

IMURA, Kohei; NAGAHARA, Tetsuhiko;
OKAMOTO, Hiromi

[*Appl. Phys. Lett.* **88**, 023104 (2006)]

We have investigated two-photon-induced photoluminescence (TPI-PL) properties of single gold nanoplates by using an apertured scanning near-field optical microscope. We found the remarkably large cross sections of TPI-PL from the gold nanoplates. It is one or two orders of magnitudes larger than those observed from the gold nanorods. The near-field PL images show characteristic spatial features. These PL images are in good agreement with the calculated spatial distribution of the electric fields adjacent to the particles at the excitation wavelength. We attribute the observed images to spatial characteristics of plasmon-mode wavefunctions. The TPI-PL images of the gold triangles are strongly dependent on the incident polarization and wavelength. We also found that the plasmon-mode excitation is the primary factor for enhancing the TPI-PL process. The result suggests that it would be possible to further improve the efficiency of TPI-PL by synthesizing the nanoparticles of controlled size and shape.

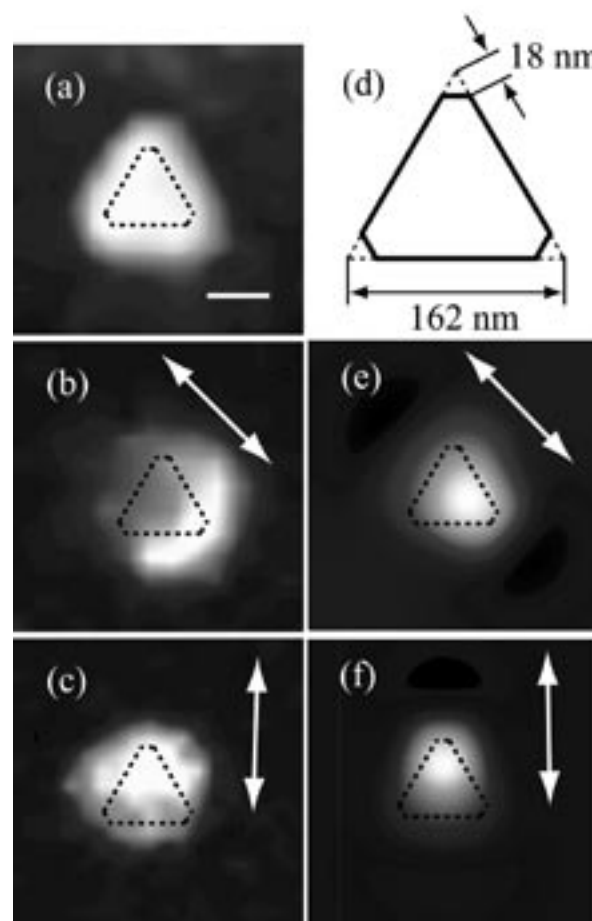


Figure 1. (a) Topography of a single gold triangle. (b), (c) Observed incident-polarization dependent TPI-PL images of the single gold triangle. (d) Schematic drawing of a snipped triangle used for calculations (e), (f). (e), (f) Calculated polarization-dependent electric field distributions near the snipped triangle. Arrows indicate the direction of the incident polarization. Dashed lines indicate approximate shape of the triangle. Scale bar: 100 nm.

II-A-2 Near-Field Imaging of SERS-Active Hot Spots on Metal-Nanoparticle Aggregates

IMURA, Kohei; OKAMOTO, Hiromi; HOSSAIN, Mohammad K.¹; KITAJIMA, Masahiro²

(¹Univ. Tsukuba and NIMS; ²NIMS, Univ. Tsukuba and IMS)

[*Chem. Lett.* **35**, 78–79 (2006)]

It is of fundamental importance to reveal the origin of the huge Raman enhancement in single-molecular level surface-enhanced Raman scattering. The major factor of the enhancement is considered to be an electromagnetic mechanism, *i.e.*, electric field enhancement induced by a plasmon resonance. For aggregated nanoparticles, strong electric field is expected in interstitial gaps between the nanoparticles (“hot spot”). Up to now, however, Raman enhancement on the hot spot site has not been directly shown by experiment. In this study, we succeeded in imaging of spatial distributions of electric-field enhancement and Raman-excitation probability for aggregates of gold nanospheres, using a scanning near-field optical microscope. To observe electric field enhancement, we used two-photon excitation probability imaging.¹⁾ The Raman excitation images were obtained by monitoring Raman band intensities while exciting the samples by cw lasers through the near-field fiber probe.

Figure 1 shows topographic, near-field two-photon excitation probability, and near-field Raman excitation probability (for dilutely doped dye molecule R6G) images, for aggregated gold nanospheres (diameter 100 nm). The two-photon image reflects spatial distribution of plasmon-induced electric field enhancement. The image shows that the aggregates, especially the gaps in the dimers, show strong electric field enhancements. Strong enhancements for the dimeric aggregates are also found in the Raman image. In contrast, the enhancements are not prominent in isolated particles. The present result gives a clear experimental proof to the theoretical prediction of hot spots.

Reference

- 1) K. Imura, T. Nagahara and H. Okamoto, *J. Phys. Chem. B* **109**, 13214 (2005).

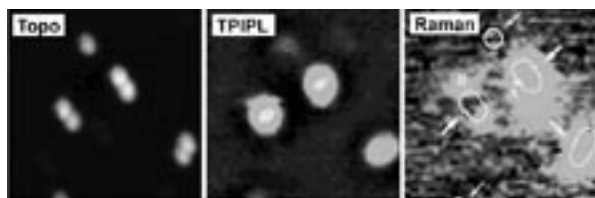


Figure 1. Topograph (left), near-field two-photon excitation (center), and near-field Raman excitation (right) images of gold nanospheres doped with R6G molecules. The Raman image was obtained for the R6G band at 1340 cm^{-1} . Image size: $1.5\text{ }\mu\text{m} \times 1.5\text{ }\mu\text{m}$.

II-A-3 Reciprocity in Scanning Near-Field Optical Microscopy: Illumination and Collection Modes of Transmission Measurements

IMURA, Kohei; OKAMOTO, Hiromi

[*Opt. Lett.* **31**, 1474–1476 (2006)]

There are two operational modes of near-field transmission experimental setup, *i.e.*, illumination (I) and collection (C) modes. In I-mode the object is illuminated through the near-field aperture probe, and the transmitted light is detected in the far field. In C-mode the object is illuminated by the far-field radiation, and the transmitted light is collected by the near-field probe. The configurations of I- and C-modes are optically reciprocal to each other. However, in the near-field experiment the reciprocity is not apparent or trivial.

We experimentally investigated the reciprocity of near-field measurements between I- and C-modes. Near-field transmission images of single gold spheres and nanorods observed by the two modes are found to be equivalent to each other in the region from visible to near infrared. This result shows that reciprocity holds for the near-field scattering problems. We found that the conventional optical selection rule for far-field excitations does not apply not only under I-mode but also with C-mode arrangements. The possible origin of this observation might be the near-field probe. The existence of the near-field probe tip close to the nanorod may perturb the electric field distribution near the gold nanorods. The local electric field generated in the presence of the near-field probe would allow SP-mode excitation at the tip position.

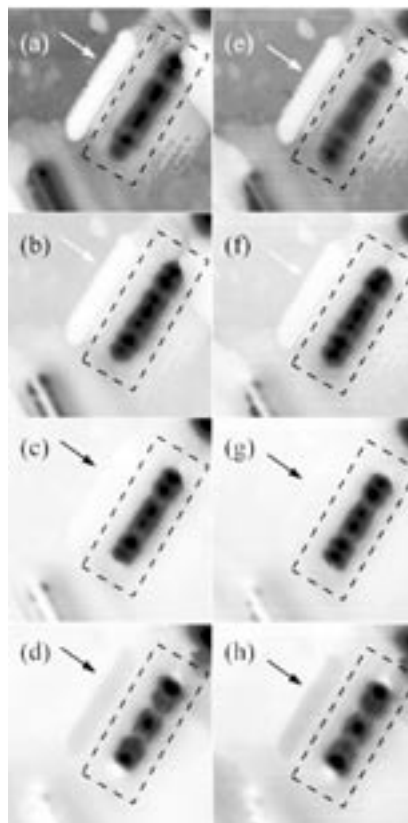


Figure 1. Transmission near-field optical images of a single gold nanorod (diameter $22 \pm 3\text{ nm}$, length $510 \pm 30\text{ nm}$): (a–d) I-mode, (e–h) C-mode. The scan area is $1\text{ }\mu\text{m} \times 1\text{ }\mu\text{m}$. Observed spectral region: (a,e) $607\text{--}627\text{ nm}$, (b,f) $647\text{--}666\text{ nm}$, (c,g) $666\text{--}686\text{ nm}$, (d,h) $705\text{--}725\text{ nm}$. Arrows indicate z -motion artifacts.

II-A-4 Near-Field Raman Study on the Close-Packed 2D Nanostructures of Gold Nanoparticles

**HOSSAIN, Mohammad K.¹; SHIMADA, Toru²;
KITAJIMA, Masahiro³; IMURA, Kohei;
OKAMOTO, Hiromi**

(¹NIMS and Univ. Tsukuba; ²NIMS; ³NIMS, Univ. Tsukuba and IMS)

Metallic nanostructure, particularly gold nanostructure is an indispensable candidate for future nanoscale science and technology for its unique properties. We have studied electromagnetic field enhancement with surface-enhanced Raman scattering (SERS) and near-field spectroscopy for well-ordered two-dimensional (2D) nanostructures of gold nanoparticles. 2D nanostructures of gold nanoparticles (diameter 100 nm) were fabricated from gold colloids without using capping reagent or surfactant on glass substrate. The individual gold nanoparticles of the 2D structure were not in contact. The over all 2D structure area ranged from several 100 μm^2 to mm^2 . Crystal violet (CV) or rhodamine 6G (R6G) molecules were dispersed on this 2D structure by spin-coating method.

The microscopic SERS spectrum of the adsorbed molecules on this Au 2D surface were measured. Several distinguishing peaks confirmed that such substrate was indeed SERS-active. The enhancement was highest at the edge of the 2D nanostructure.¹⁾ To exploit the spatial distributions of electromagnetic enhancement, scanning near-field optical measurement was performed for this 2D nanostructure. The Raman signal was enhanced at the 2D nanostructure of gold nanoparticles, especially along the edge of the 2D structure.

Reference

1) M. K. Hossain, K. Shibamoto, K. Ishioka, M. Kitajima, T. Mitani and S. Nakashima, *J. Lumin.* **122-123**, 792 (2006).

II-A-5 Enhancement and Quenching of Fluorescence from Dye Molecules by Single Gold Nanoparticles

**HORIMOTO, Noriko N.; IMURA, Kohei;
OKAMOTO, Hiromi**

We investigated the enhancement and quenching of fluorescence from dye molecules by single gold nanoparticles, and their dependence on particle shape and size, using an aperture-type scanning near-field optical microscope. Gold nanoplates (thickness ~ 20 nm) showed large enhancements, and gold nanospheres (diameter ~ 30 – 100 nm) showed a moderate enhancement. On the other hand, gold nanorods (diameter ~ 20 – 40 nm, length ~ 100 – 500 nm) showed quenching. The enhancement and quenching mechanism is discussed based on electromagnetic effects.

II-A-6 Near-Field Two-Photon-Induced Photoluminescence from Single Gold Nanorods

IMURA, Kohei; OKAMOTO, Hiromi

We investigated photoluminescence (PL) properties of single gold nanorods (diameter 20–32 nm, length 190–630 nm) by using a near-field two-photon microscope. A PL spectrum of a single gold nanorod shows two peak wavelengths. The peaks are always observed near 550 nm and 650 nm, regardless the rod dimensions and plasmon modes excited. The intensity ratio ($I_{650\text{nm}}/I_{550\text{nm}}$) of the two spectral components varies with the rod dimension, and becomes nearly zero in the spherical particle limit. The results indicate that the PL appeared in the longer wavelength (~ 650 nm) gains the intensity in resonance with the longitudinal plasmon mode. The spectral features as well as polarization characters of the PL indicate that the emission process is dominantly occurred though a radiative recombination of an electron-hole pair generated by the two-photon excitation.

II-A-7 Ultrafast Near-Field Transient Imaging of Single Gold Nanorods

IMURA, Kohei; OKAMOTO, Hiromi

We investigated ultrafast transient behaviors in single nanorods (diameter 30 nm, length 300–330 nm) after an optical excitation with a 50-nm spatial resolution and a 100-fs time resolution. We used a near-infrared pulse to excite longitudinal plasmon resonances of the nanorod. Spatial patterns of transient images of the single nanorods observed at 1 ps delay time were similar to those of plasmon wavefunctions found in the steady-state transmission measurements (Figure 1).¹⁾ However, depending on the rod dimension, the image shows either induced absorptions or absorption bleaches at end edges of the nanorod.

To get a deeper understanding for the observed features of the transient transmission images, we simulated position-dependent transient transmission change by assuming that the photoexcitation induces a homogeneous electronic temperature rise in the nanorod. In the simulation, the transient transmission change at a position was considered to be proportional to the change of the electromagnetic local density-of-states (LDOS) due to the elevation of electronic temperature. The change of LDOS was evaluated by taking the temperature dependency of the dielectric constants of the gold into account. Simulated transient images qualitatively reproduced the observations. The observed transient images were thus assignable to the change of the LDOS due to the electronic temperature rise.

Reference

1) K. Imura, T. Nagahara and H. Okamoto, *J. Phys. Chem. B* **108**, 16344 (2004).

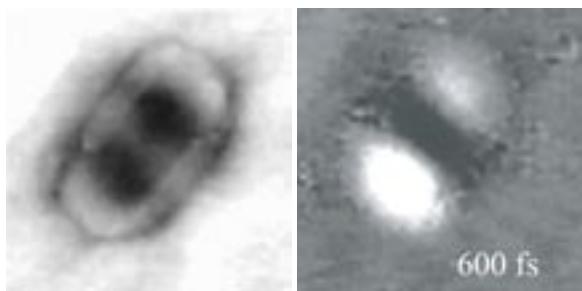


Figure 1. Typical near-field static transmission (left) and transient transmission change (right) images of gold nanorod (diameter 30 nm, length 300 nm). In the right panel, bleached and induced extinctions are indicated, respectively, in black and white.

II-A-8 Scanning Near-Field Optical Microscopic Study of Porphyrin Nanowire

**NAGAHARA, Tetsuhiko; IMURA, Kohei;
OKAMOTO, Hiromi; OZAWA, Hiroaki; OGAWA,
Takuji**

We studied optical properties of molecular nanowires of coupled zinc porphyrins with bulky dendric groups, by means of scanning near-field optical microscopy and spectroscopy. The topographic images and the near-field-excited fluorescence images gave string-like structures, and correlated well to each other. We also performed polarization dependence measurements. From the result of the analysis, it has been suggested that the photoexcitation is spatially propagated along the chain for appreciably long distance.

II-B Development of a Novel Solid-State NMR Technique

In order to alleviate an adversary effect of heating problem by irradiation of strong rf field for long duration, a novel solid state NMR technique has been explored as a means useful for a cross-polarization and separated local field NMR which enable to enhance sensitivity and determine relative orientation of the principal axes of the chemical shift and the heteronuclear dipolar interaction tensors, respectively. In the conventional approach, however, continuous rf irradiation of millisecond long rather than microsecond pulse used for conventional NMR is required. We have successfully developed a novel technique using weak rf fields without any serious loss of spectral quality. Therefore, this approach is essential for a study on biologically important molecules near under physiological conditions.

II-B-1 Remarkable Reduction of RF Power by ATANSEMA and DATANSEMA Separated Local Field in Solid-State NMR Spectroscopy

NISHIMURA, Katsuyuki; NAITO, Akira¹
(¹Yokohama Natl. Univ.)

[*Chem. Phys. Lett.* **419**, 120–124 (2006)]

We proposed a novel approach to markedly reduce rf power for both ¹H and observed nuclei during spin exchange for separated local field experiments. The rf power to satisfy the Hartmann-Hahn matching conditions during spin exchange for observed nuclei was arbitrarily reduced by alternating the directions of effective fields for ¹H nuclei with unequal duration times and amplitudes. The proposed techniques were compared experimentally with those developed previously by the authors. The rf power for observed nuclei and average ¹H were reduced by factors of 9 and 2, respectively, for ¹³C NMR signals of liquid crystalline 5CB.

References

- 1) K. Nishimura and A. Naito, *Chem. Phys. Lett.* **402**, 245–250 (2005).
- 2) C. H. Wu, A. Ramamoorthy and S. J. Opella, *J. Magn. Reson. A* **109**, 270–272 (1994).

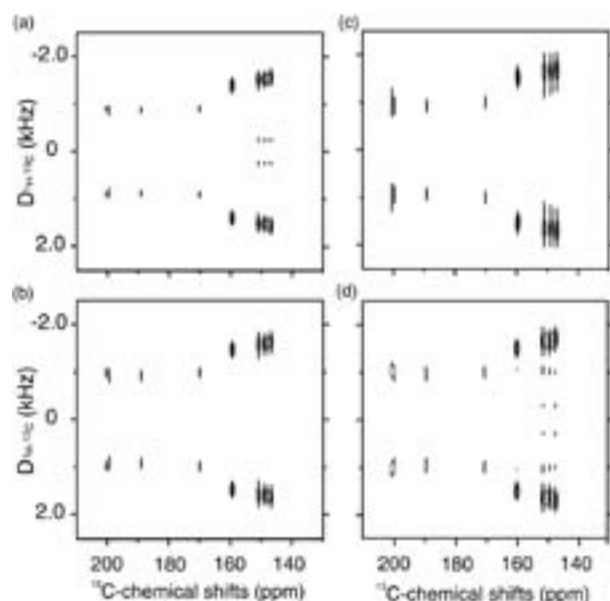


Figure 1. 2D-Separated local field ¹³C-NMR spectra aromatic region of 5CB in the liquid crystalline state at 20 °C obtained by (a) TANSEMA¹ (¹H, ¹³C = 57.7, 11 W), (b) ATANSEMA (¹H_{av}, ¹³C = 34.4, 11 W), (c) DATANSEMA (¹H_{av}, ¹³C = 25.4, 11 W), (d) PISEMA² (¹H, ¹³C = 57.7, 97 W).

II-B-2 Reduction of RF Power by Duration and Amplitude Time-Averaged Nutation Cross Polarization in Solid State NMR Spectroscopy

NISHIMURA, Katsuyuki; NAITO, Akira¹
(¹Yokohama Natl. Univ.)

We have developed a new approach to markedly reduce rf power for both ¹H and observed nuclei during cross-polarization under static condition. The rf power to satisfy the Hartmann-Hahn matching condition for observed nuclei was arbitrary reduced by alternating the direction of effective fields with unequal-duration times and -amplitudes. The proposed technique was compared theoretically and experimentally with the previously developed duration time averaged technique with and without ¹H-homonuclear dipolar decoupling. The rf power for observed nuclei and averaged power for ¹H were shown to be reduced experimentally by factors of 9 and 2, respectively, as manifested from ¹³C-NMR signals of MBBA in the liquid crystalline state without expense of reduced signals.

References

- 1) K. Nishimura and A. Naito, *Chem. Phys. Lett.* **380**, 569–576 (2003).
- 2) R. K. Hester, J. L. Ackerman, V. R. Cross and J. S. Waugh, *Phys. Rev. Lett.* **34**, 993–995 (1975).

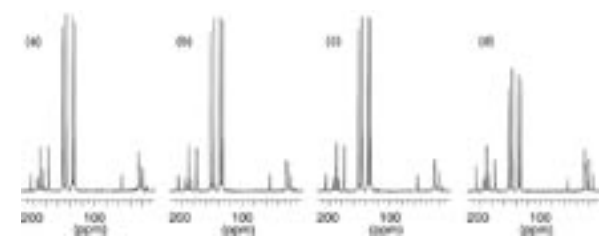


Figure 1. ¹³C-NMR spectra of MBBA in the liquid crystalline state at 20 °C obtained by (a) TANMA-CP¹ (¹H, ¹³C = 57.7, 11 W), (b) ATANMA-CP (¹H_{av}, ¹³C = 34.4, 11 W), (c) DATANMA-CP (¹H_{av}, ¹³C = 25.4, 11 W), and (d) LG-CP² (¹H, ¹³C = 57.7, 97 W).

II-C Structural Characterization of Biomolecules by Solid State NMR

Solid state NMR is an excellent technique to examine structures and dynamics of biomolecules including membrane proteins or membrane-associated peptides at physiological temperature. In particular, we have explored to reveal the functional role of membrane proteins or peptides inside or at the membrane surface of fully hydrated lipid bilayers by using solid state NMR at ambient temperature.

II-C-1 Histidines, Heart of the Hydrogen Ion Channel from Influenza A Virus: Toward an Understanding of Conductance and Proton Selectivity

HU, Jun¹; FU, Riqiang¹; NISHIMURA, Katsuyuki; ZHANG, Li¹; ZHOU, Huan-Xiang¹; BUSATH, David D.²; VIJAYYERGIYA, Viksita²; CROSS, Timothy A.¹

(¹Florida State Univ. and Natl. High Magnetic Field Laboratory; ²Brigham Young Univ.)

[*Proc. Natl. Acad. Sci. U.S.A.* **103**, 6865–6870 (2006)]

The heart of the H⁺ conductance mechanism in the homotetrameric M2 H⁺ channel from influenza A is a set of four histidine side chains. Here, we show that protonation of the third of these imidazoles coincides with acid activation of this transmembrane channel and that, at physiological pH, the channel is closed by two imidazole–imidazolium dimers, each sharing a low-barrier hydrogen bond. This unique construct succeeds in distributing a pair of charges over four rings and many atoms in a low dielectric environment to minimize charge repulsion. These dimers form with identical pK_{as} of 8.2±0.2, suggesting cooperative H⁺ binding and clearly illustrating high H⁺ affinity for this channel. The protonation behavior of the histidine side chains has been characterized by using solid-state NMR spectroscopy on the M2 transmembrane domain in fully hydrated lipid bilayers where the tetrameric backbone structure is known. Furthermore, electrophysiological measurements of multichannel and single-channel experiments confirm that these protein constructs are functional.

II-C-2 Conformational Changes of Adrenocorticotrophic Hormone, ACTH (1-24), Bound to Lipid Bilayers, Dependent upon Proportion of Lipids Composition, as Studied by Solid State NMR

NISHIMURA, Katsuyuki; MYOGA, Hiroki¹; NARITA, Muneto¹; KIRA, Atsushi²; NAITO, Akira¹
(¹Yokohama Natl. Univ.; ²ULVAC Inc.)

Local conformations of ACTH (1-24), bound to fully hydrated multibilayers consisting of neutral and anionic lipids (DMPC/DMPG) at liquid crystalline, were examined by ¹³C-solid state NMR. It turned out that ACTH (1-24) exhibited conformational changes depending upon the lipid composition of DMPC to DMPG. The binding constants of ACTH (1-24) to the lipid bilayers were determined by a quartz crystal microbalance

(QCM) for various DMPC/DMPG proportion. The local maximum was seen at the proportion of DMPG/(DMPC + DMPG) = 0.25, which is close to the composition of neutral and anionic lipids occurring in human cells. This result suggests that ACTH (1-24) has favorable lipid composition in order to bind tightly lipid bilayers prior to reach receptor, together with changing its conformation depending on the lipid composition.

II-D Structure and Function of Metalloproteins and Its Molecular Design

Metal ion is a common cofactor that is crucial for active centers of proteins involved in many biologically important processes in cells, and a relatively small number of metal-based prosthetic groups are utilized to serve numerous and diverse chemical functions. A typical metal-based prosthetic group, which represents a fascinating example in this respect, is heme. Heme promotes a variety of functions, such as dioxygen storage, activation of small molecules, electron transfer reactions, and sensing gaseous molecule. In the field of protein design and engineering, hemoproteins also make particularly attractive targets. There are many reasons for this, including the exciting possibility of engineering protein-based molecules with useful catalytic, electronic or optoelectronic properties. Based on various kinds of spectroscopies, we have functionally and structurally characterized some hemoproteins including newly identified heme-regulated proteins, and designed hemoproteins showing improved activities and new functions.

II-D-1 Absence of a Detectable Intermediate in the Compound I Formation of Horseradish Peroxidase at Ambient Temperature

SHINTAKU, Masato¹; MATSUURA, Koji¹;
TAKAHASHI, Satoshi¹; ISHIMORI, Koichiro²;
MORISHIMA, Isao¹
(¹Kyoto Univ.; ²IMS and Kyoto Univ.)

[*J. Biol. Chem.* **280**, 40934–40938 (2005)]

A microsecond-resolved absorption spectrometer was developed to investigate the elementary steps in hydrogen peroxide (H₂O₂) activation reaction of horseradish peroxidase (HRP) at ambient temperature. The kinetic absorption spectra of HRP upon the mixing with various concentrations of H₂O₂ (0.5–3 mM) were monitored in the time range from 50 to 300 μs. The time-resolved spectra in the Soret region possessed isosbestic points that were close to those between the resting state and compound I. The kinetic changes in the Soret absorbance could be well fitted by a single exponential function. Accordingly, no distinct spectrum of the putative intermediate between the resting state and compound I was identified. These results were consistent with the proposal that the O–O bond activation in heme peroxidases is promoted by the imidazolium form of the distal histidine that exists only transiently. It was estimated that the rate constant for the breakage of the O–O bond in H₂O₂ by HRP is significantly faster than 1 × 10⁴ s⁻¹.

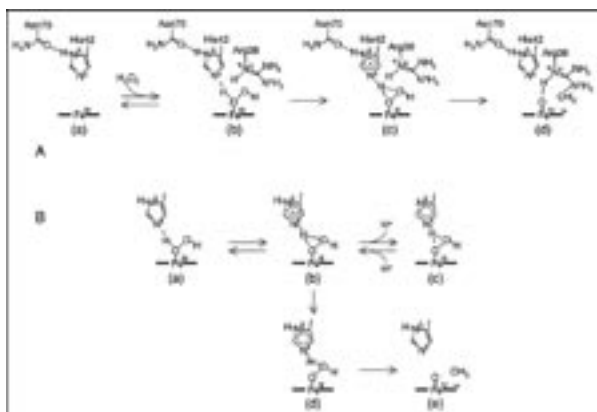


Figure 1. The proposed formation mechanisms of compound I. *A*, the formation mechanism of compound I in heme peroxidases proposed by Poulos and Kraut. The amino acid numbering is for HRP, although the original proposal was based on the structure of cytochrome *c* peroxidase. (*a*), the resting state. (*b*) and (*c*), the hypothetical intermediate and transition state structures for the compound I formation. His-42 acts as a general acid-base catalyst and translocates a proton from the proximal to the distal oxygen. (*d*), compound I. The hydrogen bonds between oxygen atoms and Arg-38 were detected in the recent crystallographic data. *B*, the generalized mechanism of hydrogen peroxide activation by heme proteins described by Egawa *et al.* (*a*), the hydrogen peroxide-bound form. (*b*), the transition state for the O–O bond heterolysis. The structure is unstable because of the doubly protonated His. (*c*), the deprotonation of the distal His causes the stabilization of the iron hydroperoxide complex. (*d*), the proton translocation occurs only from the structure ((*b*)). (*e*), compound I.

II-D-2 Dehydration in the Folding of Reduced Cytochrome *c* Revealed by the Electron-Transfer-Triggered Folding under High Pressure

KIMURA, Tetsunari¹; SAKAMOTO, Koichi²;
MORISHIMA, Isao¹; ISHIMORI, Koichiro³
(¹Kyoto Univ.; ²Kyoto Univ. and Hokkaido Univ.; ³IMS,
Kyoto Univ. and Hokkaido Univ.)

[*J. Am. Chem. Soc.* **128**, 670–671 (2006)]

We determined the activation volume associated with protein folding of reduced cytochrome *c* from the collapsed intermediate to the native state. The folding rate was followed by a change in the absorption (420 nm) at various pressures between 0.1 and 200 MPa and at various concentrations of denaturant (guanidine hydrochloride) between 3.2 and 4.0 M. Dependence of the folding rate on both these factors revealed that the activation volume at ambient pressure in the absence of denaturant is negative ($\Delta V^\ddagger = -14 \pm 7 \text{ cm}^3 \cdot \text{mol}^{-1}$). Such a negative activation volume can be accounted for by a decrease in volume resulting from the dehydration of hydrophobic groups, primarily the heme group. Dehydration, which increases the entropy of the protein system, compensates for a decrease in the entropy

accompanying the formation of the more compact and ordered transition state. We, therefore, propose that the positive change in the activation entropy for the folding reaction is due to the dehydration of hydrophobic groups. Furthermore, dehydration entropically promotes the protein folding reaction.

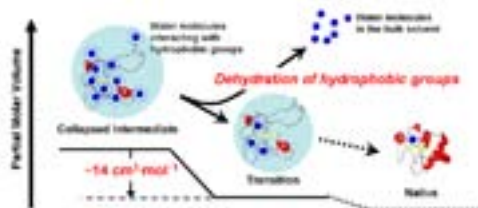


Figure 1. Volume profile for protein folding of cytochrome *c*.

II-D-3 Time-Resolved Small Angle X-Ray Scattering Investigation on the Folding Dynamics of Heme Oxygenase: Implication of the Scaling Relationship for the Submillisecond Intermediates of Protein Folding

UZAWA, Takanori¹; KIMURA, Tetsunari¹;
ISHIMORI, Koichiro²; MORISHIMA, Isao¹;
MATSUI, Toshitaka³; IKEDA-SAITO, Masao³;
TAKAHASHI, Satoshi⁴; AKIYAMA, Shuji⁵;
FUJISAWA, Tetsuro⁵

(¹Kyoto Univ.; ²IMS and Kyoto Univ.; ³Tohoku Univ.;
⁴Osaka Univ.; ⁵RIKEN)

[*J. Mol. Biol.* **357**, 997–1008 (2006)]

Polypeptide collapse is generally observed as the initial folding dynamics of proteins with more than 100 residues, and is suggested to be caused by the coil-globule transition explained by Flory's theory of polymers. To support the suggestion by establishing a scaling behavior between radius of gyration (R_g) and chain length for the initial folding intermediates, the folding dynamics of heme oxygenase (HO) was characterized by time-resolved, small-angle X-ray scattering. HO is a highly helical protein without disulfide bridges, and is the largest protein (263 residues) characterized by the method. The folding process of HO was found to contain a transient oligomerization; however, the conformation within 10 ms was demonstrated to be monomeric and to possess R_g of 26.1 ± 1.1 Å. Together with the corresponding data for proteins with different chain lengths, the seven R_g values demonstrated the scaling relationship to chain length with a scaling exponent of 0.35 ± 0.11 , which is close to the theoretical value of $1/3$ predicted for globules in solutions where monomer-monomer interactions are favored over monomer-solvent interactions (poor solvent). The finding indicated that the initial folding dynamics of proteins bears the signature of the coil-globule transition, and offers a clue to explain the folding mechanisms of proteins with different chain lengths.

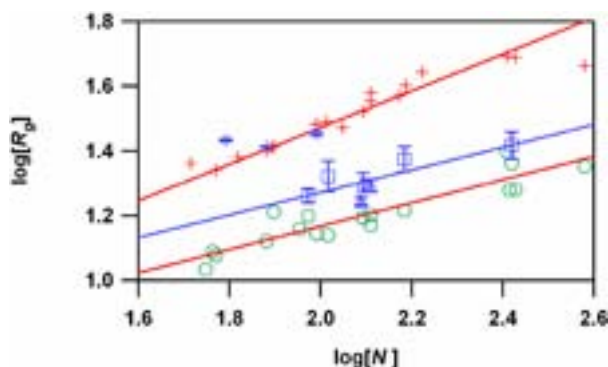


Figure 1. The correlation plots between R_g and chain length (N) for the chemically unfolded states (crosses), native states (circles) and initial collapsed intermediates (squares and triangles) of various proteins. Squares and triangles represent R_g values obtained with the submillisecond and millisecond time resolutions, respectively. Lines denote the scaling relationships for the respective states. The data for the chemically unfolded state, and for the native state, are reported elsewhere.

II-E Structure and Energy Changes during Protein Reaction Dynamics

The thermodynamic properties (enthalpy, thermal expansion coefficient, compressibility, partial molar volume, etc.) as well as the transport property (diffusion coefficient) of proteins are of fundamental importance to understand the structural fluctuation and the dynamics of protein molecules. Traditional techniques that can access to these quantities are certainly useful and powerful to characterize the proteins. However, knowledge of these properties of time-dependent or unstable (intermediate) species during biological reactions is very limited. It is most desirable to develop and use a method that can measure these properties in time domain so that reaction intermediates can be characterized in a similar way. In this project, we try to construct a method to probe energies and conformational changes as well as the diffusion coefficients of biological proteins in time domain. One of interesting applications of this technique is to detect spectral silent kinetics in reactions of biological proteins.

II-E-1 Time-Resolved Thermodynamics: Heat Capacity Change of Transient Species during Photo-Reaction of PYP

**KHAN, Javaid Shahbaz¹; IMAMOTO, Yasushi³;
KATAOKA, Mikio³; TOKUNAGA, Fumio⁴;
TERAZIMA, Masahide²**
(¹Kyoto Univ.; ²IMS and Kyoto Univ.; ³Nara Inst. Sci. Tech.; ⁴Osaka Univ.)

[*J. Am. Chem. Soc.* **128**, 1002–1008 (2006)]

Heat capacity changes of short lived transient species in different time ranges were measured for the first time by using the thermal component of the transient grating and transient lens signals at various temperatures. This method was applied to the transient intermediates of Photoactive Yellow Protein (PYP). The temperature dependence of the enthalpy change shows that the heat capacity of the short lived intermediate pR₂ (also called I₁ or PYP_L) species is the same as that of the ground state (pG) species within our experimental accuracy, whereas that of the long lived intermediate pB (I₂ or PYP_M) is much larger (2.7±0.4 kJ/mol K) than that of pG. The larger heat capacity is interpreted in terms of the conformational change of the pB species such as melted conformation and/or exposure of the non-polar residues to the aqueous phase. This technique can be used for photochemical reaction in general to investigate the conformational change and the hydrophobic interaction in time domain.

II-E-2 Conformational Changes of PYP Monitored by Diffusion Coefficient: Effect of N-Terminal α -Helices

**KHAN, Javaid Shahbaz¹; IMAMOTO, Yasushi³;
HARIGAI, Miki³; KATAOKA, Mikio³; TERAZIMA,
Masahide²**
(¹Kyoto Univ.; ²IMS and Kyoto Univ.; ³Nara Inst. Sci. Tech.)

[*Biophys. J.* **90**, 3686–3693 (2006)]

Conformational changes in the light illuminated intermediate (pB) of photoactive yellow protein (PYP) were studied from a view point of the diffusion coefficient (*D*) change of several N-truncated PYPs, which

lacked the N-terminal 6, 15, or 23 amino acid residues (T6, T15, and T23, respectively). For intact PYP (i-PYP), *D* of pB (*D*_{pB}) was *c.a.* 11% lower than that (*D*_{pG}) of the ground state (pG) species. The difference in *D* (*D*_{pG} – *D*_{pB}) decreased upon cleavage of the N-terminal region in the order of i-PYP > T6 > T15 > T23. This trend clearly showed that conformational change in the N-terminal group is the main reason for the slower diffusion of pB. This slower diffusion was interpreted in terms of the unfolding of the two α -helices in the N-terminal region, increasing the intermolecular interactions due to hydrogen bonding with water molecules. The increase in friction per one residue by the unfolding of the α -helix was estimated to be 0.3×10^{-12} kg/s. The conformational change in the N-terminal group upon photo-illumination is discussed.

II-E-3 Diffusion Coefficient and the Secondary Structure of Poly-L-Glutamic Acid in Aqueous Solution

**INOUE, Keiichi¹; BADEN, Naoki¹; TERAZIMA,
Masahide²**
(¹Kyoto Univ.; ²IMS and Kyoto Univ.)

[*J. Phys. Chem. B* **109**, 22623–22628 (2005)]

The diffusion coefficients (*D*) of poly-L-glutamic acid (PLG) at various pH were investigated by the laser induced transient grating method with a new photo-reactive probe molecule. The pH dependence of *D* was compared with that of the helical content of PLG measured by the circular dichroism. It was found that the pH dependences of both quantities are very similar. Since the frictions of the translational diffusion of charged and protonated carboxyl group were found to be similar each other, it was concluded that the conformation of the main polymer chain is a main factor to determine the diffusion process; that is, the α -helix conformation makes the molecular diffusion faster. This result indicates that the conformational change of a protein can be detected by monitoring the diffusion coefficient.

II-F Surface Magnetism of Ultrathin Films: Search of New Phenomena and Exploitation of New Techniques

Noble properties of magnetic thin films such as perpendicular magnetic anisotropy (PMA) and giant magneto-resistance (GMR) have extremely attracted scientific and technological interests. The origin of perpendicular magnetic anisotropy of ultrathin metal films is not fully understood and is an important subject in fundamental physics but is useful for high-density recording media. The GMR property is already utilized for read-heads of hard disk drives, although quantitative understanding of the GMR is still to be improved.

Our research subjects are twofold. The first one is to find out new important phenomena concerning surface magnetism. We have been investigating drastic changes of magnetic properties of ultrathin metal films by using surface chemical modification such as atoms/molecules adsorption on the surface. This is studied by several sophisticated techniques such as the synchrotron radiation x-ray magnetic circular dichroism (XMCD), the visible-light magneto-optical Kerr effect (MOKE) and the magnetization induced second harmonic generation (MSHG) techniques. A goal of these works is spin engineering by which the magnetization of ultrathin metal films and nanowires can be controlled artificially.

The second one is to exploit new techniques for the investigations of surface magnetism. Last year we discovered surprising enhancements of the magnetic circular dichroism (MCD) in the threshold photoemission, which provide the possibility of the visible and ultraviolet (UV) MCD photoemission electron microscopy (PEEM).

II-F-1 Effect of Adsorbate Carbon on Spin Reorientation Transitions in Cu-Capped Ultrathin Ni Films on Cu(001)

NAKAGAWA, Takeshi; WATANABE, Hirokazu; YOKOYAMA, Toshihiko

[*Surf. Sci.* **599**, 262–269 (2005)]

We have reinvestigated the Cu capping effect for Ni films on clean Cu(001) by means of polar and longitudinal MOKE measurements in order to account for previous discrepancies^{1,2} among the results regarding whether the Cu capping stabilizes perpendicular or in-plane magnetization. Figure 1(a) shows the Ni thickness dependence of the polar and longitudinal MOKE results of Ni/Cu(001) before and after Cu capping. The perpendicular magnetization from the polar MOKE appears at smaller thickness in Cu-capped Ni/Cu(001). We can immediately conclude that Cu capping stabilizes perpendicular magnetization.

We also found that the previous erroneous observation of in-plane stabilization could be accounted for by the presence of a small amount of C contamination, which was revealed to stabilize perpendicular magnetization surprisingly. Figure 1(b) shows the Ni thickness dependence of the polar MOKE results of Ni/Cu(001) before and after Cu capping. In contrast to the Ni films on clean Cu(001), the perpendicular magnetization is apparently unstabilized after Cu capping. The C atoms were found to act as surfactants and were always located at the top surface. As regards perpendicularly magnetized films on clean Cu(001), the enhancement of the coercivity with Cu capping was observed. This finding indicates that Cu does not act as a simple magnetism killer but effectively suppresses the surface anisotropy that favors in-plane magnetic anisotropy.

References

- 1) W. L. O'Brien and B. P. Tonner, *Phys. Rev. B* **49**, 15370 (1994).

- 2) H. W. Zhao, Y. Z. Wu, C. Won, F. Toyoma and Z. Q. Qiu, *Phys. Rev. B* **66**, 104402 (2002).

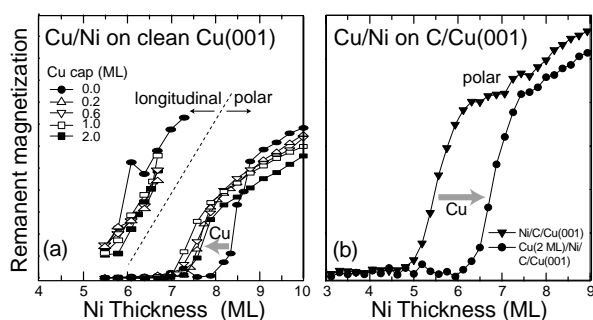


Figure 1. (a) Remanent longitudinal and polar MOKE intensities of Cu-capped Ni films grown on clean Cu(001) as a function of Ni film thickness. The critical thickness of the spin reorientation transition is shifted from ~ 8.5 ML to a thinner side (~ 7.5 ML) with increasing the amount of capped Cu. (b) Remanent polar MOKE intensities for Ni films on C-contaminated Cu(001) as a function of Ni film thickness. In contrast to (a), the critical thickness of the spin reorientation transition is shifted from ~ 5.5 ML to a thicker side (~ 7.0 ML) with Cu capping.

II-F-2 Effect of Surface Chemisorption on the Spin Reorientation Transition in Magnetic Ultrathin Fe Film on Ag(001)

MA, Xiao-Dong¹; NAKAGAWA, Takeshi; YOKOYAMA, Toshihiko
(¹SOKENDAI)

[*Surf. Sci.* **600**, 4605–4612 (2006)]

We have investigated the effect of surface chemisorption on the spin reorientation transitions in magnetic ultrathin Fe films on Ag(001) by means of the polar and longitudinal MOKE and XMCD measurements. Remanent perpendicular magnetization and the coercive fields of the Fe films on Ag(001) before and

after gas (O_2 , NO and H_2) adsorption at 100 K are shown in Figure 1. It is found by the MOKE that adsorption of O_2 and NO induces the shift of the critical thickness for the transitions to a thinner side, together with the suppression of the remanent magnetization and the coercive field of the Fe film. This implies destabilization of the perpendicular magnetic anisotropy. On the other hand, H_2 adsorption is found not to change the magnetic anisotropy, though the enhancement of the coercive field is observed. The XMCD reveals that although both the spin and orbital magnetic moments along the surface normal are noticeably reduced upon O_2 and NO adsorption, the reduction of the orbital magnetic moments are more significant. This indicates that the destabilization of the perpendicular magnetic anisotropy upon chemisorption of O_2 and NO originates from the change of the spin-orbit interaction at the surface.

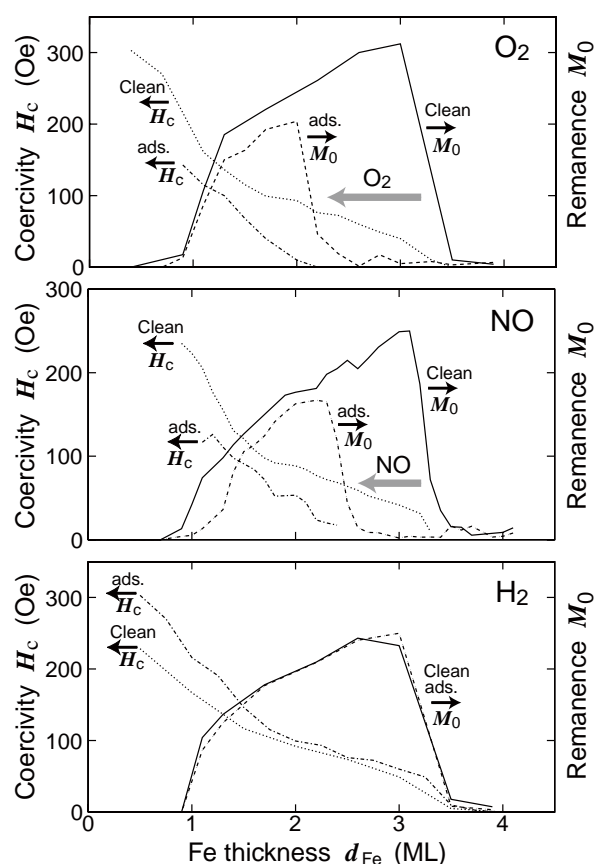


Figure 1. Remanent magnetization and the coercive field of the Fe films on $Ag(001)$ before and after gas (O_2 , NO and H_2) adsorption recorded at 100 K by the polar MOKE measurements. O_2 and NO adsorption destabilizes perpendicular magnetic anisotropy, while H_2 does not change the critical thickness.

II-F-3 Magnetic Circular Dichroism near the Fermi Level: Possibility of UV MCD PEEM

NAKAGAWA, Takeshi; YOKOYAMA, Toshihiko

[*Phys. Rev. Lett.* **96**, 237402 (2006)]

It has long been believed that the MCD in the visible and ultraviolet regions is in general too weak to apply for a noble nano-scale magnetic imaging technique of PEEM. In this study, we discovered surprising enhancement of the MCD intensity near the Fermi level using visible and ultraviolet lasers. Figure 1(a) shows the MCD asymmetry of a perpendicularly magnetized Cs-coated 12 ML Ni film on $Cu(001)$ as a function of $h\nu - \Phi$ ($h\nu$ the photon energy and Φ the work function). The work function was changed with the aid of Cs adsorption. More than 10% MCD asymmetry is achieved near the photoemission threshold. The MCD asymmetry is found to be enhanced only near the threshold and to drop down to 0.1% at the photon energy larger than the work function by 0.6 eV. A theoretical calculation also shows enhanced MCD near the photoemission threshold, qualitatively in agreement with the experimental results. Other ultrathin films of 6 ML Ni, 15 ML Co, and 3 and 15 ML Fe on $Cu(001)$ were also investigated. It is found that the perpendicularly magnetized films show much larger MCD asymmetries than the in-plane magnetized films as in the Kerr effect.

Moreover, we have performed the measurements of magnetization curves on clean Ni/ $Cu(001)$ using the free electron laser (FEL) from UVSOR-II in order to eliminate the possibility of the Cs effect. This part is a collaboration with a UVOSR machine group (Prof. M. Kato, Dr. M. Hosaka *et al.*). Figure 1(c) shows the hysteresis loop taken with the photon energy of 5.37 eV. Although the photon energy was not optimized, the MCD asymmetry is found to be as much as 5–6%. This supports the idea that the threshold photoemission provides huge enhanced MCD especially in the perpendicularly magnetized films.

This discovery enables us to exploit a new technique of UV MCD PEEM. At present, x-ray MCD PEEM is widely available for the investigations of nano-scale magnetic imaging of magnetic thin films. This technique however requires third generation synchrotron radiation light sources and cannot be used in laboratories. It is also difficult to obtain information on subpicosecond ultrafast spin dynamics due to the pulse width of the synchrotron radiation. If the UV MCD PEEM techniques can be used in near future, these difficulties can be overcome. We are now developing the new technique of UV MCD PEEM.

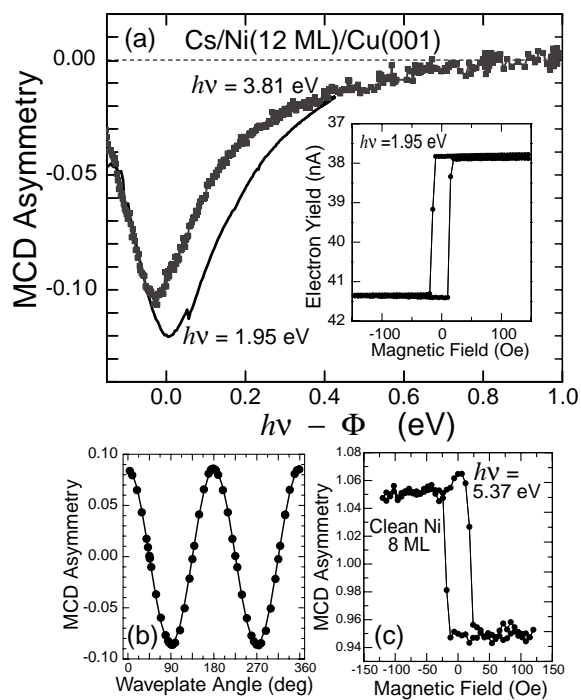


Figure 1. (a) MCD asymmetry from Cs/Ni(12ML)/Cu(001) at normal incidence as a function of $h\nu - \Phi$ ($h\nu = 1.95$ or 3.81 eV). The work function varied by changing the Cs coverage. The largest MCD asymmetries are as much as 10% near the photoemission threshold. The inset shows the typical magnetization curve. (b) Azimuthal angle dependence of the quarter-wave plate. The angles 0° , 45° and 90° correspond to the left-circularly, linearly, right-circularly polarized lights, respectively. The cosine curve clearly shows the successful observation of MCD. (c) The magnetization curve of clean Cs-free Ni/Cu(001) taken by using the FEL from UVSOR-II. Intense MCD was observed, eliminating the possibility of the Cs effect for the MCD enhancement.

II-G Development of Fluorescent and Bioluminescent Proteins for Imaging Biomolecules

Our understanding of biological systems is increasingly dependent upon the ability to quantify and image biomolecules in living animals and plants. To probe the biomolecular functions and dynamics in living organisms, we are exploring a new way for developing fluorescent and bioluminescent reporter proteins based on protein splicing. The reporter proteins can be applied to development of analytical methods for detecting protein-protein interactions, intracellular localization of proteins and their dynamics, enzyme activities, gene expression, and production of small bio-molecules. We are also currently investigating analytical techniques such as complementary DNA library screenings and proteome analysis.

II-G-1 A Short Peptide Sequence that Targets Fluorescent and Functional Proteins into the Mitochondrial Intermembrane Space

OZAWA, Takeaki; SAKO, Yusuke¹; NATORI, Yutaka¹; KUROIWA, Haruko²; KUROIWA, Tsuneyoshi²; UMEZAWA, Yoshio¹
(¹Univ. Tokyo; ²Rikkyo Univ.)

Protein-based fluorescent and functional probes are widely used for real-time visualization, purification and regulation of a variety of biological molecules. The protein-based probes can generally be targeted into subcellular compartments of eukaryotic cells by a particular short peptide sequence. Little is known, however, about the sequence that targets probes into the mitochondrial intermembrane space (IMS). To identify the IMS-targeting sequence, we developed a simple genetic screening method to discriminate the proteins localized in the IMS from those in the mitochondrial matrix, thereby revealing a sequence sorting into the IMS. An IMS-localized protein, Smac/DIABLO, was randomly mutated and mitochondrial localization of each mutant was analyzed. We found that the four residues of Ala-Val-Pro-Ile are required for the IMS localization, and a sequence of the four residues fused with matrix-targeting signals is sufficient for targeting the Smac/DIABLO in the IMS. The sequence was shown to readily direct multiple proteins of interest to the IMS, which will open avenues to elucidating IMS functions in live cells.

II-G-2 Intein-Mediated Reporter Gene Assay for Detecting Protein-Protein Interactions in Living Mammalian Cells

KANNO, Akira¹; OZAWA, Takeaki; UMEZAWA, Yoshio¹
(¹Univ. Tokyo)

[*Anal. Chem.* **78**, 556–560 (2006)]

For nondestructive analysis of chemical processes in living mammalian cells, we developed a new reporter gene assay for detecting cytosolic protein-protein interactions based on protein splicing of transcription factors with DnaE inteins. The protein splicing induces connection of a DNA-binding protein (modified LexA; mLexA) with a transcription activation domain of a herpes simplex virus protein (VP16AD). We thereby circumvented the limitation of earlier methods for moni-

toring protein-protein interactions, including the two-hybrid systems, protein complementation systems (PCS), and protein reconstitution systems, and rather combined their advantages. To test the applicability of this method, we monitored epidermal growth factor (EGF)-induced interactions on cell membranes of a known partner, an oncogenic product Ras and its target Raf-1. Ras was connected with N-terminal DnaE and mLexA, while Raf-1 was connected with C-terminal DnaE and VP16AD. Upon stimulation with EGF, the interaction between Ras and Raf-1 triggered folding of the DnaEs, thereby inducing protein splicing to form mLexA-VP16AD fusion protein, and transcription of a reporter gene, firefly luciferase. The extent of Ras-Raf-1 interaction was quantified by measuring the luciferase activity. The interaction was not able to be monitored by two-hybrid systems nor by PCS of split firefly luciferases; however, by using the protein splicing elements and the reporter gene, we obtained the bioluminescence signals sufficient for evaluation of the interactions close to cell membranes.

II-G-3 A Genetically Encoded Indicator for Assaying Bioactive Chemicals that Induce Nuclear Transport of Glucocorticoid Receptor

KIM, Sung Bae¹; OZAWA, Takeaki; UMEZAWA, Yoshio¹
(¹Univ. Tokyo)

[*Anal. Biochem.* **347**, 213–220 (2005)]

Glucocorticoids, the adrenal steroid hormones secreted during stress, are essential to homeostasis and metabolism in the human body. An impaired glucocorticoid signaling due to dysfunction of the glucocorticoid receptor (GR) by synthetic chemicals can cause diseases and disruptions of the homeostasis and metabolism. Here we demonstrate the development of a method for screening endocrine-disrupting chemicals and potent risk factors of human diseases based on the nuclear trafficking of the GR. We constructed a new assay using a pair of genetic indicators with the full length of the GR, split *Renilla* luciferase (RLuc), and split DnaE (a protein splicing element). The GR-containing fusion protein with C-terminal halves of DnaE and RLuc is localized in cytosol due to the cytosolic character of the GR, whereas the fusion protein with N-terminal halves of DnaE and RLuc stays in the nucleus due to the cofused nucleus localization signal. On being stimulated

with a ligand, the GR is translocated into the cellular nucleus. Thus, the protein splicing occurs in the nucleus by an interaction between the splicing junctions of each DnaE fragment. The enzymatic activities from the reconstituted RLuc allow the ligand-dependent luminescence intensities. The feasibility of the method was evaluated by quantifying the hormonal activities of 20 different kinds of steroids and synthetic chemicals using the NIH 3T3 cells carrying the pair of indicators. The hormonal activities of tested ligands are discussed based on the chemical structure-activity relationship. We found that androgens, testosterone, and 19-nortestosterone weakly induce the nuclear transport of the GR. The current assay allows high-throughput screening of risk chemicals and drug candidates influential to a signal transduction pathway of the GR.

II-G-4 A Method for Determining the Activities of Cytokines Based on the Nuclear Transport of Nuclear Factor- κ B

KIM, Sung Bae^{1,2}; NATORI, Yutaka¹; OZAWA, Takeaki; UMEZAWA, Yoshio¹; TAO, Hiroaki²
(¹Univ. Tokyo; ²AIST)

[Anal. Biochem. in press]

Gene expressions are controlled by regulatory proteins known as transcription factors. One important transcription factor is nuclear factor- κ B (NF- κ B), which is related to cellular proliferation, survival, differentiation, or apoptosis. We developed a method to evaluate the activities of cytokines based on the nuclear transport of NF- κ B. A pair of bioluminescent indicators were made for conferring cytokine sensitivity to cervical carcinoma-derived HeLa cells. The principle is based on reconstitution of split fragments of *Renilla* luciferase (RLuc) by protein splicing with a DnaE intein. The bioluminescence intensity of thus reconstituted RLuc in the HeLa cells was used as a measure of the activities for cytokines. The present method would be a useful high-throughput assay for determining the activities of potential biomedical inhibitors on NF- κ B trafficking.

RESEARCH ACTIVITIES III Department of Electronic Structure

III-A Synthesis and Characterization of Exotic Molecule Based Nano-Crystals of Metal Acetylides: Toward Carbon Encapsulated Metal Dot Array, Metal Nano-Networks and Metal-Carbon Hybrid Devices

Metal-carbon binary junctions are expected to exhibit interesting properties, such as Shottky barrier rectification, optical and tunneling devices, and chemical protector against oxidation. Metal acetylides have the ionic bond between the metallic cation and the acetylide anion. In the simplest case, divalent metal cations (M^{2+}) form a fcc lattice structure with a C_2^{2-} anion between the two metal cations. The introduction of alkyl or aromatic group into the C_2 unit, producing $R-C\equiv C^-$, can generate organometallic cluster compounds $((R-C\equiv C^-)_a M^{a+})_n$, ($a = 1, 2$), some of which can be isolated as a single crystal. These cluster compounds are soluble in organic solvent and provide solid films with nano-scale planarity by spin-coating method. Photoexcitation of metal-acetylides induces charge-neutralization reaction producing carbon-skinned metal particles, or metallic nanowires or nano-sheets covered with organic polymer matrices. This property leads us for application of photo-lithographical pattern generation of metallic circuits or magnetic arrays. On the other hand, the reaction mechanism of the photoreactions of the respective acetylide systems can be highly dependent on the electronic structure of metal atoms. We are also illuminating the mechanism of these reactions.

III-A-1 Electric Conductivity of Self-Assembled Copper Acetylide Nanowires and Nanocables

JUDAI, Ken; NISHIJO, Junichi; NISHI, Nobuyuki

[*Adv. Mater.* in press]

We have found that copper acetylide (C_2Cu_2) molecules self-assemble into ultra thin nanowires in an aqueous solution at room temperature, and annealing of the C_2Cu_2 nanowires converts to metallic copper nanowires encapsulated in carbon outer layers (nanocables). This copper nanocable core is extremely thin, in which only 8 Cu atoms can line up in the diameter. The electric conductivity of such thin wires becomes important for recent progress of electronic devices.

Actually, the current-voltage (I - V) measurement of the nanowires and nanocables was carried out by point-contact using an atomic force microscopy (AFM). Figure 1a illustrates a topological image of a C_2Cu_2 nanowire on Au substrate by AFM. The height observed by AFM was 5 ~ 6 nm, which corresponds to the diameter of a single C_2Cu_2 nanowire. By using a conductive cantilever, I - V properties could be observed with point-contacting through the nanowire. Figure 1b shows I - V characteristics of contacting onto the nanowire, and the nanocable after the annealing. Without nanowires and nanocables, the direct contact of the cantilever on the substrate showed a normal ohmic I - V property. As the cantilever was in contact with the nanowire, non-ohmic behavior was observed in I - V measurement. The band-gap of 0.5 ~ 1.5 eV was typically observed as the threshold voltages of the drastic increasing current.

When I - V characteristics of the converted nanocables was measured, much larger plateau of no current region was observed to be typically more than ~3 V. This

indicates that the nanocable exhibits insulating character through the point-contact by AFM. Annealing of the semiconductive C_2Cu_2 nanowires produced Cu nanowires covered with carbon outer layers. The AFM cantilever was contacting to this carbon outer layers. The measurement by AFM proves that the nanocable is coated with microscopic insulator.

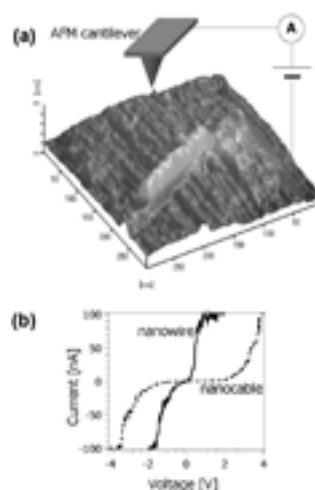


Figure 1. Electric conductive properties of C_2Cu_2 nanowires. (a) AFM image of a C_2Cu_2 nanowire on Au substrate. Schematic diagram is also supplemented for current-voltage (I - V) measurement. With using conductive cantilever (Au coated), current between the substrate and the cantilever through nanowires was measured. (b) I - V properties of nanowires and nanocables. Although the Au substrate showed ohmic I - V character, the C_2Cu_2 nanowire exhibited a non-ohmic property with a small band-gap (solid line). The converted Cu-nanocables covered with carbon provided insulating nature (dashed line).

III-A-2 Crystal Structure of C_2Cu_2 Nanowires by X-Ray Diffraction and DFT Calculation

JUDAI, Ken; NISHI, Nobuyuki

Copper acetylide (C_2Cu_2) molecules self-assemble into nanowires. The X-ray diffraction (XRD) measurement was performed to reveal stacking of C_2Cu_2 molecules in the nanowire. The sample of C_2Cu_2 nanowires exhibited several well-resolved peaks (Figure 1a). Peak widths of XRD measurement can be related to crystalline size by the Scherrer equation. Broader XRD peaks indicate smaller size. The coexistence of the sharp and broad signals for the crystals implies non-spherical crystalline structure of C_2Cu_2 .

The density functional theory (DFT) calculation was carried out to assign the XRD spectrum. Various crystal structures have been reported for alkali metal acetylide compounds. We have optimized C_2Cu_2 crystal structure from these reported structures as initial geometries. The obtained structure with the lowest energy is illustrated in Figure 1c, which is essentially the same as the structure of C_2Li_2 . The unit cell is orthorhombic (*Immm* No.71, $Z = 2$) with cell parameters of $a = 3.39 \text{ \AA}$, $b = 4.58 \text{ \AA}$, and $c = 5.57 \text{ \AA}$.

From the optimized crystal structure of C_2Cu_2 , XRD spectrum can be simulated. Peak intensity can be calculated from the Lorenz-Polarization factors and the structure factors using DFT optimized unit cell. Peak width can be estimated by the Scherrer equation depending on the size of crystal. When a needle-like crystal ($a = c = 5 \text{ nm}$, $b = 40 \text{ nm}$) was assumed for their peak broadness, the dominant peaks of the observed XRD spectrum could be reproduced by the simulation (Figure 1b). This simulation suggests that the driving force of self-assembling nanowire production is originated in the highly anisotropic character of the C_2 unit. The b -axis of C_2Cu_2 crystal is the direction of the C_2 unit. The line width in the observed spectrum suggests that the crystal grows along b -axis more rapidly than the other axes.

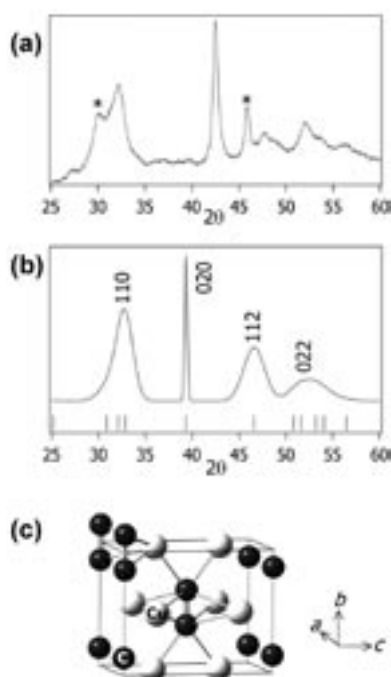


Figure 1. Crystal structure of C_2Cu_2 nanowires. (a) Powder XRD spectrum of C_2Cu_2 nanowires. The XRD results were acquired with X-ray of a Cu $K\alpha$ line (0.154 nm). (b) Simulated XRD spectrum from the DFT calculated structure. The peak widths were estimated by the Scherrer equation with assumption of a needle shape ($a = c = 5 \text{ nm}$, $b = 40 \text{ nm}$). The dominant peaks of experimental XRD can be reproduced in the simulation, however, there are still unidentified peaks (labeled with *) of another crystal form. (c) DFT optimized structure of C_2Cu_2 . The unit cell is orthorhombic and has body centered symmetry. C_2 units are coordinated with 4 Cu atoms in end-on sites and with 4 Cu atoms in side-on.

III-A-3 Photoconversion of Organometallic Cluster Thin Films to Metallic Copper-Sheets Sandwiched in Polymers

NISHI, Nobuyuki; NISHIJO, Junichi; JUDAI, Ken; OKABE, Chie; OISHI, Osamu

Generation of hot electrons in nanoparticles can be performed with efficient energy pumping from light harvesting π electron networks of organic matrices. Metallic copper is the best material for electronic conduction because of its low resistivity and enthalpy of fusion. $[Cu-C\equiv C-tBu]_{24}$ cluster molecules contain the light harvesting unit of ethynyl chromophore and the lowest excited π -d charge transfer triplet state. Photoexcitation of $[Cu-C\equiv C-tBu]_{24}$ films induces segregation of the crystals into metallic and organic phases and leads to evolve the metallic nanosheets sandwiched by organic polymers. High pressure mercury lamp irradiation for 2 hours produces copper nanoplates. KrF laser irradiation at a low power of 3 mJ/cm^2 also generates copper nanosheets, efficiently. Figure 1 displays the change of the TEM images of the film as functions of irradiated number of laser pulses, 120 shots (a), 1200 shots (b) and 9600 shots(c). In Figure 1-a, one can see the formation of nuclei of metallic particles. The wavy lattice patterns with 0.3 nm spacing are thought due to the alignment of the original cluster molecules and the disorder can be produced by the formation of metallic nuclei. Further irradiation causes planer crystals as seen in (b). The spacing of the lattice pattern is regular and the interval is 0.26 nm. At this stage, the crystals exhibit grain boundaries with several 10 nm scales. In the planes dominated with metallic plates, one can find white matrix rooms composed of segregated (*t*butyl-ethynyl) $_n$ polymers. However, further photon impact fills these spaces with joining metallic particles or plates nearby located on the lower side and made them into larger crystalline sheets as seen in Figure 1-c, where not only the (111) plane but also the (110) plane of copper fcc crystals are seen with a lattice spacing of 0.26 and 0.36 nm, respectively.

In Figure 1-d, we show schematic explanation of the evolution of small particles to a nanosheet in the photon field. The observed phenomenon can be explained by plasmon-plasmon interaction induced by the photon electromagnetic field and surface enhanced photochemical reactions of the residual ethynyl copper cluster molecules that may also supply heat for rearrangement of metal atoms in the joining particles or sheets. Energy supply to metallic particles from light harvesting organic matrices can be also important to increase the internal

temperature of the metals.

Figure 1-e displays a cross-sectional view of the film deposited on a polyimide film after the irradiation of KrF laser pulses (12000 shots). Photolithographic dot patterning observed by a SEM is shown in Figure 1-f that was made with a chromium photo-mask and washing the residual cluster molecules by hexane. Each dot is spaced at every 1 μm . The surface is covered with the polymer layer thinner than 50 nm that is easily removed by laser sputtering.

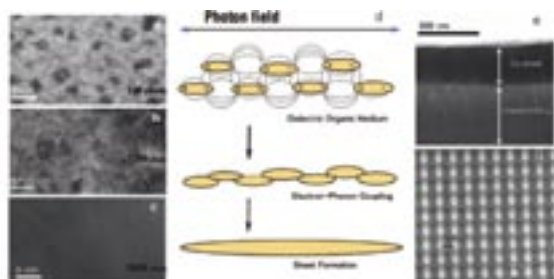


Figure 1. High resolution TEM images of the film as functions of irradiated number of laser pulses, 120 shots (a), 1200 shots (b) and 9600 shots(c). Laser energy density was 3 mJ/cm². (d) is schematic explanation of the evolution of small particles to a nanosheet in the photon field. (e) is a cross-sectional view of the film deposited on a polyimide film after the irradiation of KrF laser pulses (12000 shots). (f) is photolithographic copper-dot patterning obtained with a chromium photo-mask and washing the residual cluster molecules by hexane. Since, the copper surface is covered by thin polymer layer, copper parts look white.

III-A-4 Synthesis of Carbon-Encapsulated Nanoparticles via Thermal Decomposition of Metal Acetylide

NISHIJO, Junichi; OKABE, Chie; OISHI, Osamu; NISHI, Nobuyuki

[Carbon in press]

Carbon-encapsulated metal nanoparticles are promising materials for application in magnetic storage and battery due to their chemical stabilities. Though there are several methods of synthesizing the carbon-encapsulated nanoparticles such as arc discharge and thermal decomposition of hydrocarbons, the methods are not suitable for size-selective synthesis or mass production. Furthermore, the methods require a high temperature treatment which makes it difficult to synthesize carbon-encapsulated nanoparticles of metastable phases and low melting point metals. To solve these problems, we developed a new synthesis method for the carbon-encapsulated nanoparticles, where the carbon-encapsulated materials are formed by the low temperature thermal decomposition of the metal acetylide.

The acetonitrile suspension of metal chloride MCl_2 and calcium carbide CaC_2 sealed into the airtight vessel is heated to 240 $^\circ\text{C}$ for 12 h. In the solution, CaC_2 is gradually dissolved, and C_2^{2-} and M^{2+} form nanosized ionic cluster $(\text{M}^{2+}\text{C}_2^{2-})_n$ in the solution. Owing to the strong reducibility of C_2^{2-} , the cluster is converted into neutral metal-carbon cluster $(\text{M}^0\text{C}_2^0)_n$ by thermal

energy. This neutral cluster is unstable because it can be regarded as metal-carbon supersaturated solid solution. As a result, metal atoms exclude the excess carbons and form carbon-encapsulated carbon-saturated metal nanoparticles. Figures 1 show the TEM images of carbon-encapsulated metal nanoparticles (M@C) of Sn, Pd, Ni and Co. As shown in the figures, each particle is covered with a carbon shell with the thickness of 2–6 nm which protects the metal or metal carbide core from the oxidation even in 1 M HCl(aq). The average core sizes depend on the metals; that is, 25, 8, 14 and 15 nm for M = Sn, Pd, Ni and Co, respectively.

The XRD patterns reveal the peculiar structures of the metallic cores. The core of Sn@C is pure metallic β -Sn, which reflects the instability of tin-carbide. On the other hand, other three metals prefer the carbide phases to metallic phases. The XRD pattern of Pd@C is explained as the sum of usual *fcc* and unusual *hcp* palladium carbide phases which has not been reported. In the case of M = Ni, Ni_3C phase is formed selectively. In contrast to the crystalline core structures mentioned above, the core of Co@C is almost all amorphous cobalt-carbon solid solution.

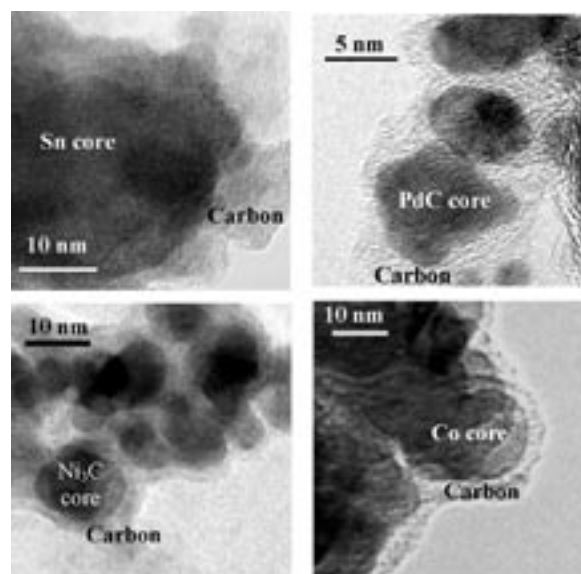


Figure 1. TEM images of carbon-encapsulated metal/metal carbide nanoparticles synthesized by thermal decomposition of metal-acetylide.

III-A-5 Synthesis, Structure and Magnetic Properties of a New Low-Spin Iron(III) Complex $[\text{FeL}_3]$ $\{\text{L} = [\text{HNC}(\text{CH}_3)]_2\text{C}(\text{CN})\}$

NISHIJO, Junichi; NISHI, Nobuyuki

[Eur. J. Inorg. Chem. 3022–3027 (2006)]

High temperature treatment of acetonitrile with CaC_2 and FeCl_2 affords the new iron (III) *S* = 1/2 low-spin complex $[\text{FeL}_3]$ ($\text{L} = [\text{HN}=\text{C}(\text{CH}_3)]_2\text{C}(\text{CN})$). The crystal structure and the inter-molecular overlap mode are largely affected by the crystal solvent ROH (R = Me, Et). In the $[\text{FeL}_3]\text{MeOH}$ crystal, each MeOH molecule attracts $[\text{FeL}_3]$ complexes and disturb ligand–ligand interaction, resulting in the small overlap between adja-

cent complexes. On the contrary, $[\text{FeL}_3]$ complexes form one-dimensional tunnel structure filled with EtOH molecules, where the inter-complex overlap is much larger as shown in Figure 1. The difference between the overlaps affects the inter-complex spin-spin interaction. The small overlap of $[\text{FeL}_3]\text{MeOH}$ brings the negligibly small interaction, resulting in the Curie-like behavior of the spin. On the other hand, $[\text{FeL}_3]\text{EtOH}$ behaves as singlet-triplet spin system with the interaction $2J/k_B = -7.5$ K caused by stronger spin-spin interaction between adjacent complexes, which is originated from the large overlap between the π -electrons of the ligands. The EtOH crystal solvent can be easily removed only by evaporation owing to the tunnel structure of $[\text{FeL}_3]\text{EtOH}$, where the inter-complex interaction is reduced to negligibly small.

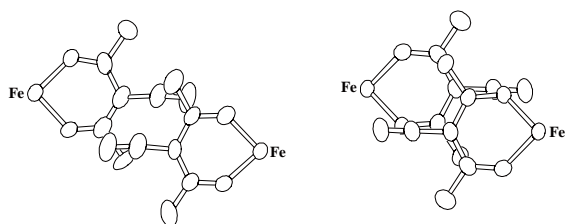


Figure 1. The inter-complex overlap mode of $[\text{FeL}_3]\text{MeOH}$ (left) and $[\text{FeL}_3]\text{EtOH}$ (right).

III-A-6 Preparation and Characterization of Gold Nanoparticles with Reactive Thiocarbonyls: A Proposal for Active Size Control of Nanoparticles

HINO, Kazuyuki¹; NAKANO, Hirofumi¹; ITO, Naomi¹; MATSUSHITA, Machiko¹; TAKAGI, Hideyuki¹; NISHI, Nobuyuki
(¹Aichi Univ. Educ.)

[*Trans. Mater. Res. Soc. Jpn.* **31**, 525–528 (2006)]

Gold nanoparticles are prepared by using methyl-substitute 1,3-oxathiole-2-thione as a stabilizing reagent in the hydride reduction of tetrachloroaurate(III) ions. UV-vis absorption spectra and electron microscope observation show that the particle size can be controlled in a wide range from subnanometer to nanometer scale. Comparison of the results for these particles with those formed using methyl-substituted 1,2,4-trithiolane leads us to attribute the initial process of the formation of subnanometer-sized particles to the dimerization of 1,3-oxathiole-2-thione derivatives. In the reaction process, nascent particle surface is passivated with dimerization intermediates and the particle growth is terminated by sulfide formation.

III-B Ultrafast Dynamics and Scanning Tunneling Microscopy

Proton transfer and geometrical isomerization processes in electronic excited states are investigated with our pico-femto dual wavelength valuable systems. For the study of molecules on metallic or crystalline surface, very low temperature Scanning Tunneling Microscope (LT STM) system are now in use for collaboration with users in universities

III-B-1 Ultrafast Dynamics of Excited States of Chromium(III) Porphyrin Complexes in Solution

INAMO, Masahiko¹; OKABE, Chie;
NAKABAYASHI, Takakazu²; HOSHINO, Mikio³;
NISHI, Nobuyuki
(¹Aichi Univ. Educ.; ²Hokkaido Univ.; ³RIKEN)

Cr(III) porphyrin complexes show variety of chemical reactivity and photophysical processes in their electronic excited states. In the present study, relaxation dynamics of the excited states following the Soret band excitation of the Cr(III) tetraphenylporphyrin complexes, $[\text{Cr}(\text{TPP})(\text{Cl})(\text{L})]$ ($\text{L} = \text{H}_2\text{O}$, Py, 1-MeIm), has been investigated using femtosecond time-resolved absorption spectroscopy in the toluene solution. The dynamics of the decay of the transient absorption spectra measured within a time domain of 400 ps is discussed with the various physical and chemical processes. In the case of $[\text{Cr}(\text{TPP})(\text{Cl})(\text{H}_2\text{O})]$, the biexponential decay of the initially populated excited state was observed with rate constants of $k_1 = 6.8 \times 10^{10} \text{ s}^{-1}$ and $k_2 = 1.6 \times 10^9 \text{ s}^{-1}$. These processes were assigned to the photodissociation of a H_2O ligand in the $^4\text{S}_1$ excited state followed by the

energy dissipation to electronically ground state $[\text{Cr}(\text{TPP})(\text{Cl})]$. On the contrary, the 1-MeIm complex $[\text{Cr}(\text{TPP})(\text{Cl})(1\text{-MeIm})]$, in which only the triplet excited state was observed using nanosecond transient spectra, shows a single exponential decay of the excited state. This was assigned to the decay of $^4\text{S}_1$ to T_1 with a rate constant of $3.8 \times 10^9 \text{ s}^{-1}$. The excitation to S_2 , the Soret band, occurs for 395 nm excitation followed by the intramolecular process of electronic, vibrational, and singlet-triplet relaxation with time scales of subfemtosecond, subpicosecond, and nanosecond, respectively, for a free base porphyrin. These findings indicate that the initially observed excited states in the present study may be $^4\text{S}_1$, and the S_2 to S_1 relaxation may be too fast to be observed in the present measurement. The lifetime of the $^4\text{S}_1$ excited states of $[\text{Cr}(\text{TPP})(\text{Cl})(1\text{-MeIm})]$ is much shorter than those of the porphyrin species that produce no paramagnetic ion due to the presence of the Cr(III) ion, but substantially longer than those of paramagnetic complexes such as $[\text{Cu}(\text{TPP})]$.

III-B-2 Scanning-Tunneling Microscopy, Near-Edge X-Ray-Absorption Fine Structure, and Density-Functional Theory Studies of N₂O Orientation on Pd(110)

WATANABE, Kazuo¹; KOKALJ, Anton²; HORINO, Hideyuki³; RZEZNICKA, Izabela I.²; TAKAHASHI, Kazutoshi³; NISHI, Nobuyuki; MATSUSHIMA, Tatsuo³

(¹Fritz-Haber-Inst Max-Planck-Gesellschaft; ²J. Stefan Inst.; ³Hokkaido Univ.)

[*Jpn. J. Appl. Phys.* **45**, 2290–2294 (2006)]

The orientation of adsorbed N₂O on Pd(110) was studied by scanning tunneling microscopy, near-edge X-ray absorption fine structure (NEXAFS), and density functional theory. Below 14 K, N₂O(a) forms clusters extending along the [110] direction as well as monomers oriented along the [001] direction. In the clusters, N₂O is tilted with the terminal nitrogen bonding to the surface. The clusters are mobile at 14 K and stable at 8 K, whereas the monomers are stable at 14 K. In NEXAFS work at 60 K, remarkable anisotropy was found in the polarization dependence of π resonance, which was consistent with a mixture of the tilted and [001]-oriented forms.

III-C Spectroscopic and Dynamical Studies of Molecular Cluster Ions

Electron deficiency of molecular cluster cations can attract electron rich groups or atoms exhibiting charge transfer or charge resonance interaction in the clusters. This causes dynamical structural change such as proton transfer or ion-core switching in hot cluster ions or clusters in solution.

III-C-1 IR Photodissociation Spectroscopy of Hydrated Noble Metal Ions: Coordination and Solvation Structures

IINO, Takuro¹; INOUE, Kazuya¹; OHASHI, Kazuhiko¹; MUNE, Yutaka¹; INOKUCHI, Yoshiya²; JUDAI, Ken; NISHI, Nobuyuki; SEKIYA, Hiroshi¹
(¹Kyushu Univ.; ²Hiroshima Univ.)

Hydrated noble metal ions, M⁺(H₂O)_n (M = Cu, Ag), are studied by infrared photodissociation spectroscopy and density functional theory calculations. The third water in Cu⁺(H₂O)₃ is hydrogen-bonded to one of the two waters coordinated to Cu⁺, while all waters in Ag⁺(H₂O)₃ are directly bonded to Ag⁺. The difference in the coordination number is attributable to the different degree of *s-d* hybridization between Cu⁺ and Ag⁺.

III-D Development of High-Precision Coherent Control and Its Applications

Coherent control is based on manipulation of quantum phases of wave functions. It is a basic scheme of controlling a variety of quantum systems from simple atoms to nanostructures with possible applications to novel quantum technologies such as bond-selective chemistry and quantum computation. Coherent control is thus currently one of the principal subjects of various fields of science and technology such as atomic and molecular physics, solid-state physics, quantum electronics, and information science and technology. One promising strategy to carry out coherent control is to use coherent light to modulate a matter wave with its optical phase. We have so far developed a high-precision wave-packet interferometry by stabilizing the relative quantum phase of the two molecular wave packets generated by a pair of femtosecond laser pulses on the attosecond time scale. We will apply our high-precision quantum interferometry to gas, liquid, solid, and surface systems to explore and control various quantum phenomena.

III-D-1 Visualizing Picometric Quantum Ripples of Ultrafast Wave-Packet Interference

KATSUKI, Hiroyuki¹; CHIBA, Hisashi¹; GIRARD, Bertrand²; MEIER, Christophe²; OHMORI, Kenji¹ (¹IMS and JST/CREST; ²Univ. Paul Sabatier (Toulouse III))

[*Science* **311**, 1589–1592 (2006)]

Interference fringes in vibrating molecules are a signature of quantum mechanics, but are often so short-lived and closely spaced that they elude visualization. We have experimentally visualized dynamical quantum interferences, which appear and disappear in less than 100 femtoseconds in the iodine molecule synchronously with the periodic crossing of two counterpropagating nuclear wave packets. The obtained images have picometer and femtosecond spatiotemporal resolution, representing a detailed picture of the quantum interference.

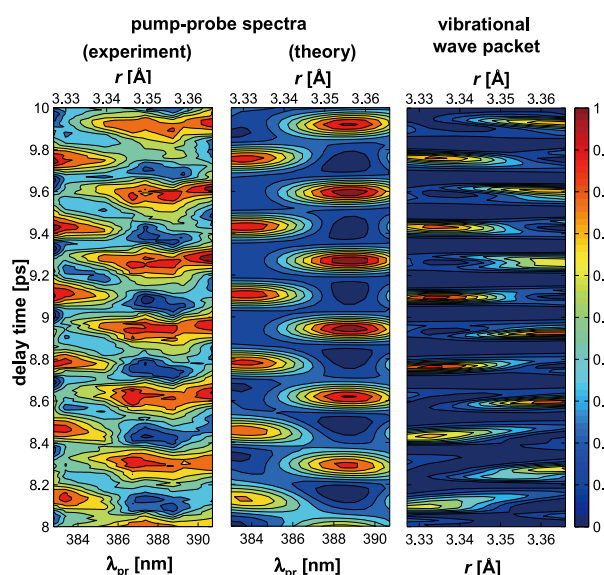


Figure 1. Contour plots of the experimental pump-probe signal (left), the simulated pump-probe signal (middle), and parts of the vibrational wave packet (right). The pump-probe spectra clearly reflect the spatiotemporal nodal structure of the wave-packet interferences.

[Reprinted with permission from *Science* **311**, 1589–

1592 (2006). Copyright (2006) American Association for the Advancement of Science.]

III-D-2 Real-Time Observation of Phase-Controlled Molecular Wave-Packet Interference

OHMORI, Kenji¹; KATSUKI, Hiroyuki¹; CHIBA, Hisashi¹; HONDA, Masahiro^{2,3}; HAGIHARA, Yusuke^{2,3}; FUJIWARA, Katsutoshi³; SATO, Yukinori^{2,3}; UEDA, Kiyoshi^{2,3} (¹IMS and JST/CREST; ²JST/CREST; ³Tohoku Univ.)

[*Phys. Rev. Lett.* **96**, 093002 (4 pages) (2006)]

The quantum interference of two molecular wave packets has been precisely controlled in the *B* electronic state of the I_2 molecule by using a pair of fs laser pulses whose relative phase is locked within the attosecond time scale and its real time evolution has been observed by another fs laser pulse. It is clearly observed that the temporal evolution changes drastically as a function of the relative phase between the locked pulses, allowing us to read both amplitude and phase information stored in the wave functions of the molecular ensemble.

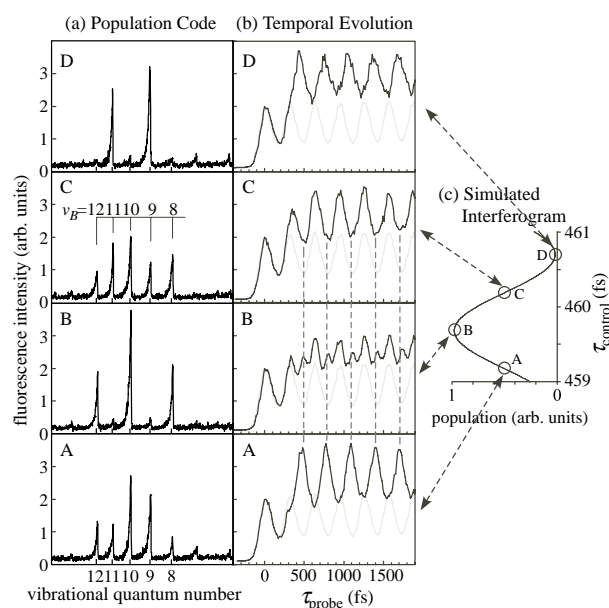


Figure 1. Wave packet interference measured and simulated with the pump and control delay τ_{control} tuned to $\sim 1.5 T_{\text{vib}}$ (~ 460 fs), where T_{vib} is a classical vibrational period of I_2 . (a) E - B excitation spectrum, which we call the “POPULATION CODE,” measured by scanning the wavelength of the ns probe pulse delayed by ~ 35 ns from the pump and control pulses. The relative phase θ_{p-c} of the pump and control pulses is increased in steps of $\sim \pi/2$ in going from code A to code D. (b) Real time evolutions of the wave-packet interference measured with the same θ_{p-c} 's as for codes A-D. The shaded trace is the evolution measured without the control pulse and is displayed for reference. Each trace is a summation of four repeated scans. The origin of the probe delay ($\tau_{\text{probe}} = 0$) denotes a position of the top of the first undulation in each measured trace. The vertical scaling of each trace is arbitrary and is normalized by the height of its first undulation. (c) Simulation of τ_{control} -dependence of the population of $v_B = 10$. The arrows stand for approximate correspondences in θ_{p-c} , and not in the absolute values of τ_{control} .

[Reprinted with permission from *Phys. Rev. Lett.* **96**, 093002 (4 pages) (2006). Copyright (2006) American Physical Society.]

III-D-3 Implementation of Quantum Gate Operations in Molecules with Weak Laser Fields

TERANISHI, Yoshiaki¹; OHTSUKI, Yukiyo¹;
 HOSAKA, Kouichi²; CHIBA, Hisashi²; KATSUKI,
 Hiroyuki²; OHMORI, Kenji²
 (¹Tohoku Univ. and JST/CREST; ²IMS and JST/CREST)

[*J. Chem. Phys.* **124**, 114110 (9 pages) (2006)]

We numerically propose a way to perform quantum computations by combining an ensemble of molecular states and weak laser pulses. A logical input state is expressed as a superposition state (a wave packet) of molecular states, which is initially prepared by a designed femtosecond laser pulse. The free propagation of the wave packet for a specified time interval leads to the specified change in the relative phases among the molecular basis states, which corresponds to a computational result. The computational results are retrieved by means of quantum interferometry. Numerical tests are implemented in the vibrational states of the B state of I_2 employing controlled-NOT gate, and 2 and 3 qubits Fourier transforms. All the steps involved in the computational scheme, *i.e.*, the initial preparation, gate operation, and detection steps, are achieved with extremely high precision.

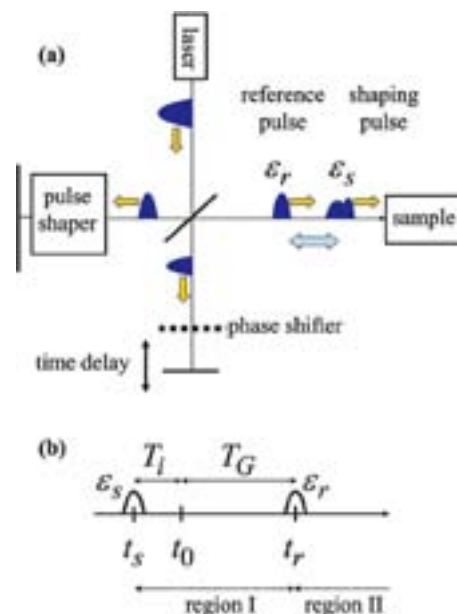


Figure 1. (a) Schematic of the experimental setup. (b) Pulse sequence for quantum computation. The times, t_s , t_0 , and t_r , specify the temporal peak of the shaping pulse, the initial separation time, and the temporal peak of the reference pulse, respectively. The time intervals are referred to as the input preparation time $T_i = t_0 - t_s$ and the gate operation time $T_G = t_r - t_0$.

[Reprinted with permission from *J. Chem. Phys.* **124**, 114110 (9 pages) (2006). Copyright (2006) American Institute of Physics.]

III-E Quantum-State Manipulation of Molecular Motions

Molecules in gas phase undergo translational, rotational and vibrational motions in a random manner, and the total molecular system is a statistical ensemble that contains a number of molecules in many different states of motions. This research group aims to establish methods to manipulate the quantum-state distribution pertinent to molecular motions, by utilizing the coherent interaction with laser lights. Three complement methods are now being explored for manipulation of molecular motions. The first method exploits an impulsive interaction with ultrafast intense laser light to transform the initial distribution into an arbitral non-equilibrium one. We have succeeded in applying the method to nonadiabatic rotational population transfer in various molecular systems. The second one employs creation and detection of molecular wavepackets by fs pump-probe experiments. Experimental methods newly developed in this laboratory have been applied to probing vibrational wavepackets associated with internal rotation of jet-cooled polyatomic systems. The third one utilizes an adiabatic interaction to achieve the complete population transfer, by which all the molecules are launched into states with high excitation of vibrations or rotation. We have constructed ns laser systems with sufficiently high frequency resolution to drive the adiabatic coherent interaction. Along the development of the instruments, appropriate candidates for the quantum-state adiabatic manipulation are searched. Laser spectroscopic studies are carried out to explore energy-level structure of the intermolecular vibrations in molecular clusters containing benzene.

III-E-1 Nonadiabatic Population Transfer by Intense Femtosecond Laser Light

HASEGAWA, Hirokazu; OHSHIMA, Yasuhiro

A new vacuum chamber was constructed for the study of nonadiabatic population transfer processes induced by intense fs laser light, and has been utilized to explore the rotational excitation of NO. A fundamental output (~800 nm, ~120 fs duration, and < 1 mJ/pulse) of a titanium-sapphire laser was introduced to transiently align NO molecules, which were initially jet-cooled to < 2 K where states with $J = 0.5$ were only populated. Rotational distribution after the impulsive excitation was monitored by two-photon resonance enhanced ionization by ns laser pulses through the A-X(0,0) transition. States with up to $J = 8.5$ were populated through the nonadiabatic transfer process, and characteristic population alternation in J was identified. A model calculation has been performed to quantitatively explain the observations. The excitation is achieved through a ladder climbing mechanism by Raman process with $\Delta J = \pm 1$ and ± 2 . Because the transition probabilities with $\Delta J = \pm 2$ are much larger than those with $\Delta J = \pm 1$ and the initial distribution is restricted only to $J = 0.5$, populations in $J = 2.5, 4.5, 6.5, \dots$ become superior.

For further detailed insight into the nonadiabatic rotational excitation, experiments utilizing double excitation pulses with an appropriate delay in time have been performed. Population of each rotational state changes oscillatory against the delay, with frequency components matching with rotational-energy differences. It has been shown the rotational states are grouped into two, in which states strongly couples *via* $\Delta J = \pm 2$ matrix elements to form the coherent superposition. The two groups are weakly coupled to each other *via* $\Delta J = \pm 1$ matrix elements. Such an excitation process is typical to molecules in degenerate states.

In addition to the simple diatomic molecule NO, much larger molecular systems, *i.e.*, benzene and styrene, have been examined for the nonadiabatic rotational excitation by intense short laser pulses. These successful applications demonstrate the potential of the present

method in manipulation of quantum-state distribution of various types of molecules.

III-E-2 Wavepacket Observation of Methyl Internal Rotation in Substituted Toluenes

KITANO, Kenta¹; MIYAZAKI, Mitsuhiko²; HASEGAWA, Hirokazu; OHSHIMA, Yasuhiro
(¹Kyoto Univ.; ²IMS and Tokyo Tech)

Femtosecond (fs) time-domain experiments have been performed in the S_1 - S_0 origin regions of jet-cooled *o*-fluorotoluene and *m*-cresol to explore the wavepacket dynamics associated with internal rotation of the methyl group. The COIN (Coherence Observation by Interference Noise) method, a variant of fs interferometry,¹ has been applied to observe quantum beats, of which frequencies correspond to differences between vibronic transitions. Time-resolved fluorescence depletion (TRFD)² has been implemented in fs domain for the first time, where change in excited-state population induced by the pump-dump process was monitored as fluorescence depletion. In *o*-fluorotoluene, quantum interferences in S_1 were exclusively observed in the TRFD spectrum. Comparison with the COIN and TRFD data allows us to reconstruct the vibronic band structure without ambiguity. On the other hand, TRFD spectrum of *m*-cresol was dominated by quantum beats in S_0 , because the separations between internal-rotation levels are smaller in S_0 than in S_1 . The modulation amplitude of the beats reached to 5% of the total fluorescence, indicating substantial coherent population transfer to excited internal-rotation states in S_0 *via* Rabi oscillation induced by the pump pulse.

References

- 1) O. Kinrot, I. Sh. Averbukh and Y. Prior, *Phys. Rev. Lett.* **75**, 3822 (1995).
- 2) M. J. Côté *et al.*, *J. Chem. Phys.* **90**, 2865 (1989); G. V. Hartland, L. L. Connell and P. M. Felker, *J. Chem. Phys.* **94**, 7649 (1991).

III-E-3 Development of High-Resolution Coherent Pulsed Lasers

OHSHIMA, Yasuhiro; SUMA, Kosuke

We are constructing a pulsed laser system with Fourier-transform (FT) limited resolution for quantum-state manipulation by coherent light-matter interaction, such as stimulated Raman adiabatic passage. In the system, the output from a cw ring titanium-sapphire laser seeds a pulsed dye amplifier pumped by a single-mode Nd:YAG laser. The laser system delivers the output power of 30 mJ/pulse at around 780 nm, with spectral bandwidth of 200 MHz ($< 0.007 \text{ cm}^{-1}$). This fundamental output is tripled by nonlinear crystals to have UV radiation at 260 nm, which is suitable to excite S_1-S_0 transitions of the benzene molecule and its van der Waals clusters.

In addition to the pulsed amplifier system, an all solid-state pulsed laser system based on the optical parametric oscillation (OPO) pumped by the Nd:YAG laser is now in under construction. The OPO system is injection-seeded by an extra-cavity cw diode laser. For stable external seeding operation, the ring-type cavity is adopted for the OPO. The frequency locking mechanism for the cavity is now designed and constructed. This OPO system will deliver the almost FT-limited ns pulse with $> 10 \text{ mJ/pulse}$ at 520 nm.

III-E-4 Laser Spectroscopy of the van der Waals Vibrations of Benzene-Water

MIYAKE, Shin-ichiro¹; MIYAZAKI, Mitsuhiro²; OHSHIMA, Yasuhiro

(¹Kyoto Univ.; ²IMS and Tokyo Tech)

Benzene-water is a prototypical system containing the π hydrogen bond. We have recently examined in detail the vibronic spectra of various isotopomers of the benzene-water 1:1 cluster pertaining to the S_1-S_0 6_0^1 transition of the benzene moiety, recorded by utilizing resonance two-photon ionization (R2PI) time-of-flight mass spectrometry. UV-UV hole-burning measurement has been performed to observe weak vibronic bands, which are buried in the R2PI excitation spectrum by background signals due to fragmentation of higher clusters. For the H_2O isotopomer, bands from the $m = 0$ and ± 1 internal-rotation states were separately observed by probing split components in the 6_0^1 origin. A dozen of bands with intermolecular mode excitation clearly appeared in the region up to 160 cm^{-1} . Observed level structure was compared with the 6D dynamical calculation by Felker and co-workers¹ based on the model potential by Karlström *et al.*² Levels pertaining to the vdW stretching and bending modes show reasonable agreements between observation and calculation, while states probably associated to the 3D internal rotation of water unit exhibit extremely large discrepancies. This result indicates the necessity for the substantial refinement in the model potential, especially for its anisotropic part (*i.e.*, angular dependence on the 3D internal-rotation coordinates).

References

- 1) W. Kim *et al.*, *J. Chem. Phys.* **110**, 8461 (1999).
- 2) G. Karlström *et al.*, *J. Am. Chem. Soc.* **105**, 3777 (1983).

III-F Spectroscopy of Jet-Cooled Aromatic Molecules and Photochemical Reaction of Aza- and Thio-Substituted Nucleobases

The phenomena of energy relaxation in isolated molecules have been essential issue in chemical dynamics over many decades. The laser spectroscopy coupled with the jet expansion gives us much information on molecular structure and relaxation processes. The substituent of the $-NH_2$ or $-SCH_3$ group should play an important role for the structure and the relaxation processes in their excited states.

Transient molecules such as excited states and chemical intermediates, which can be generated with laser irradiation, have been detected by laser flash photolysis. Time-resolved photothermal techniques are powerful to study nonradiative processes because they can detect the released heat from excited molecules directly with high sensitivity. Combination of photoexcited and photothermal methods will give us detailed information on photophysical and photochemical dynamics of intermediates, as well as excited states.

III-F-1 Conformation of 2-Aminoindan in a Supersonic Jet: The Role of N–H $\cdots\pi$ Hydrogen Bonding

IGA, Hiroshi¹; ISOZAKI, Tasuku¹; SUZUKI, Tadashi¹; ICHIMURA, Tejiro²
(¹Tokyo Tech; ²IMS and Tokyo Tech)

Weak intramolecular hydrogen bonding has attracted considerable attention of many researchers because it would govern chemical and physical properties of flexible molecules. Previously, we studied 1-aminoindan in a supersonic jet expansion, and two rotational isomers stabilized by an intramolecular N–H $\cdots\pi$ hydrogen bonding were observed. To further understand the interaction we investigate the effect of the position of the substitution. We measured laser-induced fluorescence (LIF) and dispersed fluorescence spectra of 2-aminoindan (2-AI). Three series of bands in the LIF spectrum were observed, and were assigned to the corresponding conformational isomers with the aid of *ab initio* calculation at the MP2/6-311+G(d,p). A hydrogen atom of the amino group in the most stable conformer points toward the benzene ring, suggesting the contribution of an intramolecular hydrogen bonding between the hydrogen atom and the π -electron of the benzene ring. The contribution of the extremely weak intramolecular hydrogen bonding to the molecular structure of 2-AI was elucidated. The strength of the hydrogen bonding of 2-AI was discussed in detail.

III-F-2 Conformation of Thioanisole in a Supersonic Jet

NAGASAKA, Mariko¹; ISOZAKI, Tasuku¹; SUZUKI, Tadashi¹; ICHIMURA, Tejiro²
(¹Tokyo Tech; ²IMS and Tokyo Tech)

It is suggested that thioanisole has a planar and perpendicular conformers with respect to the rotation of methylthio group around the C(sp²)–S bond. Despite of many experimental and theoretical attempts, the most stable conformer and potential energy curves are still of subject because the experimental and theoretical results are not consistent each other. In this study, to elucidate the molecular structure of thioanisole in S₀ and S₁ states

we measured the laser-induced fluorescence (LIF) and dispersed fluorescence (DF) spectra of thioanisole in a supersonic jet. We can firmly conclude that the most stable conformer in the S₀ and S₁ states is the planer conformer. In the LIF spectrum, low-frequency out-of-plane torsional mode, which is only allowed if their quantum numbers change by an even number, was observed relatively intensive. It is suggested that in the S₁ state structure of thioanisole is slightly twisted outside the benzene ring.

III-F-3 Excited-State Dynamics of 6-Azauracil with UVA Light Irradiation

KOBAYASHI, Takashi¹; HARADA, Yosuke¹; SUZUKI, Tadashi¹; ICHIMURA, Tejiro²
(¹Tokyo Tech; ²IMS and Tokyo Tech)

Analogues of nucleobases have been paid much attention because of distinct properties to originals. Aza-nucleobase, including a N atom into the skeleton of the nucleobase molecule, is one of the well-known analogues for anti-neoplastic and fungistatic properties. For the wide application, it is important to obtain information on relaxation and reaction mechanism of photo-excited nucleobase analogues.

We have measured transient absorption spectrum of 6-Azauracil (6-AU) in deaerated acetonitrile with the nanosecond 248 nm laser. Immediately after the laser shot, an absorption band peak at 320 nm and a broad absorption band at 500–700 nm were observed. The absorption bands are assigned to the lowest excited triplet (T₁) state of 6-AU (T–T absorption). The T–T absorption decayed with the rate constant of 5.0×10^6 s⁻¹. With the time-resolved thermal lensing experiment, it was found that the triplet 6-AU produces singlet oxygen (¹ Δ_g) efficiently.

III-F-4 Ultrafast Excited-State Dynamics of 4-Thiothymidine in Aqueous Solution

HARADA, Yosuke¹; SUZUKI, Tadashi¹; ICHIMURA, Tejiro²; OKABE, Chie; NISHI, Nobuyuki
(¹Tokyo Tech; ²IMS and Tokyo Tech)

Thionucleobases and thionucleosides have received renewed attention because of high sensitivity to UVA light (320–400 nm) in which region normal DNA constituents are transparent. 4-Thiothymidine (s^4 -TdR), an analogue of the naturally occurring nucleoside thymidine, has strong absorption in the UVA region. Recently it was reported that s^4 -TdR can be readily incorporated into cellular DNA and that low doses of UVA light can easily inflict lethal damage on the DNA containing s^4 -TdR, causing cell death. The synergistic use of s^4 -TdR and UVA light offers a novel approach to cancer treatment. Apparently, electronically excited state of s^4 -TdR is at the initial and crucial stage of the UVA-induced cell killing, and thus photophysical and photochemical studies of s^4 -TdR would be of great significance. Recently, we elucidated that the major process of deactivation of photoexcited s^4 -TdR is intersystem crossing (ISC) to triplet manifolds, and the quantum yield for ISC of s^4 -TdR to be unity. In this study, ultrafast transient absorption measurement was performed with the pump-probe technique in order to obtain more detailed information

on the $S \rightarrow T$ ISC process.

We have measured a time profile of the transient absorption of s^4 -TdR in aqueous solution (pH 7.4) monitored at 570 nm obtained by 263 nm femtosecond laser excitation. The transient absorption emerged within the instrumental response time (< 0.50 ps) and decayed with the decay time of 10 ps. We have also measured a time profile of the transient absorption of thymidine (TdR) under the same experimental condition for s^4 -TdR. The transient absorption emerged by the excitation decayed immediately to the initiate level, and it was found the transient should decay with time constant of equal or faster than 0.50 ps. For both cases of s^4 -TdR and TdR, the observed transients should be assigned to be their excited singlet states, and the decay rate constants of the transient absorption should be regarded as the lifetime of the excited singlet states. It was clarified that s^4 -TdR decays much slowly (10 ps) compared with TdR (0.5 ps), and the $S \rightarrow T$ ISC process of s^4 -TdR should take place with time of approximately 10 ps.

III-G Photochemical Reactions in Microreactors

In the last decade, microreaction system has developed using the features unique to microspace such as short molecular diffusion distance, excellent heat transfer characteristics, laminar flow, and large surface-to-volume ratio. Although microreaction systems are successfully examined in a wide range of applications of analytical and organic chemistry, there are only several reports on photoreactions in microreactors as described in the following section. We can expect microreactors to exhibit higher spatial illumination homogeneity and better light penetration through the entire reactor depth in comparison to large-scale reactors. Thus, we are investigating applications of microreactors on organic photoreactions.

III-G-1 Application of Microreactors for Photoreactions

**ICHIMURA, Teijiro¹; MATSUSHITA, Yoshihisa²;
SAKEDA, Kosaku²; SUZUKI, Tadashi²**
(¹IMS and Tokyo Tech; ²Tokyo Tech)

[Photoreactions, in *Microchemical Engineering in Practice*, T. R. Dietrich, Ed., Blackwell Publishing (2006)]

We investigated effects of residence time, reaction temperature, laser power, and excitation wavelength on photosensitized enantio- and diastereo-differentiating reactions in microreactors. Photonic efficiencies of model reactions were considerably larger than those in conventional batch reactors. Further, the yield of photosensitized diastereodifferentiating addition of methanol to terpenes was greatly improved in the microreactor.

Photocatalytic oxidation of endocrine disruptors, reduction of organic compounds, and amine alkylation processes were investigated in a microreactor with immobilized photocatalytic TiO₂ layer. Apparent reaction rates in microreactors were much larger than those in conventional batch reactors. A photocatalytic process of N-alkylation of benzylamine in alcohol media was successfully observed by using microreactors with immo-

bilized Pt-free TiO₂ as well as Pt-loaded TiO₂, while it has been reported that the N-alkylation didn't occur by the irradiation of Pt-free TiO₂ in conventional batch reactors. The study on the oxidation process of olefins by using a multiphase-photocatalytic microreactor was also reported.

III-G-2 Photocatalytic Reduction in Microreactors

**MATSUSHITA, Yoshihisa¹; KUMADA, Shinji¹;
WAKABAYASHI, Kazuhito¹; SAKEDA, Kosaku¹;
ICHIMURA, Teijiro²**
(¹Tokyo Tech; ²IMS and Tokyo Tech)

[*Chem. Lett.* **35**, 410–411 (2006)]

Photocatalytic reduction of benzaldehyde and nitrotoluene in microspace was investigated by using a microreactor with immobilized titanium dioxide. Since a photocatalytic reaction takes place on an irradiated titanium dioxide surface, a microfabricated reactor which has a large surface-to-volume ratio must prove its advantages on the reaction.

Photoreduction was carried out with a microreactor made of quartz which has a microchannel of 500 μm width, 100 μm depth, and 40 mm length. The bottom

and side walls of the microchannel were coated with a photocatalytic TiO₂ layer. To appear the advantages of the miniaturized reaction vessel, a light source of minimal space and lower photon cost is suitable for the microreaction system. We employed UV light emitting diodes (UV-LEDs) for the excitation light source of photocatalyst. Alcohol solutions of benzaldehyde or nitrotoluene saturated with nitrogen were introduced to the microreactor with a syringe pump and irradiated with UV-LEDs. The reactions proceeded within 60 s to yield 10.7% of benzylalcohol from benzaldehyde and 45.7% of *p*-toluidine from *p*-nitrotoluene by the excitation of 365 nm UV-LED. The results suggest the possibilities of a catalytic microreaction system on organic photoreactions.

III-H Coherent Phonon Dynamics in Crystals

III-H-1 Femtosecond Pump-Probe Study of Coherent Soft Phonon in Ferroelectric Materilas

LU, Rong¹; HASE, Muneaki¹; KITAJIMA, Masahiro²; NAKASHIMA, Shinichi³; SUGAI, Shunji⁴

(¹NIMS; ²NIMS, Univ. Tsukuba and IMS; ³AIST;

⁴Nagoya Univ.)

Structural phase transitions in solids have been investigated with X-ray- and neutron-scatterings, and especially through the “soft mode” dynamics using Raman scattering spectroscopy. However, such the soft mode is usually located at extremely low frequency or shifts to “zero” frequency when the lattice temperature approaches to the critical temperature T_c , which makes frequency-domain spectroscopic study difficult. For this point of view the time-domain spectroscopy method has advantage to study such low frequency phonon modes. The time-domain study provides also possibility of observing nonthermal phase transitions under high density photoexcitation above mJ/cm^2 pump fluences, which is inaccessible by frequency-domain techniques. Motivated by the observation of the ultrafast dynamics of structural phase transition in ferroelectric materials under the high-density photoexcitation, in this work, we have investigated the coherent soft mode in $\text{Pb}_{1-x}\text{Ge}_x\text{Te}$ ($x = 0.07$) using a pump-probe technique with amplified femtosecond laser pulses. As the pump fluence increases, the frequency of the coherent A_1 phonon becomes soften and at higher fluence it reaches saturation due to the screening effect in the electron-phonon interaction, while the large damping rate dose not show similar saturation due to the dominant anharmonic phonon-phonon coupling. The linear increase of the amplitude of the coherent phonon is ascribed to the linear increase of photo-excited carrier density under the DECP mechanism. The saturation behavior of the frequency of the soft mode implies that it will be difficult to realize the laser induced structural phase transition using single pump in $\text{Pb}_{1-x}\text{Ge}_x\text{Te}$, and multiple-pump excitation will provide a possibility for the future studies.

Reference

- 1) R. Lu, M. Hase, M. Kitajima, S. Nakashima and S. Sugai, *J. Lumin.* **378**, 119–120 (2006).

III-H-2 Temperature Dependence of Coherent A_{1g} and E_g Phonons of Bismuth

ISHIOKA, Kunie¹; KITAJIMA, Masahiro²; MISOCHKO, O. V.³

(¹NIMS and Univ. Tsukuba; ²NIMS, Univ. Tsukuba and IMS; ³Russ. Acad. Sci.)

Bismuth has been a model material to study femtosecond dynamics of coherent lattice oscillations. The generation mechanism was considered to be displacive for the totally symmetric A_{1g} mode, which was the only coherent mode observed in the conventional (isotropic) detection. The absence of the other Raman

active mode, E_g , has not been fully explained, but was phenomenologically attributed to the exclusive coupling of the hot electrons at $k < 0$ and high symmetry phonons. In the present study, we demonstrate that both A_{1g} and E_g modes are coherently excited at comparable amplitudes at low temperature, and thus proved that the coherent phonons are generated basically *via* Raman process. We found a puzzling $\pi/2$ difference in the initial phases of the two coherent oscillations, which suggests that the initial phase is not a clear-cut indication for the generation mechanism of the coherent phonons in absorbing media.

Reference

- 1) K. Ishioka, M. Kitajima and O. V. Misochko, *J. Appl. Phys.* **100**, 093501 (6 pages) (2006).

III-I In-Situ Observation of Surface Reactions by Variable Temperature Scanning Tunneling Microscopy

Chemical reactions at a well-defined single crystal surface has been intensively investigated as a prototype for heterogeneous catalytic reaction, electrochemical reaction and corrosion. The surface chemical reactions are heterogeneous in nature reflecting the structural and electronic imperfections relevant to steps, vacancies and impurities. In addition, the surface reactions are significantly influenced by the presence of reactants and products which often form ordered arrays. Therefore, in order to get better understanding of the surface reactions, it is vital to unravel the nature of these local properties which are closely linked to catalytic activity. The advent of scanning tunneling microscopy (STM) has enabled us to tackle the challenge with the ability to image the surface reactions in both real-time and real-space with atomic resolution. We investigate the reactivity of novel one-dimensional (1D) $-\text{Ag}-\text{O}-\text{Ag}-\text{O}-$ compounds formed upon the dissociative adsorption of oxygen molecule on Ag(110) using variable temperature STM (VT-STM). The 1D compounds are arranged periodically to form $(n \times 1)$ ($n = 2-7$) reconstructed structures. In addition, the 1D compounds show structural fluctuation in low O coverage regime reflecting the low dimensionality. These characteristics make them promising as a model system to explore physical and chemical properties of nano-structured materials.

III-I-1 Spontaneous Formation of Stripe Phase under the Dynamic Equilibrium between Adsorption and Desorption of H_2O on O-Covered Ag(110) Surfaces

TAKAGI, Noriaki¹; NAKAGOE, Osamu²;
WATANABE, Kazuya; MATSUMOTO, Yoshiyasu
(¹IMS and Univ. Tokyo; ²Hokkaido Univ.)

The surface structure variation under the equilibrium condition achieved by the adsorption-desorption of H_2O ($\text{H}_2\text{O} + \text{O}_{(\text{ad})} \leftrightarrow 2\text{OH}_{(\text{ad})}$) on the Ag(110)(2×1)-O surface at room temperature was investigated using VT-STM. We found that the (2×1)-O and OH phase alternately arrange to form periodic stripes. The STM observations were made by initially preparing the (2×1)-O surface and then exposing the surface to H_2O of $P_{\text{H}_2\text{O}} = 1 \times 10^{-8}$ mbar. The initial surface is the (2×1)-O structure with small bare patches that are not covered with the AgO chains. These patches are randomly distributed and appear as darker lines. When the surface was exposed to H_2O , the darker lines wander and become frizzy because the deconstruction of AgO chains upon the reaction occurs at the boundary. In addition, the lines coalesce to extend from step to step, become bright and finally arrange periodically to form a stripe pattern. The average interval between the stripes was estimated to be 6–7 nm. When H_2O was fully evacuated, the stripe pattern became disordered and finally the structure similar to the initial structure was restored. This indicates that the spontaneous formation of the stripe pattern occurs only under the equilibrium.

The formation of phase boundary is generally unfavorable because energy cost related to the phase boundary increases the surface energy. Thus, the formation of the stripe pattern needs the energy gain which overcomes the energy cost accompanied by the interface formation. According to Vanderbildt,¹⁾ the interactions characterized by $1/r^3$ scaling are responsible for the stabilizing the stripe pattern formation. The elastic and electrostatic interactions between the (2×1)-O and the OH phases are dominant candidates. Simple estimation based on the theory suggests that the energy gain originating from the electrostatic interaction is not sufficient

and thus the elastic relaxation is responsible for the formation of the stripe pattern.

Reference

1) D. Vanderbilt, *Surf. Sci.* **268**, L300 (1992).

III-I-2 Direct Observation of a Propagating Chemical Wave in Disproportionation Reactions of Water on Oxidized Ag(110) Surface by Scanning Tunneling Microscopy

TAKAGI, Noriaki¹; NAKAGOE, Osamu²;
WATANABE, Kazuya; MATSUMOTO, Yoshiyasu
(¹IMS and Univ. Tokyo; ²Hokkaido Univ.)

Scanning tunneling microscopy was used for studying spatiotemporal evolution of the disproportionation reaction of H_2O with O adatoms on oxidized Ag(110) surfaces where quasi-one dimensional AgO chains form ordered structures. Initially the reaction takes place slowly on Ag(110)-(5×1)O at the end of AgO chain, whereas the reaction accelerates explosively upon the appearance of a chemical wave that propagates along the direction perpendicular to the chain. The surface morphology of the region swept over by the chemical wave completely changes from (5×1)-O to that with many rectangular islands, indicating the formation of H_2O (OH)₂. The induction time and explosive acceleration with the propagating chemical wave imply that the reaction is autocatalytic. Water clusters hydrating OH produced likely play a central role in serving as a reservoir of H_2O to feed to the reaction and enhancing the reactivity of H_2O with O adatoms in AgO chains.

III-J High-Resolution Spectroscopy and Excited-State Dynamics of Jet-Cooled Molecules

The energy structures in the electronic excited states of isolated molecules are of great importance. The excited-state dynamics such as internal conversion to the ground state (IC), intersystem crossing to the triplet state (ISC), intramolecular vibrational redistribution (IVR), vibronic interaction, and predissociation are closely related with the irregular changes of the energy levels, *i.e.*, perturbations. High-resolution laser spectroscopy is one of the powerful methods to investigate the perturbation between the electronic states. The aims of this project are to accurately observe the fluorescence and phosphorescence excitation spectra in a supersonic jet and rotationally resolved spectra of isolated molecules using a new system of coherent narrowband pulse laser light.

In aromatic hydrocarbons such as benzene, naphthalene, and anthracene, the ISC is not expected to be a major process. In contrast with this, the triplet state plays an important role in molecules with the $n\pi^*$ lowest state such as aldehydes and ketones. The dynamical processes can be understood by analyzing rovibronic structure in the high-resolution spectrum.

III-J-1 Vibronic Structure in the S_1 - S_0 Transition of Jet-Cooled Dibenzofuran

BABA, Masaaki¹; MORI, Koichi²; YAMAWAKI, Michiru³; KASAHARA, Shunji³; YAMANAKA, Takaya
(¹IMS and Kyoto Univ.; ²Kyoto Univ.; ³Kobe Univ.)

[*J. Phys. Chem. A* **110**, 10000–10005 (2006)]

Dibenzofuran is one of the prototypical molecules of toxic dioxins.¹⁾ We have observed the fluorescence excitation spectrum and dispersed fluorescence spectrum of the S_1 - S_0 transition of jet-cooled dibenzofuran. We observed strong vibronic bands whose intensities are larger than the 0–0 band. The observed vibronic bands were assigned referring to *ab initio* calculations of the normal vibrations. The molecule is essentially planar and the structure is not much changed by the electronic excitation. It is concluded that intensities of the observed strong vibronic bands arise from vibronic interaction between the S_1 1A_1 and S_2 1B_2 $\pi\pi^*$ states. The energies of b_2 vibrational bands are decreased by the vibronic interaction. Broad component was observed in the dispersed fluorescence spectrum. It indicates that IVR occurs in the lower energy vibronic levels of the S_1 state.

Reference

1) M. Baba *et al.*, *J. Phys. Chem. A* **108**, 1388–1392 (2004).

III-J-2 Energy Levels of CH_3 Rotation in the S_1 and S_0 States of 9-Methylanthracene

BABA, Masaaki¹; MORI, Koichi²; YAMANAKA, Takaya
(¹IMS and Kyoto Univ.; ²Kyoto Univ.)

CH_3 internal rotation induces radiationless transitions of aromatic molecules. In order to understand the mechanism of excited-state dynamics of methyl containing molecules we have observed high-resolution spectra of jet-cooled 9-methylanthracene (9MA). We found several low energy bands, which are assigned to transitions between the vibrational levels of CH_3 internal rotation. The barrier height to CH_3 rotation was estimated to be

about 100 and 50 cm^{-1} in the S_0 and S_1 states, respectively. The barrier height is attributed to steric repulsion and interaction with the π orbitals. The barrier height is very small in toluene and that in 9MA is relatively larger. This increase is considered to be due to larger anisotropy of the π orbitals in 9MA.

The dispersed fluorescence spectra indicate that IVR occurs in the lower energy vibrational levels of the S_1 state. The threshold is much smaller than that of anthracene. The IVR is considered to be enhanced by CH_3 substitution. It is the effect of increase of the level density, lowering of the symmetry, and coupling of the out-of-plane vibrations.

III-J-3 High-Resolution Spectroscopy of the T_1 $^3A_u(n\pi^*)$ State of Oxalyl Chloride

BABA, Masaaki¹; HASEGAWA, Hirokazu;
OHSHIMA, Yasuhiro
(¹IMS and Kyoto Univ.)

Oxalyl Chloride is a Cl derivative of glyoxal which is a prototypical diketones. Generally energy difference between the $n\pi^*$ and $\pi\pi^*$ states are very small in diketones and ISC occurs efficiently in the S_1 state. The energy structure of the triplet state is an important factor to quantitatively understand the mechanism. In order to observe high-resolution spectrum, strong pulse laser light is necessary because the S–T transition is very weak. In particular Cl atoms enhance radiationless transitions which are called as heavy atom effect. Furthermore, there are two mass isotopes of the Cl atom and the spectrum becomes congested.

Phosphorescence of jet-cooled oxalyl chloride was observed and an S–T phosphorescence excitation spectrum has been reported using a pulse laser with the resolution of 0.2 cm^{-1} .¹⁾ Pulse amplifying of CW single-mode laser makes it possible to observe rotationally resolved spectrum. The three spin sublevels in the triplet state and the coupling with the rotation angular momentum are important to understand the mechanism of ISC.

Reference

1) T. Yoshii *et al.*, *J. Phys. Chem.* **100**, 3354–3358 (1996).

RESEARCH ACTIVITIES IV

Department of Molecular Assemblies

IV-A Optical Study of Charge Ordering States in Organic Conductors

In the organic charge-transfer salts, the charge carriers in organic crystal is located at the boundary between localized and extended (delocalized) states, mainly because the interatomic distances between the neighboring molecules are much longer than the bond length within the molecule. Therefore, charge ordering (CO) originated from the localization of the charge carriers is widely found in organic conductors through the phase transition. Recently, CO has been found in several organic conductors, and the electronic phase diagrams of typical organic conductors are re-considered taking CO into account. The CO state is drawing attention, first because a CO phase is neighbored on a superconducting phase, wherein a new type of pairing mechanism for superconductivity is theoretically predicted, second because some compounds in a CO phase shows ferroelectricity, the origin of which is expected to be electronic, third because the narrow-band compounds have an unusual intermediate state between metallic and CO state. To detect CO states, we employ infrared and Raman spectroscopy. Some molecules have charge-sensitive intramolecular vibrational modes, the frequency of which shifts depending upon the molecular charge (oxidation state of molecule). The Raman and infrared spectra change dramatically at the CO phase-transition temperature, since CO is accompanied by an inhomogeneous distribution with large amplitude. The goal of this study is (1) the understanding of the intermediate state above the CO phase transition, (2) the investigation of the optical properties related to the ferroelectric CO phase, and (3) the characterization of the insulating electronic state near the superconducting phase.

IV-A-1 Charge Ordering State of β'' -(ET) $_3$ (HSO_4) $_2$ and β'' -(ET) $_3$ (ClO_4) $_2$ by Temperature-Dependent Infrared and Raman Spectroscopy

YAMAMOTO, Takashi; URUICHI, Mikio;
YAKUSHI, Kyuya; KAWAMOTO, Atsushi¹
(¹Hokkaido Univ.)

[*Phys. Rev. B* **73**, 125116 (12 pages) (2006)]

We present the temperature-dependent infrared and Raman spectra of β'' -(ET) $_3$ X $_2$ (X = HSO_4 and ClO_4 ; ET = Bis-ethylenedithio-tetrathiafulvalene) compounds which undergo a metal-insulator transition. The infrared-active ν_{27} mode discontinuously split into two bands at the metal-insulator transition temperature of 127 K in the X = HSO_4 salt, whereas, the corresponding mode continuously changed across the metal-insulator transition temperature of \sim 170 K in the X = ClO_4 salt. In both compounds, the charge-sensitive ν_{27} mode split into two in the insulating phase. This drastic spectral change indicates that the metal-insulator transition originated in the charge ordering. Employing the frequencies of the split ν_{27} bands, the site charges are estimated to be +0.3 $_4$ and +0.8 $_1$ for X = HSO_4 and +0.3 $_6$ and +0.8 $_1$ for X = ClO_4 . We also estimated the site charges using the Raman-active ν_2 mode and obtained consistent results. Examining the selection rule of the ν_3 mode, we reached the conclusion that the unit cell with space group $P1$ has a pseudo-inversion center in the charge-ordered phase. Based on the symmetry, we propose a charge-ordering pattern for the X = HSO_4 and X = ClO_4 salts, which is quite different from that of the X = ReO_4 salt reported previously. We qualitatively discuss the differences in

the charge-ordering pattern considering the anisotropic inter-site Coulomb interaction.

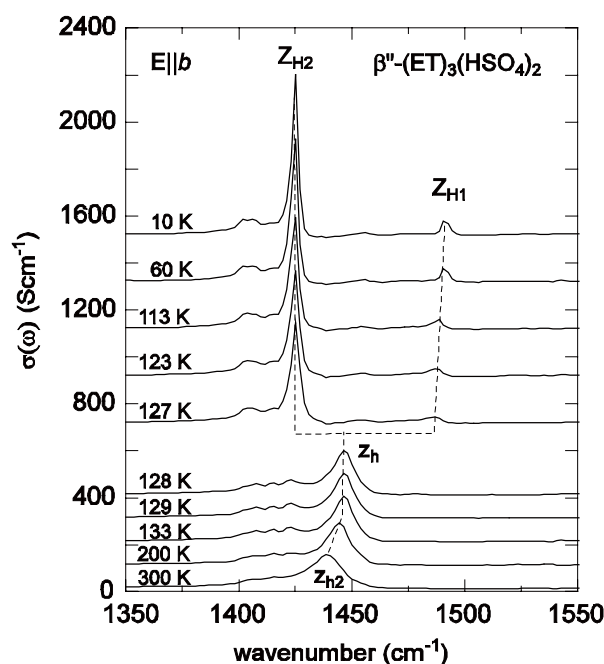


Figure 1. Temperature dependence of the conductivity spectra obtained through Kramers-Kronig transformations of the b -polarized reflectance spectra of β'' -(ET) $_3$ (HSO_4) $_2$. The infrared-active bands, z_h is the out-of-phase mode of the ring C=C stretching in highly conductive phase. The bands, denoted by Z_{H1} and Z_{H2} are respectively the ring C=C stretching modes of charge-poor and charge-rich molecules of β'' -(ET) $_3$ (HSO_4) $_2$.

IV-A-2 Infrared and Raman Studies of the Charge-Ordering Phase Transition at ~170 K in the Quarter-Filled Organic Conductor, β'' -(ET)(TCNQ)

URUICHI, Mikio; YAKUSHI, Kyuya; YAMAMOTO, Hiroshi M.¹; KATO, Reizo¹
(¹RIKEN and JST/CREST)

[*J. Phys. Soc. Jpn.* **75**, 074720 (2006)]

We present the optical conductivity, infrared- and Raman-active charge-sensitive phonon modes, and the x-ray diffraction superlattice spots of β'' -(ET)(TCNQ) [ET = bis(ethylenedithio) tetrathiafulvalene, TCNQ = 7,7,8,8-tetracyanoquinodimethane], which is characterized as a quarter-filled narrow band system. Above ~170 K, we found weak superlattice spots and splitting of the C=C and C-S stretching modes of ET. These results indicate the charge-ordering state in the ET layer. As the temperature is decreased, the superlattice spots abruptly disappeared at ~170 K and the split modes continuously merged into a single band below ~170 K. Concomitantly, the spectral weight of the optical conductivity ascribed to the ET layer significantly shifts toward lower energy. Through the analyses of these experimental results, we propose the view that the incoherent conducting electron in the ET layer shows a crossover behavior into a coherent Fermi liquid state below the structural phase transition at ~170 K.

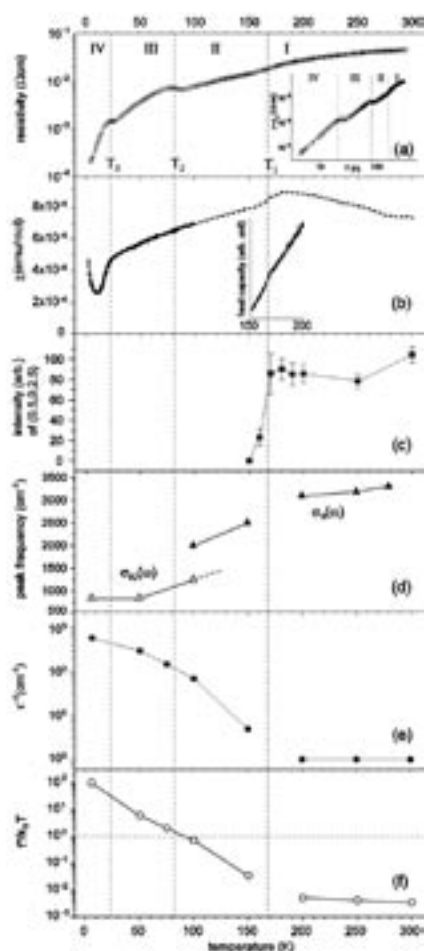


Figure 1. Comparison of (a) the dc resistivity, (b) the magnetic susceptibility and heat capacity (inset), (c) the intensity of the superlattice (1/2, 0, 21/2), (d) peak frequency in the optical conductivity of ET layer, (e) the intersite hopping rate in the ET layer, (f) the ratio of effective transfer energy to temperature.

IV-A-3 Unusual Intermediate State between Metallic and Charge-Ordered States in θ -Type ET Salts

TAKAHASHI, Toshihiro¹; NOGAMI, Yoshio²; YAKUSHI, Kyuya
(¹Gakushuin Univ.; ²Okayama Univ.)

[*J. Phys. Soc. Jpn.* **75**, 051008 (2006)]

The Raman spectrum of narrow-band θ -type ET salts in highly conducting phase exhibit a single broad band as shown in Figure 1(c). This Raman band was assigned to the ν_2 mode based on the isotope shift of the ¹³C-substituted compound. If the high-temperature phase is a metal, the ν_2 mode should appear between the ν_{2P} and ν_{2R} bands which are shown in Figure 1(a). However, the broad ν_2 band above T_{CO} is located at the ν_{2R} band. In addition, the ν_{2P} mode, the counterpart of ν_{2R} , is found in the highly conducting phase of the monoclinic TlZn salt (See Figure 1(b)). These spectra were quite different from the spectrum (Figure 1(d)) of metallic θ -(ET)₂I₃, in which the ν_2 mode nearly located at the center of ν_{2P} and ν_{2R} modes. The spectra of the narrow-band compounds in high-temperature phase rather resemble the spectrum (Figure 1(a)) of charge-ordered state. Therefore, the charges in high-temperature phase are nearly localized and hop to neighbor site slowly less than 10¹¹ Hz (~1 meV). This hopping rate is much slower than the motion of the charge carriers of organic metal. The high-temperature phase of narrow-band θ -type ET salts is considered as an intermediate state between metallic and CO states.

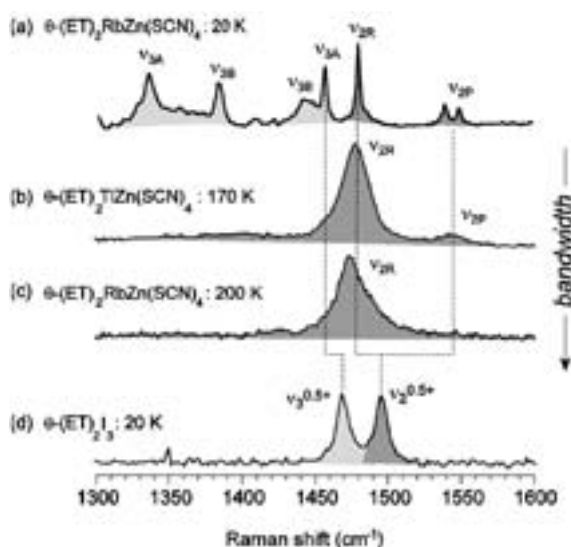


Figure 1. Comparison of the ν_2 and ν_3 bands of (a) the CO phase of RbZn, high-temperature phases of (b) TlZn, (c) RbZn, and (e) I₃ salts. Note that the ν_2 mode in high-temperature phase of (b) and (c) is already split.

IV-A-4 Photo-Gatable Second Harmonic Generation in Ferroelectric Organic Conductor with Strongly Correlated Electrons

YAMAMOTO, Kaoru; IWAI, Shinichiro^{1,2}; BOYKO, Sergiy³; KASHIWAZAKI, Akimitsu¹; HIRAMATSU, Fukiko¹; OKABE, Chie; NISHI, Nobuyuki; YAKUSHI, Kyuya
(¹Tohoku Univ.; ²JST/PREST; ³Univ. Ontario)

Ferroelectricity is characterised by the spontaneous polarisation, which shows dramatic temperature- and electric-field responses. By means of optical second-harmonic generation (SHG) measurement, we demonstrated that a two-dimensional organic metal α -(ET)₂I₃ [ET: bis(ethylenedithio)tetrathiafulvalene] undergoes ferroelectric transformation associated with Wigner-crystal like charge ordering (CO). It was found that the nonlinear electric susceptibility of the compound in the ferroelectric state was much greater than that of a nonlinear optical crystal β -BaB₂O₄ (BBO), suggesting the generation of macroscopic polarisation as in ferroelectrics. In terms of controlling the electronically induced FE polarisation, the photo-response of the macroscopic polarisation to femtosecond laser pulse was investigated. Pump-probe SHG measurement showed that the polarisation was sharply suppressed by the photo-excitation. More noteworthy is the fact that the suppressed polarisation instantaneously recovered in the time scale of 10 ps. The photo-gatable optical non-linearity based on the electron FE might be applied as a unique medium that functions as a fast optical switch in future all-optical devices.

IV-A-5 Evaluation of Charge Transfer Degree in the Bis(ethylenethio) Tetrathiafulvalene Salts by Raman Spectroscopy

KOWALSKA, Aneta¹; WOJCIECHOWSKI, Roman¹; ULANSKI, Jacek¹; MAS-TORRENT, Marta²; LAUKHINA, Elena²; ROVIRA, Concepcio²; YAKUSHI, Kyuya
(¹Univ. Lodz; ²Inst. Ciencia Mater. Barcelona)

[*Synth. Met.* **156**, 75 (2006)]

Raman spectroscopy studies for a series of charge-transfer salts based on the bis(ethylenethio)tetrathiafulvalene (BET-TTF) were carried out in order to analyze the charge distribution on the donor molecules in the unit cell of crystals. With the help of the density functional theory calculations for BET-TTF⁰ and BET-TTF⁺ molecules it was shown that the Raman spectroscopy can be applied to determine the stoichiometry in the BET-TTF salts. For salts exhibiting increase of the resistivity below *ca.* 100 K, the Raman spectra at variable temperature indicate that this behavior is not related to the charge disproportionation phenomenon.

IV-A-6 Installation of a Cryostat to the Far-Infrared Spectrometer and the Transmission Measurement of α -(BEDT-TTF)₂I₃

YAKUSHI, Kyuya; YAMAMOTO, Kaoru;

NAKANO, Chikako

The measurement of the reflectivity or transmittance in the far-infrared region of organic conductors has been conducted for very restricted materials, owing to the difficulty of the growth of a large single crystal of several mm. The optical conductivity in the far-infrared region provides the information of the electronic state near Fermi energy. For example, the incoherent conducting state is expected to give a non-Drude type optical conductivity, whereas the coherent state provides a well-defined Drude type conductivity. The absorption spectrum of insulating compounds provides the information of the low-frequency local phonons and lattice phonons, which are sometimes closely related to the mechanism of phase transition. We have installed a top-loading type of cryostat, Oxford Optistat CF, to the far-infrared spectrometer, Bruker IFS-66v, whose sample and optics chamber can be evacuated to avoid the strong absorption of water vapor. We introduced a XY stage to fix the bottom of the cryostat to adjust the sample position. Z position can be adjusted using a sample rod controlled by a micrometer. Figure 1 shows the polarized transmittance spectrum of α -(BEDT-TTF)₂I₃ of 2 mm × 2 mm. As shown in this figure, the optical gap appears abruptly at 136 K. Although this phase transition is of first order, the evolution of the gap was observed. This observation is consistent with the evolution of the SHG (second harmonic generation) signal below the phase transition temperature.

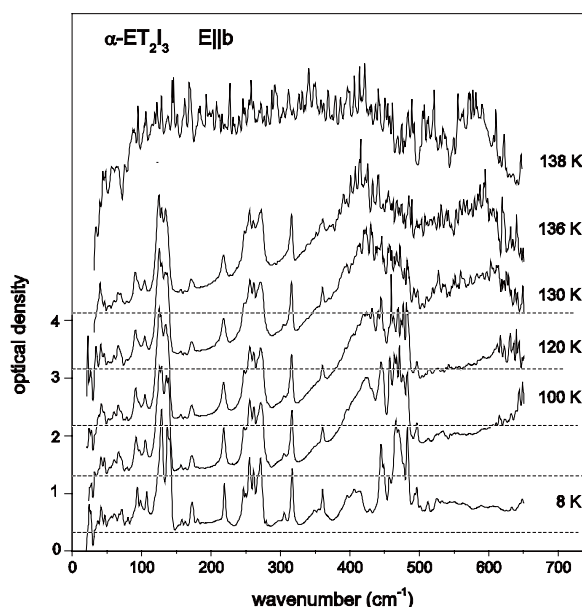


Figure 1. Temperature dependence of the *E//b* polarized transmittance of the single crystal of α -(BEDT-TTF)₂I₃. Note that the evolution of the gap is observed.

IV-A-7 Mechanism of the Phase Separation in the Monovalent-to-Divalent Phase Transition of Biferrocenium-(F₁TCNQ)₃

URUICHI, Mikio; YAKUSHI, Kyuya; MOCHIDA, Tomoyuki¹
(¹Toho Univ.)

The ionic crystal $D^+A_3^-$ (D = dineopentylbiferrocene and $A = F_1TCNQ$) undergoes a first-order phase transition, in which second ionization occurs to form a doubly ionized state, $D^{2+}A_3^{2-}$.¹⁾ This monovalent-to-divalent phase transition continuously occurs in a wide temperature range from 160 K to 100 K. X-ray diffraction and Raman spectroscopy showed that the macroscopic domains of monovalent and divalent phases coexist in this temperature range.²⁾ We investigated this unusual phase transition and elucidated the mechanism of the phase separation based on the general understanding of the first-order phase transition. According to the theory of first-order phase transition, the free-energy *vs.* order parameter has an energy barrier E_B between the two phases (monovalent and divalent phases). (See Figure 1) If E_B is smaller than the phase transition temperature kT ($T \sim 100$ – 160 K), one of the domains can be thermally activated. Therefore, the continuous phase change accompanied by the phase separation can be well explained. Interestingly, the behavior of the first-order phase transition changes from hysteretic behavior to continuous behavior on decreasing the ratio kT/E_B as shown in Figure 1. We speculate that the small energy barrier arises from the mechanism of this phase transition that the Madelung energy gain is the driving force.

References

- 1) T. Mochida, K. Takazawa, M. Takahashi, M. Takeda, Y. Nishio, M. Sato, K. Kajita, H. Mori, M. M. Matsushita and T. Sugawara, *J. Phys. Soc. Jpn.* **74**, 2214 (2005).
- 2) M. Uruichi, K. Yakushi and T. Mochida, *J. Low Temp. Phys.* in press.

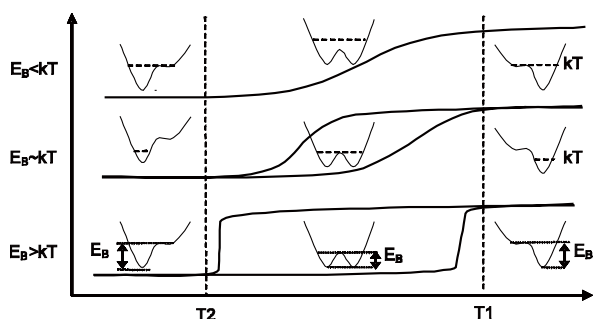


Figure 1. The behavior of first-order phase transition is classified by the ratio between the energy barrier E_B and the phase transition temperature kT . Abscissa is temperature and ordinate is the physical quantity that changes through a phase transition.

IV-B Magnetic Resonance Studies for Molecular-Based Conductors

Magnetic resonance measurements may be mature techniques as devices of the so-called chemical analyses. However, from the viewpoint of the solid state material science, magnetic resonance measurement is challenging area still in under the special condition such cases as the extreme low temperature, strong magnetic field, high pressure, electric field, optical response and so on. Moreover they are advantageous for studying the fundamental electronic properties and for understanding the detailed electronic structures of molecular based compounds. Molecular based conductors are one of the extensively studied materials. The development of the understanding of the electronic phases of these materials enables us systematic investigations of low-dimensional highly correlated electrons systems. Competition of the electronic phases in molecular based conductors has attracted much attention. The investigations of such electronic phases by means of magnetic resonance measurements are important to understand the unsolved fundamental problems in the field of solid state physics.

In this project, we performed the multi-frequency- (X-, Q- and W-bands) and pulsed-ESR, and broad-line NMR measurements for molecular based conductors to understand the electron spin dynamics in the low temperature electronic phases.

IV-B-1 Deuteration Effect and Possible Origin of the Charge-Ordering Transition of $(\text{TMTTF})_2\text{X}$

FURUKAWA, Ko; HARA, Toshifumi; NAKAMURA, Toshikazu

[*J. Phys. Soc. Jpn.* **74**, 3288–3294 (2005)]

ESR, NMR and X-ray measurements were performed for pristine and fully perdeuterio-TMTTF, $\text{TMTTF-}d_{12}$ salts. Significant enhancement by deuteration of the charge-order phase transition temperature, T_{CO} , was observed in ESR measurements for all $(\text{TMTTF})_2\text{X}$ salts measured. No obvious relation between the SbF_6 anion motion and the TMTTF charge-order was found by ^{19}F NMR. We also performed single crystal X-ray measurements to understand the deuteration effects and temperature dependence of the crystal structure. A possible relationship between the T_{CO} 's and crystallographical parameters is proposed. The deuteration effects and possible origin of the charge-ordering transition of TMTTF salts are discussed.

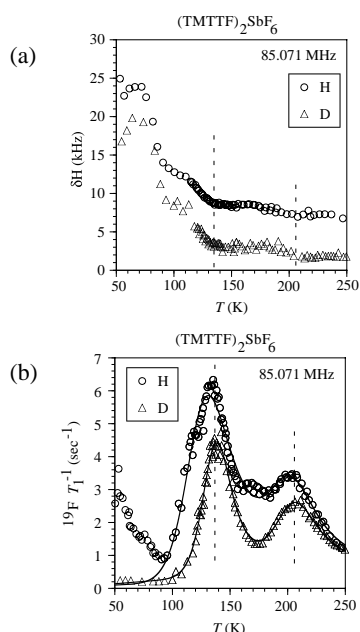


Figure 1. Temperature dependence of ^{19}F NMR, (a) absorption full width at half maximum (FWHM) linewidth, δH , and (b) spin–lattice relaxation rate, $^{19}\text{F} T_1^{-1}$, of $(\text{TMTTF-}h_{12})_2\text{SbF}_6$ (circle) and $(\text{TMTTF-}d_{12})_2\text{SbF}_6$ (triangle). The solid lines are fitted results using the BPP equation.

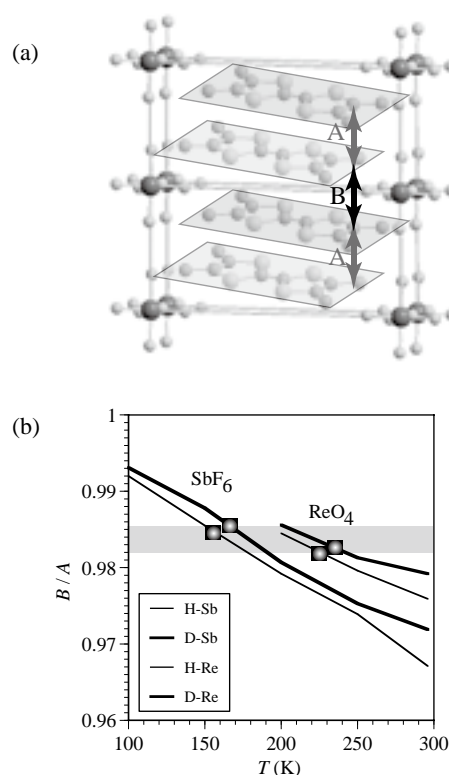


Figure 2. Crystal structure and definition of the inter-molecular distances, A and B , of $(\text{TMTTF})_2\text{SbF}_6$. Temperature dependence of inter-molecular distances and their ratio of $(\text{TMTTF-}h_{12})_2\text{SbF}_6$, $(\text{TMTTF-}d_{12})_2\text{SbF}_6$, $(\text{TMTTF-}h_{12})_2\text{ReO}_4$ and $(\text{TMTTF-}d_{12})_2\text{ReO}_4$. The measured points (every 50 K) are interpolated with a straight line. Solid circles correspond to T_{CO} 's for each of salts.

IV-B-2 ^{13}C NMR Analyses of Successive Charge Ordering in $(\text{TMTTF})_2\text{ReO}_4$

NAKAMURA, Toshikazu; FURUKAWA, Ko; HARA, Toshifumi

[*J. Phys. Soc. Jpn.* **75**, 013707 (4 pages) (2006)]

^{13}C NMR measurements were performed for a one-dimensional organic conductor, $(\text{TMTTF})_2\text{ReO}_4$. The existence of an intermediate charge ordering (CO) phase was clarified for a TMTTF salt with a Td symmetry counter anion by the ^{13}C NMR absorption line and spin-lattice relaxation rate, ^{13}C T_1^{-1} . The ^{13}C NMR spectra, which are characteristic of nuclei in equivalent molecules at room temperature, indicated two inequivalent molecules with unequal electron densities below 225 K. Moreover, the spin-singlet transition associated with ReO_4 anion ordering was confirmed at around 158 K by ^{13}C NMR. The ^{13}C NMR lines show a marked change at 158 K. The possible redistribution of the electronic charge at the anion ordering temperature as well as the origin of the charge ordering phenomena are discussed.

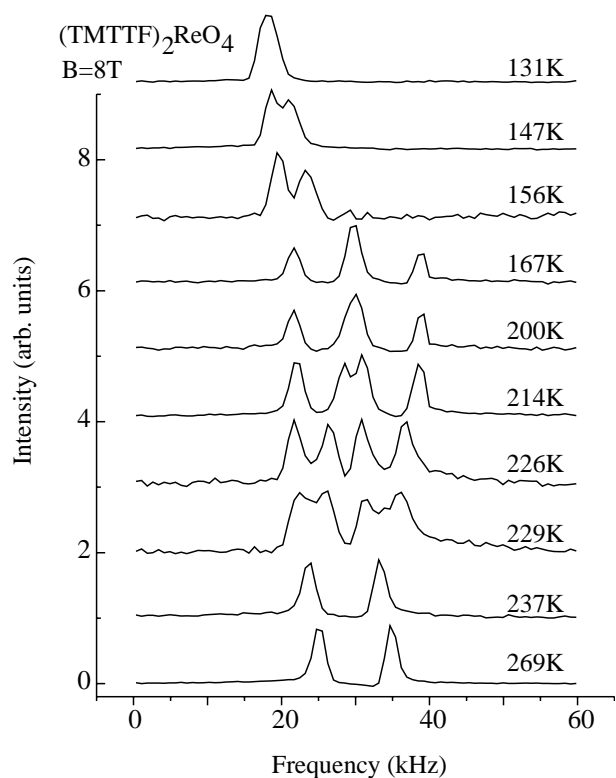


Figure 1. Temperature dependence of ^{13}C NMR spectra of $(\text{TMTTF})_2\text{ReO}_4$. Measurements were performed at the so-called magic-angle configuration.

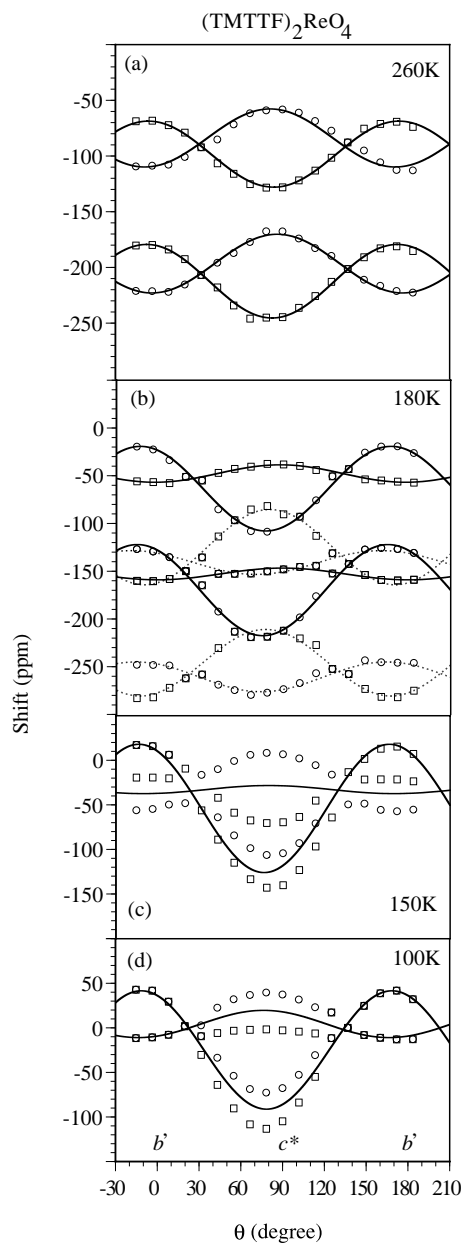


Figure 2. Angular dependence of resonance frequency of ^{13}C NMR in $(\text{TMTTF})_2\text{ReO}_4$. A single crystal of $(\text{TMTTF})_2\text{ReO}_4$ was rotated within the $b'c^*$ plane perpendicular to the external static magnetic field. The solid and dashed lines are included as guides to the eye, but are the least-squares fits to the measured data assuming the $3\cos^2\theta - 1$ formulae.

IV-B-3 Redistribution of Electronic Charges in the Spin-Peierls State in $(\text{TMTTF})_2\text{AsF}_6$ Observed by ^{13}C NMR

FUJIYAMA, Shigeki; NAKAMURA, Toshikazu

[*J. Phys. Soc. Jpn.* **75**, 014705 (7 pages) (2006)]

We report ^{13}C NMR spectra and nuclear spin lattice relaxation rate $1/T_1$ for a quasi-one-dimensional quarter-filled organic material $(\text{TMTTF})_2\text{AsF}_6$, which undergoes charge ordering ($T_{\text{CO}} = 102$ K) and spin-Peierls phase transitions ($T_{\text{SP}} = 14$ K). The ratio of two $1/T_1$ for the charge accepting and donating TMTTF sites which

grows from T_{CO} finally saturates in approaching T_{SP} , indicating one spin correlation function even in the charge ordered state. Below T_{SP} , however, the doubly split NMR lines from inequivalently charged molecules merge into one line, originated from the variation in charge densities. This shows that a rearrangement of the charge configuration occurs at T_{SP} .

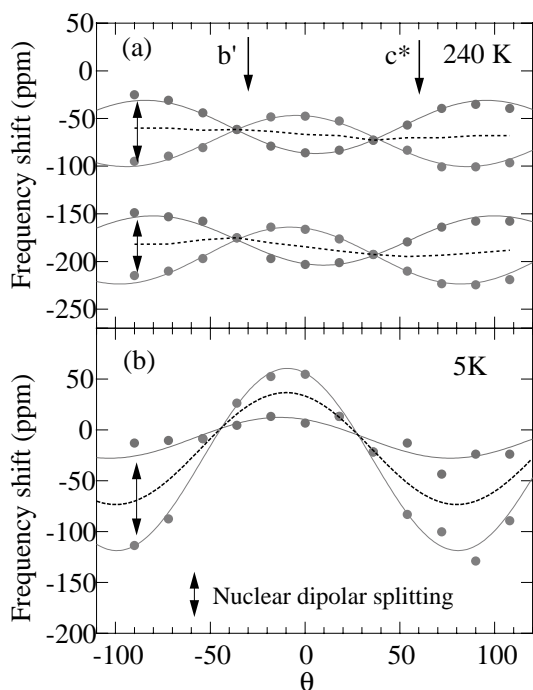


Figure 1. Angular dependence of the peak positions of the NMR spectra rotated in the b - c plane at 240 K (a) and 5 K (b).

IV-B-4 The Effect of Deuteration on the Transition into a Charge Ordered State of $(TMTTF)_2X$ Salts

NAD, Felix^{1,2}; MONCEAU, Pierre²; NAKAMURA, Toshikazu; FURUKAWA, Ko
(¹Inst. Rad. Elec., Russia; ²CNRS, France)

[*J. Phys.: Condens. Matter* **17**, L399–L406 (2005)]

From dielectric permittivity measurements, we show that deuteration yields a large increase of the transition temperature for the charge ordered state of $(TMTTF)_2X$ ($X = AsF_6, SbF_6, ReO_4$) salts. We propose an explanation of this phenomenon, suggesting that deuteration induces a modification of the $(TMTTF)_2X$ crystal unit cell.

IV-B-5 Magnetic Properties of Hexa-*peri*-hexabenzocoronene Nanotube Investigated by Magnetic Resonance

HARA, Toshifumi; FURUKAWA, Ko; NAKAMURA, Toshikazu; YAMAMOTO, Yohei¹; KOSAKA, Atsuko¹; FUKUSHIMA, Takanori^{1,2}; AIDA, Takuzo^{1,2}
(¹ERATO-SORST; ²Univ. Tokyo)

The discovery of electric conductive carbon nanotube

materials has expanded interest in exploring novel materials for functional electronic devices. Recently, new type nanotubular objects has been developed by Aida and co-workers with novel HBC (hexa-*peri*-hexabenzocoronene) amphiphiles bearing hydrophilic oxyalkylene chains and lipophilic dodecyl chains. These HBC molecules stack to form a well-defined nanotube with a helical array of a large number of π -stacked HBC units. By chemical oxidation using iodine, the HBC nanotube turns to show highly electrical conductive behavior.

In order to understand the origin of the carrier and the electronic properties, ESR and 1H NMR measurements were carried out for the iodine doped HBC nanotube. The drastic increases of the ESR intensity with the iodine doping indicates that the carrier possesses a spin-freedom. In the initial phase of doping, a narrow ESR line was observed. After additional several hours of doping, another broad ESR lines appear, and the intensity of it overcomes that of the narrow lines. The spin susceptibility evaluated from the broad ESR line shows a temperature independent behavior down to 140 K. The ESR linewidth decreases with lowering temperature. These observations are typical phenomena of itinerant spins. Below 140 K, the spin susceptibility turns to show the Curie-like behavior, following an hump of ESR linewidth. The drastic change of the ESR parameters suggests a possible semiconductor to insulator transition (or crossover) in this nanotubular system. In this paper, we describe magnetic properties of the HBC nanotube and discuss the nature of the electronic phases from a microscopic point of view.

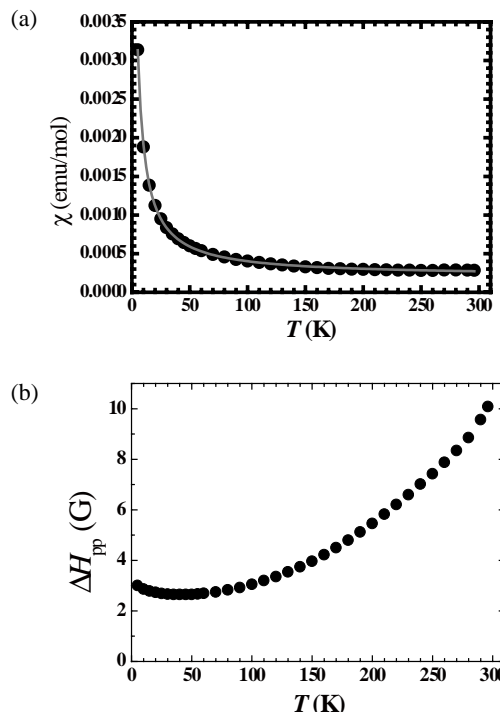


Figure 1. Temperature dependence of the spin susceptibility and ESR linewidth of the iodine doped HBC nanotube.

IV-B-6 X-Ray Structural Study of Charge and Anion Orderings of TMTTF Salts

NOGAMI, Yoshio¹; ITO, Takayoshi¹; YAMAMOTO,

Kenichiro¹; IRIE, Naoaki¹; HORITA, Shintaro¹;
KAMBE, Takashi¹; NAGAO, Nobuaki¹; OSHIMA,
Kokichi¹; IKEDA, Naoshi²; NAKAMURA,
Toshikazu
(¹Okayama Univ.; ²JASRI)

[*J. Phys. IV France* **131**, 39–42 (2005)]

High resolution X-ray structure analyses and electronic structure calculation revealed the condition for the charge ordering (CO) observed in the (TMTTF)₂X (Fabre) salts. The phase diagram of the electronic states including $2k_F$ and $4k_F$ CO has been proposed associated with magnitudes of molecular dimerization and tetramerization.

IV-B-7 Depinning of the Spin-Density Wave in (TMTTF)₂Br under Pressure

NOMURA, Kazushige¹; ISHIMURA, Kazunori¹;
FUJIMOTO, Kazuteru¹; MATSUNAGA, Noriaki¹;
NAKAMURA, Toshikazu; TAKAHASHI, Toshihiro²;
SAITO, Gunzi³
(¹Hokkaido Univ.; ²Gakushuin Univ.; ³Kyoto Univ.)

[*J. Phys. IV France* **131**, 111–114 (2005)]

We have investigated the sliding motion of the SDW in the organic compound (TMTTF)₂Br under the pressure with the measurement of the non-linear conductivity. Below the SDW transition temperature T_{SDW} , we observed the sharp increase of conductivity with the clear threshold electric field E_T , associated with the depinning of the SDW. For the typical sample, the temperature dependence of E_T shows a peak around $0.3T_{SDW}$ in each pressure. In addition, the field hysteresis with the switching appears in the dc I - V characteristics around $0.3T_{SDW}$. The excess conductivity, dominated by the kinetic friction, shows a sharp increase below $0.3T_{SDW}$. These behaviors indicate that the sliding mechanism of SDW varies across $0.3T_{SDW}$, which is almost equal to the sub-phase transition temperature. This fact suggests that the transition at $0.37T_{SDW}$ is associated with both the magnetic and charge degrees of freedom.

IV-B-8 Pulsed ESR Measurements for (TMTTF)₂X

FURUKAWA, Ko; HARA, Toshifumi; NAKAMURA,
Toshikazu

It is well known that most of TMTTF salts undergo the charge ordering (CO) transitions in the paramagnetic phase. We already demonstrated the charge configuration pattern for several TMTTF salts. However it is not clear the relationship between the CO configurations and ground states. Actually, the (TMTTF)₂SbF₆ salts undergoes an antiferromagnetic phase, while the (TMTTF)₂PF₆ and (TMTTF)₂AsF₆ salts show spin-Peierls ground states. They have common CO configuration pattern at the paramagnetic phase. So it is interesting to investigate the charge configuration at around the spin-Peierls state. So we performed the pulsed ESR measurements for one

of typical TMTTF salts, (TMTTF)₂PF₆ and (TMTTF)₂-Br. The low temperature electron spin dynamics from the ESR point of view are discussed.

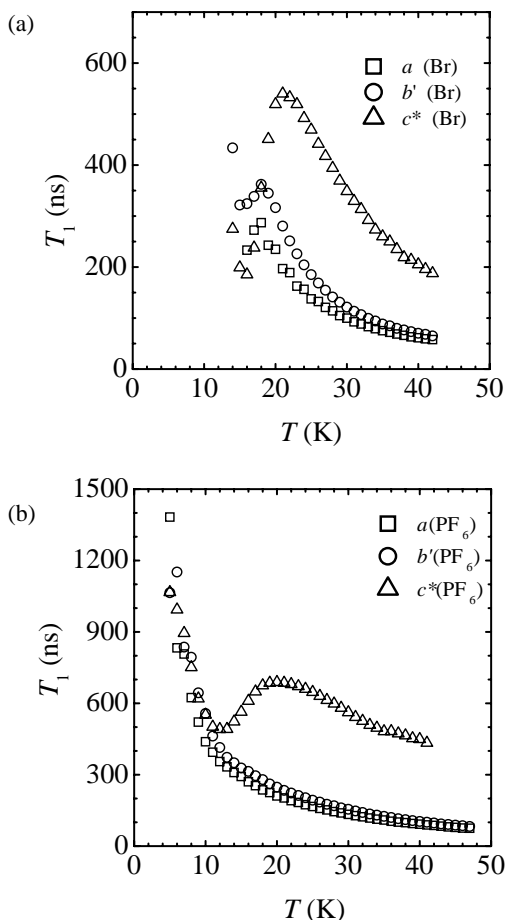


Figure 1. Temperature dependence of the ESR spin-lattice relaxation time, T_1 , for (TMTTF)₂Br (a) and (TMTTF)₂PF₆ (b).

IV-B-9 Synchrotron X-Ray Diffraction Experiments and MEM Analyses for the Charge-Ordering State of (TMTTF)₂PF₆

HARA, Toshifumi; FURUKAWA, Ko; NAKAMURA,
Toshikazu; KAKIUCHI, Toru¹; SAWA, Hiroshi²;
IZUMI, Fujio³
(¹SOKENDAI; ²KEK; ³NIMS)

TMTTF family salts have been attracting attention due to observations of their charge-ordering (CO) phenomena. ¹³C NMR indicates the existence of inequivalent TMTTF sites at low temperatures, and dielectric permittivity measurements show ferroelectric behaviors for (TMTTF)₂MF₆ ($M = P, As, Sb$) salts. We also proposed that the variation of charge-ordering patterns such as $-O-O-o-o-$ and $-O-o-O-o-$ along the stacking axes for a series of TMTTF salts by ESR linewidth analyses. The competition between the long-range Coulomb interaction and anion ordering are pointed out by experimental and theoretical investigations. However, there is no direct observation of the charge distribution for charge ordered states so far. Hence we performed synchrotron X-ray diffraction measurements and MEM

analyses (TMTTF)₂PF₆ at R.T. and 20 K. We observed apparent difference of the electric charge distributions between two TMTTF molecules in the original unit cell. This fact reveals that the charge order phase transition in (TMTTF)₂PF₆ is purely electronic one without apparent structural changes.

IV-B-10 g-Anisotropy of the S₂-State Manganese Cluster in Single Crystals of Cyanobacterial Photosystem II Studied by W-Band Electron Paramagnetic Resonance Spectroscopy

MATSUOKA, Hideto¹; FURUKAWA, Ko; KATO, Tatsuhisa²; MINO, Hiroyuki³; SHEN, Jian-Ren⁴; KAWAMORI, Asako⁵

(¹IMS and Free Univ. Berlin; ²IMS and Josai Univ.; ³Nagoya Univ.; ⁴Okayama Univ.; ⁵Kwansei Gakuin Univ.)

[*J. Phys. Chem. B* **110**, 13242–13247 (2006)]

The multiline signal from the S₂-state manganese cluster in the oxygen evolving complex of photosystem II (PSII) was observed in single crystals of a thermophilic cyanobacterium *Thermosynechococcus vulcanus* for the first time by W-band (94 GHz) electron paramagnetic resonance (EPR). At W-band, spectra were characterized by the g-anisotropy, which enabled the precise determination of the tensor. Distinct hyperfine splittings (hfs's) as seen in frozen solutions of PSII at X-band (9.5 GHz) were detected in most of the crystal orientations relative to the magnetic field. In some orientations, however, the hfs's disappeared due to overlapping of a large number of EPR lines from eight crystallographic symmetry-related sites of the manganese cluster within the unit cell of the crystal. Analysis of the orientation-dependent spectral features yielded the following g-tensor components: $g_x = 1.988$, $g_y = 1.981$, $g_z = 1.965$. The principal values suggested an approximate axial symmetry around the Mn(III) ion in the cluster.

IV-C Development of Multi-Functional Molecular Systems

Various types of molecular conductors such as organic superconducting alloys containing localized magnetic moments, single-component molecular metals with unprecedentedly high antiferromagnetic transition temperature, molecular conductors exhibiting resistivity anomaly coupled with a spin transition, and ferro- and ferri-electric porous molecular crystals were developed and their physical properties were examined. Recently, magnetic molecular conductors have attracted a considerable interest because of their possible *bi*-functional properties originated from the interaction between π conduction electrons and localized magnetic moments. But except BETS (bis(ethylenedithio)tetrathiasfulvalene) conductors with FeX_4^- ($X = \text{Cl}, \text{Br}$) anions developed more than ten years ago, there has been almost no organic superconductor (and even metal) exhibiting distinct *bi*-functional properties. In the last ten years, we have discovered unprecedented organic superconductors such as the system exhibiting “superconductor \rightarrow insulator transition,” the antiferromagnetic organic superconductors and the field-induced organic superconductors. We have recently re-examined the temperature-composition phase diagram of the alloys of organic superconductor (λ -(BETS) $_2\text{GaCl}_4$) and field-induced organic superconductor (λ -(BETS) $_2\text{FeCl}_4$) and found that the superconducting temperature phase of the alloy is stabilized by neighbouring on the antiferromagnetic insulating phase. In addition, we have reconfirmed the recently discovered peculiar “constant resistivity state” between zero-resistivity (or superconducting) state and normal metal state. It will be highly expected that new “vortex dynamics” will be disclosed in future from this unprecedented organic superconducting alloy.

Besides BETS conductors, we have developed new types of magnetic conductors such as (1) single-component molecular metal where conduction electrons and antiferromagnetic order coexists below 110 K, (2) novel system exhibiting weakly metallic behavior at high temperature and weak ferromagnetic properties at low temperature and (3) molecular conductors consisting of π molecule responsible for electron conduction and spin-crossover transition metal complex counter ion. We are also trying to synthesize new organic donors with stable radical spin parts and new functional porous molecular crystals.

We reported the improved method of four-probe resistivity measurements using diamond anvil several years ago. However we had to stop the high-pressure experiment since then. But we are now re-trying to perform the single-crystal resistivity measurements above 20 GPa.

IV-C-1 Phase Diagram and Anomalous Resistivity Behavior of λ -(BETS) $_2\text{Fe}_x\text{Ga}_{1-x}\text{Cl}_4$

CUI, HengBo; TAKAHASHI, Kazuyuki; OKANO, Yoshinori; KOBAYASHI, Hayao; KOBAYASHI, Akiko¹
(¹Nihon Univ.)

Rich variety of organic conductors provides unique chances to encounter novel systems showing unexpected conducting phenomena such as a superconductor-to-insulator (SC-I) transition and organic thyristor effect. Several years ago, we have reported that λ -(BETS) $_2\text{FeCl}_4$ undergoes a field-induced superconducting transition, where BETS (= bis(ethylenedithio)tetraselenafulvalene, $\text{C}_{10}\text{H}_8\text{S}_4\text{Se}_4$) is a π donor molecule. Since the size of FeCl_4^- anion is almost equal to that of GaCl_4^- , unprecedented alloys (λ -(BETS) $_2\text{Fe}_x\text{Ga}_{1-x}\text{Cl}_4$) of organic superconductor (λ -(BETS) $_2\text{FeCl}_4$) and field-induced organic superconductor can be prepared at arbitrary mixing ratio. We have previously reported the temperature-composition (T - x) phase diagram of λ -(BETS) $_2\text{Fe}_x\text{Ga}_{1-x}\text{Cl}_4$. However, we have recently found that x -value shows a significant difference even in one single crystal, which requested careful re-examination of the phase diagram of these novel alloy systems. The revised phase diagram showed that the superconducting phase is stabilized by neighboring on the antiferromagnetic insulating phase. In addition we have examined the resistivity behavior under magnetic field and found that constant resistivity state at $x = 0.37$ – 0.42 .

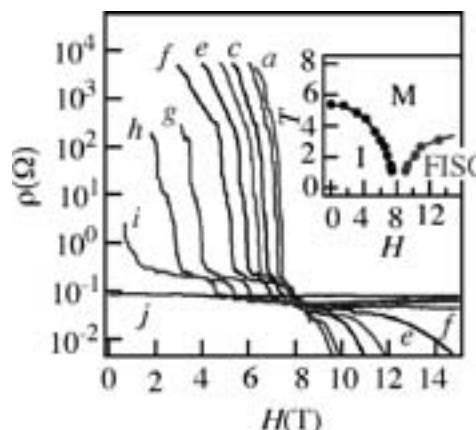


Figure 1. An example of T - H phase diagram of λ -(BETS) $_2\text{Fe}_x\text{Ga}_{1-x}\text{Cl}_4$ ($x = 0.66$), where H is applied parallel to the ac conduction plane: $a = 1.1$ K, $b = 1.5$, $c = 2.1$, $d = 2.6$, $e = 3.1$, $f = 3.6$, $g = 4.45$, $h = 4.9$, $i = 5.3$, $j = 4.1$, $k = 7.7$. It is shown that the MI transition was suppressed around 8 T and the field-induced superconducting phase begins to appear.

IV-C-2 Magnetic Transitions of Single-Component Molecular Metal [Au(tmdt) $_2$] and Its Alloy Systems

ZHOU, Biao¹; KOBAYASHI, Akiko¹;
SHIMAMURA, Mina¹; FUJIWARA, Emiko¹;
HIGASHI, Takeshi²; NISHIBORI, Eiji²; SAKATA,
Makoto²; CUI, HengBo; TAKAHASHI, Kazuyuki;
KOBAYASHI, Hayao
(¹Univ. Tokyo; ²Nagoya Univ.)

[Ni(tmdt)₂] (tmdt = trimethylenetetrafulvalenedithiolate) is the first single-component molecular metal, where the metal electrons can be automatically generated by self-assembly of single kind of molecules. Though [Au(tmdt)₂] is isostructural to [Ni(tmdt)₂], the electronic band structures is completely different from that of [Ni(tmdt)₂] because the neutral bis(dithiolato)gold complex has an odd number of total electrons. Although it had been found that [Au(tmdt)₂] undergoes a possible antiferromagnetic transition around 100 K, more detail examination was needed. We have recently succeeded to obtain high-quality sample and performed the single crystal structure determination, resistivity measurements (on compacted pellet sample) and magnetic susceptibility. As shown in Figure 1, the temperature and field dependences of the susceptibility showed antiferromagnetic transition at 110 K. Recent electrical resistivity measurements using interdigitated electrodes by Tanaka et al. confirmed that the crystal retains metallic state even below 100 K. Thus, [Au(tmdt)₂] is clarified to be the first antiferromagnetic molecular metal with magnetic transition temperature at 110 K. The metallic state below the antiferromagnetic transition temperature is consistent with the band structure calculation suggesting the possibility of the partial nesting of the Fermi surfaces.

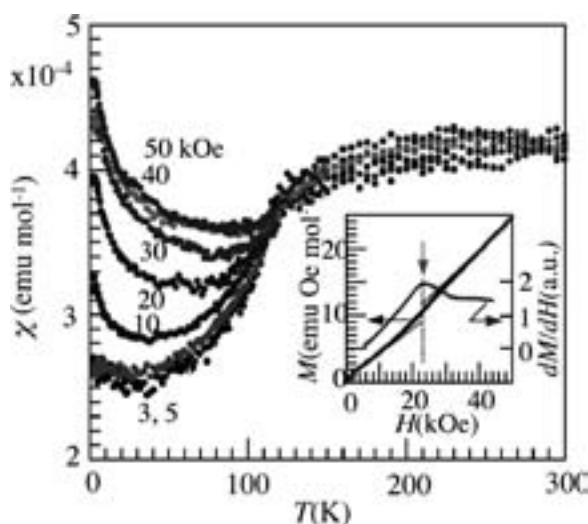


Figure 1. Temperature and magnetic field dependences of the susceptibilities of crystalline powder sample of [Au(tmdt)₂]. The inset is the H -dependences of M and dM/dH at 40 K. The gray arrow indicates the spin flop field

IV-C-3 Molecular Design and Physical Properties of Single-Component Molecular Metals

**KOBAYASHI, Akiko¹; OKANO, Yoshinori;
KOBAYASHI, Hayao**
(¹Univ. Tokyo)

[*J. Phys. Soc. Jpn.* **75**, 051002 (2006)]

The design of metallic crystals consisting of single-component molecules (*single-component molecular metal*) is explained on the basis of the examinations of frontier molecular orbitals and the simple extended-

Hückel tight-binding band pictures. To meet the conditions required to realize automatic carrier generation by self-assembly of the same kind of neutral molecules, a crystal of a transition metal complex molecule [Ni(tmdt)₂] with extended-TTF-type (TTF = tetrathiafulvalene) dithiolate ligands was synthesized, which was found to be the first single-component molecular metal. The X-ray structure analyses of the crystals of [(C₄H₉)₄N]₂[Ni(tmdt)₂] and neutral [Ni(tmdt)₂] provided information on the symmetry of the frontier molecular orbitals (the highest occupied molecular orbital (HOMO) and the lowest unoccupied molecular orbital (LUMO)) from which the metallic bands are formed. The infrared and visible spectra of a crystalline powder sample of [Ni(tmdt)₂] showed a broad electronic absorption maximum at around 2200 cm⁻¹, suggesting an extremely small HOMO-LUMO gap. The physical properties of some of the hitherto-developed single-component molecular conductors are also briefly described.

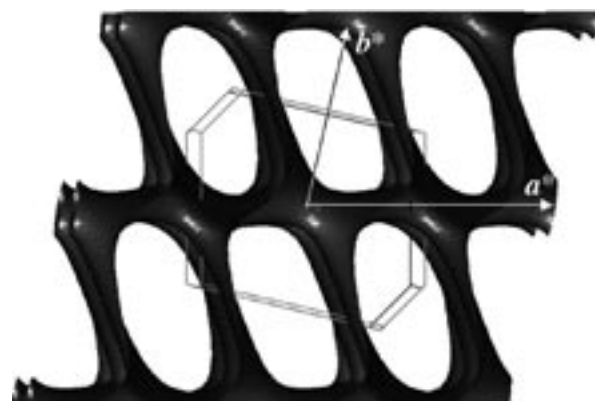


Figure 1. Fermi surfaces of single-component magnetic molecular metal, [Au(tmdt)₂] viewed along the c^* direction.

IV-C-4 A Molecular Conductor Based on Monoanionic Nickel Complex with Extended-TTF Type Ligands, (nBu₄N)[Ni(dmstfdt)₂] Exhibiting Weakly Metallic Behavior at High Temperature and Weak Ferromagnetism at Low Temperature

**FUJIWARA, Emiko¹; YAMAMOTO, Kimiko¹;
SHIMAMURA, Mina¹; ZHOU, Biao^{1,2};
KOBAYASHI, Akiko^{1,2}; CUI, HengBo;
TAKAHASHI, Kazuyuki; OKANO, Yoshinori;
KOBAYASHI, Hayao**
(¹Univ. Tokyo; ²Nihon Univ.)

A 1:1 tetrabutylammonium nickel complex with TTF-type ligands, (nBu₄N)[Ni(dmstfdt)₂] (dmstfdt = dimethyldiselenadithiafulvalenedithiolate) (**1**) is a unique molecular system with ambivalent character which exhibits weakly metallic behavior above room temperature and a weak ferromagnetism of localized electrons at low temperature. The X-ray structure analysis of **1** revealed that there are crystallographically independent two [Ni(dmstfdt)₂]⁻ anions (A and B) and two nBu₄N⁺ cations in the unit cell. The anions are arranged in a zigzag -ABA'B'- manner along the molecular side-by-side direction with a dihedral angle of molecular planes being 42.6°. The tight-binding band structure calculation

based on the extended Hückel approximation of **1** gave small three-dimensional electron and hole Fermi surfaces, which were compatible with the observed weakly metallic behavior around room temperature despite of the 1:1 stoichiometry of the complex. The χT values of **1** increased linearly from 0.129 to 0.383 emu·K·mol⁻¹ with decreasing temperature at 160–340 K, suggesting the gradual electron localization with lowering temperature. At 147 K, the complex **1** showed a sharp insulating transition associated with the localization of one electron on each nickel complex below 160 K. At 80–150 K, χ was well fitted by the Curie-Weiss law: $\chi = C/(T-\theta)$; $C = 0.383$ emu·K·mol⁻¹ and $\theta = -4$ K. A weak ferromagnetism was observed below 7 K. The coercive force was ± 1.5 kOe at 2.0 K.

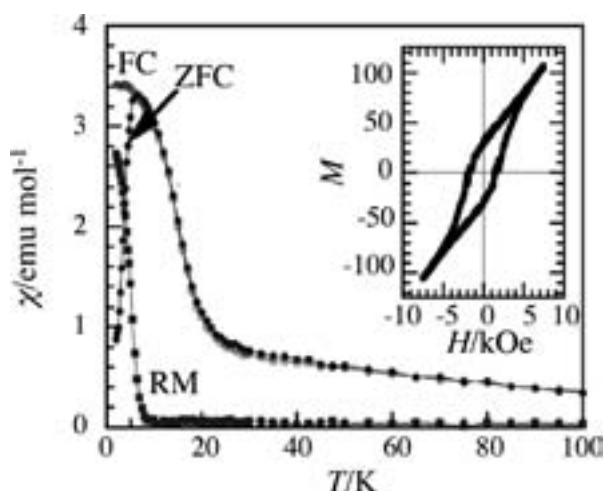


Figure 1. The zero-field-cooled (ZFC) and field-cooled (FC) susceptibilities and remnant magnetization (RM) as a function of temperature at 1 kOe for the polycrystalline sample of **1**. The insets shows the field dependence of the magnetization at 2.0 K.

IV-C-5 Ferroelectric Porous Molecular Crystal, [Mn₃(HCOO)₆](C₂H₅OH)

CUI, HengBo; WANG, Zheming¹; TAKAHASHI, Kazuyuki; OKANO, Yoshinori; KOBAYASHI, Hayao; KOBAYASHI, Akiko²
(¹Peiking Univ.; ²Nihon Univ.)

Weak interaction is the most characteristic feature in the assembling of molecules. A typical example is the host-guest interaction in the porous materials, which have recently attracted large attention because of the high potentiality in the design of new materials with novel functions. Since the polar guest molecules form small assemblies loosely confined in the porous space, the porous material will be easily converted to the highly polarizable system by inserting polar guest molecules. If the polarized guest molecules are three-dimensionally ordered, a ferro- (or antiferro-) electric state will be realized. Furthermore, if we can combine the ferroelectrically polarizable guest molecules and the host porous lattice exhibiting magnetic order, we can obtain new type of “*multiferroic* molecular materials” where ferroelectricity and ferromagnetism coexist. We have recently discovered the first example of porous molecu-

lar crystal [Mn₃(HCOO)₆](C₂H₅OH) exhibiting ferroelectric transition at 165 K and ferrimagnetic transition at 8.5 K. The temperature dependence of the dielectric constants indicated that the ferroelectric transition is the first order transition. The dielectric measurements on the crystal with deuterated ethanol showed no significant change of T_c , suggesting that H-bond is not play an important role.

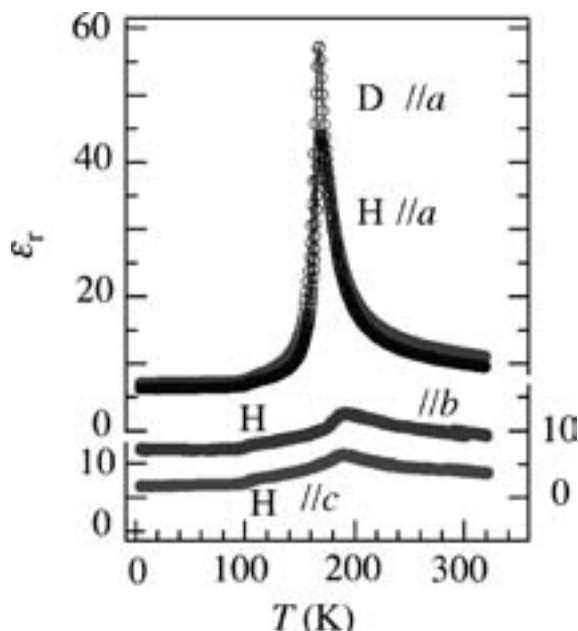


Figure 1. Dielectric constants (ϵ_r) of [Mn(HCOO)₆](C₂H₅OH) for the field $E//a$, b and c . The ϵ_r ($E//a$) of the crystal with deuterated ethanol, [Mn(HCOO)₆](C₂H₅OD) is also presented (open circles). D and H represent the dielectric constants of [Mn(HCOO)₆](C₂H₅OH) and [Mn(HCOO)₆](C₂H₅OD), respectively.

IV-C-6 Antiferroelect Porous Molecular Crystal with Guest Water Molecules

CUI, HengBo; LONG, La-Sheng¹; TAKAHASHI, Kazuyuki; OKANO, Yoshinori; KOBAYASHI, Hayao; KOBAYASHI, Akiko¹
(¹Xiamen Univ.; ²Nihon Univ.)

We have recently found that a porous molecular crystal containing guest H₂O molecules, [Cu₃La₂(imino diacetate)₃](H₂O)₈ exhibits anomalously large dielectric constants and antiferroelectric hysteresis above the room temperature. At first, we measured the dielectric constants of the crystalline powder sample. But it gave anomalously large dielectric constant. In addition, the dielectric constant increased with increasing temperature around the room temperature. Similar behaviors were observed in various powdered crystals including famous ferroelectric material such as KH₂PO₄, which of course gave normal results when the single crystal was used. Therefore the measurement using the single crystal is essential for the dielectric experiments. In the present studies, the crystal with the size of 1.4 × 1.1 × 0.55 mm³ was used. As shown in Figure 1, ϵ_r showed a characteristic temperature dependence above 150 K. Though ϵ_r of [Cu₃La₂(iminodiacetate)₃](H₂O)₈ increased above 250

K, its temperature dependence became sluggish above 340 K. It was quite surprising that the antiferroelectric hysteresis loop was observed around 350 K where the guest H₂O molecules began to escape fairly rapidly. The dielectric properties of [Cu₃La₂(iminodiacetate)₆](D₂O)₈ were also examined.

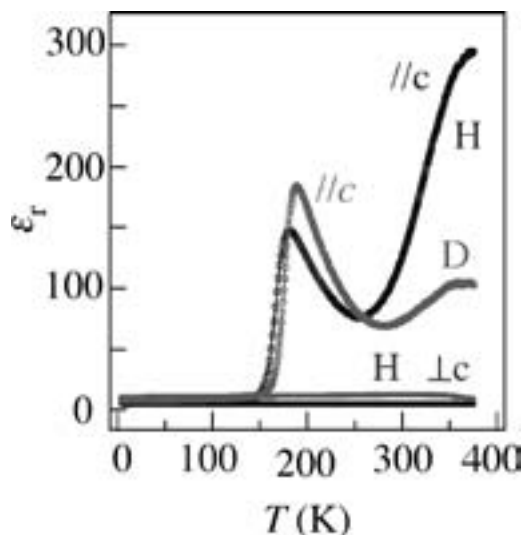


Figure 1. The dielectric constants ϵ_r of [Cu₃La₂(iminodiacetate)₆](H₂O)₈ for $E//c$ (black) and $E\perp c$ (gray). The black lines indicate ϵ_r of the guest-free crystal [Cu₃La₂(iminodiacetate)₆]. The dielectric constant of [Cu₃La₂(iminodiacetate)₆](D₂O)₈ is also presented ($E//c$ (gray)).

IV-C-7 High-Pressure Four-Probe Resistivity Measurements of Organic Crystals

CUI, HengBo; KOBAYASHI, Hayao

It is well known that resistivity measurements at extremely high pressure using diamond anvil revealed the superconductivities of various molecular materials such as hexa-iodobenzene and even O₂ which are usually considered to have no connection with electron conduction phenomena. Although the diamond anvil technique is very attractive one, its application to the four-probe resistivity measurements of the fragile organic crystals seems to contain many difficulties. Non-hydrostatic nature of the pressure medium at high pressure and anisotropic nature of molecular crystals will prevent the accurate resistivity measurements. However, the largest difficulty will exist in the method to connect four electrical leads (usually very thin gold wires) bonded to small sample crystal set in the small sample space in the diamond anvil cell with four lead terminals outside the diamond anvil. Several years ago, we have reported the superconductivity of (TMTTF)₂PF₆ discovered around 5 GPa by four-probe diamond anvil resistivity measurements and the improved method of the diamond anvil resistivity measurements. Very recently we have re-tried to perform high-pressure resistivity measurements of organic crystals by adopting the same method and found this method to be applicable at least up to 20 GPa.

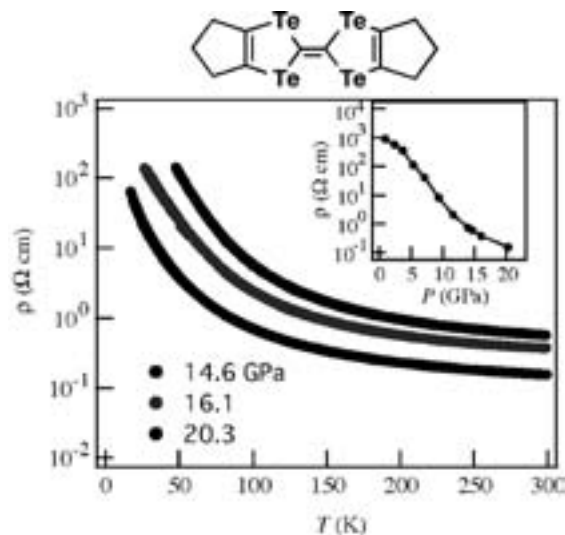


Figure 1. An example of the temperature dependence of the resistivity of molecular crystal up to 20 GPa. It should be noted that the room-temperature resistivity of the crystal of HMTTeF was reduced to about 0.15 Ωcm at 20 GPa.

IV-C-8 Electrical Conductivity Modulation Coupled to a High-Spin–Low-Spin Conversion in the Molecular System [Fe^{III}(qsal)₂][Ni(dmit)₂]₃·CH₃CN·H₂O

TAKAHASHI, Kazuyuki; CUI, HengBo; OKANO, Yoshinori; KOBAYASHI, Hayao; EINAGA, Yasuaki¹; SATO, Osamu²
(¹Keio Univ.; ²Kyushu Univ.)

[*Inorg. Chem.* **45**, 5739–5741 (2006)]

Recently considerable interest has been attracted to the development of novel multi-functional molecular conductors. We have attempted to explore the possibility of reversible control of electrical conducting states by external stimuli. It is well known that the conducting properties of molecular conductors are changed greatly by the small modification of their crystal structures. Since the spin transition between the low-spin (LS) and the high-spin (HS) states accompanies a remarkable structural change in coordination bond length and geometry, the electrical conductivity of conducting spin-crossover (SCO) complex can be expected to be controlled by a structural change involving the spin conversion. The title complex was prepared by applying a constant voltage of [Fe(qsal)₂][Ni(dmit)₂]₂·2CH₃CN in acetonitrile [qsalH = *N*-(8-quinolyl)-salicylaldehyde, dmit = 4,5-dithiolato-1,3-dithiole-2-thione]. Ni(dmit)₂ molecules are arranged in a face-to-face manner to form a six-fold column along the *b* axis. These columns are arranged in a herring-bone type side-by-side to generate layers along the transverse direction. Fe(qsal)₂ cations are dimerized by π - π interactions. The Fe(qsal)₂ dimers construct a one-dimensional chain parallel to the Fe–Fe direction of a dimer, which is the *a*+*b* direction in the present case. Thus, Fe(qsal)₂ chains were interwoven with the Ni(dmit)₂ columns. Temperature dependence of magnetic moment and electrical resistivity of the 1:3 complex were shown in Figure 1. Interestingly, a hysteresis

esis loop of resistivity was observed in the temperature range of 90–120 K, which corresponds to the temperature range of the hysteresis of magnetic behavior. The relatively low resistivity in the heating process may be due to a sort of “chemical pressure effect” associated with the spin transition. Since the smaller size of SCO ions in the LS state than in the HS state will produce the more compact molecular packing of the cationic layers; this contraction exerts a pressure to the Ni(dmit)₂ conducting layers to make the system more conducting. Thus, to the best of our knowledge, this is the first evidence of a resistivity anomaly coupled with a spin transition in the SCO-molecular conductor hybrid.

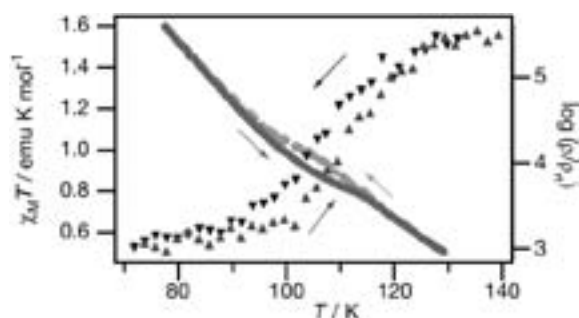


Figure 1. $\chi_M T$ vs. T plot (triangle, scale: left) and $\log(\rho/\rho_{RT})$ vs. T plot (circle, scale: right) of the 1:3 complex at the temperature range between 70 and 140 K.

IV-C-9 Structural Modifications Accompanying a Reproducible Spin-Crossover Phenomenon in [Fe(qsal)₂][Ni(dmise)₂] \cdot 2CH₃CN

TAKAHASHI, Kazuyuki; CUI, HengBo; KOBAYASHI, Hayao; EINAGA, Yasuaki¹; SATO, Osamu²
(¹Keio Univ.; ²Kyushu Univ.)

Recently we have developed novel Fe(III) spin-crossover (SCO) systems containing the Ni(dmit)₂ components: [Fe(qsal)₂][Ni(dmit)₂] \cdot 2CH₃CN showed a cooperative spin transition and a light-induced excited spin state trapping (LIESST) effect and [Fe(qsal)₂][Ni(dmit)₂] \cdot 3 \cdot CH₃CN \cdot H₂O demonstrated a conducting modulation coupled to a spin transition [qsalH = *N*-(8-quinoly)-salicylaldehyde, dmit = 4,5-dithiolato-1,3-dithiole-2-thione]. In particular, the synergic behavior between conducting and magnetic properties probably results from a sort of “chemical pressure effect” involving a spin conversion. However, it has never been successful to determine the crystal structures before and after the spin transition in both complexes. In the course of further studies to investigate more conducting systems in the related complexes, a reproducible spin transition with a small hysteresis loop that didn’t change by repeating the cooling and heating treatments was found in [Fe(qsal)₂][Ni(dmise)₂] \cdot 2CH₃CN [dmise is 4,5-dithiolato-1,3-dithiole-2-selone] (Figure 1). The crystal structure in the high temperature (HT) phase was isostructural to that of [Fe(qsal)₂][Ni(dmit)₂] \cdot 2CH₃CN at room temperature. The crystal system and symmetry does not change in the low temperature (LT) phase. Fe(qsal)₂ molecules formed one-dimensional chains through strong π – π interactions along the *b* axis and each chain was over-

lapped each other, to construct Fe(III) cation two-dimensional layers. The coordination bond lengths around the Fe atom indicated that the Fe(III) complex in the HT phase was almost in the high spin state and that in the LT phase was almost in the low spin state, respectively. These observations are consistent with the $\chi_M T$ values calculated from the SQUID data. A significant contraction in Fe(qsal)₂ two-dimensional layer was observed from the HT to the LT phases, suggesting this contraction would apply pressure to Ni(dmit)₂ layers.

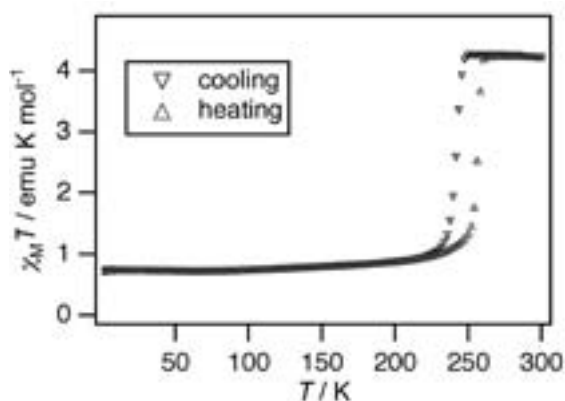


Figure 1. $\chi_M T$ vs. T plot of [Fe(qsal)₂][Ni(dmise)₂] \cdot 2CH₃CN.

IV-C-10 A Magnetic Organic Conductor Based on a π Donor with a Stable Radical and a Magnetic Anion—A Step to Magnetic Organic Metals with Two Kinds of Localized Spin Systems

OTSUBO, Saika; CUI, HengBo; LEE, HaJin; FUJIWARA, Hideki; TAKAHASHI, Kazuyuki; OKANO, Yoshinori; KOBAYASHI, Hayao

[*Chem. Lett.* **35**, 130–131 (2006)]

The synergetic action of magnetism and conductivity in the magnetic organic conductor consisting of π donor molecules and magnetic anions has recently attracted a considerable attention. On the other hand, there remains the long-standing target, that is, the magnetic organic conductor based on π donors having a stable organic radical part in the development of magnetic organic conductors. We have utilized a stable radical donor, TTP-PROXYL, which is 2,5-bis(1,3-dithiol-2-ylidene)-1,3,4,6-tetrathiapentalene (TTP) incorporating the 2,2,5,5-tetramethyl-1-pyrrolidin-1-ylloxyl (PROXYL) radical, and have obtained two isostructural conducting salts, (TTP-PROXYL)FeCl₄ and (TTP-PROXYL)GaCl₄. (TTP-PROXYL)FeCl₄ is a semiconductor with two kinds of localized spin systems which are organic radical spins and 3d spins of magnetic FeCl₄[−] ions, respectively. Compared with the isostructural GaCl₄ salt showing similar conducting properties, the π spin of the TTP-PROXYL radical cation disappears due to dimerization but the χT -value in FeCl₄ salt is 4.65 K emu mol^{−1}, indicating the coexistence of high-spin Fe³⁺ ($S = 5/2$) and PROXYL radical ($S = 1/2$). This observation will open a way to realize a new type of the magnetic organic conductors such as ferrimagnetic organic conductors.

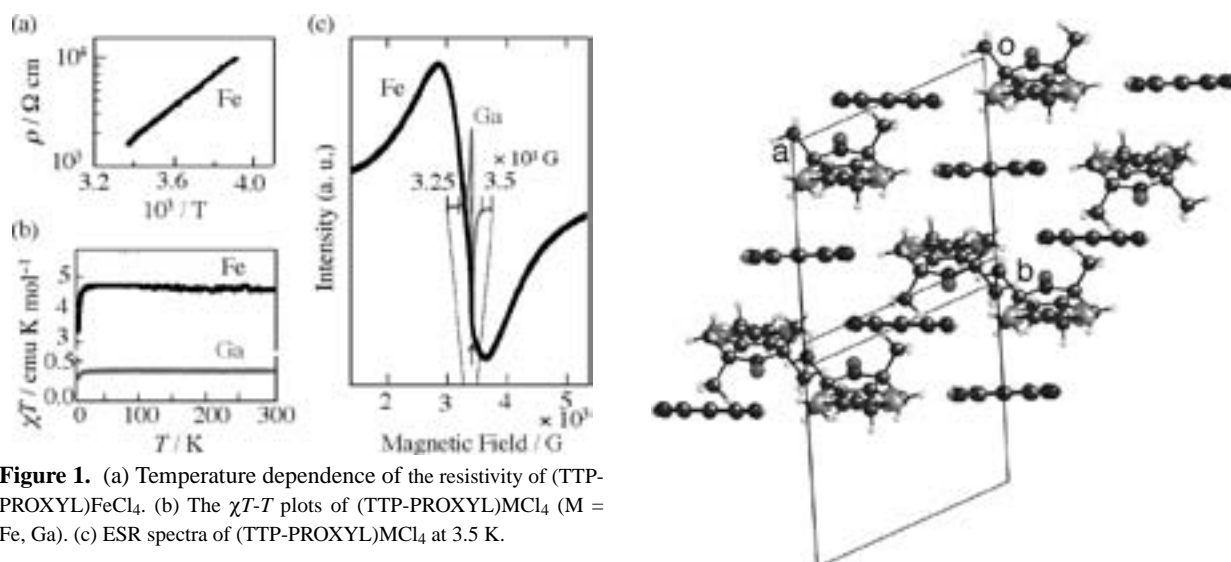


Figure 1. (a) Temperature dependence of the resistivity of (TTP-PROXYL)FeCl₄. (b) The χT - T plots of (TTP-PROXYL)MCl₄ (M = Fe, Ga). (c) ESR spectra of (TTP-PROXYL)MCl₄ at 3.5 K.

IV-C-11 Synthesis and Characterization of Novel PROXYL-Fused π -Electron Donors

TAKAHASHI, Kazuyuki; KOBAYASHI, Hayao

The development of novel magnetic molecular conductors based on the interplay between conducting electrons and localized spins has aroused a great attention in molecular materials science. To realize the coupling between conducting π -electrons and the spins on the stable organic radical in purely organic systems is one of the targets in this field. Despite several reports of syntheses and physical properties of π -electron donor or acceptor molecules with stable organic radicals and their conducting complexes, the number of well-characterized conducting complexes based on these donor or acceptor molecules is rare. Probably since the organic stable radicals are usually bulky and flexible, it is difficult to construct the conduction path based on the overlap between π -donors or acceptors and to give conducting crystals of good quality. In order to decrease a steric hindrance of a stable organic radical and to make a molecular structure rigid, we have designed and synthesized novel PROXYL radical-fused diselenadithiafulvalene (STF) derivatives. All the spectral data of new radical donors were in a good agreement with their molecular structures. Cyclic voltammograms revealed that the first and second one-electron oxidations occurred on the STF moieties, suggesting the possibility to generate cation biradical species. PROXYL-ET-STF afforded the 1:1 charge transfer complex with TCNQF₄. The radical donors (D) and acceptors (A) were alternately stacked to form irregular one-dimensional columns consisted of D-A-D trimers and A monomers (Figure 1). Bond length differences indicated that the complete charge transfer from the donor to the acceptor would occur. The magnetic data suggested that π -spins on the donor and acceptor were strongly antiferromagnetically coupled. The existence of NO radical spins was also suggested.

Figure 1. Crystal structure of (PROXYL-ET-STF)(TCNQF₄)·PhCl.

IV-D Progress of Conjugated Phenomena Coupled with Spin, Charge and Photon for Assembled Hetero-Molecular System

Intercalation of photochromic molecule into magnetic system provides fascinating multi-functionalities such as photo-magnetism, which gains much attention for their application to devices. The main subjects in this project are the development of photo-induced spin-crossover phenomena at room temperature by using the photo-isomerization of intercalated molecule, and the development of the transformation of magnetism for two-dimensional ferromagnetic system coupled with photochromic molecule.

IV-D-1 Enhancement of the Curie Temperature by Photoisomerization of Diaryl-Ethene (DAE) for an Organic-Inorganic Hybrid System: $\text{Co}_4(\text{OH})_7(\text{DAE})_{0.5}\cdot 3\text{H}_2\text{O}$

SHIMIZU, Hideharu¹; NAKAMOTO, Akio¹; ENOMOTO, Masaya¹; KOJIMA, Norimichi²
(¹Univ. Tokyo; ²IMS and Univ. Tokyo)

[*Inorg. Chem.* **45**, 10240–10247 (2006)]

Photomagnetism is one of the most attractive topics in recent research on molecular solids. Intercalation of an organic photochromic molecule into layered magnetic systems has a possibility to provide multifunctional properties such as photomagnetism. In order to build up a photosensitive multifunctional magnet, an organic-inorganic hybrid system coupled with a photochromic diarylethene anion, 2,2'-dimethyl-3,3'-(perfluorocyclopentene-1,2-diyl)bis(benzo[b]thiophene-6-sulfonate) (DAE), and cobalt LDHs (layered double hydroxides), $\text{Co}_4(\text{OH})_7(\text{DAE})_{0.5}\cdot 3\text{H}_2\text{O}$, was synthesized by the anion exchange reaction between $\text{Co}_2(\text{OH})_3(\text{CH}_3\text{COO})\cdot\text{H}_2\text{O}$ and DAE.^{1,2} In the dark and under UV (313 nm) irradiated conditions, $\text{Co}_4(\text{OH})_7(\text{DAE})_{0.5}\cdot 3\text{H}_2\text{O}$ with the open and close-forms of DAE were obtained, respectively. The magnetic susceptibility measurements elucidated ferromagnetic intra- and inter-layer interactions and Curie temperatures of $T_C = 9$ K and $T_C = 20$ K for cobalt LDHs with the open and close-forms of DAE, respectively. The enhancement of the Curie temperature from 9 K to 20 K by substituting the open-form of DAE with the close-form of DAE as intercalated molecule is attributed to the delocalization of π electrons in the close-form of DAE, which enhances the inter-layer magnetic interaction. The enhancement of the inter-layer magnetic interaction induced by the delocalization of π electrons in intercalated molecules is strongly supported by the fact that the Curie temperature (26.0 K) of cobalt LDHs with (*E,E*)-2,4-hexadienedioate having a conjugated π electron system is enormously higher than that (7.0 K) of cobalt LDHs with hexanedioate, which is shown in Figure 1.² By UV irradiation of 313 nm, $\text{Co}_4(\text{OH})_7(\text{DAE})_{0.5}\cdot 3\text{H}_2\text{O}$ shows the photoisomerization of DAE from the open-form to the close-one in solid state, which leads to the enhancement of Curie temperature, which is schematically shown in Figure 2.²

References

- 1) M. Okubo, M. Enomoto and N. Kojima, *Solid State Commun.* **134**, 777 (2005).
- 2) H. Shimizu, M. Okubo, A. Nakamoto, M. Enomoto and N. Kojima, *Inorg. Chem.* **45**, 10240 (2006).

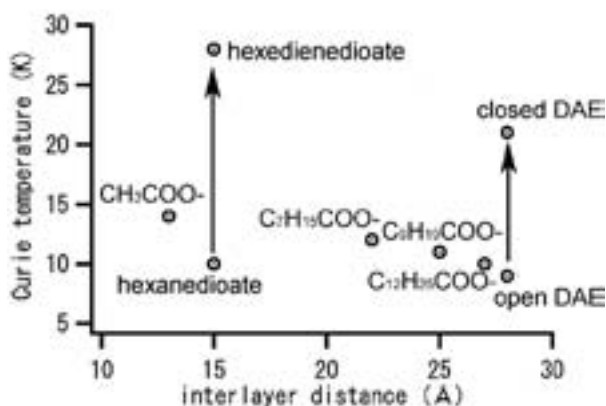


Figure 1. Relation between the interlayer distance and the Curie temperature of Co-LDHs.

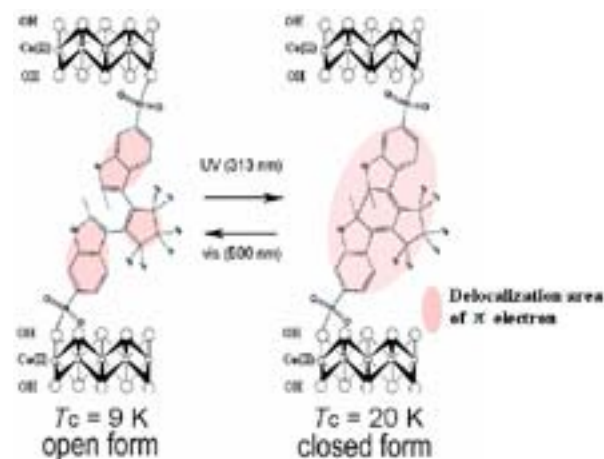


Figure 2. Schematic representation of the photoinduced conversion between Co-LDHs with open-form of DAE having $T_C = 9$ K and Co-LDHs with closed-form of DAE having $T_C = 20$ K.

IV-D-2 Charge Transfer Phase Transition and Ferromagnetism in Organic-Inorganic Hybrid System, $\text{A}[\text{Fe}^{\text{II}}\text{Fe}^{\text{III}}(\text{dto})_3](\text{A} = (\text{C}_n\text{H}_{2n+1})_4\text{N}, \text{Spiropyran}, \text{etc.}; \text{dto} = \text{C}_2\text{O}_2\text{S}_2)$

KOJIMA, Norimichi¹; HIKITA, Masanori²; KIDA, Noriyuki²; KASHIMA, Izuru²; ONO, Yuuki²; ITOI, Miho²; ENOMOTO, Masaya²
(¹IMS and Univ. Tokyo; ²Univ. Tokyo)

[*Synth. Met.* **153**, 473–476 (2005), *Eur. J. Inorg. Chem.* 1198–1207 (2006)]

In the case of mixed-valence complexes whose spin states are situated in the spin-crossover region, it is expected that new types of conjugated phenomena coupled with spin and charge take place. Recently, we have discovered a new type of first order phase transition around 120 K for $(n\text{-C}_3\text{H}_7)_4\text{N}[\text{Fe}^{\text{II}}\text{Fe}^{\text{III}}(\text{dto})_3](\text{dto} = \text{C}_2\text{O}_2\text{S}_2)$, where the thermally induced charge transfer between Fe^{II} and Fe^{III} occurs reversibly.¹⁾ $(n\text{-C}_4\text{H}_9)_4\text{N}[\text{Fe}^{\text{II}}\text{Fe}^{\text{III}}(\text{dto})_3]$ also undergoes the charge transfer phase transition around 140 K, while the charge transfer phase transition does not take place for $(n\text{-C}_n\text{H}_{2n+1})_4\text{N}[\text{Fe}^{\text{II}}\text{Fe}^{\text{III}}(\text{dto})_3](n = 5 \text{ and } 6)$, where the spin configuration of Fe^{II} ($S = 2$) and Fe^{III} ($S = 1/2$) exists between 2 K and 300 K. Moreover, $(n\text{-C}_n\text{H}_{2n+1})_4\text{N}[\text{Fe}^{\text{II}}\text{Fe}^{\text{III}}(\text{dto})_3]$ ($n = 3\text{--}6$) undergo the ferromagnetic phase transition. The Curie temperatures for $n = 3$ and 4 are 6.5 K and 6 K & 13 K, respectively, while those for $n = 5$ and 6 are 19 K and 25 K, respectively.²⁾

As mentioned above, these phase transitions remarkably depend on the size of intercalated cation, which implies a possibility to control the magnetic properties of two-dimensional honeycomb network structure of $[\text{Fe}^{\text{II}}\text{Fe}^{\text{III}}(\text{dto})_3]_\infty$ by means of the isomerization of intercalated cation. From this viewpoint, we have synthesized a photo-sensitive organic-inorganic hybrid system, $(\text{SP})[\text{Fe}^{\text{II}}\text{Fe}^{\text{III}}(\text{dto})_3](\text{SP} = \text{spiropyran})$, and investigated the photo-induced effect on the magnetic properties through the medium of photo-isomerization of spiropyran.³⁾ When the UV light is irradiated for $(\text{SP})[\text{Fe}^{\text{II}}\text{Fe}^{\text{III}}(\text{dto})_3]$ in KBr pellet between 300 K and 77 K, a new absorption spectrum with wide half-width appears around 550 nm, which corresponds to the $\pi\text{-}\pi^*$ transition in the open form of SP^+ , which implies that the photo-isomerization of SP^+ takes place even at 77 K in the solid state of $(\text{SP})[\text{Fe}^{\text{II}}\text{Fe}^{\text{III}}(\text{dto})_3]$. The zero-field cooled magnetization (ZFCM) has two peaks at 5 K and 15 K, which implies the coexistence of two ferromagnetic phases. The peak of ZFCM at 5 K disappears after UV irradiation. These UV irradiation effects on the magnetic properties imply that the photo-isomerization of SP from the closed form to the open one stabilizes the high-temperature phase with $\text{Fe}^{\text{III}}(S = 1/2)\text{--}\text{Fe}^{\text{II}}(S = 2)$ and destabilizes the low-temperature phase with $\text{Fe}^{\text{III}}(S = 5/2)\text{--}\text{Fe}^{\text{II}}(S = 0)$. Consequently, it is concluded that the charge transfer transition between Fe^{II} and Fe^{III} in $[\text{Fe}^{\text{II}}\text{Fe}^{\text{III}}(\text{dto})_3]$ is induced by the photo-isomerization of SP in $(\text{SP})[\text{Fe}^{\text{II}}\text{Fe}^{\text{III}}(\text{dto})_3]$.

References

- 1) N. Kojima, W. Aoki, M. Itoi, Y. Ono, M. Seto, Y. Kobayashi and Yu. Maeda, *Solid State Commun.* **120**, 165 (2001).
- 2) M. Itoi, Y. Ono, N. Kojima, K. Kato, K. Osaka and M. Takata, *Eur. J. Inorg. Chem.* 1198 (2006).
- 3) I. Kashima, M. Okubo, Y. Ono, M. Itoi, N. Kida, M. Hikita, M. Enomoto and N. Kojima, *Synth. Met.* **153**, 473 (2005).

IV-E Charge and Spin Dynamics of Organic Conductors

The spin and charge dynamics in organic conductors play important role in the emergence of the exotic properties in organic conductors, for example, superconductivity, magnetic ordering, charge ordering. For these purposes, it is important to reveal not only magnetic properties, the total picture of organic conductors. As known well, ^{13}C -NMR is a one of the most powerful tool in the point of the magnetism. Since nuclear magnetic moment, I , is $1/2$, ^{13}C -NMR is not sensitive to the charge properties. On the other hand, optical studies, which are sensitive to the charge properties, are complementary to NMR study. In order to study both magnetic and charge properties, we performed ^{13}C -NMR and optical works.

IV-E-1 Charge Ordering State on Organic Conductors

OGURA, T.¹; KAWAMOTO, Atsushi²; KUMAGAI, K.¹; TANIGUCHI, H.³

(¹Hokkaido Univ.; ²IMS and Hokkaido Univ.; ³Saitama Univ.)

Quasi-two-dimensional (Q2D) organic conductor (BEDT-TTF)₃Cl₂·2H₂O is metallic at 300 K and it undergoes metal–insulator transition (MIT) at $T \sim 150$ K from magnetic susceptibility and electric conductivity measurements. The MIT has been believed to be connected with charge density wave (CDW) formation. However, the formation of the charge ordering (CO) in the insulator phase was also expected. Using ^{13}C -NMR measurement, we observed the split of the NMR spectrum which corresponded to the charge rich and poor sites below the MIT temperature and could conclude the insulator state is in the CO state.

From electric conductivity measurement under pressures for this compound, it is found that the metal–insulator transition is suppressed by applying pressure and this compound shows superconductivity above 1.6 GPa. In order to inspect how CO state formed under ambient pressure is changed, we measured T_1 under pressures. Regrettably, we could get no information from NMR spectrum because of the broadening spectrum due to magnetism of the pressure cell. Below 1.4 GPa, we observed $(T_1T)^{-1} = \text{constant}$ at high temperature and decreased at low temperature, just same as ambient pressure. This indicates that the formation of the gap Δ also exists under pressures. As we have done above, we estimated the gap Δ at each pressure by means of thermal activation model fitting. We could confirm the existence of the gap Δ until 1.4 GPa. Both the gap Δ and T_g decreased with increasing pressure until 1.4 GPa. By applying pressure, transfer integral t in conductivity chain increases and enhance itinerant-electron system. As the results, the amplitude of the charge disproportionation becomes small and the gap Δ is decreasing. In addition, as compared to metal–insulator transition temperature T_{MI} estimated from electric conductivity measurement, T_g behaves in a way similar to T_{MI} , just as ambient pressure. We predict that a strong correlation between two temperatures; T_g and T_{MI} , exists. With decreasing temperature, $(T_1T)^{-1}$ shows almost constant like a metallic behavior. This indicates that the system changes an itinerant-electron system and the localization of the carrier by CO vanishes. It is important for the elucidation of the mechanism of superconductivity to consider whether the system is a simple metallic state or

an exotic metallic state in which itinerant-electron system and charge disproportionation coexist.

IV-E-2 ^{13}C -NMR Study of Single Crystal of β' -(BEDT-TTF)(TCNQ) under Pressure

ETO, Y.¹; OGURA, T.¹; KAWAMOTO, Atsushi²; KUMAGAI, K.¹; YAMAMOTO, Kaoru; YAKUSHI, Kyuya

(¹Hokkaido Univ.; ²IMS and Hokkaido Univ.)

Organic conductor β' -(BEDT-TTF)(TCNQ) is the material in which BEDT-TTF molecules form two-dimensional structure and TCNQ molecules form one-dimensional stacked structure, and both molecules are in the form of dimer. Properties of this salt shows metal insulator transition (M–I transition) at 330 K at ambient pressure, and transition temperatures decrease by applying pressure. It is known that BEDT-TTF molecule and TCNQ molecule show different magnetic properties so that an antiferromagnetic ordering occurs in the former at 20 K and the latter occurs at 3 K. In addition, properties of this salt under pressure are interested very much from the point of view that the layer structure of BEDT-TTF have the same type of structure of β' -(BEDT-TTF)₂Cl₂ which has the highest T_C under pressure among the organic conductors. So we performed ^{13}C -NMR measurements using single crystal of (BEDT-TTF)(TCNQ) where one site of the central double-bonded carbon in BEDT-TTF molecule is labeled by ^{13}C . BEDT-TTF forms a dimer in a layer. It is expected that two peaks are observed in the high temperature. Actually, two peaks were seen in the observed spectrum in the high temperature side. We can estimate a local susceptibility only for a BEDT-TTF site by using NMR at selected site. One peak was observed in the vicinity of almost knight shift 0 at antiferromagnetic transition temperature (20 K) and understood that line width increased as lowering temperature. We measured in a range of ± 1 MHz at 10 K, but the other peaks were not observed. It suggests that antiferromagnetic transition of this material is not commensurate but incommensurate. We are also going to report about the result of under pressure.

RESEARCH ACTIVITIES V

Department of Applied Molecular Science

V-A Design of Spin-Functional Nanomaterials through Molecular Programming and Nanostructuring

Metal ions with d^4 – d^7 electron configurations can adopt two different magnetic states, *i.e.*, high-spin and low-spin states, which can cross over thermally or by electronic excitation. Spin-crossover phenomena have attracted attention in relation to their potential applications in molecular electronics. A fundamentally important challenge is to synthesize soft spin-crossover materials that can respond to external stimuli such as light and electric/magnetic fields. Up to date, inorganic and crystal engineering approaches have been employed for the synthesis of crystalline spin-crossover solid, which is hardly to process and difficult to use as a component for fabricating nano devices. In contrast to the above approaches, we are developing soft nanomaterials through programmed nanostructuring of metal complexes *via* covalent and non-covalent interactions. We employ one-, two-, and three-dimensional nanoarchitectures to construct well-defined coordination nanospace with spin-active metal complex as building blocks. By altering the size of building blocks, controlling their geometry and orientation, and directing their assembly, it is possible to engineer properties in unprecedented ways. Our strategy is promising for the development of a new family of spin-active nanomaterials whose functionalities and properties are heretofore unavailable in conventional crystalline metal complexes.

V-A-1 Molecular Design and Functions of Spin-Active Dendrimers

ISHIZUKA, Tomoya; JIANG, Donglin¹
(*IIMS and JST/PRESTO*)

Dendrimers are three-dimensional hyperbranched macromolecules that provide well-defined nanoscopic objects at the single molecular level. Unlike ordinary linear polymers, star-shaped polymers, and traditional branched polymers, dendrimers are characterized by their elaborate structure, which allows for precise control of their molecular size, shape, and the numbers and positions of functional groups. Recent studies on dendritic macromolecules have extended the scope of research from synthesis to applications for catalysts, photoactive and electronic materials, medicinal and biomedical materials, and other functional materials.

In this project, we are developing dendrimeric architecture for construction of novel metallodendrimers, whose metal sites are covalently linked in three-dimensional nanospace. By taking advantage of convergent approach, metallodendrimers with different generation numbers, different morphology, and different size are synthesized. These dendrimers provide a platform for the studies on magnetic interactions and cooperativity in spin crossover, among dendritic wedges within confined dendritic nanospace.

V-A-2 Molecular Design and Functions of Spin-Active One-Dimensional Nano-Channels

HE, Zheng; JIANG, Donglin¹
(*IIMS and JST/PRESTO*)

In relation to project V-A-1, we are developing spin-active low-dimensional soft materials, in which metal sites are aligned through non-covalent interactions to assemble one-dimensional and two-dimensional arrays.

A series of triazole derivatives bearing water-soluble dendritic wedges with different generation numbers were synthesized as a bidentate ligand for coordination polymerization with iron(II). The rod-like rigid polynuclear chain appended with water-soluble dendritic wedges serves as a template for hybridization with mesoporous silicate. The hybrid consists of an iron(II) polynuclear chain that is spatially isolated within mesoporous channel, which thereby enables the investigation of magneto-optical properties at the single molecular level. Hybridized mesoporous silica thin film thus formed, due to its domain structure, functions as novel switching and high-density memory devices based on spin transition.

V-B Bioinorganic Chemistry and Structural Biology of Heme Proteins

One of research activities of my group is directed toward developing a rigorous, quantitative understanding of the biochemical function of heme proteins such as oxygenases, peroxidases and oxidases by characterization of their structural and functional properties. We use different experimental strategies including protein engineering, spectroscopic characterization of the molecular structure of the active centers, measurements of dynamics of substrates and inhibitor binding, and X-ray crystallography.

My current heme protein projects include (1) elucidation of the catalytic mechanism of heme oxygenase, one of the essential components of the heme catabolism and biosynthesis of carbon monoxide, a versatile physiological messenger molecule, (2) elucidation of the mechanism of controlling reactivity of hemoglobin and myoglobin, and (3) determination of heme sensing mechanism of Bach1, a heme-dependent transcription factor which regulates heme oxygenase gene expression. Effective clues to delineate the detailed active site structure have been obtained by X-ray crystallography, resonance Raman and magnetic resonance studies. The synergy of site-directed mutagenesis, structural biology, and spectroscopic techniques has revealed the specific roles of amino acids located in the active centers of heme proteins. Ligands and substrates binding measurements complement the structural data for our understanding functional properties displayed by heme proteins at the molecular level.

V-B-1 Compound I of Heme Oxygenase Can Not Hydroxylate Its Heme *meso*-Carbon

MATSUI, Toshitaka¹; KIM, Sum-Hee²; JIN, Toshimichi¹; HOFFMAN, Brian M.²; IKEDA-SAITO, Masao³

(¹Tohoku Univ.; ²Northwestern Univ.; ³IMS and Tohoku Univ.)

[*J. Am. Chem. Soc.* **128**, 1090–1091 (2006)]

Heme oxygenase (HO) catalyzes heme catabolism through three successive oxygenation where the substrate heme itself activates O₂. It has been thought that the reactive species responsible for the first heme oxygenation, *meso*-hydroxylation, is the hydroperoxy-ferric heme intermediate (Fe–OOH) rather than an oxo ferryl porphyrin cation radical, so called compound I. A recent theoretical study (Kamachi *et al.*, *J. Am. Chem. Soc.* **127**, 10686 (2005)), however, proposed that compound I can oxidize its *meso*-carbon atom with the assistance of a bridging water molecule. In this communication, we have reported the first direct observation of compound I of a heme–HO-1 complex, generated by reaction of ferric–HO-1 with *m*-chloroperbenzoic acid. HO compound I slowly decays to compound II without producing any *meso*-hydroxylated products. It does react with guaiacol and thioanisole, however. Our findings unambiguously rule out involvement of compound I in the HO catalysis.

V-C Electronic Structure and Phase Stability of Bulk Metallic Glass

In this project, we have investigated the electronic structure and chemical bonding of the bulk metallic glasses, bulky multi-element amorphous alloys, experimentally by means of the synchrotron light photoemission spectroscopy and theoretically by the electronic structure calculation for their characteristic clusters, in order to understand the origin of their large glass forming ability from the microscopic point of view. Bulk metallic glasses show very high resistance against the crystallization of the super-cooled melt and a clear glass transition in spite of their thermodynamically metastable phase, and they have drawn much attention as new materials possessing useful engineering properties such as high mechanical strength, high corrosion resistance, good shaping ability, and soft-magnetic properties.

V-C-1 Electronic Structure of Bulk Metallic Glass $Zr_{55}Al_{10}Cu_{30}Ni_5$

SODA, Kazuo¹; SHIMBA, Krando²; YAGI, Sinya²; KATO, Masahiko²; TAKEUCHI, Tsunehiro²; MIZUTANI, Uichiro²; ZHANG, Tao³; HASEGAWA, Masashi³; INOUE, Akihisa³; ITO, Takahiro; KIMURA, Shin-ichi
(¹IMS and Nagoya Univ.; ²Nagoya Univ.; ³Tohoku Univ.)

[*J. Electron. Spectrosc. Relat. Phenom.* **144-147**, 585–587 (2005)]

The electronic structure of a bulk metallic glass $Zr_{55}Al_{10}Cu_{30}Ni_5$ has been studied by means of photoelectron spectroscopy in order to understand the origins of its large glass formation ability and unique mechanical properties from the microscopic point of view. The valence-band photoelectron spectra show three bands ascribed to the Zr $4d$, Ni $3d$ and Cu $3d$ states. Remarkable feature of these bands is the highly-symmetric spectral shape with the high binding energy and narrow width in comparison with the d bands of the crystalline transition metals. This is attributed to the lack of the crystalline periodicity in the metallic glass as well as the reduction in the neighboring atoms to hybridize with those transition metals. High-resolution valence-band spectrum also reveals the intensity reduction near the Fermi level, which implies that the pseudo-gap in the electronic structure may be one of the important factors for the glass formation.

V-C-2 Free-Energy Estimation of the Zr-Ni-Al Bulk Metallic Glass from the Local Atomic Arrangements of the Relevant Crystals

TAKEUCHI, Tsunehiro¹; NAKANO, Sakura¹; HASEGAWA, Masashi²; SODA, Kazuo³; SATO, Hirokazu⁴; MIZUTANI, Uichiro⁵; ITOH, Keiji⁶; FUKUNAGA, Toshiharu⁶
(¹Nagoya Univ.; ²Tohoku Univ.; ³IMS and Nagoya Univ.; ⁴Aichi Univ. Educ.; ⁵Toyota Phys. Chem. Res. Inst.; ⁶Kyoto Univ.)

[*Mater. Trans.* **46**, 2791–2798 (2005)]

Free-energy of Zr-Ni-Al bulk metallic glass (BMG) was estimated by making full use of coordination clus-

ters in the relevant crystals. The clusters in the BMG were determined by using the BMG's experimentally determined radial distribution functions, and the electronic structure of the identified clusters was calculated by the DVX α cluster calculation. The local atomic arrangements in the Zr-Ni-Al BMG are found to be characterized by the prism clusters with Zr or Ni atom in their center and the Kasper polyhedrons about Al atoms. It was concluded, as a consequence of the present analysis, that the Zr-Ni-Al BMG are stabilized by the low internal energy of the constituent local atomic clusters assisted by the large entropy caused by the freedom in the bond-direction between the prism clusters and the Kasper polyhedrons.

V-C-3 Investigation of Stability of the Zr-Ni-Al Bulk Amorphous Phase from Local Atomic Arrangements of the Relevant Crystals

NAKANO, Sakura¹; TAKEUCHI, Tsunehiro¹; SODA, Kazuo²; HASEGAWA, Masashi³; MIZUTANI, Uichiro⁴; SATO, Hirokazu⁵; ITOH, Keiji⁶; FUKUNAGA, Toshiharu⁶
(¹Nagoya Univ.; ²IMS and Nagoya Univ.; ³Tohoku Univ.; ⁴Toyota Phys. Chem. Res. Inst.; ⁵Aichi Univ. Educ.; ⁶Kyoto Univ.)

[*J. Jpn. Soc. Powder Metallurgy* **53**, 100–106 (2006)]

Stability of the Zr-Ni-Al bulk metallic glass (BMG) was investigated by making full use of its relevant crystals. The local atomic arrangements (characteristic atomic clusters) commonly existing in the BMG and its relevant crystals were identified by the experimentally determined radial distribution functions. We found that the local atomic arrangements of the BMG were characterized by the prism clusters with a transition element, Zr or Ni, in their center and the Kasper polyhedron about an Al atom. Internal energy of these clusters was investigated by combinational use of the DVX α cluster calculation and the high-resolution photoemission spectroscopy. The prism clusters about the transition metal elements were confirmed to possess a low internal energy. We propose, as a consequence of present analysis, that the Zr-Ni-Al BMG is stabilized by the low internal-energy of the cluster and the large entropy caused by the freedom in the bond-direction between the clusters.

V-C-4 Electronic Structure of Zr-TM-Al (TM = Ni, Cu) Bulk Metallic Glasses

SUZUKI, Takaharu¹; MIYAZAKI, Hidetoshi¹;
SODA, Kazuo²; TAKEUCHI, Tsunehiro¹;
HASEGAWA, Masashi³; SATO, Hirokazu⁴;
MIZUTANI, Uichiro⁵

(¹Nagoya Univ.; ²IMS and Nagoya Univ.; ³Tohoku Univ.; ⁴Aichi Univ. Educ.; ⁵Toyota Phys. Chem. Res. Inst.)

[*J. Jpn. Soc. Powder Powder Metallurgy* **53**, 107–110 (2006)]

The valence-band electronic structures of Zr-TM-Al (TM = Ni, Cu) bulk metallic glasses have been investigated by means of synchrotron-radiation photoelectron spectroscopy. Their valence-band spectra show Zr 4d-

Ni 3d- and Cu 3d-derived bands at the binding energies of 0.5, 2.0 and 3.6 eV, respectively. The Zr 4d-derived band becomes prominent around the excitation photon energy $h\nu$ of 40 eV. It is found that the wider the super-cooled liquid region $\Delta T_x = T_x - T_g$ (T_x : the crystallization temperature, T_g : the glass transition temperature), the larger the peak binding energy of the Zr 4d-derived band becomes. For the photoexcitation at $h\nu \sim 18$ eV, where the Zr 4d states less contribute to the spectrum, the spectral intensity reduces towards the Fermi level. This may imply the formation of a pseudogap in the sp bands. It is also found that the width of the pseudogap for the occupied states becomes wider as ΔT_x is increased. These spectral findings suggest that both the strength of the chemical bonding around Zr and the reduction in the electronic energy because of the pseudogap formation and the chemical bonding contribute to the large glass formation ability of the Zr-Cu-Al metallic glasses.

V-D Electronic Structures of Fe₂VAl Intermetallic Compound and Its Related Alloys

In this project, we have studied the electronic structures of the Heusler-type intermetallic compound Fe₂VAl and related alloys experimentally with use of the synchrotron light photoemission spectroscopy and theoretically by both the band structure calculation with a super cell and the cluster calculation, in order to clarify the mechanisms of its unusual transport properties and of the large enhancement of their thermoelectric properties. Fe₂VAl and related alloys have been received much attention because of not only the scientific interest in the anomalous transport properties at low temperatures but also their potential application for thermoelectric materials.

V-D-1 Surface and Bulk Electronic Structures of Heusler-Type Fe₂VAl

MIYAZAKI, Hidetoshi¹; SODA, Kazuo¹; YAGI, Sinya²; KATO, Masahiko²; TAKEUCHI, Tsunehiro²;
MIZUTANI, Uichiro³; NISHINO, Yoichi⁴

(¹IMS and Nagoya Univ.; ²Nagoya Univ.; ³Toyota Phys. Chem. Res. Inst.; ⁴Nagoya Inst. Tech.)

[*J. Vac. Sci. Technol., A* **24**, 1464–1467 (2006)]

Surface and bulk electronic structures of Heusler-type ($L2_1$ -type) Fe₂VAl have been investigated by photoelectron spectroscopy, in particular, for the valence band and V 2p core level regions, in order to elucidate the changes in the valence band electronic structures for the surface and bulk regions. In the valence band spectrum, the intensity at the Fermi level E_F is increased for the surface-sensitive low photon energy excitation in comparison to the bulk-sensitive high photon energy excitation. It is also found that the intensity around a binding energy of 0.4 eV is enhanced for large photoelectron takeoff angles for the bulk-sensitive photoelectron spectrum. The V 2p core level spectrum shows a surface-derived shoulder structure on the low binding energy side of the main feature, which suggests that the valence electron concentration around V may be large in the surface layers in comparison to the bulk. These facts suggest that a pseudogap is formed around E_F in the

bulk electronic structure, as predicted by band calculations, and that it is destroyed in the surface layers by the V 3d states as well as the Fe 3d states emerging in mid pseudogap of the bulk electronic structure.

V-E Phase Dynamics under Ultra-High Pressures

Dynamics of phase transition under ultra-high pressures is investigated by using nanosecond time-resolved nonlinear Raman spectroscopy and laser shock compression. Shock wave induced by intense pulsed-laser irradiation can instantaneously generate ultra-high pressures (>1 GPa) and enable to monitor time-evolution of phase transition. By using nonlinear Raman spectroscopy such as stimulated Raman scattering and coherent anti-Stokes Raman scattering, change of molecular structure can be monitored.

V-E-1 Nanosecond Rapid Freezing of Liquid Benzene under Shock Compression Studied by Time-Resolved Coherent Anti-Stokes Raman Spectroscopy

MATSUDA, Akitaka¹; KONDO, Ken-ichi²;
NAKAMURA, Kazutaka¹
(¹IMS and Tokyo Tech; ²Tokyo Tech)

[*J. Chem. Phys.* **124**, 054501 (4 pages) (2006)]

Nanosecond time-resolved coherent anti-Stokes Raman spectroscopy is used to investigate the shock-induced liquid-solid phase transition and crystallization of liquid benzene. Temporal evolution of the Raman shift of the ring-breathing and C–H stretching mode is investigated. A metastable super-compressed state and a liquid–solid phase transition are observed under shock compression. Time-resolved Raman spectra reveal that liquid state is initially a metastable state and rapidly transforms to the solid state within 25 ns under shock compression at 4.2 GPa.

V-E-2 Time-Resolved Coherent Anti-Stokes Raman Scattering of Cyclohexane under Shock Compression

OGUCHI, Shiro¹; MATSUDA, Akitaka²; KONDO, Ken-ichi¹; NAKAMURA, Kazutaka²
(¹Tokyo Tech; ²IMS and Tokyo Tech)

[*Jpn. J. Appl. Phys.* **45**, 5817–5820 (2006)]

Time-resolved coherent anti-Stokes Raman scattering has been performed on cyclohexane under laser-driven shock compression of up to 2 GPa. The ring-breathing and C–C stretching mode exhibits blue shift, which agrees well with that obtained by static-compression experiments. The intensity increase of the shifted peak due to the propagation of the shock wave is observed. Shock velocity is obtained using anti-Stokes Raman scattering signal intensity ratio, and agrees well with that estimated from the measured particle velocity and Hugoniot.

V-F Pyrrole-Based Molecular Assemblies and Supramolecular Structures

An important class of naked-eye sensors are synthetic receptors that permit anionic guest species to be seen by visual means or *via* changes in the electronic absorption or fluorescent spectral properties. Among the various artificial host molecules reported to date, pyrroles incorporated into macrocycles are particularly attractive because they behave as essential binding units due to the presence of polarized NH sites. Although less well studied, acyclic pyrrole derivatives often potentially have even more advantages. This is because they can form the complexes with anions via the synthetic attachment of additional recognition units such as amide NH, or simply because they are easily to make their macrocyclic systems.

On the other hand, metal ion coordination enables organic ligands to form versatile discrete or infinite architectures, such as wire structures and nanospace materials, with potential applications in catalysis, optics, and biosensing. Recently, nanoscale morphologies based on coordination polymers have been reported to exist as spherical and fibrous structures. Of the coordinating ligands, dipyrrens (dipyrromethenes), consisting of two pyrroles with an sp^2 -*meso* position, are essential π -conjugated *bidentate monoanionic* ligands for metal ions in natural and artificial systems. Therefore, dipyrrens are promising planar scaffoldings for self-assemblies and would give neutral coordination oligomers and, which, in combination with various spacer units, could be used to fabricate fine-tuned nanoscale morphologies using bridging metal cations.

From the above background, we are focusing on development of nanoarchitectures based on metal coordination of dipyrren oligomers as well as efficient anion binding systems of acyclic oligopyrroles.

V-F-1 Dipyrrolyldiketone Difluoroboron Complexes: Novel Anion Sensors with C–H...X[−] Interactions

MAEDA, Hiromitsu¹; KUSUNOSE, Yukio²
(¹IMS and Ritsumeikan Univ.; ²Ritsumeikan Univ.)

[*Chem. Eur. J.* **11**, 5661–5666 (2005)]

1,3-Dipyrrolyl-1,3-propanediones, synthesized from pyrroles and malonyl chloride, form BF₂ complexes, a new class of naked-eye sensors for halide and oxoanions. Association mode with the interactions of both the pyrrolyl NH and bridging CH protons for anion was confirmed by ¹H NMR chemical shifts in CD₂Cl₂ and supported by theoretical study. Binding constants (K_a) were estimated at 8.1×10^4 , 2.0×10^3 , 3.3×10^2 , 1.3×10^4 , and 80 M^{-1} for F[−], Cl[−], Br[−], H₂PO₄[−], and HSO₄[−] by UV/vis absorption spectral changes in CH₂Cl₂. Augmentation of K_a compared to dipyrrolylquinoxaline for H₂PO₄[−] is much larger than those for other anions. F[−] quenches the emission almost completely, contrasted with other anions, detected by fluorescence spectrum as well as naked-eye. In the case of the chloride anion complex, the formation of Cl[−]-bridged 1-D networks, in which anion is associated with two BF₂ complexes, is observed in the solid state.

V-F-2 CH...Anion Interaction in BF₂ Complexes of C₃-Bridged Oligopyrroles

FUJIMOTO, Chikoto¹; KUSUNOSE, Yukio¹;
MAEDA, Hiromitsu²
(¹Ritsumeikan Univ.; ²IMS and Ritsumeikan Univ.)

[*J. Org. Chem.* **71**, 2389–2394 (2006)]

Alkyl-substituted derivatives of 1,3-dipyrrolyl-1,3-propanedione BF₂ complexes, the efficient receptors for halide and oxoanions using bridging CH as well as

pyrrole NH, are reported. BF₂ complexes with only one pyrrole NH interaction site, which exhibit less affinities than the basic structures, bind anions tightly, inferred by UV/vis absorption spectral changes, compared to the derivatives with an alkyl group at the bridging carbon or two pyrrole nitrogen sites. Using ¹H NMR and theoretical studies for anion complexes of N-blocked and N-lacked receptors, bridging CH (and one β -CH in N-blocked) as well as pyrrole NH is found to interact with anions.

V-F-3 BF₂ Complex of Fluorinated Dipyrrolyldiketone: A New Class of Efficient Receptor for Acetate Anions

MAEDA, Hiromitsu¹; ITO, Yoshihiro²
(¹IMS and Ritsumeikan Univ.; ²Ritsumeikan Univ.)

[*Inorg. Chem.* **45**, 8205–8210 (2006)]

β -Fluorinated derivative of 1,3-dipyrrolyl-1,3-propanedione BF₂ complex has been prepared from 3,4-difluoropyrrole and malonyl chloride followed by treatment with BF₃·OEt₂. Despite the simple, acyclic, and neutral structure, β -fluorinated receptor exhibits efficient 1:1 binding for anions in CH₂Cl₂ using bridging CH and pyrrole NH as interaction sites. Binding constant (K_a) for acetate (CH₃CO₂[−]), associated more effectively compared to the anions like F[−], Cl[−], Br[−], H₂PO₄[−], and HSO₄[−], is estimated as $9.6 \times 10^5 \text{ M}^{-1}$, *ca.* 9-times augmented in comparison with that of β -H derivative ($1.1 \times 10^5 \text{ M}^{-1}$). UV/vis and fluorescence spectral changes of the receptors elucidate the effective recognition of an amino acid such as phenylalanine in anionic form, also supported by CD spectral changes with mirror images by L- and D-isomers. Furthermore, in the solid state, BF₂ complex of β -F receptor provides Cl[−]-bridged supramolecular networks, and, in sharp contrast, deprotonated “anionic” self-assembled structures by F[−] binding.

V-F-4 Dipyrin-Porphyrin Hybrids: Potential π -Conjugated Platform to Fabricate Coordination Oligomers

MAEDA, Hiromitsu¹; ITO, Miki²

(¹IMS and Ritsumeikan Univ.; ²Ritsumeikan Univ.)

[*Chem. Lett.* **34**, 1150–1151 (2005)]

Bis-dipyrin-appended porphyrin derivatives are synthesized and exhibited complexation at the two dipyrin sites with BF_2 and $\text{Rh}(\text{CO})_2$. Treatment with $\text{Zn}(\text{OAc})_2$ is found to show the MALDI-TOF-MS suggesting the formation of dimer (corresponding to $2 \times$ dipyrin-porphyrin hybrid + $2 \times \text{Zn}^{2+}$) as a major product and trimetric and tetrametric structures as traces, which infers that the dipyrin moieties behave as potential scaffolds for supramolecular coordination polymers.

V-F-5 Nanoscale Spherical Architectures Fabricated by Metal Coordination of Multiple Dipyrin Moieties

MAEDA, Hiromitsu¹; HASEGAWA, Masahiro²; HASHIMOTO, Takashi²; KAKIMOTO, Takuya²; NISHIO, Satoru²; NAKANISHI, Takashi³

(¹IMS and Ritsumeikan Univ.; ²Ritsumeikan Univ.; ³NIMS)

[*J. Am. Chem. Soc.* **128**, 10024–10025 (2006)]

Phenylethynyl-bridged dipyrin “dimers” have been prepared by cross-coupling reactions of bromobenzaldehydes and diethynylbenzenes followed by condensation with pyrrole and a subsequent DDQ oxidation. The dipyrin dimers performed Zn^{II} complexation in THF, detected by UV/vis and ^1H NMR spectral changes. The coordination oligomers, according to the spacer units, provided the submicrometer-scale colloidal spherical objects observed by DLS measurements in solution and SEM, TEM, and optical microscopy on the substrate. Using mixture of THF and water, unique morphologies, such as hemispheres and bell-shaped and “golf ball”-like architectures, were observed. The coordination oligomers have emission maxima at 510–515 nm in THF, which can be ascribed to the Zn^{II} -bisdipyrin moieties, and give fluorescent spherical objects with emission at 532–543 nm in the solid state by assembly from THF. In contrast, addition of a 1:1 mixture of $\text{Zn}(\text{OAc})_2$ and $\text{Cu}(\text{OAc})_2$ into a THF solution of dipyrin dimer resulted in quenching of emission from the Zn^{II} -dipyrin units similarly to the case of the single Cu^{II} complex possibly due to intramolecular energy transfer.

RESEARCH ACTIVITIES VI

Department of Vacuum UV Photoscience

VI-A Electronic Structure and Decay Mechanism of Inner-Shell Excited Molecules

In this project, we have two major subjects: (a) resonant photoelectron spectroscopy and (b) resonant inelastic soft X-ray emission spectroscopy following inner-shell excitations of simple molecules and clusters. We have recently succeeded in development of a next-generation soft X-ray emission spectrometer.

VI-A-1 Improvement of the Energy Resolution of Transmission Grating Soft X-Ray Emission Spectrometer

HATSUI, Takaki; HORIGOME, Toshio; KOSUGI, Nobuhiro

Last year we reported the first results on the performance of a transmission-grating spectrometer (TGS) for high-resolution soft X-ray emission studies. The obtained energy resolution ($E/\Delta E$) was about 3100 at the photon energy of 110 eV, which was limited by the source size on the sample. In order to obtain higher energy resolution, an UHV-compatible entrance slit with the slit opening of 1–30 μm has been developed. The slit blades are mounted on a flexure guided stage in combination with a piezo actuator. The slit opening is feedback controlled by monitoring a capacitance sensor attached to the frame. The performance of the TGS was evaluated by introducing the new entrance slit. The elastic x-ray scattering from aluminum sample irradiated by the monochromatic x-rays (Figure 1) indicates that the overall energy resolution is now 4500 at the photon energy of 114 eV. The resolution is limited by the energy resolving power of the beamline BL3U for the incident soft x-rays, not by the TGS.

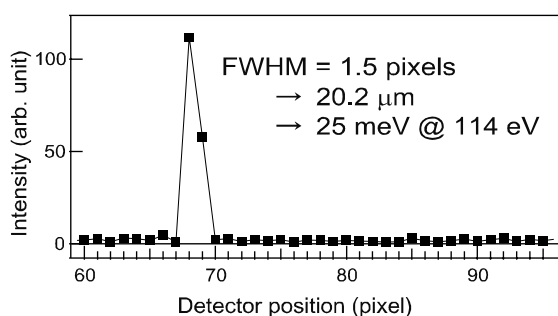


Figure 1. Line profile along dispersion direction of the CCD detector image. Full width at half maximum (FWHM) is 20.2 μm , corresponding to energy resolution of 25 meV ($E/\Delta E = 4500$).

VI-A-2 Development of a Sub-Pixel Resolution CCD for High Resolution Soft X-Ray Emission Spectrometer

HATSUI, Takaki; HOLLAND, Andrew¹; INGLEBY, Richard¹; HOLLAND, Karen²; KOSUGI, Nobuhiro

(¹Brunel Univ.; ²XCam Ltd.)

Last year we reported the performance of a transmission-grating spectrometer (TGS) for high-resolution soft X-ray emission studies. The TGS equipped with a conventional charge coupled device (CCD) detector with the pixel size of 13 μm realized an energy resolution $E/\Delta E$ up to 4500 at the photon energy of 114 eV. The observed peak has the full width at half maximum (FWHM) of 1.5 pixels under this high energy-resolution condition. The performance is hence limited dominantly by the spatial resolution of the CCD detector. In order to improve the spatial resolution of the detector, we have developed an electron multiplying CCD detection system with the pixel size of 16 μm for photon-counting detection of the soft x-rays. By amplifying the charge generated by soft x-ray photon prior to on-chip MOSFET, which is the dominant source of the readout noise, the noise is reduced less than 1 electron rms/pixel at the readout rate as high as 400 kHz/pixel. The obtained signals are analyzed to obtain the centroid of the charge, or the position of the x-ray absorption. By examining the image of a slit with a width of 10 μm (Figure 1) and assuming Gaussian profile of the point spread function (PSF) of the detector, the PSF is estimated to have FWHM of 3.0 μm . The results indicate that this new detection technique improves the special resolution by a factor of 10 compared with the conventional CCD detector without degrading the quantum efficiency.

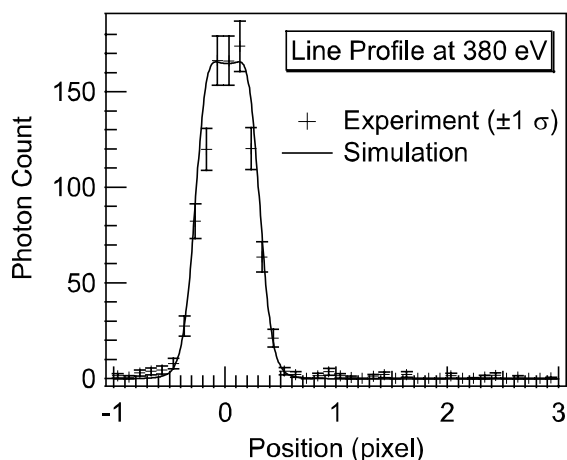


Figure 1. Line profile measured for the image of the slit and simulated profile, based on the diffraction theory assuming the detector PSF with FWHM of 3.0 μm .

VI-B Soft X-Ray Photoelectron-Photoabsorption Spectroscopy and Electronic Structure of Molecular Solids and Clusters

This project has been carried out in international collaboration. We have two subprojects: (a) molecules and radicals in condensed phase and in rare gas matrix, and (b) ionic fragmentation and photoelectron emission of atomic and molecular clusters following the inner-shell resonance excitation. In (a), we have measured excitation spectra in some matrix phases at the bending-magnet beamline BL4B of the UVSOR facility. In (b), we have measured soft X-ray photoelectron spectra of some atomic and molecular clusters on the undulator beamline BL3U.

VI-B-1 Orbital-Dependent Stabilization in the Valence Ionization of CS₂ Cluster

HATSUI, Takaki; PLENGE, Jürgen; RÜHL, Eckart; KOSUGI, Nobuhiro
(¹Freie Univ. Berlin)

Van der Waals clusters have been interested since they give opportunities to investigate the connection between isolated and condensed phases. Cluster formation is known to give the decrease or red shift in adiabatic and vertical ionization (binding) energies, which is commonly interpreted in terms of final-state polarization stabilization. The polarization stabilization is dependent on the distance to the surrounding atoms/molecules and their polarizabilities and numbers.

In the present work, we have investigated red shift dependent on the ionized state of CS₂. Figure 1 shows the spectrum measured by using the He I source, as plotted in relative energy scale, where zero energy is chosen to be the vertical energy of each ionized state of a single molecule. The band profile of the cluster spectrum indicates the abundance or size of the cluster. In the case of larger cluster size with increased stagnation pressure, the peak tops of the cluster bands show larger red shifts. The peak position can be regarded as the vertical binding energy at an average cluster size. We can assume that the vibrational progression of each ionized state does not change upon the cluster formation and is mainly determined by the intra-molecular potentials.

Figure 1 and Table 1 show that the relative binding energies are increased in order of X, A, B, and C. Charge distributions determined by a least-square fitting of the electrostatic potential evaluated by an ab initio MR-SDCI solution for each ionized state of a molecule explain different red shifts. The theoretical charge distribution of a single molecule reasonably predicts that the higher ionized state should have larger polarization stabilization by the surrounding molecules in the cluster.

Table 1. Charge Distribution of a CS₂ molecule in ground and ionized states.

State	Charge		Binding Energy (eV)	
	O	S	Theory	Exp.
Ground state	-0.258	+0.129		
X ² Π _g	-0.228	+0.614	9.65	10.06
A ² Π _u	+0.048	+0.476	12.99	12.83
B ² Σ _u ⁺	-0.598	+0.799	14.45	14.42
C ² Σ _g ⁺	-0.552	+0.776	16.56	16.19

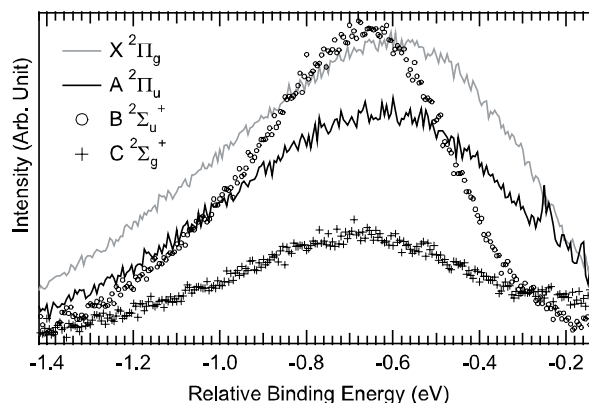


Figure 1. Valence bands for CS₂ clusters relative to the vertical binding energy of the corresponding state in a molecule.

VI-B-2 Absence of Symmetry Breaking Observed for O 1s Core-Excited SO₂ Molecule

LINDGREN, Andreas¹; KOSUGI, Nobuhiro; GISSELBRECHT, Mathieu¹; KIVIMÄKI, Antti¹; BURMEISTER, Florian²; NAVES de BRITO, Arnaldo³; SORENSEN, Stacey¹
(¹Lund Univ.; ²Uppsala Univ.; ³LNL)

Electron-ion-ion coincidence measurements of sulphur dioxide at discrete resonances near the O 1s ionization edge were carried out. The spectra are analyzed using a dynamic model based upon molecular symmetry and on the geometry of the molecule. We have found clear evidence for molecular alignment which can be ascribed to symmetry properties of the ground and core excited states. Ab initio MR-SDCI calculations indicate geometry changes in accord with the analysis of the measured coincidence spectra. For the SO₂ molecule, however, we have found that the core-hole does not produce measurable evidence for localization, in contrast to the case of ozone, O₃. The dissociation behavior calculated using symmetry-adapted orbitals is equivalent to the behavior derived using symmetry-broken orbitals.

VI-B-3 Radiation Damage Effects on the Electronic Structure of Glycine

MacNAUGHTON, Janay¹; MOEWES, Alexander¹; WILKS, Regan¹; KOSUGI, Nobuhiro
(¹Univ. Saskatchewan)

The emerging field of molecular electronics has focused research on the electronic structures of biomaterials. Soft X-ray absorption and emission spectroscopy are synchrotron-based experimental probes of the electronic states of a material. These techniques can be used to determine structural, electronic and magnetic properties. However, large biological molecules such as proteins and DNA are prone to radiation damage and understanding the mechanisms that lead to the damage is essential. Amino acids are the building blocks of proteins and their simplicity makes them ideal candidates to study the effects of radiation. Radiation damage can cause organic molecules to undergo both structural changes and chemical modifications. *Ab initio* STEX calculation has been carried out to gain insight into the spectral changes that occur after amino acids are irradiated. It is found that deprotonation is a possible change occurring during the irradiation of glycine with soft X-rays.

VI-C Molecules in Few-Cycle Intense Laser Fields

When the intensity of a laser field reaches as large as $\sim 10^{15}$ W/cm², the magnitude of the electric field component becomes comparable with that of the Coulomb field within a molecule. Thus, the electrons bound in a molecule become heavily perturbed by the external electric field to form a new class of states, often referred to as light-dressed states. Since an internuclear potential within a molecule is deformed in response to the temporal variation of the amplitude of the light field, dynamical processes of molecules such as vibration and chemical bond breaking should be controlled if the light field is properly designed. In the present study, we employed extremely short intense laser pulses with the duration less than 10 fs, to clarify the behavior of molecules through the three-dimensional momentum measurements of the fragment ions produced from a single parent ion.

VI-C-1 Electronic and Nuclear Responses of Fixed-in-Space H₂S in Ultrashort Intense Laser Fields

HISHIKAWA, Akiyoshi¹; TAKAHASHI, Eiji J.;
MATSUDA, Akitaka
(¹IMS and JST/PRESTO)

[Phys. Rev. Lett. in press]

The Coulomb explosion dynamics in non-resonant, ultrashort intense laser fields (12 fs, $\sim 10^{14}$ W/cm²) is studied for H₂S with its orientation fixed in space, to clarify how the electronic and nuclear responses change by the direction of laser polarization direction (ϵ) in the molecular frame. The momenta of the respective fragment ions, $p_1(\text{H}^+)$, $p_2(\text{H}^+)$ and $p_3(\text{S}^+)$ produced in the Coulomb explosion process, $\text{H}_2\text{S}^{3+} \rightarrow \text{H}^+ + \text{S}^+ + \text{H}^+$, were determined as three-dimensional vectors in the laboratory frame. The kinetic energy release (E_{kin}) and momentum angle (θ_{12}) distributions obtained for the respective directions revealed that the geometrical structure is almost frozen during the interaction with the laser fields for x/ϵ , while it becomes elongated along the laser polarization vector when ϵ is parallel to the y - or z -axis, demonstrating that the Coulomb explosion dynamics of H₂S in intense laser fields can be manipulated by the polarization direction in the molecular frame.

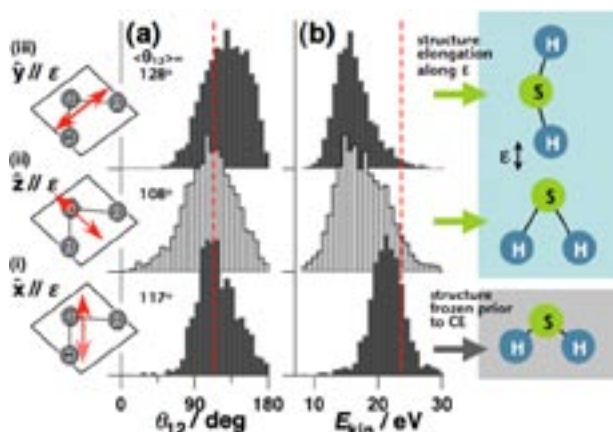


Figure 1. (a) Momentum angle θ_{12} distribution and (b) total kinetic energy E_{kin} distribution obtained for three different directions of ϵ in the molecular frame, (i) x/ϵ , (ii) z/ϵ and (iii) y/ϵ . Each distribution is normalized at the peak. The dotted lines indicate the θ_{12} and E_{kin} values obtained by a classical simulation of the Coulomb explosion on the *ab initio* PES, $\theta_{12} = 113.6^\circ$ and $E_{\text{kin}} = 23.6$ eV, which are smaller than those expected from the corresponding Coulombic PES, $\theta_{12} = 124.1^\circ$ and $E_{\text{kin}} = 29.2$ eV.

VI-C-2 Coulomb Explosion Imaging of Molecular Structures with Ultrashort Intense Laser Pulses

HISHIKAWA, Akiyoshi¹; TAKAHASHI, Eiji J.;
MATSUDA, Akitaka
(¹IMS and JST/PRESTO)

The Coulomb explosion process of CS₂ in ultrashort (<10 fs) intense laser field ($>10^{15}$ W/cm²) is investigated. At the field intensity of 5×10^{15} W/cm², six different symmetric pathways are identified in the Coulomb explosion of CS₂, $\text{CS}_2^{2+} \rightarrow \text{S}^{p+} + \text{C}^{q+} + \text{S}^{r+}$; $(p,q,r) = (1,1,1), (1,2,1), (2,1,2), (2,2,2), (3,2,3), (4,2,4)$ by the coincidence momentum imaging. A good agreement between the results obtained for the (4,2,4) pathway and the momentum distribution expected from the geometry of neutral CS₂ was obtained, indicating that the molecular structure is directly reflected in the momentum distribution when fragment ions from highly charged parent ions are monitored.

VI-D Synchrotron Radiation Stimulated High-Speed Etching on Silicon Surfaces

Synchrotron radiation (SR) stimulated process (etching, CVD) has excellent characteristics of unique material selectivity, low damage, low contamination, high spatial resolution and high precision, *etc.* We have utilized these advantages for silicon and silicon oxide substrates fabrication for bio-sensing devices. However, the slow etching rate in the SR-stimulated etching process is the bottle-neck for the through-hole type device fabrication. In this project, we are constructing a new SR-etching system using XeF_2 gas as a etching gas, in order to achieve high-speed SR-etching.

VI-D-1 Construction of High-Speed Synchrotron Radiation Etching System Using XeF_2

NAKAI, Naohito¹; CHIANG, Tsung-Yi; UNO, Hidetaka; TERO, Ryugo; SUZUI, Mitsukazu; TERAOKA, Yuden²; YOSHIGOE, Akitaka²; MAKIMURA, Tetsuya³; MURAKAMI, Kouichi³; URISU, Tsuneo
(¹SOKENDAI; ²JAEA; ³Univ. Tsukuba)

We have been constructing a new synchrotron radiation (SR) induced high-speed etching system to make a through-hole type biosensor on Si substrates. The conventional SR-etching using SF_6 has the etching rate of only $\sim 2 \text{ nm min}^{-1}$ (at 200 mA ring-current), therefore is not suitable for micrometer-order deep etching. XeF_2 is known as an etching gas for the high-speed vapor-phase etching and is used in the MEMS and μTAS fields. XeF_2 etching has, however, several disadvantages such as; an isotropic etching without directivity; material limitation, for example SiO_2 can not be etched. We expect that SR-induced etching under XeF_2 leads to the high-speed etching with good directivity. We constructed a new etching chamber with LiF window (Figure 1a), and equipped it to the UVSOR-BL4A1. The diagonal mirrors in the beam line will be adjusted to cut off the Li absorption band.

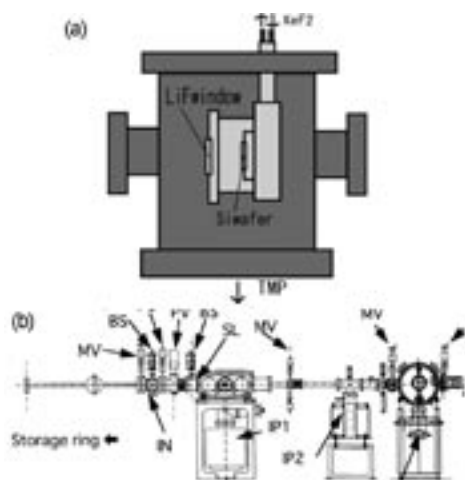


Figure 1. Schematic drawings of (a) the SR-induced XeF_2 etching chamber, and (b) the beam line equipped with the chamber (a).

VI-D-2 Vapor-Phase Etching of Silicon Substrates Using XeF_2

CHIANG, Tsung-Yi; NAKAI, Naohito¹; UNO, Hidetaka; TERO, Ryugo; SUZUI, Mitsukazu; TERAOKA, Yuden²; YOSHIGOE, Akitaka²; MAKIMURA, Tetsuya³; MURAKAMI, Kouichi³; URISU, Tsuneo
(¹SOKENDAI; ²JAEA; ³Univ. Tsukuba)

XeF_2 vapor etching without SR irradiation was performed to check our XeF_2 flow system. Test pattern of a photoresist (N-HC600) was deposited on a Si substrate, and exposed to the 300 Pa of XeF_2 for 10–120 min. Figure 1a is the SEM image of the Si substrate after the photoresist removal. The image clearly shows that isotropic etching by XeF_2 has proceeded. Figure 1b shows the line profile of the line-and-space pattern with 50 μm width after the XeF_2 etching, measured by a non-contact three-dimensional measurement instrument. The etching rate of 900 nm min^{-1} was obtained.

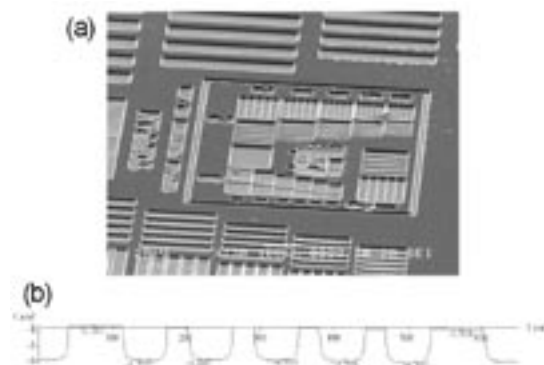


Figure 1. (a) SEM image of the Si substrate after the exposure to 300 Pa of XeF_2 for 10 min. (b) Non-contact three-dimensional measurement profile of the 50 μm wide line-and-space patterns on the Si substrate shown in (a).

VI-E Fabrication of Silicon-Based Planar Ion-Channel Biosensors

It is known that more than 50% of target proteins in the drug discovery field based on the genome information are membrane proteins. The patch clamp method is a powerful and widely used technique for the membrane protein studies, but is not suitable for the high-throughput and multi-integrated screening application. In this project, we have constructed a through-hole silicon device for the ion-channel biosensors. We succeeded to fabricate low-noise planer-type silicon device, and to detect the single ion channel current of gramicidin A.

VI-E-1 Fabrication of Circular Through-Hole on Si(100)-SOI Substrate

ZHANG, Zhen-Long¹; UNO, Hidetaka; CHIANG, Tsung-Yi; ASANO, Toshifumi¹; SUZUI, Mitsukazu; TERO, Ryugo; NAKAO, Satoshi; URISU, Tsuneo (¹SOKENDAI)

We have fabricated a circular through-hole on Si(100)-SOI substrate for channel current measurement. The through-hole is necessary for the electronic conduction, and the circular hole with sharp edge is important for the lipid bilayer membrane formation over the hole and the membrane stability. Figure 1 shows the substrate fabrication process. The Si(100)-SOI (600 μm thick) (Figure 1a) substrate was annealed at water-saturated O_2 flow at 950 $^\circ\text{C}$ for 2 h to form a 200 nm thick thermally oxidized layer (Figure 1b). A circular hole with depth of $\sim 550 \mu\text{m}$ was made by a diamond grinder on the back-side surface of the Si(100)-SOI (Figure 1c). Then the hole was etched in tetramethyl ammonium hydroxide (TMAH) until the hole reached to the oxide layer in SOI (Figure 1d). After a 20 nm thick SiO_2 layer was deposited on the top-side surface by sputtering (Figure 1e), the 2–3 μm thick $\text{SiO}_2/\text{Si}(100)$ layer was penetrated by focused ion beam (FIB) (Figure 1f). The diameter of the hole can be controlled in the range of 1–100 μm . Figure 2 shows the optical microscope image of the through-hole with 100 μm diameter. The through-hole made by the processes shown in Figure 1 had a perfect circular shape and a sharp edge.

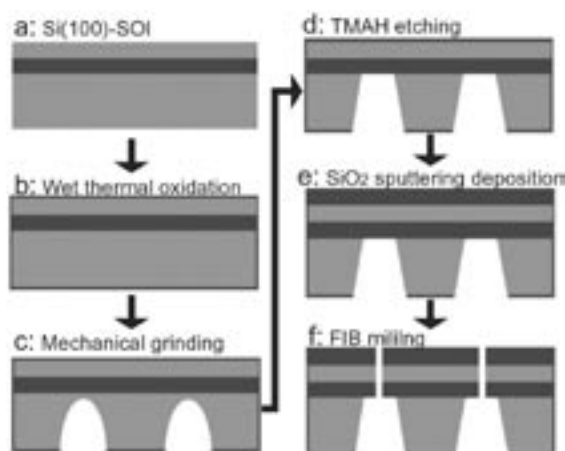


Figure 1. Schematic drawings of the through-hole fabrication processes on a Si(100)-SOI substrate.

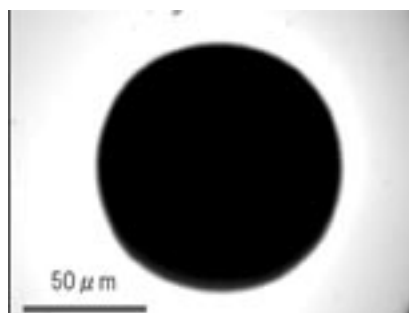


Figure 2. Optical microscope image of the through-hole with 100 μm diameter made by the processes shown Figure 1.

VI-E-2 Channel Current Measurement Using Silicon-Based Planar Type Biosensor

UNO, Hidetaka; ZHANG, Zhen-Long¹; ASANO, Toshifumi¹; CHIANG, Tsung-Yi; SUZUI, Mitsukazu; TERO, Ryugo; NAKAO, Satoshi; NONOGAKI, Youichi; URISU, Tsuneo (¹SOKENDAI)

We have formed a suspended phospholipid bilayer membrane on the Si(100)-SOI through-hole chip (Figure 1), and measured the channel current of gramicidin A (gA). We deposited octadecyltrimethoxysilane by chemical vapor deposition to make the oxidized layer surface of the chip hydrophobic. The through-hole chip was settled in a home-build Teflon chamber, and the suspended bilayer of diphytanoylphosphatidylcholine (D ϕ PC) was formed in the hole by painting method using 10 mg/ml of D ϕ PC/decane solution. The electrical property of the bilayer membrane was measured by a patch clamp amplifier (CEA-2400, Nihon Kodan, Japan). Aqueous gA solution was added to the both sides of the bilayer, to reconstitute the gA in to the bilayer. We succeeded in measuring the single channel current of gA using the through-hole silicon chip (Figure 2). Each of the step-signal in Figure 2 is the single channel current through gA.

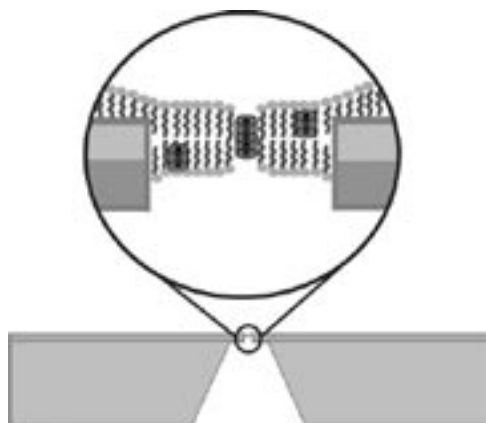


Figure 1. Schematic drawing of the through-hole silicon chip and the suspended lipid bilayer containing gA in the hole.

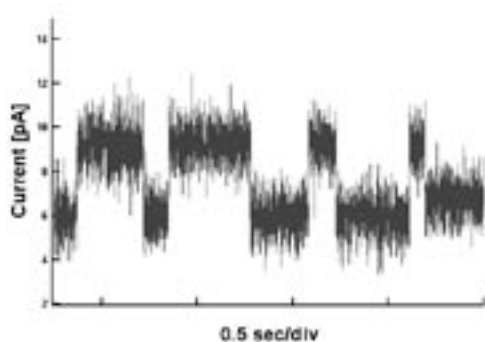


Figure 2. Single ion channel current signals of gA measured by the through-hole silicon chip. Bias voltage is 150 mV.

VI-E-3 Noise Analysis in the Planar-Type Ion-Channel Biosensors

UNO, Hidetaka; ZHANG, Zhen-Long¹; CHIANG, Tsung-Yi; SUZUI, Mitsukazu; TERO, Ryugo; NAKAO, Satoshi; NONOGAKI, Youichi; URISU, Tsuneo
(¹SOKENDAI)

[*Jpn. J. Appl. Phys.* submitted]

Low noise electronic systems in pA order is necessary for the ion channel current detection from single molecule. It has been believed that silicon is an

inept material in ion channel detecting, because its high dielectric loss causes high noise level. However, our through-hole silicon chip during the gA channel measurement showed sufficiently low noise level (1.7 pA, rms). We investigated the noise sources in our silicon chip based on the dimension parameters shown in Figure 1. The main noise sources in planar bilayer recordings are; (1) I_h : the current noise from the interaction between the head-stage input voltage noise (e_n) and the input capacitance (C_t); (2) I_{Ra} : the current noise due to the thermal voltage noise of the access resistance R_a in series with the bilayer capacitance C_m ; (3) I_d : the dielectric noise. These noise variances are expressed as

$$I_h^2 = (4/3)e_n^2 \pi^2 C_t^2 B^3 \quad (1),$$

$$I_{Ra}^2 = (4/3)k T R_a (2\pi C_m)^2 B^3 \quad (2),$$

$$I_d^2 = 4k T \pi D C_t B^2 \quad (3),$$

$$C_t = C_m + C_{sub} + C_{others} \quad (4),$$

where B is the frequency band width, C_{sub} is the capacitance of the substrate, C_{others} is the sum of other capacitances contributing to noise. The measured noise current I_m is given by

$$I^2 = I_h^2 + I_{Ra}^2 + I_d^2 \quad (5).$$

We calculated these capacitance and noise current values based on the substrate structure used in our experiments shown in Figure 1. The calculated values in $B = 5$ kHz are; $C_m = 76$ pF; $C_{sub} = 2$ pF; $C_{others} = 1.2$ pF; $C_t = 80$ pF; $I_h^2 = 5.5 \times 10^{-26}$ A² (assuming $e_n = 2.3 \times 10^{-9}$ V Hz^{0.5}); $R_a = 1.7$ k Ω ; and $I_{Ra}^2 = 2.7 \times 10^{-25}$ A². Thus the calculated noise current $I = 1.7$ pA (rms) was obtained. This value is in quite good agreement with the measured value 1.2 pA. We found that the SiO₂ disk around the hole (C_1 region in Figure 1) contributed to the low noise level in our chip.

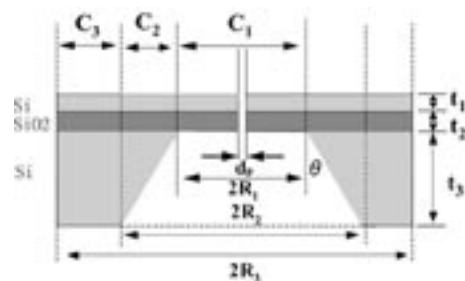


Figure 1. Schematic drawing of the through-hole silicon chip and its dimension parameters.

VI-F Integration and Characterization of Bio-Functional Materials on Silicon Surfaces

Integration of bio-functional materials on solid surfaces is an attractive research theme and important to the development of new biosensors and screening methods in which biological reactions are directly detected on electronic circuits. We have investigated the lipid bilayer membrane deposition and covalent immobilization of protein, and have characterized the properties of these bio-functional materials using atomic force microscopy infrared absorption spectroscopy. We have also developed a new infrared absorption spectroscopy system using buried-metal-layer substrate, for the in-situ measurements of water/solid interface.

VI-F-1 Supported Phospholipid Bilayer Formation on Hydrophilicity-Controlled Silicon Dioxide Surfaces

TERO, Ryugo; WATANABE, Hidekazu¹; URISU, Tsuneo
(¹RIKEN)

[*Phys. Chem. Chem. Phys.* **8**, 3885–3894 (2006)]

We investigated the influence of surface hydroxyl groups (-OHs) on the supported planar phospholipid bilayer (SPB) formation and characteristic. We prepared SiO₂ surfaces with different hydrophilicity degree by annealing the SiO₂ layer on Si(100) formed by wet chemical treatments. The hydrophilicity reduced with irreversible thermal desorption of -OHs. We formed SPB of dimyristoylphosphatidylcholine (DMPC) on the SiO₂ surfaces by incubation at a 100-nm-filtered vesicle suspension. The formation rate was faster on less hydrophilic surfaces (Figure 1). We proposed that a stable hydrogen-bonded water layer on the SiO₂ surface worked as a barrier to prevent vesicle adhesion on the surface. Theoretical calculation indicates that water molecules on vicinal surface -OHs take a stable surface-unique geometry, which disappears on an isolated -OH. The surface -OH density, however, little affected the fluidity of once formed SPBs, which was measured by the fluorescence recovery after photobleaching method. We also describe about the area-selective SPB deposition using surface patterning by the focused ion beam.

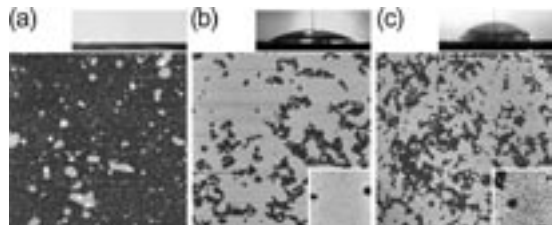


Figure 1. AFM images of DMPC-SPB on hydrophilicity-controlled SiO₂/Si(100) surfaces. The water contact angle of the SiO₂ surfaces before the DMPC deposition and the SPB coverage are; (a) 5°, 0.12; (b) 24°, 0.78; and (c) 67°, 0.67, respectively. The AFM images were obtained in a buffer solution.

VI-F-2 Orientation of Avidin Molecules Immobilized on COOH-Modified SiO₂/Si(100) Surfaces

MISAWA, Nobuo; YAMAMURA, Shusaku¹; KIM, Yong-Hoon¹; TERO, Ryugo; NONOGAKI, Youichi; URISU, Tsuneo
(¹SOKENDAI)

[*Chem. Phys. Lett.* **419**, 86–90 (2006)]

Avidin molecules were immobilized on a COOH-modified SiO₂/Si(100) surface with sub-nanometer order flatness (root-mean-square (rms) roughness ~0.1 nm) forming covalent bonds between the COOH groups on the substrate surface and the NH₂ groups of avidin molecules. The structures of avidin-immobilized sur-

faces were investigated by atomic force microscopy (AFM), ellipsometry, and infrared (IR) reflection absorption spectroscopy using buried metal layer substrate (BML-IRRAS), and transmission IR absorption spectroscopy (TIRAS). We have simulated dependence of the amide I band intensity on the avidin orientation (Figure 1), since BML-IRRAS and TIRAS are sensitive to perpendicular and parallel dipole moments to the surface, respectively. These data have evidenced that the avidin molecules are immobilized with the 2-fold symmetry axis of the tetramer almost perpendicularly to the substrate surface.

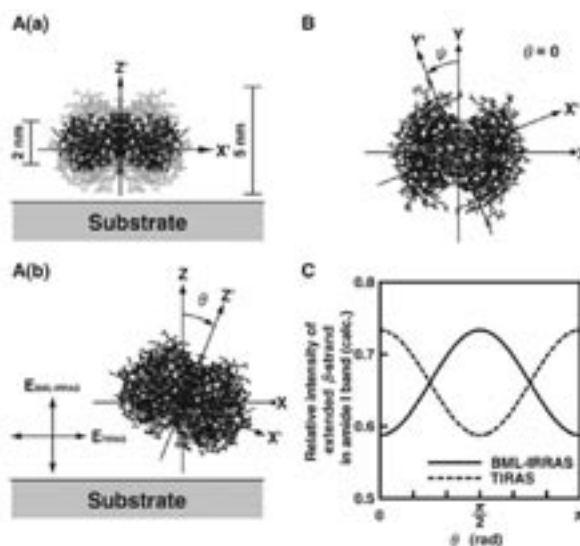


Figure 1. Schematic images of an egg white avidin molecule immobilized on the substrate surface. All component atoms are plotted using the coordinate data given in PDB (1AVD) as dots of the same size in A(a): avidin tetramer (gray) and the only β -barrel part (dark). Coordinates X, Y and Z are fixed to the substrate surface, while X', Y' and Z' are fixed to the molecule. Molecular orientation is defined by the Eulerian angles, φ ($= 0$), θ and ψ in A(b) and B. Electric fields, $E_{\text{BML-IRRAS}}$ and E_{TIRAS} , in BMLIRRAS and TIRAS are drawn in A(b). Calculated relative intensities of extended b-strand peak in the amide I band as a function of θ ($0 \leq h \leq \pi$) are shown in C.

VI-F-3 AFM Characterization of Gramicidin-A in Tethered Lipid Membrane on Silicon Surface

LEI, Sheng-Bin¹; TERO, Ryugo; MISAWA, Nobuo; YAMAMURA, Shusaku²; WAN, Li-Jun¹; URISU, Tsuneo
(¹IMS and Chinese Acad. Sci.; ²SOKENDAI)

[*Chem. Phys. Lett.* in press]

The tethered 1,2-dipalmitoyl-*sn*-glycero-3-phosphocholine (DPPC) lipid bilayer is formed on the oxidized Si surfaces using the avidin-biotin interaction to investigate the lipid-membrane protein interactions by using gramicidin-A (g-A) as a model membrane protein. The morphology of the tethered lipid bilayer, observed by the *in situ* atomic force microscopy (AFM), changes drastically by the reconstruction of g-A (Figure 1). The aggregation behavior of g-A is clearly different in the tethered membrane from those in the simple supported

membranes on mica and SiO₂ surfaces. The thick water layer under the membrane introduced by the tethered structure gives important influence on the aggregation behavior of g-A.

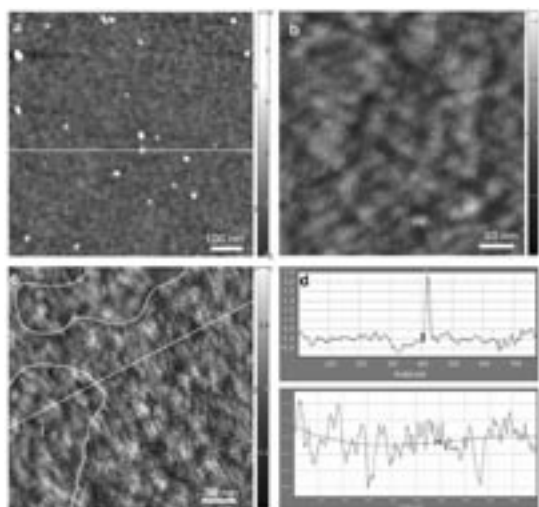


Figure 1. Topography images of (a) avidin immobilized substrate, and tethered lipid bilayers (b) without and (c) with 1 mol% g-A. (d) The line profile of marked place in (a) and (c). Color scales are (a) 7.5 nm, (b) 1.7 nm and (c) 1.5 nm full scale.

VI-F-4 In-Situ Infrared Reflection Absorption Spectroscopy System Using Buried Metal Layer Substrate (BML-IRRAS) for Biomaterials under Water

SAYED, Md. Abu¹; UNO, Hidetaka; MISAWA, Nobuo; HARADA, Kensuke²; TANAKA, Keiichi²; KONDOH, Takuhiko; TERO, Ryugo; URISU, Tsuneo
(¹SOKENDAI; ²Kyushu Univ.)

Supported membrane on biosensor surface is one of the most attractive research fields in these days. For new bioactive biosensor or biochips for diagnostics or other electronic purposes we have to study biomaterial properties on solid surfaces in different conditions. Many experimental approaches including infrared reflection absorption spectroscopy using buried metal layer (BML-IRRAS) have been performed to study the function of biomaterials on inorganic surfaces. But there are few IRRAS techniques to study the membrane surface reaction under aqueous solution. We have constructed a new BML-IRRAS system to study biomaterials under water. We used CaF₂ prism and 12 μm aluminum spacer upon BML substrate including a solution injection system (Figure 1a). We used JIR-7000 (JEOL Ltd.) with a MCT detector as a FT-IR system. Although water is necessary for biomaterials to keep life functions, but water have strong absorptivity in the IR region. We have investigated the window regions for H₂O and D₂O as shown in Figure 1b. It is concluded that 1250–4000 cm⁻¹ and 3700–4000 cm⁻¹ are applicable for IR measurements in D₂O and H₂O, respectively, in the present system.

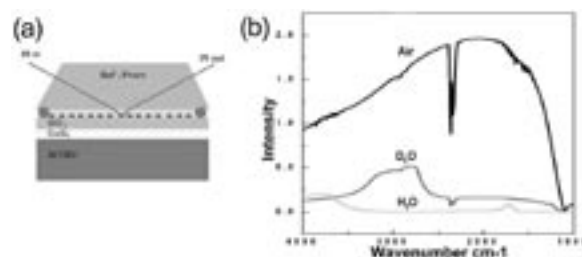


Figure 1. (a) Schematic drawings of the sample holder for the new BML-IRRAS system. (b) IR power spectra measured by the new BML-IRRAS instrument for (a) air, (b) D₂O and (c) H₂O with 12 nm thickness.

VI-G Extreme UV Photoionization Studies of Fullerenes by Using a Grazing-Incidence Monochromator and High-Temperature Mass Spectrometer

On the beam line BL2B in UVSOR a grazing incidence monochromator has been constructed which supplies photons in the energy region from 20 to 200 eV [M. Ono, H. Yoshida, H. Hattori and K. Mitsuke, *Nucl. Instrum. Methods Phys. Res., Sect. A* **467-468**, 577–580 (2001)]. This monochromator was assumed to bridge the energy gap between the beam lines BL3B and BL4B, thus providing for an accelerating demand for the high-resolution and high-flux photon beam from the research fields of photoexcitation of inner-valence electrons, *L*-shell electrons in the third-row atom, and *4d* electrons of the lanthanides.

Since 2001 we have tried taking photoion yield curves of fullerenes. Geometrical structures and electronic properties of fullerenes have attracted widespread attention because of their novel structures, novel reactivity, and novel catalytic behaviors as typical nanometer-size materials. Moreover, it has been emphasized that the potential for the development of fullerenes to superconductors ($T_c \sim 50$ K) and strong ferromagnetic substances is extremely high. In spite of such important species spectroscopic information is very limited in the extreme UV region, which has been probably due to difficulties in obtaining enough amount of sample. The situation has rapidly changed in these few years, since the techniques of syntheses, isolation, and purification have been advanced so rapidly that appreciable amount of fullerenes is obtainable from several distributors in Japan.

VI-G-1 Refinements of the Estimation of Photoabsorption Cross Sections of Metallofullerenes

KATAYANAGI, Hideki; PRODHAN, Md. Serajul Islam¹; MITSUKE, Koichiro
(¹SOKENDAI)

We have revisited the photoabsorption cross sections of endohedral metallofullerenes (Ce@C₈₂, Dy@C₈₂ and Pr@C₈₂) in the extreme ultraviolet¹⁻³) and refined the procedure of their precise estimation. In the previous studies the cross sections were evaluated by comparing normalized count rates for the metallofullerenes with those for a standard sample. The cross sections thus obtained are found to serve as only crude approximations, since no consideration was given to the detection efficiency dependence of the time-of-flight mass spectrometer on sample masses and charges.

In the present study, we adopted an alternative approach to obtain more precise cross sections of the metallofullerenes. First, multiple standard samples having different masses were utilized for correction of the detection efficiency dependence. Second, such corrections were made by applying an empirical formula proposed by Twerenbold *et al.*⁴) Table 1 summarizes refined partial photofragmentation cross sections of Pr@C₈₂ and its total photoabsorption cross sections. All these values are the means of the two cross sections that were calculated using xenon and C₆₀ as standard samples. The deviations of the values in Table 1 are at most 12%, which implies that the detection efficiency dependence is fairly corrected. Indeed, the total photoabsorption cross section of 36 Mb at 110 eV is in good agreement with that of 82 carbon atoms, 33.5 Mb. Refinements of the cross sections of other metallofullerenes using several standard samples are also in progress.

References

1) K. Mitsuke, T. Mori, J. Kou, Y. Haruyama and Y. Kubozono, *J. Chem. Phys.* **122**, 064304 (2005).

- 2) K. Mitsuke, T. Mori, J. Kou, Y. Haruyama, Y. Takabayashi and Y. Kubozono, *Int. J. Mass Spectrom.* **243**, 121 (2005).
3) H. Katayanagi, B. P. Kafle, J. Kou, T. Mori, K. Mitsuke, Y. Takabayashi, E. Kuwahara and Y. Kubozono, *J. Chem. Phys.* submitted.
4) D. Twerenbold, D. Gerber, D. Gritti, Y. Gonin, A. Netuschil, F. Rossel, D. Schenker and J. L. Vuilleumier, *Proteomics* **1**, 66 (2001).

Table 1. Partial photofragmentation cross sections of Pr@C₈₂ for the formation of Pr@C₈₂^{z+} and the total photoabsorption cross sections at the photon energies of 110 and 130 eV. All cross sections are in Mb.

Photon energy	Photofragmentation cross section		Total cross section
	Pr@C ₈₂ ⁺	Pr@C ₈₂ ²⁺	
110 eV (off-resonance)	22.2	13.8	36.0
130 eV (on-resonance)	32.7	22.6	55.3

VI-G-2 Fragmentation Mechanism of Highly Excited C₇₀ Cations in the Extreme Ultraviolet

MITSUKE, Koichiro; KATAYANAGI, Hideki; KOU, Junkei; MORI, Takanori; KUBOZONO, Yoshihiro¹
(¹Okayama Univ.)

[*AIP Conf. Proc.* **811**, 161–166 (2006)]

The ion yield curves for C_{70-2n}^{z+} ($n = 1-8$, $z = 2$ and 3) produced by photoionization of C₇₀ were measured in the photon energy ($h\nu$) range of 25–150 eV. The appearance $h\nu$ values were higher by *ca.* 34 eV than the thermochemical thresholds for dissociative ionization of C₇₀ leading to C_{70-2n}^{z+} (see Figure 1). Evaluation was made on the upper limits of the internal energies of the primary C₇₀^{z+} above which C_{70-2n+2}^{z+} fragments cannot escape from further dissociating into C_{70-2n}^{z+} + C₂. These critical internal energies agreed well with appearance internal energies of C₇₀^{z+} theoretically obtained

corresponding to the threshold for the formation of C_{70-2n}^{z+} . The photofragmentation of the parent C_{70}^{z+} ions is considered to be governed by the mechanism of internal conversion of their electronically excited states, statistical redistribution of the excess energy among a number of vibrational modes, and sequential ejection of the C_2 units.

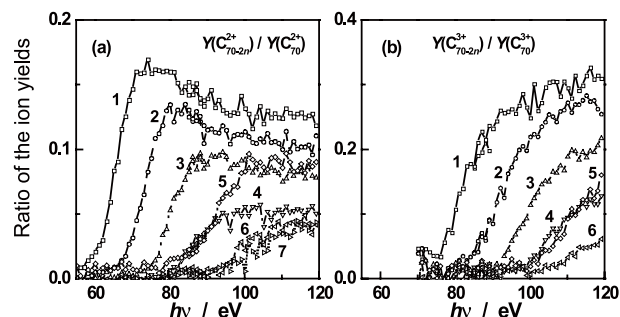


Figure 1. Relative ion yield curves of C_{70-2n}^{z+} ions obtained from time-of-flight mass spectra. (a) $z = 2$, $n = 1-7$ and (b) $z = 3$, $n = 1-6$.

VI-H Photoionization and Fragmentation Mechanisms of C_{60} and C_{70} in the Extreme Ultraviolet

When fullerenes gain enough amount of energy through photoionization processes, primarily formed ions are known to undergo decomposition into fragment ions with even numbered carbon atoms. We have measured the yield curves for C_{60-2n}^{z+} from C_{60} as a function of the internal energy E_{int} of the parent C_{60}^{z+} ions to study the mechanisms and kinetics of the above unimolecular reactions. These experimental yield curves have been compared with the theoretical fractional abundance curves. We found that the experimental and theoretical curves provide almost the same appearance internal energies for the formation of C_{60-2n}^{z+} ($n \geq 1$). This result appears to reveal that the excess energy is statistically distributed among the internal degrees of freedom of the parent ions and that C_2 units are ejected sequentially ($C_{60}^{z+} \rightarrow C_{58}^{z+} + C_2$, $C_{58}^{z+} \rightarrow C_{56}^{z+} + C_2$, ..., $C_{60-2n+2}^{z+} \rightarrow C_{60-2n}^{z+} + C_2$).

There remains ambiguity as to whether potential barrier exists along the reaction coordinate and whether resonant state participates during dissociation. Moreover, a few groups have argued that another mechanism of single-step two-fragment fission ($C_{60}^{z+} \rightarrow C_{60-2n}^{z+} + C_{2n}$) could be involved in the formation of C_{60-2n}^{z+} . To elucidate these issues, we are developing two devices which are incorporated into the present photoionization spectrometer for gaseous fullerenes: photofragment imaging analyzer and threshold photoelectron-photoion coincidence apparatus.

VI-H-1 Kinetic Energy Analysis of the Fragment Ions Produced from C_{60} and C_{70}

**KATAYANAGI, Hideki; KAFLE, Bhim Prasad¹;
PRODHAN, Md. Serajul Islam¹; YAGI, Hajime;
MITSUKE, Koichiro**
(¹SOKENDAI)

We have reported the yield curves^{1,2)} of the fragments C_{60-2n}^{z+} and C_{70-2n}^{z+} ($n = 1$, $z = 1$) produced by photoionization of solitary C_{60} and C_{70} , respectively, in the photon energy range of 45–150 eV. Then the mechanism of sequential loss of C_2 units has been proposed on a basis of comparison between the experimental ion yield curves and theoretical fractional abundance curves. The latter curves have been derived by employing the RRKM theory to individual unimolecular reactions, $C_{60-2n+2}^{z+} \rightarrow C_{60-2n}^{z+} + C_2$. More reliable calculations of the rate constants of the consecutive reactions are needed before closer comparison between the two curves. For such calculations we should know precise values of the activation energies for the reactions, together with the vibrational spectra of the transition states. This induced us to develop a new ion spectrometer for the fragment ions produced from C_{60}^{z+} and

C_{70}^{z+} . It is likely that the magnitude of the potential barriers of the reactions can be estimated from the average kinetic energy release measured by this spectrometer.

References

- 1) J. Kou, T. Mori, Y. Kubozono and K. Mitsuke, *Phys. Chem. Chem. Phys.* **7**, 119 (2005).
- 2) K. Mitsuke, H. Katayanagi, J. Kou, T. Mori and Y. Kubozono, *AIP Conf. Proc.* **811**, 161 (2006).

VI-H-2 Photofragment Imaging Apparatus for Measuring Momentum Distributions in Dissociative Photoionization of Fullerenes

KAFLE, Bhim Prasad¹; PRODHAN, Md. Serajul Islam¹; KATAYANAGI, Hideki; MITSUKE, Koichiro
(¹SOKENDAI)

[AIP Conf. Proc. in press]

We are developing a photofragment imaging apparatus based on time-of-flight (TOF) mass spectrometry to measure the kinetic energy and angular distributions

of the fragments. We have adopted the Eppink–Parker type three-element velocity focusing lens system¹⁾ (electrodes R, E, and T) to achieve high kinetic energy resolution on the photofragment images. Furthermore, we have utilized a potential switchable mass gate M and an ion reflector G inside the TOF tube as demonstrated in Figure 1, to select a bunch of fragments having the same mass-to-charge ratio m/z from neighboring bunches $(m \pm 24)/z$. As long as M is kept grounded, all fragments are reflected back by G and do not impinge against the imaging detector PSD. When an entire bunch of the fragments having an expected m/z arrives inside M, a pulsed voltage is applied there. The potential energies of the ions in this bunch are suddenly elevated, so that these ions can exclusively pass through G and reach the PSD.

For optimizing the dimensions of the setup, we have performed ion trajectory simulations utilizing the SIMION software. We considered that the dissociative ionization of C_{60} takes place within a region of rectangular parallelepiped $\Delta x \Delta y \Delta z = 1 \times 3 \times 1 \text{ mm}^3$ in the ionization region of the spectrometer. The simulated trajectories of C_{60}^+ , C_{58}^+ and C_{56}^+ at initial kinetic energy of 0.1 eV show that the trajectories of unwanted C_{60}^+ and C_{56}^+ ions are reflected completely. On the other hand, most of the trajectories of C_{58}^+ , the ion whose momentum image we wish to measure, are found to go beyond G and reach the PSD. This observation provides direct evidence for exclusive imaging detection of C_{58}^+ .

Reference

- 1) A. T. J. B. Eppink and D. H. Parker, *Rev. Sci. Instrum.* **68**, 3477 (1997).



Figure 1. Schematic view of the momentum imaging spectrometer and simulated trajectories of C_{58}^+ at initial kinetic energies of 0.1 eV. R, repeller; E, extractor; T, entrance electrode of a time-of-flight drift tube (TOF); IT, Ion trajectories; M, mass gate; G, ion reflector. The dimensions of all the electrodes are determined from the SIMION 3D software.

VI-H-3 Simulated Image of Fragment Ions Produced from C_{60}

KAFLE, Bhim Prasad¹; PRODHAN, Md. Serajul Islam¹; YAGI, Hajime; KATAYANAGI, Hideki; MITSUKE, Koichiro
(¹SOKENDAI)

Our photofragment imaging spectrometer under construction is found to realize excellent momentum imaging detection of fullerene fragments with a particular cluster size. To demonstrate its capability, we have reproduced a simulated image of fragment ions C_{58}^+ from C_{60} with different kinetic energies. Figure 1 shows the image of the C_{58}^+ ions on the PSD at the kinetic energies of 0.1 eV (triangles) and 0.11 eV (circles). We have taken into account the ion trajectories generated in

the elevation and azimuth angle ranges of 0° to $+90^\circ$ and 0° to $+180^\circ$, respectively, which cover only one quarter of the full three-dimensional trajectories over the 4π solid angle. The trajectories with a given elevation angle form a horizontal stripe, and the envelope of all the stripes makes an arc. This clearly demonstrates that scattering distribution in spherical symmetry can be successfully projected on an image plane. It is likely that the two images are almost separable if their kinetic energy difference is larger than 0.01 eV. Comparison between the simulations with and without the ion reflector G (see Figure 1 of VI-H-2) confirmed that the images are not distorted in the presence of G. The present momentum imaging spectrometer will be installed at the end station of beam line 2B in the UVSOR facility.

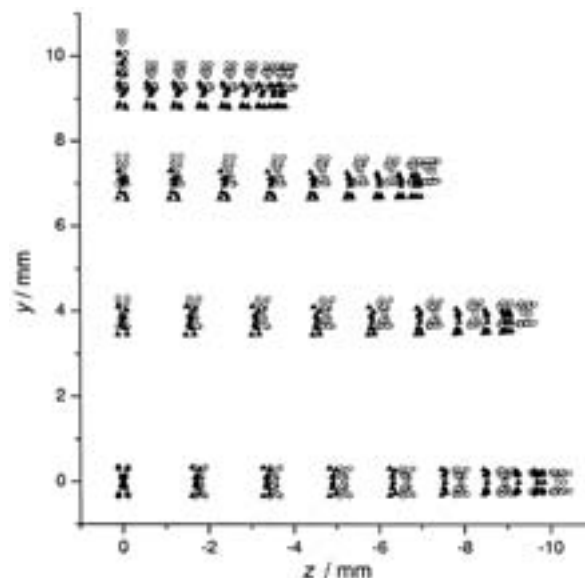


Figure 1. Simulated image of C_{58}^+ ions at the kinetic energies of 0.1 eV (▲) and 0.11 eV (○). The three-dimensional scattering distribution of the ions is projected on the PSD.

VI-H-4 Scattering Distributions of the Photofragments from C_{60} in the Extreme Ultraviolet

PRODHAN, Md. Serajul Islam¹; KAFLE, Bhim Prasad¹; YAGI, Hajime; KATAYANAGI, Hideki; MITSUKE, Koichiro
(¹SOKENDAI)

In thermodynamic equilibrium the velocity distribution of a large number of C_{60} molecules can be represented by the Maxwell-Boltzmann form of

$$f_0(\vec{v}) \propto \left[\frac{m}{2\pi kT} \right]^{\frac{3}{2}} \exp\left(\frac{-mv^2}{2kT} \right) \quad (1)$$

where the density and temperature are assumed to be independent of the positions of molecules. Therefore, the velocity distribution of the photofragments from C_{60} in the laboratory system can be expressed as that in the center-of-mass system convoluted with the initial Maxwell-Boltzmann distribution before photoionization. We will perform deconvolution procedure to derive the

velocity distribution in the center-of-mass system, which is needed to decide on a dominant mechanism in fragmentation of electronically excited C_{60} cations, from the three-dimensional velocity distributions of the fragment ions measured by using our imaging spectrometer.

VI-H-5 Why We Wish to Measure the Yield Curves of the Photofragments from C_{60} in Coincidence with Threshold Electrons

MITSUKE, Koichiro; KATAYANAGI, Hideki;
KAFLE, Bhim Prasad¹; PRODHAN, Md. Serajul
Islam¹; YAGI, Hajime
(¹SOKENDAI)

We have derived the E_{int} -dependence of the C_{60-2n}^{z+} yield from the experimental $h\nu$ -dependent yield, and then compared the former dependence with the theoretical fractional abundance near the onset region.¹⁾ Such a comparison may become less meaningful further away from the onset region. This is because, in our estimate of E_{int} of the primary C_{60}^{z+} , we have disregarded the energy transmission from a portion of $h\nu$ to the photoelectron kinetic energy, and eventually substantial errors have been produced in the E_{int} -dependence curve. To convert the $h\nu$ -dependent yield accurately to the E_{int} -dependence, we require the partial photoionization cross section of C_{60} for the formation of C_{60}^{z+} as a function of both $h\nu$ and E_{int} . However, it is far from easy to obtain the partial photoionization cross section in wide $h\nu$ and E_{int} ranges from conventional two-dimensional photoelectron spectroscopy. Thus we are planning to measure (a) the yield curve of threshold electrons and (b) that of C_{60-2n}^{z+} in coincidence with the threshold electrons. Using these two curves we will be able to calculate a proper E_{int} -dependence of the C_{60-2n}^{z+} yield.

Reference

- 1) K. Mitsuke, H. Katayanagi, J. Kou, T. Mori and Y. Kubozono, *AIP Conf. Proc.* **811**, 161 (2006).

VI-H-6 ZEKE Photoelectron Spectroscopy Utilizing the Dark Gap of UVSOR Storage Ring

KATAYANAGI, Hideki; KAFLE, Bhim Prasad¹;
PRODHAN, Md. Serajul Islam¹; YAGI, Hajime;
MITSUKE, Koichiro
(¹SOKENDAI)

Last year we constructed a threshold photoelectron spectrometer for the purpose of measuring the signal of threshold electron-photoion coincidence (TEPICO), using the dark gap of the synchrotron radiation facility. Such measurements provide us with the detailed information about the excitation/dexcitation and decay processes of gaseous fullerenes (C_{60} and C_{70}). We already succeeded in observing the threshold electron signal using He and O_2 samples, but the spectra suffered from intense background counts. The background needs to be reduced to the utmost for performing the TEPICO measurement. Also an improvement of the spectrometer in the efficiency for threshold electrons is urgently needed. For these requirements, we are now developing an

improved version of the spectrometer which has the capability to significantly reject the electrons with high kinetic energies and to guide electrons with zero or very small kinetic energies (0 to 10 meV) to the detector.

VI-H-7 New Design of a ZEKE Photoelectron Spectrometer for Photofragmentation Studies of Fullerenes

KAFLE, Bhim Prasad¹; KATAYANAGI, Hideki;
MITSUKE, Koichiro
(¹SOKENDAI)

Figure 1 shows a schematic diagram of our improved threshold photoelectron spectrometer, together with typical trajectories for 10 meV photoelectrons. Here, a voltage of $E_E = 3$ V is applied to the extraction electrode. The extraction and screening electrodes are 1 mm in thickness and central circular apertures of 7 mm in diameter are drilled. The arrangement of the electrodes was optimized by using the SIMION software.¹⁾ We have adopted penetrating field technique which was invented by King and coworkers.²⁾ In this technique a potential well is formed in the ionization region by the field penetration from the potential of the extraction electrode through the screening electrode, providing a very large solid angle of collection for slow electrons ($\sim 4\pi$ sr). Slow electrons are focused again at a crossover point inside a three-element asymmetric lens system beyond which they can reach the detector. In contrast, high energy electrons are strongly suppressed by the field of the asymmetric lens system. The proportion of the detectable trajectories is determined by simulation as a function of the electron kinetic energy. The results at $E_E = 3$ V are shown in Figure 2.

References

- 1) D. A. Dahl, SIMION 3D Version 7.0 User's Manual, Idaho falls: 2000.
- 2) R. I. Hall, A. McConkey, K. Ellis, G. Dawber, L. Avaldi, M. A. MacDonald and G. C. King, *Meas. Sci. Technol.* **3**, 316 (1992).



Figure 1. Schematic view of the threshold photoelectron spectrometer and simulated trajectories at the initial kinetic energy of 10 meV. From ionization center 36 electron trajectories were generated in the ejection angle of 0° to 360° , at an interval of 10° . R, repeller; S, screening electrode; E, extraction electrode; A, asymmetric lens system; F, front-plate electrode.

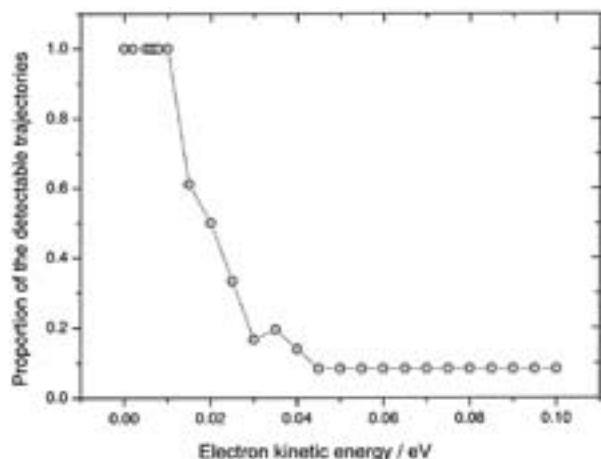


Figure 2. Proportion of the detectable trajectories determined by simulation at $E_E = 3$ V. The curve shows a sharp increase below 20 meV.

VI-H-8 High Resolution Photoelectron Spectroscopy of Gaseous Fullerenes

YAGI, Hajime; KATAYANAGI, Hideki; KAFLE, Bhim Prasad¹; PRODHAN, Md. Serajul Islam¹; MITSUKE, Koichiro
(¹SOKENDAI)

Photoemission measurements of solitary C_{60} and C_{70} have been made by several groups, but their energy resolution was *ca.* 100 meV at the best. We are developing an apparatus of high-resolution angle-resolved photoemission spectroscopy, using a helium discharge lamp or synchrotron radiation. Our goal is to carry out photoemission spectroscopy of various kinds of gaseous fullerenes with a total energy resolution of ~ 20 meV. Fullerenes have a number of degenerated bands within 40 eV from the Fermi energy. Definite assignments of the peaks in the photoemission spectra of fullerenes are expected to be easier in the gas phase than in the solid phase, since band broadening and interference of secondary electrons are substantially reduced in the gas phase. Some of the peaks arising from excitations to different vibrational states of excited C_{60}^+ ions might be distinguishable. As for metallofullerenes it is documented that electron transfer takes place from the encapsulated metal atoms to the fullerene cages. For instance, valence-band photoemission studies of the $La@C_{82}$ film showed that new peaks due to triply electron transfer emerge near the Fermi energy. Such peaks are expected to be seen more clearly in the gas phase. By measuring the photoion yield curves, we observed for the first time the $4d \rightarrow 4f$ giant dipole resonance in $Ce@C_{82}$ and $Pr@C_{82}$. Using synchrotron radiation, we will perform resonant photoemission spectroscopy of these species to confirm the presence of giant dipole resonance and to study the dynamics of the $4f$ electrons of encapsulated metal atoms.

VI-H-9 Construction of an End Station of BL2B to Study Dissociative Photoionization of Fullerenes and VUV Spectroscopy of Ionic Liquids

KATAYANAGI, Hideki; KAFLE, Bhim Prasad¹; PRODHAN, Md. Serajul Islam¹; YAGI, Hajime; MITSUKE, Koichiro
(¹SOKENDAI)

A new vacuum chamber for the end station of beam line 2B (BL2B) in UVSOR was constructed. The chamber was designed for the gas phase spectroscopy of refractory materials such as fullerenes, metalloencapsulated fullerenes and ionic liquids. The following three subjects are now under way: (1) the velocity map imaging¹⁾ of the ionic photofragments from fullerenes, (2) threshold photoelectron-photoion coincidence measurements of the fullerenes, and (3) photoelectron and photoabsorption spectroscopy of ionic liquids. The installation of the chamber at BL2B was accomplished. We are going to instrument various spectrometers into the chamber for the above experiments.

Drawing of the chamber is shown in Figure 1. The twofold μ -metal shield is put inside the chamber to prevent penetration of the geomagnetic field. The effective volume surrounded by the shield is five times as large as that of the previous chamber used at BL2B. The new chamber is equipped with 14 ports facing the ionization region, *i.e.* the focal point of the synchrotron radiation. This larger volume and versatile port arrangement enable us to incorporate many complicated devices. Moreover, we will use this chamber also at BL7U, a new beam line with a normal incidence monochromator connected with a planar undulator. Accordingly, the chamber was mounted on a micromotion stage in order to align its optical axis readily with the beam lines when the chamber is relocated.

Reference

- 1) A. T. J. B. Eppink and D. H. Parker, *Rev. Sci. Instrum.* **69**, 3477 (1997).

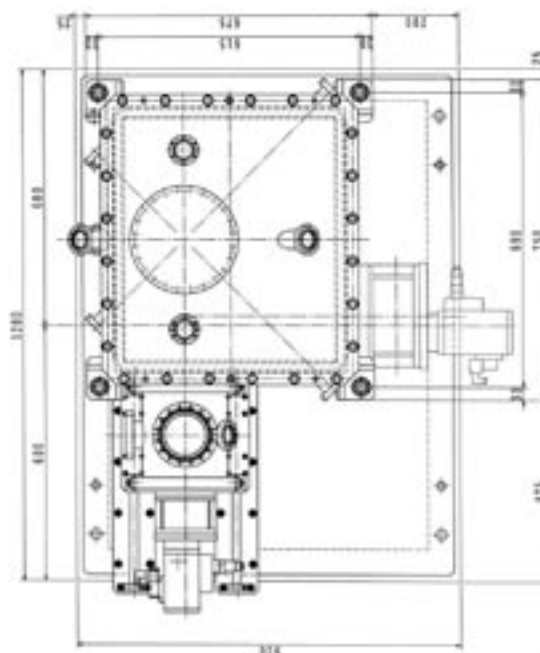


Figure 1. Drawing (top view) of the vacuum chamber on the micromotion stage (1200 × 900 mm) for the beam lines BL2B and BL7U in UVSOR.

VI-I Ray-Tracing for the Branch Beam Line of the 10-m Normal Incidence Monochromator Developed for Gas-Phase Photochemistry

Domestic synchrotron radiation facilities have no undulator beam line devoted to studies on gas-phase photochemistry in the vacuum ultraviolet (VUV) region. Kimura and coworkers in the UVSOR facility are constructing a new undulator beam line BL7U equipped with normal incidence monochromator, aiming at a maximum flux of 10^{11} photons/s (at 0.01% band width) and a maximum resolving power of 60000 [e.g. *UVSOR Activity Report* **2004**, 46 (2005)]. Our group is planning to construct a branch line to this monochromator. At the end station we will perform spectroscopic and dynamical studies of gas-phase molecules and clusters. Ray-tracing of the monochromator is in progress to determine the specifications of the branch line, with particular attention to the positions and shapes of post-focusing mirrors.

VI-I-1 Layout of the Branch Beam Line of BL7U

MITSUKE, Koichiro

The detailed design of the beam line 7U has been reported elsewhere,¹⁾ so that we will briefly describe its layout (see Figure 1). The undulator is of APPLE-II type with a periodic length of 76 mm and the number of period of 38. Kimura and coworkers have adopted the normal incidence monochromator having an off-plane eagle mount in which three spherical gratings with 10-m focal length undergo translational and rotational motions. The undulator radiation is sampled by a pinhole, deflected horizontally at planar mirrors M0 and M1 by 10° and 165° , respectively, and made to irradiate the surface of one of the spherical gratings. The undulator radiation is further deflected horizontally at the grating by 182° . The dispersion plane of the grating lies vertically and the associated incidence and diffracted angles are always the same with varying from 0° (0^{th} -order light) to 6° (the longest wavelength). The 1^{st} -order light of the grating is deflected horizontally at the planar steering mirror M2 by 30° and focused onto the exit slit in the horizontal and vertical directions simultaneously. The light is then deflected horizontally at the toroidal postfocusing mirror M4 by 20° , thereby focusing onto the ionization point in the end station.

Reference

1) S. Kimura, *UVSOR Activity Report* **2004**, 46 (2005).

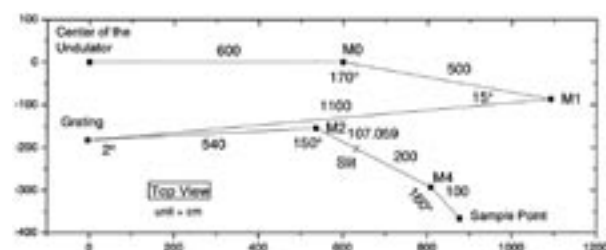


Figure 1. Layout of the beam line BL7U of UVSOR involving a 10-m normal incidence monochromator. The distances between two optical elements are in cm. Symbols M_n ($0 \leq n \leq 4$) designate the pre- and post-focusing mirrors.

VI-I-2 Ray-Tracing for the Branch Beam Line of BL7U of UVSOR

MITSUKE, Koichiro

The ray tracing is carried out at the fundamental of the undulator radiation around 17 eV at the deflection parameter of $K = 2.5$ by making use of the Shadow software. Panels a and b of Figure 1 show the spot images at the exit slit and ionization point, respectively, when 20000 rays ranging in the photon energy from 17.0497 to 17.0500 eV are generated randomly. We employed a grating with 2400 lines/mm, a slit with a 20 μm , and diffraction angle of 5.00695° . The sizes of the optical elements are taken into account, whereas their reflectivity and slope errors are neglected. The analysis showed that 6843 rays can arrive at the ionization point (Good rays) with a spot size of $20 \mu\text{m} \times 400 \mu\text{m}$. On the other hand, the number of the good rays is reduced to almost 3000, when the 20000 rays are generated in the photon energy range of either 17.0494–17.0497 eV or 17.0500–17.0503 eV. It is therefore likely that a resolving power of more than 30000 has been achieved. A resolving power of ca. 60000 is expected to be attained if we utilize a grating with 3600 lines/mm.

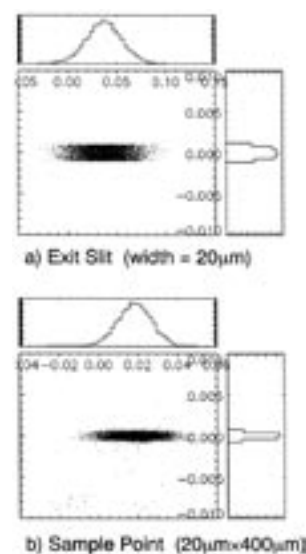


Figure 1. Spot images at the a) exit slit and b) ionization point under a 5%-coupling operation.

RESEARCH ACTIVITIES VII

Department of Computational Molecular Science

VII-A Computer Simulation of Quantum Systems in Condensed Phase

VII-A-1 A Surface Hopping Method for Chemical Reaction Dynamics in Solution Described by Diabatic Representation: An Analysis of Tunneling and Thermal Activation

YAMADA, Atsushi; OKAZAKI, Susumu

[*J. Chem. Phys.* **124**, 094110 (11 pages) (2006)]

We present a surface hopping method for chemical reaction in solution based on diabatic representation, where quantum mechanical time evolution of the vibrational state of the reacting nuclei as well as the reaction-related electronic state of the system are traced simultaneously together with the classical motion of the solvent. The method is effective in describing the system

where decoherence between reactant and product states is rapid. The diabatic representation can also give a clear picture for thereaction mechanism, *e.g.* thermal activation mechanism and tunneling one. An idea of molecular orbital theory has been applied to evaluate the solvent contribution to the electronic coupling which determines therate of reactive transition between the reactant and product potential surfaces. We applied the method to a model system which can describe complex chemical reaction of the real system. Two numerical examples are presented in order to demonstrate the applicability of the present method, where the first example traces a chemical reaction proceeded by thermal activation mechanism and the second examines tunneling mechanism mimicking a proton transfer reaction.

VII-B Molecular Dynamics Study of Classical Complex Systems

VII-B-1 A Molecular Dynamics Study of Sodium Chenodeoxycholate in an Aqueous Solution

NAKASHIMA, Toshio; IWAHASHI, Kensuke;
OKAZAKI, Susumu

[*Chem. Phys. Lett.* **420**, 489–492 (2006)]

Hydration structure and dynamics of sodium chenodeoxycholate (CDC) in water are studied by a long-time molecular dynamics calculation. Strong hydration shell around the hydrophobic region of this large solute and strong hydrogen bonds of water with both hydroxyl and carboxyl oxygen atoms have been identified. The rotation of CDC around its longitudinal axis is found to be particularly active in comparison with that around other axes of the molecule. The diffusion coefficient of CDC calculated from the slope of the meansquaredisplacement, $0.95 \times 10^{-9} \text{ m}^2/\text{s}$, is only 1/6 of that for water in the solution, $5.4 \times 10^{-9} \text{ m}^2/\text{s}$.

VII-B-2 A Molecular Dynamics Study of Free Energy of Micelle Formation for Sodium Dodecyl Sulfate in Water and Its Size Distribution

YOSHII, Noriyuki; IWAHASHI, Kensuke;
OKAZAKI, Susumu

[*J. Chem. Phys.* **124**, 184901 (6 pages) (2006)]

Free energy of micelle formation has been evaluated for spherical sodium dodecyl sulfate (SDS) in water by a thermodynamic integration method combined with a series of large-scale molecular dynamics calculations following the chemical species model. In particular, free energy change $\Delta\mu_{n+1}^0$ with respect to the addition of one surfactant molecule to the spherical micelle of size n was obtained as a function of n . The free energy profile showed a minimum followed by a maximum, which corresponds to a peak in the size distribution. The calculated peak size $n = 57$ near its critical micelle concentration is in good agreement with the experimental averaged aggregation number $n = 55\text{--}75$ of the SDS micelle. The distribution showed a rather sharp peak, indicating that the size is almost a monodisperse one. The size is likely to be insensitive to the total concentration of the surfactant.

VII-B-3 A Molecular Dynamics Study of Structural Stability of Spherical SDS Micelle as a Function of Its Size

YOSHII, Noriyuki; OKAZAKI, Susumu

[*Chem. Phys. Lett.* **425**, 58–61 (2006)]

In order to investigate stability of spherical sodium

dodecyl sulfate micelle in water, molecular dynamics calculations have been performed for the micelle of various sizes. Size-dependence of the micelle structure such as asphericity, Voronoi polyhedron, and radial density profile has been analyzed in detail from a viewpoint of geometrical instability found in it, *i.e.*, direct exposition of the hydrophobic group to water observed for small micelles and cavity formation in the center of large micelles.

VII-B-4 A Molecular Dynamics Study of Surface Structure of Spherical SDS Micelles

YOSHII, Noriyuki; OKAZAKI, Susumu

[*Chem. Phys. Lett.* **426**, 66–70 (2006)]

A series of molecular dynamics calculations have been carried out for spherical sodium dodecyl sulfate micelle of various sizes in order to investigate surface structure of the micelle as a function of its size. Two-dimensional surface pair correlation function of the hydrophilic head group projected on the sphere of the micelle showed a gas-like structure for small micelle, *e.g.* $N = 31$, and a liquid-like one for large micelles, *e.g.* $N \geq 61$, depending on the surface density of the head group. Coordination structure of the sodium ion near the surface has been analyzed in detail, too.

VII-C Development of Simulation Algorithms for Quantum Many-Body Systems

VII-C-1 Path Integral Hybrid Monte Carlo Study on Structure of Small Helium-4 Clusters Doped with a Linear Molecule

MIURA, Shinichi

[*J. Low Temp. Phys.* in press]

Microscopic structure of small helium-4 clusters doped with a carbonyl sulfide molecule, $\text{OCS}({}^4\text{He})_N$, at 0.37 K is studied by the path integral hybrid Monte Carlo method; the size of the cluster N ranges from $N = 2$ to $N = 5$. In all the cases examined in the present study, the helium atoms are localized around the carbon atom of the OCS molecule, forming a doughnut-type structure around the molecular axis. Bosonic exchange among the helium atoms is found to be promoted in the doughnut region, showing an anisotropic “superfluid” response of the clusters.

VII-D Development of Polarizable Molecular Modeling for Simulation Studies

Accuracy and reliability of molecular models are crucial for theoretical understandings of condensed phase chemistry. This year we have developed molecular models which incorporate both intramolecular vibration and electronic polarization. Such flexible and polarizable models have a number of applications to condensed phase chemistry, including electron transfer reactions. Another important purpose of the flexible and polarizable models is to describe the sum frequency generation spectroscopy by molecular dynamics simulation, as discussed in the next section.

VII-D-1 Polarizable Solute in Polarizable and Flexible Solvents: Simulation Study of Electron Transfer Reaction Systems

ISHIDA, Tateki

[*J. Phys. Chem. B* **109**, 18558–18564 (2005)]

A polarizable solute model, based on the empirical valence bond approach, is developed and applied to electron transfer (ET) reactions in polarizable and flexible water solvents. The polarization effect is investigated in comparison with a nonpolarizable solute and solvent model. With free energy curves constructed by a molecular dynamics simulation, the activation energy barrier and the reorganization energy related to ET processes are investigated. The simulation results show that the activation energy barrier becomes larger in the polarizable model than in the nonpolarizable model and that this makes the ET rate slower than that with the nonpolarizable model. It is shown that the effect of the electronic energy difference of solute molecule on free energy profiles is remarkable and that, corresponding to this effect, the reorganization energy is significantly modified. These results indicate that the process of solvent polarization by the polarized solute to enhance the solute-solvent interaction is a key factor and that treating the polarization of both solute and solvent at the same time is essential. Also, the polarization effect on the diffusive motion of the solute molecule in the polarization solvent is studied. The polarized solute molecule shows slower diffusive motion compared with that in the

nonpolarizable model.

VII-D-2 Extended Treatment of Charge Response Kernel Comprising the Density Functional Theory and Charge Regulation Procedures

ISHIDA, Tateki; MORITA, Akihiro

[*J. Chem. Phys.* **125**, 074112 (2006)]

We propose an extended treatment of the charge response kernel (CRK), $\partial Q_a/\partial V_b$, which describes the response of partial charges on atomic sites to external electrostatic potential, on the basis of the density functional theory (DFT) via the coupled perturbed Kohn-Sham equations. The present CRK theory incorporates regulation procedures in the definition of partial charges to avoid unphysical large fluctuation of the CRK on “buried” sites. The CRKs of some alcohol and organic molecules, methanol, ethanol, propanol, butanol, dimethylsulfoxide (DMSO) and tetrahydrofuran (THF) were calculated, demonstrating that the new CRK model at the DFT level has greatly improved the performance of accuracy in comparison with that at the Hartree-Fock level previously proposed. The CRK model was also applied to investigate spatial nonlocality of the charge response through alkyl chain sequences. The CRK model at the DFT level enables us to construct a non-empirical strategy for polarizable molecular modeling, with practical reliability and robustness.

VII-E Computational Analysis of Sum Frequency Generation Spectroscopy

This project aims at developing theoretical and computational methods of visible-infrared Sum Frequency Generation (SFG) spectroscopy for interface characterization. While SFG is recognized as a powerful experimental technique to optically probe a variety of interface structure, experimental spectra are not often amenable to straightforward fitting or interpretation. We have proposed theoretical methods to compute SFG directly via molecular modeling and molecular dynamics simulation, without resorting to empirical parameterization. This year, we have developed a general polarizable and flexible molecular model, called charge response kernel, on the basis of the density functional theory for the purpose of the SFG calculation. SFG spectra of aqueous electrolyte solutions are also analyzed by molecular dynamics simulation.

VII-E-1 Intermolecular Correlation Effect in Sum Frequency Generation Spectroscopy of Electrolyte Aqueous Solution

ISHIYAMA, Tatsuya; MORITA, Akihiro

[*Chem. Phys. Lett.* **431**, 78–82 (2006)]

Molecular dynamics analysis of the sum frequency generation (SFG) spectroscopy was performed to solve the recent controversial problem about liquid-vapor interface of electrolyte aqueous solution [Garrett, *Science* **303**, 1146 (2004)]. The present MD analysis revealed a crucial role of ion-water dipolar correlation in the vibrational SFG spectroscopy, which significantly distorts the general relationship between SFG intensity and surface orientational order. The experimental SFG spectra were thereby elucidated from the local structure of interface.

VII-F Theoretical Study of Condensed Phase Dynamics by Using Multi-Dimensional Spectroscopy

VII-F-1 Fifth-Order Two-Dimensional Raman Spectroscopy of Liquid Water, Crystalline Ice Ih and Amorphous Ices: Sensitivity to Anharmonic Dynamics and Local Hydrogen Bond Network Structure

SAITO, Shinji; OHMINE, Iwao¹
(¹Nagoya Univ.)

[*J. Chem. Phys.* **125**, 084506 (12 pages) (2006)]

Theoretical study of off-resonant fifth-order two-dimensional (2D)-Raman spectroscopy is made to analyze the intermolecular dynamics of liquid and solid water. The 2D-Raman spectroscopy is susceptible to the nonlinear anharmonic dynamics and local hydrogen bond structure in water. It is found that the distinct 2D-Raman response appears as the negative signal near the t_2 axis. The origin of this negative signal for $t_2 < 15$ fs is from the nonlinear polarizability in the librational mo-

tions, whereas that for $30 \text{ fs} < t_2 < 150 \text{ fs}$ is attributed to the anharmonic translational motions. It is found that the mechanical anharmonicity and nonlinear polarizability couplings among modes clearly can be observed as the sum- and difference-frequency peaks in the 2D-Raman spectrum (that is, Fourier transforms of the responses). The 2D-Raman spectroscopies of ice Ih and amorphous ices, low-density, high-density, and very high-density amorphous ices, are also investigated. It is found that the 2D-Raman spectroscopy is very sensitive to the anisotropy of the structure of ice Ih. The strong HB stretching band is seen in the 2D-Raman spectroscopy of the polarization directions parallel to the c -axis, whereas the contributions of the librational motion can be also seen in the spectrum with the polarization directions parallel to the a -axis. The 2D-Raman spectroscopy is also found to be also very sensitive to the differences in local hydrogen bond network structures in various amorphous phases.

VII-G Theoretical Study of Dynamics in Biological Systems

VII-G-1 Mechanism of Ion Permeation in Model Channel; Free Energy Surface and Dynamics of K^+ Ion Transport in Anion-Doped Carbon Nanotube

SUMIKAMA, Takashi¹; SAITO, Shinji; OHMINE, Iwao¹
(¹Nagoya Univ.)

[*J. Phys. Chem. B* **110**, 20671–20677 (2006)]

The mechanism of the ion permeation is investigated for an anion-doped carbon nanotube, as a model of the K^+ channel, by analyzing the free energy surface and the dynamics of the ion permeation through the model channel. It is found that the main rate-determining step is how an ion enters the channel. The entrance of the ion

is mostly blocked a water molecule locating at this entrance. Only a few percent of K^+ ions which reach the mouth of the channel can really enter the channel. The rejection rate sensitively depends on the location of this water molecule, which is easily controlled by the charge of the carbon nanotube; for example, the maximum permeation is obtained when the anion charge is at a certain value, $-5.4e$ in the present model. At this charge, the facile translocation of the ion inside the channel is also induced due to the number fluctuation of the ions inside the channel. Therefore, the so-called “Newton’s balls,” a toy model, combined with a simple ion diffusion model for explaining the fast ion permeation should be modified. The present analysis thus suggests that there exists an optimum combination of the length and the charge of the carbon nanotube for the most efficient ion permeation.

VII-H Theoretical Study of Origin of Slow Relaxation in Liquid Water

VII-H-1 Origin of Slow Relaxation in Liquid Water Dynamics: A Possible Scenario for the Presence of Bottleneck in Phase Space

SHUDO, Akira¹; ICHIKI, Kouichiro¹; SAITO, Shinji

(¹Tokyo Metropolitan Univ.)

[*Europhys. Lett.* **73**, 826–832 (2006)]

We study slow relaxation in dynamics of liquid water at room temperatures and propose a consistent inter-

pretation explaining why liquid-water dynamics exhibits power law relaxation behavior and can form the bottleneck in phase space even though it is a many dimensional and strongly chaotic system. Our idea is inspired by recent developments of perturbation theories of Hamiltonian systems, and is reminiscent of the so-called Boltzmann-Jeans conjecture. Within this scenario, it is natural to expect that slow relaxation is not limited to liquid-water dynamics. We found that our hypothesis works well in predicting the relaxation properties of other molecules. The relation to the potential landscape picture is also discussed.

RESEARCH ACTIVITIES VIII

Coordination Chemistry Laboratories

Prof. Hiroshi Kitagawa (Kyushu Univ.) and Assoc. Prof. Mitsuru Kondo (Shizuoka Univ.) took the position of the Laboratory of Complex Catalyst from April 2006. Prof. Kazushi Mashima (Osaka Univ.) and Assoc. Prof. Masato Kurihara (Yamagata Univ.) finished their term as Adjunct Prof. of the Laboratory of Complex Catalyst in March 2006. Their effort during their term is gratefully appreciated. Prof. Yoichi Ishii (Chuo Univ.) and Prof. Takashi Hayashi (Osaka Univ.) continue the position of Laboratory of Coordination Bond.

VIII-A Metal Complexes Aimed at Conversion between Chemical and Electrochemical Energies

Metal complexes that have an ability to oxidize organic molecules at potentials more negative than the reduction potential of dioxygen have potential uses for electro-catalysts in fuel cells. Metal-oxo complexes are possible candidates for the oxidation of organic molecules, since metal-oxo species are believed to work as active centers in various metal enzymes, which oxidize various biological substrates under very mild conditions. Mechanistic understandings of the reactivity of metal-oxo species, however, are limited due to the difficulty of preparation of reactive M–O frameworks in artificial systems. On the other hand, reactivity of high valent Ru=O complexes prepared by sequential electron and proton loss of the corresponding Ru–OH₂ ones have been extensively studied and proven to work as oxidants of organic molecules to some extent. We have succeeded reversible conversion between aqua and oxo ligands on Ru–dioxolene frameworks without using any oxidants by taking advantage of dioxolene as a redox active ligand. Along this line, we have been preparing a variety of metal–aqua and –amine complexes bearing a dioxolene ligand aiming at oxidation of hydrocarbons by the corresponding metal–oxo and –imido complexes.

VIII-A-1 Structural Characterization of Ruthenium–Dioxolene Complexes with Ru^{II}–SQ and Ru^{II}–Cat Frameworks

FUJIIHARA, Tetsuaki; OKAMURA, Rei; TANAKA, Koji

[*Chem. Lett.* **34**, 1562–1563 (2005)]

The structural and electronic properties of [Ru^{II}(trpy)(ClSQ)(PPh₃)]⁺ (trpy = 2,2':6',2''-terpyridine; ClSQ = 4-chlorobenzosemiquinonate) that is prepared from *cis*-[Ru(trpy)(PPh₃)Cl₂] and 4-chlorocatechol (HClCat), and [Ru^{II}(trpy)(ClCat)(PPh₃)] obtained by the reduction of the former were examined. Both complexes were characterized by x-ray diffractometry, UV-visible spectroscopy, ESR, and electrochemistry.

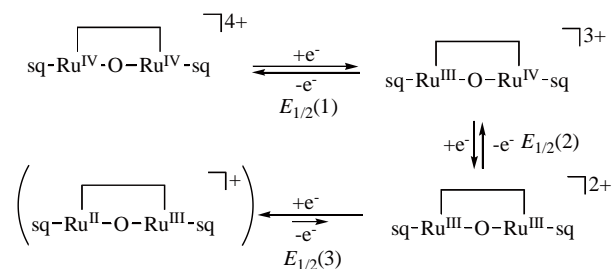
VIII-A-2 Reversible Bond Formation and Cleavage of the Oxo Bridge of [Ru₂(μ-O)(dioxolene)₂(btpyxa)]³⁺ [btpyxa = 2,7-Di-*tert*-butyl-9,9-dimethyl-4,5-bis(2,2':6',2''-terpyrid-4'-yl)xanthene] Driven by a Three-Electron Redox Reaction

WADA, Tohru; TANAKA, Koji

[*Eur. J. Inorg. Chem.* **19**, 3832–3839 (2005)]

The bis(chlororuthenium) complex [Ru₂Cl₂(3,6-*t*Bu₂sq)₂(btpyxa)](PF₆)₂ [3,6-*t*Bu₂sq = 3,6-di-*tert*-butyl-1,2-benzosemiquinone; btpyxa = 2,7-di-*tert*-butyl-9,9-dimethyl-4,5-bis(2,2':6',2''-terpyrid-4'-yl)xanthene]

and the oxo-bridged diruthenium complex [Ru₂(μ-O)(3,6-*t*Bu₂sq)₂(btpyxa)](PF₆)₃ were synthesized, and the redox behavior of these complexes, which contain a non-innocent dioxolene ligand, was investigated by electrochemistry and electro-spectrochemistry methods. Dicationic 2⁺ undergoes two successive metal-centered one-electron and a simultaneous two-electron ligand-based redox reaction at $E_{1/2} = +0.13$ and $+0.09$ and $E_{1/2} = -0.75$ V (vs. SCE), respectively, in CH₂Cl₂. The UV/Vis/NIR spectrum of tricationic 3⁺ shows an intervalence-transition (IT) band at 1333 nm ($\lambda = 1.52 \times 10^4$ M⁻¹ cm⁻¹) in a near-IR region together with two CT bands at 766 ($\lambda = 2.21 \times 10^4$ M⁻¹ cm⁻¹) and 586 nm ($\epsilon = 1.13 \times 10^4$ M⁻¹ cm⁻¹) in CH₂Cl₂. The mixed-valence complex of 3⁺ with an Ru^{IV}–O–Ru^{III} core is reversibly oxidized and reduced to the Ru^{IV}–Ru^{IV} and Ru^{III}–Ru^{III} oxidation states at $E_{1/2} = +0.63$ and -0.01 V, respectively, in CH₂Cl₂. On the other hand, three-electron redn. of (PF₆)₃ is accompanied by the cleavage of the Ru–O–Ru bond at $E_p = +0.02$ V to give [{Ru(OMe)(3,5-*t*Bu₂sq)}{Ru(OH₂)(3,5-*t*Bu₂sq)}(btpyxa)]⁺ in MeOH.



VIII-A-3 A New Series of Molybdenum-(IV), -(V), and -(VI) Dithiolate Compounds as Active Site Models of Molybdoenzymes: Preparation, Crystal Structures, Spectroscopic/Electrochemical Properties and Reactivity in Oxygen Atom Transfer

SUGIMOTO, Hideki¹; TARUMIZU, Makoto¹; TANAKA, Koji; MIYAKE, Hiroyuki¹; TSUKUBE, Hiroshi¹

(¹Osaka City Univ.)

[Dalton Trans. **21**, 3558–3565 (2005)]

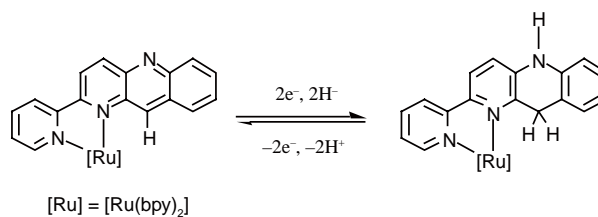
A new set of Mo-(IV), -(V), and -(VI) compounds containing 3,6-dichloro-1,2-benzenedithiolate (bdtCl₂) were isolated and characterized by crystallography and other spectroscopic techniques as active site models of arsenite oxidase, one of the molybdoenzymes. MoO₂ compounds were prepared in high yields by reaction of MoO₂Cl₂ with bdtCl₂, related dithiolene and thio-catecholates in MeOH at low temp. The bdtCl₂ ligand particularly stabilized the MoO compounds with oxidation states of +4 and +5 as well as the MoO₂ compound with an oxidation number of +6. (Et₄N)₂[Mo^{VI}O₂(bdtCl₂)₂] (**1**) (Et₄N)₂[Mo^{IV}O(bdtCl₂)₂] (**2**) and (Et₄N)[Mo^VO(bdtCl₂)₂] (**3**) were successfully isolated, whereas (Et₃NH)₂[MoO₂(thiocatecholates)] (**6**) gradually decomposed in MeCN. A distorted octahedral structure similar to that of **1** was suggested for the structure of the active site of the oxidized form of arsenite oxidase from a comparison of their bond distances and angles. The bond distances and angles around the Mo(IV) atom in **2** were similar to those around the Mo(IV) center in the reduced form of arsenite oxidase. The reversible 2/3 couple exhibited a more positive redox potential than common MoO dithiolene compounds. **1** underwent an irreversible proton-coupled reduction process to yield **2**. An O atom transfer reaction of **1** with PPh₃ afforded **2** and OPPh₃, and proceeded in second order as $v = -d/dt [\text{MoO}_2] = k[\text{MoO}_2][\text{PPh}_3]$. The structures and properties of the oxo-bridged dinuclear compound, (Et₄N)₂[Mo^{VI}O₂(bdtCl₂)₂](μ-O) (**4**), a dimer of bdtCl₂ (**5**) and **6** were also characterized.

VIII-A-4 Reversible Hydride Generation and Release from the Ligand of [Ru(pbn)(bpy)₂](PF₆)₂ Driven by a Pbn-Localized Redox Reaction

KOIZUMI, Take-aki; TANAKA, Koji

[Angew. Chem., Int. Ed. **44**, 5891–5894 (2005)]

[Ru(pbn)(bpy)₂](PF₆)₂ (**1**, pbn = 2-(2-pyridyl)benzo[b]-1,5-naphthyridine, bpy = 2,2'-bipyridine) was prepared and characterized by x-ray crystallography. Electrochemical reduction of **1** in an acidic solvent gives [Ru(pbnH₂)(bpy)₂]²⁺ (**2**), which releases the hydrogen as hydride. This catalytic system reduces substrates (for example, acetone) with two electrons and protons from water, and thus operates in a similar way to the NAD⁺/NADH redox couple.



VIII-A-5 Mononuclear Five-Coordinate Molybdenum(IV) and -(V) Monosulfide Complexes Coordinated with Dithiolene Ligands: Reversible Redox of Mo(V)/Mo(IV) and Irreversible Dimerization of [Mo^VS]⁻ Cores to a Dinuclear [Mo^V₂(μ-S)₂]²⁻ Core

SUGIMOTO, Hideki¹; SAKURAI, Takashi¹; MIYAKE, Hiroyuki¹; TANAKA, Koji; TSUKUBE, Hiroshi¹

(¹Osaka City Univ.)

[Inorg. Chem. **44**, 6927–6929 (2005)]

A mononuclear five-coordinate Mo(IV) monosulfide complex, (Et₄N)₂[MoS(L)₂] (L = cyclohexene-1,2-dithiolate) (**1**), was obtained and characterized by IR, UV-visible spectroscopic methods, and x-ray crystallography. **1** was oxidized by an equiv. ferrocenium cation to give the corresponding mononuclear Mo(V) complex, (Et₄N)[MoS(L)₂] (**2**), which was stable for a few minutes under a lower concentration than 0.3 mM and then further dimerized to (Et₄N)₂[Mo(L)₂]₂(μ-S)₂ (**3**).

VIII-A-6 Synthesis and Crystal Structures of [W(3,6-dichloro-1,2-benzenedithiolate)₃]ⁿ⁻ (n = 1, 2) and [Mo(3,6-dichloro-1,2-benzenedithiolate)₃]²⁻: Dependence of the Coordination Geometry on the Oxidation Number and Counter-Cation in Trigonal-Prismatic and Octahedral Structures

SUGIMOTO, Hideki¹; FURUKAWA, Yuuki¹; TARUMIZU, Makoto¹; MIYAKE, Hiroyuki¹; TANAKA, Koji; TSUKUBE, Hiroshi¹

(¹Osaka City Univ.)

[Eur. J. Inorg. Chem. **15**, 3088–3092 (2005)]

(Et₄N)₂[W(bdtCl₂)₃] (**1a**), (Ph₄P)₂[W(bdtCl₂)₃] (**1b**), (Et₄N)[W(bdtCl₂)₃] (**2a**), (Ph₄P)[W(bdtCl₂)₃] (**2b**), (C₅NH₆)[W(bdtCl₂)₃] (**2c**), and (Et₃NH)₂[Mo(bdtCl₂)₃] (**3a**) (bdtCl₂ = 3,6-dichloro-1,2-benzenedithiolate) were prepared and characterized by x-ray crystallography, UV/visible spectroscopic, and electrochemical methods. Versatile geometrical changes around the W centers were observed. The trigonal-prismatic structure of the W center in (Et₄N)₂[W(bdtCl₂)₃] (**1a**) is changed to an intermediate structure between trigonal prismatic and octahedral upon solid-state oxidation of the complex of **2a**. Replacement of the counteranion of **1a** with Ph₄P⁺ also resulted in geometrical changes and somewhat of an octahedral contribution is included in **1b**. However, almost the same coordination structures are present in structures **2a**, **2b**, and **2c**, with an oxidation number of

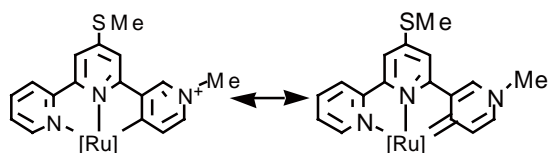
+5. These structures adopt an intermediate geometry between trigonal prismatic and octahedral. No geometrical change was observed upon changing the metal center from W to Mo in $[M(\text{bdtCl}_2)_3]^{2-}$ ($M = \text{W}$ and Mo).

VIII-A-7 Synthesis, Structures and Electrochemical Properties of Ruthenium (II) Complexes Bearing Bidentate 1,8-Naphthyridine and Terpyridine Analogous (N,N,C)-Tridentate Ligands

KOIZUMI, Take-aki; TOMON, Takashi; TANAKA, Koji

[*J. Organomet. Chem.* **690**, 4272–4279 (2005)]

1,8-Naphthyridine (napy) and terpyridine-analogous (N,N,C) tridentate ligands coordinated ruthenium (II) complexes, $[\text{RuL}(\text{napy-}\kappa\text{pa}2, \text{N}, \text{N}')(\text{dmsO})](\text{PF}_6)_2$ (**1**: $L = \text{L1} = \text{N}''\text{-methyl-4'-methylthio-2,2':6',4''-terpyridinium}$, **2**: $L = \text{L2} = \text{N}''\text{-methyl-4'-methylthio-2,2':6',3''-terpyridinium}$) were prepared and their chemical and electrochemical properties were characterized. The structure of complex **1** was determined by x-ray crystallographical study, showing that it has a distorted octahedral coordination style. The cyclic voltammogram of **1** in DMF exhibited two reversible ligand-localized redox couples. On the other hand, the CV of **2** shows two irreversible cathodic peaks, due to the Ru–C bond of **2** containing the carbenic character. The IR spectra of **1** in CO_2 -saturated CH_3CN showed the formation of Ru–(η - CO_2) and Ru–CO complexes under the controlled potential electrolysis of the solution at -1.44 V (*vs.* Fc/Fc^+). The electrochemical reduction of CO_2 catalyzed by **1** at -1.54 V (*vs.* Fc/Fc^+) in DMF (-0.1 M Me_4NBF_4) produced CO with a small amt. of HCO_2H .



VIII-A-8 Dioxo-Molybdenum(VI) and Mono-Oxo-Molybdenum(IV) Complexes Supported by New Aliphatic Dithiolene Ligands: New Models with Weakened Mo:O Bond Characters for the Arsenite Oxidase Active Site

SUGIMOTO, Hideki¹; HARIHARA, Makoto¹; SHIRO, Motoo¹; SUGIMOTO, Kunihisa¹; TANAKA, Koji; MIYAKE, Hiroyuki¹; TSUKUBE, Hiroshi¹

(¹Osaka City Univ.)

[*Inorg. Chem.* **44**, 6386–6392 (2005)]

The *cis*-dioxomolybdenum(VI) complexes, $[\text{MoO}_2(\text{LH})_2]^{2-}$ (**1b**), $[\text{MoO}_2(\text{LS})_2]^{2-}$ (**2b**), and $[\text{MoO}_2(\text{LO})_2]^{2-}$ (**3b**) ($\text{LH} = \text{cyclohexene-1,2-dithiolate}$, $\text{LS} = 2,3\text{-dihydro-2H-thiopyran-4,5-dithiolate}$, and $\text{LO} = 2,3\text{-dihydro-2H-pyran-4,5-dithiolate}$), with new aliphatic dithiolene ligands were prepared and studied by IR and

UV-visible spectroscopic and electrochemical methods. The mono-oxomolybdenum(IV) complexes, $[\text{MoO}(\text{LH})_2]^{2-}$ (**1a**), $[\text{MoO}(\text{LS})_2]^{2-}$ (**2a**), and $[\text{MoO}(\text{LO})_2]^{2-}$ (**3a**), were further characterized by x-ray crystal structural determinations. The IR and resonance Raman spectroscopic studies suggested that these *cis*-dioxo Mo(VI) complexes (**1b-3b**) have weaker Mo=O bonds than the common $\text{Mo}^{\text{VI}}\text{O}_2$ complexes. Complexes **1b-3b** also exhibited strong absorption bands in the visible regions assigned as charge-transfer bands from the dithiolene ligands to the *cis*- MoO_2 cores. Because the O atoms of the *cis*- $\text{Mo}^{\text{VI}}\text{O}_2$ cores are relatively nucleophilic, these complexes are unstable in protic solvents and protonation might occur to produce $\text{Mo}^{\text{VI}}\text{O}(\text{OH})$, as observed with the oxidized state of arsenite oxidase.

VIII-A-9 Electronic Structural Changes between Nickel(II)–Semiquinonato and Nickel(III)–Catecholato States Driven by Chemical and Physical Perturbation

OHTSU, Hideki; TANAKA, Koji

[*Eur. J. Chem. A* **11**, 3420–3426 (2005)]

The selective synthesis of tetracoordinate square-planar low-spin nickel(II)–semiquinonato ($\text{Ni}^{\text{II}}\text{-SQ}$) and nickel(III)–catecholato ($\text{Ni}^{\text{III}}\text{-Cat}$) complexes, $[\text{Ni}(\text{L})(\text{SQ}/\text{CAT})](\text{PF}_6)$ ($L = \text{dibenzyl}(2\text{-pyridylmethyl})\text{amine}$, $\text{SQ} = 3,5\text{-di-tert-butylsemiquinonato}$, $\text{CAT} = 3,5\text{-di-tert-butylcatecholato}$), **1** and **2**, respectively, was achieved by using bidentate ligands with modulated nitrogen-donor ability to the nickel ion. The electronic structures of **1** and **2** were revealed by XPS and EPR measurements. The absorption spectra of **1** and **2** in a noncoordinating solvent, dichloromethane (CH_2Cl_2), are completely different from those in THF, being a coordinating solvent. As expected the gradual addition of DMF, which is also a coordinating solvent like THF, into a solution of **1** or **2** in CH_2Cl_2 leads to color changes from blue (for **1**) or brown (for **2**) to light green, which is the same color observed for solutions of **1** or **2** in THF. Also, the same color changes are induced by varying the temp. Such spectral changes are attributable to the transformation from square-planar low-spin $\text{Ni}^{\text{II}}\text{-SQ}$ and $\text{Ni}^{\text{III}}\text{-Cat}$ complexes to octahedral high-spin $\text{Ni}^{\text{II}}\text{-SQ}$ ones, caused by the coordination of two solvent molecules to the nickel ion.

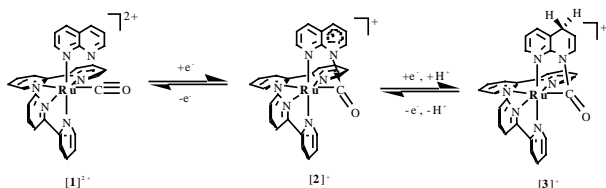
VIII-A-10 Electrochemical Hydrogenation of $[\text{Ru}(\text{bpy})_2(\text{napy-}\kappa\text{M})(\text{CO})]^{2+}$: Inhibition of Reductive Ru–CO Bond Cleavage by a Ruthenacycle

TOMON, Takashi; KOIZUMI, Take-aki; TANAKA, Koji

[*Angew. Chem., Int. Ed.* **44**, 2229–2232 (2005)]

A 5-membered metallacycle (2^+) hydrogenated at the 4-position of the naphthyridine ligand (3^+) is formed by the electrochemical reduction of $[\text{Ru}(\text{bpy})_2(\text{napy-}\kappa\text{N})(\text{CO})]^{2+}$ (1^{2+} ; bpy = 2,2'-bipyridine, napy = 1,8-naphthyridine) at -1.40 V in H_2O . Chemical or electro-

chemical oxidation of 3^+ regenerates 1^+ through 2^+ in almost quantitative yield.



VIII-A-11 Synthesis, Chemical- and Electrochemical Properties of Ruthenium(II) Complexes Bearing 2,6-Bis(2-naphthridyl)pyridine

KOIZUMI, Take-aki; TANAKA, Koji

[*Inorg. Chim. Acta* **358**, 1999–2004 (2005)]

Ruthenium complexes with a terpyridine-analogous ligand, 2,6-bis(2-naphthridyl)-pyridine (**1**, bnp), were synthesized and their chemical and electrochemical properties studied. The structures of $[\text{Ru}(\text{bnp})(\text{tpy})](\text{PF}_6)_2$ (**1**) and $[\text{Ru}(\text{bnp})_2](\text{PF}_6)_2$ (**2**) were determined by x-ray structure analysis. The bnp localized redox potentials of **1** and **2** showed significant positive shift by 260–290 mV relative to the analogous Ru–terpyridine complexes.

VIII-A-12 Synthesis and Electrochemical Properties of Bis(bipyridine)ruthenium(II) Complexes Bearing Pyridinyl- and Pyridinylidene Ligands Induced by Cyclometalation of N-Methylated Bipyridinium Analogs

KOIZUMI, Take-aki; TOMON, Takashi; TANAKA, Koji

[*J. Organomet. Chem.* **690**, 1258–1264 (2005)]

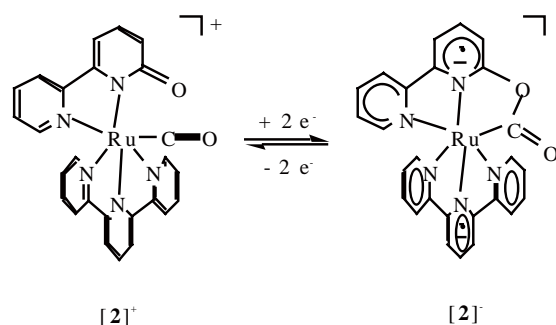
Ruthenium cyclometalated complexes with N-mono-methylated 2,4'- and 2,3'-bipyridine N,C-ligands were prepared and characterized. Reaction of $[(\text{bpy})_2\text{RuCl}_2]$ (bpy = 2,2'-bipyridine) with 1-methyl-4-(2-pyridinyl)pyridinium ($\text{HL}_1 \cdot \text{PF}_6$) and 1-methyl-3-(2-pyridinyl)pyridinium ($\text{HL}_2 \cdot \text{PF}_6$) hexafluorophosphates and AgPF_6 afforded cyclometalated complexes $[(\text{bpy})_2\text{Ru}(\text{L}_1\text{-C}_3, \text{N}^+)](\text{PF}_6)_2$ (**1**) and carbenoid complex **2**, respectively. Structure of **2** was confirmed by low-field shift of the C4-carbon of the cyclometalated bipyridinium ligand and by x-ray structure determination. The ligand-localized redox potentials of **1** and **2** also revealed the substantial difference in the electron donating ability of both ligands.

VIII-A-13 Stabilization and Destabilization of the Ru–CO Bond during the 2,2'-Bipyridin-6-Onato (bpyO)-Localized Redox Reaction of $[\text{Ru}(\text{terpy})(\text{bpyO})(\text{CO})](\text{PF}_6)$

TOMON, Takashi; KOIZUMI, Take-aki; TANAKA, Koji

[*Eur. J. Inorg. Chem.* **2**, 285–293 (2005)]

Two stereoisomers of $[\text{Ru}(\text{terpy})(\text{bpyO})(\text{CO})](\text{PF}_6)$ ($[1]^+$ and $[2]^+$; terpy = 2,2':6',2''-terpyridine, bpyO = 2,2'-bipyridin-6-onato) were prepared. The pyridonato moiety in the bpyO ligand of $[1]^+$ and $[2]^+$ is located *trans* and *cis*, respectively, to CO. Treatment of $[1]^+$ and $[2]^+$ with HPF_6 produced $[1\text{H}]^{2+}$ and $[2\text{H}]^{2+}$, both of which contain bpyOH (bpyOH = 6-hydroxy-2,2'-bipyridine). The difference in the *pK_a* values of $[1\text{H}]^{2+}$ (3.5) and $[2\text{H}]^{2+}$ (3.9) reflects the stronger electronic interaction between CO and the pyridonato moiety in the bpyO ligand in the *trans* position compared with that in the *cis* position. The molecular structures of $[1](\text{PF}_6)$, $[2](\text{PF}_6) \cdot \text{H}_2\text{O}$ and $[2\text{H}](\text{PF}_6)_2 \cdot 2\text{H}_2\text{O}$ were determined by x-ray structure analyses. $[1]^+$ and $[2]^+$ undergo one reversible reduction at $E_{1/2} = -1.65$ V and -1.51 V, respectively, and one irreversible reduction at $E_{p,c} = -2.07$ and $E_{p,c} = -2.13$ V, respectively. Both reductions are assigned to redox reactions localized at the terpy and bpyO ligands. Irreversible reduction of $[1]^0$ results from reductive cleavage of the Ru–CO bond of $[1]^-$. However, a two-electron oxidation of $[2]^-$ almost regenerates $[2]^+$ because of the depression of the reductive Ru–CO bond cleavage of $[2]^-$ due to cyclometalation formed by an attack of O of bpyO to the C of the Ru–CO bond. An unusually large shift of the $\nu(\text{C}\equiv\text{O})$ band on going from $[2]^0$ (1950 cm^{-1}) to $[2]^-$ (1587 cm^{-1}) also supports a reversible cyclometalation driven by the bpyO-localized redox reaction.



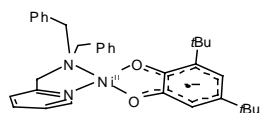
VIII-A-14 Electronic Structural Changes between Nickel(II)–Semiquinonato and Nickel(III)–Catecholato States Driven by Chemical and Physical Perturbation

OHTSU, Hideki; TANAKA, Koji

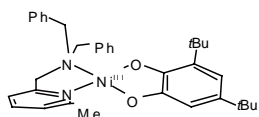
[*Eur. J. Chem. A* **11**, 3420–3426 (2005)]

The selective synthesis of tetracoordinate square-planar low-spin nickel(II)–semiquinonato ($\text{Ni}^{\text{II}}\text{-SQ}$) and nickel(III)–catecholato ($\text{Ni}^{\text{III}}\text{-Cat}$) complexes, $[\text{Ni}(\text{L})(\text{SQ}/\text{CAT})](\text{PF}_6)$ (L = dibenzyl(2-pyridylmethyl)amine, SQ = 3,5-di-*tert*-butylsemiquinonate, CAT = 3,5-di-*tert*-butylcatecholate), **1** and **2**, respectively, was achieved by using bidentate ligands with modulated nitrogen-donor ability to the nickel ion. The electronic structures of **1** and **2** were revealed by XPS and EPR measurements. The absorption spectra of **1** and **2** in a noncoordinating solvent, dichloromethane (CH_2Cl_2), are completely different from those in THF, being a coordinating sol-

vent. As expected the gradual addition of DMF, which is also a coordinating solvent like THF, into a solution of **1** or **2** in CH_2Cl_2 leads to color changes from blue (for **1**) and brown (for **2**) to light green, which is the same color observed for solutions of **1** or **2** in THF. Also, the same color changes are induced by varying the temp. Such spectral changes are attributable to the transformation from square-planar low-spin Ni^{II} -SQ and Ni^{III} -Cat complexes to octahedral high-spin Ni^{II} -SQ ones, caused by the coordination of two solvent molecules to the nickel ion.



$[\text{Ni}^{\text{II}}(\text{Py}(\text{Bz})_2)(\text{tBu}_2\text{SQ})](\text{PF}_6)$



$[\text{Ni}^{\text{III}}(\text{MePy}(\text{Bz})_2)(\text{tBu}_2\text{Cat})](\text{PF}_6)$

VIII-B Coordination Chemistry of Sterically Hindered Ligands and Multidentate Ligands, and Activation of Small Molecules

This project is focused on the design and synthesis of new ligands that are capable of supporting novel structural features and reactivity. Currently, we are investigating multidentate ligands based on aryloxy and thiolate. In addition, we set out to study metal complexes with sterically hindered aryloxy and arylthiolate ligands. Our recent efforts have been directed toward activation of small molecules.

VIII-B-1 Complexes of Tantalum with Triaryloxides: Ligand and Solvent Effects on Formation of Hydride Derivatives

KAWAGUCHI, Hiroyuki; MATSUO, Tsukasa

[*J. Organomet. Chem.* **690**, 5333–5345 (2005)]

A family of tantalum compounds supported by the triaryloxyde $[R-L]^{3-}$ ligands are reported $[H_3(R-L) = 2,6\text{-bis}(4\text{-methyl-6-}R\text{-salicyl})\text{-4-}tert\text{-butylphenol}$, where $R = \text{Me}$ or Bu^t]. The reaction of $H_3[Me-L]$ with $TaCl_5$ in toluene gave $[(Me-L)TaCl_2]_2$ (**1**). The $[Bu^t-L]$ analogue $[(Bu^t-L)TaCl_2]_2$ (**2**) was synthesized *via* treatment of $TaCl_5$ with $Li_3[Bu^t-L]$. A THF solution of $LiBHET_3$ was added to **1** in toluene to provide $[(Me-L)TaCl(THF)]_2$ (**3**), while treatment of **2** with 2 equiv of $LiBHET_3$ or potassium in toluene followed by recrystallization from DME resulted in formation of $[M(DME)_3][\{(Bu^t-L)TaCl\}_2(\mu-Cl)]$ [$M = \text{Li}$ (**4a**), K (**4b**)]. When the amount of $MBHET_3$ ($M = \text{Li, Na, K}$) was increased to 5 equiv, the analogous reactions in toluene afforded $[\{(bit-Bu^t-L)Ta\}_2(\mu-H)_3M]$ [$M = \text{Li(THF)}_2$ (**5a**), Na(DME)_2 (**5b**), K(DME)_2 (**5c**)]. During the course of the reaction, the methylene CH activation of the ligand took place. Dissolution of **5a** in DME produced $[\{(bit-Bu^t-L)Ta\}_2(\mu-H)_3Li(DME)_2]$ (**6**), indicating that the coordinated THF molecules are labile. When the **2**/ $LiBHET_3$ reaction was carried out in THF, the ring opening of THF occurred to yield $[(Bu^t-L)Ta(OBu^t)_2]_2$ (**7**) along with a trace amount of $[Li(THF)_4][\{(Bu^t-L)TaCl\}_2(\mu-OBu^t)]$ (**8**). Treatment of **2** with potassium hydride in DME yielded $[\{(Bu^t-L)TaCl_2K(DME)_2\}_2(\mu-OCH_2CH_2O)]$ (**9**), in which the ethane-1,2-diolate ligand arose from partial C–O bond rupture of DME.

VIII-B-2 A Synthetic Cycle for H_2/CO Activation and Allene Synthesis Using Recyclable Zirconium Complexes

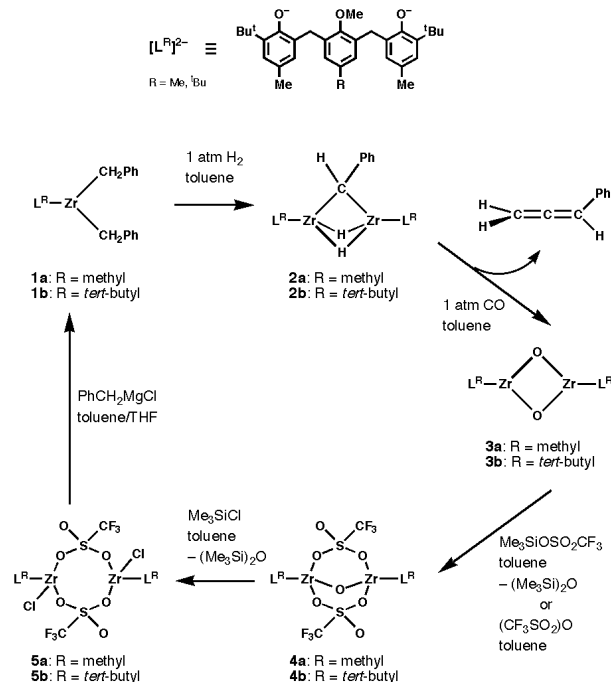
MATSUO, Tsukasa; KAWAGUCHI, Hiroyuki

[*J. Am. Chem. Soc.* **127**, 17198–17199 (2005)]

Fischer–Tropsch (F–T) synthesis is an important chemical reaction to convert H_2 and CO to hydrocarbons along with water, thereby giving access to organic chemistry on the basis of simple inorganic molecules. The impressive F–T chemical transformation has elicited extensive synthetic efforts to reach chemical understanding of the heterogeneous F–T reaction and to produce soluble metal complexes that can react with H_2 and CO to form hydrocarbons with high product selec-

tivity. Although many soluble metal compounds and reactions relevant to surface species in the heterogeneous F–T process are known, well-characterized synthetic systems capable of converting H_2/CO into hydrocarbons have been limited. To explore the transformation of H_2 and CO with metal complexes, we have sought to use zirconium complexes supported by 2,6-bis(3-*tert*-butyl-5-methyl-2-oxybenzyl)-4-*R*-anisole ligands ($[L^R]^{2-}$).

This study demonstrated a synthetic cycle having relevance to F–T chemistry, wherein zirconium alkyl complexes of the $[L^R]$ ligands serves to transform H_2 and CO into corresponding allenes *via* alkylidene intermediates. The synthetic cycle is outlined in Scheme 1. This transformation involves the activation of H_2 , and C–C, C–H bond formation, C–O bond cleavage, and deoxygenative recycling of the oxo-bridging zirconium complexes. All of the preceding reactions are spectroscopically quantitative under mild conditions. Thus there is much potential for yield optimization, including the combination of consecutive steps.



Scheme 1.

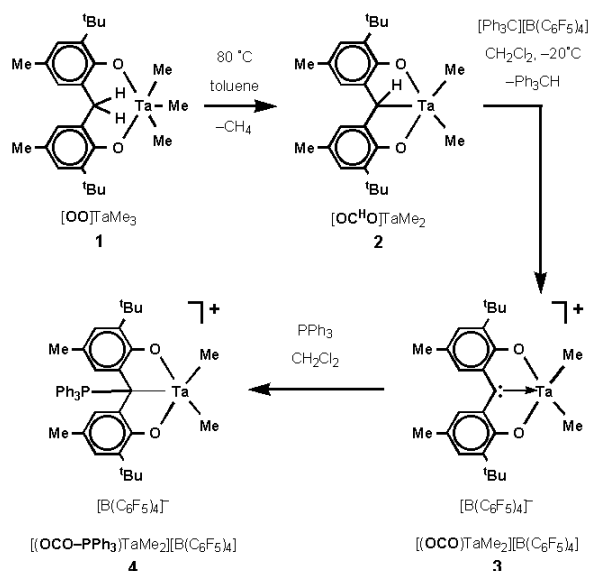
VIII-B-3 A Tantalum(V) Carbene Complex: Formation of a Carbene-Bis(phenoxide) Ligand by Sequential Proton and Hydride Abstraction

WATANABE, Takahito; MATSUO, Tsukasa;
KAWAGUCHI, Hiroyuki

[*Inorg. Chem.* **45**, 6580–6582 (2006)]

Bis(phenoxides), in which the two phenoxide rings are linked to a donor atom (X) such as sulfur and phosphorous in the *ortho* positions, have been useful dianionic ancillary ligands in coordination chemistry and homogeneous catalysis. In this type of [OXO] ligands that combine the hard phenoxide donors with the soft X donor into a chelating array, electronic and stereochemical parameters can be manipulated by modifications of X donor groups so as to accommodate many transition metals in a variety of oxidation states and induce interesting transformations. With this in mind, we have begun to study the chemistry of carbene–phenoxide hybrid ligands, where a carbene functionality is introduced at the X donor site. The strong two-electron donor ability of the carbene group was appealing to us. In addition, this ligand system would provide the opportunity to study the effect of the σ -donor carbene functionality on the properties of electron deficient metal complexes.

The present work has demonstrated the synthesis and structure of the cationic tantalum(V) dimethyl complex with the [OCO] ligand. The dianionic tridentate [OCO] ligand is formed by the sequential proton and hydride abstraction from the backbone of the [OO] ligand (Scheme 1). The carbene moiety of **3** is stabilized *via* π -bonding to the oxyphenyl groups. This kind of carbene in this circumstance could be viewed as a neutral σ -donor carbene bound to Ta(V). This is a rare example of early transition metal complexes with σ -donor carbene ligands except N-heterocyclic carbenes. The electrophilic nature of carbene **3** has been shown in the reaction with PPh₃. Extension of this work to include other transition metal complexes and reactivity studies of **3** are in progress.



Scheme 1.

VIII-C Physicochemical Properties of Hemoprotein Reconstituted with Artificially Created Hemins

Hemoprotein is one of the most versatile metalloproteins having a prosthetic group heme, *e.g.* protoheme IX, which shows various physicochemical properties. Most of hemes in hemoproteins are usually bound in the heme pocket via multiple non-covalent interactions with the several amino acid residues. Recently, we have focused on the replacement of the native hemin with an artificially created metal complex. This method is at least two advantages; First, the reconstitution with an artificial hemin gives an insight into the elucidation of hemoprotein function. Second, we have a chance to dramatically modify the function of hemoproteins. In our project, we try to prepare various artificial prosthetic groups and inserted them into apohemoproteins to obtain reconstituted proteins. For example, one of our aims is to elucidate the role of each heme-propionate side chains in a series of hemoproteins by replacing the native hemin with monoproponated hemin. Replacing the native hemin with hemin derivatives such as iron porphycene or iron corrole is also very attractive to modify the function of hemoproteins. From these projects, we wish to understand the physicochemical properties of hemoproteins based on the coordination chemistry in the protein matrix.

VIII-C-1 Preparation and O₂ Binding Study of Myoglobin Having a Cobalt Porphycene

MATSUO, Takashi¹; TSURUTA, Takashi²; MAEHARA, Keiko²; SATO, Hideaki²; HISAEDA, Yoshio²; HAYASHI, Takashi³
(¹Osaka Univ.; ²Kyushu Univ.; ³IMS and Osaka Univ.)

[*Inorg. Chem.* **44**, 9391–9396 (2005)]

Sperm whale myoglobin, an oxygen-storage hemoprotein, was reconstituted with 2,7-diethyl-3,6,12,17-tetramethyl-13,16-bis(carboxyethyl)porphycenatocobalt (II) in order to investigate the reactivities of a cobalt porphycene in a protein matrix (Figure 1). Similar to the previously reported finding for the myoglobin with the iron porphycene, the reconstituted myoglobin with the cobalt porphycene was also found to have a higher O₂ affinity by two orders of magnitude when compared to the myoglobin possessing cobalt protoporphyrin IX. The EPR spectra of the deoxy and oxy myoglobins having the cobalt porphycene at 77 K also have similar features to the myoglobin with cobalt protoporphyrin IX. These spectra suggest that the porphycene cobalt in the deoxy form is coordinated by one nitrogenous ligand postulated to be the imidazole ring of His93, and that the bond configuration of Co^{II}-O₂ is regarded as the Co^{II}-O₂⁻ species.

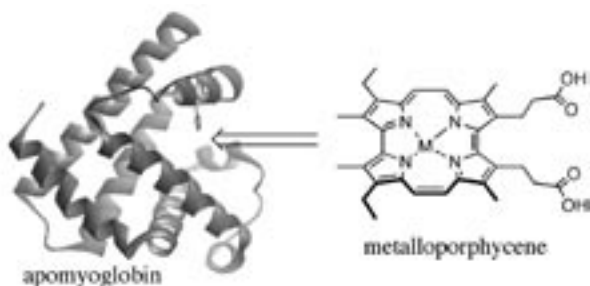


Figure 1. Incorporation of metalloporphycene into apomyoglobin.

VIII-C-2 Iron Porphyrin–Cyclodextrin Supramolecular Complex as a Functional Model of Myoglobin in Aqueous Solution

KANO, Koji¹; KITAGISHI, Hiroaki¹; DAGALLIER, Camelle¹; KODERA, Masahito¹; MATSUO, Takashi²; HAYASHI, Takashi³; HISAEDA, Yoshio⁴; HIROTA, Shun⁵

(¹Doshisha Univ.; ²Osaka Univ.; ³IMS and Osaka Univ.; ⁴Kyushu Univ.; ⁵Kyoto Pharm. Univ.)

[*Inorg. Chem.* **45**, 4448–4460 (2006)]

The 1:1 inclusion complex of 5,10,15,20-tetrakis(4-sulfonatophenyl)porphyrinatoiron(II) (Fe^{II}TPPS) and an *O*-methylated β-cyclodextrin dimer having a pyridine linker (**1**) binds dioxygen reversibly in aqueous solution. The O₂ adduct was very stable (*t*_{1/2} = 30.1 h) at pH 7.0 and 25 °C. ESI-MS and NMR spectroscopic measurements and molecular mechanics calculations indicated the inclusion of the sulfonatophenyl groups at the 5- and 15-positions of Fe^{III}TPPS or Fe^{II}TPPS into two cyclodextrin moieties of **1** to form a supramolecular 1:1 complex (hemoCD1 for the Fe^{II}TPPS complex), whose iron center is completely covered by two cyclodextrin moieties. Equilibrium measurements and laser flash photolysis provided the affinities (*P*^{O₂}_{1/2} and *P*^{CO}_{1/2}) and rate constants for O₂ and CO binding of hemoCD1 (*k*^{O₂}_{on}, *k*^{O₂}_{off}, *k*^{CO}_{on}, and *k*^{CO}_{off}). The CO affinity relative to the O₂ affinity of hemoCD1 was abnormally high. Although resonance Raman spectra suggested weak back-bonding of dπ(Fe) → π*(CO) and hence a weak CO–Fe bond, the CO adduct of hemoCD1 was very stable. The hydrophobic CO molecule dissociated from CO-hemoCD1 hardly breaks free from a shallow cleft in hemoCD1 surrounded by an aqueous bulk phase leading to fast rebinding of CO to hemoCD1. Isothermal titration calorimetry furnished the association constant (*K*^{O₂}), Δ*H*^o, and Δ*S*^o for O₂ association to be (2.71 ± 0.51) × 10⁴ M⁻¹, -65.2 ± 4.4 kJ mol⁻¹, and -133.9 ± 16.1 J mol⁻¹ K⁻¹, respectively. The autoxidation of oxy-hemoCD1 was accelerated by H⁺ and OH⁻. The inorganic anions also accelerated the autoxidation of oxy-hemoCD1. The O₂-Fe^{II} bond is equivalent to the O₂⁻-Fe^{III} bond, which is attacked by the inorganic anions or the

water molecule to produce met-hemoCD1 and a superoxide anion.

VIII-C-3 Crystal Structure and Peroxidase Activity of Myoglobin Reconstituted with Iron Porphycene

HAYASHI, Takashi¹; MURATA, Dai²; MAKINO, Masatomo³; SUGIMOTO, Hiroshi⁴; MATSUO, Takashi⁵; SATO, Hideaki²; SHIRO, Yoshitsugu⁴; HISAEDA, Yoshio²

(¹IMS and Osaka Univ.; ²Kyushu Univ.; ³Himeji Inst. Tech.; ⁴RIKEN/SPring-8; ⁵Osaka Univ.)

[Inorg. Chem. to be submitted]

The incorporation of an artificially created metal complex into an apomyoglobin is one of the attractive studies in a series of hemoprotein modifications. Single crystals of myoglobin reconstituted with 13,16-dicarboxyethyl-2,7-diethyl-3,6,12,17-tetramethylporphycenat iron(III) were obtained in the imidazole buffer and the 3D structure with a 2.25-Å resolution indicates that the artificially created prosthetic group as a heme structural isomer is located in the normal position of the heme pocket (Figure 1). Furthermore, the reconstituted myoglobin catalyzed the H₂O₂-dependent oxidations of substrates such as guaiacol, thioanisole, and styrene. At pH 7.0 and 20 °C, the initial rate of the guaiacol oxidation is 11-fold faster than that observed for the native myoglobin. Moreover, the stopped-flow studies of the reconstituted protein with H₂O₂ demonstrated that two reaction intermediates, compounds II and III, were detected in the absence of a substrate. It is a rare example that compound III is formed via compound II in myoglobin chemistry. The enhancement of the peroxidase activity and the formation of the stable compound III in myoglobin with iron porphycene could be due to the strong coordination of the Fe-His93 bond.

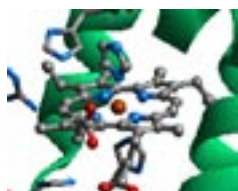


Figure 1. 3D crystal structure of iron(III)-porphycene in myoglobin matrix.

VIII-C-4 Construction of Glycosylated Myoglobin by Reconstitutive Method

MATSUO, Takashi¹; NAGAI, Hirokazu²; HISAEDA, Yoshio²; HAYASHI, Takashi³

(¹Osaka Univ.; ²Kyushu Univ.; ³IMS and Osaka Univ.)

[Chem. Commun. **29**, 3131–3133 (2006)]

An artificially created prosthetic group **1** having β-galactosyl moieties (Figure 1) was prepared and inserted into sperm whale apomyoglobin to successfully afford a glycosylated myoglobin. The glycomyoglobin was characterized by ESI-MS and UV-vis spectroscopy and

stable in a buffer solution at 4 °C over one week. The immunoprecipitation experiment was carried out to evaluate the function of the galactose units on the protein surface. The mixture of the glycomyoglobin and commercially available biotin-labelled peanut lectin was treated with streptavidin-modified sepharose to determine the affinity. From this study, the galactose units on the myoglobin surface well work as the interface for forming the myoglobin-lectin complex without any non-specific interaction.

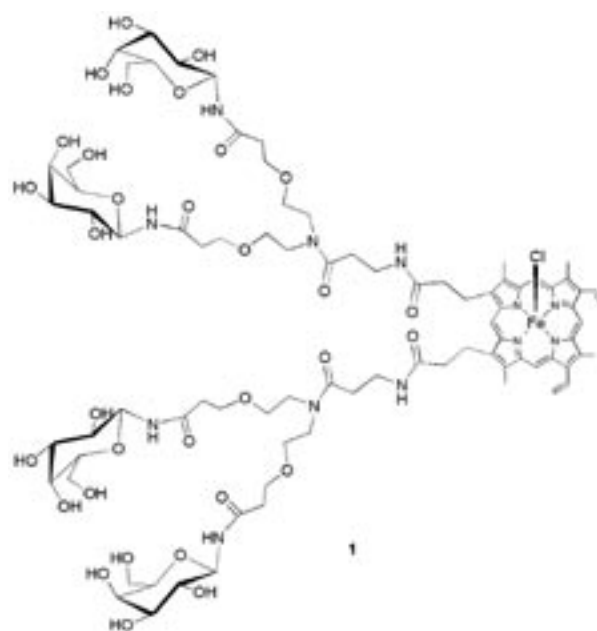


Figure 1. Galactohemin **1** as an artificial prosthetic group for myoglobin.

VIII-C-5 Structure and Ligand Binding Properties of Sperm Whale Myoglobins Reconstituted with Two Monopropionated Hemin: Role of Each Heme-Propionate Side Chain in Myoglobin

HAYASHI, Takashi¹; HARADA, Katsuyoshi²; MAKINO, Masatomo³; HIROTA, Shun⁴; SUGIMOTO, Hiroshi²; MATSUO, Takashi²; SHIRO, Yoshitsugu⁵; FUNASAKI, Noriaki⁴; HISAEDA, Yoshio⁶

(¹IMS and Osaka Univ.; ²Osaka Univ.; ³Himeji Inst. Tech.; ⁴Kyoto Pharm. Univ.; ⁵RIKEN/SPring-8; ⁶Kyushu Univ.)

[J. Am. Chem. Soc. to be submitted]

Many hemoproteins have protoheme IX as a prosthetic group. The heme bears two unique propionate side chains at 6- and 7-positions of β-pyrrolic carbons. According to a series of 3D structures of hemoproteins, the propionate side chains interact with polar amino acid residues in the protein matrix, so it has been known that the side chains play a role on the fixation of the prosthetic group in the heme pocket. However, we have recently thought that the role of the two propionate side chains are not only the fixation of heme but also the direct contribution to the regulation of the hemoprotein

function. Based on this viewpoint, we have prepared two monopropionated hemes; 6-methyl-7-carboxyethyl-heme (6M7PHE) and 6-carboxyethyl-7-methyl-heme (6P7MHE) (Figure 1). Furthermore, the hemins were incorporated into apohemoprotein by conventional method to understand each role of the defective propionate side chain.

In the case of sperm whale myoglobin, 6- and 7-propionate side chains interact with Arg45 and Ser92 via hydrogen bonding, respectively. The reconstituted myoglobins with the two monopropionated hemins, rMb(6M7PHE) and rMb(6P7MHE), were characterized by UV-vis, ESI-MS, ^1H NMR spectroscopic methods. The dissociation of O_2 from oxymyoglobin with 6M7PHE was accelerated about three times as that of the oxymyoglobin with the native heme. Furthermore, the autoxidation rate of oxymyoglobin with 6M7PHE was approximately six times faster than that of oxymyoglobin with native heme. These results indicate that the 6-propionate side chain plays an important role on the stabilization of oxymyoglobin. In contrast, the acceleration of the CO binding rate was observed for myoglobin with 6P7MHE, suggesting that the 7-propionate side chain regulates the His93-heme iron coordination in the proximal site.

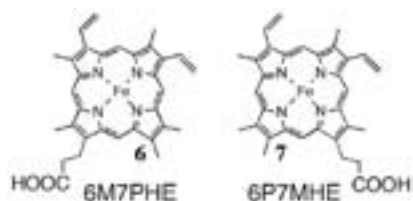


Figure 1. Structures of Two Monopropionated Heme.

VIII-C-6 Ligand Binding Properties of Two Kinds of Reconstituted Myoglobins with Iron Porphycene Having Propionates: Effect of β -Pyrrolic Position of Two Propionate Side Chains in Porphycene Framework

MATSUO, Takashi¹; IKEGAMI, Takahiro²; SATO, Hideaki²; HISAEDA, Yoshio²; HAYASHI, Takashi³
(¹Osaka Univ.; ²Kyushu Univ.; ³IMS and Osaka Univ.)

[*J. Inorg. Biochem.* **100**, 1265–1271 (2006)]

An iron porphycene containing two propionate side chains at the 12th and 17th β -pyrrolic positions of the porphycene ring was synthesized and incorporated into sperm whale apomyoglobin in order to investigate the O_2 and CO binding properties of the reconstituted ferrous myoglobin. The protein showed a slower O_2 dissociation rate by 1/20, compared to the native myoglobin, whereas the CO dissociation rates were found to be almost the same. This tendency is similar to the result of a previous study on the reconstituted myoglobin with a porphycene having the propionates at the 13th and 16th β -pyrrolic positions. However, the present myoglobin showed a faster O_2 dissociation than the previously studied myoglobin. This finding suggests that the position of the two propionates as well as the symmetry of the porphycene framework is an important factor for obtaining a stable oxygenated iron porphycene myoglobin.

VIII-D Syntheses, Structures, and Reactivities of Multinuclear Transition Metal Complexes with O- and N-Donor Ligands

Organotransition metal complexes with O- and N-donor ligands have recently been attracting considerable attention, because they often show structures, reactivities, and physicochemical properties significantly different from those of the complexes with P- and S-donor ligands. In this project it has been revealed that cyanamide (NCN^{2-}) anion effectively bridge organometallic fragments to form multinuclear complexes with characteristic structures. It has recently been found that tetranuclear C_3 -elongated cubane-like complexes of cobalt and rhodium can be synthesized from the reaction of $[\text{Cp}^*\text{MX}_2]_2$ ($M = \text{Co}, \text{Rh}; X = \text{Cl}, \text{I}$) with Na_2NCN . We have also investigated into the reactivities of coordinated NO in early and late heterobimetallic (ELHB) complexes and shown that the terminally bound NO ligand at a Rh-W bimetallic core undergoes unprecedented O-methylation.

VIII-D-1 Syntheses and Properties of NCN-Bridged Tri- and Tetranuclear Complexes of Cobalt and Rhodium

TAKAHATA, Keiichi¹; IWADATE, Noriyuki¹; KAJITANI, Hidenobu²; TANABE, Yoshiaki¹; ISHII, Youichi³

(¹Chuo Univ.; ²Univ. Tokyo; ³IMS and Chuo Univ.)

[*J. Organomet. Chem.* in press]

The reaction of $[\text{Cp}^*\text{CoI}_2]_2$ with 2 equiv of NaNCNH affords the 16-membered macrocyclic NCNH-bridged tetracobalt(III) complex $[\text{Cp}^*\text{CoI}(\mu_2\text{-NCNH-}N,N')_4]$ (**1a**), while that with 2 equiv of Na_2NCN yields the C_3 -elongated cubane-like NCN-bridged tetracobalt(III) complex $[\text{Cp}^*\text{Co}(\mu_3\text{-NCN-}N,N,N')_3(\text{CoCp}^*)_3(\mu_3\text{-NCN-}N,N,N)]$ (**2a**). Treatment of $[\text{Cp}^*\text{RhCl}_2]_2$ with 2 equiv of NaNCNH gives the C_3 -elongated cubane-like tetrarhodium(III) complex $[\text{Cp}^*\text{Rh}(\mu_3\text{-NCN-}N,N,N')_3(\text{RhCp}^*)_3(\mu_3\text{-NCN-}N,N,N)]$ (**2b**) via the macrocyclic complex $[\text{Cp}^*\text{RhCl}(\mu_2\text{-NCNH-}N,N')_4]$ (**1b**) (Figure 1). On the other hand, the reaction of $[\text{Cp}^*\text{CoCl}]_2$ with Na_2NCN affords the anionic bis(NCN)-capped tricobalt(II) complex $\text{Na}[(\text{Cp}^*\text{Co})_3(\mu_3\text{-NCN-}N,N,N)_2]$. The molecular structures of complexes **1a**· CH_2Cl_2 and **2b**· $2\text{C}_6\text{H}_6$ have been confirmed by X-ray analyses. The electrochemical properties of these types of NCN-bridged group 9 metal complexes have also been examined.

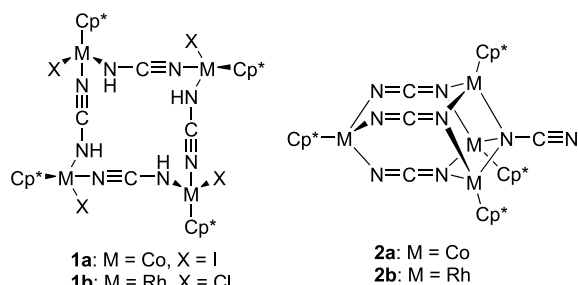


Figure 1. Structures of NCN-bridged Co and Rh tetranuclear complexes.

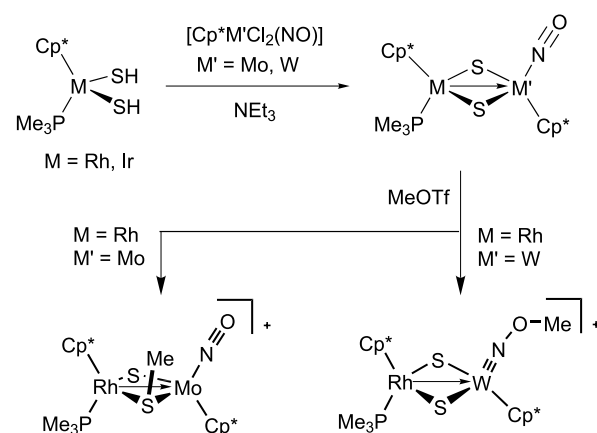
VIII-D-2 Electrophilic O-Methylation of a Terminal Nitrosyl Ligand Attained by Early-Late Heterobimetallic Effect

ARASHIBA, Kazuya¹; MATSUKAWA, Shoji²;

KUWATA, Shigeki³; TANABE, Yoshiaki¹; IWASAKI, Masakazu⁴; ISHII, Youichi⁵
(¹Chuo Univ.; ²Univ. Tokyo; ³Tokyo Tech; ⁴Saitama Inst. Tech.; ⁵IMS and Chuo Univ.)

[*Organometallics* **25**, 560–562 (2006)]

The reaction of the group 9 bis(hydrosulfido) complexes $[\text{Cp}^*\text{M}(\text{SH})_2(\text{PMe}_3)]$ ($M = \text{Rh}, \text{Ir}$) with the group 6 nitrosyl complexes $[\text{Cp}^*\text{M}'\text{Cl}_2(\text{NO})]$ ($M' = \text{Mo}, \text{W}$) in the presence of NEt_3 affords a series of the bis(sulfido)-bridged early-late heterobimetallic (ELHB) complexes $[\text{Cp}^*\text{M}(\text{PMe}_3)(\mu\text{-S})_2\text{M}'(\text{NO})\text{Cp}^*]$ ($M = \text{Rh}, \text{Ir}; M' = \text{Mo}, \text{W}$). These complexes show one strong IR absorption assignable to the NO stretching around 1500 cm^{-1} . Interestingly, this $\nu(\text{NO})$ value is 100 cm^{-1} smaller than that of the mononuclear thiolato complex $[\text{Cp}^*\text{W}(\text{NO})(\text{SPh})_2]$. This unusual IR absorption is attributable to the influx of electrons to the group 6 metal center through the $M(\text{III}) \rightarrow M'(\text{II})$ dative bond. The electron rich nature of the dinuclear complexes is reflected in its reactivities. Upon treatment of the Rh–W complex with MeOTf, the oxygen atom of the terminal nitrosyl ligand is readily methylated to form the methoxyimido complex $[\text{Cp}^*\text{Rh}(\text{PMe}_3)(\mu\text{-S})_2\text{W}(\text{NOMe})\text{Cp}^*]^+$, while methylation of the Rh–Mo complex results in S-methylation, giving the methanethiolato complex $[\text{Cp}^*\text{Rh}(\text{PMe}_3)(\mu\text{-SMe})(\mu\text{-S})\text{Mo}(\text{NO})\text{Cp}^*]^+$ (Scheme 1).



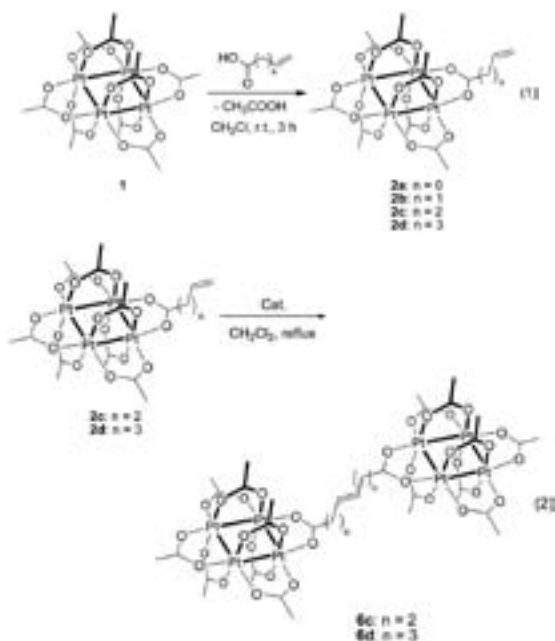
Scheme 1.

VIII-E Transition Metal Cluster Chemistry

VIII-E-1 Metathesis Approach to Linkage of Two Tetraplatinum Cluster Units: Synthesis, Characterization, and Dimerization of $[\text{Pt}_4(\mu\text{-OCOCH}_3)_7(\mu\text{-OCO}(\text{CH}_2)_n\text{CH}=\text{CH}_2)]$ ($n = 0\text{--}3$)

MASHIMA, Kazushi¹; OHASHI, Masato²; YAGYU, Akihiro²; XU, Qinghong²
(¹IMS and Osaka Univ.; ²Osaka Univ.)

Reaction of $[\text{Pt}_4(\mu\text{-OCOCH}_3)_8]$ (**1**) with 1 equiv of acrylic acid led to the selective mono-substitution of one of the four *in*-plane acetates in **1**, affording $[\text{Pt}_4(\mu\text{-OCOCH}_3)_7(\mu\text{-OCOCH}=\text{CH}_2)]$ (**2a**) (eq. 1), whereas treatment with excess amounts of acrylic acid resulted in a full-substitution of four *in*-plane acetates, yielding $[\text{Pt}_4(\mu\text{-OCOCH}_3)_4(\mu\text{-OCOCH}=\text{CH}_2)_4]$ (**3**) (Figure 1). Similarly, mono-substituted heptaacetate complexes $[\text{Pt}_4(\mu\text{-OCOCH}_3)_7\{\mu\text{-OCO}(\text{CH}_2)_n\text{CH}=\text{CH}_2\}]$ (**2b-d**; $n = 1\text{--}3$) were prepared. These complexes **2a-d** seem to be a suitable precursor for linkage of the Pt_4 units. Catalytic intermolecular coupling reactions of **2c** and **2d** assisted by Grubbs' catalysts gave the desired dimers $\{[\text{Pt}_4(\mu\text{-OCOCH}_3)_7]_2\{\mu\text{-OCO}(\text{CH}_2)_n\text{CH}=\text{CH}(\text{CH}_2)_n(\mu\text{-OCO})\}\}$ (**6c**; $n = 2$; **6d**; $n = 3$) (eq. 2), while metathesis reactions using complexes **2a** and **2b** did not proceed under the same catalytic condition.

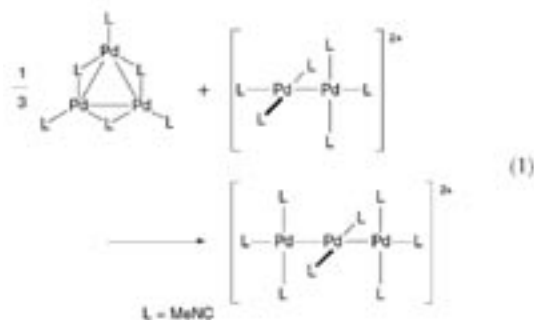


VIII-E-2 Hexapalladium Cluster: Unique Reaction of Cyclic $\text{Pd}_3(\text{CNC}_6\text{H}_3\text{Me}_2\text{-}2,6)_6$ and Linear $[\text{Pd}_3(\text{CNC}_6\text{H}_3\text{Me}_2\text{-}2,6)_8]^{2+}$

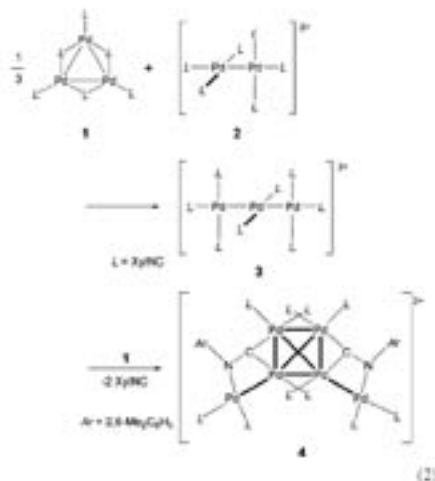
MASHIMA, Kazushi¹; YI, Jianjun²; YAMAGATA, Tsuneaki²; OHASHI, Masato²
(¹IMS and Osaka Univ.; ²Osaka Univ.)

Polynuclear clusters with metal–metal bonds have attracted research interest due to their fundamental aspect as surface model of heterogeneous catalyst, as

well as potential applications as electrochemical, photoelectric and magnetic materials. Among them, di- and trinuclear complexes with metal–metal bonds have been well documented, and have been used as starting materials to construct new clusters with high nuclearity. Many di- or trinuclear palladium and platinum complexes with isocyanide ligands have been formed by electrochemical preparation as well as by redox reactions between metal ions in different formal oxidation states. It has been reported that dicationic dinuclear palladium isocyanide complex $[\text{Pd}_2\text{L}_6]^{2+}$ ($\text{L} = \text{isocyanide}$) with d^9 configuration reacted with Pd^0L_x sources with d^{10} configuration such as cyclic trinuclear palladium isocyanide complex $(\text{Pd}^0\text{L}_2)_3$ resulted in the selective formation of dicationic linear trinuclear palladium complex $[\text{Pd}_3\text{L}_8]^{2+}$, where $\text{Pd}(0)$ formally inserted into $\text{Pd}\text{--Pd}$ bond of $[\text{Pd}_2\text{L}_6]^{2+}$ (eq. 1). However, additional reaction of $[\text{Pd}_3\text{L}_8]^{2+}$ with “ Pd^0L_2 ” species has not been reported.



Recently we used 2,6-dimethylphenyl-isocyanide as the homoleptic ligand to develop this reaction by preparing $[\text{Pd}_3(\text{CNC}_6\text{H}_3\text{Me}_2\text{-}2,6)_8][\text{PF}_6]_2$ (**3**) from $[\text{Pd}(\text{CNC}_6\text{H}_3\text{Me}_2\text{-}2,6)_2]_3$ (**1**) and $[\text{Pd}_2(\text{CNC}_6\text{H}_3\text{Me}_2\text{-}2,6)_6][\text{PF}_6]_2$ (**2**). Herein we reported that the additional reaction of **3** and **1** selectively afforded a dicationic hexanuclear palladium complex $[\text{Pd}_6(\text{CNC}_6\text{H}_3\text{Me}_2\text{-}2,6)_{10}][\text{PF}_6]_2$ (**4**) (eq. 2, $\text{L} = 2,6\text{-Me}_2\text{C}_6\text{H}_3\text{NC}$). The crystal structure of the complex **4** was determined by X-ray crystallography and spectroscopic analysis.



VIII-F Synthesis of Transition Metal Catalysts for Organic Transformations

VIII-F-1 Oxidative Addition of RCO₂H and HX to Chiral Diphosphine Complexes of Iridium(I): Convenient Synthesis of Mononuclear Halo-Carboxylate Iridium(III) Complexes and Cationic Dinuclear Triply Halogen-bridged Iridium(III) Complexes and Their Catalytic Performance in Asymmetric Hydrogenation of Cyclic Imines and 2-Phenylquinoline

MASHIMA, Kazushi¹; YAMAGATA, Tsuneaki²; TADAOKA, Hiroshi²; NAGATA, Mitsuhiro²; HIRAO, Tsukasa²; RATOVELOMANANA-VIDAL, Virginie³; GENET, Jean Pierre³
(¹IMS and Osaka Univ.; ²Osaka Univ.; ³Ecole Natl. Supérieure Chim. Paris)

Mononuclear iridium(III) complexes of the general formula IrX(H)(O₂CR)[(S)-binap] (**2**: R = CH₃; **3**: R = Ph; **4**: R = C₆H₄CH₃-*p*; **a**: X = Cl; **b**: X = Br; **c**: X = I) were prepared by one-pot reaction of [Ir(μ-X)(cod)]₂ with two equiv of (S)-BINAP [= 2,2'-bis(diphenylphosphino)-1,1'-binaphthyl] and an excess of the corresponding carboxylic acid in toluene. The structure of (S)-**2-4** bearing an (S)-BINAP was confirmed to be OC-6-23-A (Λ-conformation) by X-ray analysis of (S)-**4a-c**. In this reaction, an iridium(I) complex {Ir(μ-Cl)[(S)-binap]}₂ [(S)-**5a**] and pentacoordinated iridium(I) com-

plexes IrX(cod)[(S)-binap] [(S)-**7b**: X = Br; (S)-**7c**: X = I] were generated prior to the oxidative addition of carboxylic acid. Cationic dinuclear iridium(III) complexes of the general formula [{Ir(H)[(S)-binap]}₂(μ-X)₃]X [(S)-**8**: **a**: X = Cl; **b**: X = Br; **c**: X = I] were prepared and their cationic bifacial octahedral dinuclear structure was characterized by spectral data and combustion analysis. The anionic portion of these complexes could be replaced by NaPF₆, leading to the corresponding PF₆ salts, [{Ir(H)[(S)-binap]}₂(μ-X)₃]PF₆ [(S)-**8**: **d**: X = Cl; **e**: X = Br; **f**: X = I]. Iodo-acetate complexes of *p*-TolBINAP (= 2,2'-bis(di-4-tolylphosphino)-1,1'-binaphthyl) [(S)-**9c**] and SYNPHOS [= 2,2',3,3'-tetrahydro(5,5'-bi-1,4-benzodioxin)-6,6'-diyl]bis(diphenylphosphine)] [(S)-**10c**] were also prepared according to the method used for the BINAP complex (S)-**2c** and were characterized spectroscopically. Cationic dinuclear complexes of *p*-TolBINAP [(S)-**11c**] and SYNPHOS [(S)-**12c**] were also generated. Using these complexes, the effect of halide variation was studied by asymmetric hydrogenation of 2-phenylpyrrolidine and 2-phenyl-4,5,6,7-tetrahydro-3H-azepine along with 2-phenylquinoline, and the results indicated that iodide complexes were better catalyst precursors for catalytic activity than the corresponding chloride and bromide complexes, but were not superior in enantioselectivity.

VIII-G Early Transition Metal Complexes

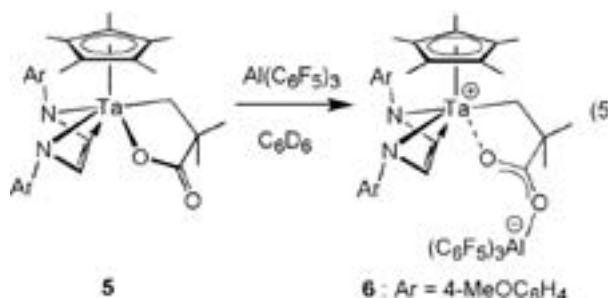
VIII-G-1 Synthesis, Structure, and Reactivity of Tantalum and Tungsten Homoenoate Complexes

MASHIMA, Kazushi¹; TSURUGI, Hayato²; OHNO, Takashi²; YAMAGATA, Tsuneaki²
(¹IMS and Osaka Univ.; ²Osaka Univ.)

Preparation and characterization of homoenoate complexes of tantalum, Cp*Cl₃Ta(CH₂CR¹₂C(=O)OR²) (**1a**: R¹ = H, R² = Et; **1b**: R¹ = R² = Me; **1c**: R¹ = Me, R² = C₆H₄CH₃-4), and tungsten, (Xyl-N=)Cl₃W(CH₂CH₂C(=O)OEt) (**7**), using zinc homoenoate reagents are described. Intramolecular coordination of the carbonyl moiety to the metal center in these complexes was confirmed by their NMR and IR spectroscopy together with X-ray analyses of **1a** and **1b**. The insertion reaction of isocyanide into the metal carbon bond of **1a** and **7**, respectively, resulted in the formation of a diazametallacycle,



Xyl] (**3a**), which possesses a metallacyclic structure with an exocyclic ketene-imine moiety, and an η²-iminoacyl tungsten complex, (Xyl-N=)W{C(=N-Xyl)CH₂CH₂CO₂Et}(CNXyl)Cl₃ (**8**). The β-proton of the homoenoate moiety of **1a** was selectively deprotonated by KN(SiMe₃)₂ to afford an η⁴-ethyl acrylate complex, Cp*Cl₂Ta(η⁴-ethyl acrylate) (**4**). In the case of complex **1b**, in which the β-positions were protected by dimethyl substituents, reaction with the dilithium salt of diazadiene afforded a tantalalactone complex **5**. The addition of Al(C₆F₅)₃ to **5** afforded a novel zwitterionic complex **6**, in which Al(C₆F₅)₃ coordinated to the exocyclic carbonyl oxygen of the tantalalactone.



VIII-H Creation of Novel Functional Nano Materials Based on Proton-Coupled Electronic Properties

Dynamics of molecules and ions in “coordination nano-space” are acted by characteristic nano-fields such as intermolecular interaction, coulomb interaction, catalytic action, *etc.* This project is to reveal a basic principle of an unusual nano-field acting on coordination space, and to create the nano space where the energy conversions can be easily operated. In particular, we aim at the construction of coordination nano space system which is able to control a series of energy operations such as generation, separation, storage, material conversion of an energy molecule H₂, or electron/ion transport. In this year, we have explored a novel hydrogen-energy functional coordination nano-space by using proton-coupled redox and electron-proton interaction. In the present project, we will create new 1) hydrogen-storage nano-materials, 2) highly proton-conductive coordination polymers, 3) highly electron-proton conductive materials, *etc.*

VIII-H-1 Most Stable Metallic Phase of the Mixed-Valence MMX-Chain, Pt₂(dtp)₄I (dtp: C₂H₅CS₂⁻) in Purely *d*-Electronic Conductors Based on the Transition-Metal Complex

OTSUBO, Kazuya¹; KOBAYASHI, Atsushi¹;
KITAGAWA, Hiroshi²; HEDO, Masato³;
UWATOKO, Yoshiya³; SAGAYAMA, Hajime⁴;
WAKABAYASHI, Yusuke⁴; SAWA, Hiroshi⁴
(¹Kyushu Univ.; ²IMS and Kyushu Univ.; ³Univ. Tokyo;
⁴KEK-PF)

[*J. Am. Chem. Soc.* **128**, 8140–8141 (2006)]

The electrical resistivity and X-ray oscillation photograph measurements for an MMX-Chain complex, Pt₂(dtp)₄I (dtp = C₂H₅CS₂⁻) under high pressure were performed. We observed the most stable metallic phase ($T_{MI} = 70$ K, under 2.2 GPa) in the 1-D purely *d*-electronic conductors and pressure-induced metal-insulator transition including structural phase transition at 3.0 GPa.

VIII-H-2 Direct Determination of Low-Dimensional Structures: Synchrotron X-Ray Scattering on One-Dimensional Charge-Ordered MMX-Chain Complexes

WAKABAYASHI, Yusuke¹; KOBAYASHI, Atsushi²;
SAWA, Hiroshi¹; OHSUMI, Hiroyuki³; IKEDA,
Naoshi³; KITAGAWA, Hiroshi⁴
(¹KEK-PF; ²Kyushu Univ.; ³JASRI; ⁴IMS and Kyushu Univ.)

[*J. Am. Chem. Soc.* **128**, 6676–6682 (2006)]

A powerful method to determine the hidden structural parameters in functional molecules has been developed. Local valence arrangements that dominate the material properties are sometimes not three-dimensionally ordered. This method that comprises diffuse X-ray scattering and resonant X-ray scattering is suitable in such cases. Using this method, we present clear evidence of the low-dimensional valence arrangement in two halogen-bridged one-dimensional metal complexes, so-called MMX chains. This family allows us to control many physical and structural parameters by chemical substitution of bridging halogen, counterions, or metal

ions, and one of our samples carries an unusual metallic phase. It is demonstrated with this complex that the present method makes it possible to have microscopic insight to low-dimensionally ordered systems.

VIII-H-3 Pressure-Induced Metal–Semiconductor–Metal Transitions in an MMX-Chain Complex, Pt₂(C₂H₅CS₂)₄I

KOBAYASHI, Atsushi¹; TOKUNAGA, Aya²;
IKEDA, Ryuichi²; SAGAYAMA, Hajime³;
WAKABAYASHI, Yusuke³; SAWA, Hiroshi³; HEDO,
Masato⁴; UWATOKO, Yoshiya⁴; KITAGAWA,
Hiroshi⁵
(¹Kyushu Univ.; ²Univ. Tsukuba; ³KEK-PF; ⁴Univ. Tokyo; ⁵IMS and Kyushu Univ.)

[*Eur. J. Inorg. Chem.* 3567–3578 (2006)]

The electrical conductivity and X-ray diffraction measurements under high pressure up to 2.5 GPa were performed for a highly-conductive halogen-bridged binuclear-metal mixed-valence complex (the so-called MMX chain), Pt₂(C₂H₅CS₂)₄I. It exhibited pressure-induced metal-semiconductor-metal transitions at 0.5 and 2.1 GPa. The X-ray diffuse scatterings were observed at $k = n + 0.5$ (n : integer) under ambient pressure, which are derived from the charge-density-wave (CDW: ...Pt²⁺–Pt²⁺...I–Pt³⁺–Pt³⁺–I...) fluctuation in the MMX chain. Above 0.5 GPa where the pressure-induced metal-semiconductor transition occurred, these scatterings disappeared. The electronic phases under high pressure (P) were found to be attributable to the metallic averaged-valence state (AV: –Pt^{2.5+}–Pt^{2.5+}–I–Pt^{2.5+}–Pt^{2.5+}–I–) with CDW fluctuation for $P < 0.5$ GPa, semi-conducting charge-polarization state (CP: ...Pt²⁺–Pt³⁺–I...Pt²⁺–Pt³⁺–I...) for $0.5 < P < 2.1$ GPa, and metallic AV state for $P > 2.1$ GPa. The electronic state of Pt₂(C₂H₅CS₂)₄I is very sensitive to pressure, implying that phase competition among the CP, CDW and AV phases is present in the MMX chain.

VIII-H-4 Synthesis of a One-Dimensional Metal-Dimer Assembled System with Interdimer Interaction, M₂(dtp)₄ (M = Ni, Pd; dtp = Dithiopropionato)

KOBAYASHI, Atsushi¹; KOJIMA, Takahiko¹;

IKEDA, Ryuichi²; KITAGAWA, Hiroshi³
 (¹Kyushu Univ.; ²Univ. Tsukuba; ³IMS and Kyushu Univ.)

[*Inorg. Chem.* **45**, 322–327 (2006)]

A metal-dimer assembled system, $M_2(dtp)_4$ ($M = Ni, Pd$; $dtp =$ dithiopropionate, $C_2H_5CS_2^-$) was synthesized and analyzed by X-ray single-crystal diffraction method, UV-Vis-Near-IR of solutions and solid state diffuse reflectance spectroscopies, and electrical conductivity measurement. The structures exhibit one-dimensional metal-dimer chains of $-M_2(dtp)_4-M_2(dtp)_4-M_2(dtp)_4-$ with moderate interdimer contact. These complexes are semiconducting or insulating, which is consistent with the fully filled d_z^2 band of $M^{II}(d^8)$. Interdimer metal-metal distances were 3.644(2) Å in $Ni_2(dtp)_4$ and 3.428(2) Å in $Pd_2(dtp)_4$, each of which is marginally longer than twice the van der Waals radius of the metal. Interdimer charge-transfer transitions were nevertheless observed in diffuse reflectance spectra. The origin of this transition is considered to be due to an overlap of two adjacent d_{σ^*} orbitals which spread out more than d_z^2 orbital due to the antibonding d_{σ^*} character of the $M(d_z^2)-M(d_z^2)$. The $Ni_2(dtp)_4$ exhibited an interdimer charge transfer band at relatively low energy region, which is derived from the Coulomb repulsion of $3d_{\sigma^*}$ orbital of Ni.

VIII-H-5 Galvanostatic Transient Studies on Copper Coordination Polymer under Hydrogen Absorption

FUJISHIMA, Musashi¹; ENYO, Michio²; KANDA, Seiichi³; IKEDA, Ryuichi⁴; KITAGAWA, Hiroshi⁵
 (¹Kinki Univ.; ²Hokkaido Univ.; ³Univ. Tokushima; ⁴Univ. Tsukuba; ⁵IMS and Kyushu Univ.)

[*Chem. Lett.* **35**, 546–547 (2006)]

Hydrogen electrode reaction (HER) was investigated for a copper coordination polymer, catena- $\mu-N,N'$ -bis(hydroxyethyl)dithiooxamidatocopper(II) (CuCP) by galvanostatic transient measurements using a palladium cathode. Individual steps in the Volmer–Tafel reaction were successfully observed for the colloidal CuCP in alkaline solution under hydrogen absorption. The Volmer step was found to be promoted with CuCP and its hydrogen-absorbed polymer (CuCPH) from shorter decay times in transient curves and smaller overpotentials in Tafel plots. In contrast, the inhibition of the Tafel step was observed, which is due to the larger overpotentials. Difference in reducibility between the polymers and plausible reduction mechanisms is discussed.

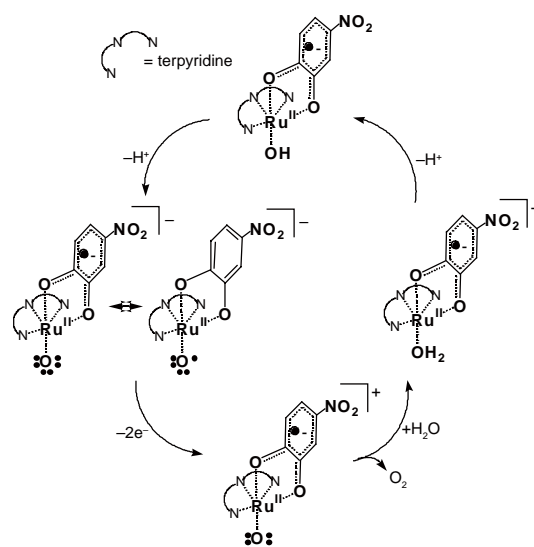
VIII-I Development of Metal-Cojugated Redox Systems in Metal-Dioxolene Complexes and Electrochemical Activation of Water Ligand

Dioxolenes function as a versatile electron-acceptor and electron-donor through the reversible two-electron redox reactions among the three oxidation states of catechol (Cat), semiquinone (SQ), and quinone (Q). A variety of metal-dioxolene complexes has appeared and the unique metal-conjugated electronic interaction has been extensively investigated. The ruthenium-terpyridine-dioxolene complexes exhibit the reversible two-electron redox behavior derived from a resonance hybrid between the metal center and the dioxolene ligand. In the ruthenium-dioxolene complex, its aqua ligand undergoes the electrochemical activation to generate a novel ruthenium-oxo bond. Fabrication of a water-soluble ruthenium-terpyridine complex having a strongly electron-withdrawing dioxolene is a particularly urgent target for the future applications as an electrochemical catalyst utilizing water molecules.

VIII-I-1 Synthesis of a Water-Soluble Ruthenium-Terpyridine-Dioxolene and the Electrochemical Activation of Water Molecules

KURIHARA, Masato¹; MIURA, Yasutaka²;
SAKAMOTO, Masatomi²; WADA, Tohru;
TANAKA, Koji
(¹IMS and Yamagata Univ.; ²Yamagata Univ.)

A ruthenium-terpyridine-dioxolene complex having a chloro ligand was synthesized using 4-nitrocatechol. The dioxolene complex, $[\text{Ru}^{\text{II}}\text{Cl}(\text{NO}_2\text{-SQ})(\text{terpy})]$ was transformed to a hydroxo complex, $[\text{Ru}^{\text{II}}(\text{OH})(\text{NO}_2\text{-SQ})(\text{terpy})]$ (**1**) by elimination of the chloro ligand with Ag^+ in acetone/water, where terpy and $\text{NO}_2\text{-SQ}$ are 2,2':6',2''-terpyridine and 4-nitrobenzosemiquinone, respectively. The hydroxo complex, **1** is soluble in water, unlike the chloro complex. The intense near-IR absorption band of **1** is ascribable to the $\text{Ru}(\text{II}) \rightarrow \text{NO}_2\text{-SQ}$ charge transfer. Both of the complexes show two-reversible redox waves of the cyclic voltammograms (CV) in the organic solvents. Based on the electrochemical measurement, the two-redox reactions correspond to $\text{Ru}(\text{II})\text{-NO}_2\text{-Cat} \leftrightarrow \text{Ru}(\text{II})\text{-NO}_2\text{-SQ} \leftrightarrow \text{Ru}(\text{III})\text{-NO}_2\text{-SQ}$ ($\text{Ru}(\text{II})\text{-NO}_2\text{-Q}$). The UV-Vis-near-IR absorption spectrum and CV of **1** are significantly changed depending on pH in water. In pH 12, a catalytic current is observed around 0.7 V vs. Ag/AgCl. When we suppose that oxygen molecules are evolved catalytically at the oxidation potential, an electrocatalytic cycle can be proposed, as shown in Scheme 1.



Scheme 1. The electrocatalytic cycle.

VIII-J Syntheses, Structures, and Redox Properties of New Multinuclear Coordination Materials with Metallocene Units

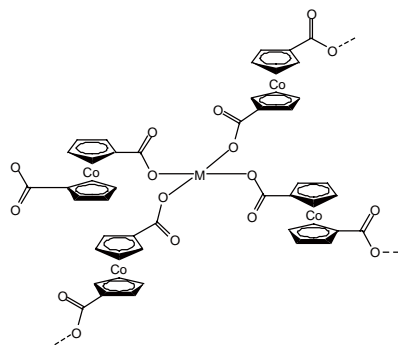
Coordination materials with metallocene are of interest for creations of new redox-active crystalline solids, in which ferrocene moieties have mainly been utilized as the redox-active units. Because other metallocene such as ruthenocene and cobaltocene are known to show quite different potentials compared to ferrocene units, coordination materials with such metallocene units in the framework are promising compounds that show different redox properties compared with those for ferrocene units. Nevertheless the coordination materials with their metallocene units are still unexplored. This project proceeds synthesis, and characterizations of new coordination materials with metallocene and metallocenium units with dicarboxylate 1,1'-dicarboxylate. These studies show that the compounds obtained demonstrate unique dynamics depending on the free rotations of the Cp-M-Cp rotations as well as the redox properties based on the metallocene units.

VIII-J-1 Synthesis of Coordination Polymers with Cobaltocenium and Rhodocenium Units

KONDO, Mitsuru¹; HAYAKAWA, Yuri²; UNOURA, Kei³; KAWAGUCHI, Hiroyuki
(¹IMS and Shizuoka Univ.; ²Shizuoka Univ.; ³Yamagata Univ.)

Four new redox-active crystalline coordination polymers with cobaltocenium-1,1'-dicarboxylate (ccdc) have been synthesized and characterized. The crystalline materials, [Cu(ccdc)₂].2MeOH (**1**) and [M(ccdc)₂].2DMF (M = Co (**2**), Zn (**3**)) were obtained by a treatment of Hccdc and Hrcdc with the corresponding M (CH₃COO)₂. Because of the charge balance, ccdc acts as monoanionic dicarboxylate ligand, yielding M(ccdc)₂ type compounds. Crystal structural analyses clearly demonstrated that these compounds have two-dimensional structure (Scheme 1). The free rotations based on the crystal structures are revealed for these compounds.

The high redox properties of **1-4** based on the ccdc components were characterized by solid-state cyclic voltammogram (CV).



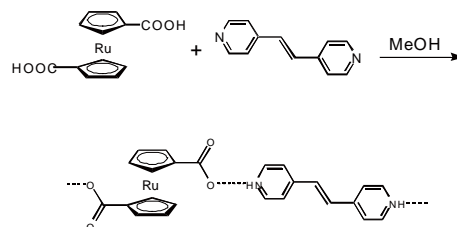
Scheme 1.

The quasi reversible redox waves ascribed to the Co(III)/Co(II) couple of the ccdc centers are observed at -933 and -831 mV (*vs.* SCE) in 1,2-dichloroethane media for **1** and **2**, respectively. Although these potentials change depending on the electrolyte solvents used for the measurements, the orders (**1** < **2** < **3**) of the potentials are retained. The correlations between the reduction processes and the LUMO levels were revealed by preliminary molecular orbital calculation.

VIII-J-2 Synthesis of Coordination Networks with Ruthenocene Units

KONDO, Mitsuru¹; KOBAYASHI, Yuko²; KAWAGUCHI, Hiroyuki
(¹IMS and Shizuoka Univ.; ²Shizuoka Univ.)

As a ruthenocene assembled complex, [(H₂bpe)(rcdc)] (bpe = 4,4'-bipyridylethylene, rcdc = ruthenocene-1,1'-dicarboxylate) was prepared and structurally characterized. Treatment of H₂rcdc with bpe yields the compound as pale pink crystals. The carboxylate groups of the rcdc form hydrogen bonds to the protonated pyridine nitrogen atom of the bpe. These interactions yield the infinite one-dimensional chain structure (Scheme 1).



Scheme 1.

RESEARCH ACTIVITIES IX

Research Center for Molecular-Scale Nanoscience

IX-A Nano-Science and Nano-Technology toward Molecular Scale Electronics

Molecular electronics is a fairly new and fascinating area of research that is firing the imagination of scientists. However, most single organic molecules are not conductive in a classical sense, long range electronic transport through single molecules can not be so effective to realize practical electronic circuits. Our group is interested in (1) construction of nano-structures made from conductive materials such as carbon nanotubes, metal particles or rods, with functional organic molecules, (2) measurements of electric or photonic properties of individual nano-structures while observing their nanometric images, and (3) conductance change of single molecules by external stimulation such as electric field, photon irradiation or chemical species.

IX-A-1 Synthesis and Self-Assembly of Novel Porphyrin Molecular Wires

KAWAO, Masahiro¹; OZAWA, Hiroaki²; TANAKA, Hirofumi³; OGAWA, Takuji³
(¹JST and Ehime Univ.; ²JST and SOKENDAI; ³IMS and JST)

[*Thin Solid Films* **499**, 23–28 (2005)]

Sub-micrometer long butadiyne-linked porphyrin wires were synthesized by oxidative coupling of diethynylporphyrin. The porphyrin wires were analyzed by analytical gel permeation chromatography, absorption spectroscopy and matrix-assisted laser desorption/ionization time of flight mass spectroscopy. Observations of the wire were performed by atomic force microscopy. Self-assembled structures of the wires were observed on highly oriented pyrolytic graphite. Self-assembling features of the porphyrin wires depended on the length of the porphyrin wires and the concentration of the depositing solution.

IX-A-2 Molecular Junctions Composed of Oligothiophene Dithiol Bridged Gold Nanoparticles Exhibiting Photoresponsive Properties

HUANG, Wei¹; MASUDA, Gou²; MAEDA, Seisuke²; TANAKA, Hirofumi³; OGAWA, Takuji³
(¹Nanjing Univ.; ²Ehime Univ.; ³IMS and JST)

[*Chem. Eur. J.* **12**, 607–619 (2005)]

Three oligothiophene dithiols with different number of thiophene rings (3, 6 or 9) were synthesized and characterized. X-ray single crystal structures of compounds 3',4'-dibutyl-5'5''-dithiocyno-2,2':5',2''-terthiophene (**2**) and 5,5''''-dithiocyno-tetrabutyl-2,2':5',2''':5''',2''''':5''''',2''''''':5''''''',2''''''''-hexathiophene (**5**) were involved herein to show the exact molecular lengths as well as the difference between their UV-vis spectra arising from the different packing modes. These dithiols with different chain lengths were then treated with *t*-dodecanethiol protected active gold nano-particles (Au-

NPs) *via* in situ thiol-to-thiol ligand exchange in the presence of 1 μm gap Au-electrodes. Thus the molecular junctions composed of self-assembled films were prepared, where oligothiophene dithiol bridged Au-NPs were attached to two electrodes by means of Au-S bonded contacts. The morphologies and *I-V* characteristics of these films were studied by SEM and AFM approaches, which suggest the thickness of the films varied within the size of one isolated Au-NPs and typical distance dependent semiconductor properties could be observed. Current-voltage (*I-V*) measurements for these devices were performed where the films served as active elements in the temperature range 6 ~ 300 K and classical Arrhenius plots and their linear fittings were carried out to give the activation energies (ΔE). Furthermore, preliminary studies on the photoresponsive properties of these junctions were explored at 80, 160 and 300 K, respectively. Physical and photochemical mechanisms were used to explain the possible processes. To the best of our knowledge, this is the first report where oligothiophene dithiols act as bridging units to link Au-NPs, and also the first report about functionalized Au-NPs exhibiting photo response properties in the solid state.

IX-A-3 Simple Preparation Method for Supramolecular Porphyrin Arrays on Mica Using Air/Water Interface

SATO, Hirokazu¹; TSUTSUMI, Osamu¹; TAKEDA, Kazuyoshi¹; TANAKA, Hirofumi²; OGAWA, Takuji²
(¹Ebara Research Co.; ²IMS and JST)

[*Jpn. J. Appl. Phys.* **45**, 2324–2327 (2006)]

The fabrication of supramolecular porphyrin arrays on the surface of a mica substrate is demonstrated. The supramolecular structures are prepared at the air–water interface from a dilute solution of porphyrin dimer and bidentate ligand and then transferred to mica by using the conventional Langmuir-Blodgett method. Isolated wire-like structures and networks of structures are observed by atomic force microscopy. From the analysis of the height histogram and average width, these structures are considered to be side-by-side arrangements of supramolecular chains of porphyrin dimer and bidentate

ligand. By changing the ligand molecule, we demonstrate that the configuration of the supramolecular structure can be controlled.

IX-A-4 Porphyrin Molecular Nanodevices Wired Using Single-Walled Carbon Nanotubes

TANAKA, Hirofumi¹; YAJIMA, Takashi; MATSUMOTO, Takuya²; OTSUKA, Yoichi²; OGAWA, Takuji¹
(¹IMS and JST; ²Osaka Univ. and JST)

[*Adv. Mater.* **18**, 1411–1415 (2006)]

For the future development of molecular electronics, we should construct nanosized molecular devices placed on nanowiring. To obtain high-quality devices composed of a few molecules, the wiring and the device should be connected well to maintain a constant interface. For this purpose, a single-walled carbon nanotube (SWNT)/porphyrin complex was prepared and then its electronic property was investigated while observing a topographic image using point-contact current imaging atomic force microscopy (PCI-AFM). Using PCI-AFM, we can measure the current along the long axis of the wiring by which the quality of the device in the circuit can be determined. The *I-V* curves were asymmetric with respect to the origin where an aggregate of several porphyrin molecules was absorbed, while they were symmetric without them. This means the porphyrin aggregation works as a rectification device on SWNT wiring. This is the first study which proves the electron property of a few porphyrin molecules absorbed on SWNT.

IX-A-5 Electronic Properties of Single-Walled Carbon Nanotube/150mer-Porphyrin System Measured by Point-Contact Current Imaging Atomic Force Microscopy

TANAKA, Hirofumi¹; YAJIMA, Takashi²; KAWAO, Masahiro²; OGAWA, Takuji¹
(¹IMS and JST; ²SOKENDAI)

[*J. Nanosci. Nanotechnol.* **6**, 1644–1648 (2006)]

The electronic properties of a porphyrin polymer wire absorbed on a single-walled carbon nanotube (SWNT) were investigated. Current-voltage (*I-V*) curves were measured simultaneously along with topographic observations using point-contact current imaging atomic force microscopy (PCI-AFM). *I-V* curves taken at the location of porphyrin polymer wire absorption were asymmetric with respect to the origin, while they were symmetric in the absence of a porphyrin polymer wire. The electron conduction mechanism of the porphyrin on the SWNT was similar to the case of SWNT/5,15-Bis(pentylporphyrinato) zinc(II) complex in our recent work.

IX-A-6 Preparation of Very Reactive Thiol-Protected Gold Nanoparticles: Revisiting the Brust-Schiffrin Method

ARAKI, Koiti¹; MIZUGUCHI, Eisuke²; TANAKA, Hirofumi³; OGAWA, Takuji³
(¹Sao Paulo Univ.; ²Ehime Univ.; ³IMS and JST)

[*J. Nanosci. Nanotechnol.* **6**, 708–712 (2006)]

Metal nanoparticles have attracted great interest in nanoscience and nanotechnology because of the many possibilities envisaged by the bottom-up approach since they possess unique optical, electrical, bonding and catalytic properties. Among them, the gold clusters are the most stable and extensively studied materials, and have been proposed for applications such as in photoelectrochemical devices, drug delivery systems and chemical and immunosensors. In all these cases, the properties of the materials should be adjusted by anchoring molecular species with suitable properties on the surface. In this sense, the availability of easily functionalizable and stable starting materials is an important aspect since there is a myriad of molecular species and other materials that can be combined with for the development of new inorganic-organic hybrid nanomaterials and applications.

The higher stability and possibility to isolate a solid that can be repeatedly isolated and redissolved in common organic solvents without decomposition and the possibility to treat them just as another organic molecular species is very convenient. However, there is a drawback for the widespread use of such a thiol protected materials: the sluggishness of the functionalization reaction by substitution of the protecting species, which can take more than a day to proceed until completion. The use of conventional organic chemistry on ω -functionalized protecting molecules is also tedious and hampers the preparation of organic-inorganic hybrid nanomaterials, for example by coordinative layer-by-layer assembly. Accordingly, we revisited the Brust-Schiffrin method envisaging the preparation of substitutionally reactive but stable enough thiol protected gold nanoparticles to isolate them as a solid.

IX-A-7 Spontaneous Resolution of Delta and Gamma Enantiomeric Pair of [Ru(phen)(bpy)₂](PF₆)₂ (phen = 1,10-phenanthroline, bpy = 2,2'-bipyridine) by Racemic Conglomerate Crystallization

HUANG, Wei¹; OGAWA, Takuji
(¹Nanjing Univ.)

[*Polyhedron* **25**, 1379–1385 (2006)]

Spontaneous resolution study is realized for a Δ and Λ enantiomeric pair of ruthenium(II) complexes obtained by racemic conglomeration from solution, crystallizing in *P4*₁ and *P4*₃ space groups. A ligand exchange reaction between phen and bpy ligands is found for these Ru(II) complexes, but racemization is accompanied which has been proved by the single-crystal structure of the product. To extend our research, counter-ion (BF₄⁻)

and 4,4'-dimethyl-2,2'-bipyridine (dmbpy) are used to synthesize similar six-coordinate Ru(II) complexes. Nevertheless, conglomerate crystallization could not be progressed in these two cases.

IX-A-8 Structural and Spectroscopic Characterizations of Low-Spin [Fe(4,4-dimethyl-2,2'-bipyridine)₃] (NCS)₂/H₂O Prepared from High-Spin Iron(II) Dithiocyanate Tetrapyrroline

HUANG, Wei¹; OGAWA, Takuji
(¹Nanjing Univ.)

[*J. Mol. Struct.* **785**, 21–26 (2006)]

Redetermination of the crystal structure of high-spin iron(II) dithiocyanate tetrapyrroline [Fe(py)₄(NCS)₂] (**1**) (pyZpyridine) at 85 and 291 K exhibits different unit cells when compared with that reported in 1967. An elongation in the compressed octahedron coordination environment around central ferrous ion is observed at low temperature, which can be verified by the DFT calculations of energy and dipole moments. **1** was then used as the Fe(II) source to synthesize [Fe(dmbpy)₃](NCS)₂·3H₂O (**2**) (dmbpyZ4,40-dimethyl-2,20-bipyridine). The X-ray diffraction studies of **2** reveal that six Fe–N bond distances are in the range 1.959(3)–1.971(3) Å suggesting the formation of the low-spin Fe(II) complex.

IX-A-9 Morphology and Electric Properties of Nonathioephene/Au Nano-Composite Thin Films Formed between 1 μm Gapped Electrodes

OGAWA, Takuji¹; HUANG, Wei²; TANAKA, Hirofumi¹
(¹IMS and JST; ²Nanjing Univ.)

[*Mol. Cryst. Liq. Cryst.* **455**, 299–303 (2006)]

A nano-composite conductive film is formed between gold electrodes by immersion of the electrode pair in a chloroform solution of nonathioephenedithiol and gold nanoparticles. The homogeneous thin film is formed over an area of 3 mm × 3 mm surrounding the 1 μm-gapped electrodes. The thickness of the film (20 nm) corresponds to 2–3 layers of the dithiol-bridged Au nanoparticles. Temperature-dependent *I*-*V* curves reveal that a thermionic mechanism dominates in the high-temperature region (>80 K), while molecular tunneling is the main transport process at lower temperatures.

IX-A-10 Synthesis of End-Functionalized π-Conjugated Porphyrin Oligomers

OZAWA, Hiroaki¹; OGAWA, Takuji²; TANAKA, Hirofumi²
(¹SOKENDAI; ²IMS and JST)

[*Tetrahedron* **62**, 4749–4755 (2006)]

4-(S-acetylthiomethyl)phenyl- and pyrenyl-functionalized π-conjugated porphyrin oligomers were syn-

thesized. The distribution of the length of the oligomers could be controlled by changing the ratio of the starting porphyrin to the capping molecules. Oligomers from dimers to heptamers were isolated using size exclusion chromatography. The spectroscopic properties of these oligomers were measured to determine the influences of the number of porphyrin units and capping molecules on the absorption and emission spectra.

IX-A-11 Fabrication of Nanoscale Gaps Using a Combination of Self-Assembled Monomolecular and Electron Beam Lithographic Techniques

NEGISHI, R.^{1,2}; HASEGAWA, T.^{1,2}; TERABE, K.^{1,2}; AONO, M.^{1,2}; EBIHARA, T.²; OGAWA, Takuji; TANAKA, Hirofumi
(¹ICORP, JST; ²NIMS)

[*Appl. Phys. Lett.* **88**, 223111 (2006)]

We describe a new method of fabricating nanogaps using a combination of the self-assembled molecular lithographic and the electron beam lithographic techniques. The method enables us to control the size of a gap with an accuracy of ~2 nm, and design the positions, where the nanogap should be formed, in the high-resolution patterning by employing an electron beam lithography. The utility of the fabricated nanogap is demonstrated by measurement of a single electron tunneling phenomenon through the dodecanethiol-coated Au nanoparticles placed in the fabricated nanogap.

IX-A-12 Synthesis and Photochemical Behavior of Metalloporphyrin Complexes Containing a Photochromic Axial Ligand

TSUTSUMI, Osamu¹; SATO, Hirokazu¹; TAKEDA, Kazuyoshi¹; OGAWA, Takuji
(¹Ebara Research Co.)

[*Thin Solid Films* **499**, 219–223 (2006)]

Metalloporphyrin complexes with a photochromic axial ligand were synthesized and photoisomerization behavior of those complexes was investigated. In this study, 3,3V-azopyridine (AZP) was used as the axial ligand. We found that the structure of the axial-coordinated complexes depended on the center metal of porphyrin. When magnesium was employed as the center metal, a 1:1 coordinated complex was obtained. On the other hand, zinc or rhodium porphyrins formed the sandwich-bonded complexes. The photoisomerization behavior also depended on the center metal of the porphyrins, and the *cis*-to-*trans* “one-way” photoisomerization of the AZP axial ligand took place in the complexes of zinc and rhodium porphyrins. The one-way isomerization may be interpreted as the results of the photoinduced electron transfer from porphyrin to AZP.

IX-B Development of Organic Semiconductors for Molecular Thin-Film Devices

Organic light-emitting diodes (OLEDs) and organic field-effect transistors (OFETs) based on π -conjugated oligomers have been extensively studied as molecular thin-film devices. Organic semiconductors with low injection barriers and high mobilities are required for highly efficient OLEDs and OFETs. Radical cations or anions of an organic semiconductor have to be generated easily at the interface with an electrode (or a dielectric), and holes or electrons must move fast in the semiconducting layer. Compared with organic p-type semiconductors, organic n-type semiconductors for practical use are few and rather difficult to develop. Recently, we found that perfluorinated aromatic compounds are efficient n-type semiconductors for OLEDs and OFETs.

IX-B-1 Synthesis and Characterization of Three Novel Perfluoro-Oligothiophenes Ranging in Length from the Trimer to the Pentamer

OSUNA, Reyes M.¹; ORTIZ, Rocío P.¹; DELGADO, Mari C. R.¹; SAKAMOTO, Youichi; SUZUKI, Toshiyasu; HERNÁNDSZ, Víctor¹; NAVARRETE, Juan T. L.¹

(¹Univ. Málaga)

[*J. Phys. Chem. B* **109**, 20737–20745 (2005)]

In this article, we report on the synthesis and full characterization of three perfluorinated oligothiophenes, ranging in length from the trimer (PF-*n*T, with *n* = 3, 4, or 5). The differential pulse voltammetry (DPV) analysis of the compounds showed that they can be both oxidized and reduced (*i.e.*, they display a dual or amphoteric electrochemical behavior), with the reduction peaks positively shifted relative to those of the corresponding unsubstituted oligothiophenes. The electrochemically determined energy gaps are in agreement with those measured from the UV-vis-NIR absorption spectra in solution. The conjugational properties have been investigated by means of FT-Raman spectroscopy, both as pure solids and as dilute solutes in CH₂Cl₂, revealing that: (i) π -conjugation does not still reach saturation with chain length for the longest oligomer, and (ii) conformational distortions from a nearly coplanar arrangement of the successive thiophene units upon solution are not too large. DFT and TDDFT quantum chemical calculations have been performed, at the B3LYP/6-31G** level, to assess information about the optimized molecular structure, equilibrium atomic charges distribution, energies and topologies of the frontier molecular orbitals (MO) around the gap, vibrational normal modes associated with the most outstanding Raman scatterings, and vertical one-electron excitations that give rise to the main optical absorptions.

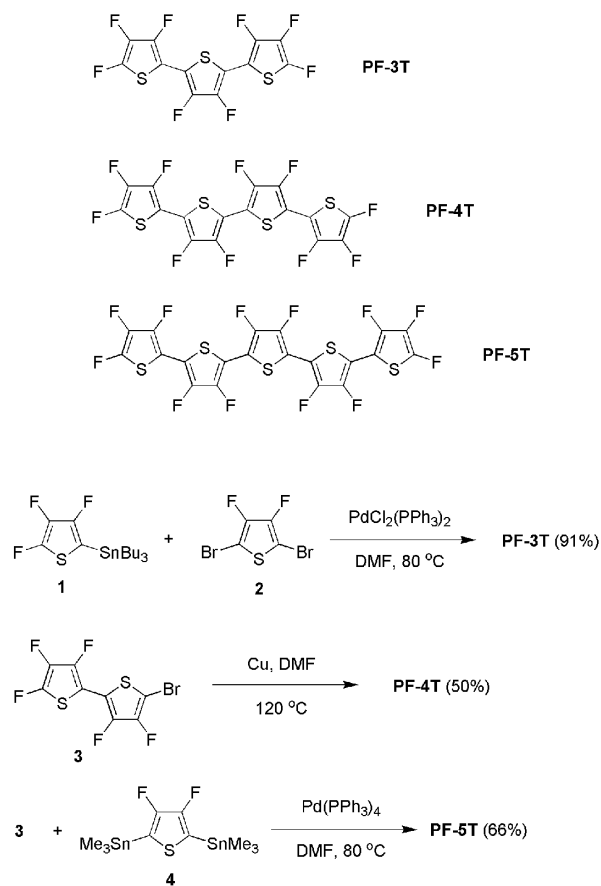


Figure 1. Structures and syntheses of perfluoro-oligothiophenes.

IX-C Development of Multi-Function Integrated Macromolecules and Their Organization on Substrate Surfaces for Planar Molecular-Scale Electronics Circuits

The concept of molecular-scale electronics is now realized for individual components such as wire, diode, switch, and memory cell, but the fabrication of complete molecular-scale circuits remains challenging because of the difficulty of connecting molecular modules to one another. Molecular monolithic technology, which integrates the wiring, transistors, and the required passive elements on a single macromolecule, has been proposed as a promising solution to this problem. In this project we have been trying to establish both the architecture of this novel class of macromolecules and the protocols for their purposive organization on metal/semiconductor substrate surfaces.

IX-C-1 Stepwise Synthesis of Molecular Wire with a Double-Tunnel Junction

TANAKA, Shoji

We have developed a synthetic protocol for precisely-defined linear macromolecules with a double-tunnel junction as shown in Figure 1. The nature of intramolecular charge transport in a π -conjugated macromolecule with tunnel junctions is of fundamental importance for single electron/hole device applications. In the field of applied physics metal–molecule–metal double junction systems have been intensively studied so far. In contrast, little attention has been paid to an intramolecular tunnel junction system because of the problem of precise fabrication of tunnel junction structures in a macromolecule. Based on our synthetic approach, a series of intramolecular junction systems will be prepared from various types of non-conjugated molecular blocks and the 1–10 nm long π -conjugated molecular blocks that we have already developed.

IX-C-2 Direct Identification of Conformational Isomers of Adsorbed Oligothiophene on Cu(100)

YOKOYAMA, Takashi¹; KURATA, Saki¹; TANAKA, Shoji
(¹Yokohama City Univ.)

[*J. Phys. Chem. B* in press]

A direct conformational analysis using scanning tunneling microscopy (STM) has been performed for individual adsorbed α -octithiophene molecules **8T-Si** on Cu(100). *s-Cis* and *s-trans* conformational isomers are induced by the rotational flexibility of individual thiophene rings. By adding bulky N-silyl substituents to octithiophene, we successfully identify the *s-cis* and *s-trans* conformational isomers using STM. The obtained relative abundances of the *s-cis* and *s-trans* conformations are analyzed using ab initio molecular orbital calculations.

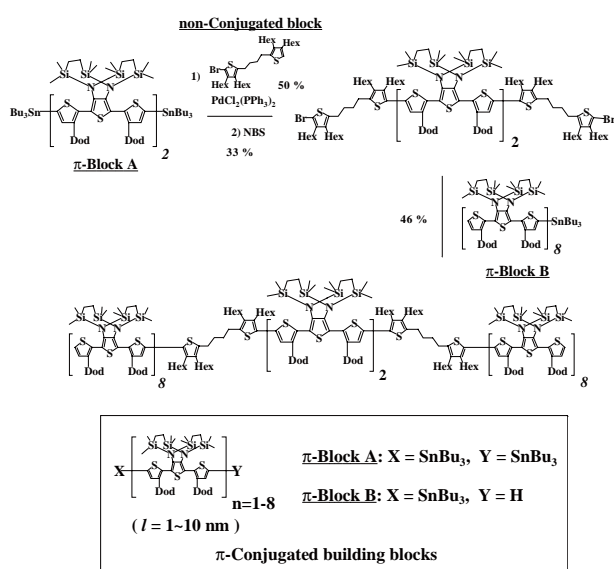


Figure 1. Synthetic scheme of 25 nm long molecular wire with a double-tunnel junction.

IX-D Nano- and Complex-Catalysis

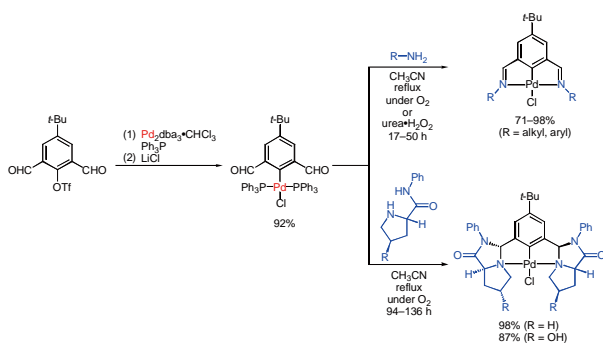
Objectives of this research group is development of nano- and complex-catalysts which exhibit novel catalytic functions, in particular, to promote efficient organic molecular transformations. Three major subjects are (1) preparation and properties of novel pincer complexes, (2) development of polymeric complex-catalysis in water, and (3) development of polymer-supported nano-metal catalysts. Representative results are shown below.

IX-D-1 NCN Pincer Palladium Complexes: Their Preparation via a Ligand Introduction Route and Their Catalytic Properties

UOZUMI, Yasuhiro; TAKENAKA, Kazuhiro; MINAKAWA, Maki

[*J. Am. Chem. Soc.* **127**, 12273–12281 (2005)]

A wide range of NCN pincer palladium complexes, [4-*tert*-2,6-bis(*N*-alkylimino)phenyl]chloropalladium (alkyl = *n*-butyl, benzyl, cyclohexyl, *t*-butyl, adamantyl, phenyl, 4-methoxyphenyl), were readily prepared from *trans*-(4-*tert*-butyl-2,6-diformyl-phenyl)chlorobis(triphenylphosphine)palladium via dehydrative introduction of the corresponding alkylimino ligand groups (ligand introduction route) in excellent yields (71–98%). NMR studies on this route for forming pincer complexes revealed the intermediacy of [4-*tert*-2,6-bis(*N*-alkylimino)phenyl]chlorobis(triphenylphosphine)palladium which is in equilibrium with the corresponding NCN pincer complexes via coordination/dissociation of the intramolecular imino groups and triphenylphosphine ligands. A series of chiral NCN pincer complexes bearing pyrroloimidazolone units as the *trans*-chelating donor groups, [4-*tert*-butyl-2,6-bis{(3*R*,7*aS*)-2-phenylhexahydro-1*H*-pyrrolo[1,2-*c*]imidazol-1-on-3-yl}phenyl]chloropalladium, were also prepared from the same precursor via condensation with proline anilides in high yields. The catalytic properties of the NCN imino and the NCN pyrroloimidazolone pincer palladium complexes were examined in the Heck reaction and the asymmetric Michael reaction to demonstrate their high catalytic activity and high enantioselectivity.

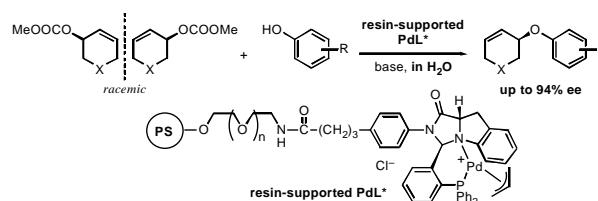


IX-D-2 Asymmetric P-Allylic Etherification of Cycloalkenyl Esters with Phenols in Water Using a Resin-Supported Chiral Palladium Complex

UOZUMI, Yasuhiro; KIMURA, Masahiro

[*Tetrahedron:Asymmetry* **17**, 161–166 (2006)]

Catalytic asymmetric allylic amination of cycloalkenyl carbonates (methyl cyclohexen-2-yl carbonate, methyl cyclohepten-2-yl carbonate, methyl 5-methoxycarbonylcyclohexen-2-yl carbonate, methyl cyclohexenyl carbonate, *t*-butyl 5-methoxycarbonyloxy-1,2,5,6-tetrahydropyridinedicarboxylate) with phenolic nucleophiles was achieved in water under heterogeneous conditions by use of a palladium complex of (3*R*,9*aS*)-3-[2-(diphenylphosphino)phenyl]-2-phenyltetrahydro-1*H*-imidazo[1,5-*a*]indole-1-one anchored on polystyrene-poly(ethylene glycol) copolymer resin (2 mol % Pd) to give the corresponding cycloalkenylamines with high enantiomeric selectivity (up to 94% *ee*).

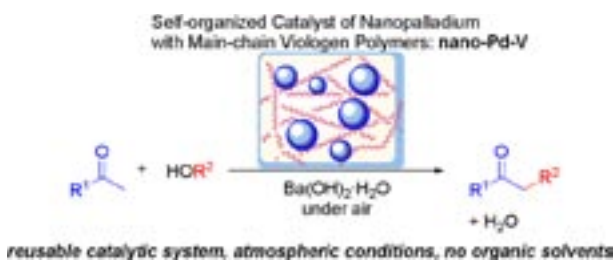


IX-D-3 A Solid-Phase Self-Organized Catalyst of Nanopalladium with Main-Chain Viologen Polymers: α -Alkylation of Ketones with Primary Alcohols

YAMADA, Yoichi; UOZUMI, Yasuhiro

[*Org. Lett.* **8**, 1375–1378 (2006)]

A novel solid-phase self-organized catalyst of palladium nanoparticles was prepared from PdCl₂ with main-chain viologen polymers via complexation and reduction. This insoluble nanocatalyst nano-Pd-V efficiently promoted α -alkylation of ketones with primary alcohols in the presence of Ba(OH)₂·H₂O under atmospheric conditions without organic solvents. The nano-Pd-V catalyst was reused without loss of catalytic activity.



IX-E Development of New Nanomaterials as Components in Advanced Molecular Systems

Nanometer-sized materials exhibit unique electronic behavior. In the quest of advanced redox catalysis, we are currently interested in combining nanometer-sized materials into molecular redox systems. As a basic architecture, composites of organic molecules and gold nanoparticles were synthesized and molecular dynamic simulations were carried out to predict the solution structures.

IX-E-1 Automated Design of Protecting Molecules for Metal Nanoparticles by Combinatorial Molecular Simulations

NAGATA, Toshi

[*J. Organomet. Chem.* in press]

New tripod oligo(dibenzyl sulfide) molecules were designed by computer modeling calculations so that they would form 1:1 complexes with an Au₁₄₇ nanoparticle. Twelve aromatic molecules containing two methylthiomethyl groups were used as construction units ("residues"). Combinations of the residues ("sequences") were examined by molecular dynamic simulations, and those sequences giving the largest interaction energies with the gold nanoparticle were sought through either full search or genetic algorithm. Best-fit sequences were found for $N = 5$ and 6 (N is the number of "residues" in one leg of the tripod molecule).

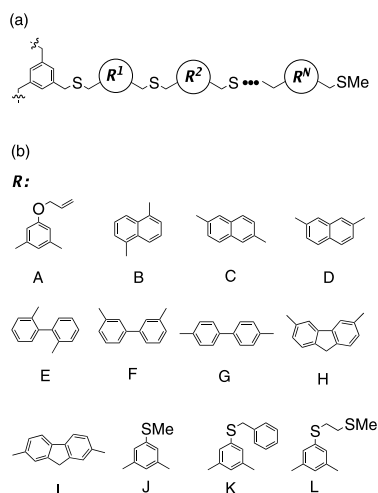


Figure 1. (a) The base structure of the protecting molecule. (b) The "residues" used in this study.

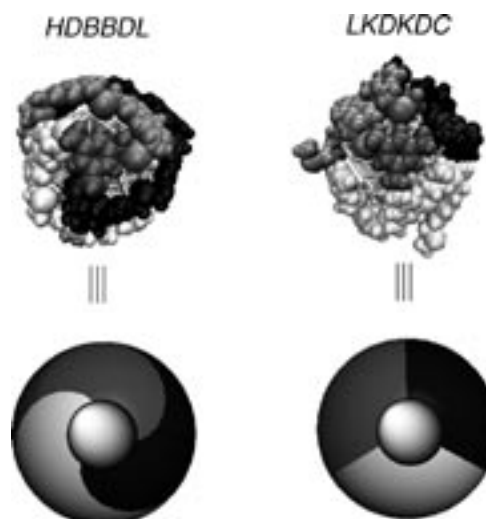


Figure 2. The surface covering schemes for the two lowest energy structures for $N = 6$. The atoms in the three "legs" are drawn in white, gray, and black, respectively.

IX-F Designing Artificial Photosynthesis at Molecular Dimensions

Photosynthesis is one of the finest piece of molecular machinery that Nature has ever created. Its ultrafast electron transfer and following well-organized sequence of chemical transformation have been, and will continue to be, challenging goals for molecular scientists. Our ultimate goal is to design artificial molecular systems that effect multiple chemical reactions triggered by light on the basis of molecular rationale.

IX-F-1 Elucidation of Solution Structures of Dendrimer-Linked Porphyrins

KIKUZAWA, Yoshihiro; NAGATA, Toshi; TAHARA, Tahei¹; ISHII, Kunihiko¹
(¹RIKEN)

[Chem. Asian J. in press]

In order to estimate the average structures of our ferrocene-dendrimer-porphyrins (Figure 1), we carried molecular-dynamic (MD) simulations of these molecules in CHCl₃ solutions. Figure 2 shows the spatial distribution of the iron atoms of all the ferrocenyl groups, in relative to the porphyrin ring at the core. Figure 3 shows the radial distribution functions of the iron atoms in the first, second, and third layers from the center of the porphyrin ring. These figures clearly show that only the ferrocenyl groups in the second layer have significant probability to approach the porphyrin ring closer than 10 Å. This observation is consistent with the results of ¹H NMR and fluorescence quenching, namely the second layer had a larger interaction with the porphyrin ring than the first and third layers.

It is also interesting to note that such layered distribution was more distinct in G3(Fc)₁₄-ZnP than in G2(Fc)₆-ZnP, the generation 2 compound with the similar architecture. The spatial distribution and radial distribution functions of the iron atoms in G2(Fc)₆-ZnP also showed similar trends as G3(Fc)₁₄-ZnP, although the distribution of the first layer Fe atoms was somewhat broader in G2(Fc)₆-ZnP than in G3(Fc)₁₄-ZnP. These results suggest that, even in the case of these “spatially relaxed” dendritic frameworks, the presence of the higher-generation branches restricts the movements of the inner layer.

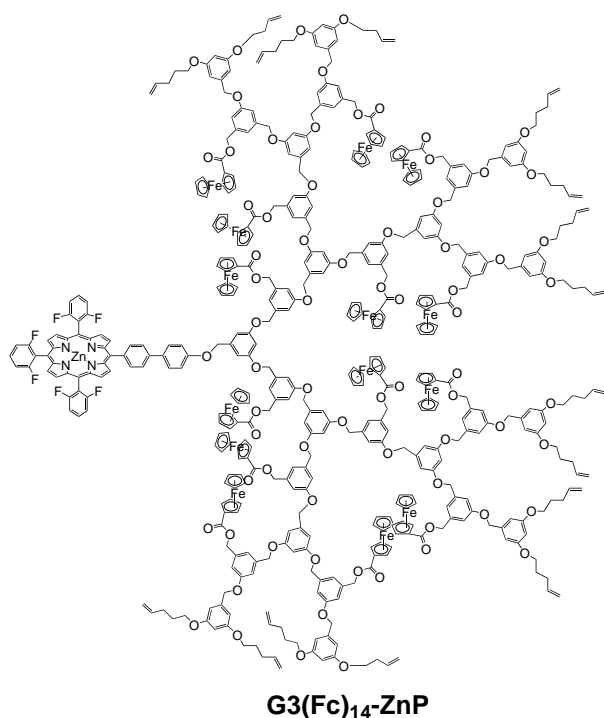


Figure 1. The structure of the ferrocene-dendrimer-linked porphyrin (generation 3).

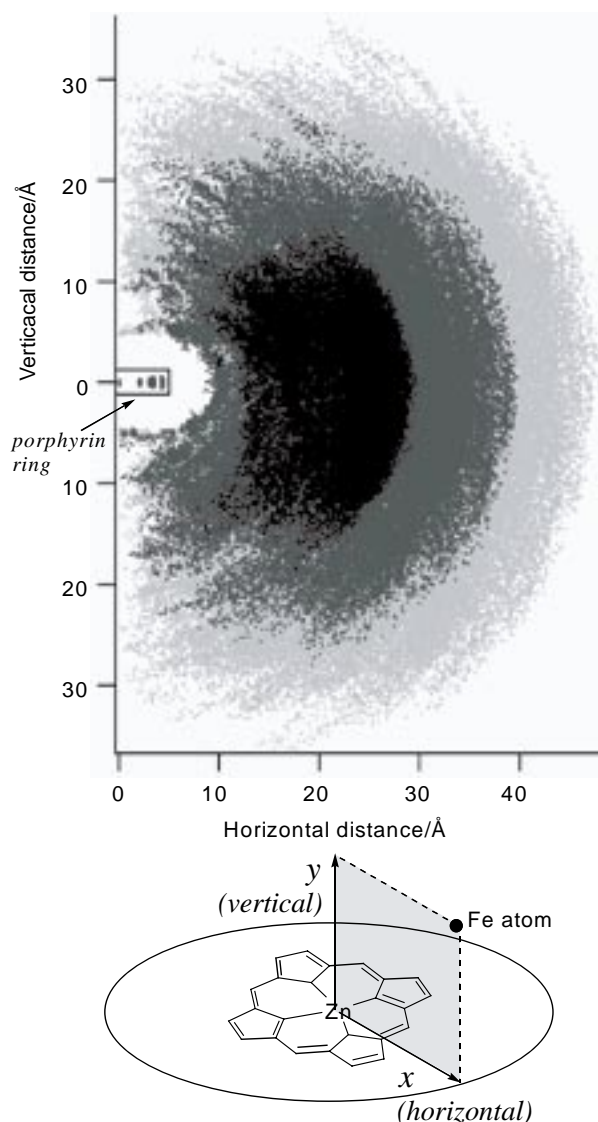


Figure 2. The calculated distribution of the iron atoms of the ferrocenyl groups in G3(Fc)₁₄-ZnP. The first, second, and third layer are represented by dark gray, medium gray, and light gray respectively.

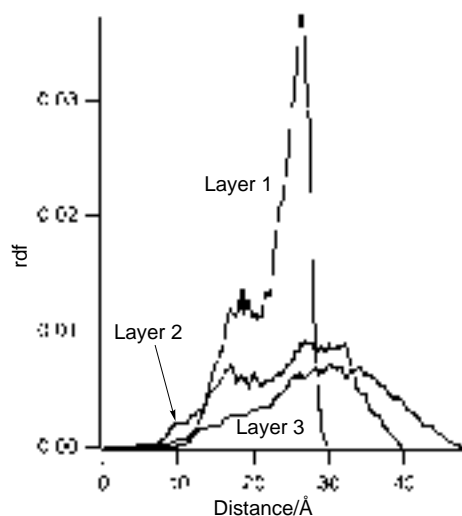


Figure 3. Radial distribution function (per single atom) of the iron atoms in each layer in G3(Fc)₁₄-ZnP.

IX-F-2 Reconstitution of the Water-Oxidizing Complex in Manganese-Depleted Photosystem II Preparations Using Binuclear Mn(II) and Mn(IV) Complexes

NAGATA, Toshi; NAGASAWA, Takayuki;
ZHARMUKHAMEDOV, Sergei K.¹;
ALLAKHVERDIEV, Suleyman I.²

(¹Inst. Basic Biological Problems, Russian Acad. Sci.;
²IMS and Inst. Basic Biological Problems, Russian Acad. Sci.)

Reconstitution of the Mn-depleted Photosystem II (PSII) particles with synthetic binuclear Mn complexes (two Mn(II)₂ complexes and one Mn(IV)₂ complex) was examined. The reconstituted PSII particles showed lower restored activities than our previous studies in photo-induced electron transfer and oxygen evolution. These results were ascribed to the "robustness" of the Mn complexes used in this study. The ESI-MS spectra of the Mn(II)₂ complexes showed that the macrocyclic ligand remained intact even after release of the Mn(II) ions, so it was proposed that the macrocyclic ligand remained in the vicinity of the PSII proteins and caused distortion of the protein structures. On the other hand, the lower activity of the Mn(IV)₂ complex was ascribed to the robustness of the bis- μ -oxo structure which caused transfer of the Mn ions to the PSII protein less efficient than the previously examined Mn complexes with mono-nuclear or mono- μ -oxo binuclear structures. These results implies that subtle balance between the stability and lability of the complexes are important in successful reconstitution of PSII.

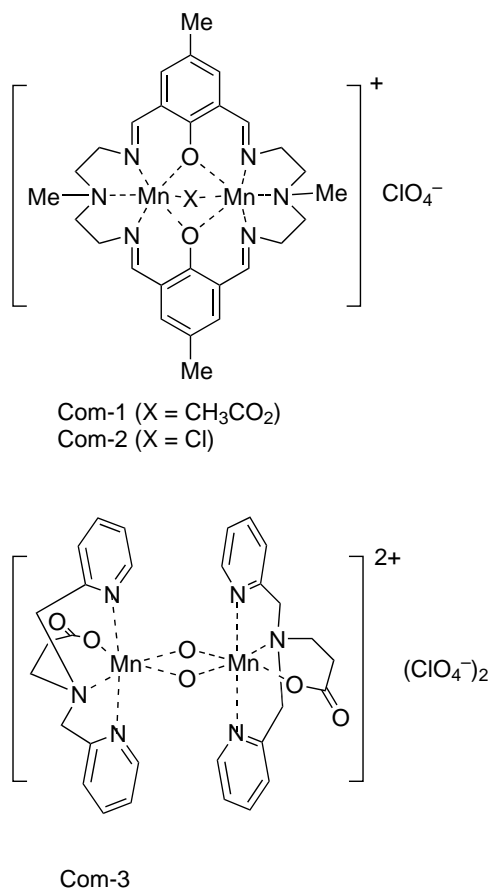


Figure 1. The structures of the synthetic dimanganese complexes.

IX-G Development of New Metal Complexes as Redox Catalysts

Redox catalysis is an important field of chemistry which translates a flow of electron into chemical transformation. It is also one of the requisites for artificial photosynthesis. This project of ours aims at developing new metal complexes that perform redox catalysis at low overpotential. Currently we are focusing our attention to the development of a series of cobalt phosphine complexes as possible catalysts for electrochemical reductions.

IX-G-1 Syntheses and Structures of Co(I) Complexes Having Cyclopentadienyl Auxiliaries and C-P Bond Cleavage of the Coordinated Phosphine

NAGASAWA, Takayuki; NAGATA, Toshi

The strong basicity of low-valent cobalt complexes are attractive in electrocatalytic organometallic chemistry. Here we report the syntheses and molecular structures of Co(I) complexes with cyclopentadienyl derivatives and an unexpected cleavage of a C-P bond in triphenylphosphine by Co(I) under mild conditions.

Reactions of ClCo(PPh₃)₃ with sodium salts of cyclopentadienyl derivatives NaCp^R (R = H, COOMe, CH₂CH₂SMe) gave five-coordinate Co(I) complexes

Cp^RCo(PPh₃)₂ (R = H, **2**; COOMe, **3**; CH₂CH₂SMe, **4**) in 60–80% yields as crystals. The structures of **2–4** were determined by X-ray crystallography (Figure 1).

On the other hand, the reaction of LiCp* (Cp* = C₅Me₅) with ClCo(PPh₃)₃ resulted in a formation of a diamagnetic dimer complex [Cp*Co(μ-Ph)(μ-PPh₂)CoCp*], **5**, which has bridging phenyl and diphenylphosphide groups. This compound was isolated from hexane solution as black crystals in 64% yield. The structure was confirmed by X-ray crystallography (Figure 2). We propose that the bridging phenyl and phosphide ligands were generated by a C-P bond cleavage caused by the action of the strongly nucleophilic Cp*Co fragment.

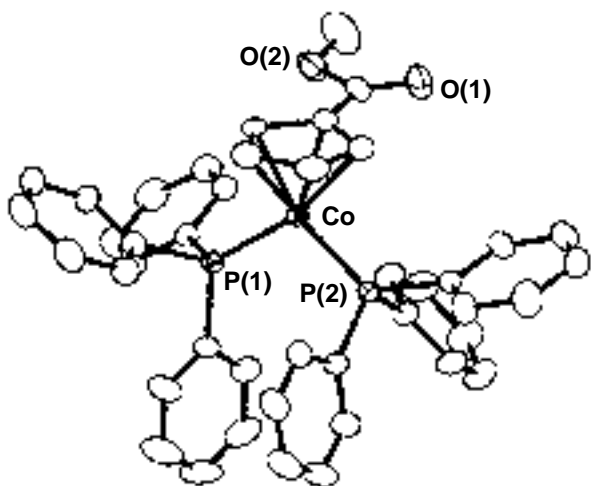


Figure 1. The ORTEP drawing of 3.

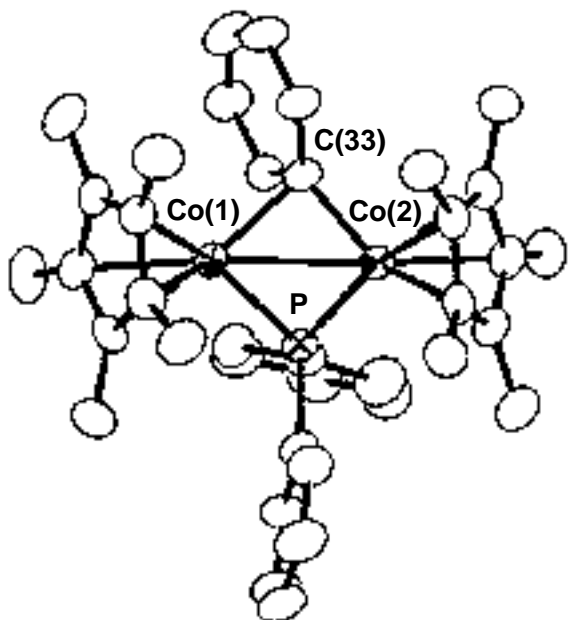


Figure 2. The ORTEP drawing of 5.

IX-H Synthesis of Buckybowls and Heterobuckybowls

Bowl-shaped π -conjugated compounds including partial structures of the fullerenes, which are called "buckybowls," are of importance not only as model compounds of fullerenes but also as their own chemical and physical properties. Heteroatom-containing buckybowls (heterobuckybowls) have also been expected to exhibit unique physical characters. For example, in solution they show the characteristic dynamic behavior such as bowl-to-bowl inversion. On the other hand, they sometimes favor stacking structure in a concave-convex fashion in the solid state, giving excellent electron conductivity. Furthermore, some buckybowls are conceivable to possess the bowl-chirality if the racemization process, as equal as bowl-to-bowl inversion, is slow enough to be isolated. However, very few buckybowls/heterobuckybowls has been achieved for preparation mainly due to their strained structure, and no report on the preparation of chiralbowls has appeared. In addition, most of thus-reported procedures are performed under severe reaction conditions, limiting the sort of the introducible atoms/functional groups.

In the present project, we develop the rational route to the various kinds of buckybowls/heterobuckybowls using the organic synthesis approach.

IX-H-1 Regio- and Stereo-Selective Synthesis of Multi-Substituted Benzene Derivatives by Cyclotrimerization of Haloalkene Derivatives

SAKURAI, Hidehiro; HIGASHIBAYASHI, Shuhei

Bridged multi-substituted benzene derivatives have been of interest because of the bond alternation of benzene ring and the utility for syntheses of cup-shaped molecules or buckybowls. The regio- and stereo-selective syntheses are important for the synthetic utility. Chiral multi-substituted benzene derivatives were synthesized from chiral halonorbornene derivatives through the regio- and stereo-selective cyclotrimerization catalyzed by palladium nanocluster. Thus prepared chiral benzene derivatives are expected to serve as the synthetic intermediates for chiral buckybowls.

IX-I Spectroscopy and Chemistry of Metal Nanoclusters on Surfaces

The structure and reactivity of metal nanoclusters are important issues because of their relevance to heterogeneous catalysis. In particular, Au nanoclusters on titanium oxide surfaces has attracted a lot of interest since the discovery of its catalytic activity on CO oxidation. We apply various surface science techniques to clarify correlations between structures and reactivity of metal nanoclusters deposited on surfaces. In this year, we use alkanethiolate-coated gold nanoclusters as a primary target in collaboration with Tsukuda (IMS) and Al-Shamery (U. Oldenburg) groups.

IX-I-1 STM Observation and Fabrication of Films of Gold Nanoclusters with and without Alkanethiolate Ligands on TiO₂(110)

MATSUMOTO, Taketoshi; NICKUT, Patricia¹; SAWADA, Takeshi; TSUNOYAMA, Hironori; WATANABE, Kazuya; TSUKUDA, Tatsuya; AL-SHAMERY, Katharina¹; MATSUMOTO, Yoshiyasu
(¹Carl v. Ossietzky U. Oldenburg)

Films of Au nanoclusters protected with alkanethiolate ligands fabricated before and after etching on the TiO₂(110) surface were investigated by scanning tunneling microscopy (STM) and X-ray photoelectron spectroscopy (XPS). The Au nanoclusters were produced by reducing HAuCl₄ in micelles and fractionalized by

size with gel permeation chromatography. Au nanoclusters with hexanethiolate formed single layers and were coated on TiO₂(110). Replacing the ligands with *n*-octadecanethiolate resulted in forming three layers. Au nanoclusters with ligands are mobile on TiO₂ at room temperature and it is possible to manipulate their positions by a STM tip. XPS spectra showed that O-atom etching removes ligands effectively and produces gold oxide on nanocluster surfaces. The oxide was reduced effectively by H atom etching. These etching procedures causes aggregation of Au nanoclusters, increasing apparent height from ~1.5 nm to 3–6 nm. Adding hexanethiol and decane to the films of Au nanocluster with hexanethiolate did not show significant changes before and after etching. No diffusion was induced by STM tips after O atom etching.

IX-J Photochemistry on Well-Defined Surfaces

Upon the irradiation of light in the wavelength range from visible to ultraviolet, a number of adsorbed molecules on metal surfaces reveal variety of photochemical processes, including photo-stimulated desorption, rearrangement of adsorbed states, photodissociation, and photo-initiated reactions with coadsorbates. A central and fundamental question in the surface photochemistry is to clarify how adsorbate-substrate systems are excited by photon irradiation. In addition, since photo-initiated reactions can be induced without any thermal activation of reactants, they may provide good opportunities for studying a new class of surface reactions that may not be induced thermally. We have studied photochemistry of various adsorption systems on well-defined metal and semiconductor surfaces mainly by temperature-programmed desorption (TPD), infrared reflection absorption spectroscopy (IRAS), x-ray photoelectron spectroscopy (XPS), work function measurements, and angular-resolved time-of-flight (TOF) mass spectrometry of photodesorbed species associated with pulsed laser irradiation. In this year, the photochemistry of cyclic alkane on Pt(111) and Cu(111) surfaces was studied mainly by TPD, XPS, and IRAS.

IX-J-1 Photochemistry of Cyclohexane on Cu(111)

YAMAGUCHI, Dai; MATSUMOTO, Taketoshi; WATANABE, Kazuya; TAKAGI, Noriaki¹; MATSUMOTO, Yoshiyasu
(¹SOKENDAI and Univ. Tokyo)

[*Phys. Chem. Chem. Phys.* **8**, 179–185 (2006)]

The photochemistry of cyclohexane on Cu(111) and its excitation mechanism have been studied by temperature-programmed desorption, ultraviolet and X-ray photoelectron spectroscopy. Cyclohexane weakly adsorbed on Cu(111) has been known to show a broadened

and redshifted CH stretching band, *i.e.*, CH vibrational mode softening. Although no dehydrogenation takes place thermally on this surface and by the irradiation of photons at 5.0 eV, adsorbed cyclohexane is dissociated to cyclohexyl and hydrogen by the irradiation of photons at 6.4 eV. This is a marked contrast to cyclohexane in the gas phase where the onset of absorption is located at 7 eV. When the surface irradiated by 6.4-eV photons is further annealed, cyclohexyl is dehydrogenated to form cyclohexene that desorbs at 230 K. The systematic measurements of photochemical cross sections at 6.4 eV with linearly polarized light as a function of incident angle indicate that the electronic transition from the highest occupied band of cyclohexane to a partially occupied hybridized band near the Fermi level is respon-

sible for the photochemistry. The hybridized band is formed by the interactions between the electronic states of cyclohexane and the metal substrate. The role of the hybridized band in the photochemistry and the CH vibrational mode softening is discussed.

IX-J-2 Photochemistry and Post-Irradiation Chemistry of Cyclohexane on Pt(111)

YAMAGUCHI, Dai; MATSUMOTO, Taketoshi; WATANABE, Kazuya; TAKAGI, Noriaki¹; MATSUMOTO, Yoshiyasu
(¹SOKENDAI and Univ. Tokyo)

Photochemistry and post-irradiation thermal chemistry of cyclohexane on Pt(111) were investigated by TPD, XPS and IRAS. From TPD results, photo-dehydrogenation of cyclohexane was confirmed on Pt(111). IRAS spectra after photo-irradiation indicate that the primary photoproduct is cyclohexyl. The photoreaction cross sections of cyclohexane on Pt(111) at 6.4 and 5.0 eV are $(3.1 \pm 0.2) \times 10^{-21}$ and $(1.1 \pm 0.6) \times 10^{-21}$ cm², respectively. The appreciable cross section at 5.0 eV suggests the larger adsorbate interactions on Pt(111)

compared with those on Cu(111). The excitation mechanism was investigated by the same procedure for Cu(111). The cross sections with p-polarized light again deviate from the absorbance of the substrate. This indicates clearly that the excitation mechanism is the same on Cu(111). On Pt(111), it has been known that cyclohexane is thermally dehydrogenated to benzene *via* C₆H₉. Benzene converted from the monolayer of cyclohexane does not desorb molecularly because benzene is further dehydrogenated to atomic C. In contrast, after photo-irradiation at 6.4 eV, the desorption of benzene in post-irradiation TPD was clearly observed. Then, the thermal reactions of the primary photoproduct, cyclohexyl, were investigated by IRAS. Absorption bands attributable to cyclohexene appeared at 200 K. This species has not been identified in the studies on thermal reactions of cyclohexane on Pt(111). UV photons can produce a larger amount of cyclohexyl than that induced thermally. In this case, the adsorption sites are largely occupied by produced cyclohexyl and hydrogen, which may increase the activation barriers for dehydrogenation of cyclohexene and benzene in the post-irradiation thermal chemistry.

IX-K Ultrafast Dynamics at Well-Defined Surfaces

To understand the mechanism of surface photochemistry, it is vital to know how photoinduced electronic excitation induces adsorbate nuclear motions that ultimately lead to chemical reactions. We demonstrate the real-time observations of surface phonons and adsorbate-substrate vibrational modes by fs time-resolved second harmonics generation (TRSHG). If an excitation light pulse has a duration sufficiently shorter than a period of a vibrational mode or a phonon mode, it can excite the mode with a high degree of temporal and spatial coherence. This coherent nuclear motion modulates the second-order susceptibility $\chi^{(2)}$. Thus, by monitoring the intensity modulation of the second harmonics (SH) generation of a probe pulse, we can observe the evolution of the coherent nuclear motion subsequent to the electronic excitation at the surfaces. This year, in particular, we have focused on K on Pt(111) and Na on Cu(111) adsorption systems.

IX-K-1 Coherent Surface Phonon Dynamics at K-Covered Pt(111) Surfaces Investigated by Time-Resolved Second Harmonic Generation

FUYUKI, Masanori¹; WATANABE, Kazuya; MATSUMOTO, Yoshiyasu
(¹SOKENDAI)

[Phys. Rev. B submitted]

We have investigated coherently excited surface phonons at K-covered Pt(111) surfaces by using femto-second time-resolved second harmonic generation spectroscopy. The frequency of the K–Pt stretching phonon mode depends on the superstructure of K: 5.0–5.3 and 4.5–4.8 THz for (2×2) and $(\sqrt{3} \times \sqrt{3})R30^\circ$ superstructures, respectively. In addition to the stretching mode, a couple of Pt surface phonon modes are simultaneously observed when the $(\sqrt{3} \times \sqrt{3})R30^\circ$ superstructure is formed. The dephasing time of the K–Pt stretching mode becomes shorter and its frequency redshifts as the absorbed fluence of a pump pulse increases. This is

in stark contrast to the Pt surface phonon modes whose frequencies are independent of fluence. The fluence dependence of the K–Pt stretching mode is interpreted to be due to anharmonic coupling between the K–Pt stretching and lateral modes.

IX-K-2 Excitation Mechanism of Coherent Surface Phonons on Na-Covered Cu(111)

FUYUKI, Masanori¹; WATANABE, Kazuya; INO, Daisuke¹; MATSUMOTO, Yoshiyasu
(¹SOKENDAI)

We observed time-resolved second harmonic signals from the Cu(111) surface with a full monolayer of Na in ultra-high vacuum and investigated the excitation-wavelength dependence of the wave packet dynamics of the coherently excited Na–Cu stretching mode. Changing the photon energy of the pump pulse (25 fs) from 2.0 to 2.5 eV, the oscillation amplitude derived from the Na–Cu stretching motion is enhanced. The careful measurements of photon-energy dependence indicates that the

excitation efficiency mimics the absorbance of bulk Cu. Holes created in the d-bands by the optical transitions could be filled by electrons in the adsorbate-induced occupied state of the metallic quantum well by an Auger-type transition. Hence, holes can be created in the adsorbate-induced occupied state. Moreover, since this Auger decay can occur significantly faster than the oscillation period of the Na–Cu stretching mode, the substrate excitation may be a possible excitation mechanism for the coherent oscillation.

IX-K-3 Electron Transfer Dynamics from Organic Adsorbate to a Semiconductor Surface: Zinc-Phthalocyanine on TiO₂(110)

INO, Daisuke¹; WATANABE, Kazuya; TAKAGI, Noriaki²; MATSUMOTO, Yoshiyasu
(¹SOKENDAI; ²Univ. Tokyo)

[*J. Phys. Chem. B* **109**, 18018–18024 (2005)]

The femtosecond time-evolutions of excited states in zinc-phthalocyanine (ZnPC) films and at the interface with TiO₂(110) have been studied by using time-resolved two-photon photoelectron spectroscopy (TR-2PPE). The excited states are prepared in the first singlet

excited state (S₁) with excess vibrational energy. Two different films are examined: ultrathin (monolayer) and thick films of ~30 Å in thickness. The decay behavior depends on the thickness of the film. In the case of the thick film, TR-2PPE spectra are dominated by the signals from ZnPC in the film. The excited states decay with $\tau = 118$ fs mainly by intramolecular vibrational relaxation. After the excited states cascaded down to near the bottom of the S₁ manifold, they decay slowly ($\tau = 56$ ps) although the states are located at above the conduction band minimum of the bulk TiO₂. The exciton migration in the thick film is the rate determining step for the electron transfer from the film to the bulk TiO₂. In the case of the ultrathin film, the contribution of electron transfer is more evident. The excited states decay faster than those in the thick film, because the electron transfer competes with the intramolecular relaxation processes. The electronic coupling with empty bands in the conduction band of TiO₂ plays an important role in the electron transfer. The lower limit of the electron transfer rate was estimated to be 1/296 fs⁻¹. After the excited states relax to the states whose energy is below the conduction band minimum of TiO₂, they decay much slowly because the electron transfer channel is not available for these states.

IX-L Vibrational Dynamics at Surfaces and Interfaces Studied by Time-Resolved Sum Frequency Spectroscopy

In addition to time-resolved second harmonic generation and two-photon photoemission spectroscopy, we have developed fs time-resolved sum frequency generation (SFG) spectroscopy to study ultrafast surface dynamics. Time-resolved SFG is a versatile tool for investigating vibrational dynamics at surfaces and interfaces. In this year, we applied this technique to probe vibrational energy transfer at the interface between Pt(111) and ice layers where CO monolayer is inserted.

IX-L-1 Vibrational Energy Relaxation at the Interface of Ice/CO/Pt(111) Studied by fs Time-Resolved Sum Frequency Generation

NAGAO, Masashi; WATANABE, Kazuya; MATSUMOTO, Yoshiyasu

We studied the vibrational excitation and relaxation dynamics of surface adsorbate for D₂O/CO/Pt(111) by the femtosecond time resolved vibrational SFG spectroscopy (VIS: 800 nm, 3 ps; IR: 3–5 μm, 130 fs; pump: 400 nm, 130 fs) under ultra vacuum condition. D₂O/CO/Pt(111) was prepared by dosing D₂O molecules on the CO covered Pt(111) surface at 140 K. Two peaks were observed in CO stretching region at 2068 and 2095 cm⁻¹ when 10 ML D₂O layer was formed on the surface, because D₂O crystals exhibit island growth on this surface. The former peak (ν*(CO)) is assigned to the adsorbed CO intact with D₂O and the latter (ν(CO)) is assigned to the CO free from D₂O. Both peaks were

redshifted and broadened by the irradiation of a pump pulse, because the frustrated translation and rotation modes of CO coupled to Pt hot electrons generated by the excitation pulse. We found the following features in the transient SFG spectra. The maximum peak shift of ν*(CO) was larger than that of ν(CO) and the peak shift of ν*(CO) shows much faster recovery than that of ν(CO) within 3 ps after the excitation. We analyze the spectra by the numerical simulation of SFG polarization based on the Bloch equations, which describe the time-dependent evolution of the density matrix for the CO stretching mode. The transient response of time-resolved SFG spectra can be characterized by the time dependent adsorbate temperature, where the key parameter is the time scale on which energy flows between substrate electrons and the CO frustrated mode, τ_e. To reproduce the experimental data, coupling times of τ_e = 0.8 ps and τ_e = 1.6 ps for ν*(CO) and ν(CO), respectively, are required, indicating that the ν*(CO) mode couples to the substrate hot electrons more effectively than ν(CO).

IX-M Chemistry of One-Dimensional Nano-Surface Compounds Studied by Scanning Tunneling Microscopy

The fluctuating configurations of low-dimensional structures can be thermodynamically favorable at finite temperatures, because the energy gain overcomes the energy cost that accompanies local structural fluctuation. In particular, one-dimensional (1D) systems have a propensity to be sensitive to these fluctuations as described by one of the maxims of condensed matter physics, *i.e.*, one chain does not make a crystal. Thus, the dynamical formation of active species and sites by these fluctuations is a key factor in establishing a microscopic model for chemical reactions at surfaces and nano-structured compounds.

IX-M-1 Direct Observation of a Propagating Chemical Wave in Disproportionation Reactions of Water on Oxidized Ag(110) Surface by Scanning Tunneling Microscopy

NAKAGOE, Osamu¹; TAKAGI, Noriaki²;
WATANABE, Kazuya; MATSUMOTO, Yoshiyasu
(¹SOKENDAI; ²Univ. Tokyo)

[*J. Phys. Chem. B* submitted]

It is well known that the adsorption of O on Ag(110) results in the formation of quasi-1D structures, AgO chains, accompanied by the mass transfer of substrate atoms. AgO chains arrange periodically to form ($n \times 1$) ($n = 2 \sim 7$) depending on the fractional O coverage due to repulsive inter-chain interactions. On the added-row reconstructed Ag(110)($n \times 1$)-O surfaces, one-dimensional -Ag-O-Ag-O- chains arrange periodically. Scanning tunneling microscopy was used for studying spatio-temporal evolution of the disproportionation reaction of H₂O with O adatoms on oxidized Ag(110) surfaces where quasi-one dimensional AgO chains form ordered structures. Initially the reaction takes place slowly on Ag(110)-(5 \times 1)O at the end of AgO chain, whereas the reaction accelerates explosively upon the appearance of a chemical wave that propagates along the direction perpendicular to the chain. The surface morphology of the region swept over by the chemical wave completely changes from (5 \times 1)-O to that with many rectangular islands, indicating the formation of H₂O(OH)₂. The induction time and explosive acceleration with the propagating chemical wave imply that the reaction is autocatalytic. Water clusters hydrating OH produced likely play a central role in serving as a reservoir of H₂O to feed to the reaction and enhancing the reactivity of H₂O with O adatoms in AgO chains.

IX-N Structures, Stabilities and Physicochemical Properties of Organometallic Hybrid Clusters

Recently, metal clusters have gained much attention because they exhibit novel physicochemical properties that are beyond the prediction made by a dimensional scaling of those of the corresponding bulk. In this regard, metal clusters protected by thiolates or stabilized by polymers are promising candidates for elementary units of nano-scale devices. Our interests are focused on the following issues on the organometallic hybrid clusters: (1) a large-scale preparation of the subnanometer-sized clusters, (2) development of size-selection method, (3) determination of chemical compositions of size-selected clusters (*i.e.* the numbers of metal atoms and organic molecules), and (4) elucidation of effect of the core size, core shape, and interaction with organic molecules on stabilities, electronic structures, and chemical properties.

IX-N-1 Aerobic Oxidation Catalyzed by Gold Nanoclusters as *quasi*-Homogeneous Catalysts: Generation of Hydrogen Peroxide Using Ammonium Formate

SAKURAI, Hidehiro; TSUNOYAMA, Hironori; TSUKUDA, Tatsuya

[*Trans. Mater. Res. Soc. Jpn.* **31**, 521–524 (2006)]

Gold(0) nanocluster with $d_{av} = 1.3 \pm 0.3$ nm stabilized by poly(*N*-vinyl-2-pyrrolidone) (Au:PVP-1) showed high catalytic activity toward the generation of hydrogen peroxide in water under ambient conditions using ammonium formate as a reductant. Generation of hydrogen peroxide was monitored by tracking the conversion of *o*-tolylboronic acid to *o*-cresol. In the presence of excess ammonium formate, *o*-cresol was obtained from *o*-tolylboronic acid with ~60% yield within 24 hours at 300 K. In order to investigate the dependence of the reactivity on cluster size, monodisperse gold nanoclusters (Au:PVP-*n*; *n* = 2–4) with average diameters up to ~5 nm were prepared by the seed-mediated growth method using Na₂SO₃ as a reductant. Smaller cluster showed superior catalytic activity compared to larger clusters, suggesting that molecular oxygen species preferentially adsorbed on small Au clusters played an essential role in the formation of hydrogen peroxide.

IX-N-2 Spectroscopic Investigation of Dendrimer-Encapsulated Gold Clusters

IMAMURA, Masaki¹; MIYASHITA, Takeho¹; TANAKA, Akinori¹; YASUDA, Hidehiro¹; YANAGIMOTO, Yasushi; NEGISHI, Yuichi; TSUKUDA, Tatsuya
(¹Kobe Univ.)

[*Trans. Mater. Res. Soc. Jpn.* **31**, 517–520 (2006)]

We have carried out the spectroscopic studies of dendrimer-encapsulated Au nanoclusters smaller than 2.4 nm. In this study, a 1.5th generation sodium carboxylate-terminated polyamidamine dendrimer was used as a template to control the size and stability of Au nanoclusters. The dendrimer-encapsulated Au nanoclusters were prepared by the chemical reduction of Au ions loaded within the dendrimer templates. The synthesized smallest nanocluster used in this work shows the

strong blue photoluminescence at 2.8 eV photon energy, while larger nanocluster shows no photoluminescence. Furthermore, we carried out the X-ray photoemission study in the valence-band region of dendrimer-encapsulated Au nanocluster. From these results, we will discuss the size dependent properties of Au nanoclusters encapsulated within the dendrimer templates.

IX-N-3 Chromatographic Isolation of “Missing” Au₅₅ Clusters Protected by Alkanethiolates

TSUNOYAMA, Hironori; NEGISHI, Yuichi; TSUKUDA, Tatsuya

[*J. Am. Chem. Soc.* **128**, 6035–6037 (2006)]

We report on the first synthesis of alkanethiolate-protected Au₅₅ (11 kDa), which has been a “missing” counterpart of Schmid’s Au₅₅(PR₃)₁₂Cl₆. Au:SC_x clusters (*x* = 12, 18) were prepared by the reaction of alkanethiol (C_xSH) with polymer-stabilized Au clusters (~1.3 nm) and subsequently incubated in neat C_xSH. The resulting clusters were successfully fractionated by recycling gel permeation chromatography into Au_{~38}:SC_x and Au_{~55}:SC_x, and identified by laser-desorption ionization mass spectrometry. The Au_{~55}:SC_x clusters exhibited structured optical spectra, suggesting molecular-like properties. The thiolate monolayers were found to be liquid-like on the basis of the IR spectrum and the monolayer thickness estimated from the hydrodynamic diameter.

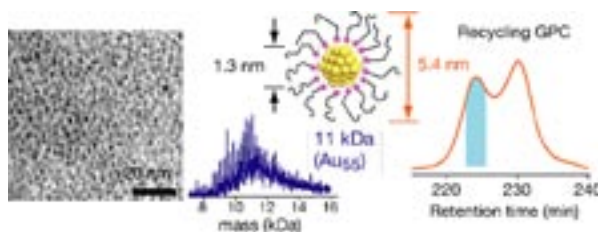


Figure 1. Isolation and characterization of Au₅₅:SC_x. [Reprinted with permission from *J. Am. Chem. Soc.* **128**, 6035–6037 (2006). Copyright (2006) American Chemical Society.]

IX-N-4 Chiroptical Activity of BINAP-Stabilized Undecagold Clusters

YANAGIMOTO, Yasushi; NEGISHI, Yuichi;

FUJIHARA, Hisashi¹; TSUKUDA, Tatsuya
(¹Kinki Univ.)

[*J. Phys. Chem. B* **110**, 11611–11614 (2006)]

Undecagold cluster compounds $[\text{Au}_{11}(\text{BINAP})_4\text{X}_2]^+$ ($\text{X} = \text{Cl}$ and Br) were synthesized by chemical reduction of the corresponding precursor complexes, Au_2X_2 (BINAP), where BINAP represents the bidentate phosphine ligand 2,2'-bis(diphenylphosphino)-1,1'-binaphthyl. The circular dichroism spectra of Au_{11} stabilized by the enantiomers $\text{Au}_{11}(\text{R-BINAP})_4\text{X}_3$ and $\text{Au}_{11}(\text{S-BINAP})_4\text{X}_3$ exhibited intense and mirror-image Cotton effect, whereas those of Au_{11}^{3+} clusters stabilized by achiral monodentate phosphine ligands did not. The origin of the chiroptical activity of $[\text{Au}_{11}(\text{BINAP})_4\text{X}_2]^+$ is discussed in the context of the structural deformation of the Au_{11}^{3+} core.

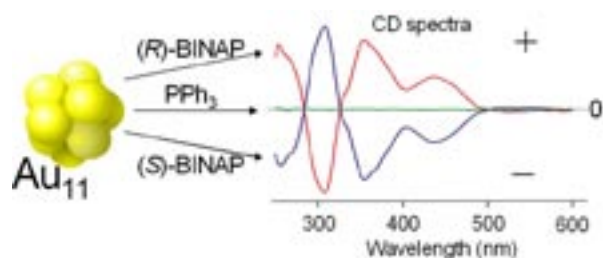


Figure 1. CD spectra of $[\text{Au}_{11}(\text{BINAP})_4\text{X}_2]^+$. [Reprinted with permission from *J. Phys. Chem. B* **110**, 11611–11614 (2006). Copyright (2006) American Chemical Society.]

IX-N-5 Kinetic Stabilization of Growing Gold Clusters by Passivation with Thiolates

NEGISHI, Yuichi; TAKASUGI, Yoshimitsu¹; SATO, Seiichi¹; YAO, Hiroshi¹; KIMURA, Keisaku¹; TSUKUDA, Tatsuya
(¹Univ. Hyogo)

[*J. Phys. Chem. B* **110**, 12218–12221 (2006)]

Small gold clusters (<1 nm), protected by monolayers of glutathione, *N*-(2-mercaptopropionyl)glycine or mercaptosuccinic acid, were prepared by reducing the corresponding Au(I)–thiolate polymers, and were fractionated by size using polyacrylamide gel electrophoresis (PAGE). Mass analysis of the fractionated clusters revealed that their core sizes varied with the molecular structures of the thiolates. This finding indicates that the reduction of the Au(I)–thiolate polymers yields small clusters whose growth is kinetically hindered by passivation with thiolates. Optical spectra of the clusters with identical compositions exhibited different profiles depending on the thiolate molecular structures, implying that deformation of the underlying gold cores is induced by inter-ligand interactions.

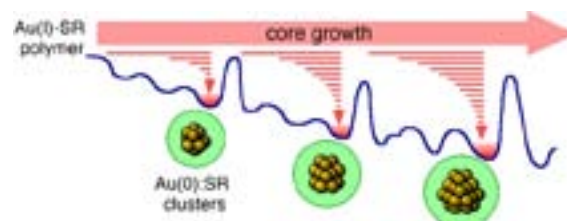


Figure 1. Kinetic stabilization of growing gold clusters by passivation with thiolates.

[Reprinted with permission from *J. Phys. Chem. B* **110**, 12218–12221 (2006). Copyright (2006) American Chemical Society.]

IX-N-6 Size Effect on the Catalysis of Gold Clusters Dispersed in Water for Aerobic Oxidation of Alcohol

TSUNOYAMA, Hironori; SAKURAI, Hidehiro; TSUKUDA, Tatsuya

[*Chem. Phys. Lett.* **429**, 528–532 (2006)]

We prepared a set of nearly monodisperse gold clusters ranging from 1.3 to 10 nm by a seed-mediated growth in the presence of poly(*N*-vinyl-2-pyrrolidone) (PVP). The seed clusters with a diameter of 1.3 ± 0.3 nm were prepared by reducing AuCl_4^- with NaBH_4 in a low-temperature aqueous solution of PVP. Subsequent reduction of more AuCl_4^- by Na_2SO_3 in the presence of the seed clusters yielded a series of larger Au:PVP clusters. Catalytic activities of the Au:PVP clusters for aerobic oxidation of *p*-hydroxybenzyl alcohol increased with decrease in the core size. The size dependence is discussed in light of the electronic structures of the cores probed by optical spectroscopy.

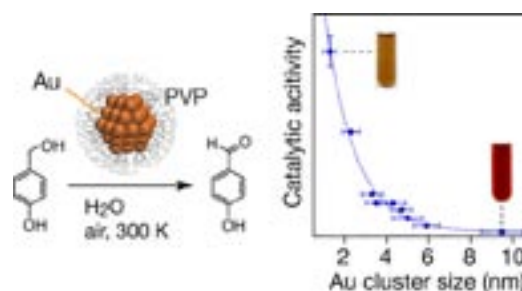


Figure 1. Catalytic activities of the Au:PVP clusters for aerobic oxidation of *p*-hydroxybenzyl alcohol increased with decrease in the core size.

[Reprinted with permission from *Chem. Phys. Lett.* **429**, 528–532 (2006). Copyright (2006) Elsevier.]

IX-N-7 X-Ray Magnetic Circular Dichroism of Size-Selected, Thiolated Gold Clusters

NEGISHI, Yuichi; TSUNOYAMA, Hironori; SUZUKI, Motohiro¹; KAWAMURA, Naomi¹; MATSUSHITA, M. Michio²; MARUYAMA, Koichi; SUGAWARA, Tadashi²; YOKOYAMA, Toshihiko; TSUKUDA, Tatsuya
(¹JASRI/SPring-8; ²Univ. Tokyo)

[*J. Am. Chem. Soc.* **128**, 12034–12035 (2006)]

We report herein the X-ray magnetic circular dichroism (XMCD) at the Au $L_{2,3}$ edges of a series of Au clusters protected by glutathione (GSH). The samples used here included $Au_N(SG)_M$ with $(N, M) = (10, 10), (15, 13), (18, 14), (22, 16), (25, 18), (29, 20), (39, 24)$ and a sodium gold(I) thiomalate (SGT) as a reference. Magnetic moments per cluster were found to be increased with size, whereas those per Au–S bond were nearly constant. This finding suggests that a localized hole created by Au–S bonding at the gold/glutathione interface, rather than the quantum size effect, is responsible for the spin polarization of gold clusters.

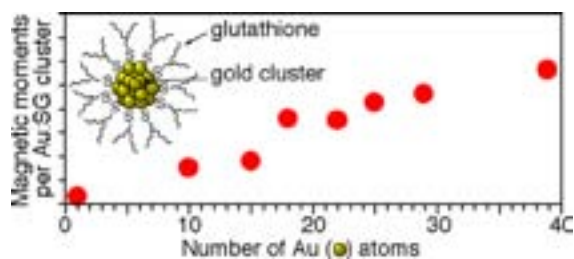


Figure 1. Magnetic moments per cluster as a function of core size.

[Reprinted with permission from *J. Am. Chem. Soc.* **128**, 12034–12035 (2006). Copyright (2006) American Chemical Society.]

IX-N-8 Mechanism of Selective Formation of Thiolated Au_{25} Clusters in Ligand Exchange of Phosphine-Stabilized Gold Clusters: Size Focusing *via* Core Etching

SHICHIBU, Yukatsu; NEGISHI, Yuichi;
TSUNOYAMA, Hironori; KANEHARA, Masayuki¹;
TERANISHI, Toshiharu¹; TSUKUDA, Tatsuya
(¹Univ. Tsukuba)

Recently, we have succeeded in large-scale selective synthesis of $Au_{25}:SG$ clusters *via* ligand exchange reactions of triphenylphosphine-stabilized Au_{11} clusters with glutathione (GSH) under optimized conditions (Shichibu, Y. *et al.* *J. Am. Chem. Soc.* **127**, 13464 (2005)). The mechanism of the selective formation of $Au_{25}:SG$ was studied by monitoring the size distribution of the ligand exchange products using electrophoresis and optical absorption spectroscopy. It was found that the core size distributions of the $Au_n:SG$ clusters extracted at the initial stage are polydisperse and are subsequently focused into $Au_{25}:SG$ in the presence of free GSH molecules. The reaction of a series of the size-selected $Au_n:SG$ clusters ($n = 10, 15, 18, 22, 25, 29, 33, 39$) with free GSH under aerobic conditions revealed that two different reaction modes are operative depending on the core size. The $Au_n:SG$ ($n < 25$) clusters are completely oxidized to $Au(I):SG$ complexes while $Au_n:SG$ ($n \geq 25$) clusters are etched into $Au_{25}:SG$ by free GSH molecules. This indicates that the “ligand exchange reaction” we referred to in our previous paper, consists of two processes, *i.e.*, a ligand exchange accompanying rapid agglomeration of Au cores and subsequent etching of the cores. We conclude that the extremely high stability of $Au_{25}:SG$ clusters against etching is the main cause for the selective formation.

Other gold clusters stabilized by polymer ($\phi = 1.3 \pm 0.3$ nm) or triphenylphosphine ($\phi = 1.5 \pm 0.4$ nm) were also converted selectively to $Au_{25}:SG$ by treatment with excess GSH, supporting the proposed mechanism.

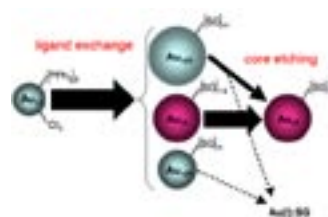


Figure 1. Mechanism of size focusing in the ligand exchange.

IX-O Structural Analyses of Biological Macromolecules by Ultra-High Field NMR Spectroscopy

Our research seeks the underlying molecular basis for the function of biological macromolecules. In particular, we are interested in the function of molecular machines that work in the cellular processes involving protein folding, transport and degradation, and of glycoproteins playing important roles in the humoral and cellular immune systems. By use of ultra-high field NMR spectroscopy, we aim to elucidate the three-dimensional structure, dynamics, and interactions of proteins and glycoconjugates at the atomic level. Here we report stable-isotope-assisted NMR studies of Ufm1, a ubiquitin-like modifier, and IgG-Fc glycoprotein.

IX-O-1 Solution Structure and Dynamics of Ufm1, a Ubiquitin-Fold Modifier 1

SASAKAWA, Hiroaki¹; SAKATA, Eri²;
YAMAGUCHI, Yoshiki¹; KOMATSU, Masaaki³;
TATSUMI, Kanako⁴; KOMINAMI, Eiki⁵; TANAKA,
Keiji⁴; KATO, Koichi¹

(¹IMS and Nagoya City Univ.; ²Nagoya City Univ.;
³Tokyo Metropolitan Inst. Medical Sci. and Juntendo
Univ.; ⁴Tokyo Metropolitan Inst. Medical Sci.;
⁵Juntendo Univ.)

[*Biochem. Biophys. Res. Commun.* **343**, 21–26 (2006)]

The ubiquitin-fold modifier 1 (Ufm1) is one of various ubiquitin-like modifiers and conjugates to target proteins in cells through Uba5 (E1) and Ufc1 (E2). The Ufm1-system is conserved in metazoa and plants, suggesting its potential roles in various multicellular organisms. Herein, we analyzed the solution structure and dynamics of human Ufm1 (hsUfm1) by nuclear magnetic resonance spectroscopy. Although the global fold of hsUfm1 is similar to those of ubiquitin (Ub) and NEDD8, the cluster of acidic residues conserved in Ub and NEDD8 does not exist on the Ufm1 surface. ¹⁵N spin relaxation data revealed that the amino acid residues of hsUfm1 exhibiting conformational fluctuations form a cluster at the C-terminal segment and its spatial proximity, which correspond to the versatile ligand-binding sites of Ub and other ubiquitin-like proteins (Ubls). We suggest that Ub and other Ubl-modifiers share a common feature of potential conformational multiplicity, which might be associated with the broad ligand specificities of these proteins.

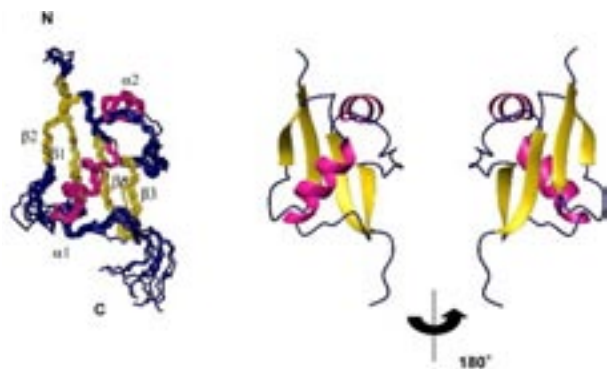


Figure 1. Backbone atom superposition of the final 10 structures (left) and ribbon representation of the lowest energy structure (right) of human Ufm1.

IX-O-2 Glycoform-Dependent Conformational Alteration of the Fc Region of Human Immunoglobulin G1 as Revealed by NMR Spectroscopy

YAMAGUCHI, Yoshiki¹; NISHIMURA, Mamiko²;
NAGANO, Mayumi¹; YAGI, Hirokazu¹;
SASAKAWA, Hiroaki¹; UCHIDA, Kazuhisa³;
SHITARA, Kenya³; KATO, Koichi¹

(¹IMS and Nagoya City Univ.; ²Nagoya City Univ.;
³Kyowa Hakko Kogyo Co., Ltd.)

[*Biochim. Biophys. Acta* **1760**, 693–700 (2006)]

The Fc portion of immunoglobulin G (IgG) expresses the biantennary complex type oligosaccharides at Asn297 of the C_H2 domain of each heavy chain with microheterogeneities depending on physiological and pathological states. These N-glycans are known to be essential for promotion of proper effector functions of IgG such as complement activation and Fcγ receptor (FcγR)-mediated activities. To gain a better understanding of the role of Fc glycosylation, we prepared a series of truncated glycoforms of human IgG1-Fc and analyzed their interactions with human soluble FcγRIIIa (sFcγRIIIa) and with staphylococcal protein A by surface plasmon resonance and nuclear magnetic resonance (NMR) methods. Progressive but less pronounced reductions in the affinity for sFcγRIIIa were observed as a result of the galactosidase and subsequent N-acetylhexosaminidase treatments of IgG1-Fc. The following endoglycosidase D treatment, giving rise to a disaccharide structure composed of a fucosylated GlcNAc, abrogated the affinity of IgG1-Fc for sFcγRIIIa. On the other hand, those glycosidase treatments did not significantly affect the affinity of IgG1-Fc for protein A. Inspection of stable-isotope-assisted NMR data of a series of Fc glycoforms indicates that the stepwise trimming out of the carbohydrate residues results in concomitant increase in the number of amino acid residues perturbed thereby in the C_H2 domains. Furthermore, the cleavage at the GlcNAcβ1-4GlcNAc glycosidic linkage induced the conformational alterations of part of the lower hinge region, which makes no direct contact with the carbohydrate moieties and forms the major FcγR-binding site, while the conformation of the C_H2/C_H3 interface was barely perturbed that is the protein A-binding site. These results indicate that the carbohydrate moieties are required for maintaining the structural integrity of the FcγR-binding site.

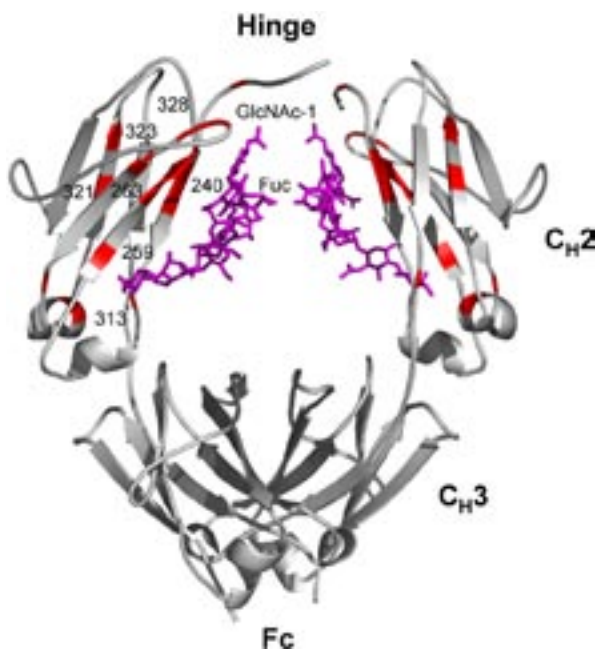


Figure 1. Mapping on the crystal structure of IgG1-Fc of the amino acid residues perturbed upon deglycosylation of carbohydrate chains attached onto Fc.

UVSOR Facility

IX-P Development of the UVSOR Light Source

IX-P-1 Design and Construction of Variably Polarized Undulator

KATOH, Masahiro; HOSAKA, Masahito; MOCHIHASHI, Akira; YAMAZAKI, Jun-ichiro; HAYASHI, Kenji; HARA, Toru¹
(¹RIKEN/SPring-8)

A new undulator was designed and constructed, which will provide bright VUV radiation to a beam-line BL7U at UVSOR-II. The period length and number of periods are 76 mm and 40, respectively. Permanent magnet blocks made of Nd-Fe-B are arranged in APPLE-II configuration. The undulator has capability of producing linear polarized light in both planes (horizontal and vertical) and circular polarized light in both directions (right handed and left handed).

A new beam duct for this undulator was also designed and constructed. The vertical aperture is 18 mm, which is narrowest in the UVSOR-II storage ring. The inner wall was covered by a Cu layer of 100 micron thick to reduce resistive wall impedance. The duct is pumped by two sputtering ion pumps and three NEG pumps.

The duct was successfully installed in the ring. Soon after finishing the field measurement, the undulator will be installed in the ring.

IX-P-2 Upgrade of Booster Synchrotron Magnet Power Supplies

KATOH, Masahiro; HOSAKA, Masahito; MOCHIHASHI, Akira; YAMAZAKI, Jun-ichiro; HAYASHI, Kenji

Top-up operation is a new technology to keep the intensity of electron beam circulating in a storage ring approximately constant by replenishing electrons frequently, typically with an interval of several minutes. The constant intensity of synchrotron radiation (SR) realized by this scheme will enable more accurate experiments.

Preparing for the top up injection, energy upgrade of the booster synchrotron is in progress at UVSOR-II. The maximum energy of the booster synchrotron had been limited at 600 MeV by the capacity of the magnet power supply, which is lower than the operation energy of the storage ring, 750 MeV. New power supplies compatible with the full energy injection were designed and constructed. In July, 2006, the power supplies were replaced. The acceleration to 600 MeV was successfully tested. Soon, full energy acceleration will be tested.

IX-P-3 One Watt Lasing in Deep UV Region of UVSOR-II Free Electron Laser

HOSAKA, Masahito; KATOH, Masahiro;

MOCHIHASHI, Akira; YAMAZAKI, Jun-ichiro; SHIMADA, Miho; TAKASHIMA, Yoshifumi¹; HARA, Toru²

(¹Nagoya Univ.; ²RIKEN/SPring-8)

The shortest wavelength of the UVSOR free electron laser (FEL) had been at 239 nm for many years. However, the low emittance owing to the new magnetic lattice introduced in 2003 and the higher peak current owing to the new RF cavity installed in 2005 have drastically increased the gain of FEL. The higher gain have made the FEL oscillate in deep UV region with high output power. The shortest wavelength is now 215 nm with output power of several milli-watt level. Lasing at shorter wavelength around 200 nm will be tried in near future. Average output power exceeding one watt was recorded at the wavelength of 230 nm. Some users experiments using this high power deep UV laser have started and a few others are under planning.

IX-P-4 Production of Coherent Terahertz Radiation by Laser Bunch Slicing Method

KATOH, Masahiro; HOSAKA, Masahito; MOCHIHASHI, Akira; YAMAZAKI, Jun-ichiro; SHIMADA, Miho; KIMURA, Shin-ichi; TAKASHIMA, Yoshifumi¹; TAKAHASHI, Toshiharu²; HARA, Toru³

(¹Nagoya Univ.; ²Kyoto Univ.; ³RIKEN/SPring-8)

Laser bunch slicing is a technology to slice out a part of an electron bunch moving with relativistic velocity in particle accelerators. At UVSOR-II, an Ti:Sa laser which can be synchronized with the RF acceleration of the electron storage ring was installed in 2005. By using the existing optical system and the optical klystron for the free electron laser experiment, we have started a laser bunch slicing experiment, aiming to produce intense terahertz radiation. As a result of the interaction between the laser pulse and the electron bunch, a dip is created on the longitudinal density structure of the electron bunch. The width of the dip is basically same as the laser pulse width; sub-pico-second in our case. An electron bunch which has such structure emits intense coherent terahertz radiation. The terahertz radiation synchronized with the laser injection was successfully observed at an existing beam-line BL6B, which is one of the most powerful infrared beam-line in the world. The observed intensity of the terahertz pulses is 10^{4-5} times higher than that of normal synchrotron radiation. The intensity was observed to be proportional to the square of the electron intensity. This clearly indicates that the observed terahertz pulses are produced by coherent radiation.

IX-P-5 Coherent Harmonic Generation by Using Ultra-Short Pulse Laser

LABAT, Marie¹; COUPRIE, Marie, Emmanuelle¹; LAMBERT, Guillaume¹; HARA, Toru²; KATOH, Masahiro; HOSAKA, Masahito; MOCHIHASHI, Akira; TAKASHIMA, Yoshifumi³
(¹CEA; ²IMS and RIKEN/SPring-8; ³Nagoya Univ.)

Coherent harmonic generation was successfully demonstrated at UVSOR-II. In the experiment, ultra-short laser pulses are injected to the storage ring. The laser pulses and the electron pulses interact in an optical klystron type undulator. The electrons are either accelerated or decelerated depending on the phase of the laser

field. As the result, a periodic energy modulation is created on the electron pulse, whose period is exactly same as the laser wavelength. This energy modulation is converted to a density modulation, which has a periodicity of laser wavelength and its higher harmonics. Electron bunches which have such a longitudinal density structure emit coherent radiation at the laser wavelength and also at its higher harmonics. Intense radiation at the third harmonic (267 nm) synchronized with the laser injection was successfully observed. The intensity of the coherent harmonics was proportional to the square of the intensity of the electron pulses. This clearly indicates that the observed radiation is a coherent harmonic radiation.

IX-Q Researches by the Use of UVSOR

IX-Q-1 Experimental Investigation of Core-Valence Double Photoionization

HIKOSAKA, Yasumasa; AOTO, Tomohiro¹; LABLANQUIE, Pascal²; PENENT, Francis²; SHIGEMASA, Eiji; ITO, Kenji¹
(¹KEK-PF; ²LCP-MR)

[*Phys. Rev. Lett.* **97**, 053003 (2006)]

Core-valence double photoionization has been observed in Ne atoms and N₂ molecules using a magnetic bottle time of flight spectrometer. The multi-electron coincidence datasets give complete information on the energy correlations between all emitted electrons, which supports a detailed description of the core-valence double photoionization process including direct spectroscopy of the core-valence doubly ionized states, the final states populated by their Auger decay and details of the dynamics of core-valence double photoionization for selected states.

IX-Q-2 Efficient Production of Metastable Fragments around the 1s Ionization Threshold in N₂

HIKOSAKA, Yasumasa; LABLANQUIE, Pascal¹; SHIGEMASA, Eiji
(¹LCP-MR)

[*J. Phys. B: At., Mol. Opt. Phys.* **38**, 3597 (2005)]

Metastable formation has been investigated in the inner-shell region of N₂. Enhanced N* formation has been observed around the 1s threshold, and is shown to result from dissociation of high N₂^{+*} Rydberg states. These N₂^{+*} states are populated by spectator Auger decay from the core-excited states, as well as by the recapture of slow photoelectrons into the Rydberg orbitals. The present measurement demonstrates that the metastable observation is a new and sensitive tool to

study the decay dynamics of core-excited states and the photoelectron recapture due to post-collision interaction.

IX-Q-3 Anisotropic Fragment Emission on Valence Photoionization of CF₄

HIKOSAKA, Yasumasa; SHIGEMASA, Eiji

[*J. Electron Spectrosc. Relat. Phenom.* **152**, 29 (2006)]

Photoion images from photoionization of CF₄ with an isotropic geometry have been measured in the photon energy range of 17–60 eV. Fragment ion emissions below 40 eV are found to be anisotropic with respect to the electric vector of the linearly polarized light. This observation directly implies that the T_d symmetry is broken on the dissociative photoionization process. The excited states associated with the transitions to the unoccupied orbitals are subject to symmetry lowering, which promotes the anisotropic fragment emissions from the highly-symmetrical molecule.

IX-Q-4 Auger Decay of Ne 1s Photoionization Satellites Studied by a Multi-Electron Coincidence Method

HIKOSAKA, Yasumasa; AOTO, Tomohiro¹; LABLANQUIE, Pascal²; PENENT, Francis²; SHIGEMASA, Eiji; ITO, Kenji¹
(¹KEK-PF; ²LCP-MR)

[*J. Phys. B: At., Mol. Opt. Phys.* **39**, 3457 (2006)]

The Auger decay of Ne 1s photoionization satellite states is studied with a magnetic-bottle multi-electron coincidence method. The energy correlations among the multi-electrons associated with the double Auger decay from the Ne⁺ satellite states are extracted from the accumulated coincidence dataset. It is concluded that the Ne²⁺ states populated through the initial Auger decays from the Ne⁺ satellite states can be excited states that lie

above the Ne^{3+} threshold. Their subsequent decay produces slow electrons in the 0–25 eV kinetic energy range. Possible assignments of the intermediate Ne^{2+} and the final Ne^{3+} states are given.

IX-Q-5 Inner-Valence States of N^{2+} and the Dissociation Dynamics Studied by Threshold Photoelectron Spectroscopy and Configuration Interaction Calculation

AOTO, Tomohiro¹; ITO, Kenji¹; HIKOSAKA, Yasumasa; SHIBASAKI, Akihiro²; HIRAYAMA, Ryo²; YAMAMOTO, Norifumi²; MIYOSHI, Eisaku² (¹KEK-PF; ²Kyushu Univ.)

[*J. Chem. Phys.* **124**, 234306 (2006)]

The N_2^+ states lying in the ionization region of 26–45 eV and the dissociation dynamics are investigated by high-resolution threshold photoelectron spectroscopy and threshold photoelectron-photoion coincidence spectroscopy. The threshold photoelectron spectrum exhibits several broad bands as well as sharp peaks. The band features are assigned to the N_2^+ states associated with the removal of an inner-valence electron, by a comparison with a configuration interaction calculation. In contrast, most of the sharp peaks on the threshold photoelectron spectrum are allocated to ionic Rydberg states converging to N_2^{2+} . Dissociation products formed from the inner-valence N_2^+ states are determined by threshold photoelectron-photoion coincidence spectroscopy. The dissociation dynamics of the inner-valence ionic states is discussed with reference to the potential energy curves calculated.

IX-Q-6 Electron Correlation in Xe 4d Auger Decay Studied by Slow Photoelectron–Auger Electron Coincidence Spectroscopy

SHEINERMAN, Sergei^{1,2}; LABLANQUIE, Pascal¹; PENENT, Francis¹; PALAUDOUX, Jerome¹; ELAND, John³; AOTO, Tomohiro⁴; HIKOSAKA, Yasumasa; ITO, Kenji⁴ (¹LCP-MR; ²St. Petersburg Univ.; ³PTCL; ⁴KEK-PF)

[*J. Phys. B: At., Mol. Opt. Phys.* **39**, 1017 (2006)]

Two different experimental methods, namely threshold electron–Auger electron coincidences and slow photoelectron–Auger electron coincidences are applied to investigate the Xe 4d Auger decay in the near-threshold region and reveal the essential role of electron correlation. The coincidences allow us to select the different channels for the 4d hole Auger decay which lead to different final states of the Xe^{2+} ion: $5s^{-2}(^1S_0)$, $5s^{-1}5p^{-1}(^1P_1)$, $5p^{-2}(^1S_0)$, $5p^{-2}(^1D_2)$, $5p^{-2}(^3P_{0,1})$ and $5p^{-2}(^3P_2)$. Measurements of the threshold electrons with the first method reveal strong PCI distortion of electron spectra in all channels. Comparison with calculations carried out in the framework of the quantum-mechanical PCI model allows us to clarify the dynamics of threshold electron production. In the $5p^{-2}(^1S_0)$ channel, the main contribution comes from the PCI retardation of slow photoelectrons. In the $5p^{-2}(^1D_2)$ and $5p^{-2}(^3P)$ final state

channels, additional processes of PCI recapture followed by valence multiplet decays play a role at and below the N_4 and N_5 thresholds. The slow photoelectron spectra measured by the second method reveal also a strong PCI distortion. Analysis within the framework of the eikonal model shows the influence of the Auger electron on the PCI distorted line shapes.

IX-Q-7 Development of Symmetry-Resolved Zero-Kinetic-Energy Photoelectron Spectroscopy for Probing Multielectron Processes

GEJO, Tatsuo¹; NAKAMURA, Eiken; SHIGEMASA, Eiji (¹Univ. Hyogo)

[*Rev. Sci. Instrum.* **77**, 036112 (2006)]

A new experimental setup for probing multielectron processes in molecular inner-shell ionization regions has been developed. Symmetry-resolved zero-kinetic-energy (ZEKE) spectra have been measured by scanning the photon energy along with monitoring the intensity of the coincidence signals between ZEKE electrons and fragment ions detected at 0° and 90° relative to the electric vector of the light. The actual performance of the method is illustrated by using it to reveal the symmetry decomposition of the multielectron processes, such as double excitations and shake-up satellites, in the K -shell ionization region of nitrogen.

IX-Q-8 Iron-Based Heavy Quasiparticles in $\text{SrFe}_4\text{Sb}_{12}$: An Infrared Spectroscopic Study

KIMURA, Shin-ichi; MIZUNO, Takafumi¹; IM, Hojun¹; HAYASHI, Katsuyuki²; MATSUOKA, Eiichi²; TAKABATAKE, Toshiro² (¹SOKENDAI; ²Hiroshima Univ.)

[*Phys. Rev. B* **73**, 214416 (5 pages) (2006)]

Temperature-dependent infrared reflectivity spectra of $\text{SrFe}_4\text{Sb}_{12}$ has been measured. A renormalized Drude peak with a heavy effective mass and a pronounced pseudogap of 10 meV develops in the optical conductivity spectra at low temperatures. As the temperature decreases below 100 K, the effective mass (m^*) rapidly increases, and the scattering rate ($1/\tau$) is quenched. The temperature dependence of m^* and $1/\tau$ indicates that the hybridization between the Fe 3d spins and the charge carriers plays an important role in determining the physical properties of $\text{SrFe}_4\text{Sb}_{12}$ at low temperatures. This result is the clear evidence of the iron-based heavy quasiparticles.

IX-Q-9 Optical Pseudogap from Iron States in Filled Skutterudites $\text{AFe}_4\text{Sb}_{12}$ ($A = \text{Yb}$ and Ca , Ba)

SICHELSCHMIDT, J.¹; VOEVODIN, V.¹; IM, Hojun²; KIMURA, Shin-ichi; ROSNER, H.¹; LEITHE-JASPER, A.¹; SCHNELLE, W.¹; BURKHARDT, U.¹; MYDOSH, J. A.¹; GRIN, Yu.¹;

STEGLICH, F.¹*(¹Max-Planck Inst.; ²SOKENDAI)**[Phys. Rev. Lett. 96, 037406 (2006)]*

Optical investigations are presented of the filled skutterudites $A\text{Fe}_4\text{Sb}_{12}$ with divalent cations $A = \text{Yb, Ca, Ba}$. For each of these compounds a very similar pseudogap structure in the optical conductivity develops in the far-infrared spectral region at temperatures below 90 K. Highly accurate local-density approximation electronic band structure calculations can consistently explain the origin of the pseudogap structure generated largely by transition metal 3d states. In particular, a 4f-conduction electron hybridization or strong correlations can be ruled out as origin for the pseudogap.

IX-Q-10 Continuity of Ce 4f Electronic Structure across the Quantum Critical Point: A Resonant Photoemission Study on $\text{CeNi}_{1-x}\text{Co}_x\text{Ge}_2$

IM, Hojun¹; ITO, Takahiro; HONG, J. B.²; KIMURA, Shin-ichi; KWON, Yong-seung²
(¹SOKENDAI; ²Sungkyunkwan Univ., Korea)

[Phys. Rev. B 72, 220405(R) (4 pages) (2005)]

Ce 3d–4f and 4d–4f resonant photoemission spectroscopies have been performed on the heavy-fermion compound $\text{CeNi}_{1-x}\text{Co}_x\text{Ge}_2$, where the ground-state properties systematically change from the magnetic ($0 < x < 0.3$) to nonmagnetic ($0.3 < x < 1.0$) regime *via* the quantum critical point (QCP, $x = 0.3$). Co-substitution dependence of the bulk Ce 4f electronic structure shows gradual evolution of Kondo resonance at the Fermi level together with the reduction of the Ce 4f⁰ final state in agreement with the single impurity Anderson model (SIAM). The SIAM analysis shows that the Kondo temperature and specific-heat coefficient change continuously from the weakly hybridized CeNiGe_2 to strongly hybridized CeCoGe_2 . These indicate that the Ce 4f electronic structure of $\text{CeNi}_{1-x}\text{Co}_x\text{Ge}_2$ changes continuously through the QCP.

IX-Q-11 Optical Study on Clathrates $\text{Sr}_8\text{Ga}_{16}\text{Ge}_{30}$ and $\beta\text{-Eu}_8\text{Ga}_{16}\text{Ge}_{30}$

SAKURAI, Yoko; NISHI, Tatsuhiko¹; KIMURA, Shin-ichi; KWON, Yong-seung²; AVILA, M. A.³; TAKABATAKE, Toshiro³
(¹SOKENDAI; ²Sungkyunkwan Univ., Korea; ³Hiroshima Univ.)

[Physica B 383, 122–123 (2006)]

The optical reflectivity spectra of clathrates $\text{Sr}_8\text{Ga}_{16}\text{Ge}_{30}$ and $\beta\text{-Eu}_8\text{Ga}_{16}\text{Ge}_{30}$ have been measured to investigate their electronic structure. A clear Drude shape was observed in the spectrum of $\text{Sr}_8\text{Ga}_{16}\text{Ge}_{30}$. On the other hand, a broad Drude shape due to magnetic scattering by Eu 4f electrons and a peak originated from Eu 4f states were observed in the spectrum of $\beta\text{-Eu}_8\text{Ga}_{16}\text{Ge}_{30}$. No clear change of optical conductivity

due to the magnetic order was observed in $\beta\text{-Eu}_8\text{Ga}_{16}\text{Ge}_{30}$ and no evidence of the rattling in $\text{Sr}_8\text{Ga}_{16}\text{Ge}_{30}$ observed in contrast to $\alpha\text{-Eu}_8\text{Ga}_{16}\text{Ge}_{30}$. These results essentially originated from the large carrier density of these materials.

IX-Q-12 Infrared Study on Electronic Structure of $\text{SrT}_4\text{Sb}_{12}$ ($T = \text{Fe, Ru}$)

KIMURA, Shin-ichi; IM, Hojun¹; SAKURAI, Yoko; MIZUNO, Takafumi¹; TAKEGAHARA, Katsuhiko²; HARIMA, Hisatomo³; HAYASHI, Katsuyuki⁴; MATSUOKA, Eiichi⁴; TAKABATAKE, Toshiro⁴
(¹SOKENDAI; ²Hirosaki Univ.; ³Kobe Univ.; ⁴Hiroshima Univ.)

[Physica B 383, 137–139 (2006)]

The temperature dependent optical conductivity spectrum of strontium filled skutterudites $\text{SrT}_4\text{Sb}_{12}$ ($T = \text{Fe, Ru}$) has been measured to investigate the origin of the heavy-fermion-like physical properties and the enhancement of the thermopower at around 50 K. The optical conductivity spectra of $T = \text{Fe}$ and Ru at the temperature of 7 K have peak structures at the photon energies of 24 and 190 meV, respectively. From the band structure calculation, the peaks correspond to the density of states (DOS) mainly originating from the Fe 3d and Ru 4d characters locating in the unoccupied states, *i.e.*, $\text{SrFe}_4\text{Sb}_{12}$ has a very narrower band near the Fermi level (E_F) than $\text{SrRu}_4\text{Sb}_{12}$. The shape of DOS near E_F is concluded to be the origin of the unconventional physical properties.

IX-Q-13 Angle-Resolved Photoemission Study on CeTe_2

ITO, Takahiro; IM, Hojun¹; KIMURA, Shin-ichi; KWON, Yong-seung²
(¹SOKENDAI; ²Sungkyunkwan Univ., Korea)

[Physica B 378-380, 767–768 (2006)]

We have used angle-resolved photoemission spectroscopy as a function of excitation energy to elucidate the three dimensionality at the electronic structure of quasi-two-dimensional strongly correlated Ce 4f electron compound CeTe_2 . We observed that there are two types of Te 5p bands along ΓZ symmetry line at the valence band, one is non-dispersive bands and the other is dispersive one. While the former is ascribed to the Te 5p bands at two-dimensional Te layer relating to the CDW formation, the latter to one at CeTe double layers.

IX-Q-14 High-Resolution Photoemission Spectroscopy of CeNiGe_2 and CeCoGe_2

IM, Hojun¹; ITO, Takahiro; KIMURA, Shin-ichi; HONG, J. B.²; KWON, Yong-seung²
(¹SOKENDAI; ²Sungkyunkwan Univ., Korea)

[Physica B 378-380, 825–826 (2006)]

We have performed the high-resolution photoemis-

sion spectroscopy on the isostructural heavy fermion compounds, CeCoGe₂ and CeNiGe₂, as the representative samples of CeNi_{1-x}Co_xGe₂ to investigate the origin of the wide Ce 4f characters from the magnetic ($x = 0$) to non-magnetic regime ($x = 1$) via the quantum critical point ($x = 0.3$). We directly observed a Kondo peak, whose width corresponds to the Kondo temperature, in both materials but the crystal field splitting only in CeNiGe₂. Both the Kondo temperature and the crystal field splitting are concluded to be affected by the hybridization between Ce 4f and Ni/Co 3d states.

IX-Q-15 Infrared Absorption in Heavy Fermion System CeNi_{1-x}Co_xGe₂

**KWON, Yong-seung¹; HONG, J. B.¹; IM, Hojun²;
NISHI, Tatsuhiko²; KIMURA, Shin-ichi**
(¹Sungkyunkwan Univ., Korea; ²SOKENDAI)

[*Physica B* **378-380**, 823–824 (2006)]

We have measured optical conductivity spectra $\sigma(\omega)$ of CeNi_{1-x}Co_xGe₂ at several temperatures. The $\sigma(\omega)$ spectra exhibit two peaks in middle infrared regions at low temperatures. The peaks show a strong temperature dependence and disappear above a characteristic temperature (T^*) at last. We suggest that the middle infrared peaks arise from transitions between d-states below E_F and c-f hybridization states just above E_F .

Laser Research Center for Molecular Science

IX-R Developments and Researches of New Laser Materials

Although development of lasers is remarkable, there are no lasers which lase in ultraviolet and far infrared regions. However, it is expected that these kinds of lasers break out a great revolution in not only the molecular science but also in the industrial world.

In this project we research characters of new materials for ultraviolet and far infrared lasers, and develop new lasers by using these laser materials.

IX-R-1 Photonic-Crystal-Fiber Pigtail Device Integrated with Lens-Duct Optics for Terahertz Radiation Coupling

DIWA, Girbert; QUEMA, Alex; ESTACIO, Elmer; POBRE, Romeric¹; MURAKAMI, Hidetoshi; ONO, Shingo; SARUKURA, Nobuhiko
(¹De La Salle Univ.)

[*Appl. Phys. Lett.* **87**, 151114 (2005)]

An integrated optics called terahertz (THz) pigtail, which is comprised of an emitter, an optically transparent launching media, and a waveguide, is devised and fabricated. The InAs emitter under a 1 T magnetic field is coupled to the launching media using silicone grease, an index matching liquid. The launching media, a lens duct made from a polymer based on poly 4-methyl pentene-1 (commonly known as TPX), is designed based on the concept of guiding THz radiation into Teflon photonic crystal fiber (PCF) waveguide by means of total internal reflection. It is found that the constructed THz lens duct is able to channel and couple the THz radiation into the PCF waveguide with a loss of < 1 dB. The results here show that the idea of using the THz pigtail can be a potential means of effectively directing THz radiation.

IX-R-2 Band-Structure Design of Fluoride Complex Materials for Deep-Ultraviolet Light-Emitting Diodes

ONO, Shingo; EL OUENZERFI, Riadh; QUEMA, Alex; MURAKAMI, Hidetoshi; SARUKURA, Nobuhiko; NISHIMATSU, Takeshi¹; TERAKUBO, Noriaki¹; MIZUSEKI, Hiroshi¹; KAWAZOE, Yoshiyuki¹; YOSHIKAWA, Akira¹; FUKUDA, Tsuguo¹
(¹Tohoku Univ.)

[*Jpn. J. Appl. Phys.* **44**, 7285 (2005)]

The design principle for fluoride-containing optical devices for applications in the deep ultraviolet range is discussed. Variations in band gap energy, band structure and lattice constant of $\text{LiBa}_x\text{Ca}_y\text{Sr}_{(1-x-y)}\text{F}_3$ and $\text{Li}_{(1-x)}\text{K}_x\text{Ba}_{(1-y)}\text{Mg}_y\text{F}_3$ have been studied. The band structure and transition type of these fluorides are predicted by ab initio band calculations based on the local density approximation. The lattice-matched double-hetero structure of direct-band-gap compounds $\text{LiBa}_x\text{Ca}_y\text{Sr}_{(1-x-y)}\text{F}_3$

on LiSrF_3 and $\text{Li}_{(1-x)}\text{K}_x\text{Ba}_{(1-y)}\text{Mg}_y\text{F}_3$ on either LiBaF_3 or KMgF_3 is sufficiently feasible to fabricate.

IX-R-3 Ce³⁺-Doped LiCaAlF₆ Crystals as a Solid-State Ultraviolet Saturable Absorber and Role of Excited State Absorption

HAI, Le Hoang¹; HUNG, Nguyen Dai¹; QUEMA, Alex; DIWA, Girbert; MURAKAMI, Hidetoshi; ONO, Shingo; SARUKURA, Nobuhiko
(¹Inst. Phys. Elect.)

[*Jpn. J. Appl. Phys.* **44**, 7984 (2005)]

Nonlinear absorption properties of Ce³⁺-doped LiCaAlF₆ (Ce:LiCAF) crystals at wavelength of 266 nm are studied using open-aperture Z-scan method and a Q-switch Nd:YAG laser. Saturable absorption of solid-state materials in ultraviolet region is demonstrated for the first time.

IX-R-4 Generation of Terahertz Radiation Using Zinc Oxide as Photoconductive Material Excited by Ultraviolet Pulses

ONO, Shingo; MURAKAMI, Hidetoshi; QUEMA, Alex; DIWA, Girbert; SARUKURA, Nobuhiko; NAGASAKA, Ryujiro¹; ICHIKAWA, Yo¹; OGINO, Hiraku²; OHSHIMA, Eriko²; YOSHIKAWA, Akira²; FUKUDA, Tsuguo²
(¹Nagoya Inst. Tech.; ²Tohoku Univ.)

[*Appl. Phys. Lett.* **87**, 261112 (2005)]

Terahertz (THz) radiation generated from photoconductive antenna fabricated on a single crystal zinc oxide (ZnO) is presented. The THz-radiation power is saturated at bias voltages above 800 V/cm and the obtained spectrum extends up to 1 THz. Moreover, ZnO is found to be highly transparent in the visible, near-infrared, mid-infrared and THz frequency regions. The results depicted here will categorically unravel the prospects of using ZnO as a material for integrated active optics.

IX-R-5 Ultraviolet Irradiation Effect of Ce³⁺-Doped BaMgF₄ Crystals

HAYASHI, Eiji¹; ITO, Kiyotaka¹; YABASHI, Satoshi¹; YAMAGA, Mitsuo¹; KODAMA, Nobuhiro²; ONO, Shingo; SARUKURA, Nobuhiko

(¹Gifu Univ.; ²Akita Univ.)

[*J. Alloys Compd.* **408**, 883 (2006)]

Ce³⁺-doped BaMgF₄ (BMF) crystals have the absorption and luminescence spectra in the vacuum ultraviolet (VUV) and ultraviolet (UV) ranges. Strong excitation of the fourth harmonic (266 nm) of a pulsed Nd:YAG laser colours the BMF crystal brown and produces a new luminescence spectrum with double peaks at 445 and 500 nm and a lifetime of less than 10 ns. When the sample temperature is elevated up to 200 degrees C, the crystal colour is changed from brown to green. The colouration is due to localized electrons and holes created by the strong UV excitation, which are identified by the electron spin-resonance (ESR) technique. This new luminescence may be due to Ce³⁺ perturbed by the colour centres.

IX-R-6 Vacuum Ultraviolet and Ultraviolet Spectroscopy of BaMgF₄ Codoped with Ce³⁺ and Na⁺

HAYASHI, Eiji¹; ITO, Kiyotaka¹; YABASHI, Satoshi¹; YAMAGA, Mitsuo¹; KODAMA, Nobuhiro²; ONO, Shingo; SARUKURA, Nobuhiko
(¹Gifu Univ.; ²Akita Univ.)

[*J. Lumin.* **119**, 69 (2006)]

Ce³⁺/Na⁺-doped BaMgF₄ (BMF) crystals with a nonlinear property show strong absorption in the vacuum ultraviolet (VUV) and ultraviolet (UV) ranges. Three different fluorescence bands (A, B, C) at 300, 340, and 430 nm were observed when pumped at different wavelengths. Under excitation of the fourth harmonic (266 nm) from a pulsed Nd:YAG laser the BMF crystal changed its colour from transparent to brown due to formation of colour centres. The A, B and C bands are assigned to three different sites of Ce³⁺: site A is Ce³⁺ substituting for perfect Ba²⁺ sites; site B is Ce³⁺ (Ba²⁺) perturbed by Na⁺ as a charge compensator; and site C is a complex composed of Ce³⁺ and F- vacancies, which trapped one or two electrons.

IX-R-7 Vacuum Ultraviolet Spectroscopy of Ce³⁺-Doped SrMgF₄ with Superlattice Structure

YAMAGA, Mitsuo¹; HAYASHI, Eiji¹; KODAMA, Nobuhiro²; ITO, Kiyotaka¹; YABASHI, Satoshi¹; MASUI, Yuki¹; ONO, Shingo; SARUKURA, Nobuhiko; HAN, T. P. J.³; GALLAGHER, H. G.³
(¹Gifu Univ.; ²Akita Univ.; ³Univ. Strathclyde)

[*J. Phys.: Condens. Matter* **18**, 6033 (2006)]

X-ray diffraction of Ce³⁺-doped SrMgF₄ (SMF:Ce) crystals shows a superlattice structure, reflecting the distribution of Ce³⁺ polyhedra centres observed in optical experiments. Optical absorption bands and fluorescence bands from the Ce³⁺ polyhedra centres overlap in the vacuum ultraviolet (VUV) and ultraviolet (UV) regions, respectively, so that wide pumping and tuning ranges are expected for laser operation. The SMF: Ce

crystals, as well as the isomorphous BaMgF₄, are candidates for a tunable laser gain material with nonlinear properties.

The optical absorption, excitation, and fluorescence bands observed in the SMF: Ce crystals at low temperatures are ascribed to five distinct fluorescent centres. Three centres have well-known Ce³⁺ optical characters, for example, fluorescence with double peaks separated by 2000 cm⁻¹ and five resolved absorption/excitation bands. These centres are assigned to Ce³⁺-polyhedra classified by weak and strong crystal fields as a consequence of the superlattice structure. The other two fluorescence bands observed in the visible region have 1.5–2 times larger linewidths than those of the former three bands. These bands are interpreted as optical transitions from complexes consisting of Ce³⁺ and one or two electrons trapped at a vacancy of the nearest neighbour F-ligand ions.

IX-S Development and Research of Advanced Tunable Solid State Lasers

Diode-pumped solid-state lasers can provide excellent spatial mode quality and narrow linewidths. The high spectral power brightness of these lasers has allowed high efficiency frequency extension by nonlinear frequency conversion. Moreover, the availability of new and improved nonlinear optical crystals makes these techniques more practical. Additionally, quasi phase matching (QPM) is a new technique instead of conventional birefringent phase matching for compensating phase velocity dispersion in frequency conversion. These kinds of advanced tunable solid-state light sources, so to speak "Chroma Chip Lasers," will assist the research of molecular science.

In this projects we are developing Chroma Chip Lasers based on diode-pumped-microchip-solid-state lasers and advanced nonlinear frequency conversion technique.

IX-S-1 300W Continuous-Wave Operation of Diode Edge-Pumped, Hybrid Composite Yb:YAG Microchip Laser

TSUNEKANE, Masaki; TAIRA, Takunori

[*Opt. Lett.* **31**, 2003–2005 (2006)]

300 W continuous-wave operation of a diode edge-pumped, hybrid (single-crystal/ceramic) composite, Yb^{3+} :YAG microchip laser with a 5-mm-diameter and 300- μm -thickness, single-crystal core uniformly bonded to a water-cooled heat-sink by the new Au–Sn soldering system has been demonstrated. The beam quality factor, M^2 follows the mode-mismatch between the core and the fundamental mode, and was improved to 17 with the maximum output power of 230 W. The thermally induced convex mirror with a spherical radius of curvature ranging from -2.5 to -1.5 m, which decreases as the pump power increases by thermal deformation of a microchip, was observed.

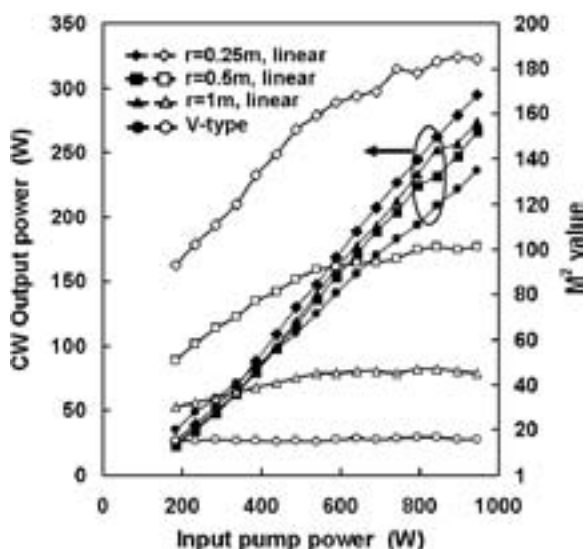


Figure 1. CW output power and the beam quality characteristics (M^2 factor) with four different cavity configurations as a function of input pump power.

IX-S-2 Spectroscopic Properties and Laser Emission in Layer-by-Layer Type Nd:Y₃ScAl₄O₁₂/Nd:Y₃Al₅O₁₂ Composite Ceramics

SATO, Yoichi; TAIRA, Takunori; IKESUE, Akio¹
(¹JFCC)

[*OSA Topical Meeting of Advanced Solid State Photonics TuB3* (2006)]

We have fabricated the all-ceramic layered composite device with Nd:YAG and Nd:YSAG, which can perform efficient laser oscillation. From its spectroscopic properties, this layer-by-layer composite device will offer new function of laser oscillation by pump wavelength tuning. For example when pumped from YSAG side at 810.5 nm, it can oscillate at 1064 nm. On the other hand, it will oscillate at 1061 nm when pumped at 808.5 nm.

Due to the difference in the dependence on the wavelength of, the portion of the pumped power absorbed in Nd:YAG-layer and in Nd:YSAG-layer depends on the pumping wavelength. This resulted in the tuning of the component ratio of the Nd:YAG and Nd:YSAG in the fluorescence. The dependence of fluorescence profiles in this composite on the pump wavelength is shown in Figure 1.

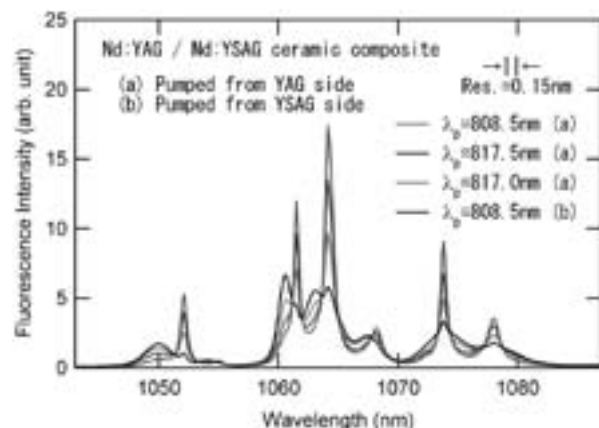


Figure 1. Measured fluorescent spectral profiles by changing pumping wavelength.

IX-S-3 Thermal Properties of Y₃Al₅O₁₂, GdVO₄, and YVO₄

SATO, Yoichi; TAIRA, Takunori

[Conf. Lasers Electro-Optics JThC30 (2006)]

We have measured thermal conductivity of $Y_3Al_5O_{12}$, $GdVO_4$, and YVO_4 . In order to avoid the miss leading from three-dimensional (3D) thermal diffusion, we developed the quasi-one-dimensional (q1D) flash method. By taking in account the heat radiation effect in transparent materials for this measurement, YVO_4 was found to have larger thermal conductivity than $GdVO_4$. The measured thermal conductivities were 12.1, 10.5, 10.1, 8.9, and 8.5 W/mK for *c*-cut YVO_4 , *c*-cut $GdVO_4$, YAG, *a*-cut YVO_4 , and *a*-cut $GdVO_4$, respectively. The measured value in the range from room temperature to 200 °C is shown in Figure 1. The dependence of Nd-conductivity coefficient (dk/dc_{Nd}) for convenient evaluation of the doping effect in thermal conductivity is also discussed.

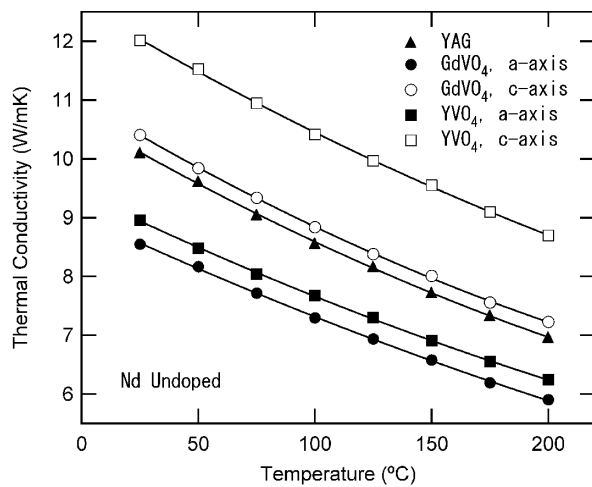


Figure 1. Thermal conductivities of undoped YAG, $GdVO_4$, and YVO_4 .

IX-S-4 Spectroscopic Properties and Laser Operation of RE³⁺-ion Doped Garnet Materials

TAIRA, Takunori; SATO, Yoichi; SAIKAWA, Jiro; IKESUE, Akio¹
(¹JFCC)

[Proc. SPIE 6216, 62160J (2006)]

Lately developed RE³⁺-ion-doped disordered laser ceramic materials, $Y_3Sc_xAl_{5-x}O_{12}$, which are a solid solution of YAG and $Y_3Sc_2Al_3O_{12}$ (YSAG), have been interested in because of its compositional tuning of parameter *x*. The disordered $Y_3ScAl_4O_{12}$ (YAG/YSAG) ceramics exhibit relatively low minimum pump intensity (I_{min}) and broad emission bandwidth. The value of I_{min} in the Yb: $Y_3ScAl_4O_{12}$ ceramics was found to be 2/3 compared with the Yb:YAG single crystal under 970nm zero-line pumping. Efficient laser oscillation of 72% slope efficiency was obtained for input power. Next, we have demonstrated passively mode-locked Yb: $Y_3ScAl_4O_{12}$ disordered ceramic laser by using a semiconductor saturable-absorber mirror. Pulses as short as 280 fs having an average power of 62 mW at 1035.8 nm was obtained as shown in Figure 1. As a conclusion, the possibility of tailored fluorescence spectral profile in

layer-by-layer type ceramic composite is also discussed.

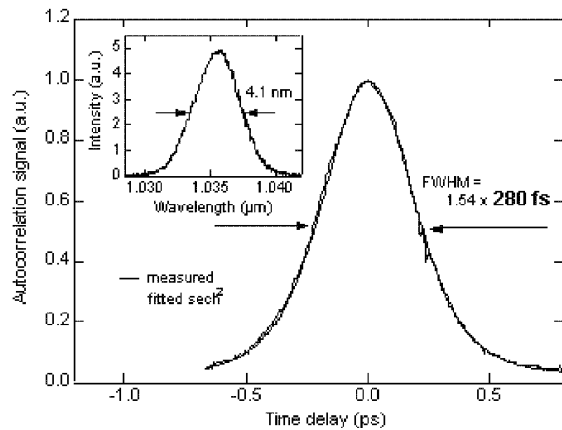


Figure 1. Second-harmonic autocorrelation trace and spectrum (inset) for the shortest-pulse generation with a 0.5% output coupler. The solid-line indicates ideal sech² shape.

IX-S-5 Comparative Study on the Spectroscopic Properties of Nd:GdVO₄ and Nd:YVO₄ with Hybrid Process

SATO, Yoichi; TAIRA, Takunori

[IEEE J. Sel. Top. Quantum Electron. 11, 613 (2005)]

We have proposed the hybrid procedure of determining spectroscopic parameters for uniaxial solid-state laser crystals. Figure 1 shows the procedure of this process. By using our procedure the spectroscopic properties of Nd:GdVO₄ were evaluated and compared to those of Nd:YVO₄. The product of stimulated emission cross section and fluorescence lifetime ($\sigma\tau$ product) of Nd:GdVO₄ was smaller than that of Nd:YVO₄ under 1.0-at.% of Nd³⁺-doping concentration. Because of the low value of radiative quantum efficiency of Nd:GdVO₄ (50%), careful cavity design is required for creating a well performing solid-state laser with Nd:GdVO₄, based on the larger $\sigma_{em}\tau_f$ product than $\sigma_{em}\tau_f$ product of Nd:YAG.

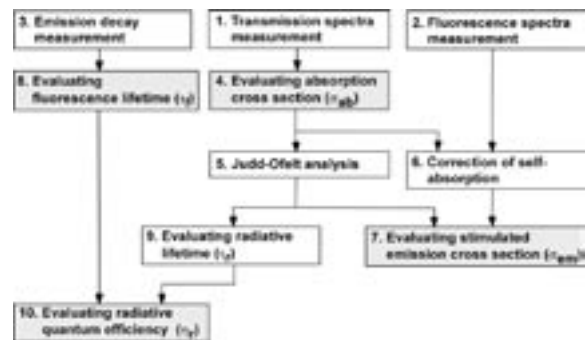


Figure 1. Flow-chart of the Hybrid process in this work.

IX-S-6 High-Energy, Narrow-Bandwidth 2-μm Optical Parametric Oscillator/Power Amplifier Based on Periodically Poled MgO:LiNbO₃

SAIKAWA, Jiro; FUJII, Masaaki¹; ISHIZUKI, Hideki; TAIRA, Takunori

(¹Tokyo Tech)

[*Conf. Lasers Electro-Optics CThG3* (2006)]

We demonstrated a high-energy, high-efficiency quasi-phase-matched optical parametric oscillator/power amplifier system based on $5 \times 5 \text{ mm}^2$ large aperture periodically poled MgO:LiNbO₃. Maximum pulse energy of 52 mJ (optical conversion efficiency of 60%) with resolution limit spectral bandwidth of $< 2 \text{ nm}$ at $2.128 \text{ }\mu\text{m}$ degeneracy point was obtained. These experimental result shows that large aperture PPMgLN device is useful for the development of the high-energy, efficient, narrowband $2\mu\text{m}$ light source.

IX-S-7 High-Energy Quasi-Phase Matched Optical-Parametric Oscillation in Periodically Poled MgO:LiNbO₃ Device with 5 mm x 5 mm Aperture

ISHIZUKI, Hideki; TAIRA, Takunori

[*Opt. Lett.* **30**, 2918–2920 (2005)]

Fabrication of 5mm-thick periodically poled MgO-doped LiNbO₃ device with $32.1\mu\text{m}$ period for mid-infrared generation was demonstrated. The periodic structure was evaluated by measurement of second-harmonic generation with d_{31} -coefficient. Optical-parametric oscillation using the device with uncoated $5 \text{ mm} \times 5 \text{ mm}$ aperture and 36mm effective length realized a high-energy output of 77 mJ for both signal (wavelength: $1.83 \text{ }\mu\text{m}$) and idler ($2.54 \text{ }\mu\text{m}$) waves with 72% slope efficiency at 110mJ pumping of Q-switched Nd:YAG laser with 12ns pulse duration.

Equipment Development Center

IX-T Development of New Instruments and Experimental Devices

The technical staff of the Equipment Development Center is partly engaged in planning, researching, designing and constructing high technology experimental instruments in collaboration with the scientific staff. And these experimental instruments are incorporated with new manufacturing technology and new mechanical idea.

IX-T-1 Manufacture of a Mold for a Microchip Using a Surface Impression Agent

AOYAMA, Masaki; SUZUI, Mitsukazu; SHINTANI, Takafumi¹; NODA, Masaharu¹
(¹NIBB)

Figure 1 shows an external photograph and an SEM photograph of a produced mold. A microchip is produced by injecting PDMS into the mold. The mold has first projections of 0.5 mm in width and 3 mm in height on both sides which form liquid sump sections, and second projections extending between the first projections each having a width of 90 μm and a height 60 μm which form passages.

The mold cannot be produced by machinery because of tool interference. Therefore, a master die is produced first by machinery, and the produced master die is transferred to make an inverse shape. In general, the transferring step is performed using an electrocasting method. However, because the electrocasting method is expensive, the master die is transferred to the inverse shape using a surface impression agent (Heraeus Kulzer GmbH & Co. Technovit 3040), which is an easier method. With the method, the mold for a PDMS microchip is produced in a short time at low cost. A produced PDMS microchip is used for making protein stripes on plastic dishes or glass coverslips as substrates for neural cell culture.

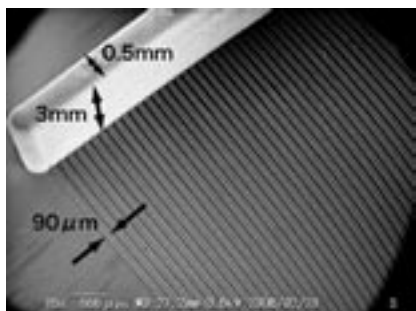
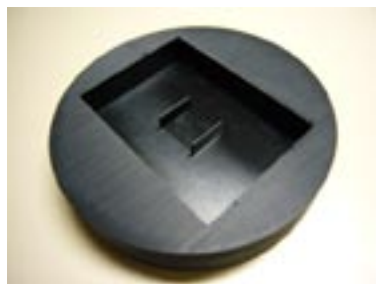


Figure 1. The externals and the SEM photographs of the mold.

IX-T-2 A Compact Mechanical Velocity Selector to Analyze Molecular Alignment

YANO, Takayuki; SUZUI, Mitsukazu; OKADA, Michio¹; KASAI, Toshio¹
(¹Osaka Univ.)

We received a request on the production of disks from Professor Kasai. (Department of Chemistry Graduate School of Science, Osaka University). As a new attempt, we expand our service to the outside researchers of universities and research institutes since October 2005. We suggested the application of the wire-cut electrical discharge machining (WEDM) to manufacturing the fine disks. However, it was difficult to apply the conventional method as it is. Therefore, we devised and made supporting tools. And we examined a routine of the production process. Selector dimensions and technical data are shown in table 1. Schematical drawing of a disk of the mechanical velocity selector is shown in Figure 1. Magnified view of fine slits on the disk is also shown in Figure 2. We used a wire of 70 micron in diameter in the processing. The slit of 100 micron in width was obtained with it. Using this fine wire enables us to make a slit of 85 micron in the minimum width.

Table 1. Selector dimensions and technical data.

Number of disks	2
Diameter of disks	72mm
Number of slits per disk	720
Length of the slits	2mm
Slit with	0.1mm
Wall width between slits	0.2mm
Disk thickness	0.1mm
Material of disks	stainless steel

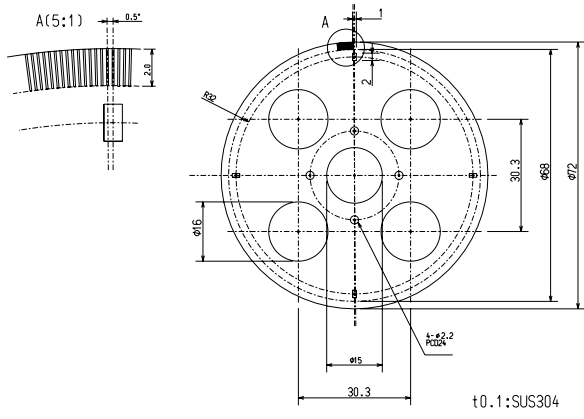


Figure 1. Schematic drawing of a disk of the mechanical velocity selector.

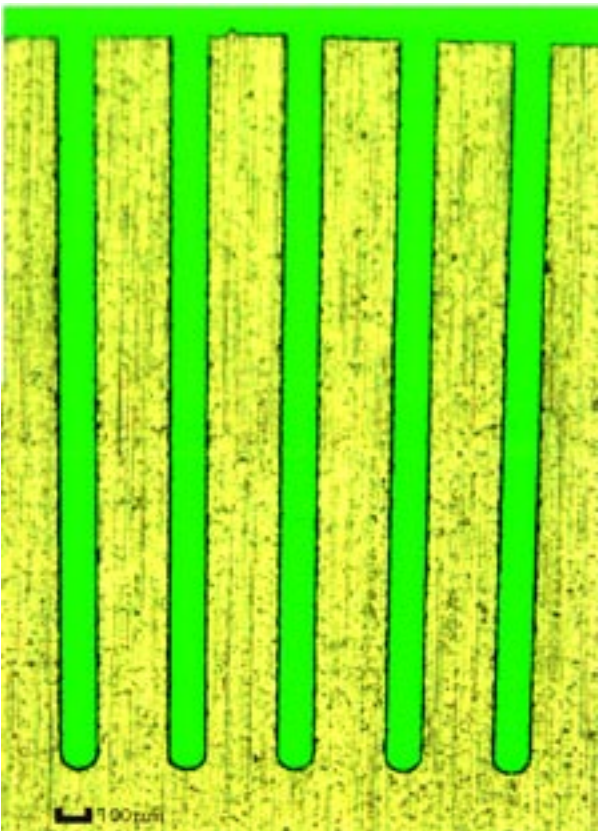


Figure 2. Photograph of the slit.

Safety Office

IX-U Development of Novel Heterocyclic Compounds and Their Molecular Assemblies for Advanced Materials

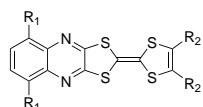
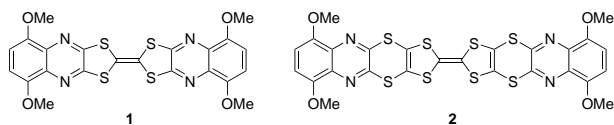
Heterocycles containing sulfur and/or nitrogen atoms are useful as components of functional materials since heteroatoms in their rings are helpful to stabilize ions or ion-radical species, and extended π -conjugation decreases Coulombic repulsion. In addition intermolecular interactions caused by heteroatom contacts can be expected to form novel molecular assemblies. In this project new electron acceptors, donors, and donor-acceptor compounds based on heterocycles such as 1,2,5-thiadiazole and 1,3-dithiole were synthesized and their properties including those of the charge-transfer complexes or ion-radical salts were investigated. Unique crystal structures were constructed by using weak intermolecular interactions such as hydrogen bonding or heteroatom contacts.

IX-U-1 TTF Derivatives Containing Fused-Pyrazine Rings for Novel Donor-Acceptor Systems

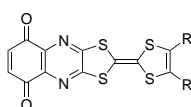
Naraso¹; NISHIDA, Jun-ichi¹; TOMURA, Masaaki;
YAMASHITA, Yoshiro²
(¹Tokyo Tech; ²IMS and Tokyo Tech)

[*Synth. Met.* **153**, 389–392 (2005)]

In this work, novel π -extended tetrathiafulvalen (TTF) derivatives **1-10** fused with electron-accepting pyrazine rings are described. We have succeeded in preparing two kinds of TTF derivatives **1** and **2** containing two pyrazine rings. Furthermore, we have prepared asymmetrical TTF derivatives **3-6** containing one pyrazine ring to increase the electron-donating properties. In some cases, hydroxyl groups were introduced to intermolecular hydrogen bonds. Oxidation of hydroquinone derivatives afforded a new type of donor-acceptor compounds **7-10** with quinone units, which showed both oxidation and reduction potentials. The electrical conductivity of the donor-acceptor compound was about 10^{-8} S/cm as single component. We have also prepared several CT complexes based on the new TTF derivatives and investigated the structures and properties.



- 3:** R₁ = OMe; R₂ = SMe
4: R₁ = OMe; R₂, R₂ = SCH₂CH₂S
5: R₁ = OH; R₂ = SMe
6: R₁ = OH; R₂, R₂ = SCH₂CH₂S



- 7:** R = SMe
8: R = SC₆H₁₃
9: R = SC₁₀H₂₁
10: R, R = SCH₂CH₂S

RESEARCH ACTIVITIES X

Okazaki Institute for Integrative Bioscience

X-A Bioinorganic Chemistry of Heme-Based Sensor Proteins

Heme-based sensor proteins show a novel function of the heme prosthetic group, in which the heme acts as an active site for sensing the external environmental signal such as diatomic gas molecules and redox change. Heme-based O₂, NO, and CO sensor proteins have now been found in which these gas molecules act as a signaling factor that regulates the functional activity of the sensor proteins. Our research interest focuses on the elucidation of structure-function relationships of CO sensor protein (CooA), O₂ sensor protein (HemAT), and redox sensor protein (DcrA).

X-A-1 Effect of Mutation on the Dissociation and Recombination Dynamics of CO in Transcriptional Regulator CooA: A Picosecond Infrared Transient Absorption Study

ZHANG, Tieqiao¹; RUBTSOV, Igor V.¹;
NAKAJIMA, Hiroshi¹; AONO, Shigetoshi;
YOSHIHARA, Keitaro¹
(¹JAIST)

[*Biochemistry* **45**, 9246–9253 (2006)]

The CO ligation process in a mutant (H77G) of CooA, the CO-sensing transcriptional regulator in *Rhodospirillum rubrum*, is studied with femtosecond time-resolved transient absorption spectroscopy in the mid-infrared region. Following photolyzing excitation, a transient bleach in the vibrational region of bound CO due to the CO photodissociation is detected. In contrast to the spectra of the wild-type (WT) CooA, the transient bleach spectra of H77G CooA show a bimodal shape with peaks shifting to the lower frequency during spectral evolution. The CO recombination dynamics show single-exponential behavior, and the CO escaping yield is higher than that of the WT CooA. A reorientation process of CO relative to the heme plane during recombination is revealed by anisotropy measurements. These phenomena indicate changes in the protein response to the CO ligation and suggest an alteration to the CO environment caused by the mutation. On the basis of these results, the role of His77 in the CO-dependent activation of CooA and a possible activation mechanism involving collaborative movement of the heme and the amino residues at both sides of the heme plane are discussed.

X-A-2 Evidence for Displacements of the C-Helix by CO Ligation and DNA Binding to CooA Revealed by UV Resonance Raman Spectroscopy

KUBO, Minoru; INAGAKI, Sayaka; YOSHIOKA, Shiro; UCHIDA, Takeshi; MIZUTANI, Yasuhisa¹;
AONO, Shigetoshi; KITAGAWA, Teizo
(¹Kobe Univ.)

[*J. Biol. Chem.* **281**, 11271–11278 (2006)]

The UV and visible resonance Raman spectra are reported for CooA from *Rhodospirillum rubrum*, which is a transcriptional regulator activated by growth in a CO atmosphere. CO binding to heme in its sensor domain causes rearrangement of its DNA-binding domain, allowing binding of DNA with a specific sequence. The sensor and DNA-binding domains are linked by a hinge region that follows a long C-helix. UV resonance Raman bands arising from Trp-110 in the C-helix revealed local movement around Trp-110 upon CO binding. The indole side chain of Trp-110, which is exposed to solvent in the CO-free ferrous state, becomes buried in the CO-bound state with a slight change in its orientation but maintains a hydrogen bond with a water molecule at the indole nitrogen. This is the first experimental data supporting a previously proposed model involving displacement of the C-helix and heme sliding. The UV resonance Raman spectra for the CooA-DNA complex indicated that binding of DNA to CooA induces a further displacement of the C-helix in the same direction during transition to the complete active conformation. The Fe–CO and C–O stretching bands showed frequency shifts upon DNA binding, but the Fe–His stretching band did not. Moreover, CO-geminate recombination was more efficient in the DNA-bound state. These results suggest that the C-helix displacement in the DNA-bound form causes the CO binding pocket to narrow and become more negative.

X-A-3 Crystallization and Preliminary X-Ray Analysis of CooA from *Carboxydotherrus hydrogeniformans*

KOMORI, Hirofumi¹; SATOMOTO, Kensuke¹;
UEDA, Yasufumi¹; SHIBATA, Naoki¹; INAGAKI,
Sayaka; YOSHIOKA, Shiro; AONO, Shigetoshi;
HIGUCHI, Yoshiki¹
(¹Univ. Hyogo)

[*Acta Crystallogr., Sect. F: Struct. Biol. Cryst. Commun.* **62**, 471–473 (2006)]

CooA, a homodimeric haem-containing protein, is responsible for transcriptional regulation in response to carbon monoxide (CO). It has a b-type haem as a CO sensor. Upon binding CO to the haem, CooA binds promoter DNA and activates expression of genes for CO metabolism. CooA from *Carboxydotherrus hydrogeniformans*

formans has been overexpressed in *Escherichia coli*, purified and crystallized by the vapour-diffusion method. The crystal belongs to space group $P2_1$, with unit-cell parameters $a = 61.8$, $b = 94.7$, $c = 92.8$ angstroms, $\beta = 104.8$ degrees. The native and anomalous difference Patterson maps indicated that two CooA dimers are contained in the asymmetric unit and are related by a translational symmetry almost parallel to the c axis.

X-A-4 Specific Hydrogen-Bonding Networks Responsible for Selective O₂ Sensing of the Oxygen Sensor Protein HemAT from *Bacillus subtilis*

YOSHIMURA, Hideaki; YOSHIOKA, Shiro; KOBAYASHI, Katsuaki; OHTA, Takehiro; UCHIDA, Takeshi; KUBO, Minoru; KITAGAWA, Teizo; AONO, Shigetoshi

[*Biochemistry* **45**, 8301–8307 (2006)]

HemAT from *Bacillus subtilis* (HemAT-Bs) is a heme-based O₂ sensor protein that acts as a signal transducer responsible for aerotaxis. HemAT-Bs discriminates its physiological effector, O₂, from other gas molecules to generate the aerotactic signal, but the detailed mechanism of the selective O₂ sensing is not obvious. In this study, we measured electronic absorption, electron paramagnetic resonance (EPR), and resonance Raman spectra of HemAT-Bs to elucidate the mechanism of selective O₂ sensing by HemAT-Bs. Resonance Raman spectroscopy revealed the presence of a hydrogen bond between His86 and the heme propionate only in the O₂-bound form, in addition to that between Thr95 and the heme-bound O₂. The disruption of this hydrogen bond by the mutation of His86 caused the disappearance of a conformer with a direct hydrogen bond between Thr95 and the heme-bound O₂ that is present in WT HemAT-Bs. On the basis of these results, we propose a model for selective O₂ sensing by HemAT-Bs as follows. The formation of the hydrogen bond between His86 and the heme propionate induces a conformational change of the CE-loop and the E-helix by which Thr95 is located at the proper position to form the hydrogen bond with the heme-bound O₂. This step-wise conformational change would be essential to selective O₂ sensing and signal transduction by HemAT-Bs.

X-A-5 Recognition and Discrimination of Gases by the Oxygen-Sensing Signal Transducer Protein HemAT as Revealed by FTIR Spectroscopy

PINAKOULAKI, Eftychia¹; YOSHIMURA, Hideaki; YOSHIOKA, Shiro; AONO, Shigetoshi; VAROTSIS, Constantinos¹
(¹Univ. Crete)

[*Biochemistry* **45**, 7763–7766 (2006)]

The determination of ligand binding properties is a key step in our understanding of gas sensing and discrimination by gas sensory proteins. HemAT is a newly discovered signal transducer heme protein that recognizes O₂ and discriminates against other gases such as CO and NO. We have used FTIR spectroscopy on CO- and NO-bound sensor domain HemAT and sensor domain distal mutants Y70F, T95A, R91A, and L92A to gain insight into the structure of the iron-bound ligand at ambient temperature. These mutations were designed to perturb the electrostatic field near the iron-bound gaseous ligand and also allow us to investigate the communication pathway between the distal residues of the protein and the heme. We show the formation of both H-bonded and non-H-bonded conformations in the CO-bound forms. In addition, we report the presence of multiple conformations in the NO-bound forms. Such distal H-bonding is crucial for ligand binding and activation by the heme. The comparison of the O₂, NO, and CO data demonstrates that Thr95 and Tyr70 are crucial for ligand recognition and discrimination and, thus, for specific sensing of gases, and L92 is crucial for controlling the conformational changes of the Thr95 and Tyr70 residues upon NO binding.

X-A-6 Biophysical Properties of a c-Type Heme in Chemotaxis Signal Transducer Protein DcrA

YOSHIOKA, Shiro; KOBAYASHI, Katsuaki; YOSHIMURA, Hideaki; UCHIDA, Takeshi; KITAGAWA, Teizo; AONO, Shigetoshi

[*Biochemistry* **44**, 15406–15413 (2005)]

Chemotaxis signal transducer protein DcrA from a sulfate-reducing bacterium *Desulfovibrio vulgaris* Hildenborough was previously shown to contain a c-type heme in its periplasmic domain (DcrA-N) for sensing redox and/or oxygen, which is the first example of a heme-based sensor protein containing a c-type heme as a prosthetic group. Optical absorption and resonance Raman spectroscopies indicates that heme *c* in DcrA-N shows a redox-dependent ligand exchange. Upon reduction, a water molecule that may be the sixth ligand of the ferric heme *c* is replaced by an endogenous amino acid. Although the reduced heme in DcrA-N is six-coordinated with two endogenous axial ligands, CO can easily bind to the reduced heme to form CO-bound DcrA-N. Reaction of the reduced DcrA-N with molecular oxygen results in autoxidation to form a ferric state without forming any stable oxygen-bound form probably due to the extremely low redox potential of DcrA-N (–250 mV). Our study supports the initial idea by Fu *et al.* that DcrA would act as a redox and/or oxygen sensor, in which the ligand exchange between water and an endogenous amino acid is a trigger for signal transduction. While the affinity of CO to DcrA-N ($K_d = 138$ μ M) is significantly weak compared to those of other heme proteins, we suggest that CO might be another physiological effector molecule.

X-B Bioinorganic Chemistry of a Novel Heme Enzyme that Catalyzes the Dehydration Reaction

Aldoxime dehydratases from various bacteria catalyze the dehydration reaction of aldoxime to produce nitrile under mild conditions. Aldoxime dehydratase from *Bacillus* sp. OxB-1 (OxdB) exists in a monomer of a 40-kDa polypeptide containing a protoheme. The heme in OxdB is thought to be the active site for the dehydration reaction. OxdB is the first example of a heme protein catalyzing the dehydration reaction physiologically, although many functions of heme proteins have been elucidated, including oxygen storage/transport, electron transfer, gas molecule sensor, and redox catalysis of various substrates. We are working on OxdB and OxdRE (aldoxime dehydratase from *Rhodococcus* sp. N-771) to elucidate the structure-function relationships of these novel heme enzymes.

X-B-1 Spectroscopic and Substrate Binding Properties of Heme-Containing Aldoxime Dehydratases, OxdB and OxdRE

KOBAYASHI, Katsuaki; PAL, Biswajit;
YOSHIOKA, Shiro; KATO, Yasuo¹; ASANO,
Yasuhisa¹; KITAGAWA, Teizo; AONO, Shigetoshi
(¹Toyama Pref. Univ.)

[*J. Inorg. Biochem.* **100**, 1069–1074 (2006)]

Phenylacetaldoxime dehydratase from *Bacillus* sp. strain OxB-1 (OxdB) catalyzes the dehydration of Z-phenylacetaldoxime (PAOx) to produce phenylacetone nitrile. OxdB contains a protoheme that works as the active center of the dehydration reaction. The enzymatic activity of ferrous OxdB was 1150-fold higher than that of ferric OxdB, indicating that the ferrous heme was the active state in OxdB catalysis. Although ferric OxdB was inactive, the substrate was bound to the ferric heme iron. Electron paramagnetic resonance spectroscopy revealed that the oxygen atom of PAOx was bound to the ferric heme, whereas PAOx was bound to the ferrous heme in OxdB via the nitrogen atom of PAOx. These results show a novel mechanism by which the activity of a heme enzyme is regulated; that is, the oxidation state of the heme controls the coordination structure of a substrate-heme complex, which regulates enzymatic activity. Rapid scanning spectroscopy using stopped-flow apparatus revealed that a reaction intermediate (the PAOx-ferrous OxdB complex) showed Soret, γ , and δ bands at 415, 555, and 524 nm, respectively. The formation of this intermediate complex was very fast, finishing within the dead time of the stopped-flow mixer (3 ms). Site-directed mutagenesis revealed that His-306 was the catalytic residue responsible for assisting the elimination of the hydrogen atom of PAOx.

X-C Reaction Mechanism of Metalloenzymes Related to Oxygen Activation

Oxygen is quite important molecule for most organisms. Oxygen is utilized for various physiological functions such as ATP synthesis, defense mechanism, oxidation reactions, and signal transduction. These diverse functions are realized by many metalloenzymes. In this project, we are studying molecular mechanisms of these metalloenzymes.

X-C-1 Oxidizing Intermediates from the Sterically Hindered Salen Iron Complexes Related to the Oxygen Activation by Nonheme Iron Enzymes

KURAHASHI, Takuya; KOBAYASHI, Yoshio¹; NAGATOMO, Shigenori; TOSHA, Takehiko; KITAGAWA, Teizo; FUJII, Hiroshi
(¹RIKEN)

[*Inorg. Chem.* **44**, 8156–8166 (2005)]

Oxidizing intermediates are generated from nonheme iron(III) complexes to investigate the electronic structure and the reactivity, in comparison with the oxoiron(IV) porphyrin π -cation radical (compound **1**) as a heme enzyme model. Sterically hindered salen iron complexes, bearing a fifth ligand Cl (**1**), OH₂ (**2**), OEt (**3**) and OH (**4**), are oxidized both electrochemically and chemically. Stepwise one-electron oxidation of **1** and **2** generates iron(III)–mono- and diphenoxyl radicals, as revealed by detailed spectroscopic investigations, including UV-Vis, EPR, Mössbauer, resonance Raman, and ESIMS spectroscopies. In contrast to the oxoiron(IV) formation from the hydroxoiron(III) porphyrin upon one-electron oxidation, the hydroxo complex **4** does not generate oxoiron(IV) species. Reaction of **2** with *m*CPBA also results in the formation of the iron(III)–phenoxyl radical. One-electron oxidation of **3** leads to oxidative degradation of the fifth EtO ligand to liberate acetaldehyde even at 203 K. The iron(III)–phenoxyl radical shows high reactivity for alcoxide on iron(III), but exhibits virtually no reactivity for alcohols including even benzyl alcohol without a base to remove an alcohol proton. The present study explains unique properties of mononuclear nonheme enzymes with Tyr residues, and also a poor epoxidation activity of Fe salen compared to Mn and Cr salens.

X-C-2 A Trigonal-Bipyramidal Geometry Induced by an External Water Ligand in a Sterically Hindered Iron Salen Complex, Related to the Active Site of Protocatechuate 3,4-Dioxygenase

KURAHASHI, Takuya; ODA, Kenji¹; SUGIMOTO, Manabu²; OGURA, Takashi¹; FUJII, Hiroshi
(¹Univ. Hyogo; ²Kumamoto Univ.)

[*Inorg. Chem.* in press]

A unique distorted trigonal-bipyramidal geometry observed for the nonheme iron center in protocatechuate 3,4-dioxygenase (3,4-PCD) was carefully examined

utilizing a sterically hindered iron salen complex, which well reproduces the endogenous His₂Tyr₂ donor set with water as an external ligand. X-ray crystal structures of a series of iron model complexes containing bis(3,5-dimesitylsalicylidene)-1,2-dimesitylethylenediamine indicate that a distorted trigonal-bipyramidal geometry is achieved upon binding of water as an external ligand. The extent of a structural change of the iron center from a preferred square-pyramidal to a distorted trigonal-bipyramidal geometry varies with the external ligand that is bound in the order Cl \ll EtO $<$ H₂O, which is consistent with the spectrochemical series. The distortion in the model system is not due to steric repulsions, but electronic interactions between the external ligand and the iron center, as evidenced from the X-ray crystal structures of another series of iron model complexes with a less-hindered bis(3-xylylsalicylidene)-1,2-dimesitylethylenediamine ligand, as well as by DFT calculations. Further spectroscopic investigations indicate that a unique distorted trigonal-bipyramidal geometry is indeed maintained even in solution. The present model study provides a new viewpoint that a unique distorted trigonal-bipyramidal iron site might not be preorganized by a 3,4-PCD protein, but could be electronically induced upon the binding of an external hydroxide ligand to the iron(III) center. The structural change induced by the external water ligand is also discussed in relation to the reaction mechanism of 3,4-PCD.

X-C-3 O₂- and H₂O₂-Dependent Verdoheme Degradation by Heme Oxygenase: Reaction Mechanisms and Potential Physiological Roles of the Dual Pathway Degradation

MATSUI, Toshitaka¹; NAKAJIMA, Aya¹; FUJII, Hiroshi; YOSHIDA, Tadashi²; IKEDA-SAITO, Masao¹
(¹Tohoku Univ.; ²Yamagata Univ.)

[*J. Biol. Chem.* **280**, 36833–36840 (2005)]

Heme oxygenase (HO) catalyzes catabolism of heme to biliverdin, CO and a free iron through three successive oxygenation steps. The third oxygenation, oxidative degradation of verdoheme to biliverdin, has been the least understood step in spite of its importance to regulate the HO activity. We have thoroughly examined degradation of a synthetic verdoheme IX α complexed with rat HO-1. Our major findings include: (1) HO degrades verdoheme through a dual pathway using either O₂ or H₂O₂; (2) the newly found H₂O₂ pathway is approximately 40-fold faster than the O₂-dependent degradation; (3) both reactions are initiated by the binding of O₂ or H₂O₂ to allow the first direct obser-

vation of degradation intermediates of verdoheme; and (4) Asp¹⁴⁰ in HO-1 is critical for the verdoheme degradation regardless of the oxygen source. On the basis of these findings, we propose that the HO enzyme activates O₂ and H₂O₂ on the verdoheme iron with the aid of a nearby water molecule linked with Asp¹⁴⁰. These mechanisms are similar to a well-established mechanism of the first oxygenation, *meso*-hydroxylation of heme, and thus, HO can utilize a common architecture to promote the first and third oxygenation steps of the heme catabolism. We also point out a possible involvement of the H₂O₂-dependent verdoheme degradation *in vivo*, and propose potential roles of the dual pathway reaction of HO against oxidative stress.

X-C-4 ¹³C and ¹⁵N NMR Studies of Iron-Bound Cyanides of Heme Proteins and Related Model Complexes: Sensitive Probe for Detecting Hydrogen Bonding Interactions at the Proximal and Distal Sides

FUJII, Hiroshi; YOSHIDA, Tadashi¹
(¹Yamagata Univ.)

[*Inorg. Chem.* **45**, 6816–6827 (2006)]

Studies of the ¹³C and ¹⁵N NMR paramagnetic shifts of the iron bound cyanides in the ferric cyanide forms of various heme proteins containing the proximal histidine and related model complexes are reported. The paramagnetic shifts of the ¹³C and ¹⁵N NMR signals of the iron bound cyanide are not significantly affected by the substitution of the porphyrin side chains. On the other hand, the paramagnetic shifts of both ¹³C and ¹⁵N NMR signals decrease with an increase in the donor effect of the proximal ligand and the ¹³C NMR signal is more sensitive to a modification of the donor effect of the proximal ligand than the ¹⁵N NMR signal. With the tilt of the iron–imidazole bond, the paramagnetic shift of the ¹³C NMR signal increases whereas that of the ¹⁵N NMR signal decreases. The hydrogen bonding interaction of the iron bound cyanide with a solvent decreases the paramagnetic shift of both ¹³C and ¹⁵N NMR signals, and the effect is more pronounced for the ¹⁵N NMR signal. Data on the ¹³C and ¹⁵N NMR signals of iron bound cyanide for various heme proteins are also reported and analyzed in detail. Substantial differences in the ¹³C and ¹⁵N NMR shifts for the heme proteins can be explained based on the results for the model complexes and structures around the heme in the heme proteins. The findings herein show that the paramagnetic shift of the ¹³C NMR signal of the iron bound cyanide is a good probe to estimate the donor effect of the proximal imidazole and that the ratio of ¹⁵N/¹³C NMR shifts allows estimating the hydrogen bonding interaction on the distal side.

X-C-5 Roles of the Heme Distal Residues of FixL in O₂ Sensing: A Single Convergent Structure of the Heme Moiety Is Relevant to the Downregulation of Kinase Activity

TANAKA, Atsunari¹; NAKAMURA, Hiro¹; SHIRO, Yoshitsugu¹; FUJII, Hiroshi

(¹RIKEN)

[*Biochemistry* **45**, 2515–2523 (2006)]

FixL is a heme-based O₂ sensor, in which the autophosphorylation is regulated by the binding of exogenous ligands such as O₂ and CN⁻. In this study, mutants of the heme distal Arg200, Arg208, Ile209, Ile210, and Arg214 residues of *Sm*FixL were characterized biochemically and physicochemically, because it has been suggested that they are significant residues in ligand-linked kinase regulation. Measurements of the autoxidation rate, affinities, and kinetics of ligand binding revealed that all of the above residues are involved in stabilization of the O₂-heme complex of FixL. However, Arg214 was found to be the only residue that is directly relevant to the ligand-dependent regulation of kinase activity. Although the wild type and R214K and R214Q mutants exhibited normal kinase regulation, R214A, R214M, R214H, and R214Y did not. ¹³C and ¹⁵N NMR analyses for ¹³C¹⁵N⁻ bound to the truncated heme domains of the Arg214 mutants indicated that, in the wild type and the foregoing two mutants, the heme moiety is present in a single conformation, but in the latter four, the conformations fluctuate possibly because of the lack of an interaction between the iron-bound ligand and residue 214. It is likely that such a rigid conformation of the ligand-bound form is important for the downregulation of histidine kinase activity. Furthermore, a comparison of the NMR data between the wild type and R214K and R214Q mutants suggests that a strong electrostatic interaction between residue 214 and the iron-bound ligand is not necessarily required for the single convergent structure and eventually for the downregulation of FixL.

X-C-6 ¹⁷O NMR Study of Oxo Metalloporphyrin Complexes: Correlation with Electronic Structure of M=O Moiety

FUJII, Hiroshi; KURAHASHI, Takuya; TOSHA, Takehiko; YOSHIMURA, Tetsuhiko¹; KITAGAWA, Teizo
(¹Yamagata Promotional Org. Industrial Tech.)

[*J. Inorg. Biochem.* **100**, 533–541 (2006)]

¹⁷O NMR spectroscopy of oxo ligand of oxo metalloporphyrin can be considered as an excellent means to derive information about structure, electronic state, and reactivity of the metal bound oxo ligand. To show the utility of ¹⁷O NMR spectroscopy of oxo ligand of oxo metalloporphyrin, ¹⁷O-NMR spectra of oxo ligands of dioxo ruthenium(VI), oxo chromium(IV), and oxo titanium(IV) porphyrins are measured. For all oxo metalloporphyrins, well-resolved ¹⁷O NMR signals are detected in far high frequency region. The ¹⁷O NMR signal of the metal bound oxo ligand shifts high frequency in order of Ru(VI) < Ti(IV) < Cr(IV), thus the ¹⁷O NMR chemical shift does not directly correlate with the oxo-transfer reactivity, Ti(IV) < Cr(IV) < Ru(VI). On the other hand, the ¹⁷O NMR shift of oxo ligand correlates with the bond strength of metal–oxo bond. This suggests that the ¹⁷O NMR signal of metal bound oxo ligand is a sensitive

probe to study the nature of metal–oxo bond in oxo metalloporphyrin. The effect of the electron-withdrawing meso-substituent on the ^{17}O NMR shift of the oxo ligand is also investigated. With increase in the electron-withdrawing effect of the meso-substituent, the ^{17}O NMR signal of the oxo ligand of oxo chromium(IV)

porphyrin shifts high frequency while that of dioxo ruthenium(VI) porphyrin hardly change resonance position. The changes in metal–oxo bonds induced by the electron-withdrawing meso-substituent are discussed on the basis of the ^{17}O NMR shifts, the strengths of the metal–oxo bonds, and the oxo-transfer reaction rates.

X-D Reaction Mechanism of Metalloenzymes Related to Global Nitrogen Cycle

For all organisms, organic nitrogen and ammonia are required as a constituent part of the cell. In order to keep the environment of the earth constant, the organic nitrogen, fixed nitrogen, must be completely reconvered into dinitrogen gas. The reverse process of the nitrogen fixing is called denitrification process. In this process, nitrate or nitrite ion is reduced to nitrogen gas *via* nitric oxide and nitrous oxide by many metalloenzymes, nitrate reductase, nitrite reductase, nitric oxide reductase, and nitrous oxide reductase. In this project, we are studying the molecular mechanism of these metalloenzymes relating to the denitrification process.

X-D-1 Kinetic Isotope Effects on the Rate-Limiting Step of Heme Oxygenase Catalysis Indicate Concerted Proton Transfer/Heme Hydroxylation

KUJIME, Masato; FUJII, Hiroshi

[*Angew. Chem., Int. Ed.* **45**, 1089–1092 (2006)]

Reduction of nitrite (NO_2^-) to gaseous nitric oxide (NO) is one of key processes in the global nitrogen cycle and carried out by bacterial copper-containing nitrite reductases (NiR). The enzymes contain two copper ion centers: the type 1 copper site for electron transfer and the type 2 copper site for the catalytic nitrite reduction. Crystallographic and spectroscopic studies of Nir have proposed the mechanism of the nitrite reduction at the type 2 copper site. The enzyme reaction is initiated by the binding of the nitrite to the reduced form of the type 2 copper site to yield a copper(I) nitrite complex. Subsequently, the copper bound nitrite is reduced to NO and water with intramolecular one electron transfer from the type 2 copper(I) ion and two protons from a conserved aspartic acid placed near the type 2 site. During the course of synthetic study of the copper(I) nitrite complexes, we found that the rapid mixing of copper(I) nitrite complex with trifluoroacetic acid (TFA) with stopped flow at low temperature allows to detect new reaction intermediates in the reduction process. Here, we report detection and characterization of new reaction intermediates in the nitrite reduction. This study shows that two protons required for the reaction are not provided to the copper bound nitrite simultaneously but stepwise and that the intramolecular electron transfer from the copper(I) ion to the copper bound nitrite occurs in the second protonation step.

X-D-2 ^{63}Cu NMR Spectroscopy of Copper(I) Complexes with Various Tridentate Ligands: CO as a Useful ^{63}Cu NMR Probe for Sharpening ^{63}Cu NMR Signals and Analyzing the Electronic Donor Effect of a Ligand

KUJIME, Masato; KURAHASHI, Takuya;
TOMURA, Masaaki; FUJII, Hiroshi

[*Inorg. Chem.* in press]

^{63}Cu NMR spectroscopic studies of copper(I) complexes with various N-donor tridentate ligands are reported. As has been previously reported for most copper(I) complexes, ^{63}Cu NMR signals, when acetonitrile is coordinated to copper(I) complexes of these tridentate ligands, are extremely broad or undetectable. However, when CO is bound the above tridentate copper(I) complexes, the ^{63}Cu NMR signals become much sharper and show a large downfield shift, compared to those for the corresponding acetonitrile complexes. Temperature dependence of ^{63}Cu NMR signals for these copper(I) complexes show that a quadrupole relaxation process is much more significant to their ^{63}Cu NMR line widths than a ligand exchange process. Therefore, an electronic effect of the copper bound CO makes the ^{63}Cu NMR signal sharp and easily detected. The large downfield shift for the copper(I) carbonyl complex can be explained by a paramagnetic shielding effect induced by the copper bound CO, which amplifies small structural and electronic changes that occur around the copper ion to be easily detected in their ^{63}Cu NMR shifts. This is evidenced by the correlation between the ^{63}Cu NMR shifts for the copper(I) carbonyl complexes and their $\nu(\text{C}\equiv\text{O})$ values. Furthermore, the ^{63}Cu NMR shifts for copper(I) carbonyl complexes with imino type tridentate ligands show a different correlation line with those for amino type tridentate ligands. On the other hand, ^{13}C NMR shifts for the copper bound ^{13}CO for these copper(I) carbonyl complexes do not correlate with the $\nu(\text{C}\equiv\text{O})$ values. The X-ray crystal structures of

these copper(I) carbonyl complexes do not show any evidence of a significant structural change around the Cu–CO moiety. The findings herein show that CO has great potential as a probe in ^{63}Cu NMR spectroscopic studies for characterizing the nature of the environment around copper ions in copper complexes.

X-E Biomolecular Science

Elucidation of a structure-function relationship of metalloproteins and structural chemistry of amyloid fibril are current subjects of this group. The primary technique used for the first project is the stationary and time-resolved resonance Raman spectroscopy excited by visible and UV lasers. Various model compounds of active site of enzymes are also examined with the same technique. IR-microscope dichroism analysis is the main techniques for the second project. The practical themes that we want to explore for the first project are (1) mechanism of oxygen activation by enzymes, (2) mechanism of active proton translocation and its coupling with electron transfer, (3) structural mechanism of signal sensing and transmission by heme-based sensory proteins, (4) higher order protein structures and their dynamics, and (5) reactions of biological NO.

In category (1), we have examined a variety of terminal oxidases in the respiratory chain, cytochrome P450s (including AOS), and peroxidases, and also treated their reaction intermediates by using the mixed-flow transient Raman apparatus and the Raman/absorption simultaneous measurement device. For (2) the third-generation UV resonance Raman (UVR) spectrometer was constructed in this laboratory and applied to a giant protein like cytochrome *c* oxidase with $M_r = 210,000$, particularly to explore the oxidation state of Tyr244 in the P_M intermediate. Furthermore, a model complex of the Cu_B -His(240)-Tyr(244) and its Tyr-radical state were investigated in detail by UVR spectroscopy. Recently, we succeeded in pursuing protein folding of apomyoglobin by combining the UV time-resolved Raman and rapid mixing techniques. With IR spectroscopy we determined the spectrum of carboxylic side chains of bovine cytochrome oxidase which undergo protonation/deprotonation changes and hydrogen-bonding status changes in response with electron transfers between metal centers or with ligand dissociation from heme a_3 . In (3) we are interested in a mechanism of ligand recognition specific to CO, NO or O_2 and a communication pathway of the ligand binding information to the functional part of the protein. Several gas sensor heme proteins including DOS, HemAT, CooA, and NAPS2 were extensively treated in this year. For (4) we developed a novel technique for UV resonance Raman measurements based on the combination of the first/second order dispersions of gratings and applied it successfully to 235-nm excited RR spectra of several proteins including mutant hemoglobins and myoglobins.

Nowadays we can carry out time-resolved UVR experiments with sub-nanosecond time resolution to discuss protein dynamics. With the system, we have succeeded in isolating the spectrum of tyrosinate in ferric Hb M Iwate, which was protonated in the ferrous state, and the deprotonated state of Tyr244 of bovine cytochrome *c* oxidase. The study is extended to a model of Tyr244, that is, imidazole-bound *para*-cresol coordinated to a metal ion, was synthesized and its UV resonance Raman was investigated. For (5) we purified soluble guanylate cyclase from bovine lung and observed its RR spectra in the presence of allosteric effector, YC-1. The CO and NO adducts in the presence of YC-1 were examined. To further investigate it, we are developing an expression system of this protein. For the amyloid study, we examined FTIR spectra of β_2 -microglobulin and its fragment peptides of #11-21, K3, and K3-K7 which form a core part of amyloid fibril of β_2 -microglobulin. The effect of seed upon the fibril structure and the chemical interactions of peptides in the growth process of amyloid fibril were focused in this year.

X-E-1 Kinetics and DFT Studies on the Reaction of Copper(II) Complexes and H_2O_2

OSAKO, Takao¹; NAGATOMO, Shigenori²;
KITAGAWA, Teizo; CHRISTOPHER, J. Cramer³;
ITO, Shinobu¹

(¹Osaka City Univ.; ²IMS and Univ. Tsukuba; ³Univ. Minnesota)

[*J. Biol. Inorg. Chem.* **10**, 581–590 (2005)]

Copper(II) complexes supported by bulky tridentate ligands $L1^H$ (*N,N*-bis(2-quinolylmethyl)-2-phenylethylamine) and $L1^{Ph}$ (*N,N*-bis(2-quinolylmethyl)-2,2-diphenylethylamine) have been prepared and their crystal structures as well as some physicochemical properties have been explored. Each complex exhibits a square pyramidal structure containing a coordinated solvent molecule at an equatorial position and a weakly coordinated counter anion (or water) at an axial position. The copper(II) complexes reacted readily with H_2O_2 at a low temperature to give mononuclear hydroperoxo copper(II) complexes. Kinetics and DFT studies have suggested that, in the initial stage of the reaction, deprotonated hydrogen peroxide attacks the cupric ion, presumably at

the axial position, to give a hydroperoxo copper(II) complex retaining the coordinated solvent molecule ($H^R \cdot S$). $H^R \cdot S$ then loses the solvent to give a tetragonal copper(II)-hydroperoxo complex (H^R), in which the -OOH group may occupy an equatorial position. The copper(II)-hydroperoxo complex H^R exhibits a relatively high O–O bond stretching vibration at 900 cm^{-1} compared to other previously reported examples.

X-E-2 Detection of the His-Heme Fe^{2+} -NO Species in the Reduction of NO to N_2O by ba_3 -Oxidase from *Thermus thermophilus*

PINAKOULAKI, Eftychia¹; OHTA, Takehiro²;
SOULIMANE, Tewfik³; KITAGAWA, Teizo;
VAROTSIS, Constantinos¹

(¹Univ. Crete; ²IMS and Stanford Univ.; ³Paul Scherrer Inst.)

[*J. Am. Chem. Soc.* **127**, 15161–15167 (2005)]

Reaction pathways in the enzymatic formation and cleavage of the N–N and N–O bonds, respectively, are difficult to verify without the structure of the intermediates, but we now have such information on the

heme a_3^{2+} -NO species formed in the reaction of ba_3 -oxidase with NO from resonance Raman spectroscopy. We have identified the His-heme a_3^{2+} -NO/ Cu_B^{1+} species by its characteristic Fe-NO and N-O stretching frequencies at 539 and 1620 cm^{-1} , respectively. The Fe-NO and N-O frequencies in ba_3 -oxidase are 21 and 7 cm^{-1} lower and higher, respectively, than those observed in Mb-NO. From these results and earlier Raman and FTIR measurements, we demonstrate that the protein environment of the proximal His384 that is part of the Q-proton pathway controls the strength of the Fe-His384 bond upon ligand (CO vs NO) binding. We also show by time-resolved FTIR spectroscopy that Cu_B^{1+} has a much lower affinity for NO than for CO. We suggest that the reduction of NO to N_2O by ba_3 -oxidase proceeds by the fast binding of the first NO molecule to heme a_3 with high-affinity, and the second NO molecule binds to Cu_B with low-affinity, producing the temporal co-presence of two NO molecules in the heme-copper center. The low-affinity of Cu_B for NO binding also explains the NO reductase activity of the ba_3 -oxidase as opposed to other heme-copper oxidases. With the identification of the His-heme a_3^{2+} -NO/ Cu_B^{1+} species, the structure of the binuclear heme a_3 - Cu_B^{1+} center in the initial step of the NO reduction mechanism is known.

X-E-3 Structural Studies Reveal that the Diverse Morphology of β_2 -Microglobulin Aggregates is a Reflection of Different Molecular Architectures

KARDOS, Jozsef¹; OKUNO, Daichi²; KAWAI, Tomoji³; HAGIHAWA, Yoshihisa⁴; YUMOTO, Noboru⁴; KITAGAWA, Teizo; ZAVODSZKY, Peter⁵; NAIKI, Hironobu⁶; GOTO, Yuji³
(¹Eötvös Lorand Univ.; ²SOKENDAI and Osaka Univ.; ³Osaka Univ.; ⁴AIST; ⁵HAS; ⁶Univ. Fukui)

[*Biochim. Biophys. Acta* **1753**, 108–120 (2005)]

Amyloid deposition accompanies over 20 degenerative diseases in human, including Alzheimer's, Parkinson's, and prion diseases. Recent studies revealed the importance of other type of protein aggregates, *e.g.*, non-specific aggregates, protofibrils, and small oligomers in the development of such diseases and proved their increased toxicity for living cells in comparison with mature amyloid fibrils. We carried out a comparative structural analysis of different monomeric and aggregated states of β_2 -microglobulin, a protein responsible for hemodialysis-related amyloidosis. We investigated the structure of the native and acid-denatured states, as well as that of mature fibrils, immature fibrils, amorphous aggregates, and heat-induced filaments, prepared under various *in vitro* conditions. Infrared spectroscopy demonstrated that the β -sheet compositions of immature fibrils, heat-induced filaments and amorphous aggregates are characteristic of antiparallel intermolecular β -sheet structure while mature fibrils are different from all others suggesting a unique overall structure and assembly. Filamentous aggregates prepared by heat treatment are of importance in understanding the *in vivo* disease because of their stability under physiological conditions, where amyloid fibrils and protofibrils

formed at acidic pH depolymerize. Atomic force microscopy of heat-induced filaments represented a morphology similar to that of the low pH immature fibrils. At a pH close to the pI of the protein, amorphous aggregates were formed readily with association of the molecules in native-like conformation, followed by formation of intermolecular β -sheet structure in a longer time-scale. Extent of the core buried from the solvent in the various states was investigated by H/D exchange of the amide protons.

X-E-4 Biophysical Properties of a c-Type Heme in Chemotaxis Signal Transducer Protein DcrA

YOSHIOKA, Shiro; KOBAYASHI, Katsuaki¹; YOSHIMURA, Hideaki; UCHIDA, Takeshi²; KITAGAWA, Teizo; AONO, Shigetoshi
(¹IMS and Chuo Univ.; ²IMS and Hokkaido Univ.)

[*Biochemistry* **44**, 15406–15413 (2005)]

Chemotaxis signal transducer protein DcrA from a sulfate-reducing bacterium *Desulfovibrio vulgaris* Hildenborough was previously shown to contain a c-type heme in its periplasmic domain (DcrA-N) for sensing redox and/or oxygen [Fu *et al. J. Bacteriol.* **176**, 344–350 (1994)], which is the first example of a heme-based sensor protein containing a c-type heme as a prosthetic group. Optical absorption and resonance Raman spectroscopies indicate that heme c in DcrA-N shows a redox-dependent ligand exchange. Upon reduction, a water molecule that may be the sixth ligand of the ferric heme c is replaced by an endogenous amino acid. Although the reduced heme in DcrA-N is six-coordinated with two endogenous axial ligands, CO can easily bind to the reduced heme to form CO-bound DcrA-N. Reaction of the reduced DcrA-N with molecular oxygen results in autoxidation to form a ferric state without forming any stable oxygen-bound form probably due to the extremely low redox potential of DcrA-N (–250 mV). Our study supports the initial idea by Fu *et al.* that DcrA would act as a redox and/or oxygen sensor, in which the ligand exchange between water and an endogenous amino acid is a trigger for signal transduction. While the affinity of CO to DcrA-N ($K_d = 138 \mu M$) is significantly weak compared to those of other heme proteins, we suggest that CO might be another physiological effector molecule.

X-E-5 Discovery of a Reaction Intermediate of Aliphatic Aldoxime Dehydratase Involving Heme as an Active Center

KONISHI, Kazunobu¹; OHTA, Takehiro²; OINUMA, Ken-Ichi¹; HASHIMOTO, Yoshiteru¹; KITAGAWA, Teizo; KOBAYASHI, Michihiko¹
(¹Univ. Tsukuba; ²IMS and Stanford Univ.)

[*Proc. Natl. Acad. Sci. U.S.A.* **103**, 564–568 (2006)]

Recently, we discovered an intriguing hemoprotein [aliphatic aldoxime dehydratase (OxDa)] that catalyzes the dehydration of aliphatic aldoximes [R-CH=N-OH] to the corresponding nitriles [R-CN] in the industrial

Pseudomonas chlororaphis B23 strain. Unlike the utilization of H₂O₂ or O₂ as a mediator of the catalysis by other heme-containing enzymes (e.g., P450), OxdA is notable for the direct binding of a substrate to the heme iron, experimental evidence of which was obtained here by means of resonance Raman (RR) analysis with an isotope technique. We found that the addition of a large amount of butyraldoxime (final concentration, 200 mM) to ferrous OxdA with a low enzyme concentration (final concentration, 5 μM) yields a long-lived OxdA-substrate complex (named OS-II), whose UV-vis spectrum is different from the corresponding spectra of the OxdA-substrate complex I and CO-bound, ferrous, and ferric forms of OxdA. Intriguingly, the RR analysis demonstrated that OS-II includes a highly oxidized heme with strong bonding between a substrate and the heme iron, as judged from the heme oxidation state marker_{v4} band at 1,379 cm⁻¹ and the ¹⁵N-isotope-substituted butyraldoxime sensitive band at 857 cm⁻¹ in the RR spectra. It is noteworthy that OS-II has a highly oxidized heme like the ferryl-oxo heme species (e.g., compound II) formed by some general hemoproteins, although the function of OxdA is different from those (transport of electrons, transport of oxygen, sensing of oxygen or carbon monoxide, and catalysis of redox reactions) of general hemoproteins.

X-E-6 Intramolecular Arene Hydroxylation versus Intermolecular Olefin Epoxidation by (μ-η²:η²-Peroxo)dinickel(II) Complex Supported by Dinucleating Ligand

MATSUMOTO, Takahiro¹; FURUTACHI, Hideki¹; KOBINO, Masashi¹; TOMII, Masato¹; NAGATOMO, Shigenori²; TOSHA, Takehiko; OSAKO, Takao³; FUJINAMI, Shuhei¹; ITOH, Shinobu³; KITAGAWA, Teizo; SUZUKI, Masatatsu¹ (¹Kanazawa Univ.; ²IMS and Univ. Tsukuba; ³Osaka City Univ.)

[*J. Am. Chem. Soc.* **128**, 3874–3875 (2006)]

A discrete (μ-η²:η²-peroxo)Cu(II)₂ complex, [Cu₂(O₂)(H-L)]²⁺, is capable of performing not only intramolecular hydroxylation of a *m*-xylyl linker of a dinucleating ligand but also intermolecular epoxidation of styrene *via* electrophilic reaction to the C=C bond and hydroxylation of THF by H-atom abstraction.

X-E-7 Significance of the Molecular Shape of Iron Corrphycene in a Protein Pocket

NEYA, Saburo¹; IMAI, Kiyohiro²; HIRAMATSU, Yoshitsugu³; KITAGAWA, Teizo; HOSHINO, Tyuji⁴; HATA, Masayuki¹; FUNASAKI, Noriaki⁵ (¹Chiba Univ.; ²Sapporo Med. Univ.; ³Okayama Univ.; ⁴Hamamatsu ENT Surgicenter; ⁵Kyoto Pharm. Univ.)

[*Inorg. Chem.* **45**, 4238–4242 (2006)]

The iron complex of a new type of corrphycene bearing two ethoxycarbonyl (-CO₂C₂H₅) groups on the bipyrrrole moiety was introduced into apomyoglobin. The reconstituted ferric myoglobin has a coordinating

water molecule that deprotonates to hydroxide with a pK_a value of 7.3 and exhibits 3–10-fold higher affinities for anionic ligands when compared with a counterpart myoglobin with the same substituents on the dipyrroethene moiety. In the ferrous state, the oxygen affinity of the new myoglobin was decreased to 1/10 of the native protein. The anomalies in the ligand binding, notably dependent on the side-chain location, were interpreted in terms of a characteristic core shape of corrphycene that produces the longer and shorter Fe–N(pyrrole) bonds. The spin-state equilibrium analysis of the ferric azide myoglobin containing the new iron corrphycene supported the nonequivalence of the Fe–N(pyrrole) bonds. These results demonstrate that the trapezoidal molecular shape of corrphycene exerts functional significance when the iron complex is placed in a protein pocket.

X-E-8 Sequential Reaction Intermediates in Aliphatic C–H Bond Functionalization Initiated by a Bis(μ-oxo)dinickel(III) Complex

CHO, Jaeheung¹; FURUTACHI, Hideki¹; FUJINAMI, Shuhei¹; TOSHA, Takehiko; OHTSU, Hideki; IKEDA, Osamu¹; SUZUKI, Akane²; NOMURA, Masaharu²; URUGA, Tomoya³; TANIDA, Hajime³; KAWAI, Toshihide³; TANAKA, Koji; KITAGAWA, Teizo; SUZUKI, Masatatsu¹ (¹Kanazawa Univ.; ²KEK; ³JASRI)

[*Inorg. Chem.* **45**, 2873–2885 (2006)]

Reaction of [Ni₂(OH)₂(Me₂-tpa)₂]²⁺ (**1**) (Me₂-tpa = bis(6-methyl-2-pyridylmethyl)(2-pyridylmethyl)amine) with H₂O₂ causes oxidation of a methylene group of Me₂-tpa ligand to give N-dealkylated ligand and oxidation of a methyl group to afford ligand-based carboxylate and alkoxide as final oxidation products. A series of the sequential reaction intermediates produced in the oxidation pathways, a bis(μ-oxo)dinickel(III) ([Ni₂(O)₂(Me₂-tpa)₂]²⁺ (**2**)), a bis(μ-superoxo)dinickel(II) ([Ni₂(O₂)₂(Me₂-tpa)₂]²⁺ (**3**)), a (μ-hydroxo)(μ-alkylperoxo)dinickel(II) ([Ni₂(OH)(Me₂-tpa)(Me-tpa-CH₂OO)]²⁺ (**4**)), and a bis(μ-alkylperoxo)dinickel(II) ([Ni₂(Me-tpa-CH₂OO)₂]²⁺ (**5**)), was isolated and characterized by various physicochemical measurements including X-ray crystallography and their oxidation pathways were investigated. Reaction of **1** with H₂O₂ in methanol at -40 °C generates **2**, which is extremely reactive with H₂O₂ to produce **3**. **2** was isolated only from disproportionation of **3** in the absence of H₂O₂ at -40 °C. Thermal decomposition of **2** under N₂ generated an N-dealkylated ligand Me-dpa ((6-methyl-2-pyridylmethyl)(2-pyridylmethyl)amine) and a ligand-coupling dimer (Me-tpa-CH₂)₂. The formation of (Me-tpa-CH₂)₂ suggests that a ligand-based radical Me-tpa-CH₂• is generated as a reaction intermediate produced probably by H-atom abstraction by the oxo group. Isotope labeling experiment revealed that intramolecular coupling occurs for the formation of the coupling dimer. The results indicates that rebound of oxygen to the Me-tpa-CH₂• is slower compared to those observed for various high-valent bis(μ-oxo)dimetal complexes. In contrast, decomposition of **2** and **3** in the presence of O₂ gave

carboxylate and alkoxide ligands (Me-tpa-COO⁻ and Me-tpa-CH₂O⁻) instead of (Me-tpa-CH₂)₂, indicating that the reaction of the Me-tpa-CH₂• with O₂ is faster than the coupling of Me-tpa-CH₂• to generate a ligand-based peroxy radical Me-tpa-CH₂OO•. Although there is a possibility that the Me-tpa-CH₂OO• species could undergo various reactions, one of possible reactive intermediates, **4**, was isolated from the decomposition of **3** under O₂ at -20 °C. The alkylperoxy ligands in **4** and **5** can be converted to a ligand-based aldehyde by either homolysis or heterolysis of the O-O bond and disproportionation of the aldehyde gives carboxylate and alkoxide *via* the Cannizzaro reaction.

X-E-9 ¹⁷O NMR Study of Oxo Metalloporphyrin Complexes: Correlation with Electronic Structure of M=O Moiety

FUJII, Hiroshi; KURAHASHI, Takuya; TOSHA, Takehiko; YOSHIMURA, Tetsuaki; KITAGAWA, Teizo

[*J. Inorg. Biochem.* **100**, 533–541 (2006)]

¹⁷O NMR spectroscopy of oxo ligand of oxo metalloporphyrin can be considered as an excellent means to derive information about structure, electronic state, and reactivity of the metal bound oxo ligand. To show the utility of ¹⁷O NMR spectroscopy of oxo ligand of oxo metalloporphyrin, ¹⁷O NMR spectra of oxo ligands of dioxo ruthenium(VI), oxo chromium(IV), and oxo titanium(IV) porphyrins are measured. For all oxo metalloporphyrins, well-resolved ¹⁷O NMR signals are detected in far high frequency region. The ¹⁷O NMR signal of the metal bound oxo ligand shifts high frequency in order of Ru(VI) < Ti(IV) < Cr(IV), thus the ¹⁷O NMR chemical shift does not directly correlate with the oxo-transfer reactivity, Ti(IV) < Cr(IV) < Ru(VI). On the other hand, the ¹⁷O NMR shift of oxo ligand correlates with the bond strength of metal-oxo bond. This suggests that the ¹⁷O NMR signal of metal bound oxo ligand is a sensitive probe to study the nature of metal-oxo bond in oxo metalloporphyrin. The effect of the electron-withdrawing meso-substituent on the ¹⁷O NMR shift of the oxo ligand is also investigated. With increase in the electron-withdrawing effect of the meso-substituent, the ¹⁷O NMR signal of the oxo ligand of oxo chromium(IV) porphyrin shifts high frequency while that of dioxo ruthenium(VI) porphyrin hardly change resonance position. The changes in metal-oxo bonds induced by the electron-withdrawing meso-substituent are discussed on the basis of the ¹⁷O NMR shifts, the strengths of the metal-oxo bonds, and the oxo-transfer reaction rates.

X-E-10 Nonheme Iron(II) Complexes of Macrocyclic Ligands in the Generation of Oxoiron(IV) Complexes and the Catalytic Epoxidation of Olefins

SUH, Yumi¹; SEO, Mi Sook¹; KIM, Kwan Mook¹; KIM, Youn Sang¹; JANG, Ho G.²; TOSHA, Takehiko; KITAGAWA, Teizo; KIM, Jinheung¹; NAM, Wonwoo¹
(¹Ewha Womans Univ.; ²Korea Univ.)

[*J. Inorg. Biochem.* **100**, 627–633 (2006)]

Mononuclear nonheme oxoiron(IV) complexes bearing 15-membered macrocyclic ligands were generated from the reactions of their corresponding iron(II) complexes and iodosylbenzene (PhIO) in CH₃CN. The oxoiron(IV) species were characterized with various spectroscopic techniques such as UV-vis spectrophotometer, electron paramagnetic resonance, electrospray ionization mass spectrometer, and resonance Raman spectroscopy. The oxoiron(IV) complexes were inactive in olefin epoxidation. In contrast, when iron(II) and oxoiron(IV) complexes are combined with PhIO in the presence of olefins, high yields of oxygenated products were obtained. These results indicate that in addition to the oxoiron(IV) species, there must be at least one more active oxidant (*e.g.*, Fe^{IV}-OIPh adduct and oxoiron(V) species) that is responsible for the olefin epoxidation. We have also demonstrated that the ligand environment of iron catalysts is an important factor in controlling the product selectivity as well as the catalytic activity in the catalytic epoxidation of olefins.

X-E-11 Resonance Raman Enhancement of Fe^{IV}=O Stretch in High-Valent Iron Porphyrins: An Insight from TD-DFT Calculations

KOZLOWSKI, Pawel M.¹; KUTA, Jadwiga¹; OHTA, Takehiro²; KITAGAWA, Teizo
(¹Louisvill Univ.; ²IMS and Stanford Univ.)

[*J. Inorg. Biochem.* **100**, 744–750 (2006)]

Density functional theory (DFT) has been applied to explain the origin of resonance Raman enhancement associated with the Fe^{IV}=O stretch observed in iron(IV) oxo porphyrins. To accomplish this electronic excitations of the Im-(Por) Fe^{IV}=O model were computed in the 1.5–4.0 eV spectral range using time-dependent DFT (TD-DFT). All electronic transitions having dominant π → π* character were analyzed and assigned in terms of one-electron excitations. It was found that the most intense Soret band has a multi-component character, but the π (a_{2u}) → π* (d_{xz}, d_{yz}) and π (a_{1u}) → π* (d_{xz}, d_{yz}) electronic excitations are primarily responsible for observed resonance enhancement of the Fe^{IV}=O stretch.

X-E-12 Spectroscopic and Substrate Binding Properties of Heme-Containing Aldoxime Dehydratases, OxdB and OxdRe

KOBAYASHI, Katsuaki¹; PAL, Biswajit²; YOSHIOKA, Shiro; KATO, Yasuo³; ASANO, Yasuhisa³; KITAGAWA, Teizo; AONO, Shigetoshi
(¹IMS and Chuo Univ.; ²IMS and CCMB; ³Toyama Pref. Univ.)

[*J. Inorg. Biochem.* **100**, 1069–1074 (2006)]

Aldoxime dehydratase (Oxd) is a novel hemeprotein that catalyzes the dehydration reaction of aldoxime to produce nitrile. In this study, we studied the spectroscopic and substrate binding properties of two Oxds, OxdB from *Bacillus* sp. strain OxB-1 and OxdRE from

Rhodococcus sp. N-771, that show different quaternary structures and relatively low amino acid sequence identity. Electronic absorption and resonance Raman spectroscopy revealed that ferric OxdRE contained a six-coordinate low-spin heme, while ferric OxdB contained a six-coordinate high-spin heme. Both ferrous OxdRE and OxdB included a five-coordinate high-spin heme to which the substrate was bound via its nitrogen atom for the reaction to occur. Although the ferric Oxds were inactive for catalysis, the substrate was bound to the ferric heme via its oxygen atom in both OxdB and OxdRE. Electronic paramagnetic resonance (EPR) and rapid scanning spectroscopy revealed that the flexibility of the heme pocket was different between OxdB and OxdRE, which might affect their substrate specificity.

X-E-13 Spectroscopic and DNA-Binding Characterization of the Isolated Heme-Bound Basic Helix-Loop-Helix-PAS-A Domain of Neuronal PAS Protein 2 (NPAS2), a Transcription Activator Protein Associated with Circadian Rhythms

MUKAIYAMA, Yuji¹; UCHIDA, Takeshi²; SATO, Emiko¹; SASAKI, Ai¹; SATO, Yuko¹; IGARASHI, Jotaro¹; KUROKAWA, Hirofumi¹; SAGAMI, Ikuko³; KITAGAWA, Teizo; SHIMIZU, Toru¹
(¹Tohoku Univ.; ²IMS and Hokkaido Univ.; ³Tohoku Univ. and Kyoto Pref. Univ.)

[*FEBS J.* **273**, 2528–2539 (2006)]

Neuronal PAS domain protein 2 (NPAS2) is a circadian rhythm-associated transcription factor with two heme-binding sites on two PAS domains. In the present study, we compared the optical absorption spectra, resonance Raman spectra, heme-binding kinetics and DNA-binding characteristics of the isolated fragment containing the N-terminal basic helix-loop-helix (bHLH) of the first PAS (PAS-A) domain of NPAS2 with those of the PAS-A domain alone. We found that the heme-bound bHLH-PAS-A domain mainly exists as a dimer in solution. The Soret absorption peak of the Fe(III) complex for bHLH-PAS-A (421 nm) was located at a wavelength 9 nm higher than for isolated PAS-A (412 nm). The axial ligand *trans* to CO in bHLH-PAS-A appears to be His, based on the resonance Raman spectra. In addition, the rate constant for heme association with apo-bHLH-PAS ($3.3 \times 10^7 \text{ mol}^{-1}\cdot\text{s}^{-1}$) was more than two orders of magnitude higher than for association with apo-PAS-A ($< 10^5 \text{ mol}^{-1}\cdot\text{s}^{-1}$). These results suggest that the bHLH domain assists in stable heme binding to NPAS2. Both optical and resonance Raman spectra indicated that the Fe(II)–NO heme complex is five-coordinated. Using the quartz-crystal microbalance method, we found that the bHLH-PAS-A domain binds specifically to the E-box DNA sequence in the presence, but not in the absence, of heme. On the basis of these results, we discuss the mode of heme binding by bHLH-PAS-A and its potential role in regulating DNA binding.

X-E-14 Specific Hydrogen-Bonding Networks Responsible for Selective O₂ Sensing of the Oxygen Sensor Protein HemAT from *Bacillus subtilis*

YOSHIMURA, Hideaki; YOSHIOKA, Shiro; KOBAYASHI, Katsuaki¹; OHTA, Takehiro²; UCHIDA, Takeshi³; KUBO, Minoru; KITAGAWA, Teizo; AONO, Shigetoshi
(¹IMS and Chuo Univ.; ²IMS and Stanford Univ.; ³IMS and Hokkaido Univ.)

[*Biochemistry* **45**, 8301–8307 (2006)]

HemAT from *Bacillus subtilis* (HemAT-Bs) is a heme-based O₂ sensor protein that acts as a signal transducer responsible for aerotaxis. HemAT-Bs discriminates its physiological effector, O₂, from other gas molecules to generate the aerotactic signal, but the detailed mechanism of the selective O₂ sensing is not obvious. In this study, we measured electronic absorption, electron paramagnetic resonance (EPR), and resonance Raman spectra of HemAT-Bs to elucidate the mechanism of selective O₂ sensing by HemAT-Bs. Resonance Raman spectroscopy revealed the presence of a hydrogen bond between His86 and the heme propionate only in the O₂-bound form, in addition to that between Thr95 and the heme-bound O₂. The disruption of this hydrogen bond by the mutation of His86 caused the disappearance of a conformer with a direct hydrogen bond between Thr95 and the heme-bound O₂ that is present in WT HemAT-Bs. On the basis of these results, we propose a model for selective O₂ sensing by HemAT-Bs as follows. The formation of the hydrogen bond between His86 and the heme propionate induces a conformational change of the CE-loop and the E-helix by which Thr95 is located at the proper position to form the hydrogen bond with the heme-bound O₂. This stepwise conformational change would be essential to selective O₂ sensing and signal transduction by HemAT-Bs.

X-E-15 Raman Evidence for Specific Substrate-Induced Structural Changes in the Heme Pocket of Human Cytochrome P450 Aromatase during the Three Consecutive Oxygen Activation Steps

TOSHA, Takehiko; KAGAWA, Norio¹; OHTA, Takehiro²; YOSHIOKA, Shiro; WATERMAN, Michael R.¹; KITAGAWA, Teizo
(¹Vanderbilt Univ.; ²IMS and Stanford Univ.)

[*Biochemistry* **45**, 5631–5640 (2006)]

Specific substrate-induced structural changes in the heme pocket are proposed for human cytochrome P450 aromatase (P450arom) which undergoes three consecutive oxygen activation steps. We have experimentally investigated this heme environment by resonance Raman spectra of both substrate-free and substrate-bound forms of the purified enzyme. The Fe–CO stretching mode ($\nu_{\text{Fe-CO}}$) of the CO complex and Fe³⁺–S stretching mode ($\nu_{\text{Fe-S}}$) of the oxidized form were monitored as a structural marker of the distal and proximal sides of the

heme, respectively. The $\nu_{\text{Fe-CO}}$ mode was upshifted from 477 to 485 and to 490 cm^{-1} by the binding of androstenedione and 19-aldehyde-androstenedione, substrates for the first and third steps, respectively, whereas $\nu_{\text{Fe-CO}}$ was not observed for P450arom with 19-hydroxy-androstenedione, a substrate for the second step, indicating that the heme distal site is very flexible and changes its structure depending on the substrate. The 19-aldehyde-androstenedione binding could reduce the electron donation from the axial thiolate, which was evident from the low-frequency shift of $\nu_{\text{Fe-S}}$ by 5 cm^{-1} compared to that of androstenedione-bound P450arom. Changes in the environment in the heme distal site and the reduced electron donation from the axial thiolate upon 19-aldehyde-androstenedione binding might stabilize the ferric peroxo species, an active intermediate for the third step, with the suppression of the formation of compound I ($\text{Fe}^{4+}=\text{O}$ porphyrin $^{+}$) that is the active species for the first and second steps. We, therefore, propose that the substrates can regulate the formation of alternative reaction intermediates by modulating the structure on both the heme distal and proximal sites in P450arom.

X-E-16 Evidence for Displacement of the C-Helix by CO Ligation and DNA Binding to CoxA Revealed by UV Resonance Raman Spectroscopy

KUBO, Minoru; INAGAKI, Sayaka¹; YOSHIOKA, Shiro; UCHIDA, Takeshi²; MIZUTANI, Yasuhisa³; AONO, Shigetoshi; KITAGAWA, Teizo
(¹IMS and CERM; ²IMS and Hokkaido Univ.; ³IMS and Osaka Univ.)

[*J. Biol. Chem.* **281**, 11271–11278 (2006)]

The UV and visible resonance Raman spectra are reported for CoxA from *Rhodospirillum rubrum*, which is a transcriptional regulator activated by growth in a CO atmosphere. CO binding to heme in its sensor domain causes rearrangement of its DNA-binding domain, allowing binding of DNA with a specific sequence. The sensor and DNA-binding domains are linked by a hinge region that follows a long C-helix. UV resonance Raman bands arising from Trp-110 in the C-helix revealed local movement around Trp-110 upon CO binding. The indole side chain of Trp-110, which is exposed to solvent in the CO-free ferrous state, becomes buried in the CO-bound state with a slight change in its orientation but maintains a hydrogen bond with a water molecule at the indole nitrogen. This is the first experimental data supporting a previously proposed model involving displacement of the C-helix and heme sliding. The UV resonance Raman spectra for the CoxA-DNA complex indicated that binding of DNA to CoxA induces a further displacement of the C-helix in the same direction during transition to the complete active conformation. The Fe–CO and C–O stretching bands showed frequency shifts upon DNA binding, but the Fe–His stretching band did not. Moreover, CO–geminaterecombination was more efficient in the DNA-bound state. These results suggest that the C-helix displacement in the DNA-bound form causes the CO binding pocket to narrow and become more negative.

X-E-17 On the Relationship of Coral Allene Oxide Synthase to Catalase: A Single Active Site Mutation that Induces Catalase Activity in Coral Allene Oxide Synthase

TOSHA, Takehiko; UCHIDA, Takeshi¹; BRASH, Alan R.²; KITAGAWA, Teizo
(¹IMS and Hokkaido Univ.; ²Vanderbilt Univ.)

[*J. Biol. Chem.* **281**, 12610–12617 (2006)]

A heme domain of coral allene oxide synthase (cAOS) catalyzes the formation of allene oxide from fatty acid hydroperoxide. Although cAOS has a similar heme active site to that of catalase, cAOS is completely lacking in catalase activity. A close look at the hydrogen-bonding possibilities around the distal His in cAOS suggested that the imidazole ring is rotated by 180° relative to that of catalase because of the hydrogen bond between Thr-66 and the distal His-67. This could contribute to the functional differences between cAOS and catalase, and to examine this possibility, we mutated Thr-66 in cAOS to Val, the corresponding residue in catalase. In contrast to the complete absence of catalase activity in wild type (WT) cAOS, T66V had a modest catalase activity. On the other hand, the mutation suppressed the native enzymatic activity of the formation of allene oxide to 14% of that of WT cAOS. In the resonance Raman spectrum, whereas WT cAOS has only a 6-coordinate/high spin heme, T66V has a 5-coordinate/high spin heme as a minor species. Because catalase adopts a 5-coordinate/high spin structure, probably the 5-coordinate/high spin portion of T66V showed the catalase activity. Furthermore, in accord with the fact that the CN affinity of catalase is higher than that of WT cAOS, the CN affinity of T66V was 8-fold higher than that of WT cAOS, indicating that the mutation could mimic the heme active site in catalase. We, therefore, propose that the hydrogen bond between Thr-66 and distal His-67 could modulate the orientation of distal His, thereby regulating the enzymatic activity in cAOS.

X-E-18 Similarities and Differences between Cyclobutane Pyrimidine Dimer (CPD) Photolyase and (6-4) Photolyase as Revealed by Resonance Raman Spectroscopy: Electron Transfer from FAD Cofactor to UV-Damaged DNA

LI, Jiang¹; UCHIDA, Takeshi²; TODO, Takeshi³; KITAGAWA, Teizo
(¹SOKENDAI; ²IMS and Hokkaido Univ.; ³Kyoto Univ.)

[*J. Biol. Chem.* **281**, 25551–25559 (2006)]

Cyclobutane pyrimidine dimer (CPD) and (6-4) photoproduct, two major types of DNA damage caused by ultraviolet (UV) light, are repaired under illumination with near-UV/visible light by CPD photolyase and (6-4) photolyase, respectively. To understand the mechanism of DNA repair, we examined the resonance Raman spectra of complexes between damaged DNA and the neutral semiquinoid and oxidized forms of (6-4) and CPD photolyases. The marker band for a neutral semi-

quinoid flavin and band I of the oxidized flavin, which are derived from the vibrations of the benzene ring of FAD, were shifted to lower frequencies upon binding of damaged DNA by CPD photolyase but not by (6-4) photolyase, indicating that CPD interacts with the benzene ring of FAD directly but that (6-4) photoproduct does not. Bands II and VII of the oxidized flavin and the 1398/1391 cm^{-1} bands of the neutral semiquinoid flavin, which may reflect the bending of the U-shaped FAD, were altered upon substrate binding, suggesting that CPD and (6-4) photoproduct interact with the adenine ring of FAD. When substrate is bound, there is an upshifted 1528 cm^{-1} band of the neutral semiquinoid flavin in CPD photolyase, indicating a weakened hydrogen bond at N5-H of FAD, and in (6-4) photolyase, band X seems to be downshifted, indicating a weakened hydrogen bond at N3-H of FAD. These Raman spectra led us to conclude that the two photolyases have different electron transfer mechanisms as well as different hydrogen bonding environments, which account for the higher redox potential of CPD photolyase.

X-E-19 Structure of Interacting Segments in the Growing Amyloid Fibril of β_2 -Microglobulin Probed with IR Spectroscopy

LU, Ming¹; HIRAMATSU, Hirotsugu²; GOTO, Yuji³; KITAGAWA, Teizo
(¹SOKENDAI; ²IMS and Tohoku Univ.; ³Osaka Univ.)

[*J. Mol. Biol.* **362**, 355–364 (2006)]

Inter-segmental interaction at the growing tip of the amyloid fibril of β_2 -microglobulin ($\beta_2\text{m}$) was investigated using IR microscopy. Cross-seeded fibril formation was implemented, in which the amyloid fibril of the #21-31 fragment of $\beta_2\text{m}$ (fA[#21-31]) was generated on $\beta_2\text{m}$ amyloid fibril (fA[$\beta_2\text{m}$]) as a seed. Differences between the IR spectra of the cross-seeded fibril and the seed were attributed to the contribution from the tip, whose structure is discussed. The results indicated that 6.5 ± 1.0 out of 11 residues of the fA[#21-31] tip on fA[$\beta_2\text{m}$] are contained in a β -sheet at pH 2.5, which was smaller than the corresponding value (7.5 ± 1.1 residues) of the spontaneous fA[#21-31] at pH 2.5. The tip was suggested to have a planar structure, indicating the planarity of the interacting segment. The N-terminal region of fA[#21-31] in the fibril is more exposed to the solvent than that in the tip, and *vice versa* for the C-terminal region. This is consistent with the different protonation levels of these regions, and from these results the direction of peptide in the fibrils is determined.

X-E-20 Pathway of Information Transmission from Heme to Protein upon Ligand Binding/Dissociation in Myoglobin Revealed by UV Resonance Raman Spectroscopy

GAO, Ying¹; EL-MASHTOLY, Samir F.; PAL, Biswajit²; HAYASHI, Takashi³; HARADA, Katsuyoshi⁴; KITAGAWA, Teizo
(¹SOKENDAI; ²IMS and CCMB; ³IMS and Osaka Univ.; ⁴Osaka Univ.)

[*J. Biol. Chem.* **281**, 24637–24646 (2006)]

Gas sensory heme proteins respond to their environment by binding a specific gas molecule to heme and transmitting this primary binding signal to the protein. How the binding signal is transmitted from the heme to the protein remains to be clarified. Using UV resonance Raman (UVRR) spectroscopy, we investigated this pathway in sperm whale myoglobin as a model gas sensory heme protein. Based on the UVRR data and the effects of deleting one of three important pathways (His93, 6-propionate, or 7-propionate), we determined the changes in the conformation of globin that occur upon binding of CO, NO, or O₂ to heme and how they are transmitted from heme to globin. The UVRR results show that heme discriminates different ligands, resulting in different conformations in the globin protein. Specifically, NO induces changes in the spectrum of Trp residues in the A-helix that are significantly different from those induced by O₂ or CO binding. On the other hand, binding of O₂ to heme produces changes in the Tyr residues of the H-helix that are different from those induced by CO or NO binding. Furthermore, we found that cleavage of the Fe–His93 covalent bond eliminates communication to the terminal region of the H-helix and that the 7-propionate hydrogen-bonding network is essential for transmitting the CO or NO binding signal to the N- and C-termini. Finally, the 6-propionate is important only for NO binding. Thus, the hydrogen-bonding network in the protein appears to be critical for intramolecular signal transduction in gas sensory heme proteins.

X-E-21 Characteristic Structure and Environment in FAD Cofactor of (6-4) Photolyase along Function Revealed by Resonance Raman Spectroscopy

LI, Jiang¹; UCHIDA, Takeshi²; OHTA, Takehiro³; TODO, Takeshi⁴; KITAGAWA, Teizo
(¹SOKENDAI; ²IMS and Hokkaido Univ.; ³IMS and Stanford Univ.; ⁴Kyoto Univ.)

[*J. Phys. Chem. B* **110**, 16724–16732 (2006)]

A pyrimidine-pyrimidone (6-4) photoproduct and a cyclobutane pyrimidine dimer (CPD) are major DNA lesions induced by ultraviolet irradiation, and (6-4) photolyase, an enzyme with flavin adenine dinucleotide (FAD) as a cofactor, repairs the former specifically by light illumination. We investigated resonance Raman spectra of (6-4) photolyase from *Arabidopsis thaliana* having neutral semiquinoid and oxidized forms of FAD, which were selectively intensity enhanced by excitations at 568.2 and 488.0 nm, respectively. DFT calculations were carried out for the first time on the neutral semiquinone. The marker band of a neutral semiquinone at 1606 cm^{-1} in H₂O, whose frequency is the lowest among various flavoenzymes, apparently splits into two comparable bands at 1594 and 1608 cm^{-1} in D₂O, and similarly that at 1522 cm^{-1} in H₂O does into three bands at 1456, 1508, and 1536 cm^{-1} in D₂O. This D₂O effect was recognized only after being oxidized once and photoreduced to form a semiquinone again, but not by simple H/D exchange of solvent. Some Raman bands of

the oxidized form were observed at significantly low frequencies (1621, 1576 cm^{-1}) and with band splittings (1508/1493, 1346/1320 cm^{-1}). These Raman spectral characteristics indicate strong H-bonding interactions (at N5-H, N1), a fairly hydrophobic environment, and an electron-lacking feature in benzene ring of the FAD cofactor, which seems to specifically control the reactivity of (6-4) photolyase.

X-E-22 Time-Resolved Raman Evidence for Energy Funneling through Propionate Side Chains in Heme Cooling Upon Photolysis of Carbonmonoxy Myoglobin

GAO, Ying¹; KOYAMA, Mai²; EL-MASHTOLY, Samir F.; HAYASHI, Takashi³; HARADA, Katsuyoshi⁴; MIZUTANI, Yasuhisa³; KITAGAWA, Teizo
(¹SOKENDAI; ²Kobe Univ.; ³IMS and Osaka Univ.; ⁴Osaka Univ.)

[*Chem. Phys. Lett.* **429**, 239–243 (2006)]

The heme “cooling” following CO photolysis was investigated with picosecond time-resolved anti-Stokes Raman spectroscopy on modified myoglobins (Mb), in which the 6- or 7-propionate is selectively replaced by a methyl group. The time constants of population decay of vibrationally excited states for two modified Mbs became significantly larger compared with those of native Mb. This is the first experimental evidence for appreciable contribution of each heme-propionate side chain to the vibrational energy transfer from the heme to the surroundings.

X-E-23 Characterization of the Phenoxyl Radical in Model Complexes for the Cu_B Site of Cytochrome *c* Oxidase: Steady-State and Transient Absorption Measurements, UV Resonance Raman Spectroscopy, EPR Spectroscopy, and DFT Calculations for M^{II}-BIAIP

NAGANO, Yasutomo; LIU, Jin-Gang¹; NARUTA, Yoshinori¹; IKOMA, Tadaaki²; TERO-KUBOTA, Shozo²; KITAGAWA, Teizo
(¹Kyushu Univ.; ²Tohoku Univ.)

[*J. Am. Chem. Soc.* **128**, 14560–14570 (2006)]

Physicochemical properties of the covalently cross-linked tyrosine-histidine-Cu_B (Tyr-His-Cu_B) unit, which is a minimal model complex [M^{II}-BIAIPBr]Br (M = Cu^{II}, Zn^{II}) for the Cu_B site of cytochrome *c* oxidase, were investigated with steady-state and transient absorption measurements, UV resonance Raman (UVRR) spectroscopy, X-band continuous-wave electron paramagnetic resonance (EPR) spectroscopy, and DFT calculations. The pH dependency of the absorption spectra reveals that the pK_a of the phenolic hydroxyl is *ca.* 10 for the Cu^{II} model complex (Cu^{II}-BIAIP) in the ground state, which is similar to that of *p*-cresol (tyrosine), contrary to expectations. The bond between Cu^{II} and nitrogen of cross-linked imidazole cleaves at pH 4.9. We

have successfully obtained UVRR spectra of the phenoxyl radical form of BIAIPs, and have assigned bands based on the previously reported isotope shifts of Im-Ph (2-(1-imidazolyl)-4-methylphenol) (Aki, M.; Ogura, T.; Naruta, Y.; Le, T. H.; Sato, T.; Kitagawa, T. *J. Phys. Chem. A* **106**, 3436–3444 (2002)) in combination with DFT calculations. The upshifts of the phenoxyl vibrational frequencies for 8a (C–C stretching), 7a' (C–O stretching), and 19a, and the Raman-intensity enhancements of 19b, 8b, and 14 modes indicate that UVRR spectra are highly sensitive to imidazole-phenol covalent linkages. Both transient absorption measurements and EPR spectra suggest that the Tyr-His-Cu_B unit has only a minor effect on the electronic structure of the phenoxyl radical form, although our experimental results appear to indicate that the cross-linked Tyr radical exhibits no EPR. The role of the Tyr-His-Cu_B unit in the enzyme is discussed in terms of the obtained spectroscopic parameters of the model complex.

X-E-24 Ultraviolet Resonance Raman Evidence for Utilization of the Heme 6-Propionate Hydrogen Bond Network in Signal Transmission from Heme to Protein in *Ec* DOS Protein

EL-MASHTOLY, Samir F.; TAKAHASHI, Hiroto¹; SHIMIZU, Toru¹; KITAGAWA, Teizo
(¹Tohoku Univ.)

[*J. Am. Chem. Soc.* in press]

The direct oxygen sensor protein from *Escherichia coli* (*Ec* DOS) is a heme-based signal transducer protein responsible for phosphodiesterase (PDE) activity. Binding of either O₂ or CO molecule to a reduced heme enhances the PDE activity towards 3',5'-cyclic diguanylic acid. We report ultraviolet resonance Raman (UVRR) spectroscopic investigations of the reduced, O₂- and CO-bound forms of heme-bound PAS domain (*Ec* DOSH) of *Ec* DOS. The UVRR results show that heme discriminates different ligands, resulting in altered conformations in the protein moiety. Specifically, the environment around Trp53 that contacts heme 2-vinyl group, shifts towards more hydrophobic upon O₂ binding, while towards more hydrophilic upon the CO-binding. In addition, the PDE activity of the O₂- and CO-bound forms for Trp53Phe is significantly decreased compared with that of WT, demonstrating the importance of Trp53 for the catalytic reaction. On the other hand, binding of O₂ or CO to the heme produces drastic changes in the Tyr126 of I_β-strand at the surface of the sensor domain. Furthermore, we found that Asn84 forms a hydrogen bond with Tyr126 either in the O₂- or CO-bound forms but not in the reduced form. Finally, the PDE activities of the ligand bound forms for Asn84Val and Tyr126Phe mutants are significantly reduced compared with that of WT, suggesting the importance of the hydrogen bonding network from heme 6-propionate to Tyr 126 through Asn84 in signal transmission.

X-E-25 Identification of an “End-on” Nickel-Superoxo Adduct, [Ni(tmc)(O₂)]⁺

KIEBER-EMMONS, Matthew T.¹; ANNARAJ,

Jamespandi²; SEO, Mi Sook²; VAN HEUVELEN, Katherine M.³; TOSHA, Takehiko; KITAGAWA, Teizo; BRUNOLD, Thomas C.³; NAM, Wonwoo²; RIORDAN, Charles G.¹

(¹Univ. Delaware; ²Ewha Womans Univ.; ³Univ. Wisconsin-Madison)

[*J. Am. Chem. Soc.* in press]

An “end-on” Ni²⁺-superoxo adduct has been prepared *via* two independent synthetic routes and its structure ascertained by spectroscopic and computational methods. The new structure type in nickel coordination chemistry is supported by resonance Raman and EPR spectroscopic features, the former displaying a high frequency ν(O–O) mode (1131 cm⁻¹) consistent with significant superoxo character. The Ni²⁺-superoxo adduct reacts with PPh₃, thereby generating OPPh₃.

X-E-26 Regioselective Arene Hydroxylation Mediated by a (μ-Peroxo)diiron(III) Complex: A Functional Model for Toluene Monooxygenase

YAMASHITA, Mai¹; FURUTACHI, Hideki¹; FUJINAMI, Shuhei¹; TOSHA, Takehiko; TAKAHASHI, Kenji¹; TANAKA, Koji; KITAGAWA, Teizo; SUZUKI, Masatatsu¹

(¹Kanazawa Univ.)

[*J. Am. Chem. Soc.* in press]

Diiron(II) complexes, [Fe₂(Ph₄-tidp)(RCO₂)₂]² (R = Ph or Ph₃CCO₂), react with dioxygen to generate peroxo–diiron(III) complexes [Fe₂(Ph₄-tidp)(RCO₂)(O₂)₂]². Dioxygen affinity can be greatly controlled by the stereochemistry of the bridging carboxylates. Thermal decomposition of a peroxo complex with Ph₃CCO₂ resulted in regioselective hydroxylation of one of phenyl groups of the supporting ligand, which mimics toluene monooxygenase activity.

X-E-27 A Novel Mononuclear Ligand-Based Alkylperoxo Copper(II) Complex as a Reaction Intermediate in the Oxidation of the Methyl Group of the Supporting Ligand

MIZUNO, Masayasu¹; HONDA, Kaoru¹; CHO, Jaeheung¹; FURUTACHI, Hideki¹; TOSHA, Takehiko; MATSUMOTO, Takahiro¹; FUJINAMI, Shuhei¹; KITAGAWA, Teizo; SUZUKI, Masatatsu¹

(¹Kanazawa Univ.)

[*Angew. Chem., Int. Ed.* in press]

Functionalization of aliphatic C–H bond mediated by copper complexes with O₂ and/or H₂O₂ is of great interest in biological significance and industrial applicability. In this communication we report the formation, structure, and reactivity of a novel ligand-based alkylperoxo copper(II) complex, [Cu(Me-tpa-CH₂OO)]⁺, which is produced by the reaction of [Cu(Me₂-tpa)]⁺ with excess of H₂O₂. The complex is the first example of a structurally characterized ligand-based alkylperoxo-copper(II) complex isolated as a reaction intermediate,

which is further converted into ligand-based alkoxo, carboxylato complexes, and some other species upon decomposition. We believe that the findings in this study provide fundamental basis for functionalization of aliphatic C–H bond by Cu–O_n species and are of great interest to wide audience.

X-E-28 Synthesis, Characterization, and Reactivities of Manganese(V)-Oxo Porphyrin Complexes

SONG, Woon Ju¹; SEO, Mi Sook¹; GEORGE, Serena DeBeer²; OHTA, Takehiro³; SONG, Rita¹; KANG, Min Jung¹; TOSHA, Takehiko; KITAGAWA, Teizo; SOLOMON, Edward I.²; NAM, Wonwoo¹
(¹Ewha Womans Univ.; ²Stanford Univ.; ³IMS and Stanford Univ.)

[*J. Am. Chem. Soc.* in press]

The reactions of manganese(III) porphyrin complexes with terminal oxidants, such as *m*-chloroperbenzoic acid, iodosylarenes, and H₂O₂, produced high-valent manganese(V)-oxo porphyrins in the presence of base in organic solvents at room temperature. The manganese(V)-oxo porphyrins have been characterized with various spectroscopic techniques, including UV-vis, EPR, ¹H and ¹⁹F NMR, resonance Raman, and X-ray absorption spectroscopy. The combined spectroscopic results indicate that the manganese(V)-oxo porphyrins are diamagnetic low-spin (*S* = 0) species with a longer, weaker Mn–O bond than in previously reported Mn(V)-oxo complexes of non-porphyrin ligands. This is indicative of double bond character between the manganese(V) ion and the oxygen atom. The [(Porp)Mn^V=O]⁺ species are stable in the presence of base at room temperature. The stability of the intermediates is dependent on base concentration. In the absence of base, (Porp)Mn^{IV}=O is generated instead of the [(Porp)Mn^V=O]⁺ species. The stability of the [(Porp)Mn^V=O]⁺ species also depends on the electronic nature of porphyrin ligands; [(Porp)Mn^V=O]⁺ complexes bearing electron-deficient porphyrin ligands are more stable than those bearing electron-rich porphyrins. Reactivity studies of manganese(V)-oxo porphyrins revealed that the intermediates are capable of oxygenating PPh₃ and thioanisoles, but not olefins and alkanes at room temperature. These results indicate that the oxidizing power of [(Porp)Mn^V=O]⁺ is low in the presence of base. However, when the [(Porp)Mn^V=O]⁺ complexes were associated with iodosylbenzene in the presence of olefins and alkanes, high yields of oxygenated products were obtained in the catalytic olefin epoxidation and alkane hydroxylation reactions. Mechanistic aspects, such as oxygen exchange between [(Porp)Mn^V=¹⁶O]⁺ and H₂¹⁸O, are also discussed.

RESEARCH FACILITIES

The Institute for Molecular Science includes five research facilities. This section describes their latest equipment and activities. For further information please refer to older IMS Annual Review issues (1978–2005).

Research Center for Molecular-scale Nanoscience

This center was established in April 2002 after reorganization including the Research Center for Molecular Materials, the Department of Electronic Structure and the Department of Molecular Assemblies. The Center is supposed to play a principal role to integrate the innovative progress that IMS has achieved in the fields of molecular science and material science. Its mission is to develop a new field of science systematizing new finding in physical and chemical properties of new molecular materials and nano structures, by elucidation and controlling the structure and function of the materials at the atom/molecular level. In addition, the center promote colaboration with internal and external researchers by providing technical services of common research facilities which are indispensable for nano science research.

The center is comprised of four divisions: (A) Molecular-scale electronics, (B) Nanocatalysis and biomolecular devices, (C) Nano-scale photoscience, and (D) Advanced molecular science, where the last division consists of visiting faculty members. The respective research activities of each divisions are reported in other sections in this Review. Technical staffs are also important members of the center, who manage the common equipments and facilities of the center, provide liquid nitrogen and helium, and take care of the elemental analyses.

UVSOR Facility

The UVSOR accelerator complex consists of a 15 MeV injector linac, a 600 MeV booster synchrotron, and a 750 MeV storage ring. The magnet lattice of the storage ring is the so-called double-bend achromat. The double RF system is routinely operated for the user beam time, and the lifetime of the electron beam has been improved to around 6 hours at 200 mA. The storage ring is normally operated under multi-bunch mode with partial filling. The single bunch operation is also conducted about two weeks per year, which provides pulsed synchrotron radiation (SR) for time-resolved experiments. Initial beam currents stored under multi-bunch and single-bunch modes are 350 mA and 70 mA, respectively.

Eight bending magnets and three insertion devices are available for utilizing SR. The bending magnet with its radius of 2.2 m provides SR, whose critical energy is 425 eV. After completing the upgrade project, there are 14 beamlines available in total (13 operational, and 1 under construction) at UVSOR, which can be classified into two categories. 9 of them are the so-called "Open beamlines," which are open to scientists of universities and research institutes belonging to the government, public organizations, private enterprises and those of foreign countries. The rest of the 5 beamlines are the so-called "In-house beamlines," which are dedicated to the use of the research groups within IMS. We have 1 soft X-rays (SX) station equipped with a double-crystal monochromator, 7 EUV and SX stations with a grazing incidence monochromator, 3 VUV stations with a normal incidence monochromator, 1 (far) infrared station equipped with FT interferometers, 1 station with a multi-layer monochromator, and 1 non-monochromatized station for the irradiation of white-light.

Discussion with users, concerning the improvements and upgrades of the beamlines at UVSOR, has been continuously held as series of UVSOR workshops. The upgrade project of the UVSOR storage ring, in which the creation of four new straight sections and the achievement of much smaller emittance (27 nm-rad) were planned, has been approved in the fiscal year of 2002 and has been accomplished on schedule. Keeping pace with this project, a new in-vacuum undulator and high performance monochromator for BL3U, and a new high-resolution photoelectron energy analyzer for the end station at BL5U, have been installed without any troubles. Thanks to the successful installation of the so-called magic mirror, as the first mirror of the IR beamline, BL6B, the highest intensity in the world has been achieved in the wavelength range from sub-milli to near IR region. Two vacant lots at BL2A and BL6A are available for constructing novel undulator beamlines. A new RF cavity has been installed to the short straight section between B01 and B02 before the end of March 2005; BL2A will be a bending-magnet beamline while BL6A is to be an undulator one, which will be called BL6U. From a viewpoint of radiation safety, the experiments carried out at the experimental stations on the second floor such as BL3B and BL7B, and the fine tunings of the laser system installed inside the shield walls during machine study, seem to become quite risky after introducing the so-called top-up operation of the UVSOR storage ring in the near future. Accordingly we have decided to put two old beamlines, BL8A and BL3B, out of service until the middle of March 2006. The experimental station for BL7B will be constructed at the vacant space after removing BL8A. All the beamline components have been completely removed from BL3B before the third week of March 2006. The laser system will be moved to the corresponding empty lot of BL3B by the machine group. Regarding the utilization for the long straight section between B06 and B07, a UVSOR workshop has been held in March 2005. On the basis of the review and evaluation report on the present status of UVSOR in 2004, a high resolution and high flux variable polarization beamline BL7U for spectroscopy in the VUV range has been proposed. The construction of the new beamline BL7U has begun in summer 2006, and the beamline commissioning will be started after the installation of a new variable polarization

undulator at the end of October 2006. Further discussion toward utilizing the available straight sections most effectively and formulating a basic plan on the beamline construction, will be continued.

All users are required to refer to the beam-line manuals and the UVSOR guidebook (latest revision in 1999), on the occasion of conducting actual experimental procedures. Those wishing to use the open and in-house beamlines are recommended to contact with the stationmaster/supervisor and the representative, respectively. For updated information of UVSOR, <http://www.uvsor.ims.ac.jp/>.

Laser Research Center for Molecular Science

This center was established in 1997 by reorganization of a part of the Instrument Center. The Center is aimed at developing new lasers suitable for pioneering researches in the new field of molecular science and now plays a central role in promoting the special research project on "Extreme Photonics."

In addition to promoting researches, this Center maintains laser systems and supplies them to other community members. The laser systems are excimer lasers and solid-state light sources in various temporal and spectral regions, including femtosecond optical parametric oscillators (OPO), and the synchronously pumped femtosecond (OPO) (OPAL; Spectra Physics) tunable from 1.1 μm up to 1.6 μm . The Center also has general instruments and spectrophotometers, including a fluorescence spectrophotometer (Fluorolog II; Spex) composed of a xenon lamp house for excitation, double and single monochromators for spectroscopy, and changeable detectors (CCD and photomultiplier tube), UV-VIS and IR spectrophotometers, circular dichroism dispersion photometer, and general-purpose electronic instruments. Using these instruments, researchers can carry out various experiments not only in the ultrafast temporal region but also in the steady state regime.

Equipment Development Center

R & D of the new instruments necessary for the molecular science research including the conventional services for the design and fabrication of the instruments, are the mission of this center, which consists of the mechanical, electronic and glass work sections.

We expanded our service to researchers in other universities and research institutes since 2005. The main aim of this new attempt is to improve the technology level of the center staffs, together with contributing to the molecular science community.

In this fiscal year, the total number of the services based on this new program were 14, and we consider that the original aim of this new service was filled both in quality and quantity.

Design and fabrication works of this fiscal year

- Diebonding system for laser crystal
- Electrode assembly for the threshold electron-photoion coincidence spectrometer
- Poling instrument
- Flexure stage
- Mounting bracket for ESR cryostat
- Gas nozzle and optical port for photoelectron spectrometer
- Measurement chamber of biosensor
- Reflection chamber
- Measurement chamber of patch-clamp
- Experimental compact laser module
- Measurement chamber of single ion channel recording
- Electron yield detector with adjustment of Z-axis

Research and developments of the new instruments

- Manufacture of a mold for a microchip using a surface impression agent
- A compact mechanical velocity selector to analyze molecular alignment
- Activities are described in detail in the section "RESEARCH ACTIVITIES"

Safety Office

The Safety Office was established in April 2004. The Office is supposed to play a principal role in the institute to secure the safety and health of the staffs by achieving a comfortable workplace environment, and improvement of the working conditions. In concrete terms, it carries out planning, work instructions, fact-findings, and other services for safety and health in the institute. The office is comprised of the following staffs: the director of the office, safety and health administrators, safety and health office personnel, operational chiefs, and other staff members appointed by the Director General.

Okazaki Research Facilities (related to IMS) Research Center for Computational Science

The Research Center for Computational Sciences, Okazaki Research Facilities, National Institutes of National Science, provides up-to-date computational resources to academic researchers in molecular science and related fields. As of March 2006, this facility is used by 520 scientists in 132 project groups.

The computer systems, currently consisting of Fujitsu PRIMEQUEST, SGI Altix4700, NEC SX-7, and NEC TX-7, cover a wide range of computational requests in quantum chemistry, molecular simulation, chemical reaction dynamics and solid state physics. These systems are linked to international networks through Super Science Information Network (super SINET). Detailed information on the hardware and software of the Center is available on the web site (<http://ccinfo.ims.ac.jp/>).

The Center provides a number of program suites, including Gaussian 03, GAMESS, Molpro2002, Hondo2003, AMBER, *etc.*, which are installed to the computer systems and kept updated for immediate use of the users. The Center also maintains and offers the Quantum Chemistry Literature Database (QCLDB, <http://qcldb2.ims.ac.jp/>), which has been developed by the Quantum Chemistry Database Group in collaboration with staff members of the Center. The latest release, QCLDB Release 2005, contains 82,017 data of quantum chemical studies.

In addition to offering computer resources to wide range of molecular scientists, another vital aspect of the Center is to perform leading computational researches with massive computations. In 2003, the Center participated the National Research Grid Initiative (NAREGI) project, a three-year national project by National Institute of Informatics (NII) and IMS. This joint project aimed at developing grid computing system (NII) and thereby realizing extremely large-scale computational studies in the frontier of nanoscience (IMS). For these purposes, two supercomputer systems, Hitachi SR11000 and HA8000, were introduced to the Center in 2004, with combined performance exceeding 10 TFlops. In 2006, the NAREGI project was reformed to join a new national project, Development & Application of Advanced High-Performance Supercomputer Project, by RIKEN where IMS plays an important role in the application of the PFlops-scale supercomputer to nanoscience. Further information on next-generation supercomputer project and computer systems at the Center is found on the web site (<http://nanogc.ims.ac.jp/nanogc/>).

SPECIAL RESEARCH PROJECTS

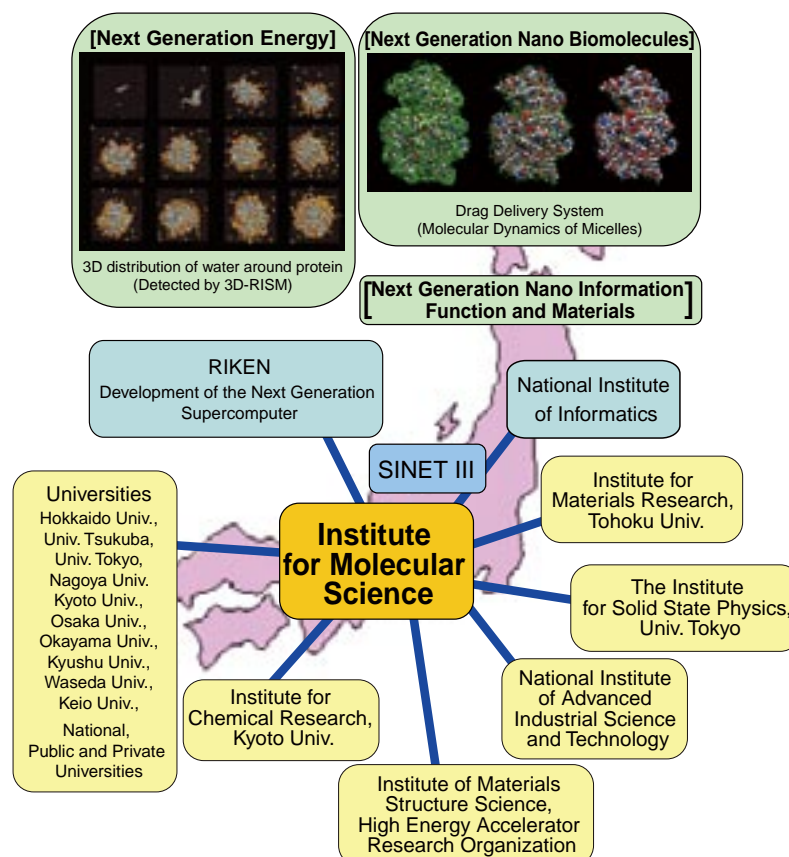
IMS has special research projects supported by national funds. Four projects in progress are:

- (a) —Grand Challenge in Nanoscience— Next Generation Integrated Nanoscience Simulation Software Development & Application of Advanced High-Performance Supercomputer Project
- (b) Formation of Interdisciplinary and International Bases for Natural Sciences, NINS
“Development of New Computational Methods for Large-Scale Systems and Establishment of Advanced Simulation Center for Molecules and Materials”
- (c) Nanotechnology Support Project: Molecular Synthesis and Analysis Group
- (d) Extreme Photonics

These four projects are being carried out with close collaboration between research divisions and facilities. Collaborations from outside also make important contributions. Research fellows join these projects.

(a) —Grand Challenge in Nanoscience— Next Generation Integrated Nanoscience Simulation Software Development & Application of Advanced High-Performance Supercomputer Project

A national project named, “Next Generation Integrated Nanoscience Simulation Software” was initiated on April 1, 2006 at Institute for Molecular Science (IMS). The project is a part of the “Development & Application of Advanced High-Performance Supercomputer Project” of MEXT, which aims to develop a next generation supercomputer and application software to meet the nation’s computational science needs. The primary mission of our project is to resolve following three fundamental problems in the field of nanoscience, all of which are crucial to supporting society's future scientific and technological needs: (1) “Next Generation Energy” (*e.g.*, effective utilization of the solar energy), (2) “Next Generation Nano Biomolecules” (*e.g.*, scientific contributions toward overcoming obstinate diseases), and (3), “Next Generation Nano Information Function and Materials” (*e.g.*, molecular devices). In these fields, new computational methodologies and programs are to be developed to clarify the properties of nanoscale substances such as catalysts (enzymes), bio-materials, molecular devices, and so forth, by making the best use of the next generation supercomputer.



(b) Formation of Interdisciplinary and International Bases for Natural Sciences, NINS

“Development of New Computational Methods for Large-Scale Systems and Establishment of Advanced Simulation Center for Molecules and Materials”

This project aims to establish a core computational science center for molecular and material systems and to develop advanced methodologies for large-scale calculations. The project has been organized by five institutes of the National Institutes of Natural Sciences, *i.e.* Institute for Molecular Science, National Astronomical Observatory of Japan, National Institute for Fusion Science, National Institute for Basic Biology, and National Institute for Physiological Sciences, and other universities and research institutes. We are trying to create a new interdisciplinary field by integrating the different views and methodologies traditionally associated with each field that belongs to a different hierarchy of natural sciences. Structures and dynamics of large-scale complex systems, such as nanomaterials and biological systems, are investigated by using a variety of sophisticated computational methods based on theories of electronic structure, molecular dynamics method, statistical mechanics, and so on. The development of new computational methods utilizing parallel computation has also been furthered organizing the members having different scientific backgrounds. Seminars and workshops for the advanced calculations and for the development of human resources are also conducted by this project.

OKAZAKI, Susumu	Large-Scale Molecular Dynamics Calculations for Aqueous Solution of Amphiphilic Molecules
HIRATA, Fumio	Theoretical Study of Molecular Recognition Based on the 3D-RISM Theory
NAGASE, Shigeru	Quantum Chemistry Calculations of Nanomolecules
SAITO, Shinji	Theoretical Analyses of Condensed Phase Dynamics by Using Molecular Dynamics Simulation
YONEMITSU, Kenji	Theory for Nonequilibrium Control of Collective Dynamics in Quantum-Classical Hybrid Many-Particle Systems
MORITA, Akihiro	Theory and Computation of Interfacial Nonlinear Optical Phenomena
NOBUSADA, Katsuyuki	Theoretical Calculations for Electron Dynamics Strongly Coupled to the Electromagnetic Field

(c) Nanotechnology Support Project: Molecular Synthesis and Analysis

The Ministry of Education, Culture, Sports, Science and Technology, Japan (MEXT) started the “Nanotechnology Support Project” from 2002 for the purpose of supporting nanotechnology research initiatives. In order to effectively utilize the large facilities and specialized equipment that is required for this research, all of which are difficult for individual research organizations or projects to maintain, we provide nanotechnology researchers with the opportunity to use these facilities and equipment as well as provide the necessary technical support. We also promote the exchange of ideas and research between different fields or across boundaries, extending beyond the spheres of industry, academia and government research groups in our efforts to encourage developments within nanotechnology.

List of Supports

Preparation of Molecular Electronic Devices and Electric Conductivity Measurements	OGAWA, Takuji; URISU, Tsuneo
Automated Molecular Synthesis for Molecular Electronic Devices	OGAWA, Takuji; SUZUKI, Toshiyasu; NAGATA, Toshi; SAKURAI, Hidehiro
Space- and Time-Resolved Near-Field Microspectroscopy	OKAMOTO, Hiromi
Ultrafast and Raman Spectroscopic Measurement of Nanosystems	NISHI, Nobuyuki
Mass Spectrometric Analysis of Nanoclusters	TSUKUDA, Tastuya
MicroESCA Spectrometer	YOKOYAMA, Toshihiko
920 MHz NMR Spectrometer	UOZUMI, Yasuhiro
High Sensitive Magnetic Measurements	NISHIJO, Jun-ichi
Electron Microscopy (i) 300kV Transmission Analytical Electron Microscope, (ii) Field Emission Scanning Electron Microscope, and (iii) Focus Ion Beam System	NISHI, Nobuyuki; TSUKUDA, Tastuya
Computational Support to Molecular Design	NAGASE, Shigeru
Preparation and Characterization of Organic Electronic Devices	OGAWA, Takuji; TADA, Hirokazu

(d) Extreme Photonics

Institute for Molecular Science has a long-standing tradition of promoting spectroscopy and dynamics of molecules and molecular assemblies. Accordingly, photo-molecular science is one of major disciplines in molecular science. This field is not confined in the traditional spectroscopy, but makes solid basis for other disciplines including nanoscience and bioscience, *etc.* Therefore, continuing developments in spectroscopy and microscopy are vital to enhance our abilities to elucidate more complex systems in time and spatial domains. In order to achieve full developments of photo-molecular science, we need to pursue three branches in developing: (1) new light source, (2) new spatio-temporally resolved spectroscopy, and (3) new methods to control chemical reactions. Since 2005, we have started the program of "Extreme Photonics" in collaborating with the RIKEN institute. Currently 8 groups in IMS are involved in this program, and the specific research titles are as follows:

(1) Development of new light sources

TAIRA, Takunori	Micro Solid-State Photonics
SARUKURA, Nobuhiko	New Coherent Vacuum Ultraviolet Light Source

(2) Development of new spatio-temporally resolved spectroscopy

OKAMOTO, Hiromi	Development of Extreme Time-Resolved Near-Field Spectroscopy
MATSUMOTO, Yoshiyasu	Development of Spatio-Temporally Resolved Spectroscopy for Surfaces and Interfaces
OZAWA, Takeaki	Developments of Luminescent Probes based on Protein Structures and Analysis System of Biological Functions

(3) Development of new methods to control chemical reactions

OHMORI, Kenji	Development of Attosecond Coherent Control and Its Applications
HISHIKAWA, Akiyoshi	Reaction Imaging and Control with Extremely Short Laser Pulses
OHSHIMA, Yasuhiro	Quantum-State Manipulation of Molecular Motions by Intense Coherent Laser Pulses

OKAZAKI CONFERENCE

The 66th Okazaki Conference

Soft X-Ray Raman Spectroscopy and Related Phenomena

(August 17-19, 2006)

Organizers: KOSUGI, Nobuhiro (*IMS*)
OKAMOTO, Hiromi (*IMS*)
SHIGEMASA, Eiji (*IMS*)
HATSUI, Takaki (*IMS*)

The scope of the workshop was to discuss leading-edge study on resonant and non-resonant X-ray Raman scattering and related phenomena, especially in the soft X-ray domain, covering fundamentals, applications, and technical advances. The participants enthusiastically took part in the discussions through 18 invited talks by leading experts in the field and 11 poster presentations, as well as informal conversations in small groups at the workshop. No timekeepers were assigned for any of the sessions, which helped bring a friendly and relaxed atmosphere into the workshop.

The workshop started on Thursday afternoon (**August 17**) with a brief welcome and introduction by Kosugi (*IMS*), who chaired the first session which was devoted to the fundamental aspects. The first speaker, **Joseph Nordgren** (*Uppsala Univ., Foreign Councilor of IMS*), provided an overview of the history, general concept, and future development of soft x-ray emission spectroscopy. **Shik Shin** (*Univ. Tokyo and RIKEN/SPring-8*) described d-d excitations of the transition metals ranging from oxide compounds to metalloproteins with special emphasis on the ability of soft x-ray emission spectroscopy. **Uwe Bergmann** (*Stanford Univ.*) discussed hard X-ray Raman spectroscopy and its advantage and recent advances in the instrumentations, showing interesting applications to science on water, cold and deuterized water, and transition metal compounds as well as industrial applications to the assessment of crude oil. **Kenji Ohmori** (*IMS*) illustrated the state-of-art control in the attosecond regime and observation of "quantum ripple" of the molecular vibrational wavepackets. This kind of coherent control by using X-ray free-electron lasers will become a great challenge in the near future. Then, a small Get-together Party was held.

The first session in the morning of the second day (**August 18**), focusing on molecular spectroscopy and dynamics, chaired by Takaki Hatsui (*IMS*), started with a talk on the welcoming address and introduction of IMS by Hiroki Nakamura (*Director General of IMS*). As the first scientific talk of the day, **Marc Simon** (*LCP-MR, France*) discussed dynamics during the resonant Raman scattering process near the Cl 1s core of HCl molecules. Simon was followed by a talk on the same topic delivered by **Stephane Carniato** (*LCP-MR*), who illustrated how the vibrationally resolved Resonant Inelastic X-ray Scattering (RIXS) spectra in the tender X-ray region can be described and computed theo-

retically. **Victor Kimberg** (*KTH Stockholm and now IMS*) continued the discussion of RIXS from a theoretical point of view, and presented his recent result on decay dynamics on the soft x-ray emission of LiF and the photoemission of N₂. **Alexander Föhlisch** (*Univ. Hamburg*) reported recent advances of soft x-ray emission spectroscopy in the studies of the adsorbates on silicon as well as heating effect on resonant soft X-ray Raman scattering of silicon. During the two hours kept for lunch, time was used efficiently in which a poster session on several relevant topics was included.

The session on materials science and experimental techniques on Friday afternoon, chaired by Eiji Shigemasa (*IMS*), began with a talk on RIXS studies for nano-structured strongly correlated materials by **Jinghua Guo** (*ALS/LBNL*), who reported an overview of the endstation on Beamline 7.0.1 at ALS and his recent results obtained. **Munetaka Taguchi** (*RIKEN/SPring-8*) discussed theoretical aspects in soft x-ray emission of transition metal compounds. He presented how d-d excitations, charge-Transfer effects and their interplay can be observed in the RIXS spectra. **Hisashi Hayashi** (*Tohoku Univ. and now Japan Women's Univ.*) introduced his lifetime-broadening-suppressed X-ray absorption spectroscopy based on the X-ray Raman scattering process. Successful application of this method to transition metal oxides was reported. After a coffee break, **Takashi Tokushima** (*RIKEN/SPring-8*) started the session on recent instrumentational development, with a talk on the good performance of the varied-line-spacing (VLS) spectrometer installed at SPring-8. He extended his experimental techniques to measure liquid samples and discussed his temperature dependent spectra of liquid water. **Takaki Hatsui** (*IMS*) showed his originally developed transmission-grating spectrometer installed at UVSOR and its performance, as a challenge to achieving higher energy resolution up to $E/\Delta E = 5000$ with increasing throughput in the soft X-ray region. The last talk in the session was given by **Coryn Hague** (*LCP-MR*), who introduced his VLS spectrometer with a premirror, which is to be installed at SOLEIL. He initiated his talk appraising the wine selection for the previous night, on behalf of our French participants. A nice summary of the performances for various spectrometers available so far throughout the world, in comparison to his now-developing one, was presented. After the session, the participants and host enjoyed an informal conference dinner. Close and in-depth discussions were conducted till the late hours of the night.

The session of the final day (**August 19**) was focused on water and related topics, chaired by Okamoto (*IMS*). **Lars G. M. Pettersson** (*Stockholm Univ.*) talked about various kinds of x-ray spectroscopic investigations applied to the study of the liquid water structure. His efforts with collaborators were shown to settle controversial debates from the experimental and theoretical

point of view. **Shinji Saito** (*IMS*) discussed, as one of other techniques to explore water property and structure, two-dimensional Raman spectroscopy from the viewpoint of the theoretical advances. **Susumu Okazaki** (*IMS*) continued the discussion and reported recent theoretical progress on the molecular vibrational relaxation and decoherence of water, deuterized water, and solutions. The last talk was given by **Shaul Mukamel** (*UC Irvine*), who spoke about non-linear spectroscopy and its future possibilities in combination with X-ray free-electron lasers. He succeeded in comprehensible discussion by showing only one viewgraph containing complex equations.

JOINT STUDIES PROGRAMS

As one of the important functions of an inter-university research institute, IMS undertakes joint studies programs for which funds are available to cover research expenses as well as travel and living expenses of individuals. The proposals from domestic scientists are reviewed and controlled by an inter-university committee.

The programs are carried out under one of the following categories:

- (1) Joint Studies on Special Projects (a special project of significant relevance to the advancement of molecular science can be carried out by a team of several groups of scientists).
- (2) Research Symposia (a symposium on timely topics organized by collaboration between outside and IMS scientists).
- (3) Cooperative Research (a research program carried out by outside scientists with collaboration from an IMS scientist).
- (4) Use of Facility (a research program carried out by outside scientists at the research facilities of IMS except the UVSOR facility).
- (5) Joint Studies Programs using beam lines of UVSOR Facility.
- (6) Use of Facility Program of the Computer Center (research programs carried out by outside scientists at research facilities in Computer Center).

In 2005 Oct.–2006 Sep., the numbers of joint studies programs accepted for the categories (1)–(6) were 2, 12, 95, 48, 115, and 238, respectively.

(1) Special Projects

A. Integration of Recognition Reaction System with Biomolecules on Solid Surfaces and Structure Analysis

URISU, Tsuneo; TERO, Ryugo; MISAWA, Nobuo; UNO, Hidetaka; ZHANG, Zheng-Lon¹; ABU, Sayed¹; WATANABE, Hidekazu²; WAN, Li-Jun³; LEI, Sheng-Bin³
(¹SOKENDAI; ²RIKEN; ³Chin. Acad. Sci.)

Membrane proteins play important roles in signaling of life systems and have relation with many intractable diseases such as central nervous system diseases, neuronal degeneration diseases and many circulatory organs system disease *etc.* Integration of membrane proteins and lipid bilayer on the solid surfaces are not only interesting subjects in the surface science field but also an important elementary technique for the fabrication of membrane protein biosensors. In this project, we have established several elementary techniques for fabrication of membrane protein biosensors.

A-1 Supported Phospholipid Bilayer Formation on Hydrophilicity-Controlled Silicon Dioxide Surfaces

We investigated the influence of surface hydroxyl groups (-OHs) on the supported planar phospholipid bilayer (SPB) formation and characteristic.¹⁾ We prepared SiO₂ surfaces with different hydrophilicity degree by annealing the SiO₂ layer on Si(100) formed by wet chemical treatments. The hydrophilicity reduced with irreversible thermal desorption of -OHs. We formed SPB of dimyristoylphosphatidylcholine on the SiO₂ surfaces by incubation at a 100-nm-filtered vesicle suspension.

The formation rate was faster on less hydrophilic surfaces. We proposed that a stable hydrogen-bonded water layer on the SiO₂ surface worked as a barrier to prevent vesicle adhesion on the surface. Theoretical calculation indicates that water molecules on vicinal surface -OHs take a stable surface-unique geometry, which disappears on an isolated -OH. The surface -OH density, however, little affected the fluidity of once formed SPBs, which was measured by the fluorescence recovery after photobleaching method. We also describe about the area-selective SPB deposition using surface patterning by the focused ion beam.

A-2 Orientation of Avidin Molecules Immobilized on COOH-Modified SiO₂/Si(100) Surfaces

Avidin molecules were immobilized on COOH-modified SiO₂/Si(100) surfaces with subnano-level flatness ($R_a < 0.1$ nm) forming covalent bonds between COOH groups on the substrate surface and NH₂ groups of the avidin molecules. Structures of avidin-immobilized surfaces were investigated by atomic force microscopy (AFM), ellipsometry, infrared reflection absorption spectroscopy using buried metal layer substrate (BML-IRRAS), and transmission infrared absorption spectroscopy (TIRAS). It is concluded from these data that the avidin molecules are immobilized with the symmetry axis of the tetramer almost perpendicular to the substrate surface.

A-3 AFM Characterization of Gramicidin-A in Tethered Lipid Membrane on Silicon Surface

Tethered lipid bilayers were formed on oxidized Si surfaces using the avidin-biotin interaction to investigate the lipid-membrane protein interactions by using gramicidin-A (g-A) as a model membrane protein. The morphology of the tethered lipid bilayer, observed by in situ atomic force microscopy (AFM), changed drastically by the reconstruction of g-A. The aggregation behavior of

g-A was clearly different in the tethered membrane from those in simple supported membranes on mica and SiO₂ surfaces.

References

- 1) R. Tero, H. Watanabe and T. Urisu, *Phys. Chem. Chem. Phys.* **8**, 3885 (2006).
- 2) N. Misawa, S. Yamamura, K. Yong-Hoon, R. Tero, Y. Nonogaki and T. Urisu, *Chem. Phys. Lett.* **419**, 86 (2006).
- 3) S. B. Lei, R. Tero, N. Misawa, S. Yamamura, L. J. Wan and T. Urisu, *Chem. Phys. Lett.* **429**, 244 (2006).

(2) Research Symposia

(From 2005 Oct. to 2006 Sep.)

1. Frontiers and Perspectives of Nanoscience Using Ultra-High Field NMR Spectroscopy
(Nov. 15, 2005)
Chair: **KATO, Koichi; UOZUMI, Yasuhiro**
2. New Developments in Research of Endohedral Metallofullerenes
(Nov. 20–21, 2005)
Chair: **KUBOZONO, Yoshihiro**
3. Molecular Catalysis for the Future Generation
(Dec. 6–7, 2005)
Chair: **SAWAMURA, Masaya**
4. The 1st Nanomedicine Symposium—from Molecular Science to Clinical-Medical Science
(Feb. 12–13, 2006)
Chair: **URISU, Tsuneo**
5. Chirality in Crystals and Magnetism: Correlation between Magnetic Structures and Properties
(Feb. 18–19, 2006)
Chair: **INOUE, Katsuya**
6. Coherent Control and Ultrafast Dynamics in the Condensed Phase
(March 2–3, 2006)
Chair: **NAKAMURA, Kazutaka**
7. The Role and Utilization of Metal Ions in Biological System
(March 18–20, 2006)
Chair: **WATANABE, Yoshito**
8. Structures and Functions of the Active Reaction Centers Involving Metal Ions—Methodologies of Constructing their Molecular Structures—
(March 23–24, 2006)
Chair: **MASUDA, Hideki**
9. Future Frontier of Molecular Science
(June 2–3, 2006)
Chair: **OKAMOTO, Hiromi**

10. Physical Chemistry Symposium for Young Researchers in Molecular Science
(June 12, 2006)
Chair: **KIMURA, Yoshifumi**
11. Creation of Molecular Systems Having Highly Functionalized Metal Centers, their Structures and Functions
(June 15–16, 2006)
Chair: **KODERA, Masato**
12. New Frontiers of NMR Molecular Science
(July 31, 2006)
Chair: **KATO, Koichi; UOZUMI, Yasuhiro**

(3) Cooperative Research

This is one of the most important categories that IMS undertakes for conducting its own research of the common interest to both outside and IMS scientists by using the facilities at IMS. In 2005 Oct.–2006 Mar., 120 outside scientists from 50 research groups joined the Cooperative Research programs, and 115 outside scientists from 45 research groups in 2006 Apr.–2006 Sep. The names and affiliations of those collaborations are found in the Research Activities sections in this Review.

(4) Use of Facility

The number of projects accepted for the Use of Facility in 2005 Oct.–2006 Mar. amounted 4, 16, and 9 for the Laser Research Center for Molecular Science (LRCMS), for the Research Center for Molecular-scale Nanoscience (RCMN) and for the Equipment Development Center (EDC), respectively. In 2006 Apr.–2006 Sep., the number of projects accepted amounted 3, 16, and 1 for LRCMS, for RCMN, and for EDC, respectively.

(5) Use of UVSOR Projects

In the UVSOR Facility with the 750 MeV electron storage ring, there are sixteen beam lines available for synchrotron radiation research (see UVSOR ACTIVITY REPORT 2005). Under the Use of UVSOR Projects, many synchrotron radiation experiments have been carried out by outside scientists on eight beam lines in close cooperation with the UVSOR staff. The total number of the projects in this category was 115 (65 in 2005 Oct.–2006 Mar., and 50 in 2006 Apr.–2006 Sep.).

(6) Use of Facility Program of the Computer Center

Computer Center provides two types of research programs for outside scientists: (a) Use-of-Facility Program; (b) Cooperative Research Program. The numbers of projects accepted for each programs during the fiscal year of 2005 were (a) 113 with 467 users, (b) 5 with 10 users. Computer time distributed for these projects amounted to 98% of the total annual CPU time available.

COLLABORATION PROGRAMS

(a) IMS International Program

IMS has accepted many foreign scientists and held many international conferences since its foundation and is now universally recognized as the institute open for foreign countries. In 2004, IMS has started a new program to promote further the international collaborations. In this new program, the faculty members of IMS can propose (1) the short-term invitation of senior foreign scientists, (2) the long-term stay of young scientists and (3) their overseas visits to carry out the international collaborations.

Leader	Title	Partner
URISU, Tsuneo	Integration of Biological Signal Transducing System on the Si Substrate and Molecular-Level Functional Analysis	China: Prof. WAN, Li-Jun Prof. WANG, Chan-shun Prof. MO, Yu-jun U.S.A.: Dr. WEI, Chiming
OHMORI, Kenji	Development of Ultrahigh-Precision Coherent Control and Its Applications	France: Prof. GIRARD, Bertrand and his group members
SHIGEMASA, Eiji	Deep Inner-Shell Photoexcitations in Molecules and Their Subsequent Dissociation Dynamics	France: Dr. SIMON, Marc Dr. GUILLEMIN, R. Dr. JOURNEL, L. Dr. CARNIATO, S. Dr. HAGUE, C.
KIMURA, Shin-ichi	Resonant Optical and Photoelectrical Studies on Electronic Structure near a Quantum Critical Point	Korea: Prof. KWON, Yong-Seung and group member Germany: Dr. SICHELSCHMIDT, Joerg and group member
TAIRA, Takunori	Development of Angular Quasi-Phase Matched Nonlinear Wavelength Conversion	France: Prof. AKA, Gerard Dr. PETIT, Yannick
KATOH, Masahiro	Beam Dynamics in Free Electron Laser	France: Dr. COUPRIE, Marie Emmanuelle and group member Dr. BIELAWSKI, Serge and group member
KOSUGI, Nobuhiro	Resonant Soft X-Ray Spectroscopic Study at UVSOR BL3U	Germany: Prof. RUEHL, Eckart and group members Sweden: Prof. AGREN, Hans Prof. PETERSSON, Lars G. M. Prof. NORDGREN, Joseph and group member U.S.A.: Dr. GUO, Jinghua
MATSUMOTO, Yoshiyasu	Electron-Phonon Dynamics at Solid Surfaces	U.S.A.: Prof. PETEK, H. and group members
OKAMOTO, Hiromi	Near-Field Spectroscopy of Plasmon-Induced Enhanced Photon Fields in Metal Nanoparticle Aggregates	Korea: Prof. JEONG, Dae Hong and a student

TANAKA, Koji	Photochemical Water Oxidation and Multi-Electron Reduction of Carbon Dioxide	U.S.A.: Dr. FUJITA, Etsuko Dr. MUCKERMAN, James T.
JIANG, Donglin	Studies on Molecular Design and Self-Assembly of Light-Harvesting Antennae	China: Prof. WANG, Changchun and group members
KOBAYASHI, Hayao	Development and Characterization of Multi-Functional Molecular Systems	France: Dr. KURMOO, Mohamedally

(b) Asian Core Program “Frontiers of Material, Photo- and Theoretical Molecular Sciences”

Asian Core Program is a multilateral international collaboration program carried out by JSPS (Japan Society for the Promotion of Science). It is designed to create world-class research hubs in selected fields within the Asian region, while fostering the next generation of leading researchers. The program is based on a principle of equal partnership among core institutions in Japan and other Asian countries, so that each institution is expected to secure its own matching fund. Institute for Molecular Science has launched a new collaboration project “material, photo- and theoretical molecular sciences” (2006–2011) within the framework of this Asian Core Program with three key institutes in east Asian countries: Institute of Chemistry, Chinese Academy of Science (China); The College of Natural Science, Korea Advanced Institute of Science and Technology (Korea); and Institute of Atomic and Molecular Sciences, Academia Sinica (Taiwan). At present, six joint researches are in progress, and three joint seminars have been carried out in Japanese Fiscal-Year 2006.

FOREIGN SCHOLARS

Visitors from abroad are always welcome at IMS and they have always played an important role in the research activities of the Institute. The foreign scientists who visited IMS during the past year (September 2005–August 2006) are listed below.

The mark ^{*1} indicates attendance at an Okazaki IMS Conference; ^{*2} a MONKASHO (Ministry of Education, Culture, Sports, Science and Technology, Japan) or JSPS (Japan Society for the Promotion of Science) Invited Fellow; ^{*3} an IMS councillor; ^{*4} an IMS visiting professor or associate professor from abroad (period of stay from 3 to 12 months); ^{*5} a JSPS Post-Doctoral or Ronpaku Fellow; ^{*6} an IMS visiting scientist and ^{*7} a visitor to IMS.

Scientists who would like to visit IMS under programs ^{*2} and ^{*4} are invited to make contact with IMS staff in their relevant field.

Dr. Sun Hao-Ling ^{*6}	Beijing Univ.	(China)	Sep. '05–Mar. '07
Prof. Li Zhengqiang ^{*6}	Jilin Univ.	(China)	Sep. '05–Dec. '05
Dr. Koutsoupakis Konstantinos ^{*5}	Univ. of Crete	(Greece)	Oct. '05–Oct. '07
Prof. Kushch Natalia ^{*6}	Inst. of Problems of Chem. Phys.	(Russia)	Oct. '05
Prof. Gao Yongli ^{*7}	Univ. of Rochester	(China)	Oct. '05
Dr. More Sam Dylan ^{*6}	Infineon	(Germany)	Oct. '05
Prof. Varotsis Constantinos ^{*6}	Univ. of Crete	(Greece)	Oct. '05–Nov. '05
Dr. Eckardt Robert C. ^{*6}	Cleveland Crystals, Inc.	(U.S.A.)	Oct. '05–Nov. '05
Dr. Chaki Kumar Nirmalya ^{*6}	Natl. Chem. Lab.	(India)	Oct. '05–Mar. '08
Prof. Wang Baolin ^{*6}	Huaiyin Inst. of Tech.	(China)	Oct. '05–Mar. '06
Prof. Araki Koichi ^{*4}	Univ. of Sao Paulo	(Brazil)	Oct. '05–Feb. '06
Mr. Hellingh Steven ^{*7}	The Royal Inst. of Tech.	(Holland)	Oct. '05–Dec. '05
Prof. Frenking Gernot ^{*6}	Philipps Univ.	(Germany)	Nov. '05
Prof. Yarwood Jack ^{*7}	Sheffield Hallam Univ.	(U.K.)	Nov. '05
Prof. Saykally Richard J. ^{*7}	Univ. of California	(U.S.A.)	Nov. '05
Prof. Prassides Kosmas ^{*7}	Univ. of Durham	(U.K.)	Nov. '05
Prof. Khabashesk Valery ^{*7}	Rice Univ.	(U.S.A.)	Nov. '05
Dr. Kim Yonfoon ^{*6}	Hunkuk Univ.	(Korea)	Nov. '05
Prof. Wei Chiming ^{*6}	Johns Hopkins Univ.	(U.S.A.)	Nov. '05
Prof. Righini Roberto ^{*7}	Univ. of Florence	(Italy)	Nov. '05
Dr. Volkov Victor ^{*7}	Univ. of Florence	(Italy)	Nov. '05
Prof. Couprie Marie-Emmanuelle ^{*6}	Commissariat for Atomic Energy	(France)	Nov. '05
Mr. Luis Fernando de Oliveira Furtado ^{*7}	Univ. of Sao Paulo	(Brazil)	Nov. '05–Jan. '06
Prof. Quiroga Reuben ^{*6}	De La Salle Univ.	(Philippines)	Nov. '05–Dec. '05
Prof. Pobre Romeric ^{*6}	De La Salle Univ.	(Philippines)	Nov. '05–Dec. '05
Prof. Eckart Gunther Adolf ^{*6}	Wuerzburg Univ.	(Germany)	Nov. '05–Dec. '05
Prof. Bielawski Serge ^{*6}	Lille Univ. of Sci. and Tech.	(France)	Nov. '05–Dec. '05
Prof. Christophe Szwaj ^{*2}	Lille Univ. of Sci. and Tech.	(France)	Nov. '05–Dec. '05
Dr. Pal Biswajit ^{*6}	Cent. for Cellular and Molecular Biology	(India)	Dec. '05–Jan. '06
Prof. Lee Jin Yong ^{*6}	Sungkyunkwan Univ.	(Korea)	Dec. '05–Feb. '06
Dr. Plenge Juergen ^{*6}	Wuerzburg Univ.	(Germany)	Dec. '05
Prof. Girard Bertrand ^{*5}	Univ. of Paul Sabatier	(France)	Dec. '05
Prof. Karplus Martin ^{*7}	Harvard Univ.	(U.S.A.)	Jan. '06
Prof. Doster Wolfgang ^{*7}	Technische Univ. Munchen	(Germany)	Jan. '06
Prof. Levy Ronald ^{*7}	Rutgers Univ.	(U.S.A.)	Jan. '06
Prof. Dobson Christopher ^{*7}	Univ. of Cambridge	(U.K.)	Jan. '06
Prof. Lee Jooyoung ^{*7}	Korea Inst.	(Korea)	Jan. '06
Dr. Lee Jinwoo ^{*7}	Korea Inst.	(Korea)	Jan. '06
Dr. Joo Keehyoung ^{*7}	Korea Inst.	(Korea)	Jan. '06
Dr. Butler Ian Robert ^{*7}	Univ. of Wales, Bangor	(U.K.)	Jan. '06
Prof. Swietlik Roman ^{*4}	Polish Acad. of Sci.	(Poland)	Feb. '06–Sep. '06
Dr. Delagnes Jean-christophe ^{*6}	Univ. of Paul Sabatier	(France)	Feb. '06–Mar. '06
Dr. Petit Yannick ^{*6}	Univ. Jeseoph Fourier	(France)	Feb. '06–Mar. '06
Prof. Jungwirth Pavel ^{*7}	The Acad. of Sci. of the Czech Republic	(Czech)	Feb. '06
Prof. Lee Yuan T ^{*7}	Acad. Sinica	(Taiwan)	Feb. '06
Prof. Mukamel Shaul ^{*7}	Univ. of California at Irvine	(U.S.A.)	Feb. '06
Dr. Liu Kopin ^{*7}	Inst. of Atomic and Molecular Sci. Acad. Sinica	(Taiwan)	Feb. '06
Prof. Kozlowski M. Pawel ^{*7}	Univ. of Louisville	(U.S.A.)	Feb. '06
Prof. Kaminskii Alexander ^{*7}	Inst. of Crystallography, Russian Acad. of Sci.	(Russia)	Feb. '06
Prof. Wei Chiming ^{*7}	Johns Hopkins Univ.	(U.S.A.)	Feb. '06
Prof. Balanov Nikolai ^{*7}	Ural State Univ.	(Russia)	Feb. '06
Dr. Ghalsasi Prasanna ^{*7}	Hiroshima Univ.	(Japan)	Feb. '06

Prof. Pradeep Thalappil ^{*2}	Indian Inst. of Tech. Madras	(India)	Apr. '06–May '06
Prof. Wang Wenping ^{*4}	Hefei Univ. of Tech.	(China)	Apr. '06–Mar. '07
Dr. Delagnes Jean-Christophe ^{*6}	IMS(CREST)	(Japan)	Apr. '06–Mar. '07
Prof. Allakhverdiev Suleyman ^{*4}	Inst. of Basic Biological Problems Russian Acad. of Sci.	(Russia)	Apr. '06–Jun. '07
Prof. Monceau Pierre ^{*6}	CNRS	(France)	Apr. '06
Prof. Ruhman Sanford ^{*7}	Hebrew Univ.	(Israel)	Apr. '06
Prof. Levis Robert J. ^{*7}	Temple Univ.	(U.S.A.)	May '06
Dr. Bruce Garrett ^{*7}	Pacific Northwest Natl. Lab.	(U.S.A.)	May '06
Prof. Ingolf Hertel ^{*5}	Max Born Inst.	(Germany)	May '06
Dr. Myers Lawrence ^{*7}	JDS Uniphase Corp.	(U.S.A.)	May '06
Dr. Marabella Len ^{*7}	JDS Uniphase Corp.	(U.S.A.)	May '06
Prof. Roesch Notker ^{*7}	TU Munchen	(Germany)	May '06
Prof. Thiel Walter ^{*7}	Max-Planck-Inst. fur Kohlenforschung	(Germany)	May '06
Prof. Shaik Sason ^{*7}	Hebrew Univ.	(Israel)	May '06
Prof. Frenking Gernot ^{*7}	Philipps- Univ. Marburg	(Germany)	May '06
Prof. Hall Michael B. ^{*7}	Texas A&M Univ.	(U.S.A.)	May '06
Prof. Siegbahn Per E. M. ^{*7}	Stockholm Univ.	(Sweden)	May '06
Dr. Dedieu Alain ^{*7}	Univ. Louis Pasteur	(France)	May '06
Dr. MUSAEV Djamaladdin G. ^{*7}	Emory Univ.	(U.S.A.)	May '06
Dr. Maseras Felix ^{*7}	ICIQ	(Spain)	May '06
Prof. Sauer Joachim ^{*7}	Humboldt Univ. zu Berlin	(Germany)	May '06
Prof. Borden Weston Thatcher ^{*7}	Univ. of Washington	(U.S.A.)	May '06
Prof. Radom Leo ^{*7}	Univ. of Sydney	(Australia)	May '06
Prof. Gadre Shridhar R. ^{*7}	Univ. of Pune	(India)	May '06
Prof. Gordon Mark ^{*7}	Iowa State Univ.	(U.S.A.)	May '06
Dr. Fedorov Dmitri G. ^{*7}	AIST	(Japan)	May '06
Dr. Selvarengan Paranthaman ^{*7}	Univ. of Rennes	(France)	May '06
Prof. Simas Alfredo Mayall ^{*7}	Univ. Federal de Penabuco	(Brazil)	May '06
Prof. Sastry G. Narahari ^{*7}	Indian Inst. of Chem. Tech.	(India)	May '06
Dr. Schaefer Ansgar ^{*7}	BASF	(Germany)	May '06
Prof. Agren Hans ^{*6}	The Royal Inst. of Tech.	(Sweden)	May '06
Ms. Labat Marie ^{*6}	CEA	(France)	May '06–Jun. '06
Mr. Lambert Guillaume ^{*6}	CEA	(France)	May '06–Jun. '06
Dr. Schmidt Mike ^{*6}	Iowa State Univ.	(U.S.A.)	May '06–Jul. '06
Prof. Wu Yun-Dong ^{*4}	The Hong Kong Univ. of Sci. and Tech.	(China)	May '06–Aug. '06
Prof. Pal Tarasankar ^{*4}	India Inst. of Tech.	(India)	May '06–Aug. '06
Prof. Holland Andrew ^{*6}	Brunel Univ.	(U.K.)	Mar. '06
Mr. Ingley Richard ^{*6}	Brunel Univ.	(U.K.)	Mar. '06
Prof. Wei Chiming ^{*7}	Johns Hopkins Univ.	(U.S.A.)	Mar. '06
Prof. Aka Gerard ^{*6}	Univ. Pierre & Marie Curie (Paris 6)	(France)	Mar. '06
Prof. Bethell Donald ^{*7}	Univ. of Liverpool	(U.K.)	Mar. '06
Prof. Zhang Guobin ^{*7}	Univ. of Sci. and Tech. of China	(China)	Mar. '06
Prof. Sheng Liusi ^{*7}	Univ. of Sci. and Tech. of China	(China)	Mar. '06
Prof. Kwon Yong Seung ^{*6}	Sungkyunkwan Univ.	(Korea)	Mar. '06
Prof. Gao Yongli ^{*4}	Rochester Univ.	(U.S.A.)	Jun. '06–Sep. '06
Prof. Lu Xin ^{*4}	Xiamen Univ.	(China)	Jun. '06–Sep. '06
Prof. Girard Bertrand ^{*6}	Univ. Paul Sabatier	(France)	Jun. '06
Prof. Yakovlev Vladislav ^{*7}	Univ. of Wisconsin-Milwaukee	(U.S.A.)	Jun. '06
Dr. Dah-Yen Yang ^{*7}	Inst. of Atomic and Molecular Sci.	(Taiwan)	Jun. '06
Prof. Paul Madden ^{*7}	Univ. of Edinburgh	(U.K.)	Jun. '06
Prof. Zhao Yi ^{*6}	Univ. of Sci. and Tech. of China	(China)	Jun. '06–Jul. '06
Mr. Larsson Gustav ^{*6}	The Royal Inst. of Tech.	(Sweden)	Jun. '06–Aug. '06
Ms. Macnaughton Janay B. ^{*5}	Univ. of Saskatchewan	(Canada)	Jun. '06–Aug. '06
Prof. Kwon Yong Seung ^{*6}	Sungkyunkwan Univ.	(Korea)	Jul. '06
Prof. Chin See Leang ^{*7}	Laval Univ.	(Canada)	Jul. '06
Prof. Boo Bong Hyun ^{*2}	Chungnam Natl. Univ.	(Korea)	Jul. '06
Dr. Richter Robert ^{*6}	Elettra Natl. Synchrotron Light Lab.	(Italy)	Jul. '06
Prof. Wennemers Helma ^{*6}	Univ. of Basel	(Swiss)	Jul. '06
Dr. Feifel Raimund ^{*6}	Uppsala Univ.	(Sweden)	Jul. '06
Ms. Yoon Hee ^{*6}	Sungkyunkwan Univ.	(Korea)	Jul. '06
Ms. Lee Kyeng Eun ^{*6}	Sungkyunkwan Univ.	(Korea)	Jul. '06
Prof. Pielichowski Jan ^{*7}	Cracow Univ. of Tech.	(Poland)	Jul. '06
Dr. Sutrisno Widayami ^{*7}	Inst. Tech. Bandung	(Indonesia)	Jul. '06
Dr. Horak Daniel ^{*7}	Inst. of Macromolecular Chem.	(Czech)	Jul. '06

Prof. Nagieb Zenat ^{*7}	Natl. Research Center	(Egypt)	Jul. '06
Ms. Gibson Gillian ^{*7}	Univ. of Greenwich at Medway	(U.K.)	Jul. '06
Prof. Bogoczek Romuald ^{*7}	Univ. of Economics	(Poland)	Jul. '06
Dr. Agag Tavelc ^{*7}	Tanta Univ.	(Egypt)	Jul. '06
Prof. Stover Harald ^{*7}	McMaster Univ.	(Canada)	Jul. '06
Dr. Kang Phil Hyun ^{*7}	Korea Atomic Energy Research Inst.	(Korea)	Jul. '06
Prof. Bergbreiter David E. ^{*7}	Texas A&M Univ.	(U.S.A.)	Jul. '06
Prof. Ding Kuiling ^{*7}	Chinese Acad. of Sci.	(China)	Jul. '06
Prof. Luis Santiago ^{*7}	Univ. Jaumel	(Spain)	Jul. '06
Prof. Lee Yoon-Sik ^{*7}	Seoul Natl. Univ.	(Korea)	Jul. '06
Prof. Wennemers Helma ^{*7}	Univ. of Basel	(Swiss)	Jul. '06
Dr. Dnal Pradeep ^{*7}	Genzyme Corporation	(U.S.A.)	Jul. '06
Dr. Almutari Adah ^{*7}	Univ. of California Berkeley	(U.S.A.)	Jul. '06
Dr. AlMaadeed Mariam ^{*7}	Qatar Univ.	(Qatar)	Jul. '06
Prof. Li Mingchun ^{*7}	Huaqiao Univ.	(China)	Jul. '06
Prof. Frechet Jean M. J. ^{*7}	Univ. of California Berkeley	(U.S.A.)	Jul. '06
Prof. Akelah Ahmed ^{*7}	Tanta Univ.	(Egypt)	Jul. '06
Prof. Toy Patrick H. ^{*7}	Univ. of Hong Kong	(Hong Kong)	Jul. '06
Prof. Cunill Fidel ^{*7}	Univ. of Barcelona	(Spain)	Jul. '06
Dr. Nho Young-Chang ^{*7}	Korea Atomic Energy Research Inst.	(Korea)	Jul. '06
Prof. Chen Yun ^{*7}	Natl. Cheng Kung Univ.	(Taiwan)	Jul. '06
Prof. Khastgir Dipak ^{*7}	Rubber Tech. Centre	(India)	Jul. '06
Prof. Shea Kenneth J. ^{*7}	Univ. of California Irvine	(U.S.A.)	Jul. '06
Prof. Skene Will G. ^{*7}	Univ. of Montreal	(Canada)	Jul. '06
Prof. Zhu Julian X. X. ^{*7}	Univ. of Montreal	(Canada)	Jul. '06
Ms. Jakubiak Anna ^{*7}	Wroclaw Univ. of Tech.	(Poland)	Jul. '06
Ms. Kan Jovi Tze-Wai ^{*7}	Univ. of Hong Kong	(Hong Kong)	Jul. '06
Ms. He Helen Song ^{*7}	Univ. of Hong Kong	(Hong Kong)	Jul. '06
Ms. Chung Cecilia Wan-Ying ^{*7}	Univ. of Hong Kong	(Hong Kong)	Jul. '06
Prof. Tsai Yu-chen ^{*7}	Natl. Chung Hsing Univ.	(Taiwan)	Jul. '06
Prof. Suen Shing-Yi ^{*7}	Natl. Chung Hsing Univ.	(Taiwan)	Jul. '06
Ms. Ronka Sylwia ^{*7}	Wroclaw Univ. of Tech.	(Poland)	Jul. '06
Prof. Chen Dorg-Hwang ^{*7}	Natl. Cheng Kung Univ.	(Taiwan)	Jul. '06
Dr. Toman Petr ^{*7}	Acad. of Sci. of the Czech Republic	(Czech)	Jul. '06
Mr. Bartholome Danny ^{*7}	Friedrich Schiller Univ.	(Germany)	Jul. '06
Mr. Cheung Sin-Yin ^{*7}	Chinese Univ. of Hong Kong	(Hong Kong)	Jul. '06
Dr. Krajnc Peter ^{*7}	Univ. of Maribor	(Slovenia)	Jul. '06
Mr. Hager Martin ^{*7}	Friedrich Schiller Univ.	(Germany)	Jul. '06
Prof. Syu Mei-Jywan ^{*7}	Natl. Cheng Kung Univ.	(Taiwan)	Jul. '06
Dr. Adhikari Airody Vasudeva ^{*7}	Natl. Inst. of Tech. Karnataka	(India)	Jul. '06
Prof. Bogdal Dariusz ^{*7}	Cracow Univ. of Tech.	(Poland)	Jul. '06
Dr. Amer Riad ^{*7}	El nasr Company for Pharmaceutical Chem.	(Egypt)	Jul. '06
Dr. Burguete Maria ^{*7}	Univ. Jaume I	(Spain)	Jul. '06
Prof. Cheng Chien-Chung ^{*7}	Tamkang Univ.	(Taiwan)	Jul. '06
Ms. Choi Ji Ah ^{*7}	Soongsil Univ.	(Korea)	Jul. '06
Prof. Chun Keun Ho ^{*7}	Soongsil Univ.	(Korea)	Jul. '06
Dr. El-Sharnouby Ayman ^{*7}	El nasr Company for Pharmaceutical Chem.	(Egypt)	Jul. '06
Dr. Katar Ibrahim ^{*7}	El nasr Company for Pharmaceutical Chem.	(Egypt)	Jul. '06
Dr. Mir Mohamad Sadeghi Gity ^{*7}	Amirkabir Univ. of Tech.	(Iran)	Jul. '06
Mr. Nam Woo ^{*7}	Soongsil Univ.	(Korea)	Jul. '06
Prof. Ulrich Anne ^{*6}	Univ. of Karlsruhe	(Germany)	Jul. '06–Aug. '06
Prof. Griesinger Christian ^{*6}	Max Plank Inst. for Biophysical Chem.	(Germany)	Jul. '06–Aug. '06
Prof. Cormack Peter ^{*7}	Univ. of Strathclyde	(U.K.)	Jul. '06–Aug. '06
Prof. Zhao Xiang ^{*6}	Xi'an Jiaotong Univ.	(China)	Jul. '06–Aug. '06
Dr. Gao Xingfa ^{*6}	Inst. of High Energy Phys., Chinese Acad. of Sci.	(China)	Aug. '06–Mar. '07
Dr. Kimberg Victor ^{*5}	Inst. of Molecular Sci.	(Japan)	Aug. '06–Aug. '08
Prof. Jeong Dae Hong ^{*6}	Seoul Natl. Univ.	(Korea)	Aug. '06
Ms. Kim Yougchae ^{*6}	Seoul Natl. Univ.	(Korea)	Aug. '06
Prof. Varotsis Constantinos ^{*6}	Univ. of Crete	(Greece)	Aug. '06
Mr. Petrossian Leo ^{*6}	Arizona State Univ.	(U.S.A.)	Aug. '06
Prof. Nordgren Joseph ^{*6}	Uppsala Univ.	(Sweden)	Aug. '06
Prof. Pettersson Lars G. M. ^{*6}	Stockholm Univ.	(Sweden)	Aug. '06
Dr. Stuart C. Althorpe ^{*7}	Univ. of Cambridge	(U.K.)	Aug. '06
Dr. Sichelschmidt Joerg ^{*6}	Max-Planck-Inst. für Plasmaphysic	(Germany)	Aug. '06

Dr. Guo Jinghua ^{*1}	Univ. of California	(U.S.A.)	Aug. '06
Prof. Uwe Bergmann ^{*1}	Stanford Univ.	(U.S.A.)	Aug. '06
Prof. Simon Marc ^{*1}	Univ. Pierre et Marie Curie	(France)	Aug. '06
Prof. Hague Coryn ^{*1}	Univ. Pierre et Marie Curie	(France)	Aug. '06
Prof. Carniato Stephane ^{*1}	Univ. Pierre et Marie Curie	(France)	Aug. '06
Dr. Foehlich Alexander ^{*1}	Hamburg Univ.	(Germany)	Aug. '06
Prof. Mukamel Shaul ^{*1}	Univ. California	(U.S.A.)	Aug. '06
Dr. Feifel Raimund ^{*1}	Uppsala Univ.	(Sweden)	Aug. '06

AWARDS

Professor Emeritus Kaya's Scientific Achievements

Professor Emeritus Koji Kaya, the former Director General of IMS, was selected as “the Person of Cultural Merit in 2005” for his outstanding contributions to “nano-materials science.”

Professor Kaya started his scientific career with an aim to understand the details of interaction between atoms and molecules. He has determined the structures of van der Waals complexes precisely by high-resolution laser spectroscopy. On the basis of the fundamental knowledge of intermolecular interaction, he has devoted himself to the research of clusters, aggregates of atoms and molecules. Various types of molecular assemblies with novel structures and properties have been produced size selectively by using laser vaporization and molecular beam techniques. One of the representative systems is a one-dimensional organo-metallic cluster, in which metal atoms and organic molecules are stacked alternately. Unique behavior of the electrons within these “sandwich clusters” has gained wide interests from both experimental and theoretical viewpoints. These clusters are potential candidates of building blocks of functional nano-materials. He has developed a method, referred to as a soft-landing method, to assemble these unique clusters onto a surface, which will open the door to a new research field of nano-materials science.

As described above, Professor Kaya has played a significant role as a forerunner in establishing a new research field of nano-materials science.

Professor Emeritus Tanaka's Scientific Achievements

Dr. Ikuzo Tanaka, former president and professor emeritus of Tokyo Institute of Technology, received the Person of Cultural Merit for 2005 in recognition of his contributions to both research and education in the field of physical chemistry, in particular photochemistry. He made outstanding research achievements and fostered many excellent scientists. He also contributed greatly to enhancement of higher education serving as the president of academic organizations including Tokyo Institute of Technology and the National Institution of Academic Degrees.

Having started the photochemistry research in 1950's, Dr. Tanaka was one of the pioneers in the field. He initiated development of photoionization mass spectrometry by utilizing the vacuum ultraviolet light irradiation in stead of conventional electron impact. This original work was highly evaluated in the international scientific community. He also introduced using lasers in the chemical research. The laser-driven pump and probe method resulted in improvement of energy and time resolution for the studies of excited state creation and chemical reactions.

Dr. Tanaka devoted himself to the advancement of the study. He took leadership in founding a new academic society on photochemistry: the Japanese Photochemistry Association, and was selected as the first president. His presidency in other academic societies includes the Chemical Society of Japan and the Japan Society of Energy and Resources. In addition, he chaired many domestic and international scientific committees.

Japan is one of the world-leading states in photochemistry with the highest standards of research in both basic and applied fields such as functional materials, environment, energy, and information and communication technology. Dr. Tanaka, as a pioneer and front-runner of the research, played an important role in promotion of science and human development.

Dr. Tanaka received Order of the Rising Sun with Gold and Silver Star in 2001, Medal with Purple Ribbon in 1989, Toray Science and Technology Prize in 1985, The Chemical Society of Japan Award in 1977, The Matsunaga Prize in 1970, and The Chemical Society of Japan Award for Young Chemist in 1959.

Professor Kobayashi's Scientific Achievements

Prof. Hayao Kobayashi of the Department of Molecular Assemblies received a Chemical Society of Japan Award in 2006 for his contributions to “Studies on Magnetic Organic Superconductors and Single-component Molecular Metals.” By highly sophisticated physical measurements, Prof. Kobayashi have developed various new functional molecular materials such as magnetic organic superconductors and single-component molecular conductors. The followings are the summary of his scientific achievements related to the award.

1) *Magnetic Organic Superconductors*

Itinerant and localized hybrid spin systems are candidates for possible new cooperative phenomena. However, most of the researches could not obtained functions beyond those of individual spin species. Prof. Kobayashi focused on BETS, bis(ethylenedithio)tetraselenafulvalene, molecules, and discovered field induced organic superconductors in λ -(BETS)₂FeCl₄, λ -(BETS)₂Fe_xGa_{1-x}Cl₄, κ -(BETS)₂FeBr₄. This observation is beyond our expectation since

superconducting phases are not stable under magnetic field. By a series of researches following this, he discovered new phenomena such as colossal magneto-resistance effects and noble metal-superconductivity-insulator transition. They are cooperative phenomena which cannot be realized by the individual conduction electron and magnetic ion. He established the new field “magnetic organic conductors.”

2) *Single-component Molecular Metals*

Conventional organic conductors are composed of two components to create conduction electrons. So single-component molecular metals like copper or gold has been one of the chemist’s dreams. Prof. Kobayashi and co-worker focused on the system which possesses significant three-dimensional inter-molecular interactions and a small HOMO-LUMO gap, and developed a series of the π extended transition metal complexes. Prof. Kobayashi developed the first single-component molecular metals based on the transition metal with extended-TTF ligands, Ni(tmdt)₂ and Au(tmdt)₂. After this discovery, extensive investigations for single-component molecular metals are performed. The very precision magnetization measurement under a strong magnetic field revealed the existence of the Fermi surface, which is a clear evidence of metal. The evaluated cross-section of the Fermi surfaces are coincided with the first-principle calculation result. The metallic properties of these single-component molecular metals are considered to be realized as compensated-metals such as Mg or Al. This discovery just realizes the dream which chemists are giving up, has big and international influence also on a lot of researchers.

These achievement mentioned here captured the high spotlight internationally from a viewpoint of new functionality molecular materials.

Professor Matsumoto’s Scientific Achievements

Professor Yoshiyasu Matsumoto received “The CSJ Award for Creative Work” in the spring of 2006 from Chemical Society of Japan for his achievements on “Ultrafast dynamics in surface photochemistry.”

Photochemistry at well-defined surface is an important subject from the viewpoint of application such as photocatalysts as well as fundamental science. Professor Matsumoto has investigated dynamics of photochemical processes by employing time-resolved non-linear spectroscopy. The major achievements are (1) elucidation of the excitation mechanism in photochemistry of adsorbates on surfaces, (2) real-time probing of dynamics of electron transfer and (3) photo-induced nuclear dynamics at surfaces. These achievements have contributed to the development of new areas in surface science and related research fields such as nanoscience and photoscience.

Dr. Tahara’s Scientific Achievements

Dr. Tahei Tahara, Chief Scientist of Molecular Spectroscopy Laboratory, RIKEN (Institute for Chemical Research), a former associate professor (1995–2001) of Department of Vacuum UV Photoscience, IMS, has been awarded the Japan Society for the Promotion of Science Prize in 2005 for his contribution, “Studies of Molecular Dynamics in the Condensed Phase by Ultrafast Time-Resolved Spectroscopy.” Dr. Tahara has performed systematic studies on the real-time observation on the intramolecular nuclear dynamics in ultrafast photoreaction, such as unimolecular dissociation, proton transfer, isomerization, by developing novel techniques/instruments. All his recent scientific accomplishments have made a large contribution to the deep understanding of elementary processes in photochemical reactions in condensed phase.

Associate Professor Donglin Jiang’s Scientific Achievement

Professor Donglin Jiang of Department of Applied Molecular Science received two awards. One is the *Young Scientist Award* from the Minister of Ministry of Education, Culture, Sports, Science and Technology of Japan (MEXT). The award title is “Study of functional nano-materials in polymer science.” Another one is the *Wiley Award* from the Society of Polymer Science, Japan. The award title is “Synthesis and functions of polymers with tree-like morphology.” Both awards are given for the original synthetic work on dendrimer. Dr. Jiang synthesized various kinds of highly functional materials employing nano-scale molecule called a dendrimer, which consists of core and dendron. First, he synthesized a heme-dendrimer with iron porphyrin as the core, and demonstrated that this molecule reversibly absorbs and desorbs oxygen molecules. Second, he synthesized a spherical dendrimer that works as a light-harvesting antenna. This finding has drawn much attention of all material scientists around the world. Third, he synthesized a columnar dendrimer that acts as a highly efficient catalyst for the generation of hydrogen molecules through the photo-reduction of water molecule. Fourth, he synthesized an amphiphilic dendron with photo-functional groups, and found that the dendrons are self-assembled to form a nano-scale organic tube with a narrow size distribution. Since the tube consists of a donor and acceptor layers, a highly efficient photoconduction is

expected. Fifth, he synthesized a polymer iron complex with dendron-type ligands. This complex changes the spin state of the iron ion depending upon the temperature. As described above, the work of Dr. Jiang has given a strong impact to the field of material science.

Associate Professor Morita's Scientific Achievement

Prof. Akihiro Morita, Department of Computational Molecular Science, received the Morino Science Award in 2006 for his contributions to "Theoretical study on structure and dynamics of solutions and solution interfaces." He has made pioneering contributions to solution chemistry and heterogeneous chemistry associated to liquid interfaces and atmospheric aerosols, using *ab initio* electronic structure theory and molecular dynamics simulation.

He has developed an *ab initio* theory of electronic polarization, called the charge response kernel, and thereby elucidated several mechanisms of experimental novel phenomena, including diffusion of radical species and vibrational relaxation of azide ions, where the electronic polarization turned out to play crucial roles. In the field of heterogeneous chemistry, one of the most noticeable achievements is the development of theory and first-principle computational methods of vibrational sum frequency generation (SFG) spectroscopy. This work opened a new avenue of detailed and unambiguous analysis of SFG spectra with the help of molecular simulation.

Associate Professor Tsukuda's Scientific Achievement

Associate Professor Tatsuya Tsukuda of Research Center for Molecular-Scale Nanoscience was awarded for best oral presentation at the GOLD2006 conference (September, 2006). The title of his paper was "Polymer-stabilized gold clusters as quasi-homogeneous catalysts for aerobic oxidation in water." He demonstrated that the gold clusters stabilized by polymer act as efficient catalysts for aerobic oxidation of alcohols in water and that the activity is increased with decrease in size. The size-dependent activity was explained in terms of quasi-molecular electronic structures of the small clusters.

Research Associate Dr. Hatsui's Scientific Achievement

Research Associate Dr. Takaki Hatsui of Department of Vacuum UV Photoscience has received the Japanese Society for Synchrotron Radiation Research (JSSRR) Award 2006 for his contribution to the promotion of synchrotron radiation research in January 2006. The title of his work is "Development of a Novel High-Resolution Spectrometer for Soft X-ray Emission Studies." His design consists of a Wolter type I mirror, a free-standing transmission grating, and a back-illuminated CCD, and is completely different from conventional types of soft X-ray emission spectrometers. His spectrometer can achieve >5000 ($E/\Delta E$) energy resolution; on the other hand, a typical energy resolution of conventional ones is <2000 . His spectrometer will be a most-promising one for the next-generation soft X-ray emission spectrometer using high brilliant synchrotron radiation.

Research Associate Dr. Higashibayashi's Scientific Achievement

Dr. Shuhei Higashibayashi, Research Associate of Research Center for Molecular-Scale Nanoscience, received the Young Scientist's Research Award in Natural Product Chemistry in the 40th Young Scientist Meeting on Natural Product Chemistry (2005) for his contribution to "Creation of Universal NMR Database for the Stereochemical Assignment of Acyclic Natural Products." This award is given to a young scientist (younger than 34 years of age) who has made notable contributions to the field of natural product chemistry or bioorganic chemistry. Dr. Higashibayashi developed Universal NMR Database approach to determine the stereochemical configurations of acyclic organic molecules. This methodology realized direct determination of the stereochemical configurations of acyclic organic molecules with the ^1H and ^{13}C chemical shifts and the vicinal $^1\text{H}/^1\text{H}$ spin-coupling constant of NMR spectra without chemical degradation or derivatization. Universal NMR Database can be applied to any acyclic organic molecules and determine the stereochemical configurations of the corresponding common structural units in the molecules at once. Universal NMR Database approach has been already utilized for the stereochemical assignment of many natural products.

Research Associate Dr. Negishi's Scientific Achievement

Dr. Negishi, a research associate of Research Center for Molecular-Scale Nanoscience, received the Best Young Presenter Award for the presentation of an Excellent paper in the 4th Annual Meeting of Society of Nano Science and Technology. The title of the paper was "Au₂₅(SR)₁₈: discovery and the origin of the stability." He established precise synthesis method of thiolated gold (Au:SR) clusters, based on polyacrylamide gel electrophoresis and electrospray ionization mass spectrometry. Among various Au:SR clusters thus synthesized, it was found that the Au₂₅(SR)₁₈ clusters exhibit extraordinarily high stability against size-reducing processes. He also developed a large-scale synthesis method for Au₂₅ clusters utilizing the high stability against thiol-mediated etching.

Research Associate Tanaka's Scientific Achievement

Dr. Hirofumi Tanaka, Research Associate of Research Center for Molecular Scale Nanoscience, received the Best Young Presenter Award for the presentation titled "Porphyrin Molecules Working as Nanodevice on Single-walled Carbon Nanotube" in the 4th annual meeting of Society of Nano Science and Technology held in Kyoto University.

He succeeded to fabricate the arrangement of 2-3-nm-size porphyrin aggregations adsorbed on single-walled carbon nanotube (SWCNT) using self-assembly. He also succeeded the direct measurement for the electric property of each aggregation by newly developed method of Point-contact Current Imaging (PCI-) AFM. Results showed that *I-V* curves on the exposed SWCNT were symmetric with respect to the origin but that through the porphyrin aggregation was asymmetric. The results indicate that the porphyrin aggregation on SWCNT works as a nano-rectification device which is one of the smallest organic devices at the present time. These results will assist to develop the new field of molecular electronics and nanoelectronics.

Dr. Iwahashi's Scientific Achievement

Dr. Iwahashi received the poster prize of Annual Meeting of EMLG/JMLG 2005 held in Prague on September 4–8, 2005. The poster was entitled "Molecular dynamics study of extension of α -helical peptides."

Extension-force curves for polyalanine and polyglutamic acid in water have been calculated based upon molecular dynamics calculation combined with thermodynamic integration method. The calculation is of higher accuracy than that obtained by other conventional methods such as steered MD. Based upon this method, he successfully showed a molecular picture for the force which originates in conformational entropy of the peptide chain.

Dr. Tsunoyama's Scientific Achievement

Dr. Hironori Tsunoyama, an IMS fellow in Research Center for Molecular-Scale Nanoscience, received Best Young Presenter Award in the 4th Annual Meeting of Society of Nano Science and Technology (May, 2006). The title of his paper was "Isolation of Alkanethiolate-Protected Au₅₅ Clusters by Recycling Gel Permeation Chromatography (GPC)." He succeeded in synthesis of alkanethiolate-protected Au₅₅ clusters by size separation with recycling GPC out of the crude samples prepared by thiolation of polymer-stabilized Au clusters. The newly prepared Au₅₅ provides a prototypical system for fundamental study of nano-scale material and application in nano-device.

Mr. M. Fuyuki's Scientific Achievement

Mr. Masanori Fuyuki, a graduate student of SOKENDAI, received the Student Award for the presentation of an excellent poster entitled "Excitation mechanism of coherent phonons on alkali-metal adsorbed metal surfaces" in the 46th IUVSTA Workshop & 5th International Symposium on Ultrafast Surface Dynamics, which was held at Abashiri in 21–25 May 2006. He performed observations of coherent phonons on alkali-metal on metal surfaces by femtosecond time-resolved second harmonic generation. He succeeded in measuring the action spectra of coherent amplitude as a function of photon energy of pump pulses in Na/Cu(111) and K/Pt(111) adsorption systems, which allowed him to pin down the excitation mechanism for the coherent phonons.

Graduate Student Shiratori's Scientific Achievement

Mr. Kazuya Shiratori, a graduate student of Department of Structural Molecular Science, School of Physical Sciences, The Graduate University for Advanced Studies, received the Young Scientist Award for the presentation of an excellent paper in the 22nd Symposium on Chemical Kinetics and Dynamics (June, 2006). The title of the paper was "Electronic structure calculations of adsorbate-surface systems based on finite-temperature density functional theory." He developed the method of quantum chemistry calculations based on finite temperature density functional theory to describe the electronic structures of (sulfur-gold) adsorbate-surface systems. He investigated the electronic structures depending on temperature and the size of the cluster model.

Graduate Student Yoshimura's Scientific Achievement

Mr. Hideaki Yoshimura, a graduate student of Department of Structural Molecular Science, School of Physical Sciences, the Graduate University for Advanced Studies received the Graduate Student Award for the Presentation of an Excellent Paper in the Annual Meeting of The Chemical Society of Japan held on March, 2006. The title of his paper was "Selective Oxygen Sensing Mechanism in the Oxygen Sensor Protein HemAT by means of hydrogen bonding network." 85 papers were selected for this award out of 290 of the applications.

LIST OF PUBLICATIONS

Department of Theoretical Studies

- Y. -K. CHOE and S. NAGASE**, "Effect of the Axial Cysteine Ligand on the Electronic Structure and Reactivity of High-Valent Iron (IV) Oxo-Porphyrins (Compound I): A Theoretical Study," *J. Comput. Chem.* **26**, 1600–1611 (2005).
- Z. SLANINA and S. NAGASE**, "Sc₃N@C₈₀: Computations on the Two-Isomer Equilibrium at High Temperatures," *ChemPhysChem* **6**, 2060–2063 (2005).
- M. SAITO, R. HAGA, M. YOSHIOKA, K. ISHIMURA and S. NAGASE**, "The Aromaticity of the Stannole Dianion," *Angew. Chem., Int. Ed.* **44**, 6553–6556 (2005).
- Y. MAEDA, J. MIYASHITA, T. HASEGAWA, T. WAKAHARA, T. TSUCHIYA, T. NAKAHODO, T. AKASAKA, N. MIZOROGI, K. KOBAYASHI, S. NAGASE, T. KATO, N. BAN, H. NAKAJIMA and Y. WATANABE**, "Reversible and Regioselective Reaction of La@C₈₂ with Cyclopentadiene," *J. Am. Chem. Soc.* **127**, 12190–12191 (2005).
- Y. IIDUKA, T. WAKAHARA, T. NAKAHODO, T. TSUCHIYA, A. SAKURABA, Y. MAEDA, T. AKASAKA, K. YOZA, E. HORN, T. KATO, M. T. H. LIU, N. MIZOROGI, K. KOBAYASHI and S. NAGASE**, "Structural Determination of Metallofullerene Sc₃C₈₂ Revisited: A Surprising Finding," *J. Am. Chem. Soc.* **127**, 12500–12501 (2005).
- M. FUJITSUKA, O. ITO, Y. MAEDA, T. WAKAHARA, T. TSUCHIYA, T. NAKAHODO, T. AKASAKA, N. MIZOROGI and S. NAGASE**, "Photophysical and Photochemical Properties of the La@C₈₂ Anion," *Chem. Lett.* 1600–1601 (2005).
- W. SONG, M. NI, J. LU, Z. GAO, S. NAGASE, D. YU, H. YE and X. ZHANG**, "Electronic Structures of Semiconducting Double-Walled Carbon Nanotubes: Important Effect of Interlayer Interaction," *Chem. Phys. Lett.* **414**, 429–433 (2005).
- M. YAMADA, T. NAKAHODO, T. WAKAHARA, T. TSUCHIYA, Y. MAEDA, T. AKASAKA, M. KAKO, K. YOZA, E. HORN, N. MIZOROGI, K. KOBAYASHI and S. NAGASE**, "Positional Control of Encapsulated Atoms inside a Fullerene Cage by Exohedral Addition," *J. Am. Chem. Soc.* **127**, 14570–14571 (2005).
- L. FANG, T. NAKAHODO, T. WAKAHARA, T. TSUCHIYA, Y. MAEDA, T. AKASAKA, T. KATO, E. HORN, K. YOZA, N. MIZOROGI and S. NAGASE**, "A Singly Bonded Derivative of Endohedral Metallofullerene: La@C₈₂CB_r(COOC₂H₅)₂," *J. Am. Chem. Soc.* **127**, 17136–17137 (2005).
- H. NIKAWA, T. NAKAHODO, T. TSUCHIYA, T. WAKAHARA, G. M. A. RAHMAN, T. AKASAKA, Y. MAEDA, M. T. H. LIU, A. MEGURO, S. KYUSHIN, H. MATSUMOTO, N. MIZOROGI and S. NAGASE**, "S-Heterocyclic Carbene with a Disilane Backbone," *Angew. Chem., Int. Ed.* **44**, 7567–7570 (2005).
- M. KARNI, Y. APELOIG, N. TAKAGI and S. NAGASE**, "Ab Initio and DFT Study of the ²⁹Si NMR Chemical Shifts in RSi≡SiR," *Organometallics* **24**, 6319–6330 (2005).
- Z. SLANINA, F. UHLIK, L. ADAMOWICZ and S. NAGASE**, "Computing Fullerene Encapsulation of Non-Metallic Molecules: N₂@C₆₀ and NH₃@C₆₀," *Mol. Sim.* **31**, 801–806 (2005).
- K. ISHIMURA, P. PULAY and S. NAGASE**, "A New Parallel Algorithm of MP2 Energy Calculations," *J. Comput. Chem.* **27**, 407–413 (2006).
- Y. SUGIYAMA, T. SASAMORI, Y. HOSOI, Y. FURUKAWA, N. TAKAGI, S. NAGASE and N. TOKITOH**, "Synthesis and Properties of a New Kinetically Stabilized Digermyne: New Insights for a Germanium Analogue of an Alkyne," *J. Am. Chem. Soc.* **128**, 1023–1031 (2006).
- Z. SLANINA, F. UHLIK, S. -L. LEE and S. NAGASE**, "Computational Modelling for the Clustering Degree in the Saturated Steam and the Water-Containing Complexes in the Atmosphere," *J. Quant. Spectrosc. Radiat. Transfer* **97**, 415–423 (2006).
- Z. SLANINA, F. UHLIK, S. -L. LEE, L. ADAMOWICZ and S. NAGASE**, "Enhancement of Fullerene Stabilities from Excited Electronic States," *Comput. Lett.* **1**, 313–321 (2006).
- M. YAMADA, T. WAKAHARA, Y. LIAN, T. TSUCHIYA, T. AKASAKA, M. WAELCHLI, N. MIZOROGI, S. NAGASE and K. M. KADISH**, "Analysis of Lanthanide-Induced NMR Chemical Shifts of the Ce@C₈₂ Anion," *J. Am. Chem. Soc.* **128**, 1400–1401 (2006).
- M. YAMADA, T. WAKAHARA, T. NAKAHODO, T. TSUCHIYA, Y. MAEDA, T. AKASAKA, K. YOZA, E. HORN, N. MIZOROGI and S. NAGASE**, "Synthesis and Structural Characterization of Endohedral Pyrrolidino-dimetallofullene: La₂@C₈₀(CH₂)₂NTrt," *J. Am. Chem. Soc.* **128**, 1402–1403 (2006).
- Z. SLANINA, Z. CHEN, P. V. R. SCHLEYER, F. UHLIK, X. LU and S. NAGASE**, "La₂@C₇₂ and Sc₂@C₇₂: Computational Characterizations," *J. Phys. Chem. A* **110**, 2231–2234 (2006).
- J. KOBAYASHI, K. GOTO, T. KAWASHIMA, M. W. SCHMIDT and S. NAGASE**, "Reactivity of 1-Hydro-5-Carbaphosphatrane Based on Tautomerization between Pentavalent Phosphorane and Trivalent Cyclic Phosphonite," *Chem. Eur. J.* **12**, 3811–3820 (2006).
- J. LU, D. WANG, S. NAGASE, M. NI, X. ZHANG, Y. MAEDA, T. WAKAHARA, T. NAKAHODO, T. TSUCHIYA, T. AKASAKA, Z. GAO, D. YU, H. YE, Y. ZHOU and W. N. MEI**, "Evolution of the Electronic Properties of Metallic Single-Walled Nanotubes with the Degree of CCl₂ Covalent Functionalization," *J. Phys. Chem. B* **110**, 5655–5658 (2006).

- Z. SLANINA and S. NAGASE, "Stability Computations for Ba@C₇₄ Isomers," *Chem. Phys. Lett.* **422**, 133–136 (2006).
- Z. SLANINA, F. UHLIK, K. ISHIMURA and S. NAGASE, "Computations of the Energetics of C₆₀F₃₆ Isomers," *Fullerenes, Nanotubes, Carbon Nanostruct.* **14**, 57–65 (2006).
- G. FRENKING, A. KRAPP, S. NAGASE, N. TAKAGI and A. SEKIGUCHI, "Comment on Disproving a Silicon Analog of an Alkyne with the Aid of Topological Analyses of the Electronic Structure and Ab Initio Molecular Dynamics Calculations," *ChemPhysChem* **7**, 799–800 (2006).
- J. LU, S. NAGASE, X. ZHANG, D. WANG, M. NI, Y. MAEDA, T. WAKAHARA, T. NAKAHODO, T. TSUCHIYA, T. AKASAKA, Z. GAO, D. YU, H. YE, W. N. MEI and Y. ZHOU, "Selective Interaction of Larger or Charge-Transfer Aromatic Molecules with Metallic Single-Wall Carbon Nanotubes: Critical Role of the Molecular Size and Orientation," *J. Am. Chem. Soc.* **128**, 5114–5118 (2006).
- Z. SLANINA, S. -L. LEE, F. UHLIK, L. ADAMOWICZ and S. NAGASE, "Excited Electronic States and Relative Stabilities of C₈₀ Isomers," *Int. J. Quantum Chem.* **106**, 2222–2228 (2006).
- Y. MATSUNAGA, Y. MAEDA, T. WAKAHARA, T. TSUCHIYA, M. O. ISHITSUKA, T. AKASAKA, N. MIZOROGI, K. KOBAYASHI, S. NAGASE and K. M. KADISH, "NMR Study of La@C₈₂ (Ad) Anion," *ITE Lett. Batt. New Tech. Med.* **7**, 43–49 (2006).
- L. FENG, T. TSUCHIYA, T. WAKAHARA, T. NAKAHODO, Q. PIAO, Y. MAEDA, T. AKASAKA, T. KATO, K. YOZA, E. HORN, N. MIZOROGI and S. NAGASE, "Synthesis and Characterization of a Bisadduct of La@C₈₂," *J. Am. Chem. Soc.* **128**, 5990–5991 (2006).
- Y. IIDUKA, T. WAKAHARA, K. NAKAJIMA, T. TSUCHIYA, T. NAKAHODO, Y. MAEDA, T. AKASAKA, N. MIZOROGI and S. NAGASE, "¹³C NMR Spectroscopic Study of Scandium Dimetallofullerene, Sc₂@C₈₄ vs. Sc₂C₂@C₈₂," *Chem. Commun.* 2057–2059 (2006).
- Z. SLANINA, P. PULAY and S. NAGASE, "H₂, Ne, and N₂ Energies of Encapsulation into C₆₀ Evaluated with the MPWB1K Functional," *J. Chem. Theory Comput.* **2**, 782–785 (2006).
- T. TSUCHIYA, K. SATO, H. KURIHARA, T. WAKAHARA, T. NAKAHODO, Y. MAEDA, T. AKASAKA, K. OHKUBO, S. FUKUZUMI, T. KATO, N. MIZOROGI, K. KOBAYASHI and S. NAGASE, "Host-Guest Complexation of Endohedral Metallofullerene with Azacrown Ether and Its Application," *J. Am. Chem. Soc.* **128**, 6699–6703 (2006).
- M. SAITO, M. SHIMOSAWA, M. YOSHIOKA, K. ISHIMURA and S. NAGASE, "Synthesis of Stannaindenyl Anions and a Dianion," *Organometallics* **25**, 2967–2971 (2006).
- L. FENG, T. WAKAHARA, T. NAKAHODO, T. TSUCHIYA, Q. PIAO, Y. MAEDA, Y. LIAN, T. AKASAKA, E. HORN, K. YOZA, T. KATO, N. MIZOROGI and S. NAGASE, "The Bingel Monoadducts of La@C₈₂: Synthesis, Characterization, and Electrochemistry," *Chem. Eur. J.* **12**, 5578–5586 (2006).
- K. IWANAGA, J. KOBAYASHI, T. KAWASHIMA, N. TAKAGI and S. NAGASE, "Syntheses, Structures, and Reactions of Heptacoordinate Trihalogermanes Bearing a Triarylmethyl-Type Tetradentate Ligand," *Organometallics* **25**, 3388–3393 (2006).
- L. LAI, W. SONG, J. LU, Z. GAO, S. NAGASE, M. NI, W. N. MEI, J. LIU, D. YU and H. YE, "Structural and Electronic Properties of Fluorinated Boron Nitride Nanotubes," *J. Phys. Chem. B* **110**, 14092–14097 (2006).
- T. WAKAHARA, Y. IIDUKA, O. IKENAGA, T. NAKAHODO, A. SAKURABA, T. TSUCHIYA, Y. MAEDA, M. KAKO, T. AKASAKA, K. YOZA, E. HORN, N. MIZOROGI and S. NAGASE, "Characterization of the Bis-Silylated Endofullerene Sc₃N@C₈₀," *J. Am. Chem. Soc.* **128**, 9919–9925 (2006).
- M. SAITO, M. SHIMOSAWA, M. YOSHIOKA, K. ISHIMURA and S. NAGASE, "Synthesis and Characterization of Dimetallostannafluorenes," *Chem. Lett.* 940–941 (2006).
- S. -I. IWAMATSU, C. M. STANISKY, R. J. CROSS, M. SAUNDERS, N. MIZOROGI, S. NAGASE and S. MURATA, "Carbon Monoxide inside an Open-Cage Fullerene," *Angew. Chem., Int. Ed.* **45**, 5337–5340 (2006).
- A. KONDORSKIY, G. V. MIL'NIKOV and H. NAKAMURA, "Semiclassical Guided Optimal Control of Molecular Dynamics," *Phys. Rev. A* **72**, 041401 (2005).
- G. V. MIL'NIKOV, S. ZOU and H. NAKAMURA, "Incorporation of Nonadiabatic Transition into Wave-Packet Dynamics," *J. Chem. Phys.* **123**, 141101 (2005).
- H. YAMADA, K. YOKOYAMA, Y. TERANISHI, A. SUGITA, T. SHIRAI, M. AOYAMA, Y. AKAHANE, N. INOUE, H. UEDA, K. YAMAKAWA, A. YOKOYAMA, M. KAWASAKI and H. NAKAMURA, "Selective Transition to the Closely-Lying States Cs (7D_{3/2}) and Cs (7D_{5/2}) by Femtosecond Laser Pulses," *Phys. Rev. A* **72**, 063404 (5 pages) (2005).
- H. TAMURA, S. NANBU, T. ISHIDA and H. NAKAMURA, "Ab Initio Nonadiabatic Quantum Dynamics of Cyclohexadiene/Hexatriene Ultrafast Photoisomerization," *J. Chem. Phys.* **124**, 084313 (13 pages) (2006).
- P. OLOYEDE, G. V. MIL'NIKOV and H. NAKAMURA, "Generalized Trajectory Surface Hopping (TSH) Method Based on the Zhu-Nakamura Theory," *J. Chem. Phys.* **124**, 144110 (11 pages) (2006).
- G. V. MIL'NIKOV, T. ISHIDA and H. NAKAMURA, "Tunneling Splitting of Energy Levels and Rotational Constants in the Vinyl Radical C₂H₃," *J. Phys. Chem. A* **110**, 5430–5435 (2006).
- S. NANBU, T. ISHIDA and H. NAKAMURA, "Atomic Hydrogen Transmission through Five-Membered Carbon Ring by the Mechanism of Nonadiabatic Tunneling," *Chem. Phys.* **324**, 721–732 (2006).
- H. TAMURA, S. NANBU, T. ISHIDA and H. NAKAMURA, "Laser Control of Reactions of Photo-Switching Functional Molecules," *J. Chem. Phys.* **125**, 034307 (10 pages) (2006).

Y. ZHAO, W. LIANG and H. NAKAMURA, "Semiclassical Treatment of Thermally Activated Electron Transfer in the Intermediate to Strong Electronic Coupling Regime under the Fast Dielectric Relaxation," *J. Phys. Chem. A* **110**, 8204–8212 (2006).

Y. ZHAO and H. NAKAMURA, "Electron Transfer Rate Uniformly Valid from Nonadiabatic to Adiabatic Regime Based on the Zhu-Nakamura Theory," *J. Theor. Comput. Chem.* **5**, 299–306 (2006).

K. SHIRATORI, K. NOBUSADA and K. YABANA, "Multiple Ionization of a Silver Diatomic Molecule in an Intense Laser Field," *Chem. Phys. Lett.* **404**, 365–369 (2005).

Y. NEGISHI, K. NOBUSADA and T. TSUKUDA, "Glutathione-Protected Gold Clusters Revisited: Bridging the Gap between Gold(I)-Thiolate Complexes and Thiolate-Protected Gold Nanocrystals," *J. Am. Chem. Soc.* **127**, 5261–5270 (2005).

T. IMAI, R. HIRAOKA, A. KOVALENKO and F. HIRATA, "Water Molecules in a Protein Cavity Detected by a Statistical-Mechanical Theory," *J. Am. Chem. Soc.* **127**, 15334–15335 (2005).

I. OMEL'YAN, F. HIRATA and A. KOVALENKO, "Criticality of a Liquid-Vapor Interface from an Inhomogeneous Integral Equation Theory," *Phys. Chem. Chem. Phys.* **7**, 4132–4137 (2005).

R. ISHIZUKA and F. HIRATA, "Conformational Equilibria in Liquids Consisting of Small Chain Molecules," *Chem. Phys. Lett.* **420**, 135–139 (2006).

N. YOSHIDA and F. HIRATA, "A New Method to Determine Electrostatic Potential Around a Macromolecule in Solution from Molecular Wave Function," *J. Comput. Chem.* **27**, 453–462 (2006).

N. YOSHIDA, R. ISHIZUKA, H. SATO and F. HIRATA, "Ab Initio Theoretical Study of Temperature and Density Dependence of Molecular and Thermodynamic Properties of Water in the Entire Fluid Region: Autoionization Processes," *J. Phys. Chem.* **110**, 8451–8458 (2006).

A. E. KOBRYN, T. YAMAGUCHI and F. HIRATA, "Study of Anomalous Mobility of Polar Molecular Solutions by Means of the Site-Site Memory Equation Formalism," *J. Mol. Liq.* **125**, 14–21 (2006).

T. IMAI, H. ISOGAI, T. SETO, A. KOVALENKO and F. HIRATA, "Theoretical Study of Volume Changes Accompanying Xenon-Lysozyme Binding: Implication for Molecular Mechanism of Pressure Reversal of Anesthesia," *J. Phys. Chem. B*, **110**, 12149–12154 (2006).

T. IMAI, Y. HARANO, M. KINOSHITA, A. KOVALENKO and F. HIRATA, "A Theoretical Analysis on Hydration Thermodynamics of Proteins," *J. Chem. Phys.* **125**, 024911 (7 pages) (2006).

J. Y. LEE, N. YOSHIDA and F. HIRATA, "Conformational Equilibrium of 1,2-Dichloroethane in Water: Comparison of PCM and RISM-SCF Methods," *J. Phys. Chem. B* **110**, 16018–16025 (2006).

K. YONEMITSU, "Mechanism of Ambipolar Field-Effect Carrier Injections in One-Dimensional Mott Insulators," *J. Phys. Soc. Jpn.* **74**, 2544–2553 (2005).

K. YONEMITSU, "Photoinduced Dynamics and Nonequilibrium Characteristics in Quasi-One-Dimensional Electron Systems: Mott Insulators vs. Band Insulators," *J. Phys.: Conf. Series* **21**, 30–37 (2005).

N. MAESHIMA and K. YONEMITSU, "Optical Responses of Photoexcited States in the One-Dimensional Ionic Hubbard Model," *J. Phys.: Conf. Series* **21**, 183–188 (2005).

Y. YAMASHITA and K. YONEMITSU, "Quantum Ising Model Coupled with Conducting Electrons," *J. Phys.: Conf. Series* **21**, 232–236 (2005).

N. MAESHIMA and K. YONEMITSU, "Photoinduced Metallic Properties of One-Dimensional Strongly Correlated Electron Systems," *J. Phys. Soc. Jpn.* **74**, 2671–2674 (2005).

J. KISHINE, T. OHARA, T. LUTY and K. YONEMITSU, "Inter-Chain Coulomb-Lattice Relaxation and Multicriticality in Charge Transfer Organic Complexes," *Synth. Met.* **154**, 257–260 (2005).

K. YONEMITSU and K. NASU, "Theory of Photoinduced Phase Transitions," *J. Phys. Soc. Jpn.* **75**, 011008 (8 pages) (2006).

B. HÜLSEN, F. X. BRONOLD, H. FEHSKE and K. YONEMITSU, "Phase Diagram of the Excitonic Insulator," *Physica B* **378-380**, 267–268 (2006).

K. YONEMITSU, "Interchain Coupling Effects on Photoinduced Phase Transitions between Neutral and Ionic Phases in an Extended Hubbard Model with Alternating Potentials and an Electron-Lattice Coupling," *Phys. Rev. B* **73**, 155120 (7 pages) (2006).

N. MAESHIMA, K. OKUNISHI, K. OKAMOTO, T. SAKAI and K. YONEMITSU, "Possibility of Field-Induced Incommensurate Order in a Quasi-One-Dimensional Frustrated Spin System," *J. Phys.: Condens. Matter* **18**, 4819–4826 (2006).

K. FUCHIZAKI, "Murnaghan's Equation of State Revisited," *J. Phys. Soc. Jpn.* **75**, 034601 (4 pages) (2006).

C. -B. LI, Y. MATSUNAGA, M. TODA and T. KOMATSUZAKI, "Phase Space Reaction Network on a Multisaddle Energy Landscape: HCN Isomerization," *J. Chem. Phys.* **123**, 184301 (13 pages) (2005).

C. -B. LI, A. SHOJIGUCHI, M. TODA and T. KOMATSUZAKI, "Dynamical Hierarchy in Transition States of Reactions," *Few-Body Systems* **38**, 173–179 (2006).

C. -B. LI, A. SHOJIGUCHI, M. TODA and T. KOMATSUZAKI, "Definability of No-Return Transition States in High Energy Regime above Threshold," *Phys. Rev. Lett.* **97**, 028302 (4 pages) (2006).

A. SHOJIGUCHI, A. BABA, C. -B. LI, T. KOMATSUZAKI and M. TODA, “Wavelet Analysis and Arnold Web Picture for Detecting Energy Transfer in Hamiltonian Dynamical System,” *Laser Phys.* **16**, 1097–1106 (2006).

H. SATO and S. SAKAKI, “Analysis on Solvated Molecule with a New Energy Partitioning Scheme for Intra- and Intermolecular Interactions,” *J. Phys. Chem. B* **110**, 12714–12720 (2006).

A. IKEDA, Y. NAKAO, H. SATO and S. SAKAKI, “A New Analysis of Molecular Orbital Wavefunctions Based on Resonance Theory,” *J. Phys. Chem. A* **110**, 9028–9030 (2006).

A. IKEDA, D. YOKOGAWA, H. SATO and S. SAKAKI, “Solvation Effect on Resonance Structure. Extracting Valence Bond-like Character from Molecular Orbitals,” *Chem. Phys. Lett.* **424**, 449–452 (2006).

D. YOKOGAWA, H. SATO and S. SAKAKI, “A New Method to Reconstruct Three-dimensional Spatial Distribution Function from Radial Distribution Function in Solvation Structure,” *J. Chem. Phys.* **123**, 211102–211107 (2005).

N. YOSHIDA, R. ISHIZUKA, H. SATO and F. HIRATA, “Ab Initio Theoretical Study of Temperature and Density Dependence of Molecular and Thermodynamic Properties of Water in the Entire Fluid Region: Autoionization Processes,” *J. Phys. Chem. B* **110**, 8451–8458 (2006).

Department of Molecular Structure

T. NAGAHARA, K. IMURA, H. OKAMOTO, A. OGURO and H. IMAHORI, “Morphological and Spectroscopic Properties of Thin Films of Self-Assembling Amphiphilic Porphyrins on a Hydrophilic Surface as Revealed by Scanning Near-Field Optical Microscopy,” *J. Phys. Chem. B* **109**, 19839–19844 (2005).

K. IMURA, H. OKAMOTO, M. K. HOSSAIN and M. KITAJIMA, “Near-Field Imaging of Surface Enhanced Raman Active Sites in Aggregated Gold Nanoparticles,” *Chem. Lett.* **35**, 78–79 (2006).

K. IMURA, T. NAGAHARA and H. OKAMOTO, “Photoluminescence from Gold Nanoparticles Induced by Near-Field Two-Photon Absorption,” *Appl. Phys. Lett.* **88**, 023104 (3 pages) (2006).

K. IMURA and H. OKAMOTO, “Reciprocity in Scanning Near-Field Optical Microscopy: Illumination and Collection Modes of Transmission Measurements,” *Opt. Lett.* **31**, 1474–1476 (2006).

K. INOUE, N. BADEN and M. TERAZIMA, “Diffusion Coefficient and the Secondary Structure of Poly-L-Glutamic Acid in Aqueous Solution,” *J. Phys. Chem. B* **109**, 22623–22628 (2005).

J. S. KHAN, Y. IMAMOTO, M. KATAOKA, F. TOKUNAGA and M. TERAZIMA, “Time-Resolved Thermodynamics: Heat Capacity Change of Transient Species during Photo-Reaction of PYP,” *J. Am. Chem. Soc.* **128**, 1002–1008 (2006).

J. S. KHAN, Y. MAMOTO, M. HARIGAI, M. KATAOKA and M. TERAZIMA, “Conformational Changes of PYP Monitored by Diffusion Coefficient: Effect of N-Terminal α -Helices,” *Biophys. J.* **90**, 3686–3693 (2006).

T. NAKAGAWA, H. WATANABE and T. YOKOYAMA, “Effect of Adsorbate Carbon on Spin Reorientation Transitions in Cu-Capped Ultrathin Ni Films on Cu(001),” *Surf. Sci.* **599**, 262–269 (2005).

D. MATSUMURA, K. AMEMIYA, S. KITAGAWA, T. SHIMADA, H. ABE, T. OHTA, H. WATANABE and T. YOKOYAMA, “Surface Structure of CO on Co/Pd(111) Magnetic Thin Films and Its Effect on the Spin Reorientation Transition of the Film,” *Phys. Rev. B* **73**, 174423 (9 pages) (2006).

H. ABE, K. AMEMIYA, D. MATSUMURA, S. KITAGAWA, H. WATANABE, T. YOKOYAMA and T. OHTA, “Spin Reorientation Transitions of Fe/Ni/Cu(001) Studied by Using the Depth-Resolved X-Ray Magnetic Circular Dichroism Technique,” *J. Magn. Magn. Mater.* **302**, 86–95 (2006).

T. NAKAGAWA and T. YOKOYAMA, “Magnetic Circular Dichroism near the Fermi Level,” *Phys. Rev. Lett.* **96**, 237402 (4 pages) (2006).

A. KANNO, T. OZAWA and Y. UMEZAWA, “Intein-Mediated Reporter Gene Assay for Detecting Protein-Protein Interactions in Living Mammalian Cells,” *Anal. Chem.* **78**, 556–560 (2006).

S. B. KIM, R. TAKAO, T. OZAWA and Y. UMEZAWA, “Quantitative Determination of Protein Nuclear Transport Induced by Phosphorylation or by Proteolysis,” *Anal. Chem.* **77**, 6928–6934 (2005).

S. B. KIM, T. OZAWA and Y. UMEZAWA, “A Genetically Encoded Indicator for Assaying Bioactive Chemicals that Induce Nuclear Transport of Glucocorticoid Receptor,” *Anal. Biochem.* **347**, 213–220 (2005).

Department of Electronic Structure

J. NISHIJO, K. KOSUGI, H. SAWA, C. OKABE, K. JUDAI and N. NISHI, “Water-Induced Ferromagnetism in Cobalt Acetylde CoC_2 Nanoparticles,” *Polyhedron* **24**, 2148–2152 (2005).

K. JUDAI, J. NISHIJO, C. OKABE, O. OHISHI, H. SAWA and N. NISHI, “Carbon-Skinned Metallic Wires and Magnetic Nanocrystals Prepared from Metal Acetylides,” *Synth. Met.* **155**, 352–356 (2005).

K. WATANABE, A. KOKALI, H. HORINO, I. I. RZEZNICKA, K. TAKAHASHI, N. NISHI and T. MATSUSHIMA, “Scanning-Tunneling Microscopy, Near-Edge X-Ray-Absorption Fine Structure, and Density-Functional Theory Studies of N_2O Orientation on Pd(110),” *Jpn. J. Appl. Phys.* **45**, 2290–2294 (2006).

K. HINO, H. NAKANO, N. ITO, M. MATSUSHITA, H. TAKAGI and N. NISHI, "Preparation and Characterization of Gold Nanoparticles with Reactive Thiocarbonyls: A Proposal for Active Size Control of Nanoparticles," *Trans. Mater. Res. Soc. Jpn.* **31**, 525–528 (2006).

J. NISHIJO and N. NISHI, "Synthesis, Structure and Magnetic Properties of a New Low-Spin Iron(III) Complex $[\text{FeL}_3]$ $\{\text{L} = [\text{HNC}(\text{CH}_3)_2\text{C}(\text{CN})\}$," *Eur. J. Inorg. Chem.* 3022–3027 (2006).

H. KATSUKI, H. CHIBA, B. GIRARD, C. MEIER and K. OHMORI, "Visualizing Picometric Quantum Ripples of Ultrafast Wave-Packet Interference," *Science* **311**, 1589–1592 (2006).

K. OHMORI, H. KATSUKI, H. CHIBA, M. HONDA, Y. HAGIHARA, K. FUJIWARA, Y. SATO and K. UEDA, "Real-Time Observation of Phase-Controlled Molecular Wave-Packet Interference," *Phys. Rev. Lett.* **96**, 093002 (4 pages) (2006).

Y. TERANISHI, Y. OHTSUKI, K. HOSAKA, H. CHIBA, H. KATSUKI and K. OHMORI, "Implementation of Quantum Gate Operations in Molecules with Weak Laser Fields," *J. Chem. Phys.* **124**, 114110 (9 pages) (2006).

Y. MATSUSHITA, S. KUMADA, K. WAKABAYASHI, K. SAKEDA and T. ICHIMURA, "Photocatalytic Reduction in Microreactors," *Chem. Lett.* **35**, 410–411 (2006).

R. LU, M. HASE, M. KITAJIMA, S. NAKASHIMA and S. SUGAI, "Femtosecond Pump-Probe Study of Coherent Soft Phonon in $\text{Pb}_{1-x}\text{Ge}_x\text{Te}$ Ferroelectrics," *J. Lumin.* **119-120**, 378–382 (2006).

D. YAMAGUCHI, T. MATSUMOTO, K. WATANABE, N. TAKAGI and Y. MATSUMOTO, "Photochemistry of Cyclohexane on $\text{Cu}(111)$," *Phys. Chem. Chem. Phys.* **8**, 179–185 (2006).

Y. MATSUMOTO, K. WATANABE and N. TAKAGI, "Excitation Mechanism and Ultrafast Vibrational Wavepacket Dynamics of Alkali-Metal Atoms on $\text{Pt}(111)$," *Surf. Sci.* **593**, 110–115 (2005).

D. INO, K. WATANABE, N. TAKAGI and Y. MATSUMOTO, "Electron Transfer Dynamics from Organic Adsorbate to a Semiconductor Surface: Zinc-Phthalocyanine on $\text{TiO}_2(110)$," *J. Phys. Chem. B* **109**, 18018–18024 (2005).

M. BABA, K. MORI, M. YAMAWAKI, K. AKITA, M. ITO, S. KASAHARA and T. YAMANAKA, "Vibronic Structure in the S_1-S_0 Transition of Jet-Cooled Dibenzofuran," *J. Phys. Chem. A* **110**, 10000–10005 (2006).

Department of Molecular Assemblies

K. SUZUKI, K. YAMAMOTO, K. YAKUSHI and A. KAWAMOTO, "Infrared and Raman Studies of θ -(BEDT-TTF) $_2\text{CsZn}(\text{SCN})_4$: Comparison with the Rapidly Cooled State of θ -(BEDT-TTF) $_2\text{RbZn}(\text{SCN})_4$," *J. Phys. Soc. Jpn.* **74**, 2631–2639 (2005).

T. KUBO, A. SHIMIZU, M. SAKAMOTO, M. URUICHI, K. YAKUSHI, M. NAKANO, D. HIOMI, K. SATO TAKUI, Y. MORITA and K. NAKASUJI, "Synthesis, Intermolecular Interaction, and Semiconductive Behavior of a Delocalized Singlet Biradical Hydrocarbon," *Angew. Chem., Int. Ed.* **44**, 6564–6568 (2005).

A. KOWALSKA, R. WOJCIECHOWSKI, J. ULANSKI, M. MAS-TORRENT, E. LAUKHINA, C. ROVIRA and K. YAKUSHI, "Evaluation of Charge Transfer Degree in the Bis(ethylenethio)tetrathiafulvalene Salts by Raman Spectroscopy," *Synth. Met.* **156**, 75–80 (2006).

T. YAMAMOTO, M. URUICHI and K. YAKUSHI, "Charge Ordering State of β'' -(ET) $_3(\text{HSO}_4)$ and β'' -(ET) $_3(\text{ClO}_4)_2$ by Temperature-Dependent Infrared and Raman Spectroscopy," *Phys. Rev. B* **73**, 125116 (12 pages) (2006).

T. TAKAHASHI, K. YAKUSHI and Y. NOGAMI, "Charge Ordering in Organic Conductors," *J. Phys. Soc. Jpn.* **75**, 051008 (17 pages) (2006).

M. URUICHI, K. YAKUSHI, H. M. YAMAMOTO and R. KATO, "Infrared and Raman Study of the Charge-Ordering Phase Transition at ~170 K in a Quarter-Filled Narrow-Band System, β'' -(ET)(TCNQ)," *J. Phys. Soc. Jpn.* **75**, 074720 (10 pages) (2006).

K. MAEDA, T. HARA and T. NAKAMURA, "ESR Study on Low-Dimensional Antiferromagnet α -(BEDT-TTF) $_2\text{PF}_6$ and ζ -(BEDT-TTF) $_2\text{PF}_6(\text{THF})$," *Synth. Met.* **152**, 453–456 (2005).

K. NOMURA, K. ISHIMURA, N. MATSUNAGA, T. NAKAMURA, T. TAKAHASHI and G. SAITO, "Non-Linear Transport in the Incommensurate SDW Phase of (TMTTF) $_2\text{Br}$ under Pressure," *Synth. Met.* **153**, 433–436 (2005).

S. FUJIYAMA, M. TAKIGAWA, J. KIKUCHI, K. KODAMA, T. NAKAMURA, E. FUJIWARA, H. FUJIWARA, H. CHUI and H. KOBAYASHI, "Nuclear Spin-Lattice Relaxation in κ -(BETS) $_2\text{FeBr}_4$," *Synth. Met.* **154**, 253–256 (2005).

F. NAD, P. MONCEAU, T. NAKAMURA and K. FURUKAWA, "The Effect of Deuteration on the Transition into a Charge Ordered State of (TMTTF) $_2X$ Salts," *J. Phys.: Condens. Matter* **17**, L399–L406 (2005).

K. FURUKAWA, T. HARA and T. NAKAMURA, "Deuteration Effect and Possible Origin of the Charge-Ordering Transition of (TMTTF) $_2X$," *J. Phys. Soc. Jpn.* **74**, 3288–3294 (2005).

- F. NAD, P. MONCEAU, M. NAGASAWA and T. NAKAMURA, “ $4k_F$ CDW Induced by Long Range Coulomb Interactions,” *J. Phys. IV France* **131**, 15–19 (2005).
- S. FUJIYAMA and T. NAKAMURA, “ ^{13}C NMR Spectral Study of Q1D Organic Conductor $(\text{TMTTF})_2\text{AsF}_6$,” *J. Phys. IV France* **131**, 33–37 (2005).
- Y. NOGAMI, T. ITO, K. YAMAMOTO, N. IRIE, S. HORITA, T. KAMBE, N. NAGAO, K. OSHIMA, N. IKEDA and T. NAKAMURA, “X-Ray Structural Study of Charge and Anion Orderings of TMTTF Salts,” *J. Phys. IV France* **131**, 39–42 (2005).
- K. NOMURA, K. ISHIMURA, K. FUJIMOTO, N. MATSUNAGA, T. NAKAMURA, T. TAKAHASHI and G. SAITO, “Depinning of the Spin-Density Wave in $(\text{TMTTF})_2\text{Br}$ under Pressure,” *J. Phys. IV France* **131**, 111–114 (2005).
- T. NAKAMURA, K. FURUKAWA and T. HARA, “ ^{13}C NMR Analyses of Successive Charge-Ordering in $(\text{TMTTF})_2\text{ReO}_4$,” *J. Phys. Soc. Jpn.* **75**, 013707 (4 pages) (2006).
- S. FUJIYAMA and T. NAKAMURA, “Redistribution of Electronic Charges in the Spin-Peierls State in $(\text{TMTTF})_2\text{AsF}_6$ Observed by ^{13}C NMR,” *J. Phys. Soc. Jpn.* **75**, 014705 (7 pages) (2006).
- Y. YAMAMOTO, T. FUKUSHIMA, W. JIN, A. KOSAKA, T. HARA, T. NAKAMURA, A. SAEKI, S. SEKI, S. TAGAWA and T. AIDA, “A Glass Hook Allows Fishing of Hexa-*peri*-hexabenzocoronene Graphitic Nanotubes: Fabrication of a Macroscopic Fiber with Anisotropic Electrical Conduction,” *Adv. Mater.* **18**, 1297–1300 (2006).
- H. MATSUOKA, K. FURUKAWA, T. KATO, H. MINO, J. R. SHEN and A. KAWAMORI, “*g*-Anisotropy of the S_2 -State Manganese Cluster in Single Crystals of Cyanobacterial Photosystem II Studied by W-Band Electron Paramagnetic Resonance Spectroscopy,” *J. Phys. Chem. B* **110**, 13242–13247 (2006).
- H. B. CUI, K. TAKAHASHI, Y. KANO, H. KOBAYASHI, Z. M. WANG and A. KOBAYASHI, “Dielectric Properties of Porous Molecular Crystals that Contain Polar Molecules,” *Angew. Chem., Int. Ed.* **44**, 6508–6512 (2005).
- E. FUJIWARA, H. FUJIWARA, B. Z. NARYMBETOV, H. KOBAYASHI, M. NAKATA, H. TORII, A. KOBAYASHI, K. TAKIMIYA, T. OTSUBO and F. OGURA, “Molecular Conductors Based on Peri-Ditellurium-Bridged Donors, 2,3-DMTTeA and TMTTeN,” *Eur. J. Inorg. Chem.* 3435–3449 (2005).
- S. FUJIYAMA, M. TAKIGAWA, J. KIKUCHI, K. KODAMA, T. NAKAMURA, E. FUJIWARA, H. FUJIWARA, H. B. CUI and H. KOBAYASHI, “Nuclear Spin-Lattice Relaxation in κ -(BETS) $_2$ FeBr $_4$,” *Synth. Met.* **154**, 253–256 (2005).
- A. KOBAYASHI, B. ZHOU and H. KOBAYASHI, “Development of Metallic Crystals Composed of Single-Component Molecules,” *J. Mater. Chem.* **15**, 3449–3451 (2005).
- T. KONOIKE, S. UJI, T. TERASHIMA, M. NISHIMURA, S. YASUZUKA, K. ENOMOTO, H. FUJIWARA, E. FUJIWARA, B. ZHANG and H. KOBAYASHI, “Fermi Surface Reconstruction in the Magnetic-Field-Induced Superconductor κ -(BETS) $_2$ FeBr $_4$,” *Phys. Rev. B* **72**, 184505 (5 pages) (2005).
- Y. OSHIMA, E. JOBILIONG, J. S. BROOKS, S. A. ZVYAGIN, J. KRZYSTEK, H. TANAKA, A. KOBAYASHI, H. B. CUI and H. KOBAYASHI, “EMR Measurements of Field-Induced Superconductor λ -(BETS) $_2$ Fe $_x$ Ga $_{1-x}$ Cl $_4$,” *Synth. Met.* **153**, 365–368 (2005).
- S. OTSUBO, K. TAKAHASHI, H. B. CUI, Y. OKANO and H. KOBAYASHI, “Organic Metals Based on an Asymmetric π Donor PEDT-TSF, $(\text{PEDT-TSF})_2\text{FeX}_4$ (PEDT-TSF = pyrazinoethylenedithiotetraselenafulvalene; X = Cl, Br),” *Chem. Lett.* **34**, 1598–1599 (2005).
- K. TAKAHASHI, H. B. CUI, H. KOBAYASHI, Y. EINAGA and O. SATO, “The Light-Induced Excited Spin State Trapping Effect on Ni(dmit) $_2$ Salt with an Fe(III) Spin-Crossover Cation: $[\text{Fe}(\text{qsal})_2][\text{Ni}(\text{dmit})_2] \cdot 2\text{CH}_3\text{CN}$,” *Chem. Lett.* **34**, 1240–1241 (2005).
- M. TOKUMOTO, H. TANAKA, T. OTSUKA, H. KOBAYASHI and A. KOBAYASHI, “Observation of Spin-Flop Transition in Antiferromagnetic Organic Molecular Conductors Using AFM Micro-Cantilever,” *Polyhedron* **24**, 2793–2795 (2005).
- S. UJI, S. YASUZUKA, M. TOKUMOTO, H. TANAKA, A. KOBAYASHI, B. ZHANG, H. KOBAYASHI, E. S. CHOI, D. GRAF and J. S. BROOKS, “Magnetic-Field-Induced Superconductivity and Phase Diagrams of λ -(BETS) $_2$ FeCl $_{4-x}$ Br $_x$,” *Phys. Rev. B* **72**, 184505 (5 pages) (2005).
- K. YAMAMOTO, E. FUJIWARA, A. KOBAYASHI, Y. FUJISHIRO, E. NISHIBORI, M. SAKATA, M. TAKATA, H. TANAKA, Y. OKANO and H. KOBAYASHI, “Single-Component Molecular Conductor $[\text{Zn}(\text{tmtd})_2]$ and Related Zn Complexes,” *Chem. Lett.* **34**, 1090–1091 (2005).
- S. FUJIYAMA, M. TAKIGAWA, J. KIKUCHI, H. B. CUI, H. FUJIWARA and H. KOBAYASHI, “Compensation of Effective Field in the Field-Induced Superconductor κ -(BETS) $_2$ FeBr $_4$ Observed by ^{77}Se NMR,” *Phys. Rev. Lett.* **96**, 217001 (4 pages) (2006).
- Y. J. JO, H. KANG, W. KANG, S. UJI, T. TERASHIMA, T. TANAKA, M. TOKUMOTO, A. KOBAYASHI and H. KOBAYASHI, “Field- and Angular-Dependent Resistance of λ -(BETS) $_2$ FeCl $_4$ under Pressure,” *Phys. Rev. B* **73**, 214532 (2006).
- A. KOBAYASHI, Y. OKANO and H. KOBAYASHI, “Molecular Design and Physical Properties of Single-Component Molecular Metals,” *J. Phys. Soc. Jpn.* **75**, 051002 (12 pages) (2006).
- T. KUSAMOTO, E. FUJIWARA, A. KOBAYASHI, H. B. CUI, T. OTSUKA, Y. OKANO, H. FUJIWARA and H. KOBAYASHI, “BDT-TTP-Based π Conductors Containing Divalent Magnetic and Non-Magnetic Inorganic Anions, $[\text{M}^{\text{II}}\text{Cl}_4]^{2-}$ (M = Co, Mn, Zn),” *Bull. Chem. Soc. Jpn.* **79**, 527–536 (2006).

S. OTSUBO, H. B. CUI, H. J. LEE, H. FUJIWARA, K. TAKAHASHI, Y. OKANO and H. KOBAYASHI, "A Magnetic Organic Conductor Based on a π Donor with a Stable Radical and a Magnetic Anion—A Step to Magnetic Organic Metals with Two Kinds of Localized Spin Systems," *Chem. Lett.* **35**, 130–131 (2006).

K. TAKAHASHI, H. B. CUI, Y. OKANO, H. KOBAYASHI, Y. EINAGA and O. SATO, "Electrical Conductivity Modulation Coupled to a High-Spin–Low-Spin Conversion in the Molecular System $[\text{Fe}^{\text{III}}(\text{qsal})_2][\text{Ni}(\text{dmit})_2]_3 \cdot \text{CH}_3\text{CN} \cdot \text{H}_2\text{O}$," *Inorg. Chem.* **45**, 5739–5741 (2006).

B. ZHANG, Z. M. WANG, Y. ZHANG, K. TAKAHASHI, Y. OKANO, H. B. CUI, H. KOBAYASHI, K. INOUE, M. KURMOO, F. L. PRATT and D. B. ZHU, "Hybrid Organic-Inorganic Conductor with a Magnetic Chain Anion: κ -BETS₂ $[\text{Fe}^{\text{III}}(\text{C}_2\text{O}_4)\text{Cl}_2]$ [BETS = bis(ethylenedithio)tetraselenafulvalene]," *Inorg. Chem.* **45**, 3275–3280 (2006).

B. ZHOU, M. SHIMAMURA, E. FUJIWARA, A. KOBAYASHI, T. HIGASHI, E. NISHIBORI, M. SAKATA, H. B. CUI, K. TAKAHASHI and H. KOBAYASHI, "Magnetic Transitions of Single-Component Molecular Metal $[\text{Au}(\text{tmdt})_2]$ and Its Alloy Systems," *J. Am. Chem. Soc.* **128**, 3872–3873 (2006).

N. MATSUSHITA, F. FUKUHARA and N. KOJIMA, "A Three-Dimensional Bromo-Bridged Mixed-Valence Gold(I,III) Compound, $\text{Cs}_2\text{Au}^{\text{I}}\text{Au}^{\text{III}}\text{Br}_6$," *Acta Crystallogr., Sect. E: Struct. Rep. Online* **61**, i123–i125 (2005).

N. MATSUSHITA, A. TANAKA and N. KOJIMA, "A Three-Dimensional Iodo-Bridged Mixed-Valence Gold(I,III) Compound, $\text{Rb}_2[\text{Au}^{\text{I}}\text{I}_2][\text{Au}^{\text{III}}\text{I}_4]$," *Acta Crystallogr., Sect. E: Struct. Rep. Online* **61**, i201–i203 (2005).

T. KAJIWARA, M. NAKANO, Y. KANEKO, S. TAKAISHI, T. ITO, M. YAMASHITA, A. IGASHIRAKAMIYAMA, H. NOJIRI, Y. ONO and N. KOJIMA, "A Single-Chain Magnet Formed by a Twisted Arrangement of Ions with Easy-Plane Magnetic Anisotropy," *J. Am. Chem. Soc.* **127**, 10150–10151 (2005).

J. Y. SON, T. MIZOKAWA, J. W. QUILTY, K. TAKUBO, K. IKEDA and N. KOJIMA, "Photoinduced Valence Transition in Gold Complexes $\text{Cs}_2\text{Au}_2\text{X}_6$ (X = Cl and Br) Probed by X-Ray Photoemission Spectroscopy," *Phys. Rev. B* **72**, 235105 (4 pages) (2005).

Y. MORITOMO, M. KAMIYA, A. NAKAMURA, A. NAKAMOTO and N. KOJIMA, "Cooperative Formation of High-Spin Species in a Photoexcited Spin-Crossover Complex," *Phys. Rev. B* **73**, 012103 (4 pages) (2006).

M. ITOI, Y. ONO, N. KOJIMA, K. KATO, K. OSAKA and M. TAKATA, "Charge Transfer Phase Transition and Ferromagnetism of Iron Mixed-Valence Complexes, $(n\text{-C}_n\text{H}_{2n+1})_4\text{N}[\text{Fe}^{\text{II}}\text{Fe}^{\text{III}}(\text{dto})_3]$ ($n = 3\text{--}6$; $\text{dto} = \text{C}_2\text{O}_2\text{S}_2$)," *Eur. J. Inorg. Chem.* 1198–1207 (2006).

M. FERBINTEANU, T. KAJIWARA, K. Y. CHOI, H. NOJIRI, A. NAKAMOTO, N. KOJIMA, F. CIMPOES, Y. FUJIMURA, S. TAKAISHI and M. YAMASHITA, "A Binuclear Fe(III)Dy(III) Single Molecular Magnet. Quantum Effects and Models," *J. Am. Chem. Soc.* **128**, 9008–9009 (2006).

Department of Applied Molecular Science

D. -L. JIANG, "Design of Drug Delivery Carriers Based on Dendritic Macromolecules," *Bionics* (in Japanese) **8**, 50–55 (2006).

T. MATSUI, S. -H. KIM, H. JIN, B. M. HOFFMAN and M. IKEDA-SAITO, "Compound I of Heme Oxygenase Can Not Hydroxylate Its Heme *meso*-Carbon," *J. Am. Chem. Soc.* **128**, 1090–1091 (2006).

K. SODA, K. SHIMBA, S. YAGI, M. KATO, T. TAKEUCHI, U. MIZUTANI, T. ZHANG, M. HASEGAWA, A. INOUE, T. ITO and S. KIMURA, "Electronic Structure of Bulk Metallic Glass $\text{Zr}_{55}\text{Al}_{10}\text{Cu}_{30}\text{Ni}_5$," *J. Electron. Spectrosc. Relat. Phenom.* **144-147**, 585–587 (2005).

T. TAKEUCHI, S. NAKANO, M. HASEGAWA, K. SODA, H. SATO, U. MIZUTANI, K. ITOH and T. FUKUNAGA, "Free-Energy Estimation of the Zr-Ni-Al Bulk Metallic Glass from the Local Atomic Arrangements of the Relevant Crystals," *Mater. Trans.* **46**, 2791–2798 (2005).

S. NAKANO, T. TAKEUCHI, K. SODA, M. HASEGAWA, U. MIZUTANI, H. SATO, K. ITOH and T. FUKUNAGA, "Investigation of Stability of the Zr-Ni-Al Bulk Amorphous Phase from Local Atomic Arrangements of the Relevant Crystals," *J. Jpn. Soc. Powder Powder Metallurgy* **53**, 100–106 (2006).

T. SUZUKI, H. MIYAZAKI, K. SODA, T. TAKEUCHI, M. HASEGAWA, H. SATO and U. MIZUTANI, "Electronic Structure of Zr-TM-Al (TM = Ni, Cu) Bulk Metallic Glasses," *J. Jpn. Soc. Powder Powder Metallurgy* **53**, 107–110 (2006).

H. MIYAZAKI, K. SODA, S. YAGI, M. KATO, T. TAKEUCHI, U. MIZUTANI and Y. NISHIO, "Surface and Bulk Electronic Structures of Heusler-type Fe_2VAl ," *J. Vac. Sci. Technol., A* **24**, 1464–1467 (2006).

A. MATSUDA, K. KONDO and K. NAKAMURA, "Nanosecond Rapid Freezing of Liquid Benzene under Shock Compression Studied by Time-Resolved Coherent Anti-Stokes Raman Spectroscopy," *J. Chem. Phys.* **124**, 054501 (4 pages) (2006).

S. OGUCHI, A. MATSUDA, K. KONDO and K. NAKAMURA, "Time-Resolved Coherent Anti-Stokes Raman Scattering of Cyclohexane under Shock Compression," *Jpn. J. Appl. Phys.* **45**, 5817–5820 (2006).

H. MAEDA, M. HASEGAWA, T. HASHIMOTO, T. KAKIMOTO, S. NISHIO and T. NAKANISHI, "Nanoscale Spherical Architectures Fabricated by Metal Coordination of Multiple Dipyrin Moieties," *J. Am. Chem. Soc.* **128**, 10024–10025 (2006).

Department of Vacuum UV Photoscience

T. HATSUI, H. SETOYAMA, N. KOSUGI, B. WASSERMANN, I. L. BRADEANU and E. RÜHL, "Photoionization of Small Krypton Clusters in the Kr 3d Regime: Evidence for Site-Specific Photoemission," *J. Chem. Phys.* **123**, 154304 (6 pages) (2005).

N. KOSUGI, "Orbital Picture in Molecular Inner-Shell Excited States of Rydberg-Valence Mixed Character," *Brazilian J. Phys.* **35**, 957–960 (2005).

M. HIYAMA and N. KOSUGI, "Application of R Matrix/MQDT Method to Valence and Core Excitations in NO," *J. Phys. B* **39**, 1797–1811 (2006).

I. L. BRADEANU, R. FLESCHE, N. KOSUGI, A. A. PAVLYCHEV and E. RÜHL, "C 1s \rightarrow π^* Excitation in Variable Size Benzene Clusters," *Phys. Chem. Chem. Phys.* **8**, 1906–1913 (2006).

M. UEYAMA, H. HASEGAWA, A. HISHIKAWA and K. YAMANOUCHI, "Concerted and Sequential Coulomb Explosion Processes of N₂O in Intense Laser Fields by Coincidence Momentum Imaging," *J. Chem. Phys.* **123**, 154305 (8 pages) (2005).

K. HOSHINA, A. HISHIKAWA, K. KATO, T. SAKO, K. YAMANOUCHI, E. J. TAKAHASHI, Y. NABEKAWA and K. MIDORIKAWA, "Dissociative ATI of H₂ and D₂ in Intense Soft X-Ray Laser Fields," *J. Phys. B* **39**, 813–829 (2006).

T. URISU, Md. M. RAHMAN, H. UNO, R. TERO and Y. NONOGAKI, "Formation of High-Resistance Supported Lipid Bilayer on the Surface of a Silicon Substrate with Microelectrodes," *Nanomedicine* **1**, 317–322 (2005).

Y. NONOGAKI and T. URISU, "Synchrotron Radiation Induced Si–H Dissociation on H-Si(111)-1 \times 1 Surfaces Studied by In Situ Monitoring in the Undulator-Scanning Tunneling Microscope System," *J. Vac. Sci. Technol., Sect. A* **23**, 1364–1366 (2005).

Md. M. RAHMAN, Y. NONOGAKI, R. TERO, Y. H. KIM, H. UNO, Z. L. ZHANG, T. YANO, M. AOYAMA, R. SASAKI, H. NAGAI, M. YOSHIDA and T. URISU, "Giant Vesicle Fusion on Microelectrodes Fabricated by Femtosecond Laser Ablation Followed by Synchrotron Radiation Etching," *Jpn. J. Appl. Phys.* **44**, L1207–L1210 (2005).

H. WATANABE, Z. H. WANG, S. NANBU, J. MAKI, T. URISU, M. AOYAGI and K. OOI, "H Atom-Induced Oxidation Reaction on Water-Terminated Si Surface, 2H+H₂O/Si(100)-(2 \times 1): A Theoretical Study," *Chem. Phys. Lett.* **412**, 347–352 (2005).

Y. H. KIM, Md. M. RAHMAN, Z. L. ZHANG, N. MISAWA, R. TERO and T. URISU, "Supported Lipid Bilayer Formation by the Giant Vesicle Fusion Induced by Vesicle-Surface Electrostatic Attractive Interaction," *Chem. Phys. Lett.* **420**, 569–573 (2006).

N. MISAWA, S. YAMAMURA, Y. H. KIM, R. TERO, Y. NONOGAKI and T. URISU, "Orientation of Avidin Molecules Immobilized on COOH-Modified SiO₂/Si(100) Surfaces," *Chem. Phys. Lett.* **419**, 86–90 (2006).

R. TERO, H. WATANABE and T. URISU, "Supported Phospholipid Bilayer Formation on Hydrophilicity-Controlled Silicon Dioxide Surfaces," *Phys. Chem. Chem. Phys.* **8**, 3885–3894 (2006).

K. MITSUKE, H. KATAYANAGI, J. KOU, T. MORI and Y. KUBOZONO, "Fragmentation Mechanism of Highly Excited C₇₀ Cations in the Extreme Ultraviolet," *AIP Conf. Proc.* **811**, 161–166 (2006).

B. P. KAFLE, I. RUBINSTEIN and E. A. KATZ, "Analytical Model of Electrodifusion of Metals in Fullerene Thin Films," *Jpn. J. Appl. Phys.* **44**, 2803–2805 (2005).

T. YOSHIDA, K. TANAKA, H. YAGI, A. INO, H. EISAKI, A. FUJIMORI and Z. -X. SHEN, "Direct Observation of the Mass Renormalization in SrVO₃ by Angle Resolved Photoemission Spectroscopy," *Phys. Rev. Lett.* **95**, 146404 (4 pages) (2005).

H. YAGI, T. YOSHIDA, A. FUJIMORI, Y. KOHSAKA, M. MISAWA, T. SASAGAWA, H. TAKAGI, M. AZUMA and M. TAKANO, "Chemical Potential Shift in Lightly Doped to Optimally Doped Ca_{2-x}Na_xCuO₂Cl₂," *Phys. Rev. B* **73**, 172503 (4 pages) (2006).

Department of Computational Molecular Science

A. YAMADA and S. OKAZAKI, "A Surface Hopping Method for Chemical Reaction Dynamics in Solution Described by Diabatic Representation: An Analysis of Tunneling and Thermal Activation," *J. Chem. Phys.* **124**, 094110 (11 pages) (2006).

T. NAKASHIMA, K. IWAHASHI and S. OKAZAKI, "A Molecular Dynamics Study of Sodium Chenodeoxycholate in an Aqueous Solution," *Chem. Phys. Lett.* **420**, 489–492 (2006).

N. YOSHII, K. IWAHASHI and S. OKAZAKI, "A Molecular Dynamics Study of Free Energy of Micelle Formation for Sodium Dodecyl Sulfate in Water and Its Size Distribution," *J. Chem. Phys.* **124**, 184901 (6 pages) (2006).

N. YOSHII and S. OKAZAKI, "A Molecular Dynamics Study of Structural Stability of Spherical SDS Micelle as a Function of Its Size," *Chem. Phys. Lett.* **425**, 58–61 (2006).

N. YOSHII and S. OKAZAKI, "A Molecular Dynamics Study of Surface Structure of Spherical SDS Micelles," *Chem. Phys. Lett.* **426**, 66–70 (2006).

S. MIURA, "Quantum Rotation of Carbonyl Sulfide Molecules in Superfluid Helium Clusters: A Path Integral Hybrid Monte Carlo Study," *J. Phys.: Condens. Matter* **17**, S3259–S3264 (2005).

T. ISHIDA, "Polarizable Solute in Polarizable and Flexible Solvents: Simulation Study of Electron Transfer Reaction Systems," *J. Phys. Chem. B* **109**, 18558–18564 (2005).

A. MORITA and T. ISHIDA, "Charge Response Kernel Theory Based on Ab Initio and Density Functional Calculations," *Lecture Series on Computer and Computational Sciences* **4**, 663–666 (2005).

A. MORITA, "Improved Computation of Sum Frequency Generation Spectrum of Water Surface," *J. Phys. Chem. B* **110**, 3158–3163 (2006).

T. ISHIDA and A. MORITA, "Extended Treatment of Charge Response Kernel Comprising the Density Functional Theory and Charge Regulation Procedures," *J. Chem. Phys.* **125**, 074112 (2006).

A. SHUDO, K. ICHIKI and S. SAITO, "Origin of Slow Relaxation in Liquid-Water Dynamics: A Possible Scenario for the Presence of Bottleneck in Phase Space," *Europhys. Lett.* **73**, 826–832 (2006).

S. SAITO and I. OHMINE, "Fifth-Order Two-Dimensional Raman Spectroscopy of Liquid Water, Crystalline Ice Ih and Amorphous Ices: Sensitivity to Anharmonic Dynamics and Local Hydrogen Bond Network Structure," *J. Chem. Phys.* **125**, 084506 (12 pages) (2006).

Coordination Chemistry Laboratories

T. FUJIHARA, R. OKAMURA and K. TANAKA, "Structural Characterization of Ruthenium–Dioxolene Complexes with Ru^{II}–SQ and Ru^{II}–Cat Frameworks," *Chem. Lett.* **34**, 1562–1563 (2005).

T. WADA and K. TANAKA, "Reversible Bond Formation and Cleavage of the Oxo Bridge of [Ru₂(μ-O)(dioxolene)₂(btpyxa)]³⁺ [btpyxa = 2,7-Di-tert-butyl-9,9-dimethyl-4,5-bis-(2,2':6',2''-terpyrid-4'-yl)xanthene] Driven by a Three-Electron Redox Reaction," *Eur. J. Inorg. Chem.* **19**, 3832–3839 (2005).

H. SUGIMOTO, M. TARUMIZU, K. TANAKA, H. MIYAKE and H. TSUKUBE, "A New Series of Molybdenum-(IV), -(V), and -(VI) Dithiolate Compounds as Active Site Models of Molybdoenzymes: Preparation, Crystal Structures, Spectroscopic/Electrochemical Properties and Reactivity in Oxygen Atom Transfer," *Dalton Trans.* **21**, 3558–3565 (2005).

T. KOIZUMI and K. TANAKA, "Reversible Hydride Generation and Release from the Ligand of [Ru(pbn)(bpy)₂](PF₆)₂ Driven by a Pbn-Localized Redox Reaction," *Angew. Chem., Int. Ed.* **44**, 5891–5894 (2005).

H. SUGIMOTO, T. SAKURAI, H. MIYAKE, K. TANAKA and H. TSUKUBE, "Mononuclear Five-Coordinate Molybdenum(IV) and -(V) Monosulfide Complexes Coordinated with Dithiolene Ligands: Reversible Redox of Mo(V)/Mo(IV) and Irreversible Dimerization of [Mo^VS]⁻ Cores to a Dinuclear [Mo^V₂(μ-S)₂]²⁻ Core," *Inorg. Chem.* **44**, 6927–6929 (2005).

H. SUGIMOTO, Y. FURUKAWA, M. TARUMIZU, H. MIYAKE, K. TANAKA and H. TSUKUBE, "Synthesis and Crystal Structures of [W(3,6-dichloro-1,2-benzenedithiolate)₃]ⁿ⁻ (n = 1, 2) and [Mo(3,6-dichloro-1,2-benzenedithiolate)₃]²⁻: Dependence of the Coordination Geometry on the Oxidation Number and Counter-Cation in Trigonal-Prismatic and Octahedral Structures," *Eur. J. Inorg. Chem.* **15**, 3088–3092 (2005).

T. KOIZUMI, T. TOMON and K. TANAKA, "Synthesis, Structures and Electrochemical Properties of Ruthenium (II) Complexes Bearing Bidentate 1,8-Naphthyridine and Terpyridine Analogous (N,N,C)-Tridentate Ligands," *J. Organomet. Chem.* **690**, 4272–4279 (2005).

H. SUGIMOTO, M. HARIHARA, M. SHIRO, K. SUGIMOTO, K. TANAKA, H. MIYAKE and H. TSUKUBE, "Dioxo-Molybdenum(VI) and Mono-oxo-Molybdenum(IV) Complexes Supported by New Aliphatic Dithiolene Ligands: New Models with Weakened Mo:O Bond Characters for the Arsenite Oxidase Active Site," *Inorg. Chem.* **44**, 6386–6392 (2005).

H. OHTSU and K. TANAKA, "Electronic Structural Changes between Nickel(II)–Semiquinonato and Nickel(III)–Catecholato States Driven by Chemical and Physical Perturbation," *Eur. J. Chem. A* **11**, 3420–3426 (2005).

T. TOMON, T. KOIZUMI and K. TANAKA, "Electrochemical Hydrogenation of [Ru(bpy)₂(napy-κN)(CO)]²⁺: Inhibition of Reductive Ru–CO Bond Cleavage by a Ruthenacycle," *Angew. Chem., Int. Ed.* **44**, 2229–2232 (2005).

T. KOIZUMI and K. TANAKA, "Synthesis, Chemical- and Electrochemical Properties of Ruthenium(II) Complexes Bearing 2,6-Bis(2-naphthyridyl)pyridine," *Inorg. Chim. Acta* **358**, 1999–2004 (2005).

T. TOMON, T. KOIZUMI and K. TANAKA, "Stabilization and Destabilization of the Ru–CO Bond during the 2,2'-Bipyridin-6-onato (bpyO)-Localized Redox Reaction of [Ru(terpy)(bpyO)(CO)](PF₆)," *Eur. J. Inorg. Chem.* **2**, 285–293 (2005).

H. KAWAGUCHI and T. MATSUO, “Complexes of Tantalum with Triaryloxides: Ligand and Solvent Effects on Formation of Hydride Derivatives,” *J. Organomet. Chem.* **690**, 5333–5345 (2005). (special issue “*Organometallic Chemistry—The Next Generation*”)

Z. -H. ZHANG, T. OKAMURA, Y. HASEGAWA, H. KAWAGUCHI, L. -Y. KONG, W. -Y. SUN and N. UEYAMA, “Syntheses, Structures, and Luminescent and Magnetic Properties of Novel Three-Dimensional Lanthanide Complexes with 1,3,5-Benzenetriacetate,” *Inorg. Chem.* **44**, 6219–6227 (2005).

T. MATSUO and H. KAWAGUCHI, “A Synthetic Cycle for H₂/CO Activation and Allene Synthesis Using Recyclable Zirconium Complexes,” *J. Am. Chem. Soc.* **127**, 17198–17199 (2005).

T. WATANABE, T. MATSUO and H. KAWAGUCHI, “A Tantalum(V) Carbene Complex: Formation of a Carbene-Bis(phenoxide) Ligand by Sequential Proton and Hydride Abstraction,” *Inorg. Chem.* **45**, 6580–6582 (2006).

T. MATSUO, T. TSURUTA, K. MAEHARA, H. SATO, Y. HISAEDA and T. HAYASHI, “Preparation and O₂ Binding Study of Myoglobin Having a Cobalt Porphycene,” *Inorg. Chem.* **44**, 9391–9396 (2005).

K. KANO, H. KITAGISHI, C. DAGALLIER, M. KODERA, T. MATSUO, T. HAYASHI, Y. HISAEDA and S. HIROTA, “Iron Porphyrin–Cyclodextrin Supramolecular Complex as a Functional Model of Myoglobin in Aqueous Solution,” *Inorg. Chem.* **45**, 4448–4460 (2006).

T. MATSUO, H. NAGAI, Y. HISAEDA and T. HAYASHI, “Construction of Glycosylated Myoglobin by Reconstitutive Method,” *Chem. Commun.* **29**, 3131–3133 (2006).

T. MATSUO, T. IKEGAMI, H. SATO, Y. HISAEDA and T. HAYASHI, “Ligand Binding Properties of Two Kinds of Reconstituted Myoglobins with Iron Porphycene Having Propionates: Effect of β-Pyrrolic Position of Two Propionate Side Chains in Porphycene Framework,” *J. Inorg. Biochem.* **100**, 1265–1271 (2006).

T. HAYASHI, “Metalloporphycene is an Attractive Prosthetic Group for Hemoproteins,” *J. Porphyrins Phthalocyanines* **10**, 292 (2006).

Y. GAO, S. F. EL-MASHTOLY, B. PAL, T. HAYASHI, K. HARADA and T. KITAGAWA, “Pathway of Information Transmission from Heme to Protein upon Ligand Binding/Dissociation in Myoglobin Revealed by UV Resonance Raman Spectroscopy,” *J. Biol. Chem.* **281**, 24637–24646 (2006).

K. ARASHIBA, S. MATSUKAWA, S. KUWATA, Y. TANABE, M. IWASAKI and Y. ISHII, “Electrophilic O-Methylation of a Terminal Nitrosyl Ligand Attained by Early–Late Heterobimetallic Effect,” *Organometallics* **25**, 560–562 (2006).

Y. FUKUDA, M. SAKUMOTO, Y. TANABE, Y. ISHII, W. SUZUKI and A. NAKAO, “Observation of the New κ²C,O:κ²C',O' Coordination Mode of 1,1,2,2-Tetraacetyletanato Ligand in a Dinuclear 1,1,1,5,5,5-Hexafluoroacetylacetonato Palladium(II) Complex,” *Chem. Lett.* **35**, 936–937 (2006).

T. YAMAGATA, H. TADAOKA, M. NAGATA, T. HIRAO, Y. KATAOKA, V. RATOVELOMANANA-VIDAL, J. P. GENET and K. MASHIMA, “Oxidative Addition of RCO₂H and HX to Chiral Diphosphine Complexes of Iridium(I): Convenient Synthesis of Mononuclear Halo-carboxylato-iridium(III) Complexes and Cationic Dinuclear Halogen-triply-bridged Iridium(III) Complexes and Their Catalytic Performance for Asymmetric Hydrogenation of Cyclic Imines and 2-Phenylquinoline,” *Organometallics* **25**, 2505–2513 (2006).

H. TSURUGI, T. OHNO and K. MASHIMA, “Synthesis and Characterization of Homoenoate Complexes of Tantalum and Tungsten,” *Organometallics* **25**, 3179–3189 (2006).

T. OHSHIMA, T. IWASAKI and K. MASHIMA, “Direct Conversion of Esters, Lactones, and Carboxylic Acids to Oxazolines Catalyzed by Tetranuclear Zinc Cluster,” *Chem. Commun.* 2711–2713 (2006).

H. TSURUGI, Y. MATSUO and K. MASHIMA, “Preparation and Characterization of Iminopyrrolyl Hafnium Complexes as Catalyst Precursors for α-Olefin Polymerization,” *J. Mol. Catal. A: Chem.* **254**, 131–137 (2006).

M. OHASHI, J. -J. YI, D. SHIMIZU, T. YAMAGATA, T. OHSHIMA and K. MASHIMA, “Hexapalladium Cluster: Unique Cluster Construction Reaction of Cyclic Pd₃(CNC₆H₃Me₂-2,6)₆ and Linear [Pd₃(CNC₆H₃Me₂-2,6)₈]²⁺,” *J. Organomet. Chem.* **691**, 2457–2464 (2006).

M. OHASHI, A. YAGYU and K. MASHIMA, “Metathesis Approach to Linkage of Two Tetraplatinum Cluster Units: Synthesis, Characterization, and Dimerization of Pt₄(μ-OCOCH₃)₇[μ-OCO(CH₂)_nCH=CH₂] (n = 0–3),” *Chem. Lett.* **35**, 954–955 (2006).

M. OHASHI, S. TAKABAYASHI, K. MASHIMA and Y. NAKATO, “Modification of the n-Si(111) Surface with Alkyl Chains Having the Terminal C=C Double Bond,” *Chem. Lett.* **35**, 956–957 (2006).

K. OTSUBO, A. KOBAYASHI, H. KITAGAWA, M. HEDO, Y. UWATOKO, H. SAGAYAMA, Y. WAKABAYASHI and H. SAWA, “Most Stable Metallic Phase of the Mixed-Valence MMX-Chain, Pt₂(dtp)₄I (dtp: C₂H₅CS₂⁻) in Purely d-Electronic Conductors Based on the Transition-Metal Complex,” *J. Am. Chem. Soc.* **128**, 8140–8141 (2006).

Y. WAKABAYASHI, A. KOBAYASHI, H. SAWA, H. OHSUMI, N. IKEDA and H. KITAGAWA, “Direct Determination of Low-Dimensional Structures—Synchrotron X-Ray Scattering on One-Dimensional Charge-Ordered MMX-Chain Complexes—,” *J. Am. Chem. Soc.* **128**, 6676–6682 (2006).

M. TADOKORO, S. FUKUI, T. KITAJIMA, Y. NAGAO, S. ISHIMARU, H. KITAGAWA, K. ISOBE and K. NAKASUJI, "Structures and Phase Transition of Multi-Layered Water Nanotube Confined to Nanochannels," *Chem. Commun.* 1274–1276 (2006).

A. KOBAYASHI, T. KOJIMA, R. IKEDA and H. KITAGAWA, "Synthesis of a One-Dimensional Metal-Dimer Assembled System with Interdimer Interaction, $M_2(\text{dtp})_4$ ($M = \text{Ni}, \text{Pd}$; $\text{dtp} = \text{dithiopropionato}$)," *Inorg. Chem.* **45**, 322–327 (2006).

M. FUJISHIMA, M. ENYO, S. KANDA, R. IKEDA and H. KITAGAWA, "Galvanostatic Transient Studies on Copper Coordination Polymer under Hydrogen Absorption," *Chem. Lett.* **35**, 546–547 (2006).

M. FUJISHIMA, M. YAMAUCHI, R. IKEDA, T. KUBO, K. NAKASUJI and H. KITAGAWA, "Powder XRD and Solid-State $^2\text{H-NMR}$ Studies of RAP-Protected Palladium Nanoparticle (RAP = Rubeanic Acid Polymer)," *Solid State Phenomena* **111**, 107–110 (2006).

T. KAWAMOTO, T. MORI, T. KONOIKE, K. ENOMOTO, T. TERASHIMA, S. UJI, H. KITAGAWA, K. TAKIMIYA and T. OTSUBO, "Charge Transfer Degree and Superconductivity of the Incommensurate Organic Superconductor $(\text{MDT-TSF})(\text{I}_3)_{0.422}$," *Phys. Rev. B* **73**, 094513 (2006).

Research Center for Molecular-scale Nanoscience List of Publications

M. KAWAO, H. OZAWA, H. TANAKA and T. OGAWA, "Synthesis and Self-Assembly of Novel Porphyrin Molecular Wires," *Thin Solid Films* **499**, 23–28 (2006).

O. TSUTSUMI, H. SATO, K. TAKEDA and T. OGAWA, "Synthesis and Photochemical Behavior of Metalloporphyrin Complexes Containing a Photochromic Axial Ligand," *Thin and Solid Films* **499**, 219–223 (2006).

W. HUANG, G. MASUDA, S. MAEDA and T. OGAWA, "Molecular Junctions Composed of Oligothiophene Dithiols Bridged Gold Nanoparticles Exhibiting Photo Response Properties," *Chem. Eur. J.* **12**, 607–619 (2006).

H. SATO, O. TSUTSUMI, K. TAKEDA, H. TANAKA and T. OGAWA, "Simple Preparation Method for Supramolecular Porphyrin Arrays on Mica Using Air–Water Interface," *Jpn. J. Appl. Phys.* **45**, 2324–2327 (2006).

H. TANAKA, T. YAJIMA, T. MATSUMOTO, Y. OTSUKA and T. OGAWA, "Porphyrin Molecular Nanodevices Wired Using Single-Walled Carbon Nanotubes," *Adv. Mater.* **18**, 1411–1415 (2006).

W. HUANG and T. OGAWA, "Spontaneous Resolution of Δ and Λ Enantiomeric Pair of $[\text{Ru}(\text{phen})(\text{bpy})_2](\text{PF}_6)_2$ ($\text{phen} = 1,10\text{-phenanthroline}$, $\text{bpy} = 2,2'\text{-bipyridine}$) by Racemic Conglomerate Crystallization," *Polyhedron* **25**, 1379–1385 (2006).

W. HUANG and T. OGAWA, "Structural and Spectroscopic Characterizations of Low-Spin $[\text{Fe}(4,4\text{-dimethyl-2,2-bipyridine})_3](\text{NCS})_2/\text{H}_2\text{O}$ Prepared from High-Spin Iron(II) Dithiocyanate Tetrapyrindine," *J. Mol. Struct.* **785**, 21–26 (2006).

K. ARAKI, E. MIZUGUCHI, H. TANAKA and T. OGAWA, "Preparation of Very Reactive Thiol-Protected Gold Nanoparticles: Revisiting the Brust-Schiffrin Method," *J. Nanosci. Nanotechnol.* **6**, 708–712 (2006).

T. OGAWA, W. HUANG and H. TANAKA, "Morphology and Electric Properties of Nonathiophene/Au Nano-Composite Thin Films Formed between $1\ \mu\text{m}$ Gapped Electrodes," *Mol. Cryst. Liq. Cryst.* **455**, 299–303 (2006).

H. TANAKA, T. YAJIMA, M. KAWAO and T. OGAWA, "Electronic Properties of Single-Walled Carbon Nanotube/150mer Porphyrin System Measured by Point-Contact Current Imaging Atomic Force Microscopy," *J. Nanosci. Nanotechnol.* **6**, 1644–1648 (2006).

H. OZAWA, M. KAWAO, H. TANAKA and T. OGAWA, "Synthesis of End-Functionalized π -Conjugated Porphyrin Oligomers," *Tetrahedron* **62**, 4749–4755 (2006).

R. NEGISHI, T. HASEGAWA, K. TERABE, M. AONO, T. EBHARA, H. TANAKA and T. OGAWA, "Fabrication of Nanoscale Gaps Using a Combination of Self-Assembled Monolecular and Electron Beam Lithographic Techniques," *Appl. Phys. Lett.* **88**, 223111 (2006).

R. M. OSUNA, R. P. ORTIZ, M. C. R. DELGADO, Y. SAKAMOTO, T. SUZUKI, V. HERNÁNDEZ and J. T. L. NAVARRETE, "Synthesis and Characterization of Three Novel Perfluoro-Oligothiophenes Ranging in Length from the Trimer to the Pentamer," *J. Phys. Chem. B* **109**, 20737–20745 (2005).

R. NAKAO, H. RHEE and Y. UOZUMI, "Hydrogenation and Dehalogenation under Aqueous Conditions with an Amphiphilic Polymer-Supported Nanopalladium Catalyst," *Org. Lett.* **7**, 163–165 (2005).

Y. NAKAI and Y. UOZUMI, "Cycloisomerization of 1,6-Enynes: Asymmetric Multistep Preparation of a Hydrindane Framework in Water with Polymeric Catalysts," *Org. Lett.* **7**, 291–293 (2005).

Y. UOZUMI and M. KIKUCHI, "Controlled Monoarylation of Dibromoarenes in Water with a Polymeric Palladium Catalyst," *Synlett* 1775–1778 (2005).

K. TAKENAKA, M. MINAKAWA and Y. UOZUMI, "NCN Pincer Palladium Complexes: Their Preparation via a Ligand Introduction Route and Their Catalytic Properties," *J. Am. Chem. Soc.* **127**, 12273–12281 (2005).

Y. UOZUMI and M. KIMURA, "Asymmetric Allylic Etherification of Cycloalkenyl Esters with Phenols in Water Using a Resin-Supported Chiral Palladium Complex," *Tetrahedron: Asymmetry* **17**, 161–166 (2006).

Y. YAMADA and Y. UOZUMI, "A Solid-Phase Self-Organized Catalyst of Nanopalladium with Main-Chain Viologen Polymers: α -Alkylation of Ketones with Primary Alcohols," *Org. Lett.* **8**, 1375–1378 (2006).

T. KUBOTA, Y. SAKUMA, K. SHIMBO, M. TSUDA, M. NAKANO, Y. UOZUMI and J. KOBAYASHI, "Ampehazonol A, a Novel Polyhydroxy Metabolite from Marine Dinoflagellate Amphidinium sp.," *Tetrahedron Lett.* **47**, 4369–4371 (2006).

Y. HOSOKAWA, S. MAKI and T. NAGATA, "Gold Nanoparticles Stabilized by Tripod Thioether Oligomers: Synthesis and Molecular Dynamics Studies," *Bull. Chem. Soc. Jpn.* **78**, 1773–1782 (2005).

Y. MATSUMOTO, K. WATANABE and N. TAKAGI, "Excitation Mechanism and Ultrafast Vibrational Wavepacket Dynamics of Alkali-Metal Atoms on Pt(111)," *Surf. Sci.* **593**, 110–115 (2005).

D. INO, K. WATANABE, N. TAKAGI and Y. MATSUMOTO, "Electron Transfer Dynamics from Organic Adsorbate to a Semiconductor Surface: Zinc-Phthalocyanine on TiO₂(110)," *J. Phys. Chem. B* **109**, 18018–18024 (2005).

D. YAMAGUCHI, T. MATSUMOTO, K. WATANABE, N. TAKAGI and Y. MATSUMOTO, "Photochemistry of Cyclohexane on Cu(111)," *Phys. Chem. Chem. Phys.* **8**, 179–185 (2006).

Y. SHICHIBU, Y. NEGISHI, T. TSUKUDA and T. TERANISHI, "Large-Scale Synthesis of Thiolated Au₂₅ Clusters via Ligand Exchange Reactions of Phosphine-Stabilized Au₁₁ Clusters," *J. Am. Chem. Soc.* **127**, 13464–13465 (2005).

Y. NEGISHI, H. TSUNOYAMA, Y. YANAGIMOTO and T. TSUKUDA, "Subnanometer-Sized Gold Clusters with Dual Molecular Receptors: Synthesis and Assembly in One-Dimensional Arrangements," *Chem. Lett.* **34**, 1638–1639 (2005).

T. MAEYAMA, Y. NEGISHI, T. TSUKUDA, I. YAGI and N. MIKAMI, "Electron Localization in Negatively Charged Formamide Clusters Studied by Photodetachment Spectroscopy," *Phys. Chem. Chem. Phys.* **8**, 827–833 (2006).

H. SAKURAI, H. TSUNOYAMA and T. TSUKUDA, "Aerobic Oxidation Catalyzed by Gold Nanocluster as a Quasi-Homogeneous Catalyst: Generation of Hydrogen Peroxide Using Ammonium Formate," *Trans. Mater. Res. Soc. Jpn.* **31**, 521–524 (2006).

M. IMAMURA, T. MIYASHITA, A. TANAKA, H. YASUDA, Y. YANAGIMOTO, Y. NEGISHI and T. TSUKUDA, "Spectroscopic Investigation of Dendrimer-Encapsulated Gold Nanoclusters," *Trans. Mater. Res. Soc. Jpn.* **31**, 517–520 (2006).

H. TSUNOYAMA, Y. NEGISHI and T. TSUKUDA, "Chromatographic Isolation of "Missing" Au₅₅ Clusters Protected by Alkanethiolates," *J. Am. Chem. Soc.* **128**, 6036–6037 (2006).

Y. YANAGIMOTO, Y. NEGISHI, H. FUJIHARA and T. TSUKUDA, "Chiroptical Activity of BINAP-Stabilized Undecagold Clusters," *J. Phys. Chem. B* **110**, 11611–11614 (2006).

Y. NEGISHI, Y. TAKASUGI, S. SATO, H. YAO, K. KIMURA and T. TSUKUDA, "Kinetic Stabilization of Growing Gold Clusters by Passivation with Thiolates," *J. Phys. Chem. B* **110**, 12218–12221 (2006).

Y. YAMAGUCHI, M. NISHIMURA, M. NAGANO, H. YAGI, H. SASAKAWA, K. UCHIDA, K. SHITARA and K. KATO, "Glycoform-Dependent Conformational Alteration of the Fc Region of Human Immunoglobulin G1 as Revealed by NMR Spectroscopy," *Biochim. Biophys. Acta* **1760**, 693–700 (2006).

H. SASAKAWA, E. SAKATA, Y. YAMAGUCHI, M. KOMATSU, K. TATSUMI, E. KOMINAMI, K. TANAKA and K. KATO, "Solution Structure and Dynamics of Ufm1, a Ubiquitin-Fold Modifier 1," *Biochem. Biophys. Res. Commun.* **343**, 21–26 (2006).

S. TASHIRO, M. TOMINAGA, Y. YAMAGUCHI, K. KATO and M. FUJITA, "Peptide Recognition. Encapsulation and α -Helix Folding of 9-Residue Peptide within a Hydrophobic Dimeric Capsule of a Bowl-Shaped Host," *Chem. Eur. J.* **12**, 3211–3217 (2006).

C. A. SANDOVAL, Y. YAMAGUCHI, T. OHKUMA, K. KATO and R. NOYORI, "Solution Structures and Behavior of Trans-RuH(η 1-BH₄)(binap)(1,2-diamine) Complexes," *Magn. Reson. Chem.* **44**, 66–75 (2006).

S. TASHIRO, M. TOMINAGA, Y. YAMAGUCHI, K. KATO and M. FUJITA, "Folding of a De Novo Designed Peptide into an α -Helix through Hydrophobic Binding by a Bowl-Shaped Host," *Angew. Chem., Int. Ed.* **45**, 241–244 (2006).

Y. KAMIYA, Y. YAMAGUCHI, N. TAKAHASHI, Y. ARATA, K. KASAI, Y. IHARA, I. MATSUO, Y. ITO, K. YAMAMOTO and K. KATO, "Sugar-Binding Properties of VIP36, an Intracellular Animal Lectin Operating as a Cargo Receptor," *J. Biol. Chem.* **280**, 37178–37182 (2005).

UVSOR Facility

Y. HIKOSAKA, T. AOTO, P. LABLANQUIE, F. PENENT, E. SHIGEMASA and K. ITO, "Experimental Investigation of Core-Valence Double Photoionization," *Phys. Rev. Lett.* **97**, 053003 (2006).

T. GEJO, E. NAKAMURA and E. SHIGEMASA, "Development of Symmetry-Resolved Zero-Kinetic-Energy Photoelectron Spectroscopy for Probing Multielectron Processes," *Rev. Sci. Instrum.* **77**, 036112–036114 (2006).

Y. HIKOSAKA and E. SHIGEMASA, "Anisotropic Fragment Emission on Valence Photoionization of CF₄," *J. Electron Spectrosc. Relat. Phenom.* **152**, 29–32 (2006).

- Y. HIKOSAKA, T. AOTO, P. LABLANQUIE, F. PENENT, E. SHIGEMASA and K. ITO**, "Auger Decay of Ne 1s Photoionization Satellites Studied by a Multi-Electron Coincidence Method," *J. Phys. B* **39**, 3457–3464 (2006).
- T. AOTO, K. ITO, Y. HIKOSAKA, A. SHIBASAKI, R. HIRAYAMA, N. YAMAMOTO and E. MIYOSHI**, "Inner-Valence States of N_2^+ and the Dissociation Dynamics Studied by Threshold Photoelectron Spectroscopy and Configuration Interaction Calculation," *J. Chem. Phys.* **124**, 234306 (2006).
- S. SHEINERMAN, P. LABLANQUIE, F. PENENT, J. PALAUDOUX, J. H. D. ELAND, T. AOTO, Y. HIKOSAKA and K. ITO**, "Electron Correlation in Xe 4d Auger Decay Studied by Slow Photoelectron-Auger Electron Coincidence Spectroscopy," *J. Phys. B* **39**, 1017–1034 (2006).
- D. CÉOLIN, C. MIRON, K. LE GUEN, R. GUILLEMIN, P. MORIN, E. SHIGEMASA, P. MILLÉ, M. AHMAD, P. LABLANQUIE, F. PENENT and M. SIMON**, "Photofragmentation Study of Hexamethyldisiloxane Following Core Ionization and Direct Double Ionization," *J. Chem. Phys.* **123**, 234303 (8 pages) (2005).
- Y. HIKOSAKA, P. LABLANQUIE and E. SHIGEMASA**, "Efficient Production of Metastable Fragments around the 1s Ionization Threshold in N_2 ," *J. Phys. B* **38**, 3597–3605 (2005).
- Y. SAKURAI, T. NISHI, S. KIMURA, Y. S. KWON, M. A. AVILA and T. TAKABATAKE**, "Optical Study on Clathrates $Sr_8Ga_{16}Ge_{30}$ and $\beta-Eu_8Ga_{16}Ge_{30}$," *Physica B* **383**, 122–123 (2006).
- S. KIMURA, H. J. IM, Y. SAKURAI, T. MIZUNO, K. TAKEGAHARA, H. HARIMA, K. HAYASHI, E. MATSUOKA and T. TAKABATAKE**, "Infrared Study on Electronic Structure of SrT_4Sb_{12} ($T = Fe, Ru$)," *Physica B* **383**, 137–139 (2006).
- T. ITO, H. J. IM, S. KIMURA and Y. S. KWON**, "Angle-Resolved Photoemission Study on $CeTe_2$," *Physica B* **378-380**, 767–768 (2006).
- H. J. IM, T. ITO, S. KIMURA, J. B. HONG and Y. S. KWON**, "High-Resolution Photoemission Spectroscopy of $CeNiGe_2$ and $CeCoGe_2$," *Physica B* **378-380**, 825–826 (2006).
- Y. S. KWON, J. B. HONG, H. J. IM, T. NISHI and S. KIMURA**, "Infrared Absorption in Heavy Fermion System $CeNi_{1-x}Co_xGe_2$," *Physica B* **378-380**, 823–824 (2006).
- S. KIMURA, T. MIZUNO, H. J. IM, K. HAYASHI, E. MATSUOKA and T. TAKABATAKE**, "Iron-Based Heavy Quasiparticles in $SrFe_4Sb_{12}$: An Infrared Spectroscopic Study," *Phys. Rev. B* **73**, 214416 (5 pages) (2006).
- J. SICHELSCHMIDT, V. VOEVODIN, H. J. IM, S. KIMURA, H. ROSNER, A. LEITHE-JASPER, W. SCHNELLE, U. BURKHARDT, J. A. MYDOSH, YU. GRIN and F. STEGLICH**, "Optical Pseudogap from Iron States in Filled Skutterudites AFe_4Sb_{12} ($A = Yb$ and Ca, Ba)," *Phys. Rev. Lett.* **96**, 037406 (2006).
- H. J. IM, T. ITO, J. B. HONG, S. KIMURA and Y. S. KWON**, "Continuity of Ce 4f Electronic Structure across the Quantum Critical Point: A Resonant Photoemission Study on $CeNi_{1-x}Co_xGe_2$," *Phys. Rev. B* **72**, 220405(R) (4 pages) (2005).

Laser Research Center for Molecular Science

- G. DIWA, A. QUEMA, E. ESTACIO, R. POBRE, H. MURAKAMI, S. ONO and N. SARUKURA**, "Photonic-Crystal-Fiber Pigtail Device Integrated with Lens-Duct Optics for Terahertz Radiation Coupling," *Appl. Phys. Lett.* **87**, 151114 (2005).
- S. ONO, H. MURAKAMI, A. QUEMA, G. DIWA, N. SARUKURA, R. NAGASAKA, Y. ICHIKAWA, E. OHSHIMA, H. OGINO, A. YOSHIKAWA and T. FUKUDA**, "Generation of Terahertz Radiation Using Zinc Oxide as Photoconductive Material Excited by Ultraviolet Pulses," *Appl. Phys. Lett.* **87**, 261112 (2005).
- L. H. HAI, N. D. HUNG, A. QUEMA, G. DIWA, H. MURAKAMI, S. ONO and N. SARUKURA**, " Ce^{3+} -Doped $LiCaAlF_6$ Crystals as a Solid-State Ultraviolet Saturable Absorber and Role of Excited State Absorption," *Jpn. J. Appl. Phys.* **44**, 7984–7986 (2005).
- E. HAYASHI, K. ITO, S. YABASHI, M. YAMAGA, N. KODAMA, S. ONO and N. SARUKURA**, "Ultraviolet Irradiation Effect of Ce^{3+} -Doped $BaMgF_4$ Crystals," *J. Alloys Compd.* **408-412**, 883–885 (2006).
- E. HAYASHI, K. ITO, S. YABASHI, M. YAMAGA, N. KODAMA, S. ONO and N. SARUKURA**, "Vacuum Ultraviolet and Ultraviolet Spectroscopy of $BaMgF_4$ Codoped with Ce^{3+} and Na^+ ," *J. Lumin.* **119**, 69–74 (2006).
- M. YAMAGA, E. HAYASHI, N. KODAMA, K. ITO, S. YABASHI, Y. MASUI, S. ONO, N. SARUKURA, T. P. J. HAN and H. G. GALLAGHER**, "Vacuum Ultraviolet Spectroscopy of Ce^{3+} -Doped $SrMgF_4$ with Superlattice Structure," *J. Phys.: Condens. Matter* **18**, 6033–6044 (2006).
- J. YI, H. ISHIZUKI, I. SHOJI, T. TAIRA and S. KURIMURA**, "Infrared Laser Spectra from an Optical Parametric Oscillator Using 5 mol.% MgO -doped Periodically Poled Lithium Niobate," *J. Korean Phys. Soc.* **47**, 439–443 (2005).
- A. MORIKAWA, K. MIZUUCHI, T. SUGITA, K. YAMAMOTO, N. PAVEL and T. TAIRA**, "Efficient Green and Blue Light Generation Using SHG Devices With Periodically Poled Structures," *Rev. Laser Eng.* **33**, 671–675 (2005).
- H. ISHIZUKI and T. TAIRA**, "High-Energy Quasi-Phase-Matched Optical Parametric Oscillation in a Periodically Poled $MgO:LiNbO_3$ Device with a $5\text{mm} \times 5\text{mm}$ Aperture," *Opt. Lett.* **30**, 2918–2920 (2005).
- T. DASCALU and T. TAIRA**, "Highly Efficient Pumping Configuration for Microchip Solid-State Laser," *Opt. Express* **14**, 670–677 (2006).

N. PAVEL, V. LUPEI, J. SAIKAWA, T. TAIRA and H. KAN, “Neodymium Concentration Dependence of 0.94-, 1.06- and 1.34- μm Laser Emission and of Heating Effects Under 809- and 885-nm Diode Laser Pumping of Nd:YAG,” *Appl. Phys. B* **82**, 599–605 (2006).

J. YI, H. ISHIZUKI, I. SHOJI, T. TAIRA and S. KURIMURA, “Generation of 6 μm Radiation by Optical Parametric Oscillator and Difference Frequency Generation in Periodically Poled LiNbO₃,” *Jpn. J. Appl. Phys.* **45**, 111–115 (2006).

N. PAVEL and T. TAIRA, “Continuous-Wave High-Power Multi-Pass Pumped Thin-Disc Nd:GdVO₄ Laser,” *Opt. Commun.* **260**, 271–276 (2006).

M. TSUNEKANE and T. TAIRA, “Efficient, Water-Cooled Heat-Sink for High-Power Edge-Pumped Microchip Lasers,” *Rev. Laser Eng.* **34**, 181–187 (2006).

M. TSUNEKANE and T. TAIRA, “300 W Continuous-Wave Operation of a Diode Edge-Pumped, Hybrid Composite Yb:YAG Microchip Laser,” *Opt. Lett.* **31**, 2003–2005 (2006).

L. GHEORGHE, V. LUPEI, P. LOISEAU, G. AKA and T. TAIRA, “Second-Harmonic Generations of Blue Light in Nonlinear Optical Crystals of Gd_{1-x}Lu_xCa₄O(BO₃)₃ and Gd_{1-x}Sc_xCa₄O(BO₃)₃ through Noncritical Phase Matching,” *J. Opt. Soc. Am. B* **23**, 1630–1634 (2006).

Safety Office

NARASO, J. NISHIDA, M. TOMURA and Y. YAMASHITA, “TTF Derivatives Containing Fused-Pyrazine Rings for Novel Donor-Acceptor Systems,” *Synth. Met.* **153**, 389–392 (2005).

Okazaki Institute for Integrative Bioscience

H. KOMORI, K. SATOMOTO, Y. UEDA, N. SHIBATA, S. INAGAKI, S. YOSHIOKA, S. AONO and Y. HIGUCHI, “Crystallization and Preliminary X-Ray Analysis of CooA from *Carboxydotherrmus hydrogenoformans*,” *Acta Crystallogr., Sect. F: Struct. Biol. Cryst. Commun.* **62**, 471–473 (2006).

T. ZHANG, I. V. RUBTSOV, H. NAKAJIMA, S. AONO and K. YOSHIHARA, “Effect of Mutation on the Dissociation and Recombination Dynamics of CO in Transcriptional Regulator CooA: A Picosecond Infrared Transient Absorption Study,” *Biochemistry* **45**, 9246–9253 (2006).

H. YOSHIMURA, S. YOSHIOKA, K. KOBAYASHI, T. OHTA, T. UCHIDA, M. KUBO, T. KITAGAWA and S. AONO, “Specific Hydrogen Bonding Networks Responsible for Selective O₂ Sensing for the Oxygen Sensor Protein HemAT from *Bacillus subtilis*,” *Biochemistry* **45**, 8301–8307 (2006).

E. PINALLOULAKI, H. YOSHIMURA, S. YOSHIOKA, S. AONO and C. VAROTSIS, “Recognition and Discrimination of Gases by the Oxygen-Sensing Signal Transducer Protein HemAT as Revealed by FTIR Spectroscopy,” *Biochemistry* **45**, 7763–7766 (2006).

M. KUBO, S. INAGAKI, S. YOSHIOKA, T. UCHIDA, Y. MIZUTANI, S. AONO and T. KITAGAWA, “Evidence for Displacements of the C-Helix by CO Ligation and DNA Binding to CooA Revealed by UV Resonance Raman Spectroscopy,” *J. Biol. Chem.* **281**, 11271–11278 (2006).

K. KOBAYASHI, B. PAL, S. YOSHIOKA, Y. KATO, Y. ASANO, T. KITAGAWA and S. AONO, “Spectroscopic and Substrate Binding Properties of Heme-Containing Aldoxime Dehydratases, OxdB and OxdRE,” *J. Inorg. Biochem.* **100**, 1069–1074 (2006).

S. YOSHIOKA, K. KOBAYASHI, H. YOSHIMURA, T. UCHIDA, T. KITAGAWA and S. AONO, “Biophysical Properties of a c-Type Heme in Chemotaxis Signal Transducer Protein DcrA,” *Biochemistry* **44**, 15406–15413 (2005).

T. MATSUI, A. NAKAJIMA, H. FUJII, K. M. MATERA, C. T. MIGITA, T. YOSHIDA, and M. IKEDA-SAITO, “O₂- and H₂O₂-Dependent Verdoheme Degradation by Heme Oxygenase. Reaction Mechanisms and Potential Physiological Roles of the Dual Pathway Degradation,” *J. Biol. Chem.* **280**, 36833–36840 (2005).

T. KURAHASHI, Y. KOBAYASHI, S. NAGATOMO, T. TOSHA, T. KITAGAWA and H. FUJII, “Oxidizing Intermediates from the Sterically Hindered Salen Iron Complexes Related to the Oxygen Activation by Nonheme Iron Enzymes,” *Inorg. Chem.* **44**, 8156–8166 (2005).

M. KUJIME and H. FUJII, “Spectroscopic Characterization of Reaction Intermediates in Nitrite Reduction of Copper(I) Nitrite Complex as a Reaction Model for Copper Nitrite Reductase,” *Angew. Chem., Int. Ed.* **45**, 1089–1092 (2006).

A. TANAKA, H. NAKAMURA, Y. SHIRO and H. FUJII, “Roles of the Heme Distal Residues of FixL in O₂ Sensing: A Single Convergent Structure of the Heme Moiety Is Relevant to the Down-Regulation of Kinase Activity,” *Biochemistry* **45**, 2515–2523 (2006).

H. FUJII, T. KURAHASHI, T. TOSHA, T. YOSHIMURA and T. KITAGAWA, “¹⁷O NMR Study of Oxo Metalloporphyrin Complexes: Correlation with Electronic Structure of M=O Moiety,” *J. Inorg. Biochem.* **100**, 533–541 (2006).

H. FUJII and T. YOSHIDA, “ ^{13}C and ^{15}N NMR Studies of Iron-Bound Cyanides of Heme Proteins and Related Model Complexes: Sensitive Probe for Detecting Hydrogen Bonding Interactions at the Proximal and Distal Sides,” *Inorg. Chem.* **45**, 6816–6827 (2006).

T. OHTA, B. PAL and T. KITAGAWA, “Excited State Property of Hardly Photodissociable Heme-CO Adduct Studied by Time-Dependent Density Functional Theory,” *J. Phys. Chem. B* **109**, 21110–21117 (2005).

T. OSAKO, S. NAGATOMO, T. KITAGAWA, C. J. CRAMER and S. ITOH, “Kinetics and DFT Studies on the Reaction of Copper(II) Complexes and H_2O_2 ,” *J. Biol. Inorg. Chem.* **10**, 581–590 (2005).

E. PINAKOULAKI, T. OHTA, T. SOULIMANE, T. KITAGAWA and C. VAROTSIS, “Detection of the His-Heme Fe^{2+} -NO Species in the Reduction of NO to N_2O by ba_3 -Oxidase from *Thermus thermophilus*,” *J. Am. Chem. Soc.* **127**, 15161–15167 (2005).

C. V. SASTRI, M. J. PARK, T. OHTA, T. A. JACKSON, A. STUBNA, M. S. SEO, J. LEE, J. KIM, T. KITAGAWA, E. MUNCK, L. QUE, Jr. and W. NAM, “Axial Ligand Substituted Nonheme $\text{Fe}^{\text{IV}}=\text{O}$ Complexes: Observation of New near UV LMCT Bands and $\text{Fe}=\text{O}$ Raman Vibrations,” *J. Am. Chem. Soc.* **127**, 12494–12495 (2005).

J. KARDOS, D. OKUNO, T. KAWAI, Y. HAGIHAWA, N. YUMOTO, T. KITAGAWA, P. ZAVODSZKY, H. NAIKI and Y. GOTO, “Structural Studies Reveal that the Diverse Morphology of β_2 -Microglobulin Aggregates is a Reflection of Different Molecular Architectures,” *Biochim. Biophys. Acta* **1753**, 108–120 (2005).

T. OSAKO, S. TERADA, T. TOSHA, S. NAGATOMO, H. FURUTACHI, S. FUJINAMI, T. KITAGAWA, M. SUZUKI and S. ITOH, “Structure and Dioxygen-Reactivity of Copper(I) Complexes Supported by Bis(6-methylpyridin-2-yl-methyl)amine Tridentate Ligands,” *Dalton Trans.* 3514–3521 (2005).

T. KURAHASHI, Y. KOBAYASHI, S. NAGATOMO, T. TOSHA, T. KITAGAWA and H. FUJII, “Oxidizing Intermediates from the Sterically Hindered Iron Salen Complexes Related to the Oxygen Activation by Nonheme Iron Enzymes,” *Inorg. Chem.* **44**, 8156–8166 (2005).

H. SAWAI, M. MAKINO, Y. MIZUTANI, T. OHTA, H. SUGIMOTO, T. UNO, N. KAWADA, K. YOSHIZATO, T. KITAGAWA and Y. SHIRO, “Structural Characterization of the Proximal and Distal Histidine Environment of Cytoglobin and Neuroglobin,” *Biochemistry* **44**, 13257–13265 (2005).

S. YOSHIOKA, K. KOBAYASHI, H. YOSHIMURA, T. UCHIDA, T. KITAGAWA and S. AONO, “Biophysical Properties of a *c*-Type Heme in Chemotaxis Signal Transducer Protein DcrA,” *Biochemistry* **44**, 15406–15413 (2005).

K. KONISHI, T. OHTA, K. OINUMA, Y. HASHIMOTO, T. KITAGAWA and M. KOBAYASHI, “Discovery of a Reaction Intermediate of Aliphatic Aldoxime Dehydratase Involving Heme as an Active Center,” *Proc. Natl. Acad. Sci. U.S.A.* **103**, 564–568 (2006).

T. MATSUMOTO, H. FURUTACHI, M. KOBINO, M. TOMII, S. NAGATOMO, T. TOSHA, T. OSAKO, S. FUJINAMI, S. ITOH, T. KITAGAWA and M. SUZUKI, “Intramolecular Arene Hydroxylation versus Intermolecular Olefin Epoxidation by $(\mu-\eta^2:\eta^2\text{-Peroxo})\text{dicopper(II)}$ Complex Supported by Dinucleating Ligand,” *J. Am. Chem. Soc.* **128**, 3874–3875 (2006).

J. M. STEVENS, T. UCHIDA, O. DALTRUP, T. KITAGAWA and S. J. FERGUSON, “Dynamic Ligation Properties of the *Escherichia coli* Heme Chaperone Ccme to Non-Covalently Bound Heme,” *J. Biol. Chem.* **281**, 6144–6151 (2006).

S. NEYA, K. IMAI, Y. HIRAMATSU, T. KITAGAWA, T. HOSHINO, M. HATA and N. FUNASAKI, “Significance of the Molecular Shape of Iron Corrophene in a Protein Pocket,” *Inorg. Chem.* **45**, 4238–4242 (2006).

J. CHO, H. FURUTACHI, S. FUJINAMI, T. TOSHA, H. OHTSU, O. IKEDA, A. SUZUKI, M. NOMURA, T. URUGA, H. TANIDA, T. KAWAI, K. TANAKA, T. KITAGAWA and M. SUZUKI, “Sequential Reaction Intermediates in Aliphatic C–H Bond Functionalization Initiated by a Bis(μ -oxo)dinickel(III) Complex,” *Inorg. Chem.* **45**, 2873–2885 (2006).

H. FUJII, T. KURAHASHI, T. TOSHA, T. YOSHIMURA and T. KITAGAWA, “ ^{17}O NMR Study of Oxo Metalloporphyrin Complexes: Correlation with Electronic Structure of $\text{M}=\text{O}$ Moiety,” *J. Inorg. Biochem.* **100**, 533–541 (2006).

Y. SUH, M. S. SEO, K. M. KIM, Y. S. KIM, H. G. JANG, T. TOSHA, T. KITAGAWA, J. KIM and W. NAM, “Nonheme Iron(II) Complexes of Macrocyclic Ligands in the Generation of Oxoiron(IV) Complexes and the Catalytic Epoxidation of Olefins,” *J. Inorg. Biochem.* **100**, 627–633 (2006).

P. M. KOZŁOWSKI, J. KUTTA, T. OHTA and T. KITAGAWA, “Resonance Raman Enhancement of $\text{Fe}^{\text{IV}}=\text{O}$ Stretch in High-valent Iron Porphyrins: an Insight from TD-DFT Calculations,” *J. Inorg. Biochem.* **100**, 744–750 (2006).

K. KOBAYASHI, B. PAL, S. YOSHIOKA, Y. KATO, Y. ASANO, T. KITAGAWA and S. AONO, “Spectroscopic and Substrate Binding Properties of Heme-Containing Aldoxime Dehydratases, OxdB and OxdRe,” *J. Inorg. Biochem.* **100**, 1069–1074 (2006).

Y. MUKAIYAMA, T. UCHIDA, E. SATO, A. SASAKI, Y. SATO, J. IGARASHI, H. KUROKAWA, I. SAGAMI, T. KITAGAWA and T. SHIMIZU, “Spectroscopic and DNA-Binding Characterization of the Isolated Heme-Bound Basic Helix-Loop-Helix-PAS-A Domain of Neuronal PAS Protein 2 (NPAS2), a Transcription Activator Protein Associated with Circadian Rhythms,” *FEBS J.* **273**, 2528–2539 (2006).

H. YOSHIMURA, S. YOSHIOKA, K. KOBAYASHI, T. OHTA, T. UCHIDA, M. KUBO, T. KITAGAWA and S. AONO, "Specific Hydrogen-Bonding Networks Responsible for Selective O₂ Sensing of the Oxygen Sensor Protein HemAT from *Bacillus Subtilis*," *Biochemistry* **45**, 8301–8307 (2006).

T. TOSHA, N. KAGAWA, T. OHTA, S. YOSHIOKA, M. R. WATERMAN and T. KITAGAWA, "Raman Evidence for Specific Substrate-Induced Structural Changes in the Heme Pocket of Human Cytochrome P450 Aromatase during the Three Consecutive Oxygen Activation Steps," *Biochemistry* **45**, 5631–5640 (2006).

M. KUBO, S. INAGAKI, S. YOSHIOKA, T. UCHIDA, Y. MIZUTANI, S. AONO and T. KITAGAWA, "Evidence for Displacement of the C-Helix by CO Ligation and DNA Binding to CooA Revealed by UV Resonance Raman Spectroscopy," *J. Biol. Chem.* **281**, 11271–11278 (2006).

T. TOSHA, T. UCHIDA, A. R. BRASH and T. KITAGAWA, "On the Relationship of Coral Allene Oxide Synthase to Catalase: A Single Active Site Mutation that Induces Catalase Activity in Coral Allene Oxide Synthase," *J. Biol. Chem.* **281**, 12610–12617 (2006).

J. LI, T. UCHIDA, T. TODO and T. KITAGAWA, "Similarities and Differences between Cyclobutane Pyrimidine Dimer (CPD) Photolyase and (6-4) Photolyase as Revealed by Resonance Raman Spectroscopy: Electron Transfer from the FAD Cofactor to UV-Damaged DNA," *J. Biol. Chem.* **281**, 25551–25559 (2006).

M. LU, H. HIRAMATSU, Y. GOTO and T. KITAGAWA, "Structure of Interacting Segments in the Growing Amyloid Fibril of β_2 -Microglobulin Probed with IR Spectroscopy," *J. Mol. Biol.* **362**, 355–364 (2006).

Y. GAO, S. F. EL-MASHTOLY, B. PAL, T. HAYASHI, K. HARADA and T. KITAGAWA, "Pathway of Information Transmission from Heme to Protein Upon Ligand Binding/Dissociation in Myoglobin Revealed by UV Resonance Raman Spectroscopy," *J. Biol. Chem.* **281**, 24637–24646 (2006).

J. LI, T. UCHIDA, T. OHTA, T. TODO and T. KITAGAWA, "Characteristic Structure and Environment in FAD Cofactor of (6-4) Photolyase along Function Revealed by Resonance Raman Spectroscopy," *J. Phys. Chem. B* **110**, 16724–16732 (2006).

REVIEW ARTICLES AND TEXTBOOKS

Department of Theoretical Studies

T. AKASAKA and S. NAGASE, "Structural Analysis of Endohedral Metallofullerenes—Recent Topics and Development," *Kagaku* (in Japanese) **60**, 68–69 (2005).

T. AKASAKA and S. NAGASE, "The Structure of Endohedral Metallofullerene Sc_3C_{82} ," *Kotai Butsuri* (in Japanese) **40**, 962–963 (2005).

T. AKASAKA and S. NAGASE, "Chemical Functionalization of Endohedral Metallofullerene," *Gendai Kagaku* (in Japanese) **No. 422**, 51–56 (2006).

T. AKASAKA and S. NAGASE, "Structures of Endohedral Metallofullerene," *J. Crystallography Soc. Jpn.* (in Japanese) **48**, 230–236 (2006).

S. ZOU, A. KONDORSKIY, G. V. MIL'NIKOV and H. NAKAMURA, "Laser Control of Chemical Dynamics. I. Control of Electronic Transitions by Quadratic Chirping," in *Progress in Ultrafast Intense Laser Science*, Springer-Verlag (2006).

A. KONDORSKIY, G. V. MIL'NIKOV and H. NAKAMURA, "Laser Control of Chemical Dynamics. II. Control of Wave Packet Motion," in *Progress in Ultrafast Intense Laser Science*, Springer-Verlag (2006).

Department of Molecular Structure

H. OKAMOTO and K. IMURA, "Imaging of Plasmons in Gold Nano-Particles by Dynamic Near-Field Spectroscopy," *Laser Kenkyu (Rev. Laser Eng.)* (in Japanese) **34**, 224–229 (2006).

K. IMURA and H. OKAMOTO, "Plasmon Wavefunction Imaging and Dynamic Near-Field Optical Microscopy of Noble Metal Nanoparticles," *Bunko Kenkyu (J. Spectrosc. Soc. Jpn.)* (in Japanese) **55**, 161–172 (2006).

T. NAKAGAWA and T. YOKOYAMA, "X-Ray Magnetic Circular Dichroism and Magneto-Optical Kerr Effect Studies of Spin Reorientation Transitions in Magnetic Ultrathin Films," *Hyomen Kagaku (J. Surf. Sci. Soc. Jpn.)* (in Japanese) **27**, 272–277 (2006).

T. OZAWA, "Designing Split Reporter Proteins for Analytical Tools," *Anal. Chim. Acta* **556**, 58–68 (2006).

M. TAKEUCHI and T. OZAWA, "Frontiers in Bioimaging," *ACS Chem. Biol.* **1**, 333–334 (2006).

T. OZAWA and Y. UMEZAWA, "Inteins for Split-Protein Reconstitutions and Their Applications," *Nucleic Acids and Molecular Biology*, Springer-Verlag, Berlin, **16**, 307–323 (2005).

Department of Electronic Structure

T. ICHIMURA, Y. MATSUSHITA, K. SAKEDA and T. SUZUKI, "Photoreactions," in *Microchemical Engineering in Practice*, T. R. Dietrich, Ed., Blackwell Publishing (2006).

Department of Molecular Assemblies

N. KOJIMA, "Photo-Induced Spin Crossover Phenomena," in *Inorganic Chromotropism*, Y. Fukuda, Ed., Kodansha/Springer, pp. 257–272 (2006).

N. KOJIMA and K. IKEDA, "Magneto-Chromism of Inorganic Materials," in *Inorganic Chromotropism*, Y. Fukuda, Ed., Kodansha/Springer, pp. 351–363 (2006).

Department of Computational Molecular Science

B. C. GARRETT, G. K. SCHENTER and A. MORITA, "Molecular Simulation of the Transport of Molecules across the Liquid/Vapor Interface of Water," *Chem. Rev.* **106**, 1355–1374 (2006).

Research Center for Molecular-scale Nanoscience

T. OGAWA, "Measurement of Electric Properties," in *Introduction to Engineering for Nano-Technology* (in Japanese), Chapter 4. (2006).

T. OGAWA, "Future of Molecular Orientation Technology," *Kinouzairyō* (in Japanese) **2**, 28–34 (2006).

K. WATANABE and Y. MATSUMOTO, “Ultrafast Dynamics of Coherent Surface Phonon,” *Oyobuturi* (in Japanese) **74**, 1316–1321 (2005).

K. WATANABE and Y. MATSUMOTO, “Vibrational Dynamics of Surface Adsorbates Studied by Femtosecond Time-Resolved Second Harmonic Generation,” *Hyomenkagaku* (in Japanese) **26**, 662–666 (2005).

Okazaki Institute for Integrative Bioscience

H. HIRAMATSU and T. KITAGAWA, “FT-IR Approaches on Amyloid Fibril Structure,” *Biochem. Biophys. Acta* **1753**, 100 (2005).

AUTHOR INDEX

to “Research Activities”

- | | | | | | |
|----------------------------|------------------------|------------------------|--------------|------------------------|------------------|
| A | | E | | GOTO, Kei | 18 |
| ADAMOWICZ, Ludwik | 19 | EBIHARA, T. | 143 | GOTO, Yuji | 183, 188 |
| AIDA, Takuzo | 81 | EINAGA, Yasuaki | 87–88 | GRIN, Yu. | 163 |
| AKAHANE, Y. | 23 | EL-MASHTOLY, Samir F. | 188–189 | H | |
| AKASAKA, Takeshi | 15–20 | ELAND, John | 163 | HAGA, Ryuta | 15 |
| AKIYAMA, Shuji | 52 | EL OUENZERFI, Riadh | 166 | HAGIHARA, Yusuke | 64 |
| AL-SHAMERY, Katharina | 152 | ENOMOTO, Masaya | 90 | HAGIHAWA, Yoshihisa | 183 |
| ALLAKHVERDIEV, Suleyman I. | 149 | ENYO, Michio | 137 | HAI, Le Hoang | 166 |
| ANNARAJ, Jamespandi | 189 | ESTACIO, Elmer | 166 | HAMAYA, Nozomu | 35 |
| AONO, M. | 143 | ETO, Y. | 92 | HAN, T. P. J. | 167 |
| AONO, Shigetoshi | 175,–177, 183, 185–187 | F | | HARA, Toru | 161–162 |
| AOTO, Tomohiro | 162–163 | FENG, Lai | 16, 19–20 | HARA, Toshifumi | 79–82 |
| AOYAMA, M. | 23 | FRENKING, Gernot | 18 | HARADA, Katsuyoshi | 131, 188–189 |
| AOYAMA, Masaki | 171 | FU, Riqiang | 50 | HARADA, Kensuke | 109 |
| APELOIG, Yitzhak | 17 | FUCHIGAMI, Sotaro | 37 | HARADA, Yosuke | 68 |
| ARAKI, Koiti | 142 | FUCHIZAKI, Kazuhiro | 35–36 | HARANO, Yuichi | 30 |
| ARASHIBA, Kazuya | 133 | FUJIHARA, Hisashi | 157 | HARIGAI, Miki | 53 |
| ASANO, Toshifumi | 106 | FUJIHARA, Tetsuaki | 123 | HARIHARA, Makoto | 125 |
| ASANO, Yasuhisa | 177, 185 | FUJII, Hiroshi | 178–180, 185 | HARIMA, Hisatomo | 164 |
| AVILA, M. A. | 164 | FUJII, Masaaki | 169 | HASE, Muneaki | 71 |
| B | | FUJIMOTO, Chikoto | 98 | HASE, Takaki | 35 |
| BABA, Akinori | 39–41 | FUJIMOTO, Kazuteru | 82 | HASEGAWA, Hirokazu | 66, 73 |
| BABA, Masaaki | 73 | FUJIMURA, Yo | 40 | HASEGAWA, Masahiro | 99 |
| BADEN, Naoki | 53 | FUJINAMI, Shuhei | 184, 190 | HASEGAWA, Masashi | 95–96 |
| BAN, Noritaka | 15 | FUJISAWA, Tetsuro | 52 | HASEGAWA, T. | 143 |
| BOYKO, Sergiy | 77 | FUJISHIMA, Musashi | 137 | HASEGAWA, Tadashi | 15 |
| BRASH, Alan R. | 187 | FUJIWARA, Emiko | 84–85 | HASHIDO, Masanori | 37 |
| BRUNOLD, Thomas C. | 190 | FUJIWARA, Hideki | 88 | HASHIMOTO, Takashi | 99 |
| BURKHARDT, U. | 163 | FUJIWARA, Katsutoshi | 64 | HASHIMOTO, Yoshiteru | 183 |
| BURMEISTER, Florian | 102 | FUJIYAMA, Shigeki | 80 | HATA, Masayuki | 184 |
| BUSATH, David D. | 50 | FUKUDA, Tsuguo | 166 | HATSUI, Takaki | 101–102 |
| C | | FUKUNAGA, Toshiharu | 95 | HAYAKAWA, Yuri | 139 |
| CHEN, Zhongfang | 18 | FUKUSHIMA, Takanori | 81 | HAYASHI, Eiji | 166–167 |
| CHIANG, Tsung-Yi | 105–107 | FUKUZUMI, Shunich | 20 | HAYASHI, Katsuyuki | 163–164 |
| CHIBA, Hisashi | 64–65 | FUNAKOSHI, Ken-ichi | 35 | HAYASHI, Kenji | 161 |
| CHO, Jaeheung | 184, 190 | FUNASAKI, Noriaki | 131, 184 | HAYASHI, Takashi | 130–132, 188–189 |
| CHOE, Yoong-Kee | 15 | FURUKAWA, Ko | 79–83 | HE, Zheng | 93 |
| CHRISTOPHER, J. Cramer | 182 | FURUKAWA, Yukio | 17 | HEDO, Masato | 136 |
| COUPRIE, Marie, Emmanuelle | 162 | FURUKAWA, Yuuki | 124 | HERNÁNDSZ, Víctor | 144 |
| CROSS, R. James | 21 | FURUTACHI, Hideki | 184, 190 | HIGASHI, Takeshi | 84 |
| CROSS, Timothy A. | 50 | FUYUKI, Masanori | 153 | HIGASHIBAYASHI, Shuhei | 151 |
| CUI, HengBo | 84–88 | G | | HIGUCHI, Yoshiki | 175 |
| D | | GALLAGHER, H. G. | 167 | HIKITA, Masanori | 90 |
| DAGALLIER, Camelle | 130 | GAO, Ying | 188–189 | HIKOSAKA, Yasumasa | 162–163 |
| DELGADO, Mari C. R. | 144 | GAO, Zhengxiang | 16, 18–20 | HINO, Kazuyuki | 62 |
| DIWA, Girbert | 166 | GEJO, Tatsuo | 163 | HIRAMATSU, Fukiko | 77 |
| | | GENET, Jean Pierre | 135 | HIRAMATSU, Hirotsugu | 188 |
| | | GEORGE, Serena DeBeer | 190 | HIRAMATSU, Yoshitsugu | 184 |
| | | GIRARD, Bertrand | 64 | HIRAO, Tsukasa | 135 |
| | | GISSSELBRECHT, Mathieu | 102 | HIRAOKA, Ryusuke | 29 |
| | | | | HIRATA, Fumio | 28–31 |
| | | | | HIRAYAMA, Ryo | 163 |

- HIROTA, Shun 130–131
HISAEDA, Yoshio 130–132
HISHIKAWA, Akiyoshi 104
HOFFMAN, Brian M. 94
HOLLAND, Andrew 101
HOLLAND, Karen 101
HONDA, Kaoru 190
HONDA, Masahiro 64
HONG, J. B. 164–165
HORIGOME, Toshio 101
HORIMOTO, Noriko N. 47
HORINO, Hideyuki 63
HORITA, Shintaro 82
HORN, Ernst 16, 18–20
HOSAKA, Kouichi 65
HOSAKA, Masahito 161–162
HOSHINO, Mikio 62
HOSHINO, Tyuji 184
HOSOI, Yoshinobu 17
HOSSAIN, Mohammad K. 46–47
HU, Jun 50
HUANG, Wei 141–143
HUNG, Nguyen Dai 166
- I**
- ICHIKAWA, Yo 166
ICHIKI, Kouichiro 121
ICHIMURA, Teijiro 68–69
IGA, Hiroshi 68
IGARASHI, Jotaro 186
IIDUKA, Yuko 16, 19–20
IINO, Takuro 63
IKEDA, Atsushi 42
IKEDA, Naoshi 82, 136
IKEDA, Osamu 184
IKEDA, Ryuichi 136–137
IKEDA-SAITO, Masao 52, 94, 178
IKEGAMI, Takahiro 132
IKEGUCHI, Mitsunori 37
IKENAGA, Ozora 20
IKESUE, Akio 168–169
IKOMA, Tadaaki 189
IM, Hojun 163–165
IMAI, Kiyohiro 184
IMAI, Takashi 29–30
IMAMOTO, Yasushi 53
IMAMURA, Masaki 156
IMURA, Kohei 45–48
INAGAKI, Sayaka 175, 187
INAMO, Masahiko 62
INGLEY, Richard 101
INO, Daisuke 153–154
INOKUCHI, Yoshiya 63
INOUE, Akihisa 95
INOUE, Kazuya 63
INOUE, Keiichi 53
INOUE, N. 23
IRIE, Naoaki 82
ISHIDA, Tateki 119
ISHIDA, Toshimasa 23–24
ISHII, Kunihiko 148
ISHII, Youichi 133
- ISHIMORI, Koichiro 51–52
ISHIMURA, Kazunori 82
ISHIMURA, Kazuya 15, 17, 20–21
ISHIOKA, Kunie 71
ISHIYAMA, Tatsuya 120
ISHIZUKA, Ryosuke 28–29
ISHIZUKA, Tomoya 93
ISHIZUKI, Hideki 169–170
ISOGAI, Hideto 30
ISOZAKI, Tasuku 68
ITO, Kenji 162–163
ITO, Kiyotaka 166–167
ITO, Miki 99
ITO, Naomi 62
ITO, Takahiro 95, 164
ITO, Takayoshi 81
ITO, Yoshihiro 98
ITOH, Keiji 95
ITOH, Shinobu 182, 184
ITOI, Miho 90
IWADATE, Noriyuki 133
IWAHASHI, Kensuke 117
IWAI, Shinichiro 77
IWAMATSU, Sho-ichi 21
IWANAGA, Kohei 20
IWASA, Takeshi 27
IWASAKI, Masakazu 133
IZUMI, Fujio 82
- J**
- JANG, Ho G. 185
JIANG, Donglin 93
JIN, Toshimichi 94
JOHNSTON, Roy L. 40
JUDAI, Ken 59–60, 63
- K**
- KADISH, Karl M. 17
KAFLE, Bhim Prasad 111–114
KAGAWA, Norio 186
KAJIMOTO, Okitsugu 40
KAJITANI, Hidenobu 133
KAKIMOTO, Takuya 99
KAKIUCHI, Toru 82
KAKO, Masahiro 16, 20
KALYUZHNYI, Y. V. 36
KAMBE, Takashi 82
KANDA, Seiichi 137
KANEHARA, Masayuki 158
KANG, Min Jung 190
KANNO, Akira 57
KANO, Koji 130
KARDOS, Jozsef 183
KARNI, Miriam 17
KASAHARA, Shunji 73
KASAI, Toshio 171
KASHIMA, Izuru 90
KASHIWAZAKI, Akimitsu 77
KATAOKA, Mikio 53
KATAYAMA, Yoshinori 35
KATAYANAGI, Hideki 110–114
- KATO, Koichi 159
KATO, Masahiko 95–96
KATO, Reizo 76
KATO, Tatsuhisa 15–16, 19–20, 83
KATO, Yasuo 177, 185
KATOH, Masahiro 161–162
KATSUKI, Hiroyuki 64–65
KAWAGUCHI, Hiroyuki 128, 139
KAWAI, Shinnosuke 40
KAWAI, Tomoji 183
KAWAI, Toshihide 184
KAWAMORI, Asako 83
KAWAMOTO, Atsushi 75, 92
KAWAMURA, Naomi 157
KAWAO, Masahiro 141–142
KAWASAKI, M. 23
KAWASHIMA, Takayuki 18, 20
KAWAZOE, Yoshiyuki 166
KHAN, Javaid Shahbaz 53
KIDA, Noriyuki 90
KIDERA, Akinori 37
KIEBER-EMMONS, Matthew T. 189
KIKUZAWA, Yoshihiro 148
KIM, Jinheung 185
KIM, Kwan Mook 185
KIM, Sum-Hee 94
KIM, Sung Bae 57–58
KIM, Yong-Hoon 108
KIM, Youn Sang 185
KIMURA, Keisaku 157
KIMURA, Masahiro 146
KIMURA, Shin-ichi 95, 161, 163–165
KIMURA, Tetsunari 51–52
KINOSHITA, Kengo 37
KINOSHITA, Masahiro 30
KIRA, Atsushi 50
KISHINE, Jun-ichiro 32
KITAGAWA, Hiroshi 136–137
KITAGAWA, Teizo 175–179, 182–190
KITAGISHI, Hiroaki 130
KITAJIMA, Masahiro 46–47, 71
KITANO, Kenta 66
KIVIMÄKI, Antti 102
KOBAYASHI, Akiko 84–86
KOBAYASHI, Atsushi 136
KOBAYASHI, Hayao 84–89
KOBAYASHI, Junji 18, 20
KOBAYASHI, Kaoru 15–16, 20
KOBAYASHI, Katsuaki 176–177, 183, 185–186
KOBAYASHI, Michihiko 183
KOBAYASHI, Takashi 68
KOBAYASHI, Yoshio 178
KOBAYASHI, Yuko 139
KOBINO, Masashi 184
KOBRYN, Alexander 31
KODAMA, Nobuhiro 166–167
KODERA, Masahito 130
KOIKE, Ryotaro 37
KOIZUMI, Take-aki 124–126

- KOJIMA, Norimichi 90
 KOJIMA, Takahiko 136
 KOKALJ, Anton 63
 KOMATSU, Masaaki 159
 KOMATSUZAKI, Tamiki 39–41
 KOMINAMI, Eiki 159
 KOMORI, Hirofumi 175
 KONDO, Ken-ichi 97
 KONDO, Mitsuru 139
 KONDOH, Takuhiko 109
 KONDORSKIY, Alexey 23–25
 KONISHI, Kazunobu 183
 KOSAKA, Atsuko 81
 KOSUGI, Nobuhiro 101–102
 KOU, Junkei 110
 KOVALENKO, Andriy F. 29–31
 KOWALSKA, Aneta 77
 KOYAMA, Mai 189
 KOZLOWSKI, Pawel M. 185
 KRAPP, Andreas 18
 KUBO, Minoru 175–176, 186–187
 KUBOTA, Yoji 26
 KUBOZONO, Yoshihiro 110
 KUJIME, Masato 180
 KUMADA, Shinji 69
 KUMAGAI, K. 92
 KURAHASHI, Takuya 178–180, 185
 KURATA, Saki 145
 KURIHARA, Hiroki 20
 KURIHARA, Masato 138
 KUROIWA, Haruko 57
 KUROIWA, Tsuneyoshi 57
 KUROKAWA, Hirofumi 186
 KUSUNOSE, Yukio 98
 KUTA, Jadwiga 185
 KUWATA, Shigeaki 133
 KWON, Yong-seung 164–165
 KYUSHIN, Soichiro 16
- L**
- LABAT, Marie 162
 LABLANQUIE, Pascal 162–163
 LAI, Lin 20
 LAMBERT, Guillaume 162
 LAUKHINA, Elena 77
 LEE, HaJin 88
 LEE, Jin Yong 28
 LEE, Shyi-Long 17, 19
 LEI, Sheng-Bin 108
 LEITHE-JASPER, A. 163
 LI, Chun Bui 39–40
 LI, Jiang 187–188
 LIAN, Yongfu 17, 20
 LIANG, Wanzhen 22
 LINDGREN, Andreas 102
 LIU, Jianjun 20
 LIU, Jin-Gang 189
 LIU, Michael T. H. 16
 LONG, La-Sheng 86
 LU, Jing 16, 18–20
 LU, Ming 188
 LU, Rong 71
- LU, Xin 18
 LUTY, Tadeusz 32
- M**
- MA, Xiao-Dong 54
 MacNAUGHTON, Janay 102
 MAEDA, Hiromitsu 98–99
 MAEDA, Seisuke 141
 MAEDA, Yutaka 15–16, 18–20
 MAEHARA, Keiko 130
 MAESHIMA, Nobuya 33
 MAKIMURA, Tetsuya 105
 MAKINO, Masatomo 131
 MARUYAMA, Koichi 157
 MARUYAMA, Yutaka 30
 MAS-TORRENT, Marta 77
 MASHIMA, Kazushi 134–135
 MASUDA, Gou 141
 MASUI, Yuki 167
 MATSUDA, Akitaka 97, 104
 MATSUI, Toshitaka 52, 94, 178
 MATSUKAWA, Shoji 133
 MATSUMOTO, Hideyuki 16
 MATSUMOTO, Takahiro 184, 190
 MATSUMOTO, Taketoshi 152–153
 MATSUMOTO, Takuya 142
 MATSUMOTO, Yoshiyasu 72, 152–155
 MATSUNAGA, Noriaki 82
 MATSUNAGA, Yasuhiro 40
 MATSUO, Takashi 130–132
 MATSUO, Tsukasa 128
 MATSUOKA, Eiichi 163–164
 MATSUOKA, Hideto 83
 MATSUSHIMA, Tatsuo 63
 MATSUSHITA, M. Michio 157
 MATSUSHITA, Machiko 62
 MATSUSHITA, Yoshihisa 69
 MATSUURA, Koji 51
 MEGURO, Akira 16
 MEI, W. N. 18–20
 MEIER, Christophe 64
 MIL'NIKOV, Gennady V. 22–25
 MINAKAWA, Maki 146
 MINO, Hiroyuki 83
 MISAWA, Nobuo 108–109
 MISOCHKO, O. V. 71
 MITSUKE, Koichiro 110–115
 MIURA, Shinichi 118
 MIURA, Yasutaka 138
 MIYAKE, Hiroyuki 124–125
 MIYAKE, Shin-ichiro 67
 MIYASHITA, Jun 15
 MIYASHITA, Satoshi 33
 MIYASHITA, Takeho 156
 MIYAZAKI, Hidetoshi 96
 MIYAZAKI, Mitsuhiro 66–67
 MIYOSHI, Eisaku 163
 MIZOROGI, Naomi 15–21
 MIZUGUCHI, Eisuke 142
 MIZUNO, Masayasu 190
 MIZUNO, Takafumi 163–164
- MIZUSEKI, Hiroshi 166
 MIZUTANI, Uichiro 95–96
 MIZUTANI, Yasuhisa 175, 187, 189
 MOCHIDA, Tomoyuki 77
 MOCHIHASHI, Akira 161–162
 MOEWES, Alexander 102
 MONCEAU, Pierre 81
 MORI, Koichi 73
 MORI, Takanori 110
 MORISHIMA, Isao 51–52
 MORITA, Akihiro 119–120
 MUKAIYAMA, Yuji 186
 MUNE, Yutaka 63
 MURAKAMI, Hidetoshi 166
 MURAKAMI, Kouichi 105
 MURATA, Dai 131
 MURATA, Shizuaki 21
 MYDOSH, J. A. 163
 MYOGA, Hiroki 50
- N**
- NAD, Felix 81
 NAGAHARA, Tetsuhiko 45, 48
 NAGAI, Hirokazu 131
 NAGANO, Mayumi 159
 NAGANO, Yasutomo 189
 NAGAO, Masashi 154
 NAGAO, Nobuaki 82
 NAGASAKA, Mariko 68
 NAGASAKA, Ryujiro 166
 NAGASAWA, Takayuki 149
 NAGASE, Shigeru 15–21
 NAGATA, Mitsuhiro 135
 NAGATA, Toshi 147–149
 NAGATOMO, Shigenori 178, 182, 184
 NAIKI, Hironobu 183
 NAITO, Akira 49–50
 NAKABAYASHI, Takakazu 62
 NAKAGAWA, Takeshi 54–55
 NAKAGOE, Osamu 72, 155
 NAKAHODO, Tsukasa 15–16, 18–20
 NAKAI, Naohito 105
 NAKAJIMA, Aya 178
 NAKAJIMA, Hiroshi 15, 175
 NAKAJIMA, Koji 19
 NAKAMOTO, Akio 90
 NAKAMURA, Eiken 163
 NAKAMURA, Hiro 179
 NAKAMURA, Hiroki 22–25
 NAKAMURA, Kazutaka 97
 NAKAMURA, Toshikazu 79–82
 NAKANISHI, Takashi 99
 NAKANO, Chikako 77
 NAKANO, Hirofumi 62
 NAKANO, Sakura 95
 NAKAO, Satoshi 106–107
 NAKAO, Yoshihide 42
 NAKASHIMA, Shinichi 71
 NAKASHIMA, Toshio 117
 NAM, Wonwoo 185, 190

- NANBU, Shinkoh 24
 Naraso 173
 NARITA, Muneto 50
 NARUTA, Yoshinori 189
 NATORI, Yutaka 57–58
 NAVARRETE, Juan T. L. 144
 NAVES de BRITO, Arnaldo 102
 NEGISHI, R. 143
 NEGISHI, Yuichi 156–158
 NEYA, Saburo 184
 NEZBEDA, Ivo 36
 NI, Ming 16, 18–20
 NICKUT, Patricia 152
 NIKAWA, Hidefumi 16
 NISHI, Nobuyuki 59–63, 68, 77
 NISHI, Tatsuhiko 164–165
 NISHIBORI, Eiji 84
 NISHIDA, Jun-ichi 173
 NISHIJO, Junichi 59–61
 NISHIMATSU, Takeshi 166
 NISHIMURA, Katsuyuki 49–50
 NISHIMURA, Mamiko 159
 NISHINO, Yoichi 96
 NISHIO, Satoru 99
 NOBUSADA, Katsuyuki 26–27
 NODA, Masaharu 171
 NOGAMI, Yoshio 76, 81
 NOMURA, Kazushige 82
 NOMURA, Masaharu 184
 NONOGAKI, Youichi 106–108
- O**
- ODA, Kenji 178
 OGAWA, Takuji 48, 141–143
 OGINO, Hiraku 166
 OGUCHI, Shiro 97
 OGURA, T. 92
 OGURA, Takashi 178
 OHARA, Tomoaki 32
 OHASHI, Kazuhiko 63
 OHASHI, Masato 134
 OHKUBO, Kei 20
 OHMINE, Iwao 121
 OHMORI, Kenji 64–65
 OHNO, Takashi 135
 OHSHIMA, Eriko 166
 OHSHIMA, Yasuhiro 66–67, 73
 OHSUMI, Hiroyuki 136
 OHTA, Takehiro 176, 182–183, 185–186, 188, 190
 OHTSU, Hideki 125–126, 184
 OHTSUKI, Yukiyoshi 65
 OINUMA, Ken-Ichi 183
 OISHI, Osamu 60–61
 OKABE, Chie 60–62, 68, 77
 OKADA, Michio 171
 OKAMOTO, Hiromi 45–48
 OKAMURA, Rei 123
 OKANO, Yoshinori 84–88
 OKAZAKI, Susumu 117–118
 OKUNO, Daichi 183
 OLOYEDE, Ponmile 22
 OMELYAN, Igor 31
- OMORI, Satoshi 37
 ONO, Shingo 166–167
 ONO, Yuuki 90
 ORTIZ, Rocío P. 144
 OSAKO, Takao 182, 184
 OSHIMA, Kokichi 82
 OSUNA, Reyes M. 144
 OTSUBO, Kazuya 136
 OTSUBO, Saika 88
 OTSUKA, Yoichi 142
 OZAWA, Hiroaki 48, 141, 143
 OZAWA, Takeaki 57–58
- P**
- PAL, Biswajit 177, 185, 188
 PALAUDOUX, Jerome 163
 PENENT, Francis 162–163
 PHONGPHANPHANEE, Saree 30
 PIAO, Qiuyue 19–20
 PINAKOULAKI, Eftychia 176, 182
 PLENGE, Jürgen 102
 POBRE, Romeric 166
 PRODHAN, Md. Serajul Islam 110–114
 PULAY, Peter 17, 19
- Q**
- QUEMA, Alex 166
- R**
- RAHMAN, G. M. Aminur 16
 RATOVELOMANANA-VIDAL, Virginie 135
 RIORDAN, Charles G. 190
 ROSNER, H. 163
 ROVIRA, Concepcio 77
 RUBTSOV, Igor V. 175
 RÜHL, Eckart 102
 RYLANCE, Gareth J. 40
 RZEZNICKA, Izabela I. 63
- S**
- SAGAMI, Ikuko 186
 SAGAYAMA, Hajime 136
 SAIKAWA, Jiro 169
 SAITO, Gunzi 82
 SAITO, Masaichi 15, 20–21
 SAITO, Shinji 121
 SAKAKI, Shigeyoshi 42–43
 SAKAMOTO, Koichi 51
 SAKAMOTO, Masatomi 138
 SAKAMOTO, Youichi 144
 SAKATA, Eri 159
 SAKATA, Makoto 84
 SAKEDA, Kosaku 69
 SAKO, Yusuke 57
 SAKURABA, Akihiro 16, 20
 SAKURAI, Hidehiro 151, 156–157
- SAKURAI, Takashi 124
 SAKURAI, Yoko 164
 SARUKURA, Nobuhiko 166–167
 SASAKAWA, Hiroaki 159
 SASAKI, Ai 186
 SASAMORI, Takahiro 17
 SATO, Emiko 186
 SATO, Hideaki 130–132
 SATO, Hirofumi 28, 42–43
 SATO, Hirokazu 95–96, 141, 143
 SATO, Kumiko 20
 SATO, Osamu 87–88
 SATO, Seiichi 157
 SATO, Yoichi 168–169
 SATO, Yukinori 64
 SATO, Yuko 186
 SATOMOTO, Kensuke 175
 SAUNDERS, Martin 21
 SAWA, Hiroshi 82, 136
 SAWADA, Takeshi 152
 SAYED, Md. Abu 109
 SCHLEYER, Paul v. R. 18
 SCHMIDT, Michael W. 18
 SCHNELLE, W. 163
 SEKIGUCHI, Akira 18
 SEKIYA, Hiroshi 63
 SEO, Mi Sook 185, 190
 SETO, Tomoyoshi 30
 SHEINERMAN, Sergei 163
 SHEN, Jian-Ren 83
 SHIBASAKI, Akihiro 163
 SHIBATA, Naoki 175
 SHICHIBU, Yukatsu 158
 SHIGEMASA, Eiji 162–163
 SHIMADA, Miho 161
 SHIMADA, Toru 47
 SHIMAMURA, Mina 84–85
 SHIMBA, Krando 95
 SHIMIZU, Hideharu 90
 SHIMIZU, Toru 186, 189
 SHIMOSAWA, Masakazu 20–21
 SHINTAKU, Masato 51
 SHINTANI, Takafumi 171
 SHIRAI, T. 23
 SHIRATORI, Kazuya 27
 SHIRO, Motoo 125
 SHIRO, Yoshitsugu 131, 179
 SHITARA, Kenya 159
 SHOUJIGUCHI, Akira 39–40
 SHUDO, Akira 121
 SICHELSCHEMIDT, J. 163
 SLANINA, Zdenek 15, 17–19
 SODA, Kazuo 95–96
 SOLOMON, Edward I. 190
 SONG, Rita 190
 SONG, Wei 16, 20
 SONG, Woon Ju 190
 SORENSEN, Stacey 102
 SOULIMANE, Tewfik 182
 STANISKY, Christopher M. 21
 STEGLICH, F. 164
 SUGAI, Shunji 71
 SUGAWARA, Tadashi 157
 SUGIMOTO, Hideki 124–125

- SUGIMOTO, Hiroshi 131
 SUGIMOTO, Kunihisa 125
 SUGIMOTO, Manabu 178
 SUGITA, A. 23
 SUGIYAMA, Yusuke 17
 SUH, Yumi 185
 SUMA, Kosuke 67
 SUMIKAMA, Takashi 121
 SUZUI, Mitsukazu 105–107, 171
 SUZUKI, Akane 184
 SUZUKI, Masatatsu 184, 190
 SUZUKI, Motohiro 157
 SUZUKI, Tadashi 68–69
 SUZUKI, Takaharu 96
 SUZUKI, Toshiyasu 144
- T**
- TADAOKA, Hiroshi 135
 TAHARA, Tahei 148
 TAIRA, Takunori 168–170
 TAKABATAKE, Toshiro 163–164
 TAKAGI, Hideyuki 62
 TAKAGI, Noriaki 72, 152–155
 TAKAGI, Nozomi 17–18, 20
 TAKAHASHI, Eiji J. 104
 TAKAHASHI, Hiroto 189
 TAKAHASHI, Kazutoshi 63
 TAKAHASHI, Kazuyuki 84–89
 TAKAHASHI, Kenji 190
 TAKAHASHI, Satoshi 51–52
 TAKAHASHI, Toshiharu 161
 TAKAHASHI, Toshihiro 76, 82
 TAKAHATA, Keiichi 133
 TAKASHIMA, Yoshifumi 161–162
 TAKASUGI, Yoshimitsu 157
 TAKEDA, Kazuyoshi 141, 143
 TAKEGAHARA, Katsuhiko 164
 TAKENAKA, Kazuhiro 146
 TAKEUCHI, Tsunehiro 95–96
 TAMURA, Hiroyuki 24
 TANABE, Yoshiaki 133
 TANAKA, Akinori 156
 TANAKA, Atsunari 179
 TANAKA, Hirofumi 141–143
 TANAKA, Keiichi 109
 TANAKA, Keiji 159
 TANAKA, Koji 123–126, 138, 184, 190
 TANAKA, Shoji 145
 TANIDA, Hajime 184
 TANIGUCHI, H. 92
 TAO, Hiroaki 58
 TARUMIZU, Makoto 124
 TATSUMI, Kanako 159
 TERABE, K. 143
 TERAOKA, Noriaki 166
 TERANISHI, Toshiharu 158
 TERANISHI, Y. 23
 TERANISHI, Yoshiaki 65
 TERAOKA, Yuden 105
 TERAZIMA, Masahide 53
 TERO, Ryugo 105–109
- TERO-KUBOTA, Shozo 189
 TODA, Mikito 39–40
 TODO, Takeshi 187–188
 TOKITOH, Norihiro 17
 TOKUNAGA, Aya 136
 TOKUNAGA, Fumio 53
 TOMII, Masato 184
 TOMON, Takashi 125–126
 TOMURA, Masaaki 173, 180
 TOSHA, Takehiko 178–179, 184–187, 190
 TSUCHIYA, Takahiro 15–20
 TSUKUBE, Hiroshi 124–125
 TSUKUDA, Tatsuya 152, 156–158
 TSUNEKANE, Masaki 168
 TSUNOYAMA, Hironori 152, 156–158
 TSURUGI, Hayato 135
 TSURUTA, Takashi 130
 TSUTSUMI, Osamu 141, 143
- U**
- UCHIDA, Kazuhisa 159
 UCHIDA, Takeshi 175–176, 183, 186–188
 UEDA, H. 23
 UEDA, Kiyoshi 64
 UEDA, Yasufumi 175
 UHLIK, Filip 17–19
 ULANSKI, Jacek 77
 UMEZAWA, Yoshio 57–58
 UNO, Hidetaka 105–107, 109
 UNOURA, Kei 139
 UOZUMI, Yasuhiro 146
 URISU, Tsuneo 105–109
 URUGA, Tomoya 184
 URUICHI, Mikio 75–77
 UWATOKO, Yoshiya 136
 UZAWA, Takanori 52
- V**
- VAN HEUVELEN, Katherine M. 190
 VAROTSIS, Constantinos 176, 182
 VIJAYYERGIYA, Viksita 50
 VOEVODIN, V. 163
- W**
- WADA, Tohru 123, 138
 WAELCHLI, Markus 17
 WAKABAYASHI, Kazuhito 69
 WAKABAYASHI, Yusuke 136
 WAKAHARA, Takatsugu 15–20
 WAN, Li-Jun 108
 WANG, Dan 18–19
 WANG, Zheming 86
 WATANABE, Hidekazu 108
 WATANABE, Hirokazu 54
 WATANABE, Kazuo 63
- WATANABE, Kazuya 72, 152–155
 WATANABE, Takahito 128
 WATANABE, Yoshihito 15
 WATERMAN, Michael R. 186
 WILKS, Regan 102
 WOJCIECHOWSKI, Roman 77
- X**
- XU, Qinghong 134
- Y**
- YABANA, Kazuhiro 26
 YABASHI, Satoshi 166–167
 YAGI, Hajime 111–114
 YAGI, Hirokazu 159
 YAGI, Sinya 95–96
 YAGYU, Akihiro 134
 YAJIMA, Takashi 142
 YAKUSHI, Kyuya 75–77, 92
 YAMADA, Akihiro 35
 YAMADA, Atsushi 117
 YAMADA, H. 23
 YAMADA, Michio 16–18
 YAMADA, Yoichi 146
 YAMAGA, Mitsuo 166–167
 YAMAGATA, Tsuneaki 134–135
 YAMAGUCHI, Dai 152–153
 YAMAGUCHI, T. 31
 YAMAGUCHI, Yoshiki 159
 YAMAKAWA, K. 23
 YAMAMOTO, Hiroshi M. 76
 YAMAMOTO, Kaoru 77, 92
 YAMAMOTO, Kenichiro 81
 YAMAMOTO, Kimiko 85
 YAMAMOTO, Norifumi 163
 YAMAMOTO, Takashi 75
 YAMAMOTO, Yohei 81
 YAMAMURA, Shusaku 108
 YAMANAKA, Takaya 73
 YAMASHITA, Mai 190
 YAMASHITA, Takefumi 40
 YAMASHITA, Yasufumi 32
 YAMASHITA, Yoshiro 173
 YAMAWAKI, Michiru 73
 YAMAZAKI, Jun-ichiro 161
 YANAGIMOTO, Yasushi 156
 YANO, Takayuki 171
 YAO, Hiroshi 157
 YASUDA, Hidehiro 156
 YASUIKE, Tomokazu 26
 YE, Hengqiang 16, 18–20
 YI, Jianjun 134
 YOKOGAWA, Daisuke 42–43
 YOKOYAMA, A. 23
 YOKOYAMA, K. 23
 YOKOYAMA, Takashi 145
 YOKOYAMA, Toshihiko 54–55, 157
 YONEMITSU, Kenji 32–33
 YOSHIDA, Norio 28, 30
 YOSHIDA, Tadashi 178–179

YOSHIGOE, Akitaka 105
YOSHIHARA, Keitaro 175
YOSHII, Noriyuki 117–118
YOSHIKAWA, Akira 166
YOSHIMURA, Hideaki
176, 183, 186
YOSHIMURA, Tetsuaki 185
YOSHIMURA, Tetsuhiko 179
YOSHIOKA, Michikazu 15, 20–21
YOSHIOKA, Shiro
175–177, 183, 185–187
YOZA, Kenji 16, 18–20
YU, Dapeng 16, 18–20
YUMOTO, Noboru 183

Z

ZAVODSZKY, Peter 183
ZHANG, Li 50
ZHANG, Tao 95
ZHANG, Tieqiao 175
ZHANG, Xinwei 16, 18–19
ZHANG, Zhen-Long 106–107
ZHAO, Yi 22
ZHARMUKHAMEDOV, Sergei K.
149
ZHOU, Biao 84–85
ZHOU, Huan-Xiang 50
ZHOU, Yunsong 18–19
ZOU, Shiyang 22, 24